Wear Rate of TiN Coatings:
Wear and Hardness Determination

AALBORG UNIVERSITY

DENMARK

P10

Physics Nanophysics

Aalborg University

Submitted: 31-10-2025

Title Sheet

10th Term Physics Nanophysics
Department of Materials and Production
Pontoppidanstræde 103
Aalborg 9220

Title:

Wear Rate of TiN Coatings:
Wear and Hardness Determination

Project:

P10

Project Period:

February 2025 - October 2025

Participants:

Claudia Larsen
Maciej Bartosz Skucha

Supervisor:

Lars Diekhöner

Number of Pages:

255

Abstract:

Titanium nitride (TiN) thin films with a thickness of 1500 nm were deposited onto stainless steel substrates and evaluated through tribological testing, scanning electron microscopy (SEM), and X-ray diffraction (XRD). Tribometer results showed that under moderate and high loads, the wear depth frequently exceeded the coating thickness, reaching up to 6000 nm in some cases. This led to complete coating penetration and exposure of the stainless steel substrate, resulting in uncontrolled wear and relatively high measured wear rates. SEM imaging confirmed mechanical degradation at the wear track edges, including cracking indicative of coating failure. XRD analysis identified a nanocrystalline TiN structure with strong (111) preferred orientation and a lattice parameter of approximately 4.24 Å, consistent with reference values. The stainless steel substrate peaks remained visible due to X-ray penetration through the thin coating, and their sharpness indicated a well-crystallized substrate. Overall, the results demonstrate that while the deposited TiN coatings exhibit the expected crystalline structure and wear protective behavior, their limited thickness and adhesion restricts load bearing capability. Increasing coating thickness and adhesion would likely improve wear resistance and more clearly reveal the capabilities of the TiN layer.

Summary

The purpose of this project is to investigate the wear behavior of titanium nitride (TiN) coatings deposited on stainless steel substrates using direct current (DC) magnetron sputtering. The study aims to understand how TiN film thickness and deposition parameters influence mechanical performance, coating adhesion, and wear resistance, and to compare the coated samples to uncoated (virgin) stainless steel as a reference.
The TiN coatings were deposited via DC magnetron sputtering under controlled vacuum conditions. The sputtering process was analyzed in detail, including plasma generation, ion–target interactions, and the role of the magnetic confinement field in enhancing deposition efficiency. Stainless steel 304 samples, both coated and uncoated, were subjected to tribological testing using a TRB-3 tribometer at various loads and cycle counts to determine wear rates and specific wear coefficients. Surface profiles were obtained using an Ambios XP-2 line profiler to measure wear track geometry, while additional characterization such as scanning electron microscopy (SEM) and X-ray diffraction (XRD) was used to examine microstructure and crystal orientation.
The theoretical framework covers the physical vapor deposition (PVD) mechanism, focusing on the fundamental principles of DC magnetron sputtering, plasma physics, and the film growth. The structure and properties of TiN are discussed in relation to its cubic NaCl-type crystal lattice and mechanical hardness. Mechanistic explanations are provided to describe how increased coating thickness contributes to reduced delamination and crack propagation, leading to enhanced wear durability.
The findings show that TiN coatings somewhat improve the wear resistance of stainless steel substrates, attributed most likely due to their high hardness and strong adhesion when deposited under optimized sputtering conditions. Thicker TiN layers could possibly provide improved stress distribution and inhibit crack growth, thereby preventing delamination during sliding wear. Overall, the study highlights the effectiveness of DC magnetron sputtering as a precise and controllable method for producing coatings and it establishes a correlation between coating parameters, film structure, and tribological performance.

Preface

This masters project was carried out by 10th semester physics and nanophysics students of Aalborg University - Department of Materials and Production, with Lars Diekhöner acting as supervisor.

The sources are referenced to with the apalike method and are found in the bibliography in alphabetical order. Furthermore, references to equations are noted with parenthesis around the equation number and all vectors are denoted by bold-face letters.

We would like to give a special thanks to Peter Kjær Kristensen for providing invaluable advice/guidance and materials necessary for the project.

ChatGPT was used in this project. ChatGPT was used to help create and troubleshoot the code for the figures and graphs. ChatGPT has not written any sentences in the project directly, however, its feedback on some of the grammar corrections or formulations has been used to ensure a better understanding of what has been written.

Claudia Larsen
clar20@student.aau.dk

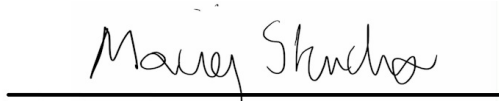

Maciej Bartosz Skucha
mskuch23@student.aau.dk

Contents

Chapter 1

Introduction

Titanium nitride (TiN) coatings have emerged as a leading choice for enhancing the surface properties of engineering materials, particularly stainless steels, due to their exceptional hardness, corrosion resistance and wear resistance. These coatings, typically golden in appearance, are widely used in cutting tools, biomedical devices and decorative applications. When deposited onto stainless steel, TiN significantly improves surface durability, making it highly relevant for industrial components exposed to mechanical stress and aggressive environments.[Vallejo-Otero et al., 2025]

The physical vapor deposition (PVD) method, specifically reactive magnetron sputtering—is a well-established technique for depositing TiN thin films. This technique provides excellent control over film thickness, composition, and structure, while maintaining relatively low substrate temperatures, which is critical when working with thermally sensitive substrates like stainless steel. In this project, TiN coatings were deposited onto stainless steel substrates using the Flextura 200 sputtering system, a versatile PVD platform that enables precise tuning of sputtering parameters such as power, pressure, gas flow and deposition time. This allows optimization of coating characteristics for targeted performance metrics.[Baptista et al., 2018a]

The coated samples were subjected to a comprehensive suite of characterization techniques to assess their mechanical and topographical properties. Tribological testing using a tribometer evaluated the friction and wear behavior of the TiN films under controlled sliding conditions. This is crucial because wear resistance is one of the most desirable properties of TiN coatings and is a key performance indicator in applications such as tools and bearings.[Novak and Polcar, 2014]

To investigate hardness and mechanical performance on a microscale, the samples were tested using a Duramin microhardness tester. The Vickers microhardness data provides insights into the resistance of the coatings to plastic deformation, which is directly related to their durability under real-world operational conditions. Meanwhile, surface topography and roughness were examined using a line profiler and Atomic Force Microscopy (AFM). These tools offer complementary data: the line profiler provides fast, quantitative measurements of roughness over longer lateral distances, while AFM delivers nanoscale 3D surface morphology, capturing fine features that may affect friction or adhesion.[Sakaguchi and Powers, 2012]

Further structural and morphological analysis was performed using a Scanning Electron Microscope (SEM). SEM imaging enables high-resolution visualization of the film's microstructure, such as grain size, porosity and coating defects. These features are crucial in understanding the correlation between deposition conditions and coating performance. In addition, cross-sectional SEM imaging can provide insight into film thickness, layer adhesion and interface quality between the coating and the substrate.[Mohammed and Abdullah, 2019]

The broader motivation for this project lies in the continuous demand for more durable, corrosion-resistant and mechanically robust surfaces in industrial and medical applications. Stainless steel, while inherently corrosion resistant, lacks the hardness and wear resistance required in high-performance scenarios. By applying a hard, inert TiN layer through an optimized sputtering process, the functional lifetime of stain-

less steel components can be significantly extended. Moreover, tailoring the surface characteristics via PVD parameters could lead to tunable coatings that can be adapted to specific mechanical or chemical requirements.[Wisbey et al., 1987]

The findings from this study contribute to the growing body of knowledge on PVD TiN coatings, offering insights into how deposition conditions affect coating performance on stainless steel substrates. By leveraging multiple advanced surface characterization techniques, this work aims to establish a robust relationship between the deposition process, microstructure and functional properties of TiN films.

Theory

2.1 Crystal Structure and Defects in TiN

This section describes the crystal structure and defects in TiN coating.

Titanium nitride (TiN) is a transition metal nitride with a face-centered cubic (fcc) crystal structure of the NaCl (B1) type. Titanium atoms occupy the fcc lattice points, while nitrogen atoms fill the octahedral interstitial sites. The lattice constant a_0 for stoichiometric TiN is approximately 4.24 Å.

2.1.1 Atomic Arrangement and Bonding

The Ti–N bond is partly covalent and partly metallic in character, which gives TiN its combination of high hardness, good electrical conductivity and thermal stability. The bonding energy can be approximated as:

$$E_{bond} = \chi Ti * \chi N + \frac{1}{2} E_{metallic} \tag{2.1.1}$$

, where χ Ti and χ N represent electronegativities of titanium and nitrogen, respectively. The mixed bonding nature makes TiN harder than pure titanium yet still conductive.

2.1.2 Crystal Geometry

In the NaCl structure, each Ti atom is surrounded by six N atoms at distance $a_0/2$ and vice versa. The interplanar spacing for cubic crystals is given by:

$$d_{hkl} = \frac{a_0}{\sqrt{h^2 + k^2 + l^2}} \tag{2.1.2}$$

This relationship allows determination of preferred crystal orientations, for example (111), (200), or (220) from X-ray diffraction (XRD) data. Orientation affects mechanical behavior: the (111) planes have higher packing density and lower surface energy. This often means that they have higher hardness.[Steneteg et al., 2013]

2.1.3 Dislocations and Burgers Vector

Dislocations are line defects in the crystal lattice that play a crucial role in determining the mechanical properties of materials, including TiN. The main types are point defects, line defects, and planar defects. The Burgers vector b characterizes the magnitude and direction of the lattice distortion associated with a dislocation. In cubic crystals such as TiN, which crystallizes in a NaCl-type face-centered cubic structure, the Burgers vector typically corresponds to the shortest lattice translation vector, often along the [110] direction. It can be expressed as:

$$\mathbf{b} = \frac{a_0}{2}\langle 110 \rangle \tag{2.1.3}$$

, where a_0 is the lattice constant of TiN. The presence of dislocations enables plastic deformation under applied stress, as they allow atomic planes to slip relative to one another without the need to simultaneously break all atomic bonds along a plane. The density of dislocations, ρ_d, is defined as the total dislocation line length per unit volume and is inversely related to the square of the average spacing between dislocations:

$$\rho_d = \frac{1}{L^2} \tag{2.1.4}$$

, where L represents the average distance between dislocations. Dislocation motion is resisted by lattice friction, quantified by the Peierls–Nabarro stress τ_p, which depends on the shear modulus G, Poisson's ratio ν, the width of the dislocation w, and the Burgers vector b:

$$\tau_p = \frac{2G}{1-\nu} \exp\left(-\frac{2\pi w}{b}\right) \tag{2.1.5}$$

These dislocation mechanisms are fundamental in understanding how TiN coatings respond to mechanical loads, as they directly influence hardness, residual stress accommodation, and the onset of plastic deformation during wear. [Joós and Duesbery, 1997]

Ti or N vacancies occur when atoms are missing from lattice sites. Nitrogen deficiency leads to metallic behavior and slightly lower hardness. The vacancy concentration N_v can be expressed with this equation:

$$\frac{N_v}{N} = \exp\left(-\frac{Q_v}{k_B T}\right) \tag{2.1.6}$$

, where Q_v is the vacancy formation energy. Stacking faults and twin boundaries form during rapid film growth and can also influence hardness.

The presence of defects in TiN significantly affects its physical and mechanical properties. For instance, electrical conductivity tends to increase in the presence of titanium or nitrogen vacancies, as these defects introduce additional free carriers, making the material more metallic in character. Hardness is also influenced by defects, particularly dislocations; an increase in dislocation density generally enhances hardness due to the obstruction of slip, although excessive dislocation accumulation can lead to defect coalescence, which ultimately reduces hardness. Furthermore, residual stress in sputtered TiN films often arises from a combination of lattice mismatch between the film and the substrate and the accumulation of defects during the deposition process. This stress can influence adhesion, fracture behavior, and the overall mechanical performance of the coating.[Tewary, 2002]

2.2 Mechanical Properties and Anisotropy

This section describes the mechanical properties and anisotropy of TiN coating.

The mechanical response of a TiN crystal to an applied stress is described by Hooke's law in its general tensor form, which relates the stress tensor σ_{ij} to the strain tensor ϵ_{kl} via the stiffness tensor C_{ijkl}:

$$\sigma_{ij} = C_{ijkl}\,\varepsilon_{kl} \tag{2.2.1}$$

, where, C_{ijkl} contains the elastic constants of the material and captures the anisotropic nature of the crystal lattice. For a cubic crystal such as TiN, the Young's modulus along an arbitrary crystallographic direction [hkl] can be expressed in terms of the elastic compliance constants S_{11}, S_{12}, S_{44}

$$\frac{1}{E_{[hkl]}} = S_{11} - 2\left(S_{11} - S_{12} - \frac{1}{2}S_{44}\right)\frac{h^2k^2 + k^2l^2 + l^2h^2}{(h^2+k^2+l^2)^2} \tag{2.2.2}$$

This relationship highlights the anisotropy of elastic properties, where the stiffness depends on the orientation of the applied stress relative to the crystal axes. The onset of plastic deformation occurs when the applied stress resolves onto a slip system and reaches the critical resolved shear stress, τ_{CRSS}. It is given by:

$$\tau_{\text{CRSS}} = \sigma_y \cos\phi \cos\lambda \tag{2.2.3}$$

, where ϕ is the angle between the stress direction and the slip direction and λ is the angle between the stress direction and the normal to the slip plane. This formulation is central to understanding dislocation motion and plasticity in anisotropic materials.[Yang et al., 2017] In polycrystalline TiN coatings, individual grains are oriented randomly, so the effective Young's modulus of the film is an average over all crystallographic directions:

$$E_{\text{film}} = \sum_i f_i E_{[hkl]_i} \tag{2.2.4}$$

, where f_i is the fraction of grains oriented along $[hkl]_i$ and $E_{[hkl]_i}$ is the directional Young's modulus for that orientation. Residual stress in TiN films arises both from thermal mismatch between the film and substrate and from internal stresses due to lattice defects. In anisotropic films, the residual stress can be expressed as:

$$\sigma_{\text{res}} = \frac{E_f}{1-\nu_f}(\alpha_s - \alpha_f)\Delta T + \sigma_{\text{int}} \tag{2.2.5}$$

, where E_f and ν_f are the Young's modulus and Poisson's ratio of the film, α_s and α_f are the thermal expansion coefficients of the substrate and film, Δ T is the temperature difference, and σ_{int} accounts for stress due to defects. The hardness of TiN can vary depending on the crystal orientation and the distribution of defects. The relationship between hardness $H_{[hkl]}$ and anisotropy is often reflected in models linking hardness to the resolved stress on slip systems, where higher resistance to dislocation motion leads to higher hardness. Finally, the wear behavior of TiN coatings is strongly influenced by anisotropic mechanical properties such as directional hardness and residual stress. A simplified proportional relationship can be written as:

$$W \propto \frac{1}{H_{[hkl]}} \cdot f_{\text{stress}}(\sigma_{\text{res}}) \tag{2.2.6}$$

,where W is the wear rate, $H_{[hkl]}$ is the directional hardness and stress $f_{(stress)}$ (σ_{res}) is a function accounting for the influence of residual and applied stresses on material removal.[Kim et al., 1992]

2.3 Physical Vapor Deposition - Sputtering

This section describes the physical vapor deposition method for coating a substrate/sample with a given material.

Physical Vapour Deposition (PVD) represents a class of vacuum-based coating techniques used to produce thin films and surface layers with precise control over composition and structure. Among various PVD methods, sputtering is one of the most widely employed due to its versatility and capability to deposit high-quality coatings on a wide range of substrates. In PVD processes, material is physically transferred from a solid source (target) to a substrate through a vapour or plasma phase within a vacuum or low-pressure gas environment. The process involves three main stages: vaporisation of the target material, transport of the vapour species through the gas phase, and condensation of these species onto the substrate surface to

form a thin film. Unlike Chemical Vapour Deposition (CVD), PVD is solely based on physical mechanisms, without the involvement of chemical reactions.[Depla and Mahieu, 2008]
To initiate sputtering, the chamber is first evacuated to a low base pressure to minimize contamination and enable efficient momentum transfer. Subsequently, an inert gas (typically argon) is introduced at a controlled flow rate. When a high voltage is applied between the negatively charged cathode (target) and the anode (substrate holder or chamber wall), the electric field ionises the argon atoms, creating a plasma composed of positively charged Ar^+ ions and free electrons. The ions are accelerated toward the target surface, where their impact ejects atoms or clusters from the target material. These sputtered atoms then travel through the low-pressure gas and condense on the substrate, forming a thin film.
Sputtering is a key technique in thin-film manufacturing, with applications ranging from optical coatings and anti-reflective layers to microelectronics and semiconductor fabrication. In this project, the direct current (DC) magnetron sputtering configuration is employed, as it enables efficient deposition from conductive targets while ensuring stable plasma generation and uniform film growth. [Baptista et al., 2018a]
Sputtering has some advantages over other methods, for example simple evaporation. First of all it has better control over film composition (for example in alloys or compounds) because sputtering can eject material with more stoichiometric fidelity. Also we can achieve better film adhesion and denser films. Additionally more uniform coatings can be deposited onto the substrate. It is especially possible in magnetron sputtering. We can also able to deposit a wider range of materials (for example metals, dielectrics or compounds), including those with high melting points. [A. Mubarak et al., 2018]
The sputtering process consists of a few steps. It starts up with a ramp up. It is the initial phase where the vacuum chamber is prepared for deposition. This procedure stabilizes the plasma prior to the onset of deposition, thereby ensuring consistent plasma conditions that contribute to improved film quality and reproducibility. It involves the activation of vacuum pumps to lower the pressure to a process level and gradual increase in temperature. Also, to establish a stable plasma, the power is ramped up to the target. It is done typically in small increments over several minutes, which prevents any damages to the target for example thermal shock from sudden and uneven heating. A slower ramp-up is crucial for conditioning a target. On the other hand, process control plays a key role in defining the maximum stable power and the corresponding deposition rate, parameters that directly influence the accuracy and uniformity of the resulting film thickness.[Steinmann and Hintermann, 1985]
The next stage involves etching, which functions as a form of cathodic cleaning to remove surface contaminants prior to deposition. The substrate in this procedure is bombardment by ions from plasma. This step is important before a deposition because it increases adhesion. The adhesion of a coating to the substrate is largely determined by the physical and chemical properties of the substrate itself. The substrate material defines parameters such as surface energy, thermal expansion coefficient and chemical compatibility with the deposited layer. The hardness of the substrate affects its resistance to plastic deformation during deposition and cooling, which can help to minimize the formation of stresses and cracks at the interface. In turn, the surface quality, which is characterized by its roughness, cleanliness and the presence of defects, directly influences the number of active adhesion sites, and consequently, the strength of the bond between the coating and the substrate.[Barshilia et al., 2012]
The third step is coating. The material that is going to be deposited is projected to the substrate surface. There are few materials that can be used for example titanium, chromium, zirconium and nitrides or oxides among others. There are some limitations of which material can be used with which method. The coating properties also depend on the different methods and procedure settings. The last step is ramp downstage. It is the ending stage, where the vacuum chamber is returning to the room temperature and ambient pressure.

Coating properties shouldn't be damaged by any equipment during unloading and cooling.[Wasa et al., 2004]

2.3.1 Physical mechanism of sputtering

2.3.2 Plasma Generation and Ion Bombardment

The target and substrate are put into a sputtering equipment. Inert gas such as Ar is introduced at low pressure in the vacuum chamber. High voltage is applied to the target (cathode) relative to substrate or ground. Glow discharge plasma initiates, electrons are accelerated and ionization of argon atoms is generated. The Ar^+ ions are created. These ions are then accelerated towards the negatively biased target, aforementioned cathode. When the ions impact the target surface with sufficient kinetic energy (typically in the range of tens to hundreds of electronvolts), momentum is transferred through collision cascades to the atoms within the target lattice. As a result, some of these atoms acquire enough energy to overcome the surface binding forces and are ejected into the surrounding vacuum or gas phase. Secondary electrons are emitted from the target surface as a result of ion bombardment. These electrons play a crucial role in sustaining the plasma by further ionising the inert gas atoms. In magnetron sputtering systems, a magnetic field is applied near the target to confine these electrons close to the surface, thereby enhancing the ionisation efficiency of the plasma and enabling stable operation at lower working pressures.[Musin, 2025]

2.3.3 Sputtering Yield and Ejection of Target Atoms

The sputtering yield is defined as the number of atoms ejected from the target per incident ion. The yield depends on several factors. First of all it depends on the energy of the incident ion. The energy of the incident ions, provided it exceeds a certain threshold, has a significant influence on the sputtering yield. Generally, the yield increases with ion energy up to an optimal value, as higher energies promote more effective momentum transfer and deeper collision cascades within the target material. Also, if masses of ion and target atom are comparable the target is effectively knocked-out and better momentum transfer occurs. The sputtering yield is also strongly influenced by several intrinsic and geometrical factors related to the target material and ion incidence conditions. The binding energy of the target atoms (both surface binding and lattice binding energy) plays a crucial role, as higher binding energies require more momentum transfer for atom ejection. Additionally, the crystallographic orientation, grain structure, and the presence of surface or near-surface defects affect the ease with which atoms can be dislodged from the lattice. The angle of ion incidence relative to the target surface further impacts the yield. Typically, an oblique incidence increases the sputtering yield up to an optimal angle, as ions produce more efficient, shallow collision cascades near the surface. However, at excessively large angles, the yield may decrease due to reflection or reduced energy transfer.[Sigmund, 1969]
During the ejection process, sputtered atoms or clusters are emitted with a characteristic energy and angular distribution (typically in the range of several tens of electronvolts). These particles then travel through the low-pressure gas environment toward the substrate. Depending on the working pressure, some atoms undergo scattering collisions with gas atoms, leading to trajectory deviations and energy losses. At higher pressures, this transport becomes increasingly diffusive rather than purely line-of-sight.[Falcone, 1988]

2.3.4 Transport and Condensation Onto the Substrate

The sputtered atoms travel from the target toward the substrate through the low-pressure environment of the deposition chamber. At low working pressures, their motion is predominantly ballistic, allowing the atoms

to maintain relatively high kinetic energies and direct trajectories. As the pressure increases, collisions with background gas atoms become more frequent, leading to scattering, energy loss and broader angular distributions of the arriving species.[Baptista et al., 2018b]
Upon reaching the substrate surface, the atoms condense and contribute to film formation. Depending on their kinetic energy, the substrate temperature, deposition parameters, and any applied substrate bias, the adatoms may diffuse across the surface, nucleate into clusters and subsequently coalesce into islands or continuous layers, eventually forming a coherent thin film. The comparatively high energy of sputtered atoms (often much greater than that in thermal evaporation) enhances adatom mobility, promoting the growth of denser films with improved adhesion and reduced porosity.[Fox-Rabinovich et al., 2016]

2.3.5 Role of Substrate Bias, Target Bias, Magnetron Geometry

In many sputtering systems, a bias voltage (either direct current (DC), pulsed-DC or radio frequency (RF)) is applied to the substrate. This bias accelerates positive ions from the plasma toward the substrate surface, increasing the kinetic energy of the arriving species and resulting in controlled ion bombardment of the growing film. Such bombardment can enhance film density, reduce void formation and improve adhesion by promoting adatom mobility and interfacial mixing. However, excessive ion energy may lead to film damage, re-sputtering of surface atoms or the introduction of stress within the growing layer.[Pei et al., 2021]
The target is powered by an external supply whose configuration depends on the electrical properties of the target material. In DC magnetron sputtering, a constant DC voltage is applied, suitable for conductive targets, whereas RF or pulsed-DC power is employed for insulating or partially conductive materials to prevent charge buildup. Increasing the applied power generally enhances the sputtering rate by generating more ions and ejecting a greater number of target atoms. Nevertheless, higher power can also induce undesirable effects such as target overheating, stress development or target poisoning in reactive sputtering environments.[Azibi et al., 2019]
In magnetron sputtering, the application of a magnetic field near the target surface confines electrons within closed drift paths, increasing plasma density and ionisation efficiency. This configuration not only improves sputtering rate and film uniformity but also enables stable operation at lower pressures, reducing gas-phase scattering and facilitating more ballistic transport of sputtered atoms toward the substrate.[Borowski and Myśliwiec, 2025]

2.3.6 Process Parameters Influences on Film Properties

The key process parameters in sputtering significantly influence the resulting film properties, including its composition, microstructure, thickness, adhesion and surface roughness. One of the most critical factors is the working gas pressure. At low pressures, the mean free path of sputtered atoms is relatively long, allowing them to reach the substrate with higher kinetic energy and more direct, line-of-sight trajectories. This typically promotes the formation of dense films with smooth surfaces and well-adhered microstructures. However, if the pressure is too low, the plasma may become unstable or spatially non-uniform, leading to process inconsistency. Conversely, at higher pressures, increased scattering of sputtered species reduces their energy and directionality, which can result in lower film density and a more porous or rough surface morphology. Other important parameters include the applied power, the target–substrate distance and the target size. Increasing the applied power raises the ion flux toward the target, thereby enhancing the sputtering yield and deposition rate. However, excessively high deposition rates may limit adatom surface diffusion on the substrate, potentially producing coarser grain structures or higher defect densities. The spacing between the target and substrate determines the angular distribution and scattering extent of sputtered atoms. A larger

separation generally increases scattering and reduces the uniformity of film deposition. Finally, employing a larger-area target facilitates improved thickness uniformity over the substrate surface, which is particularly advantageous for large-scale or industrial coating applications.[Kusano, 2018]
Another crucial set of parameters influencing film growth and properties are the substrate temperature and substrate bias. Increasing the substrate temperature enhances the surface mobility of adatoms, which promotes improved crystallinity, larger grain size and higher film density. However, excessive heating can lead to undesirable effects such as increased residual stress or interdiffusion between the film and the substrate. Applying a bias voltage to the substrate introduces additional ion bombardment during deposition. This controlled bombardment can densify the growing film, minimize void formation and improve interfacial adhesion. Nevertheless, an excessively high bias may induce surface damage, cause re-sputtering of deposited material or lead to unwanted film heating. Finally, in reactive sputtering, the introduction of reactive gases (such as nitrogen or oxygen) enables the formation of compound films (such as nitrides or oxides) through chemical reactions at the target and substrate surfaces. While this approach allows for precise tailoring of film composition, it also introduces complexities including target poisoning (the formation of a compound layer on the target surface that reduces the sputtering rate), challenges in maintaining film stoichiometry and the development of intrinsic stresses within the deposited layer.[Sproul et al., 2005]

2.3.7 Film Growth, Structure and Stress in Sputtered Films

2.3.8 Microstructure: Nucleation, Growth and Densification

During the initial stages of thin film formation, adatoms arriving on the substrate surface diffuse and aggregate to form nuclei. The extent of adatom migration depends strongly on their kinetic energy and the substrate temperature. These nuclei subsequently grow and coalesce, eventually forming a continuous film layer. In sputtering processes, the arriving species typically possess non-thermal kinetic energies on the order of tens of electronvolts compared to less than 1 eV in thermal evaporation. This enhanced energy promotes greater adatom mobility and can facilitate film densification through localized bombardment effects.
Ion bombardment, whether originating from an applied substrate bias or from backscattered ions, contributes further to film compaction by filling voids and reducing columnar porosity (“shadowing”). However, excessive energetic bombardment may also introduce defects, induce atomic intermixing at the film – substrate interface or generate residual stresses. When the deposition rate is high relative to surface diffusion, the resulting film tends to exhibit smaller grains, higher defect density and a columnar microstructure with voids. Conversely, slower deposition rates or elevated substrate temperatures enhance adatom mobility, enabling larger grain growth and more relaxed, dense film structures.[Luis et al., 2020]

2.3.9 Residual Stress

Residual stress in sputtered thin films originates from multiple sources: intrinsic stress, arising from microstructural defects, grain boundary formation and impurity incorporation during growth; thermal stress, due to mismatches in the coefficients of thermal expansion between the film and substrate during cooling; and extrinsic stress, resulting from energetic bombardment or applied substrate bias.
Energetic particle bombardment can lead to atom implantation and peening effects, which compact the film and induce compressive stresses. In contrast, tensile stresses may arise from columnar growth modes, void formation or grain boundary shrinkage during coalescence. Managing these stresses is critical, as

excessive stress can lead to cracking, delamination or substrate curvature. Careful adjustment of deposition parameters such as ion energy, substrate temperature, bias voltage and cooling rate, enables control over the magnitude and nature of residual stresses. Compared to thermal evaporation, sputtering provides superior stress control due to the higher kinetic energy and tunability of the arriving species.[Li et al., 2022]

2.3.10 Film Uniformity, Composition and Adhesion

Film thickness uniformity is primarily governed by the geometry of the target – substrate arrangement, target dimensions, plasma uniformity and gas flow distribution within the chamber. Reactor design considerations such as substrate rotation, target scanning and multi - cathode configurations, play an essential role in achieving uniform coatings. Studies have demonstrated that the substrate rotation speed and configuration can significantly influence the resulting surface morphology and film texture.
Control over film composition is equally important, particularly in reactive sputtering processes used to deposit compounds such as oxides or nitrides. The reactive gas partial pressure, target poisoning effects and overall deposition kinetics determine the final stoichiometry and phase composition of the film. Maintaining an optimal balance among these parameters ensures reproducible film composition, good adhesion and stable long-term performance.[Berg and Nyberg, 2005]

2.3.11 Theoretical Background of Plasma Discharge and Sputtering Mechanisms in PVD

When these ions strike the target, they transfer momentum to the target atoms, ejecting them from the surface: sputtering. While keeping the discharge current constant, another gas, like nitrogen or oxygen, is added in steps. After each step, the process parameters are recorded once the system reaches a steady state. When the target becomes fully poisoned, the process is reversed: the gas flow is stepwise reduced until it returns to pure argon. The discharge voltage (2.3.1) should be monitored during this process. Note that this voltage is technically negative, however, its absolute value is usually displayed. [Serway and Jewett, 2013]
To ionize a neutral gas atom, an electron must provide an average energy W_0 (effective ionization energy: Higher W_0 means more energy required per ion i.e. higher voltage needed to maintain plasma). But not every electron successfully causes ionization so we define ε_e which is the efficiency with which electrons generate ions and m which is the electron multiplication factor (average number of ionizations an electron causes before being lost). The total energy needed to sustain the plasma per ion is then:

$$E_n = \frac{W_0}{\varepsilon_e m}$$

In a plasma discharge, when positive gas ions hit the negatively charged target, they transfer energy to the surface. This impact can knock out electrons from the target atoms. These knocked-out electrons are called secondary electrons. Each ion hitting the target ejects γ_{ISEE} secondary electrons, but only a fraction ε_i of the generated ions reach the target.[Zheng et al., 2015]
The number of electrons emitted per original electron is then equal to the secondary electron gain, which is $\gamma_{ISEE}\varepsilon_i$. Higher γ_{ISEE} means more electrons emitted per ion hit which in turn means a lower voltage needed to maintain plasma. For a stable discharge, each emitted electron must cause ionizations that ultimately lead to at least one ion returning to the target and releasing another electron, thus the energy that needs to be supplied by the discharge should be the energy required to maintain plasma per ion over number of secondary electrons per ion:

$$V_dis = \frac{\frac{W_0}{\varepsilon_e m}}{\gamma_{ISEE}\varepsilon_i} = \frac{W_0}{\gamma_{ISEE}\varepsilon_e\varepsilon_i m}.$$

To this expression we add the effective ionization probability factor for a gas atom E, which adjusts the effectiveness of the ionization process based on pressure, gas type, and electron energy distribution by scaling the number of successful ionization events. The discharge voltage is thus:

$$V_dis = \frac{W_0}{\gamma_{ISEE}\varepsilon_e\varepsilon_i Em}, \tag{2.3.1}$$

In magnetron sputtering, a magnetic field is applied near the target surface. This magnetic field is oriented so that it traps electrons close to the target by forcing them into spiral paths via the Lorentz force. These trapped electrons circle around the magnetic field lines, staying near the surface much longer than in a regular discharge. Since ε_e is the fraction of the theoretical maximum number of ions that an electron can actually produce before it is lost from the discharge and because the electrons are trapped and forced to collide many times, they are highly efficient at ionizing gas atoms before escaping, thus $\varepsilon_e \approx 1$. Consequently, trapping the electrons near the target surface also causes most of the ions to reach the target surface, thus $\varepsilon_i \approx 1$ also.[Pittman and Lu, 2020]

The ion current density (I) tells us how many ions hit the target per unit area per second, and f is the fraction of the reactive gas (gas that reacts with deposited material) in the plasma. This reactive gas forms molecular ions, each ion contains two reactive atoms and thus, for each ion, two atoms are delivered to the target. So the total number of reactive atoms hitting the target per second per unit area is $2fI$. The assumptions here are that the argon and reactive gases are ionized equally in the plasma, the ions have much more energy than the energy binding the atoms in the molecule (So when a molecular ion hits the target, it splits into two atoms, each carrying about half the original energy) and that argon atoms that hit the target are ignored because they don't contribute chemically.[Shapovalov, 2023]

The probability of a particle stopping somewhere inside the target is given by the probability density function.

$$\int_0^D p(x)\mathrm{d}x = 1 - B,$$

where $p(x)\mathrm{d}x$ gives the probability that a particle will stop between a depth of x and $x + \mathrm{d}x$ inside the target, D is the implantation depth and B is a scattering coefficient accounting for reflected ions.

When sputtered atoms move through the gas in the vacuum chamber, they can collide with gas atoms randomly. This randomness follows a Poisson distribution, which describes random events happening over time. The distance a sputtered atom travels before hitting a gas atom (free path length, λ^*), varies randomly but can be determined stochastically from the Poisson distribution by using Monte Carlo simulations. This simulation picks a random number x between 0 and 1 and calculates the free path length of the atom using:

$$\lambda^* = \lambda \ln\left(\frac{1}{1-x}\right),$$

where λ is the mean free path of the atom. λ can be found if we consider the atom to have a diameter d. Then the effective collision area is given by $A = \pi d^2$.[Berg et al., 1987]

$$\lambda = \frac{RT}{\sqrt{2}\pi d^2 P}$$

This equation describes the mean free path (λ) of gas atoms or molecules. That is, the average distance a particle travels between successive collisions with other particles in a gas. It is a key parameter in understanding the behavior of sputtered atoms as they travel through the background gas in the sputtering chamber.
The denominator contains $\sqrt{2}\pi\mathbf{d^2}$, which represents the effective collision cross-section, the area in which two gas atoms are likely to collide. The presence of pressure P in the denominator shows that the mean free path is inversely proportional to the gas pressure: as pressure increases, gas atoms are closer together, leading to more frequent collisions and a shorter λ. Conversely, at lower pressures, the mean free path increases, allowing sputtered atoms to travel farther without scattering.
In the context of magnetron sputtering, this relationship is crucial for determining whether the transport of sputtered atoms from target to substrate is ballistic or diffusive. At very low pressures (long λ), the atoms move almost directly in line-of-sight trajectories to the substrate, preserving their kinetic energy. At higher pressures (short λ), multiple collisions cause energy loss and angular broadening, which can significantly influence film morphology, density, and uniformity.[Kuffel et al., 2000]

2.3.12 DC Magnetron Sputtering Process Step by Step

The list below shows each step in order of the DC magnetron sputtering process. The image below the list is a sputtering chamber scheme with all the key parts and processes, which occurs there.

1. Vacuum chamber evacuation: The deposition chamber is initially evacuated to achieve a low base pressure, minimizing contamination from residual gases and ensuring stable plasma conditions during the sputtering process.

2. Gas introduction: After evacuation, an inert process gas (typically argon) is introduced into the chamber at a controlled pressure to serve as the medium for plasma generation.

3. Target and substrate configuration: The sputtering target (cathode), composed of the material to be deposited, is mounted opposite the substrate (anode), which serves as the surface for thin-film growth.

4. Application of DC power: A negative direct-current (DC) potential is applied to the target, while the substrate is held at ground or a positive potential. This potential difference initiates the movement of charged particles necessary for plasma formation.

5. Plasma generation: Electrons emitted from the negatively biased target collide with argon atoms, causing ionisation and resulting in the formation of a stable plasma composed of positively charged Ar^+ ions and free electrons.

6. Ion bombardment of the target: The positively charged argon ions are accelerated toward the negatively biased target surface, where their impact transfers momentum to target atoms, ejecting them through the sputtering process.

7. Magnetron confinement: Magnets positioned behind the target generate a magnetic field that confines electrons near the target surface. This increases their path length and enhances ionisation efficiency, thereby enabling a high-density plasma and higher deposition rates at lower operating pressures.

8. Film growth on the substrate: The sputtered atoms travel through the low-pressure atmosphere and condense on the substrate surface, where they nucleate and grow into a thin, adherent film.[Martin, 2010]

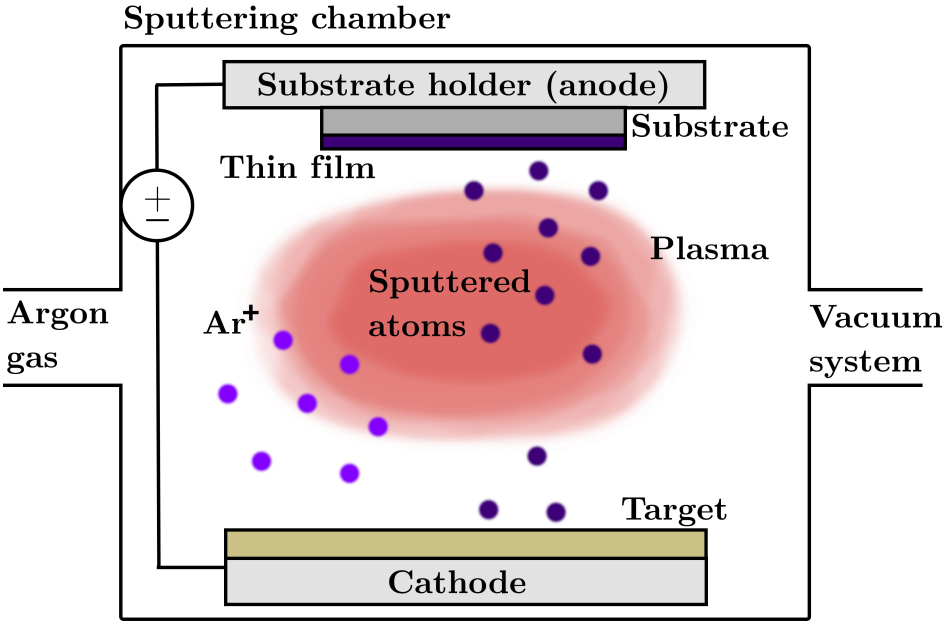

Figure 2.1: This diagram shows a sputtering chamber with all the key parts and processes that occur during the sputtering process.[Borowski and Myśliwiec, 2025]

2.4 Wear Rate

This section describes the wear, its mechanisms, where it originates from and what it can cause. There are some derivations of how to calculate wear rate.

It is important to understand how different materials undergo wear. This factor is one of the essential properties for understanding each material role and lifetime in any mechanical component. Wear combined with other processes in machine elements, causes its functional surfaces to degrade and eventually can lead to loss of functionality or material failure. It may occur due to various reasons, for example, environmental factors, mechanically changing the surface such as scratching it, processes like fatigue and creep and the physical and chemical nature of the material. We can minimize wear the same as friction by using a lubricant to separate two bodies from directly touching each other.

There are two most common types of wear: abrasive and adhesive. In first one a harder material removes a softer material. In the second one, material is transferred from one to other, in other words two bodies adhere to one another locally. Abrasive wear tends to more severe the other one in most cases. In adhesive wear, sliding surfaces or to be more precise their microscopic high points known as asperities, can temporarily bond, forming junctions between the two materials. As relative motion continues, these junctions must be broken. If the bond is weak, shear occurs along the original interface, causing minimal material loss. However, if the junction is stronger than one of the materials involved, shear may take place within the material itself, leading to adhesive wear.[Novak and Polcar, 2014]

The behavior of wear within different materials is known by calculating the wear rate. It is defined as the amount of material removed per unit of time. To measure this, we can use a tribometer in which we can set up parameters such as sliding distance, applied load, etc. Combining these with what we know about wear rate can give us the equation below.

$$W_s = \frac{\Delta V}{LD},$$

where W_s is the specific wear rate, ΔV is the volume difference of the material after wear, L is the applied normal load and D is the sliding distance.
If we want to link friction and force with wear rate. We can use this equation below.

$$W = kFD,$$

where W is the wear rate, k is a wear constant (which can be determined experimentally), F is the normal force applied and D is the sliding distance.
The force applied can also be linked to the normal force and coefficient of friction. Equation below shows this link up.

$$F = \mu N,$$

where N is the normal force, μ is the friction coefficient.
So if we combine all the equations above to express wear rate in terms of friction coefficient, we get this:

$$W = k\mu ND$$

Other ways of measuring the wear involve measurement of either mass change or the size of a worn region. The second option is more common since it can be applied for any case where there is a large enough to measure worn region (wear scar). The size of the scar can be measured using an optical image or using profilometry. Optical image can be used to measure the dimensions of the wear scar. With that and the geometry of the contacting body, which is known we can calculate parameters such as wear depth or wear volume. In case of using a profiler, we can get direct measurement of the depth of the wear scar and the in-plane dimensions. The results of this can be presented as volume or as one of the in-plane dimensions of the wear scar.[Ray et al., 2023]
Expression to calculate parameters that affect wear rate is called Archard's wear law. The wear rate in this law is expressed by this equation:

$$W = \frac{\Delta V}{D}$$

where ΔV is change of the volume and D is the sliding distance. Then Archard's wear law is expressed by this equation:

$$\frac{\Delta V}{D} = \frac{K_w P}{H}$$

where K_w is wear coefficient specific for every material, P is the total normal load on the surface and H is the hardness of the material.
From this expression, we know that as expected, the higher the load and softer the material there will be more wear. The wear rate is often normalized by the load to enable easier comparison between tests performed at different loads. So the wear is reported in units of volume per distance per load. K_w is highly dependent on surface features, materials as well as operating and environment conditions. However, the trends predicted by the simple Archard wear equation have been found to describe experimental observations well in many cases.[Hu et al., 2022]

2.5 Hardness

This section describes the hardness, how is ti measured and different methods of doing it.

Hardness of the material can be described as its ability to resist permanent surface deformation. To expand this one can say that deformation is localized plastic deformation such as cutting, indentation and scratching. To formulate a more precise definition of hardness may be difficult as every testing method interacts with the material's microstructure and induces complex stress and deformation fields. Consequently, a single hardness measurement inevitably reflects a combination of several material properties rather than an isolated characteristic. Despite this, difference between hard and soft materials comes from their relative resistance to deformation. Hardness is measured as force per unit area of indentation. There are few different hardness scales using different indenter and calculating hardness in distinct way. Although, after measuring hardness with one method, one can recalculate it into different scales. So, there is a way on how to compare results from different scales.[Sakaguchi and Powers, 2012]

Chapter 3

Material, Equipment and Method

This section provides an overview of the material and equipment used to perform the experiments and the approach to each piece of equipment.

3.1 Material

3.1.1 Stainless Steel 304 Samples

This section provides information about the material that we used for our samples. The source used in this section was provided by the producer of 304H stainless steel - Tang Eng Iron Works Co. Ltd.

For our experiments, we used stainless steel 304H. Type 304 steel is a 3xx series stainless steel. Our samples were cut from a big sheet, which measured 138.9 cm x 127.4 cm x 0.096 cm [Length x Width x Thickness (LxWxT)], to a small square 2 cm x 2 cm (Length x Width). Chemical composition was provided by the producer and is shown in the table 3.1. The density of 304 stainless steel is approximately 8 $\frac{g}{cm^3}$.[Dam,]

Element	Composition (%)
C	0.048
Si	0.45
Mn	0.88
P	0.033
S	0.002
Cr	18.02
Ni	8.10
N	0.060

Table 3.1: Chemical composition of stainless steel 304H used for our project.[Dam,]

The producer also provided mechanical properties and they are shown in the table 3.2.

Mechanical property	Value
Tensile strength [$\frac{N}{mm^2}$]	625
Yield strength (0.2%) [$\frac{N}{mm^2}$]	258
Elongation [%]	60.3
Hardness - Rockwell B hardness scale [HRBW]	76.9
Yield point (1%) [$\frac{N}{mm^2}$]	288

Table 3.2: Mechanical properties of stainless steel 304H used for our project.[Dam,]

3.2 Experiments

The experiments consisted of coating TiN on stainless steel 304H in Flextura 200 from Polyteknik. Elipsometry was used on some initial samples to determine thickness. Some of the initial samples were cleaned

with ethanol, isopropanol and Milli-Q water in ultrasonic bath. Virgin steel samples and coated ones were then used in tribometer TRB-3 from Anton Paar. On this machine wear tracks were made and friction coefficient was obtained. Then hardness test was conducted on Duramin-40. After that, Ambios XP-2 line profiler was used to determine profiles of wear track. It was necessary to later calculate wear rate. XRD was used to determine if the TiN is being properly deposited on steel. It was also used for Ti and N proportion.

3.3 Cleaning

Initial samples were cleaned before they were coated to clean the surface form any unwanted residues and particles. They were cleaned using ultrasonic bath using different chemicals. It was cleaned using Milli-Q water, acetone, isopropanol and ethanol. After that they were dried with compressed-air. Although after cleaning we noticed that the samples were visibly damaged on the steel surface. Due to that we did not clean other samples before coating them. For future samples, only ethanol and optic paper were used to get rid of residue from the sticky sample covers. Some cleaning was done in between tribometry measurement to remove debris and residue from samples. Also, compressed-air was used before line profiling to moreover clean the debris and residues.

3.4 Equipment

3.4.1 Flextura 200

This section provides information about the Flextura 200 from Polyteknik that we used to sputter TiN coating on our steel samples and parameters that we used in this machine.

Flextura 200 is an automated coating system with two separate chambers: an E-beam evaporator and a sputtering chamber. For this project, we used a sputtering chamber. Flextura is designed for 100 mm samples and due to our samples having different dimensions (20 x 20 mm), we were using two adapters. We could produce 2 samples at once.
TiN coating was sputtered by writing a recipe and putting the parameters of the process into the software. We got our recipe from previous work done on Flextura. We have to adjust the recipe in collaboration with Peter Kjær Kristensen. Adjustment was made to N_2 and O_2 flows and Ar flow and ignition flow. It was done after first few trials, because plasma was not upholding and the deposition process couldn't begin. The table below shows all the procedure parameters we input into recipe to make our coated samples. The thickness was at 0 and the time was changed for different thicknesses of samples, because the part of Flextura that measure thickness wasn't precise enough. An elipsometer was used for a few initial samples to confirm that we are getting the desired thickness. [Polyteknik AS, 2023]

Procedure property	Value
Thickness [nm]	0
Time [s]	1800, 3600 or 18000
Rotation speed [rpm]	10
Cleaning time [s]	20
Bipolar power (mag 3 + 4) [W]	300
Output mode (0 = pulsed, 1 = DC Mag3, 2 = DC Mag4)	2
Ramp level (1 - 80 A) [A]	20
Ramp time [min]	30
Temperature setpoint [°C]	300
Pre heating time [min]	30
Max PID current (1 - 80 A) [A]	50
Material	Ti sputtering
Material name	Ti sputter
Density [g/cm^3]	4.5
Tooling [%]	500
Z - ratio	0.63
Base pressure [mbar]	1.00E-6
Process pressure [mbar]	0.00E+0
N2 pressure [mbar]	0.00E+0
O2 pressure [mbar]	0.00E+0
N2 percent [%]	0
O2 percent [%]	0
Ar ignition flow [sccm]	80
Ar flow [sccm]	15
N2 flow [sccm]	20
O2 flow [sccm]	0
Reactive gas timer [sec]	20

Table 3.3: Procedure properties we input into Flextura software to coat our steel samples.[Polyteknik AS, 2023]

Ramp level, ramp time, temperature setpoint, pre heating time and max PID current values are only there if we meant to be using heater, which in our case was not in use. Some values at the table are exactly copied from the recipe and are not written mathematically correct. We already explain how flextura works and explain each step in sputtering part of theory section. The Figure 2.1 shows parts and process that occurs inside the machine.

3.4.2 DURAMIN-40

This section provides information about the Duramin-40 that we used to test the hardness of virgin and TiN-coated steel samples. The machine and parameters of our process were described.

Duramin-40 was used to test the hardness of our virgin stainless steel samples and samples coated with TiN (various thicknesses). The samples tested are the virgin polished steel sample, polished steel sample with a 150 nm thick TiN coating, polished steel samples with a 300 nm TiN coating and sample with a 1500 nm TiN. It uses the Vickers hardness scale. The test involves pressing a diamond-shaped indenter or in other words pyramid-shaped indenter with a square base, into the surface of the material using a specific load. The diamond pyramid has a 136 ° angle between opposite faces.[Dur, 2023][ISO, 2018] We choose 5 different loads: 10, 20, 50, 100 and 500 gf for our samples. Each sample was tested in 5 different places for each load to ensure accuracy of the measurement and investigate the consistency of the coating. The

indents are made at approximately the same locations for the varying samples. Below is a figure 3.1 of the places where each indent was made.

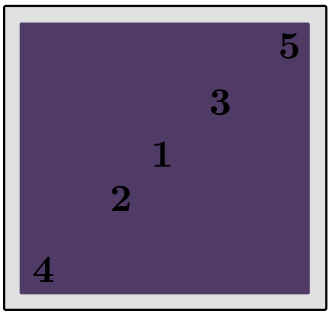

Figure 3.1: This figure depicts the places on the sample where the indents for the hardness test were made.

The table 3.4 explains the numbers that were used in the figure 3.1. For sample 1 and 2 the test was done before the samples went into the tribometer as well to investigate whether this could somehow impact the results, however, as expected it did not.

Number of Measurement	Virgin Steel Sample	Coated Steel Sample
1	Center	Center
2	Center - closer to the edge	Center - closer to track from tribometer
3	In the middle of the distance between edge and center	Between two tracks from tribometer
4	Edge	Edge
5	Different edge	Different edge

Table 3.4: Locations of DURAMIN-40 measurements on virgin and TiN coated steel samples.

In this test, hardness is measured from the size of the indentation. To be precise, two diagonals of the square indentation are being measured under a microscope. There are a few different microscopes: 2,5x, 5x, 10x and 40x to look at the sample surface and choose an appropriate spot to make an indent. Indents are not supposed to be very close to each other, so it is important to move a bit from the previous indent. [Dur, 2023]
To calculate hardness, this equation was used:

$$HV = \frac{1.854F}{d^2} \tag{3.4.1}$$

where HV is Vickers hardness, F is the applied load in kilograms-force and d is the average diagonal length in millimetres.[ISO, 2018], [Dur, 2023]
The picture below shows a Duramin-40 hardness tester machine. The indenter and microscopes with sample holder can be seen on the left. The sample holder can be moved up or down to adjust the measurement field for any sample. The monitor on the right is used for choosing the measurement place and calculating the hardness via lines that can be manually or automatically adjust to the indent boundaries.

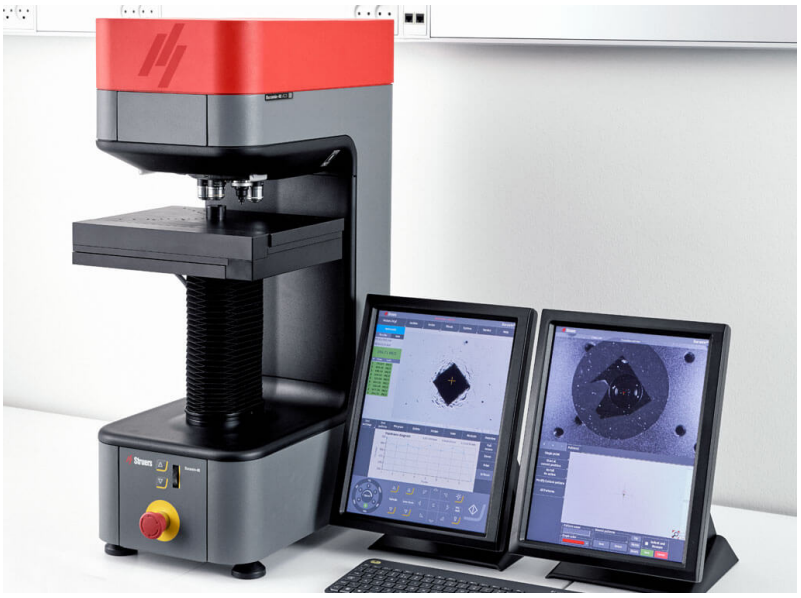

Figure 3.2: This picture depicts the Duramin-40 hardness tester machine.[Struers,]

3.4.3 Tribometer-3

This section provides information about the TRB-3 that we used to made the wear tracks and test the wear rates of virgin and TiN-coated steel samples. The machine and parameters of our process were described.

Tribometry measurements were made using TRB-3 from Anton Paar. The virgin steel samples and TiN coated samples were tested in this machine. The samples tested are the virgin polished steel sample, polished steel sample with a 150 nm thick TiN coating, polished steel samples with a 300 nm TiN coating and sample with a 1500 nm TiN. The machine uses ball of ceramic or alumina to scratch a mounted sample under controlled load. The ball can be 6 or 10 mm. The machine has an option to change loads for the measurement. One can choose between few loads varing from 0,25 N up to 10 N. The picture below, Figure 3.5, shows TRB-3.

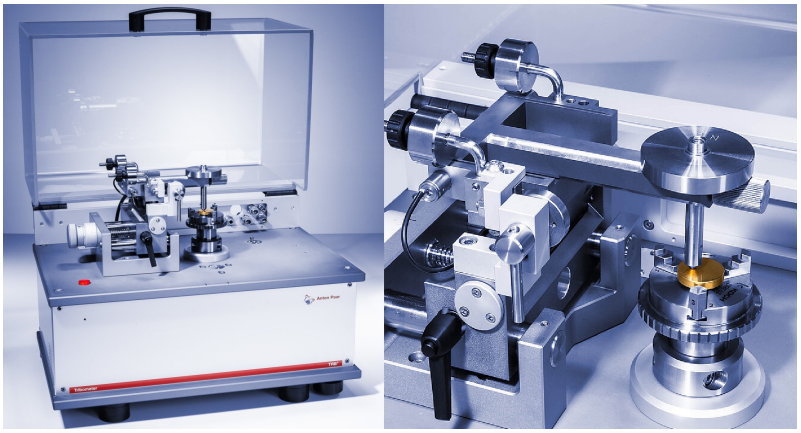

Figure 3.3: This picture depicts the TRB-3 machine.[Paar,]

In this picture we can see where the load and sample are mounted. The two weights, on the handles, visible on the left side of the right picture can be adjusted so the machine is balanced and ball is in proper contact with the sample. This is to ensure a the load applied to the sample is true and the machine is not adding or subtracting anything. There is also an option to choose the radius of the wear track which can be changed

depending on where we need the measurement to take place. The table below shows every parameter we used during our project.

Procedure property	Value
Ball material	Alumina
Ball diameter [mm]	6 and 10
Linear speed [m/s]	2
Cycles	from 1 up to 5000 (1, 10, 50, 100, 250, 350, 500, 1000, 2000, 3000 and 5000)
Load [N]	from 0.25 N up to 10 N (0.25 N, 1 N, 2 N, 5 N and 10 N)

Table 3.5: Procedure properties inputted into the TRB-3 software.[TriTec,]

3.4.4 XP-2 Line Profiler

This section provides information about the Ambios XP-2 line profiler that we used to measure wear tracks of virgin and TiN-coated steel samples. The machine and parameters of our process were described.

Line profiling was performed on Ambios XP-2 line profiler to record the profile of every wear track we got from our tribometry measurements. The samples used for this were the same as in TRB-3 section. The line profiler uses a tip that goes along our samples topography and register every hole or elevation on the sample. We choose to record each wear track separately even though we could record them at once, because the results can be shown and plot better in that way. We choose that the machine speed would be 0.03 mm/s and that the measurement only goes for 0.8 mm. Stilus force was 2 mg. There is a filter that be used to reduce or increase the data points we got from each measurements. After getting few different measurements it was chosen so that we got enough data points but not to much so the results are still visible.[Ambios Technology, 2003] Picture below shows the machine. The disk is the sample stage, which can be moved around during procedure. The sample is tested with the tip visible above the sample stage.

Figure 3.4: This picture depicts the Ambios XP-2 line profiler.[Ambios,]

3.4.5 X-Ray Diffraction

This section provides information about the XRD that we used to test composition of virgin and TiN-coated steel samples. The machine and parameters of our process were described.

X-ray diffraction (XRD) was made on Empyrean XRD instrument from Malvern Panalytical. Those measurements were performed to ensure the TiN being deposited properly on the steel sample and to get the proportion of Ti and N. It was carry out on two samples: an uncoated stainless steel sample and a 1500 nm TiN coated stainless steel sample. The scans were obtained using Cu $\kappa\alpha$ radiation (λ = 1.5406 Å) in a conventional θ – 2θ geometry over a range of approximately 5–70 ° 2θ, with a step size of about 0.013 °. Below we can see the machine. There are few parts that are adjustable like masks and filters, where change to fit our experiment. The mask was 8 mm, nickel filter was choose and two anti-scatter slits were put into the machine that were marked 1/2 °. [Panalytical, 2023]

Figure 3.5: This picture depicts the Malvern Panalytical Empyrean XRD machine.[malvern Panalytical,]

Chapter 4

Results and Data Analysis

This chapter provides the results and subsequent data analysis of the experiments described in the above section.

4.1 Hardness Measurements Results

Below are the results for 10 gf and 500 gf, for the different samples; the least and most extreme case tested. The Vickers hardness (HV) used to asses hardness is calculated by dividing the applied force by the surface area of the indentation. On each graph for every result, there is an error bar. The error was calculate as an average error from other measurements done on this samples.

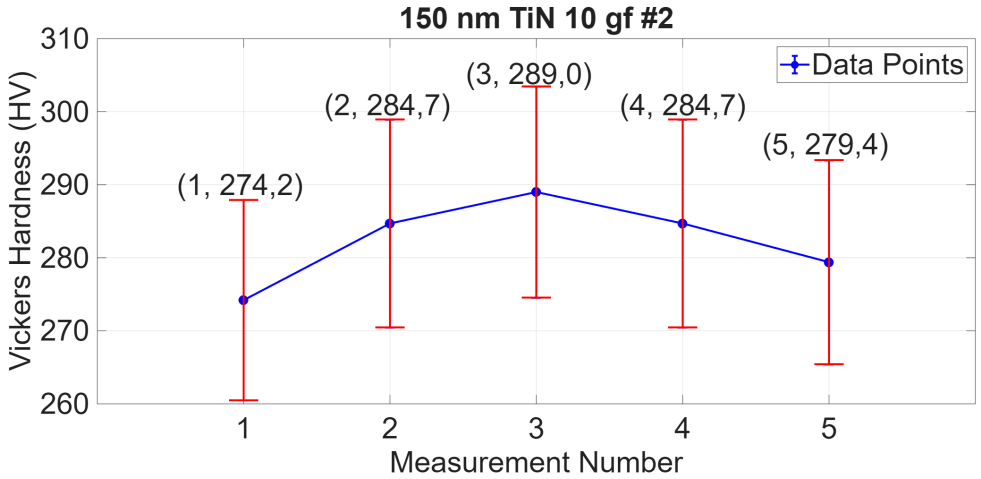

Figure 4.1: This figure depicts the results of the hardness test with 10 gf load of 150 nm TiN sample.

Figure 4.1 shows the five hardness measurements for 150 nm TiN sample. The figure is numerated #2 because this is the second batch of measurements. The hardness on this sample varies between 275 and 290, which are variations within the norm.[Hidayat et al., 2020][Sundgren, 1985] The DURAMIN-40 ensures this since it has a function that judges what the normal rage is based on the previous results and shows this by displaying the result either in a red, orange or green color.

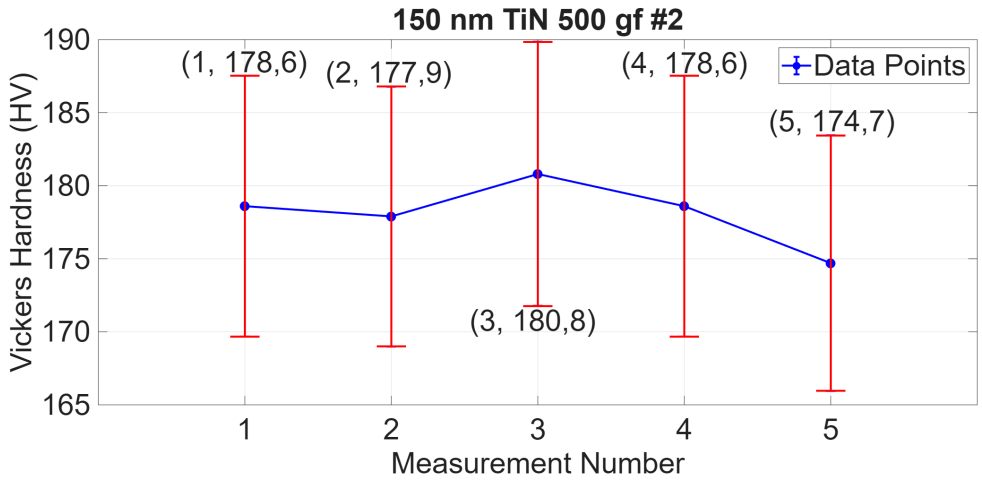

Figure 4.2: This figure depicts the results of the hardness test with 500 gf load of 150 nm TiN sample.

Figure 4.2 depicts the same sample with a greater load. The variations of the greater load tested are smaller than Figure 4.1; within 10 HV.

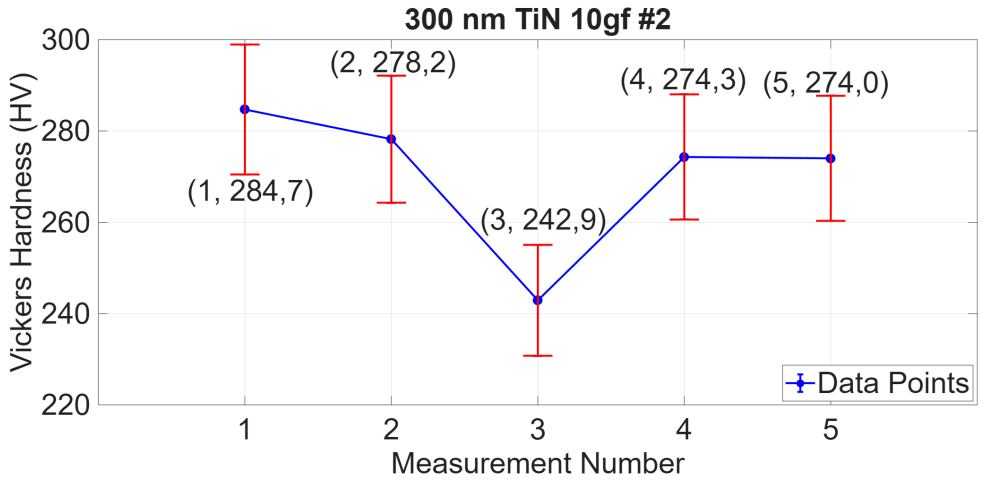

Figure 4.3: This figure depicts the results of the hardness test with 10 gf load of 300 nm TiN sample.

Figure 4.3 depicts the 10 gf hardness test for 300 nm TiN sample. These results have much greater variation with the lowest being 242 and the highest being 285. While these variations are still within the norm based on the DURAMIN-40 software they are not within the norm when referring to [Dur, 2023] and [ISO, 2018]. Additionally, occasionally we experienced warped indents and in some instances, the resulting pyramid-shaped indents appeared misaligned, which may indicate inconsistencies in surface or Duramin-40 error.

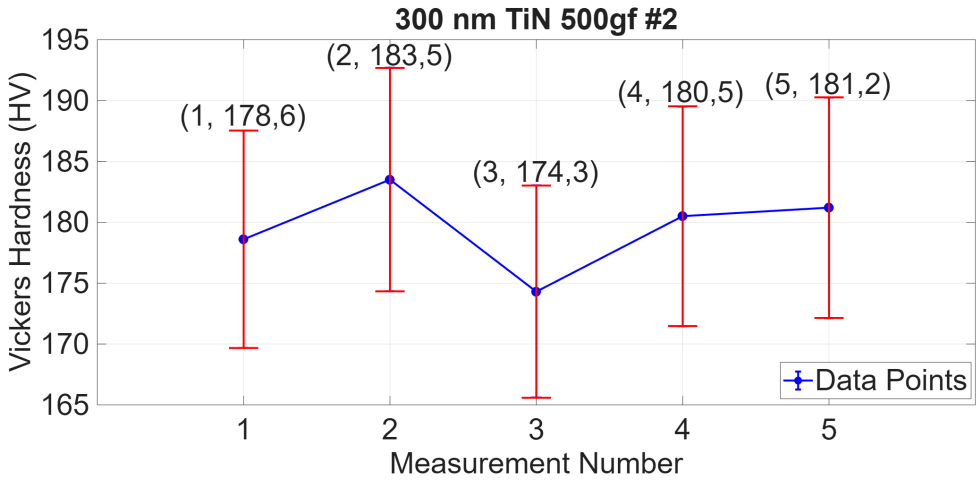

Figure 4.4: This figure depicts the results of the hardness test with 500 gf load of 300 nm TiN sample.

The variation in hardness for 300 nm TiN sample Figure 4.4, however, is in a very similar range as the 500 gf measurement for 150 nm TiN sample Figure 4.2. To compare the results from the TiN coated samples a test on a virgin stainless steel sample was done as well.

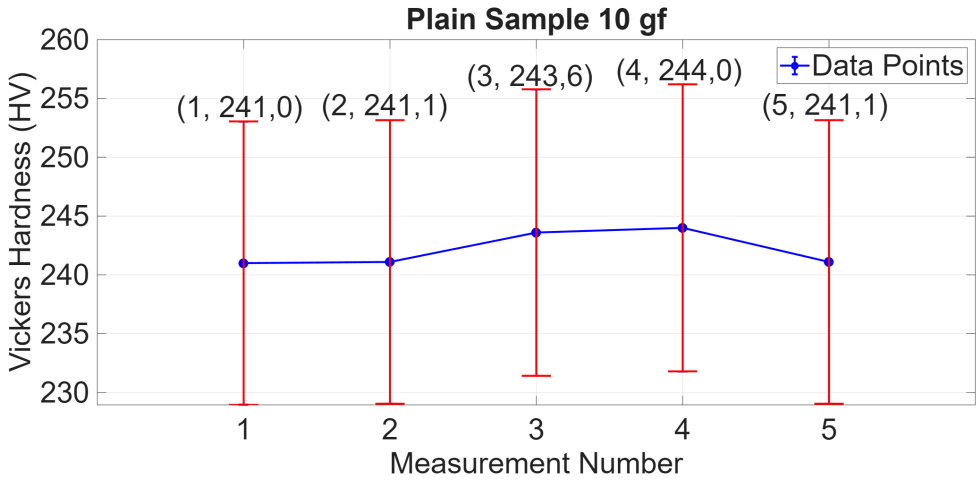

Figure 4.5: This figure depicts the results of the hardness test with 10 gf load of virgin sample.

For the 10 gf load hardness test on virgin sample Figure 4.5 the variation is slightly lower than for 150 nm TiN and 300 nm TiN samples under the same load. For the 500 gf test on virgin sample, seen in Figure 4.8, the variation is similar to 150 nm and 300 nm TiN samples. The results for the plain sample can be compared to this in the article[Barcelos et al., 2017] and from sheet of producer of steel sample [Dam,]. We can see that our results are very similar to both of those sources.

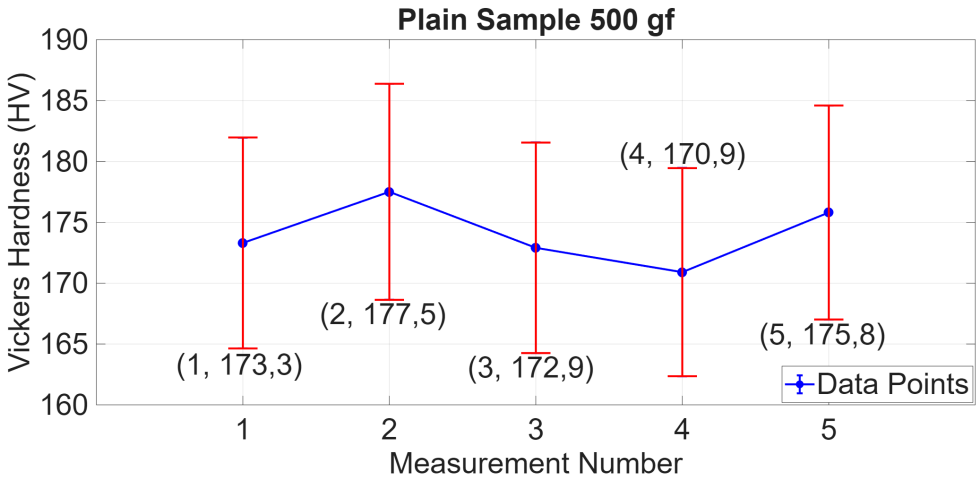

Figure 4.6: This figure depicts the results of the hardness test with 500 gf load of virgin sample.

Next two figures represent the 1500 nm TiN coated stainless steel samples. For the 10 gf the maximum and minimum results are 22 HV apart. For the 500 gf this number is a little bit lower being only 15 HV. This is consistent in each sample regardless of material and thickness of coating.

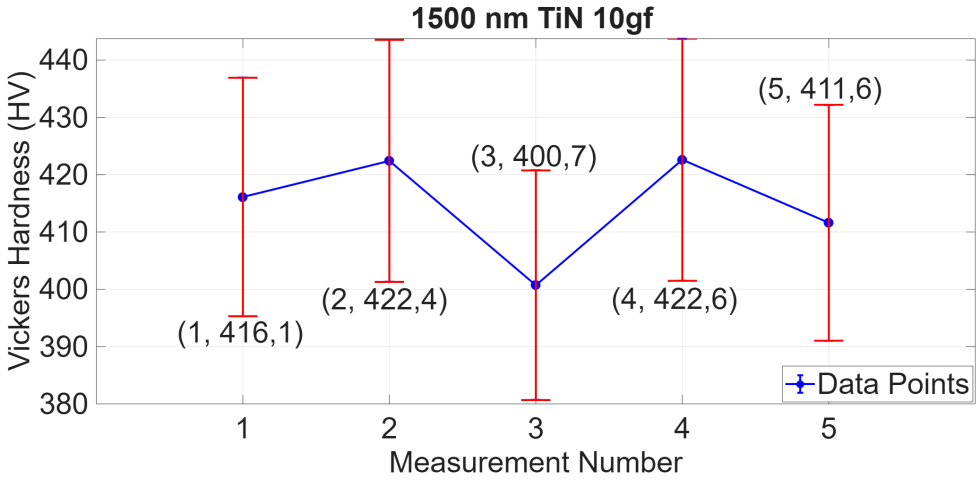

Figure 4.7: This figure depicts the results of the hardness test with 500 gf load of virgin sample.

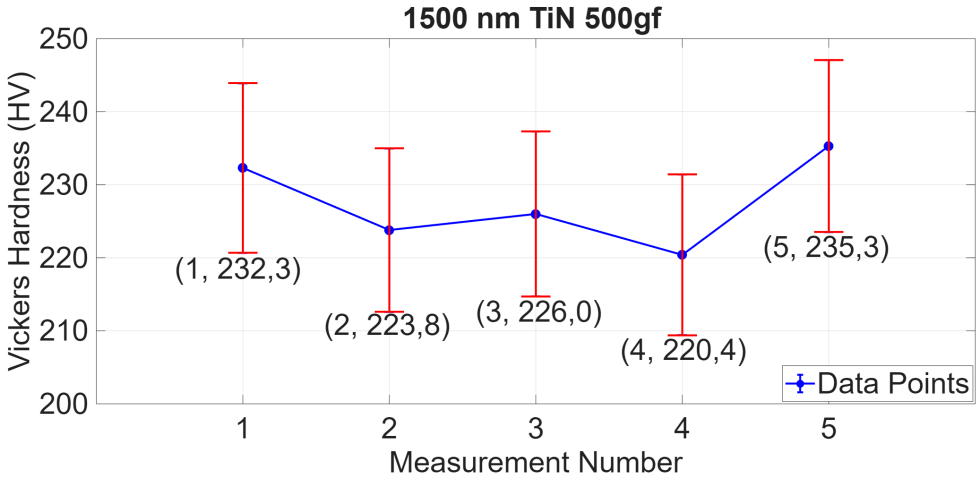

Figure 4.8: This figure depicts the results of the hardness test with 500 gf load of virgin sample.

This results shows the same pattern as the previous coated results. The main difference that can be seen is that the hardness has increased as suspected with thicker coating. However, the hardness values should still be higher for this thickness.
From these results we can see that with increasing load, the hardness of our sample is decreasing. The hardness of the 304 steel shows that our results are comparable to results from [Dam,] and [Dewangan and Mishra, 2024]. In the case of the 150 nm and 300 nm TiN coated samples, we can see that our results are a few times smaller than those in [Sundgren, 1985]. This can be a case of too thin coatings, which are getting pierced through by our indenter, thus we are essentially measuring the steel underneath instead of the TiN coating itself. For the 1500 nm TiN coated samples, we can see the results are approximately or very close to lower limit as those in [Sundgren, 1985], [Nakamura et al., 1977] and [Sundgren et al., 1983]. It can be a sign that increasing the thickness of the coating increase the sample resistance to deformation. Although, the results still shown signs of the coating being too thin and not hard enough to withstand higher loads. Generally a trend of lesser variation in HV values with higher loads is seen throughout the samples.
It is hard to asses the depth of the indentation because the hole is too deep for the Atomic Force Microscope (AFM) and difficult to locate for the XR-2 line profiler. The manual of the DURAMIN-40 states that it is dependent on the load and the material of the sample [Dur, 2023].

4.2 Line profiles of Wear Tracks

4.2.1 Virgin Stainless Steel

The experimental results described in this section are for the 2 cm x 2 cm stainless steel 304 samples without any coating.

The samples in this section were all subjected to wear using the pin-on-disk tribometer with a 0.6 cm diameter alumina ball. This type of ball was chosen since this was the most common type of ball used for TiN coated sample experiments in literature and thus this makes for the best comparison with virgin stainless steel samples. The initial tests on the first few samples were done with various load changes, however, due to issues with debris on the sample not more than 1 cycle. It is worth noting that cleaning these debris was attempted with both air and isopropyl, however, to no avail. Below is a figure, Figure 4.9, showing the line profile of a virgin stainless steel sample wear track when using a load of 5 N and at 1 cycle.

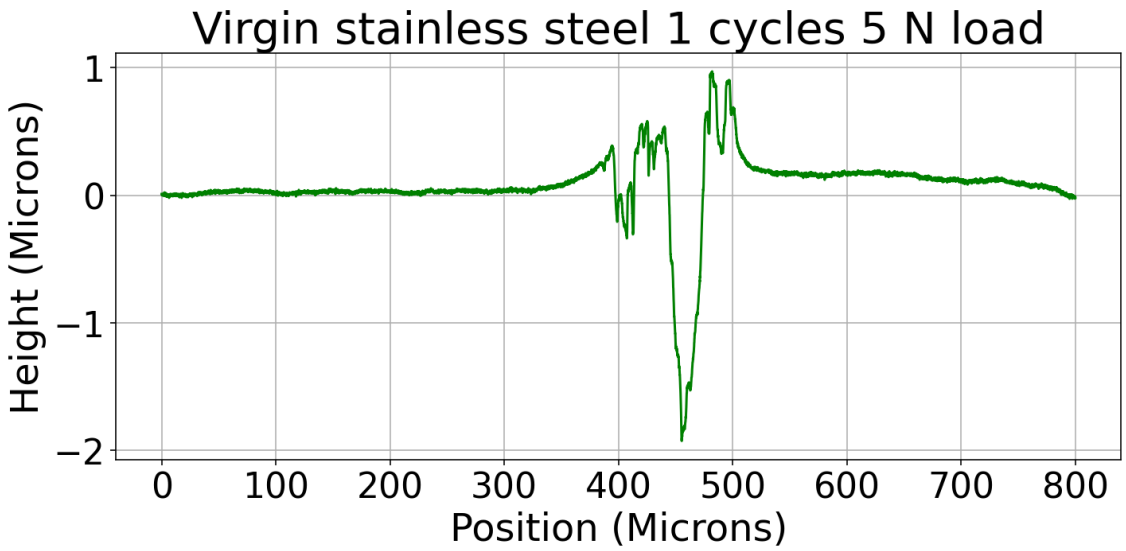

Figure 4.9: This figure shows a stainless steel sample. This figure shows the wear track the TRB makes in the sample when equipped with a load of 5 N and during 1 cycle.

The wear rate of Figure 4.9 is 1.884 x 10^{-3} $mm^3/(Nm)$ which is lower than the expected range, however, when considering the line profile seen in the graph it is clear that the reason is because a lesser amount of material than expected was removed. Generally this figure shows a very sharp and deep indent where the wear track was made. This trend continues when increasing the number of cycles as seen in figures Figure 4.10, Figure 4.11 and Figure 4.12. However, with an increasing number of cycles the track becomes broader and thus revealing a shape that is somewhat reminiscent of the characteristic half sphere shape one expects from this type of wear track. The depth increases as well going from around 2000 nm for 1 cycle to around 6000 nm for 5000 cycles, all for a load of 5 N. The wear rate of Figure 4.10, Figure 4.11 and Figure 4.12 is 5.813 x 10^{-4} $mm^3/(Nm)$, 4.201 x 10^{-5} $mm^3/(Nm)$ and 1.030 x 10^{-4} $mm^3/(Nm)$, respectively. These wear rates are in accordance with expected wear rates for stainless steel wear tracks under these conditions.[Kalin and Vižintin, 2000] [Awan et al., 2020] [Novak and Polcar, 2014]

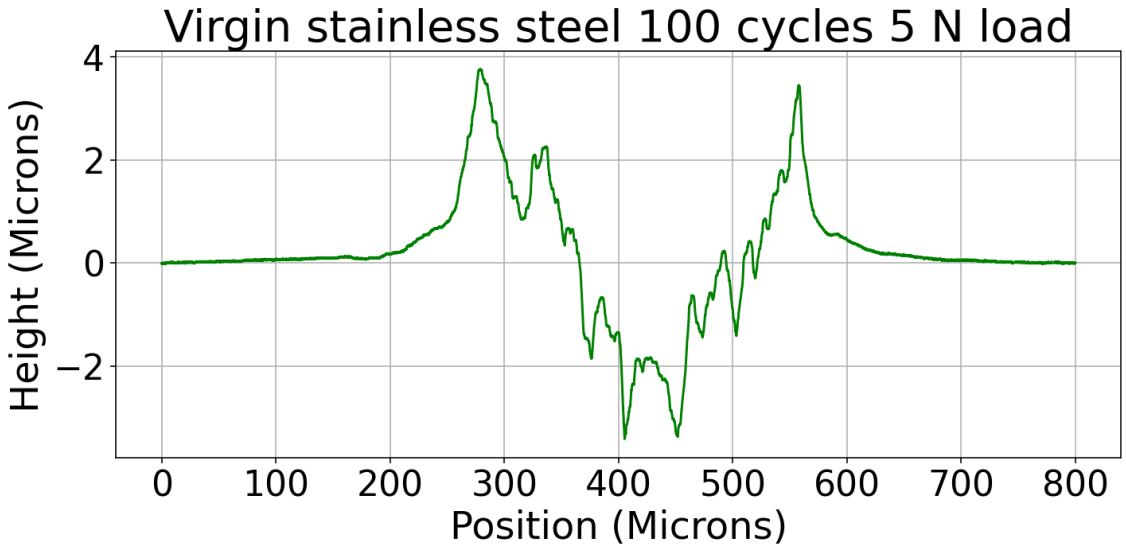

Figure 4.10: This figure shows a stainless steel sample. This figure shows the wear track the TRB makes in the sample when equipped with a load of 5 N and during 100 cycles.

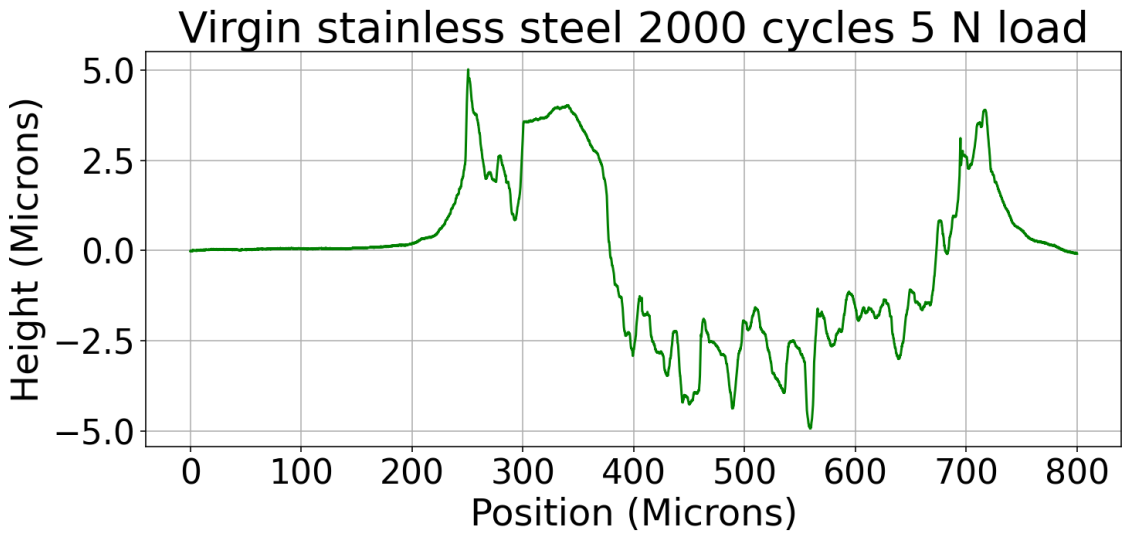

Figure 4.11: This figure shows a stainless steel sample. This figure shows the wear track the TRB makes in the sample when equipped with a load of 5 N and during 2000 cycles.

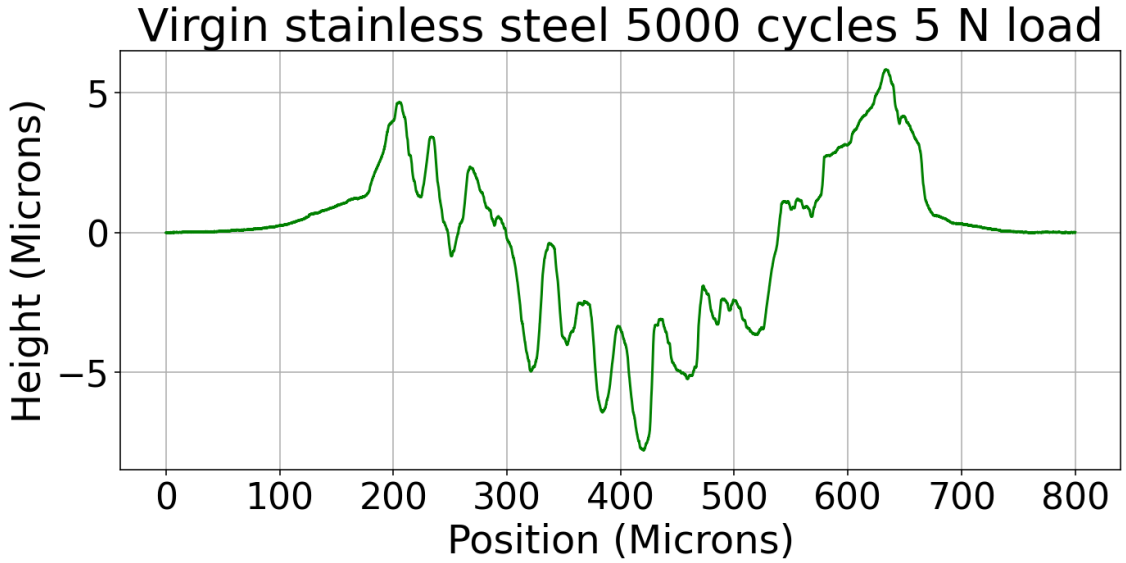

Figure 4.12: This figure shows a stainless steel sample. This figure shows the wear track the TRB makes in the sample when equipped with a load of 5 N and during 5000 cycles.

The same kind of broadening is seen for a sample subjected to a lesser load of 1 N. For this sample a cycle count of 1 shows very little material removed and a fairly shallow wear track of around 260 nm. This is seen in Figure 4.13. The figures Figure 4.14, Figure 4.15 and Figure 4.16 show this broadening with increased cycles going from around around 150 microns, for 100 cycles, to 400 microns, for 5000 cycles. For Figure 4.13 the wear rate was calculated to be 3.110 x 10^{-3} $mm^3/(Nm)$. For Figure 4.14, Figure 4.15 and Figure 4.16 it was 1.891 x 10^{-4} $mm^3/(Nm)$, 1.198 x 10^{-4} $mm^3/(Nm)$ and 4.307 x 10^{-5} $mm^3/(Nm)$, respectively. These wear rates are slightly lower than what is expected for TiN coatings, however, perfectly normal for virgin stainless steel. It is still clear from visually inspecting the line profiles that there is alot of debris on the track itself, even if the wear rate is in accordance with literature. [Kalin and Vižintin, 2000] [Awan et al., 2020] [Novak and Polcar, 2014]

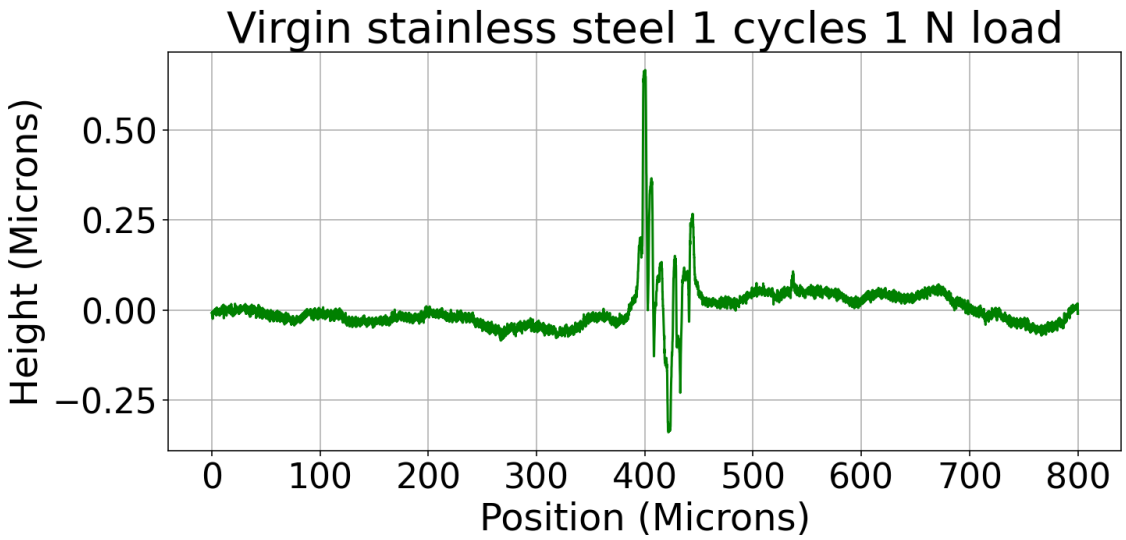

Figure 4.13: This figure shows a stainless steel sample. This figure shows the wear track the TRB makes in the sample when equipped with a load of 1 N and during 1 cycle.

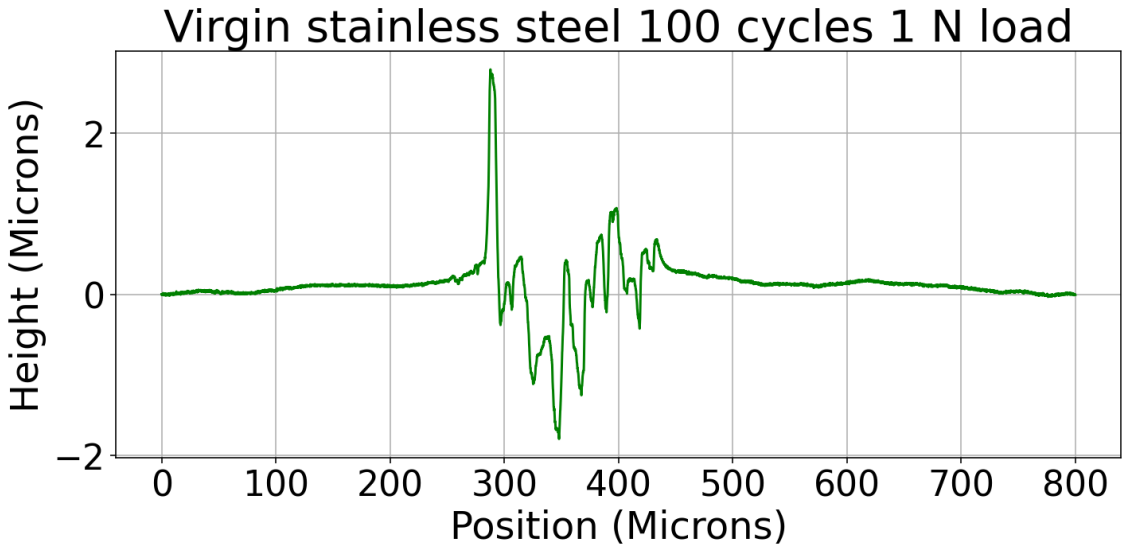

Figure 4.14: This figure shows a stainless steel sample. This figure shows the wear track the TRB makes in the sample when equipped with a load of 1 N and during 100 cycles.

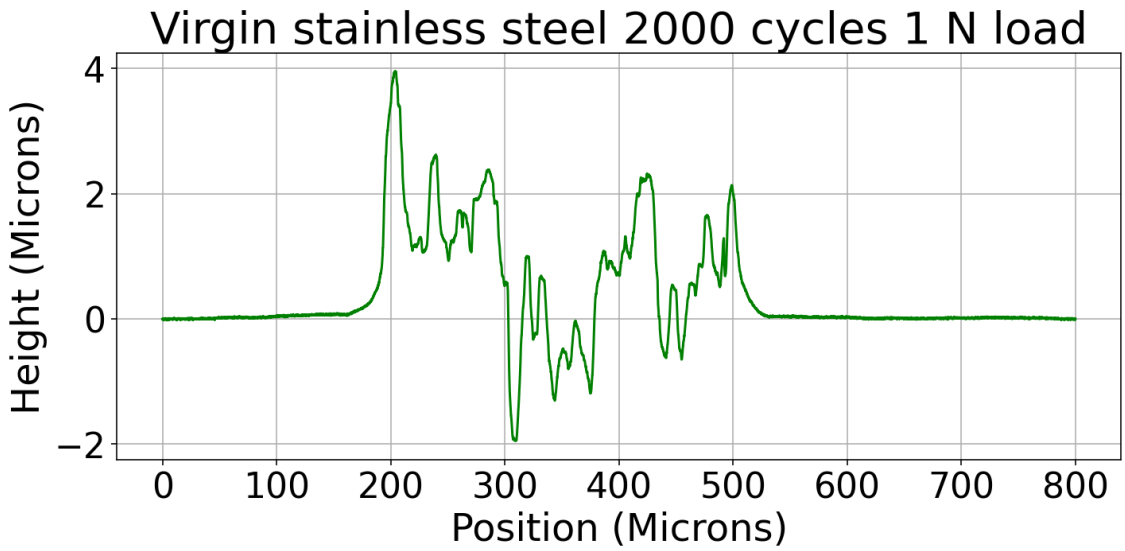

Figure 4.15: This figure shows a stainless steel sample. This figure shows the wear track the TRB makes in the sample when equipped with a load of 1 N and during 2000 cycles.

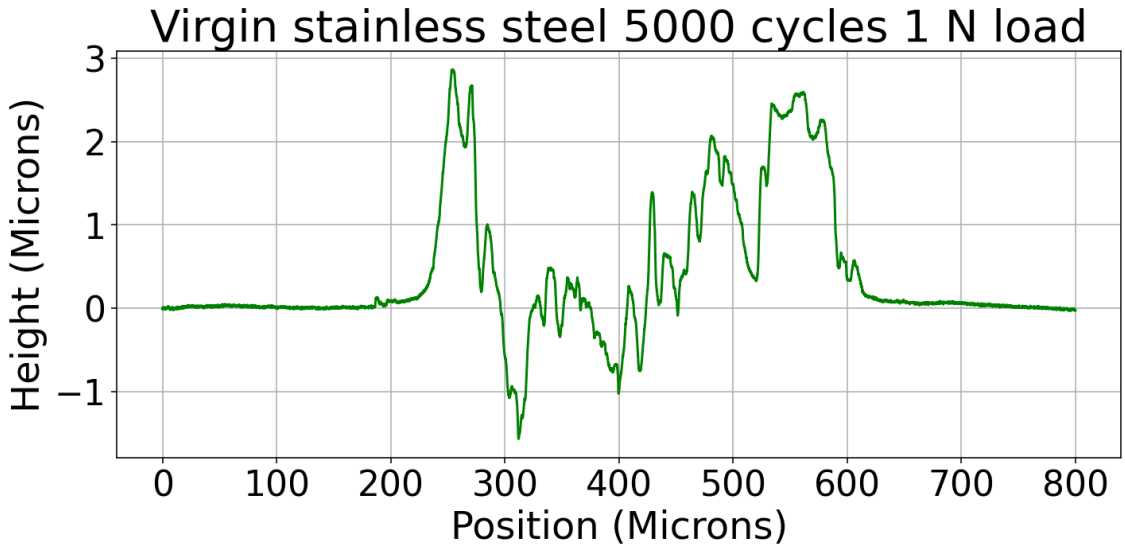

Figure 4.16: This figure shows a stainless steel sample. This figure shows the wear track the TRB makes in the sample when equipped with a load of 1 N and during 5000 cycles.

While it may look like very little material was removed on the 1 N 1 cycle track this could in fact be due to an accumulation of debris on the sample. This is not very expected at 1 cycle since no dragging of debris along the track is occurring. It is possible to visually inspect the sample to check wether the line profilers indications for little material removed are correct or if the track is full of debris showing a not true representation of the actual wear. This was done by using a scanning electron microscope. The image taken of this specific wear track is seen in Figure 4.17.

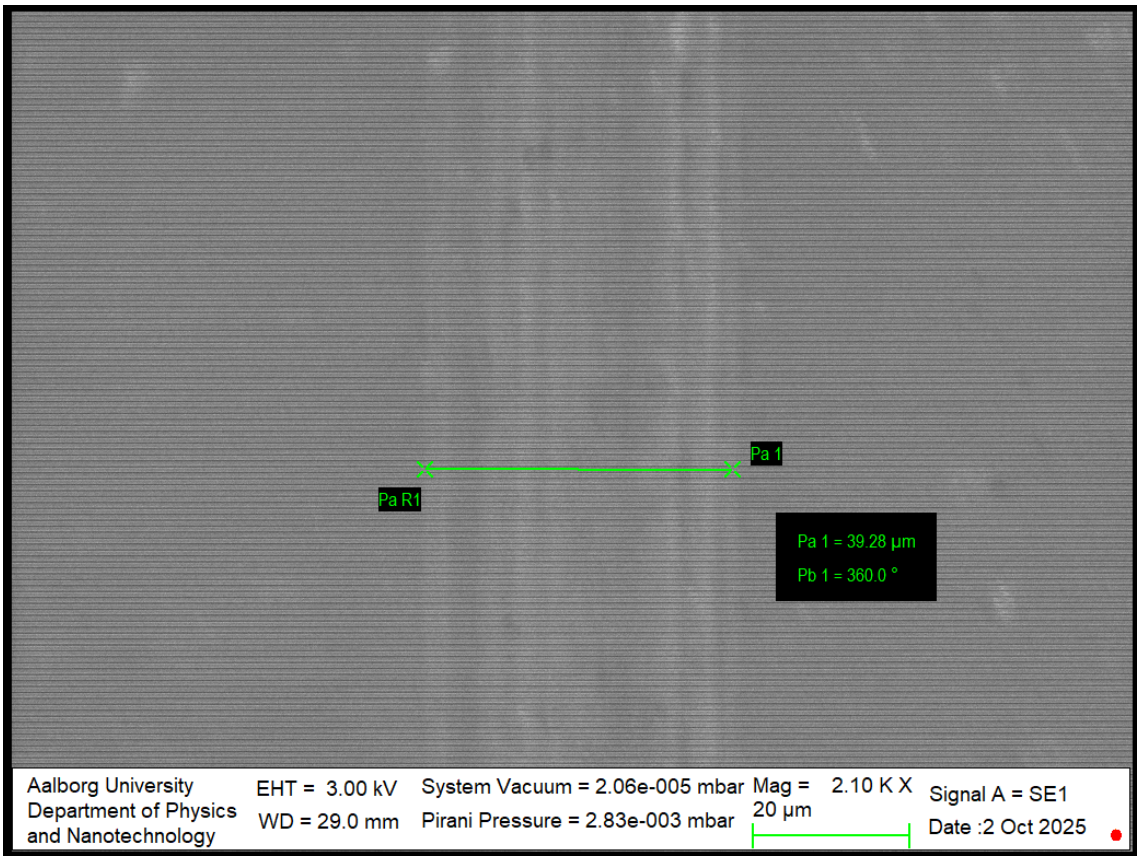

Figure 4.17: This image shows a stainless steel sample. This image shows the wear track done on the sample by the TRB3 tribometer when equipped with a load of 1 N and during 1 cycle.

This image confirms that the wear track is indeed very subtle and very little debris is generally seen on the track. The width of 39 micrometers shown by the SEM matches the width detected by the line profiler. Debris on SEM images would be seen as small particles our discolorations obstructing the clean wear track of a sample. An example of quite significant debris on a sample is seen in the image below Figure 4.18 and an example of smaller debris on top of the wear track itself is seen in Figure 4.19.

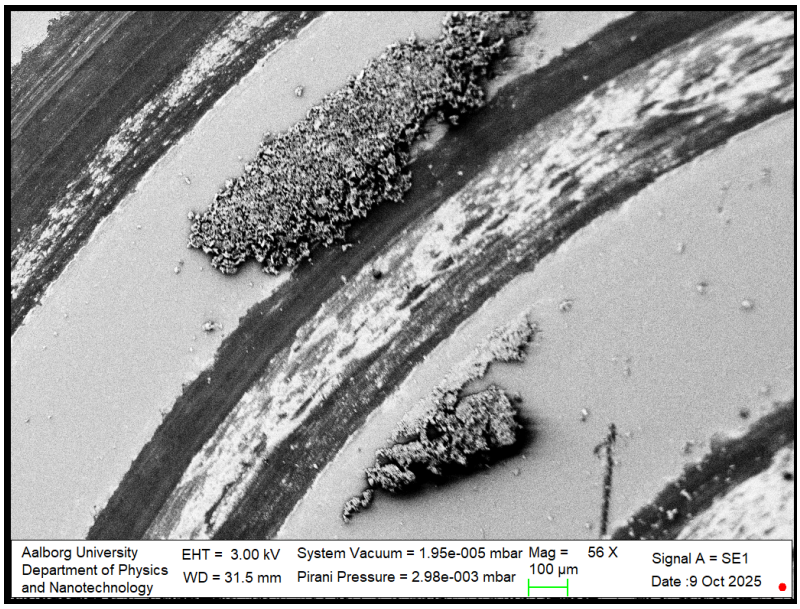

Figure 4.18: This image shows a TiN coated stainless steel sample. This image shows the wear track done on the sample by the TRB3 tribometer and surrounding debris.

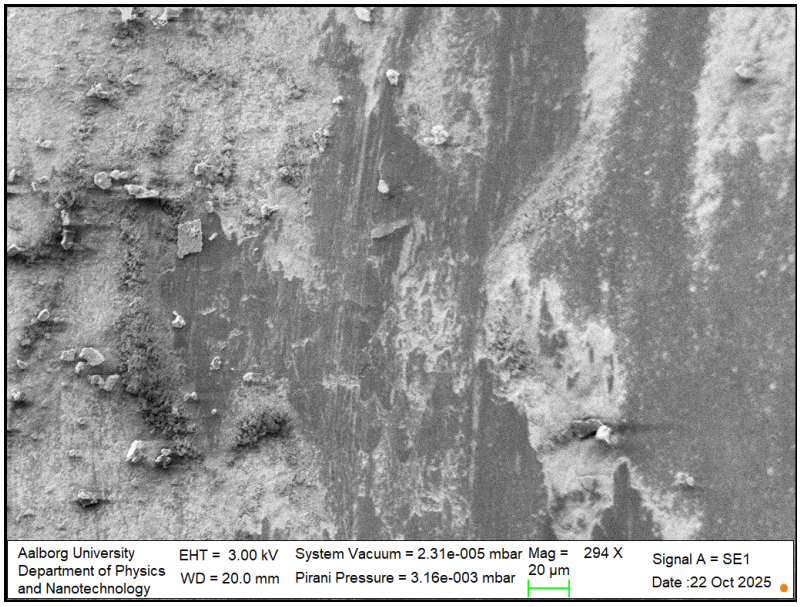

Figure 4.19: This image shows a TiN coated stainless steel sample. This image shows a close up of the wear track done on the sample by the TRB3 tribometer and smaller debris on this track.

The same can be done for the increased amounts of cycles. We inspect the 100, 2000 and 5000 cycle wear tracks, in Figure 4.20, Figure 4.21 and Figure 4.22, because we notice that the 100 and 2000 cycle tracks are deeper, both at around 2000 nm, than the 5000 cycle wear track which has a depth of around 1200 nm.

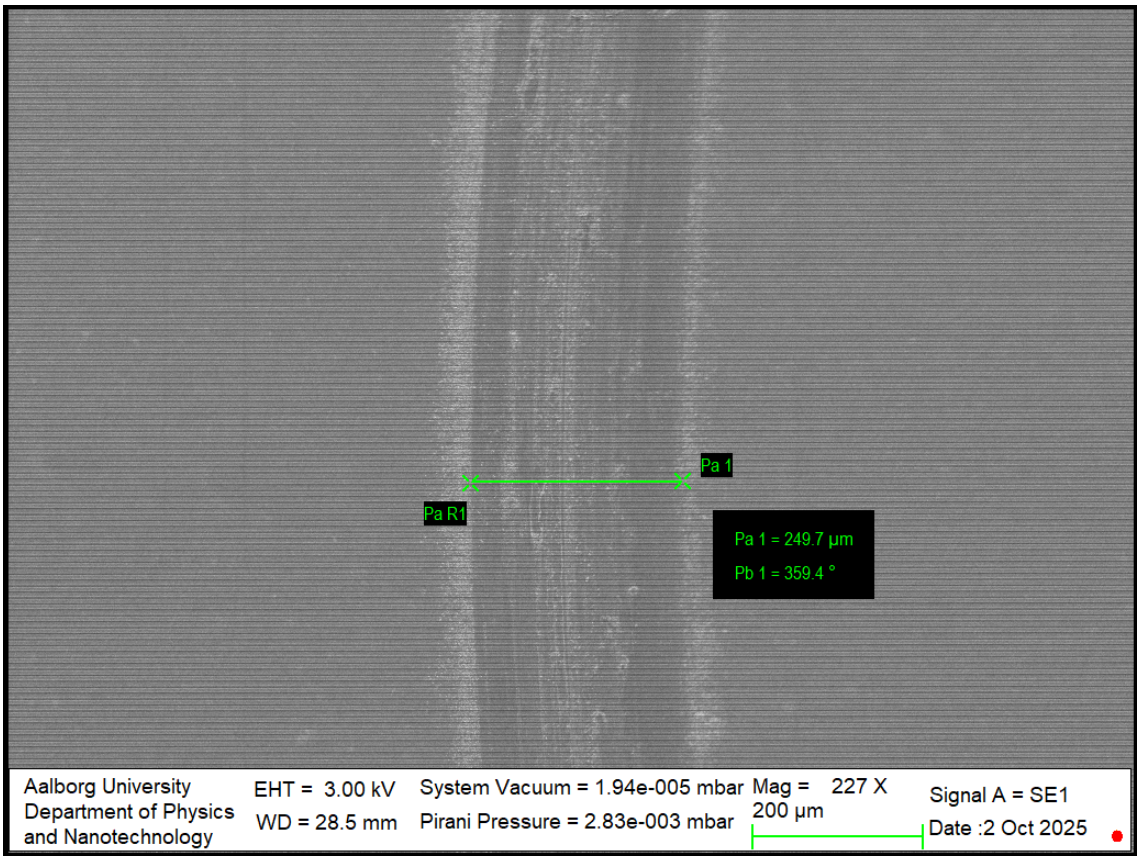

Figure 4.20: This image shows a TiN coated stainless steel sample. This image shows the wear track done on the sample by the TRB3 tribometer when equipped with a load of 1 N and during 100 cycles.

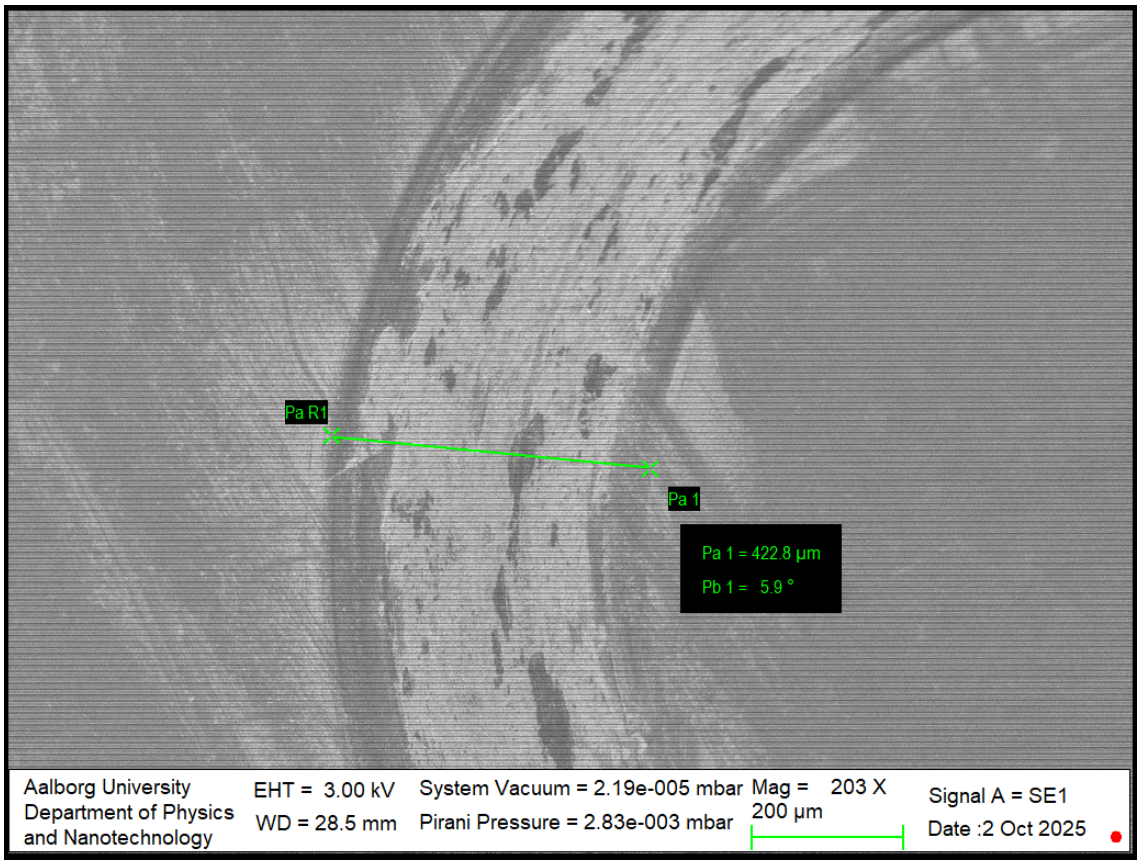

Figure 4.21: This image shows a TiN coated stainless steel sample. This image shows the wear track done on the sample by the TRB3 tribometer when equipped with a load of 1 N and during 2000 cycles.

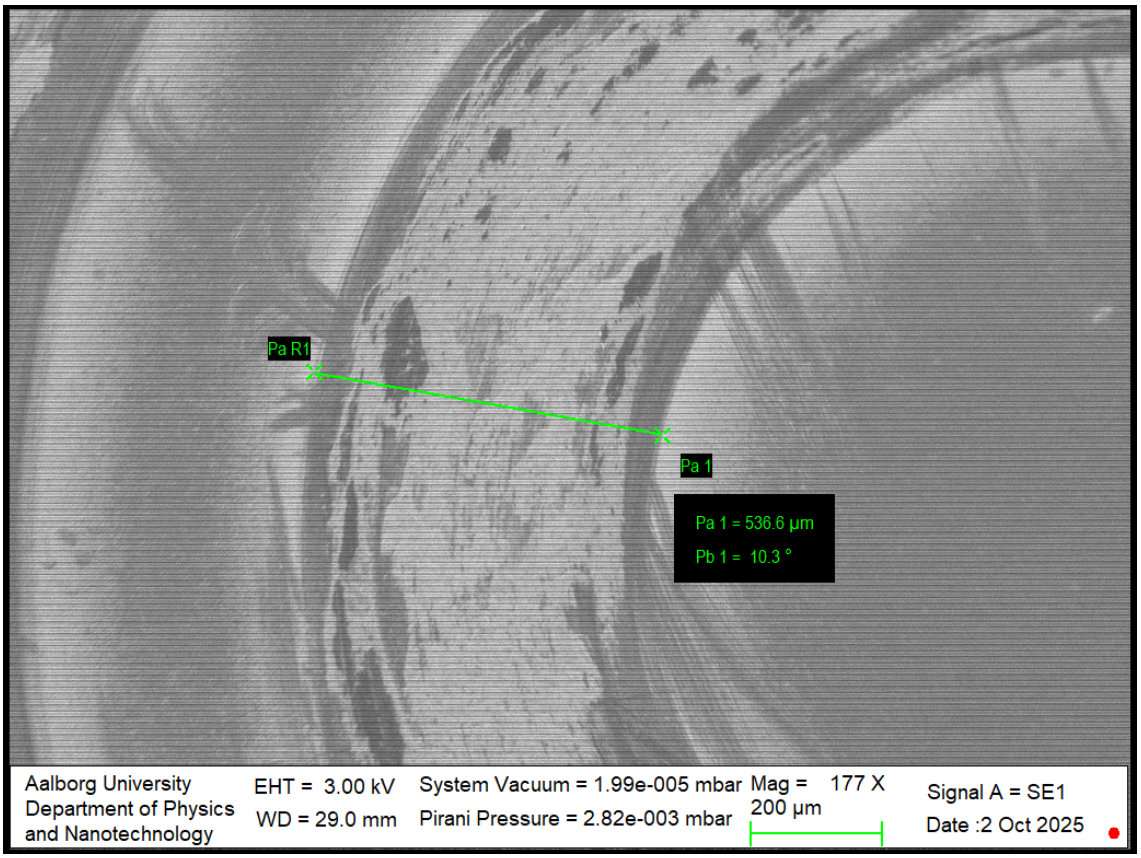

Figure 4.22: This image shows a TiN coated stainless steel sample. This image shows the wear track done on the sample by the TRB3 tribometer when equipped with a load of 1 N and during 5000 cycles.

From these images the 2000 cycle and 5000 cycle tracks look quite similar. The width of the tracks is 249.7 micrometers, 422.8 micrometers and 536.6 micrometers, respectively. These are in agreement with the track width observed by the profiler.

1500 nm TiN Coated Stainless Steel

The experiments for 1500 nm TiN coated samples were performed on different 1500 nm TiN coated samples made under the same conditions, however, yielding wildly different results.
The samples in this section were all subjected to wear using the pin-on-disk tribometer with a 0.6 cm diameter alumina ball. This type of ball was chosen since this was the most common type of ball used for these experiments in literature. The initial tests on the first few 1500 nm samples were done with various load changes, however, due to issues with debris on the sample not more than 1 cycle. It is worth noting that cleaning these debris was attempted with both air and isopropyl, however, to no avail.
The figures below, Figure 4.23 and Figure 4.2.1, show the line profiling for two 1500 TiN coated 2 cm x 2 cm stainless steel samples at 5 N and 1 cycle made under the same conditions.

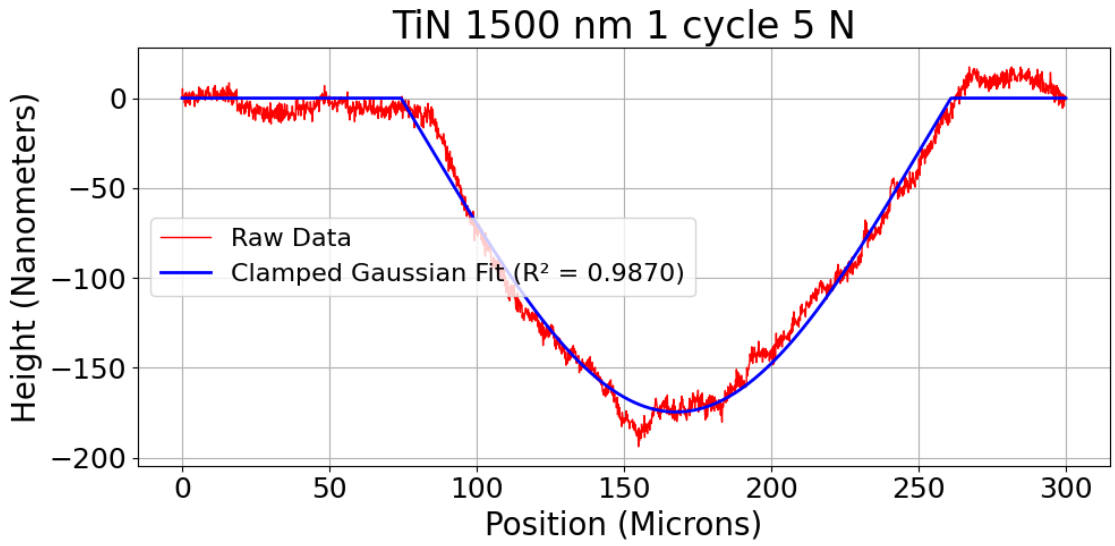

Figure 4.23: This figure shows a 1500 nm TiN coated stainless steel sample. This figure shows the wear track the TRB makes in the sample when equipped with a load of 5 N and during 1 cycle. Raw profile (red) with Gaussian fit (blue).

The first figure, Figure 4.23, shows a wear track in the shape one would expect it to be i.e. a somewhat spherical track. The wear track from this figure has a wear rate of 4.343 x 10^{-6}, which is expected for TiN coatings. The second figure, Figure 4.2.1, shows an improper wear track and complete delamination of the coating. This is seen because the line profiler shows the depth of the track to be around 500 nm more than the coating thickness itself. The suspected reason is improper coating adhesion. The wear rate of the track on Figure 4.2.1 is 2.869 x 10^{-3} $mm^3/(Nm)$ which is too high for TiN, however, when inspecting the figure it is clear that this high wear rate is due to the complete delamination of the coating that occurred.

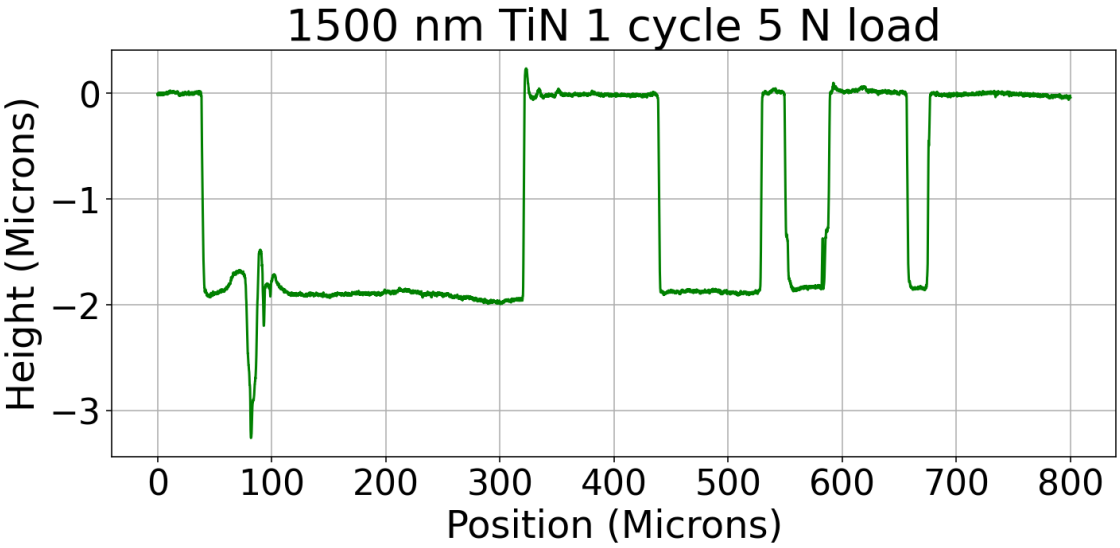

Figure 4.24: T
his figure shows a 1500 nm TiN coated stainless steel sample. This figure shows the wear track the TRB makes in the sample when equipped with a load of 5 N and during 1 cycle. Raw profile (green). This figure shows an improper wear track.

The wear track profiles for 5 N but an increased amount of cycles are seen in Figure 4.25, Figure 4.26 and Figure 4.27. All of these figures exhibit a huge amount of deformation and complete delamination beyond

the coating thickness 1500 nm. Their respective wear rates are 1.238 x 10^{-4} $mm^3/(Nm)$, 3.979 x 10^{-5} $mm^3/(Nm)$ and 2.793 x 10^{-5} $mm^3/(Nm)$. All too large for TiN but stemming from the delamination of the coating. [Kalin and Vižintin, 2000] [Awan et al., 2020] [Novak and Polcar, 2014]

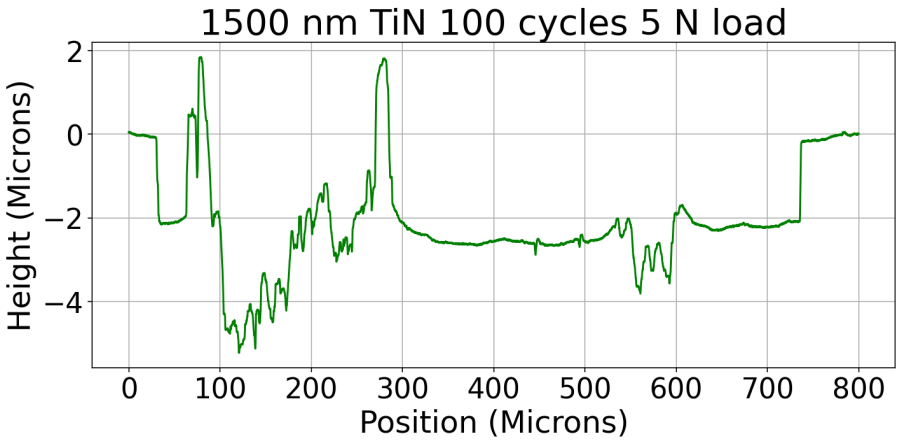

Figure 4.25: This figure shows a 1500 nm TiN coated stainless steel sample. This figure shows the friction coefficient recorded during tribometry measurement when equipped with a load of 5 N and during 100 cycles.

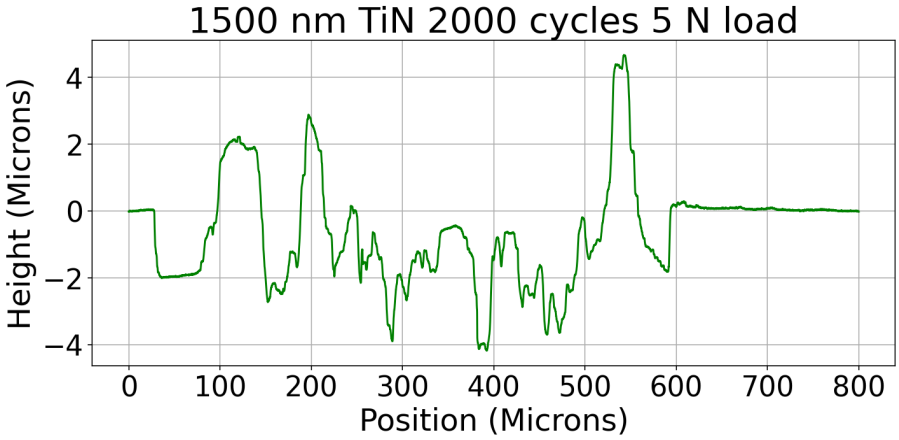

Figure 4.26: This figure shows a 1500 nm TiN coated stainless steel sample. This figure shows the friction coefficient recorded during tribometry measurement when equipped with a load of 5 N and during 2000 cycles.

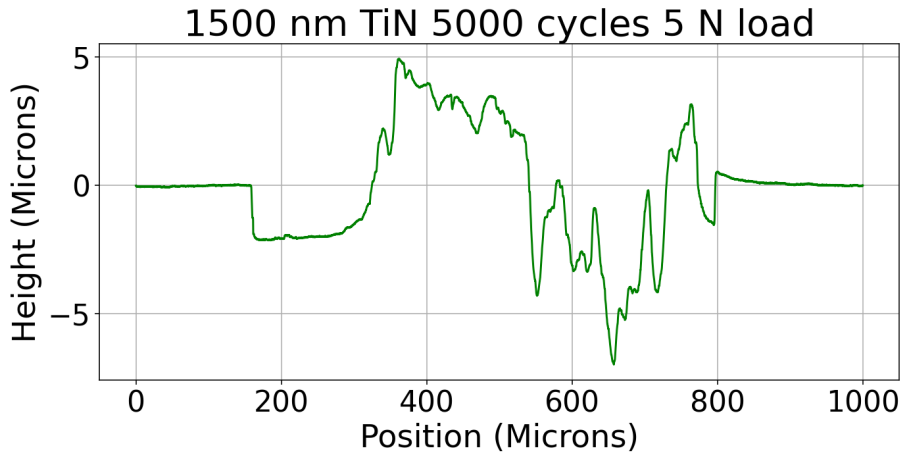

Figure 4.27: This figure shows a 1500 nm TiN coated stainless steel sample. This figure shows the friction coefficient recorded during tribometry measurement when equipped with a load of 5 N and during 5000 cycles.

Both Figure 4.28 and Figure 4.29 show an accumulation of debris in the central part of the wear tracks. These debris are confirmed to be true by SEM imaging seen on Figure 4.30. This image shows a brighter middle section with darker outer sections indicating a depth difference between these two, with the brighter being taller.

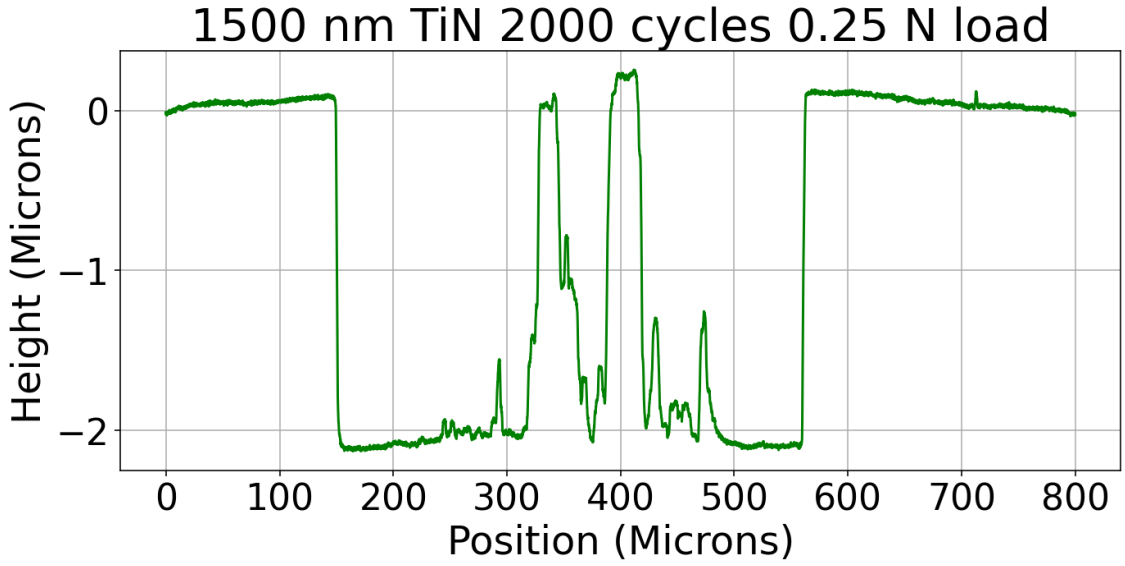

Figure 4.28: This figure shows a 1500 nm TiN coated stainless steel sample. This figure shows the wear track the TRB makes in the sample when equipped with a load of 0.25 N and during 2000 cycles.

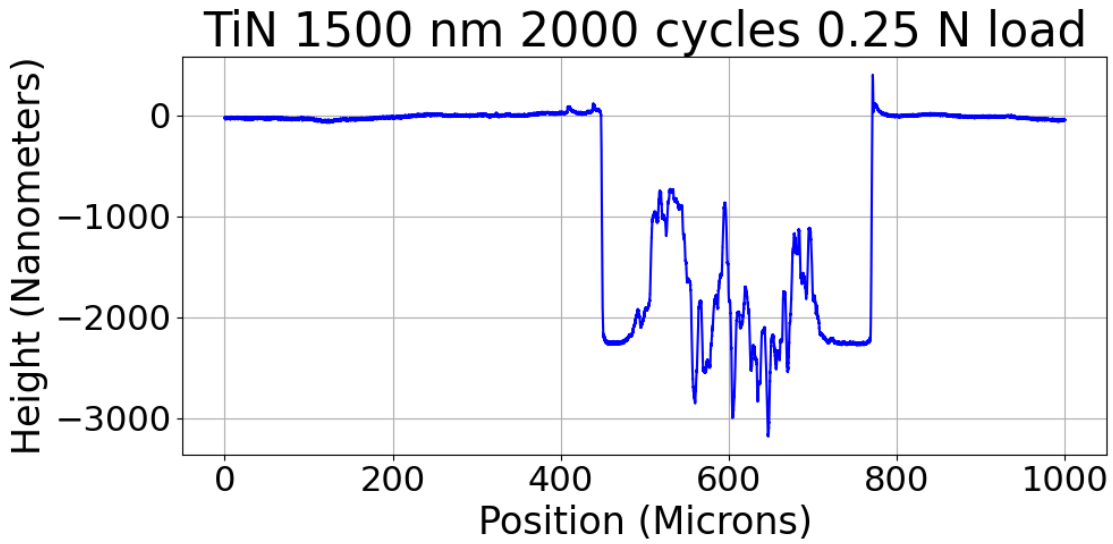

Figure 4.29: This figure shows an older 1500 nm TiN coated stainless steel sample. This figure shows the wear track the TRB makes in the sample when equipped with a load of 0.25 N and during 2000 cycles.

The SEM imaging of the 2000 cycle 0.25 N load wear track shows a width of 439 microns, which is in accordance with the width detected by the line profiler.

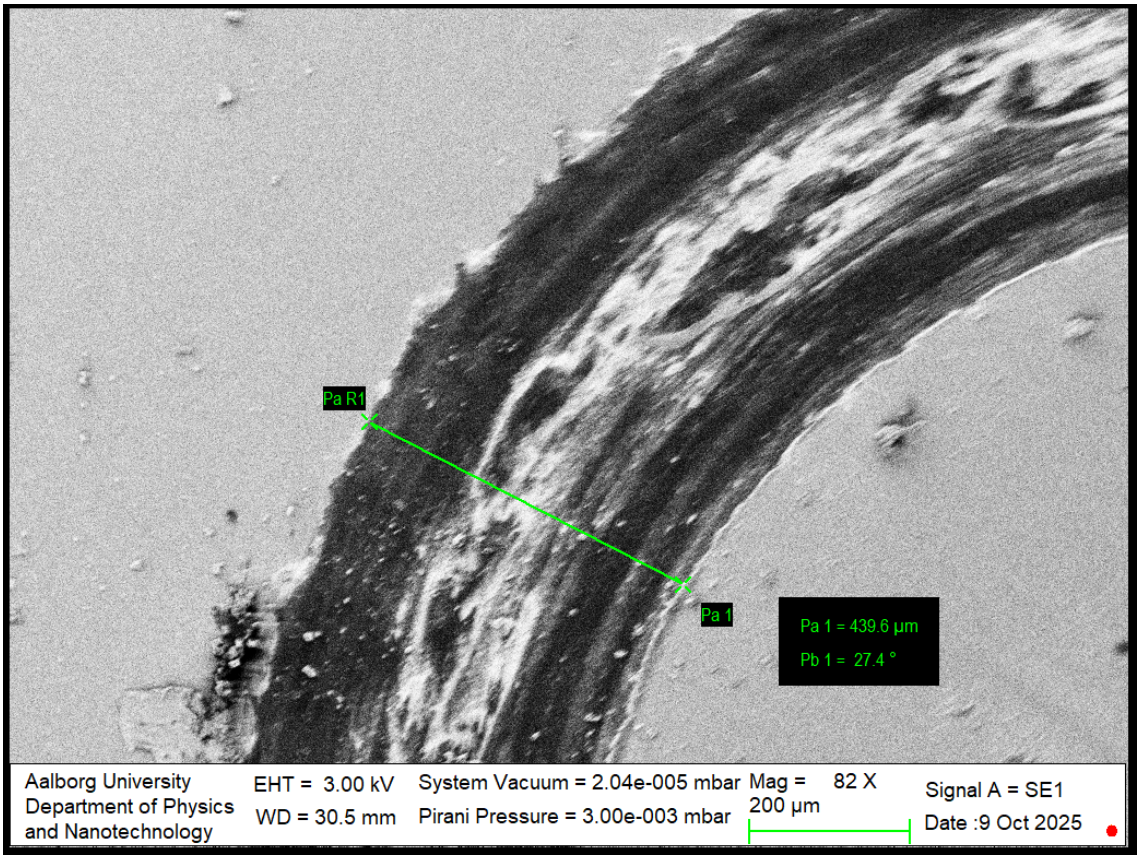

Figure 4.30: This image shows a TiN coated stainless steel sample. This image shows the wear track done on the sample by the TRB3 tribometer when equipped with a load of 0.25 N and during 2000 cycles.

The delamination is also present in loads of 1 N as seen below. The delamination is present for 1 N throughout a cycle count from 1 to 5000 cycles, but the depth of penetration is increased from slightly below

2000 nm to around 3000 nm. This is twice the coating thickness. The delamination generally stays around a maximum depth of 2000 nm even if the penetration goes deeper. The fact that the delamination does not go much deeper than 2000 nm for any load or cycle count even though the penetration might can indicate some possible inconsistency in the substrate surface. The stainless steel substrate is polished before the samples arrive at our disposition. This polishing might affect the substrate surface until a depth of around 500 nm into the substrate.

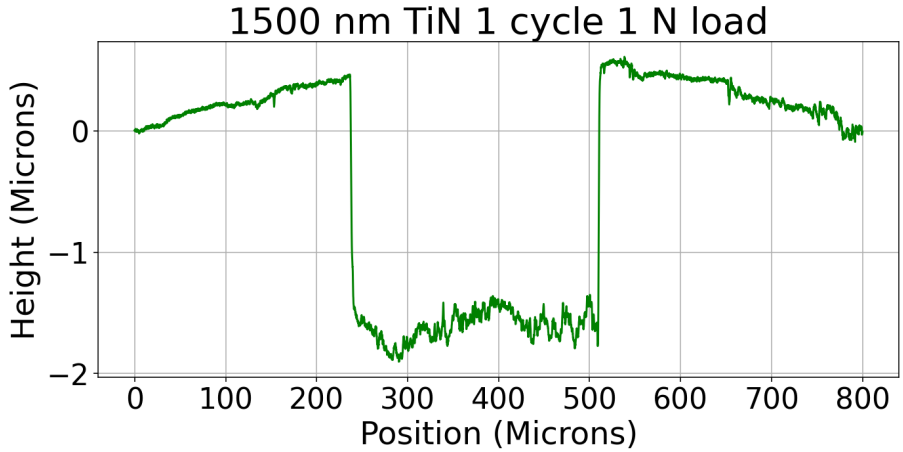

Figure 4.31: This figure shows a 1500 nm TiN coated stainless steel sample. This figure shows the wear track the TRB makes in the sample when equipped with a load of 1 N and during 1 cycle.

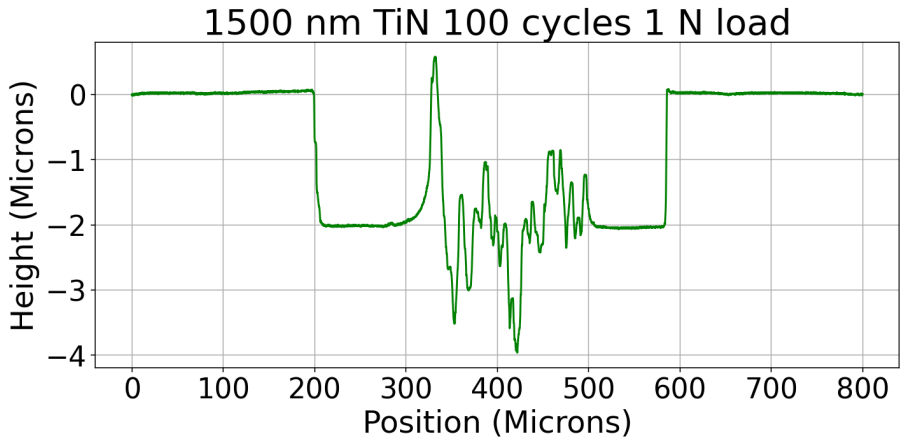

Figure 4.32: This figure shows a 1500 nm TiN coated stainless steel sample. This figure shows the wear track the TRB makes in the sample when equipped with a load of 1 N and during 100 cycles.

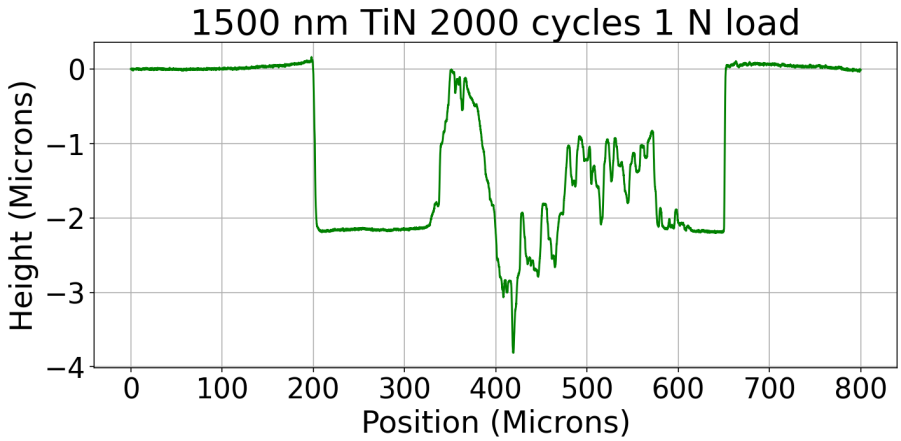

Figure 4.33: This figure shows a 1500 nm TiN coated stainless steel sample. This figure shows the wear track the TRB makes in the sample when equipped with a load of 1 N and during 2000 cycles.

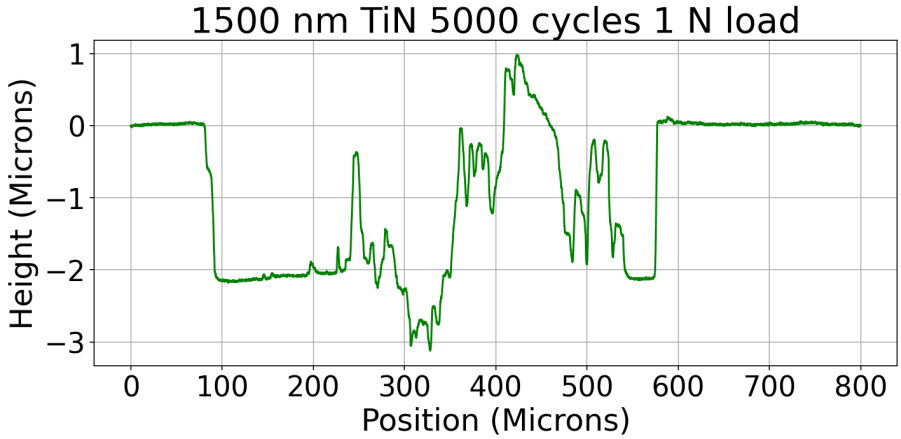

Figure 4.34: This figure shows a 1500 nm TiN coated stainless steel sample. This figure shows the wear track the TRB makes in the sample when equipped with a load of 1 N and during 5000 cycles.

At a load of above 5 N the delamination is constant throughout all cycle counts. This is seen on the 10 N wear tracks, some of which are shown below on Figure 4.35 and Figure 4.36.

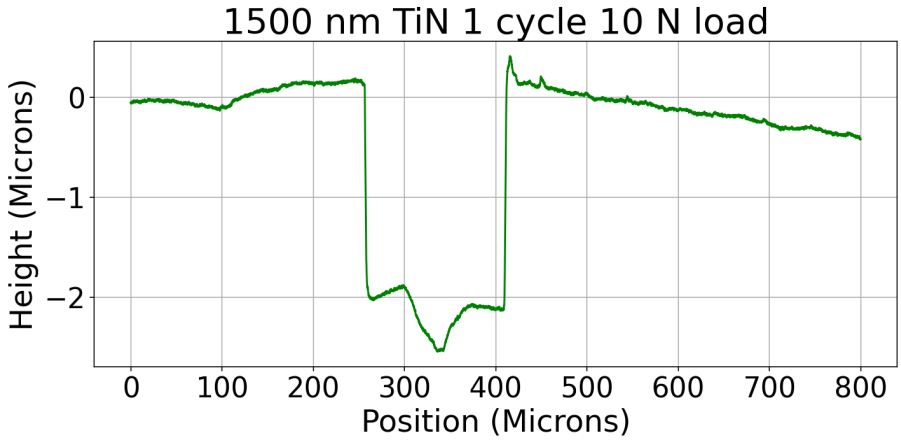

Figure 4.35: This figure shows a 1500 nm TiN coated stainless steel sample. This figure shows the wear track the TRB makes in the sample when equipped with a load of 10 N and during 1 cycle.

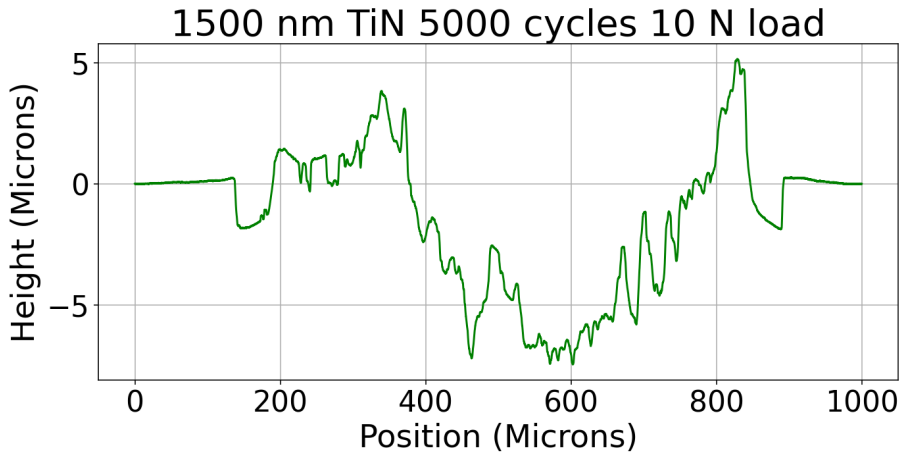

Figure 4.36: This figure shows a 1500 nm TiN coated stainless steel sample. This figure shows the wear track the TRB makes in the sample when equipped with a load of 10 N and during 5000 cycles.

In this study, the TiN coatings have a thickness of 1500 nm, which is significantly thinner than the more typical 4000-5000 nm coatings often used in [Kalin and Vižintin, 2000] [Awan et al., 2020] [Novak and Polcar, 2014]. During the tribometer tests, many of the wear track depths reached around 2000 nm and even up to 6000 nm for higher loads or more cycles, indicating that the coating was fully penetrated and that the wear process extended into the underlying steel substrate. Once the coating is breached, the wear resistance decreases because the steel, which is is softer and less resistant to abrasion, becomes exposed. This also explains the relatively high measured wear rate, comparable to that of the usual TiN coated wear rates. Increasing the TiN coating thickness would likely provide a more effective protective barrier ensuring that the coating can withstand the applied load and sliding distance without being completely penetrated. This is because a thicker coating would provide a larger load bearing volume and thus be able to redistribute contact stresses more. A thicker coating would thus most likely improve the overall wear performance, reduce substrate exposure, and more accurately demonstrate the intrinsic wear resistance of the TiN layer itself. The surface contact pressure would also be spread more evenly through the thickness of the coating, reducing the intensity of the stress peaks at the interface.

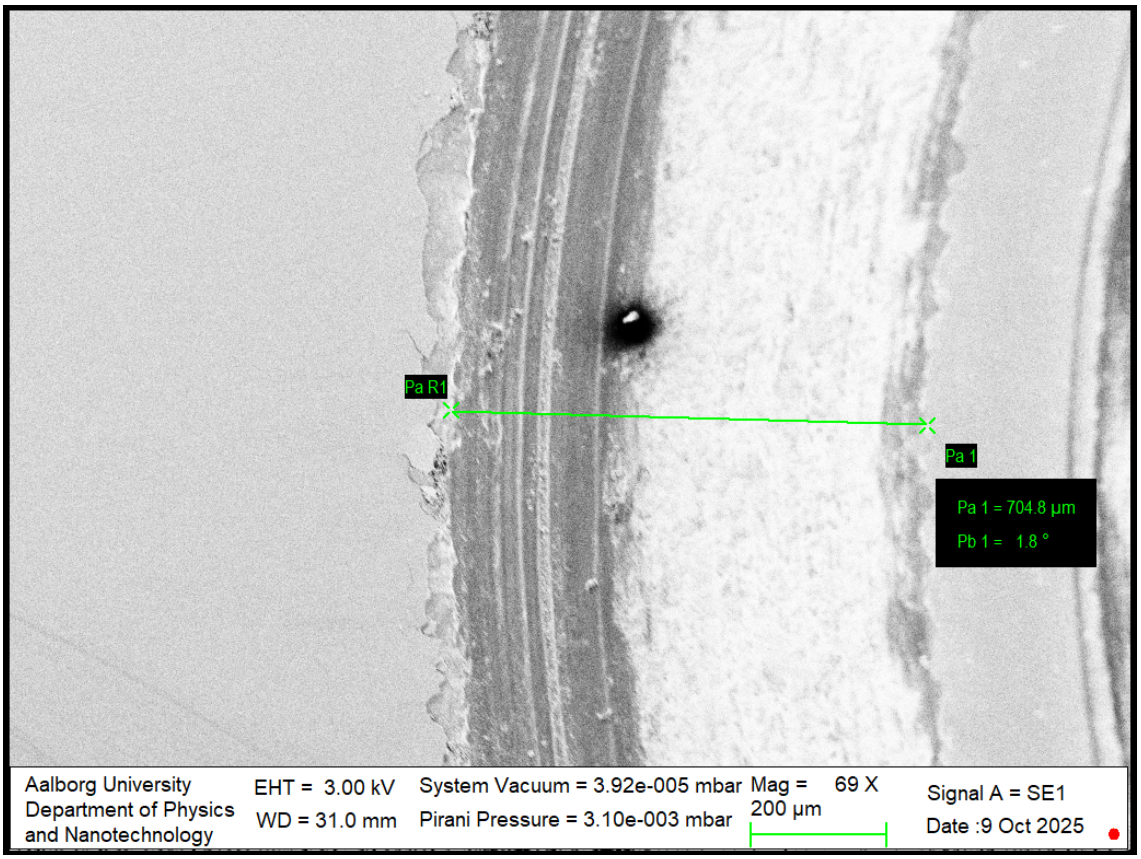

Figure 4.37: This image shows a 1500 nm TiN coated stainless steel sample. This image shows the wear track done on the sample by the TRB3 tribometer when equipped with a load of 10 N and during 1000 cycles. This image shows an example of the TiN coating cracking on the edges of the wear track.

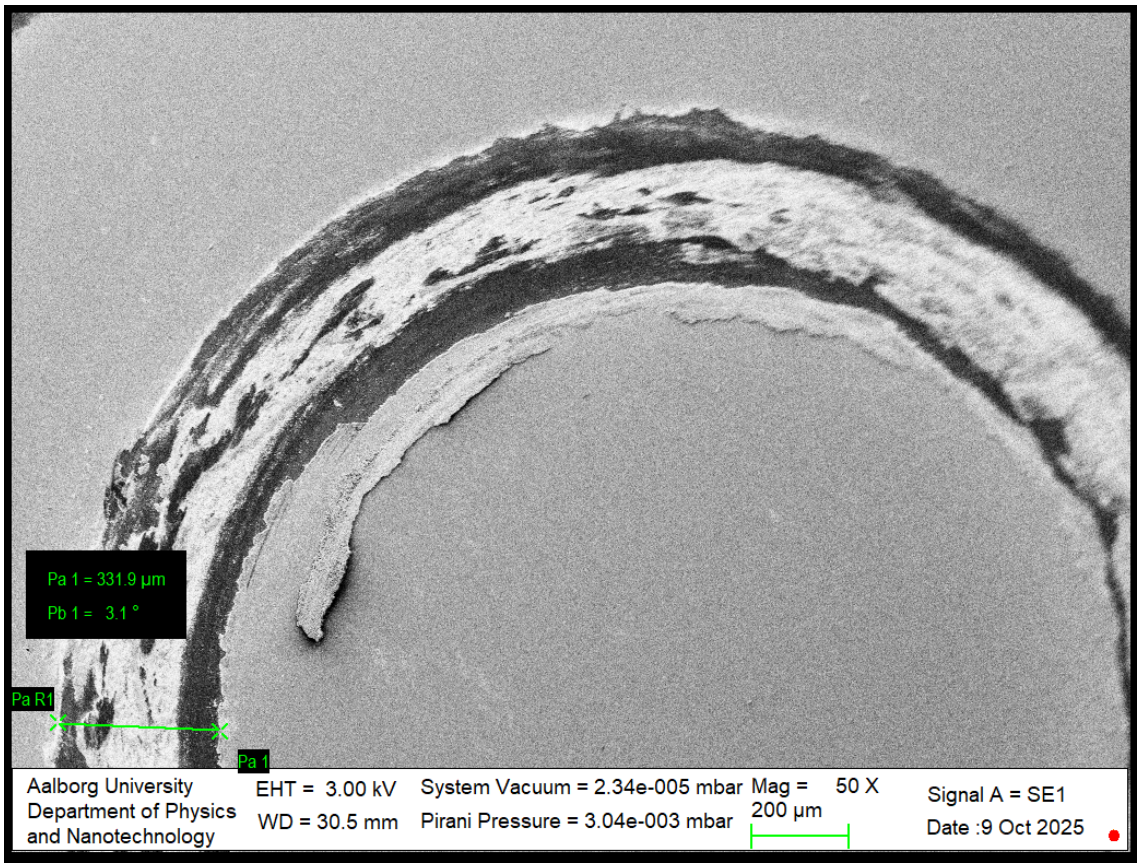

Figure 4.38: This image shows a 1500 nm TiN coated stainless steel sample. This image shows the wear track done on the sample by the TRB3 tribometer when equipped with a load of 0.25 N and during 5000 cycles. This image shows an example of the TiN coating cracking on the edges of the wear track.

When inspecting the SEM images of the wear tracks some images show clear cracks along the edges of the tracks. Their presence indicates that the coating is experiencing mechanical failure rather than purely abrasive wear. This can indeed be due to the aforementioned reason. An example of such cracks is seen in Figure 4.37 and Figure 4.38 which are for a load of 10 N and 0.25 N, respectively.
Furthermore, inspecting the friction coefficient recorded by the TRB3 can help identify the time at which the coating is being penetrated. Figure 4.39 is the friction coefficient corresponding to the line profile seen in Figure 4.27. The graph in Figure 4.39 shows a sudden drop in the friction coefficient going from around 0.9 to 0.6. This sudden drop happens around 800 seconds into the wear track being made. This change in friction coefficient could point to the time at which the coating experienced failure. [Ma et al., 2015]

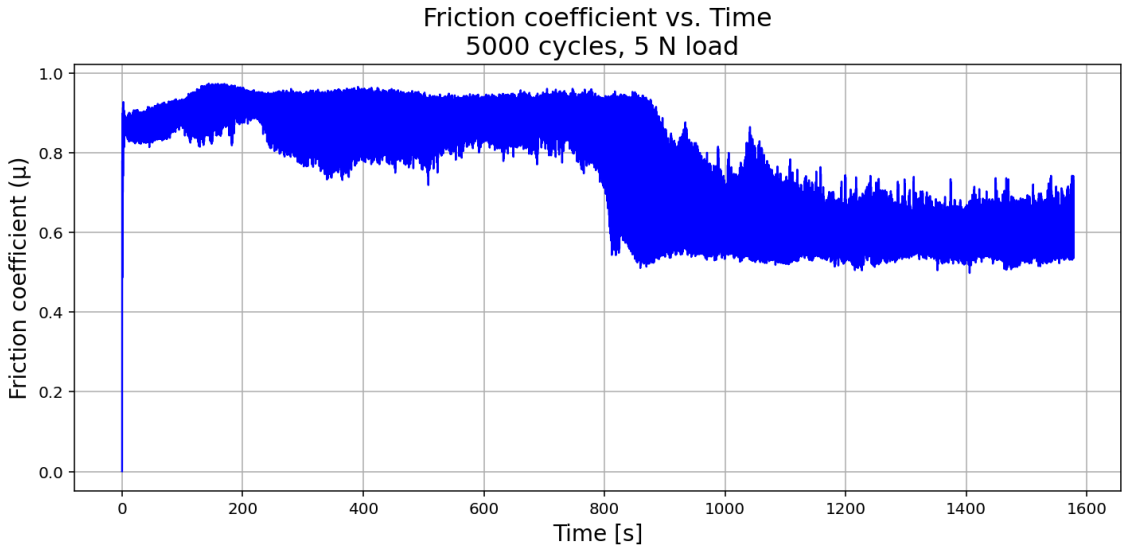

Figure 4.39: This figure shows a 1500 nm TiN coated stainless steel sample. This figure shows the friction coefficient the TRB records while making a wear track on the sample when equipped with a load of 5 N and during 5000 cycles.

4.2.2 X-Ray Diffraction

XRD measurements were performed on two samples: an uncoated stainless steel sample, Figure 4.40, and a 1500 nm TiN coated stainless steel sample, Figure 4.41. The scans were obtained using Cu $\kappa\alpha$ radiation (λ = 1.5406 Å) in a θ - 2θ geometry over a range of 5–70 ° 2θ, with a step size of about 0.013 °. Since the samples are continuous thin films rather than powders, the diffraction intensities represent reflections from crystallographic planes that are oriented parallel to the surface, rather than the random orientations assumed in powder diffraction.

TiN crystallizes in a fcc lattice, where titanium atoms occupy the fcc lattice positions and nitrogen atoms occupy the octahedral sites. The notation hkl used in XRD refers to the Miller indices of the lattice planes responsible for each diffraction peak. For cubic systems such as TiN, the most intense reflections are usually the (111), (200) and (220) planes. In this structure, the (111) plane corresponds to the most densely packed atomic layer and often represents the lowest surface energy orientation, which frequently becomes the preferred growth direction in thin film deposition. [Steneteg et al., 2013]

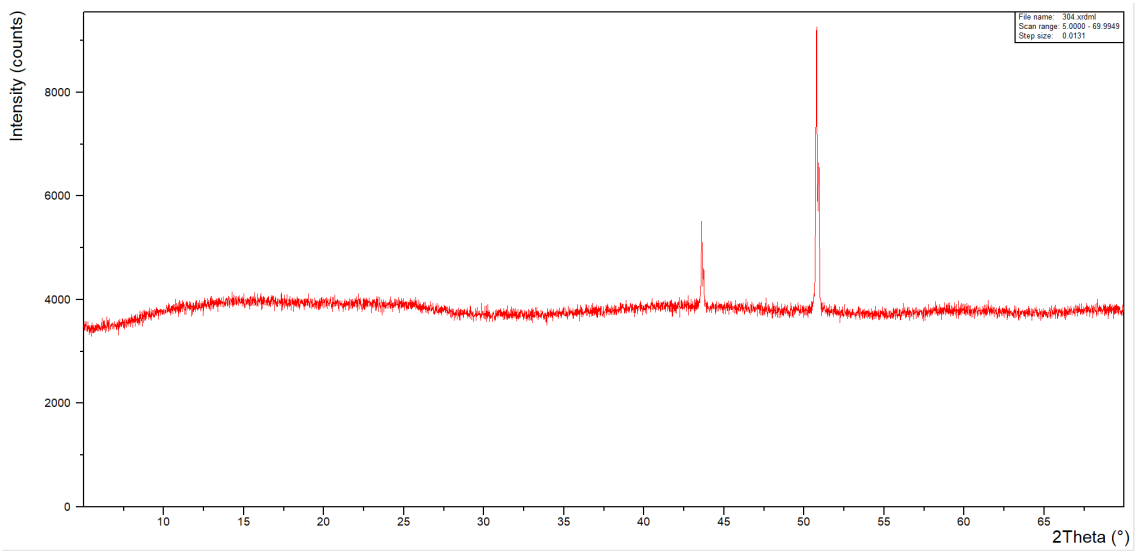

Figure 4.40: This figure shows the graph made by the XRD when scanning stainless steel 304. The graph has two sharp and intense peaks located at approximately 43.0 ° and 50.2 ° in 2θ.

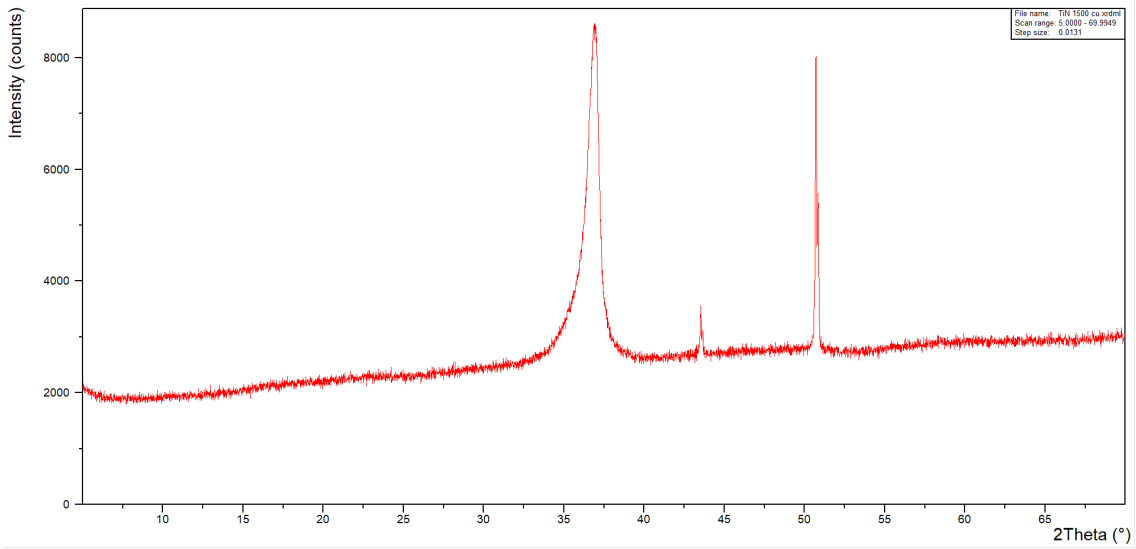

Figure 4.41: This figure shows the graph made by the XRD when scanning TiN coated stainless steel. The graph has two sharp and intense peaks located at approximately 43.0 ° and 50.2 ° in 2θ also seen when scanning pure stainless steel and one additional peak at around 36.7 °.

The XRD pattern of the uncoated 304 stainless steel, in Figure 4.40, shows two sharp and intense peaks located at approximately 43.0 ° and 50.2 ° in 2θ. These correspond to the (111) and (200) reflections of the γ-Fe phase (fcc structure) for the 304 steel. From these peak positions, the calculated lattice parameter is about 3.63–3.64 Å, consistent with literature values for stainless steel 304.[Steneteg et al., 2013] The narrow and symmetric peak shapes indicate that the substrate is highly crystalline [Richter et al., 2023].

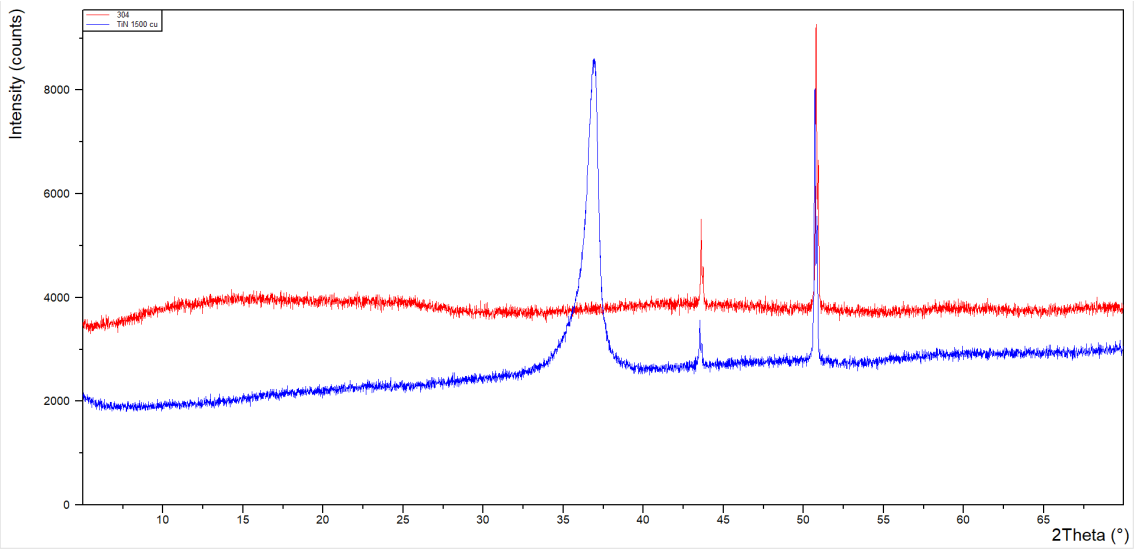

Figure 4.42: This figure shows the overlap of the graph made by the XRD when scanning stainless steel 304 (red) and TiN coated stainless steel (blue). The blue graph has two sharp and intense peaks located at approximately 43.0 ° and 50.2 ° in 2θ also seen when scanning pure stainless steel (red) and one additional peak at around 36.7 °.

The TiN coated sample shows an additional prominent peak located at approximately 36.7 ° 2θ, which can be indexed to the TiN (111) reflection. This position corresponds to a spacing of 2.45 Å, giving a cubic lattice parameter of about 4.24 Å, in agreement with the reported value for TiN (a ≈ 4.24 Å). The (111) reflection of TiN was the dominant feature in the TiN coated sample, while higher order reflections such as (200) and (220) were not apparent. This indicates a strong preferred orientation, or texture, with the (111) planes aligned parallel to the surface.

For the TiN coated sample, the diffraction pattern changes. In addition to the substrate reflections, a new peak appeared at approximately 36.7° 2θ. This peak was assigned to the (111) reflection of cubic TiN, which has the NaCl fcc structure. Using Bragg's law and the cubic lattice relation:

$$d = \frac{\lambda}{2\sin\theta} \tag{4.2.1}$$

, where λ is the wavelength of the x-ray equals 1.5406 Å (Cu κ α, d is the spacing of the crystal layers (path difference), θ is the incident angle (the angle between incident ray and the scatter plane), which is half of the reported 2 θ. The corresponding lattice parameter of the TiN phase was calculated to be approximately 4.24 Å.

A notable feature of the TiN (111) peak is its broadness relative to the sharp stainless steel peaks. This broadening can originate from several factors. In this case, the broad yet well defined TiN peak suggests that the film is nanocrystalline, composed of small grains typically tens to a few hundred nanometers in size, and that it may contain lattice strain or inhomogeneity. The peak has a clear maximum, which distinguishes the material from an amorphous phase that would produce only a broad diffuse hump.

Applying the Scherrer equation,

$$D = \frac{K\lambda}{\beta\cos\theta} \tag{4.2.2}$$

, where D is the coherent domain size, β is the full width at half maximum in radians, θ is the Bragg angle, and K is a shape factor (≈0.9), gives an estimate of the nanocrystalline domain dimensions. A typical TiN (111) peak with a width of about 0.5–1.0° 2θ would correspond to domain sizes on the order of 80–170

nm. These values would be consistent with a dense nanocrystalline film structure rather than large columnar grains. The comparison between the TiN coated and uncoated sample shows that, despite the presence of the TiN, the stainless steel peaks remain visible. This can be expected for a 1500 nm coating because Cu $\kappa\ \alpha$ X-rays penetrate on the order of a micron in dense materials. The presence of sharp substrate peaks alongside a broad TiN reflection further supports the interpretation that the coating is nanocrystalline while the substrate remains crystallized.

Overall, the diffraction data shows that the deposited layer is a nanocrystalline TiN thin film with strong (111) preferred orientation. The broadness of the TiN (111) peak reveals small coherent domain sizes, while the substrate peaks indicate partial X-ray penetration through the film. The calculated lattice parameter matches TiN, suggesting that the film has the expected cubic NaCl structure. [Thomsen et al., 1998]

Chapter 5

Conclusion

The TiN coatings deposited in this study had a thickness of approximately 1500 nm, which is significantly thinner than the typical 4000-5000 nm TiN layers usually reported. Tribological testing revealed that under moderate to high normal loads and extended sliding distances, the wear depth often exceeded the coating thickness, in some cases the depth reached up to 6000 nm. This indicates complete penetration of the TiN film and subsequent wear of the underlying stainless steel substrate. Once the coating was breached, the softer steel substrate contributed to accelerated material removal and elevated wear rates, thus masking the intrinsic wear resistance of the TiN layer itself. Increasing the coating thickness would therefore be expected to improve load bearing capacity, delay film failure, and more clearly isolate the coating's protective performance.

SEM observations corroborated these findings, showing crack formation at the edges of the wear tracks for both high load and low load conditions, suggesting mechanical failure mechanisms in addition to abrasion. Monitoring of the friction coefficient further supported coating failure progression by sudden changes in friction.

X-ray diffraction analysis indicates that the TiN coatings were crystalline and predominantly oriented along the (111) plane. The TiN (111) peak exhibited significant broadening relative to the sharp reflections of the stainless steel substrate, indicating a nanocrystalline structure with small coherent domain sizes. The steel peaks also show that the X-rays penetrated the 1500 nm coating thickness, as expected for Cu $\kappa\alpha$ radiation. The calculated lattice parameter of approximately 4.24 Å for TiN and approximately 3.63–3.64 Å for stainless steel align well with reference values, confirming successful deposition of crystalline TiN with the expected NaCl type structure.

Overall, the combined tribological, microscopic, and structural characterization shows that the deposited TiN films are nanocrystalline, textured, and mechanically protective, but their limited thickness and perhaps adhesion issues allowed substrate exposure under the applied test conditions. A thicker coating and or increased adhesion would likely enhance durability and show the wear resistant capabilities of the TiN layer more clearly.

Chapter 6

Outlook

Future studies could focus on using alternative sample material or coating material. For example the substrate can be something such as silicon. Coating can be changed to different nitrides such as Titanium Aluminum Nitride (TiAlN) or Aluminum Nitride (AlN). Additionally, thicker coatings might be used for better comparison of the results with literature. This may help with adhesion problems and it may be used as reference samples on how to properly produce and test such thin films. Furthermore, testing with multilayer coatings could be done.

Another useful direction would be to optimize deposition parameters such as substrate bias, gas composition, and deposition temperature. These variables strongly affect residual stress, grain size, and preferred orientation, and therefore mechanical and tribological properties. Performing studies with different process parameters, followed by XRD and SEM characterization, would help establish correlations between microstructure and wear behavior.

Furthermore, unfortunately, due to unexpected equipment failure line profiles of the TiN coated samples with a load of 2 N where not made. Including these would provide a more thorough look into the intermediate loads used in experiments.

Bibliography

[Dam,] Damstahl mirror steel no. 8. https://damstahl.com/da. Accessed: 02 May, 2025.

[ISO, 2018] (2018). ISO 6507-1:2018 metallic materials — vickers hardness test — part 1: Test method. Available from https://www.iso.org/standard/67145.html.

[Dur, 2023] (2023). *Duramin-40 - Instruction Manual*.

[A. Mubarak et al., 2018] A. Mubarak, A. M., E. Hamzah, E. H., and M. R. M. Tofr, M. R. M. T. (2018). Review of physical vapour deposition (pvd) techniques for hard coating. *Jurnal Mekanikal*, 20(2).

[Ambios,] Ambios. Ambios xp-2 line profiler image. https://www.kla.com/products/instruments/stylus-profilers/innovation-history. Accessed: 12 September, 2025.

[Ambios Technology, 2003] Ambios Technology, I. (2003). *XP Series Stylus Profiler User's Manual (XP-1/XP-2)*. Santa Cruz, CA, USA. User's Manual.

[Awan et al., 2020] Awan, A., Pasha, R. A., Butt, M. S., Malik, R. A., Alarifi, I. M., Alzaid, M., Latif, M., Naseer, A., Saleem, M., and Alrobei, H. (2020). Corrosion and wear behavior of tin pvd coated 304 stainless-steel. *Journal of Mechanical Science and Technology*.

[Azibi et al., 2019] Azibi, M., Saoula, N., and Aknouche, H. (2019). The influence of substrate bias voltage on the electrochemical properties of zrn thin films deposited by radio-frequency magnetron sputtering: Biomedical application. *Journal of Electrical Engineering*, 70(7):112–116.

[Baptista et al., 2018a] Baptista, A., Silva, F., Porteiro, J., Míguez, J., and Pinto, G. (2018a). Sputtering physical vapour deposition (pvd) coatings: A critical review on process improvement and market trend demands. *Coatings*, 8(11).

[Baptista et al., 2018b] Baptista, A., Silva, F., Porteiro, J., Míguez, J., Pinto, G., and Fernandes, L. (2018b). On the physical vapour deposition (pvd): Evolution of magnetron sputtering processes for industrial applications. *Procedia Manufacturing*, 17:746–757. 28th International Conference on Flexible Automation and Intelligent Manufacturing (FAIM2018), June 11-14, 2018, Columbus, OH, USAGlobal Integration of Intelligent Manufacturing and Smart Industry for Good of Humanity.

[Barcelos et al., 2017] Barcelos, M., Barcelos, M., Araujo, J., Jr, A., and Vieira, E. (2017). Wear resistance of aisi 304 stainless steel submitted to low temperature plasma carburizing. *REM - International Engineering Journal*, 70:293–298.

[Barshilia et al., 2012] Barshilia, H. C., Ananth, A., Khan, J., and Srinivas, G. (2012). Ar + h2 plasma etching for improved adhesion of pvd coatings on steel substrates. *Vacuum*, 86(8):1165–1173.

[Berg et al., 1987] Berg, S., Blom, H., Larsson, T., and Nender, C. (1987). Modeling of reactive sputtering of compound materials. *Journal of Vacuum Science Technology A*, 5(2):202–207.

[Berg and Nyberg, 2005] Berg, S. and Nyberg, T. (2005). Fundamental understanding and modeling of reactive sputtering processes. *Thin Solid Films*, 476(2):215–230.

[Borowski and Myśliwiec, 2025] Borowski, P. and Myśliwiec, J. (2025). Recent advances in magnetron sputtering: From fundamentals to industrial applications. *Coatings*, 15(8).

[Depla and Mahieu, 2008] Depla, D. and Mahieu, S., editors (2008). *Reactive Sputter Deposition*, volume 109 of *Springer Series in Materials Science*. Springer-Verlag Berlin Heidelberg, Berlin, Heidelberg.

[Dewangan and Mishra, 2024] Dewangan, S. and Mishra, S. (2024). Analysing microstructure and hardness of ss-304 under annealed, normalized, quenched and step cooled conditions. *Journal of The Institution of Engineers (India): Series D*.

[Falcone, 1988] Falcone, G. (1988). Sputtering transport theory: The mean energy. *Phys. Rev. B*, 38:6398–6401.

[Fox-Rabinovich et al., 2016] Fox-Rabinovich, G., Paiva, J. M., Gershman, I., Aramesh, M., Cavelli, D., Yamamoto, K., Dosbaeva, G., and Veldhuis, S. (2016). Control of self-organized criticality through adaptive behavior of nano-structured thin film coatings. *Entropy*, 18(8).

[Hidayat et al., 2020] Hidayat, H., Jufriyanto, M., Permata Ningtyas, A. H., and Yusron, R. (2020). Analysis of load variations on ST60 Steel using vickers method. *International Journal of Science, Engineering and Information Technology*, 5(1):231–235.

[Hu et al., 2022] Hu, J., Song, H., Sandfeld, S., Liu, X., and Wei, Y. (2022). Breakdown of archard law due to transition of wear mechanism from plasticity to fracture. *Tribology International*, 173.

[Joós and Duesbery, 1997] Joós, B. and Duesbery, M. S. (1997). The peierls stress of dislocations: An analytic formula. *Phys. Rev. Lett.*, 78:266–269.

[Kalin and Vižintin, 2000] Kalin, M. and Vižintin, J. (2000). Use of equations for wear volume determination in fretting experiments. *Wear*, 237(1–2):39–48.

[Kim et al., 1992] Kim, J. O., Achenbach, J. D., Shinn, M., and Barnett, S. A. (1992). Effective elastic constants and acoustic properties of single-crystal tin/nbn superlattices. *Journal of Materials Research*, 7(8):2248–2256.

[Kuffel et al., 2000] Kuffel, E., Zaengl, W., and Kuffel, J. (2000). Chapter 5 - electrical breakdown in gases. pages 281–366.

[Kusano, 2018] Kusano, E. (2018). Revisitation of the structure zone model based on the investigation of the structure and properties of ti, zr, and hf thin films deposited at 70–600°c using dc magnetron sputtering. *Journal of Vacuum Science Technology A*, 36(4):041506.

[Li et al., 2022] Li, X., Bakhit, B., Johansson Jõesaar, M. P., Petrov, I., Hultman, L., and Greczynski, G. (2022). Dense, single-phase, hard, and stress-free ti0.32al0.63w0.05n films grown by magnetron sputtering with dramatically reduced energy consumption. *Scientific Reports*, 12.

[Luis et al., 2020] Luis, E. E. M., Carrasco, I. S. S., de Assis, T. A., and Reis, F. D. A. A. a. (2020). Statistics of adatom diffusion in a model of thin film growth. *Phys. Rev. E*, 102:012805.

[Ma et al., 2015] Ma, G., Wang, L., Gao, H., Zhang, J., and Reddyhoff, T. (2015). The friction coefficient evolution of a tin coated contact during sliding wear. *Applied Surface Science*, 345:109–115.

[malvern Panalytical,] malvern Panalytical. Empyrean image. https://www.malvernpanalytical.com/en/products/product-range/empyrean-range/empyrean. Accessed: 25 May, 2025.

[Martin, 2010] Martin, P. M. (2010). *Handbook of deposition technologies for films and coatings: science, applications and technology*. Elsevier, 3rd ed. edition.

[Mohammed and Abdullah, 2019] Mohammed, A. and Abdullah, A. (2019). Scanning electron microscopy (sem): A review.

[Musin, 2025] Musin, A. I. (2025). Sputtering of solids by ion bombardment: Analytical models for the formation of angular and energy distributions of sputtered atoms. *Current Physics*, 2:1–9.

[Nakamura et al., 1977] Nakamura, K., Inagawa, K., Tsuruoka, K., and Komiya, S. (1977). Applications of wear-resistant thick films formed by physical vapor deposition processes. *Thin Solid Films*, 40:155–167.

[Novak and Polcar, 2014] Novak, R. and Polcar, T. (2014). Tribological analysis of thin films by pin-on-disc: Evaluation of friction and wear measurement uncertainty. *Tribology International*, 74:154–163.

[Paar,] Paar, A. Trb3 image. anton-paar.com. Accessed: 12 September, 2025.

[Panalytical, 2023] Panalytical, M. (2023). *Empyrean Series 3 User Guide (English)*. Almelo, The Netherlands. User's Manual – Empyrean Series 3 XRD System.

[Pei et al., 2021] Pei, D., Wang, L., Ding, M.-H., Hu, Z.-N., Zhao, J.-Y., Zhou, G.-Y., and Feng, Z.-R. (2021). The effects of substrate bias on the properties of hfc coatings deposited by rf magnetron sputtering. *Coatings*, 11(8).

[Pittman and Lu, 2020] Pittman, N. and Lu, T.-M. (2020). Growth front smoothing effects in extremely high pressure vapor deposition. *Scientific Reports*, 10.

[Polyteknik AS, 2023] Polyteknik AS (2023). *FLEXTURA 200 Cluster — The Most Flexible 200 mm Platform*. Polyteknik AS, Farum, Denmark. Product datasheet.

[Ray et al., 2023] Ray, S. K., Banerjee, A., Bhangi, B. K., Pyne, D., and Dutta, B. (2023). *Tribology of Polymers, Polymer Composites, and Polymer Nanocomposites*. Elsevier Series on Tribology and Surface Engineering. Elsevier.

[Richter et al., 2023] Richter, N., Yang, B., Barnard, J., Niu, T., Sheng, X., Shaw, D., Watanabe, M., Rane, G., Krause, U., Dürrenfeld, P., Wang, H., and Zhang, X. (2023). Significant texture and wear resistance improvement of tin coatings using pulsed dc magnetron sputtering. *Applied Surface Science*, 635:157709.

[Sakaguchi and Powers, 2012] Sakaguchi, R. L. and Powers, J. M. (2012). Chapter 4 - fundamentals of materials science. pages 33–81.

[Serway and Jewett, 2013] Serway, R. A. and Jewett, J. W. (2013). *Physics for Scientists and Engineers with Modern Physics*. Cengage Learning, 9 edition.

[Shapovalov, 2023] Shapovalov, V. I. (2023). Modeling of reactive sputtering—history and development. *Materials*, 16(8).

[Sigmund, 1969] Sigmund, P. (1969). Theory of sputtering. i. sputtering yield of amorphous and polycrystalline targets. *Phys. Rev.*, 184:383–416.

[Sproul et al., 2005] Sproul, W., Christie, D., and Carter, D. (2005). Control of reactive sputtering processes. *Thin Solid Films*, 491:1–17.

[Steinmann and Hintermann, 1985] Steinmann, P. A. and Hintermann, H. E. (1985). Adhesion of tic and ti(c,n) coatings on steel. *Journal of Vacuum Science Technology A*, 3(6):2394–2400.

[Steneteg et al., 2013] Steneteg, P., Hellman, O., Vekilova, O. Y., Shulumba, N., Tasnádi, F., and Abrikosov, I. A. (2013). Temperature dependence of tin elastic constants from ab initio molecular dynamics simulations. *Phys. Rev. B*, 87:094114.

[Struers,] Struers. Duramin 40 image. `https://www.struers.com/it-IT/Products/Hardness-testing/Hardness-testing-equipment/Duramin-40`. Accessed: 25 May, 2025.

[Sundgren, 1985] Sundgren, J.-E. (1985). Structure and properties of tin coatings. *Thin Solid Films*, 128(1):21–44.

[Sundgren et al., 1983] Sundgren, J.-E., Johansson, B.-O., Karlsson, S.-E., and Hentzell, H. (1983). Mechanisms of reactive sputtering of titanium nitride and titanium carbide ii: Morphology and structure. *Thin Solid Films*, 105(4):367–384.

[Tewary, 2002] Tewary, V. (2002). Theory of elastic wave propagation in an anisotropic film on an anisotropic substrate: Tin film on single crystal si. (112).

[Thomsen et al., 1998] Thomsen, N., Horsewell, A., Mogensen, K., Eskildsen, S., Mathiasen, C., and Bøttiger, J. (1998). Residual stress determination in pecvd tin coatings by x-ray diffraction: a parametric study. *Thin Solid Films*, 333(1):50–59.

[TriTec,] TriTec, A. P. *User Manual Tribometer TRB*.

[Vallejo-Otero et al., 2025] Vallejo-Otero, V., Crespo-Monteiro, N., Gamet, E., Ollier, N., Donnet, C., Valour, A., and Jourlin, Y. (2025). Advancements in nitridation of tio2 layers: Mechanisms, techniques, and applications for tin thin films. *Journal of the European Ceramic Society*, 45(10):117330.

[Wasa et al., 2004] Wasa, K., Kitabatake, M., and Adachi, H. (2004). 4 - sputtering systems. In Wasa, K., Kitabatake, M., and Adachi, H., editors, *Thin Film Materials Technology*, pages 115–189. William Andrew Publishing, Norwich, NY.

[Wisbey et al., 1987] Wisbey, A., Gregson, P., and Tuke, M. (1987). Application of pvd tin coating to co-cr-mo based surgical implants. *Biomaterials*, 8(6):477–480.

[Yang et al., 2017] Yang, Zhu, Wei, Xiao, and Du (2017). First-principles study of optical, elastic anisotropic and thermodynamic properties of tin under high temperature and high pressure. *Condensed Matter Physics*, 20(2):23601.

[Zheng et al., 2015] Zheng, B. C., Meng, D., Che, H. L., and Lei, M. K. (2015). On the pressure effect in energetic deposition of cu thin films by modulated pulsed power magnetron sputtering: A global plasma model and experiments. *Journal of Applied Physics*, 117(20):203302.

Appendix

A.1 All Stainless Steel Line Profilings

A.1.1 Stainless Steel Line Profiling at 0.25 N

This section provides the remainder of the line profile graphs not included in the main project. Note that the stainless steel wear track profiling was not possible at 1 and 10 cycles for 0.25 N, since the line profiler did not detect any wear track due to its small size.

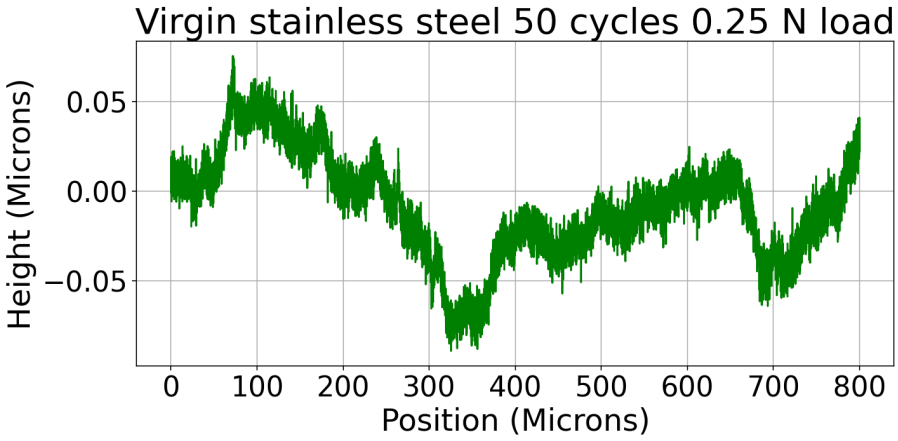

Figure A.1: This figure shows a virgin stainless steel sample. This figure shows the wear track recorded during line profiling measurement when equipped with a load of 0.25 N and during 50 cycles.

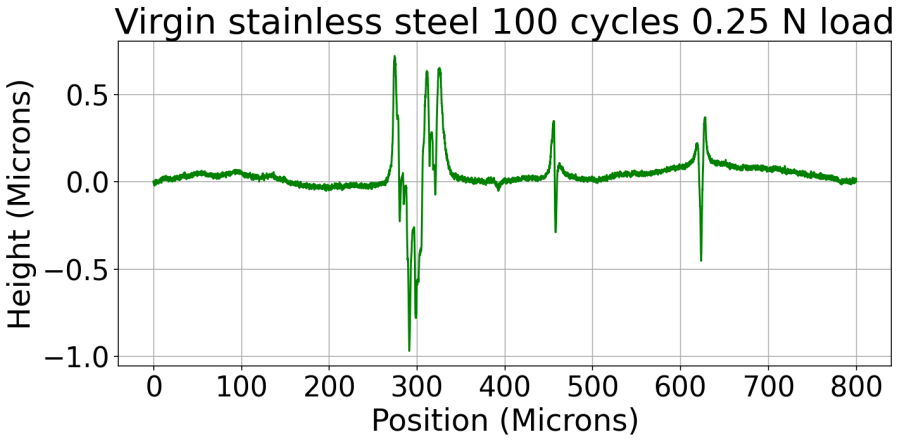

Figure A.2: This figure shows a virgin stainless steel sample. This figure shows the wear track recorded during line profiling measurement when equipped with a load of 0.25 N and during 100 cycles.

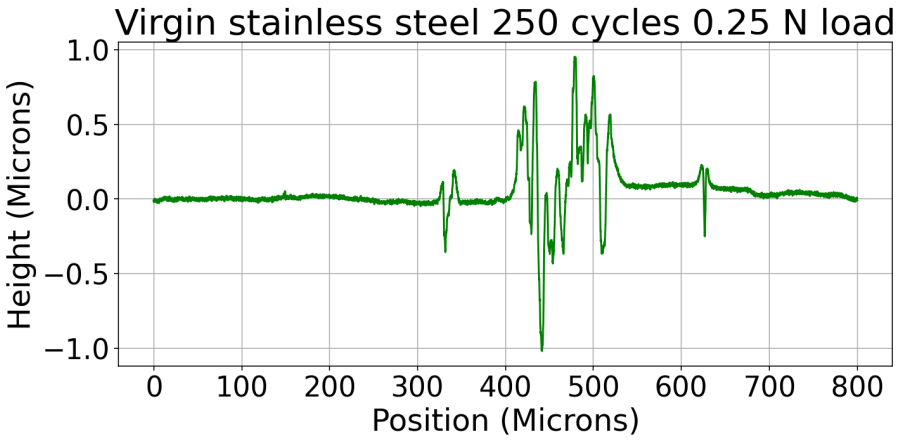

Figure A.3: This figure shows a virgin stainless steel sample. This figure shows the wear track recorded during line profiling measurement when equipped with a load of 0.25 N and during 250 cycles.

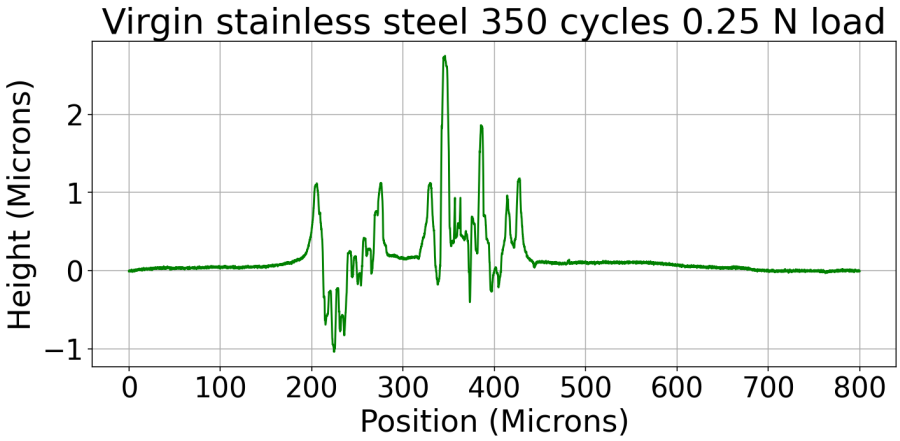

Figure A.4: This figure shows a virgin stainless steel sample. This figure shows the wear track recorded during line profiling measurement when equipped with a load of 0.25 N and during 350 cycles.

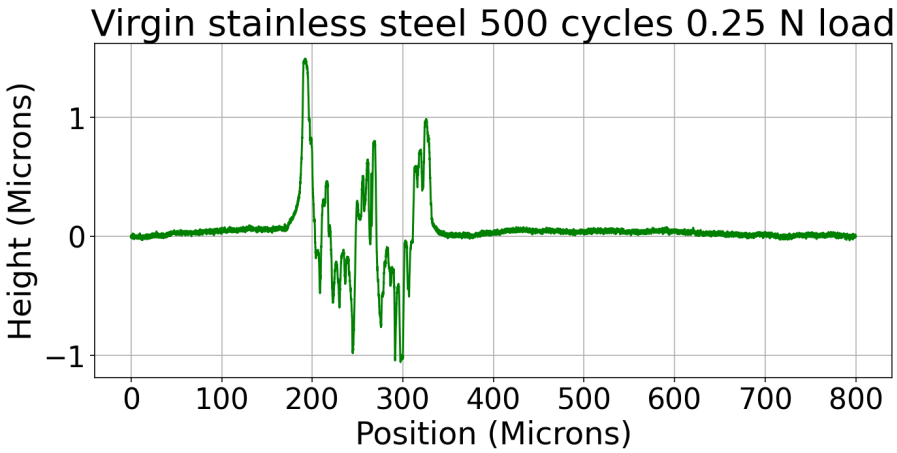

Figure A.5: This figure shows a virgin stainless steel sample. This figure shows the wear track recorded during line profiling measurement when equipped with a load of 0.25 N and during 500 cycles.

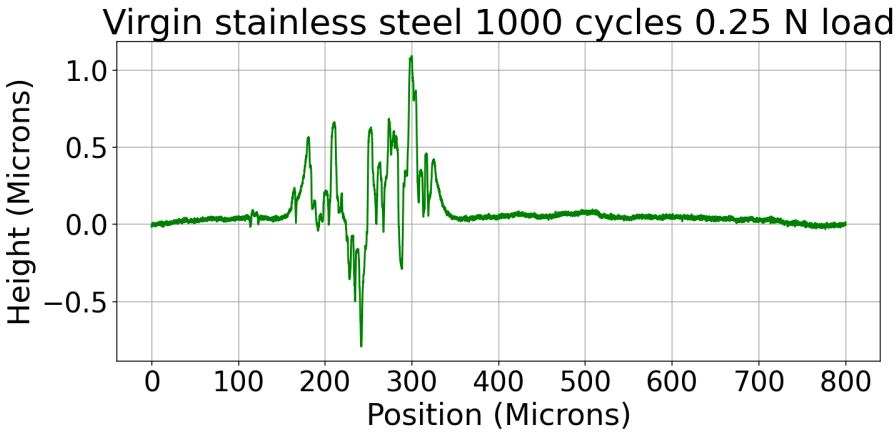

Figure A.6: This figure shows a virgin stainless steel sample. This figure shows the wear track recorded during line profiling measurement when equipped with a load of 0.25 N and during 1000 cycles.

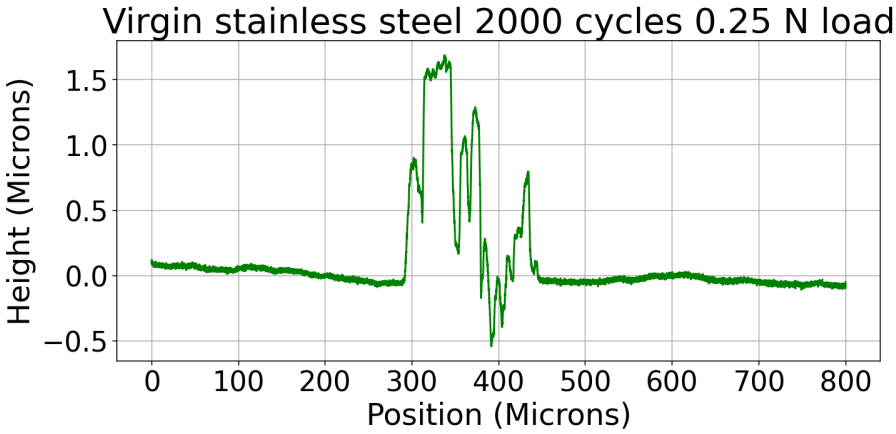

Figure A.7: This figure shows a virgin stainless steel sample. This figure shows the wear track recorded during line profiling measurement when equipped with a load of 0.25 N and during 2000 cycles.

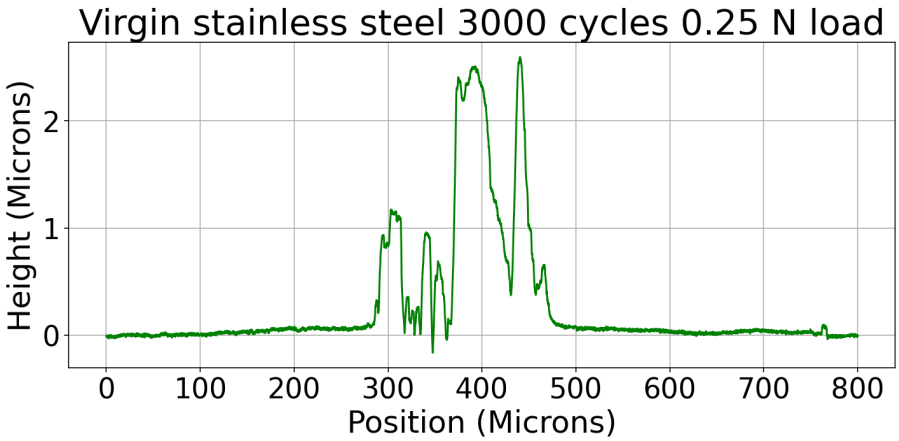

Figure A.8: This figure shows a virgin stainless steel sample. This figure shows the wear track recorded during line profiling measurement when equipped with a load of 0.25 N and during 3000 cycles.

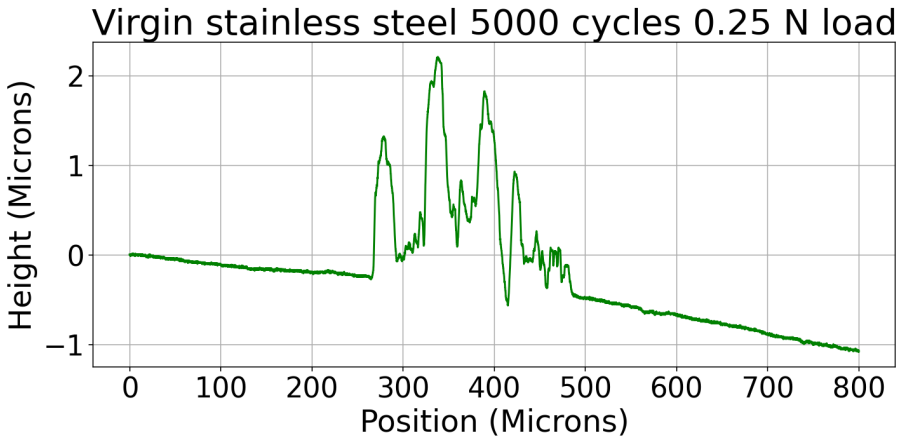

Figure A.9: This figure shows a virgin stainless steel sample. This figure shows the wear track recorded during line profiling measurement when equipped with a load of 0.25 N and during 5000 cycles.

A.1.2 Stainless Steel Line Profiling at 1 N

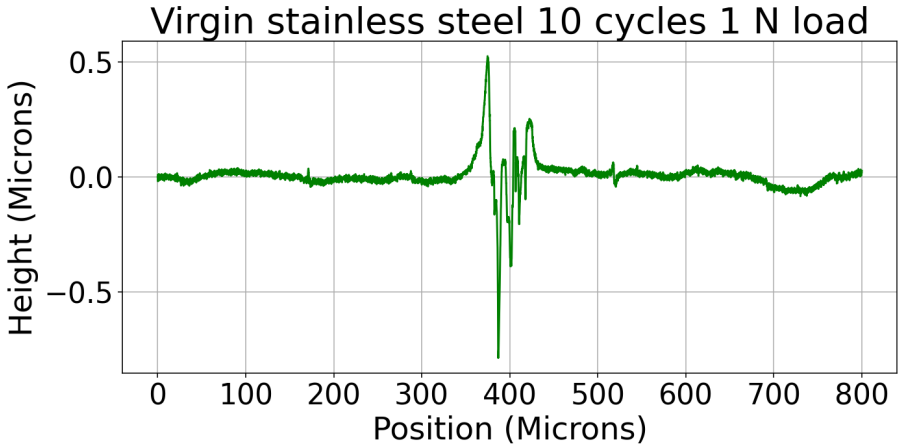

Figure A.10: This figure shows a virgin stainless steel sample. This figure shows the wear track recorded during line profiling measurement when equipped with a load of 1 N and during 10 cycles.

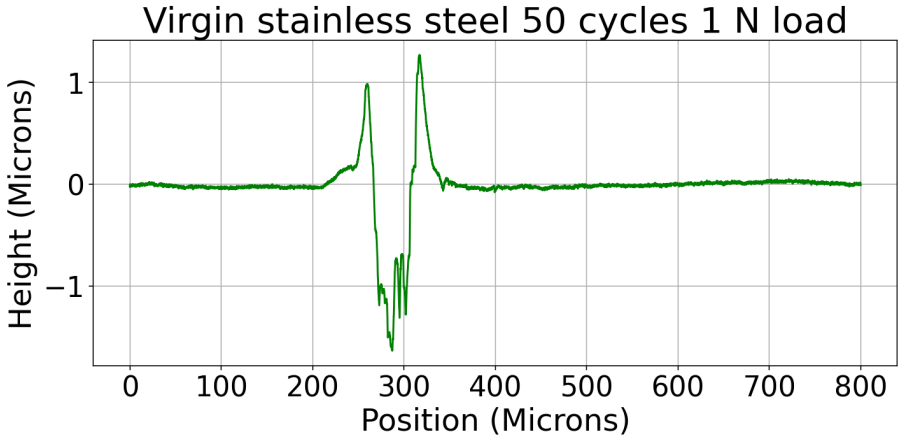

Figure A.11: This figure shows a virgin stainless steel sample. This figure shows the wear track recorded during line profiling measurement when equipped with a load of 1 N and during 50 cycles.

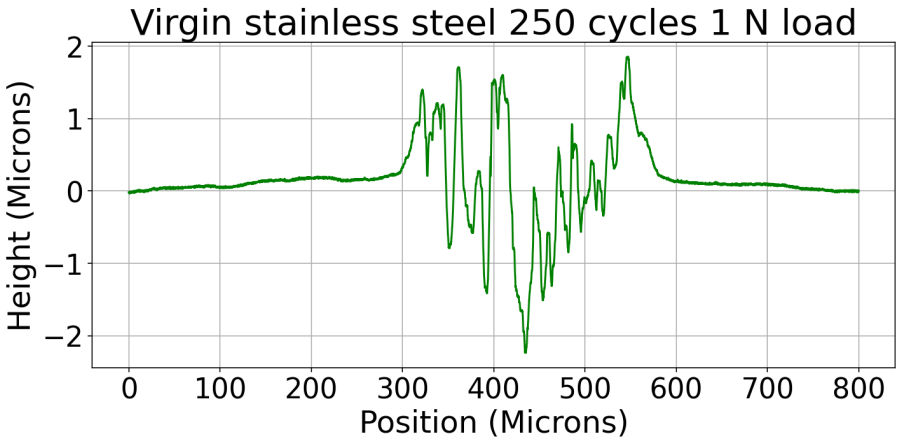

Figure A.12: This figure shows a virgin stainless steel sample. This figure shows the wear track recorded during line profiling measurement when equipped with a load of 1 N and during 250 cycles.

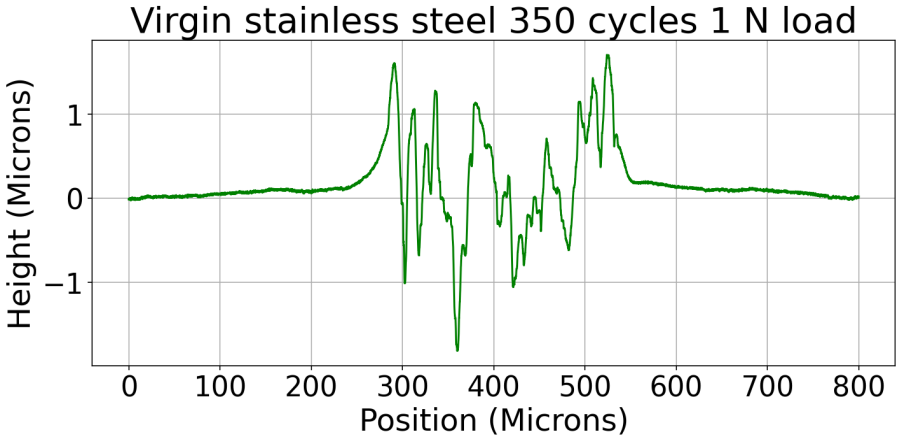

Figure A.13: This figure shows a virgin stainless steel sample. This figure shows the wear track recorded during line profiling measurement when equipped with a load of 1 N and during 350 cycles.

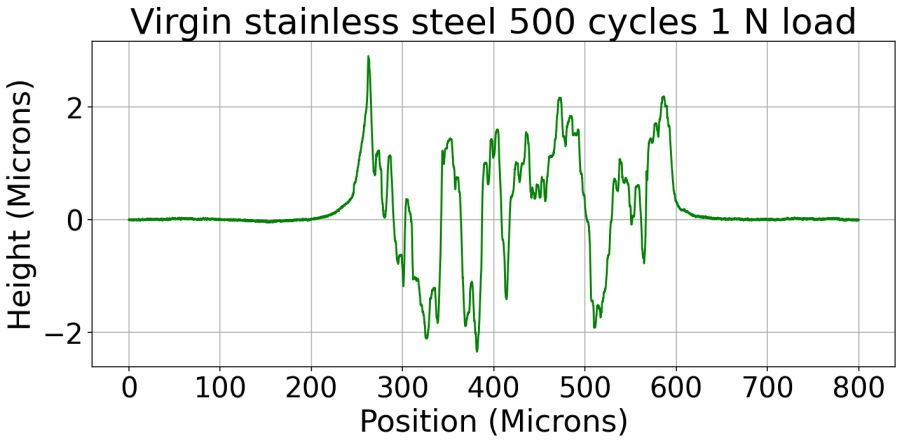

Figure A.14: This figure shows a virgin stainless steel sample. This figure shows the wear track recorded during line profiling measurement when equipped with a load of 1 N and during 500 cycles.

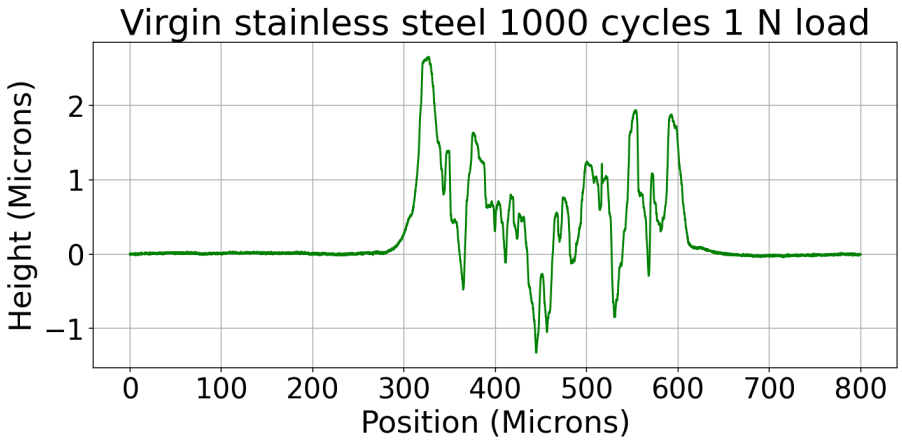

Figure A.15: This figure shows a virgin stainless steel sample.This figure shows the wear track recorded during line profiling measurement when equipped with a load of 1 N and during 1000 cycles.

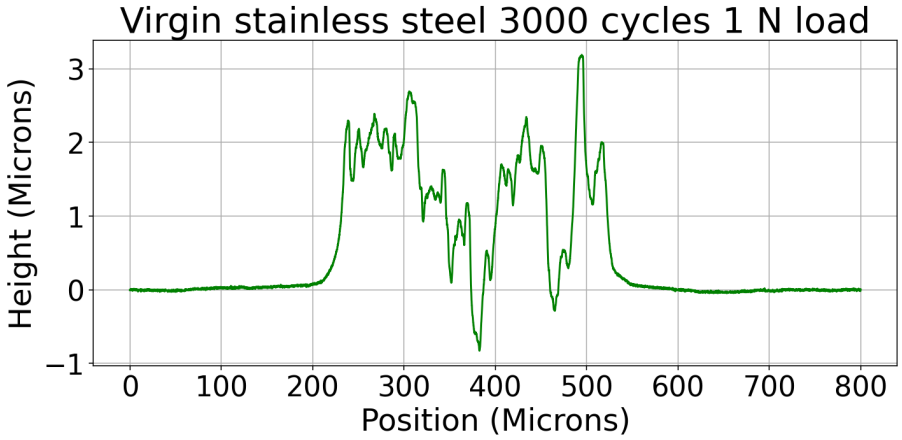

Figure A.16: This figure shows a virgin stainless steel sample. This figure shows the wear track recorded during line profiling measurement when equipped with a load of 1 N and during 3000 cycles.

A.1.3 Stainless Steel Line Profiling at 2 N

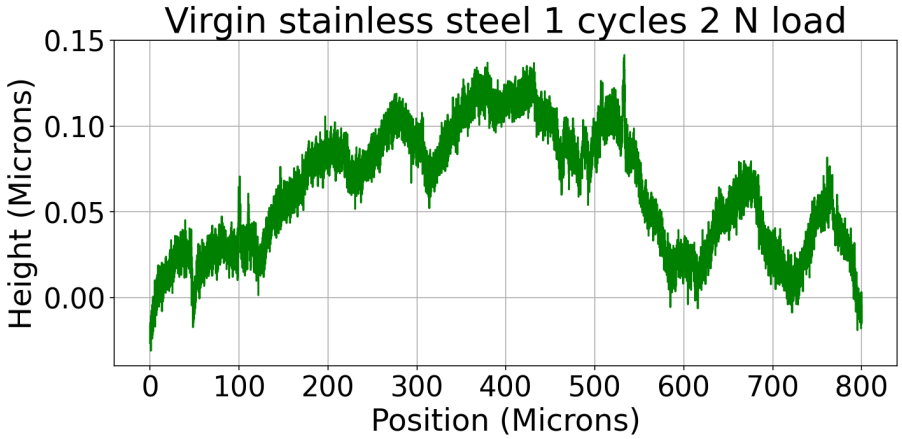

Figure A.17: This figure shows a virgin stainless steel sample. This figure shows the wear track recorded during line profiling measurement when equipped with a load of 2 N and during 1 cycle.

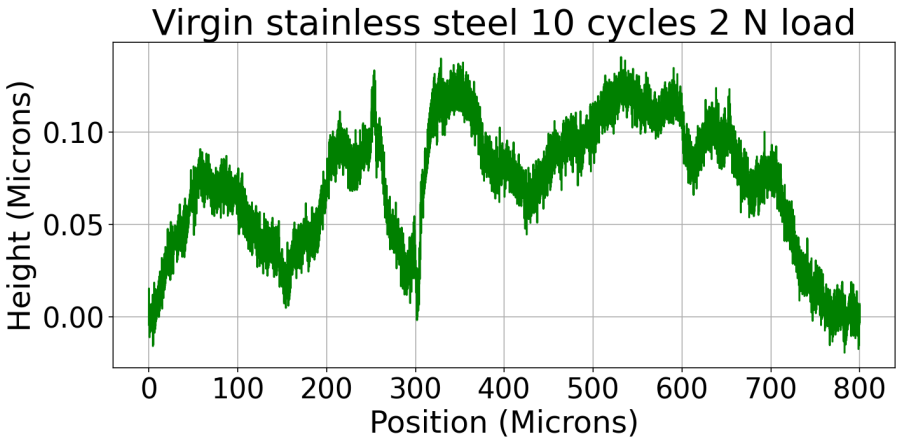

Figure A.18: This figure shows a virgin stainless steel sample. This figure shows the wear track recorded during line profiling measurement when equipped with a load of 2 N and during 10 cycles.

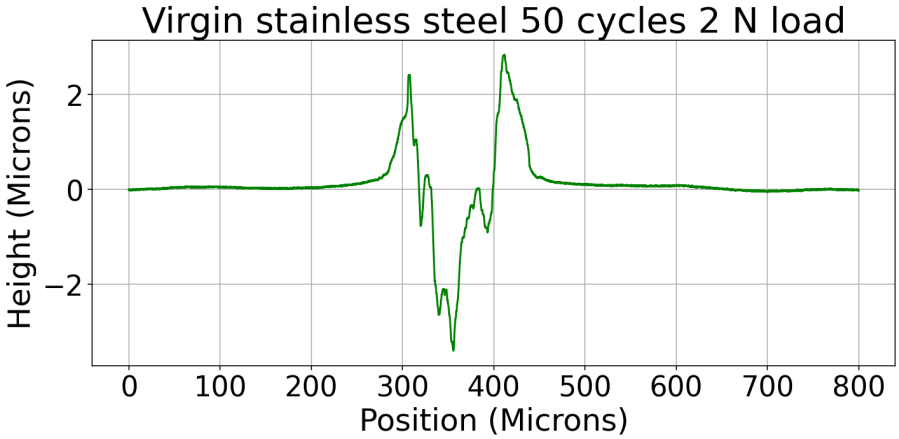

Figure A.19: This figure shows a virgin stainless steel sample. This figure shows the wear track recorded during line profiling measurement when equipped with a load of 2 N and during 50 cycles.

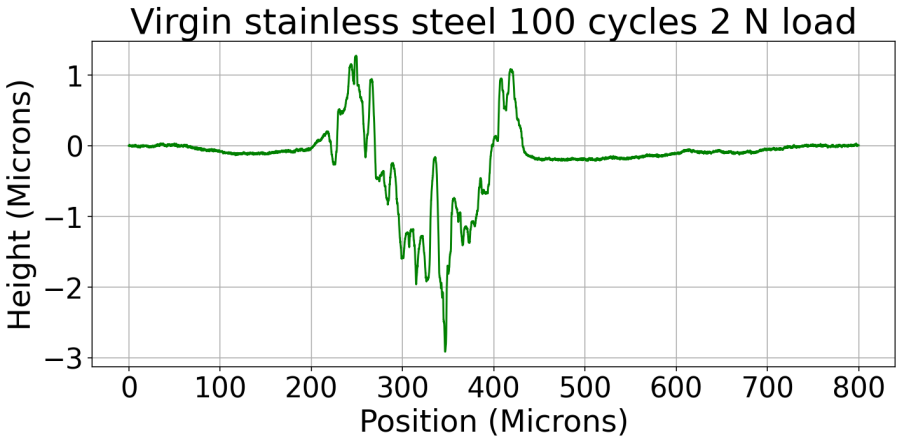

Figure A.20: This figure shows a virgin stainless steel sample. This figure shows the wear track recorded during line profiling measurement when equipped with a load of 2 N and during 100 cycles.

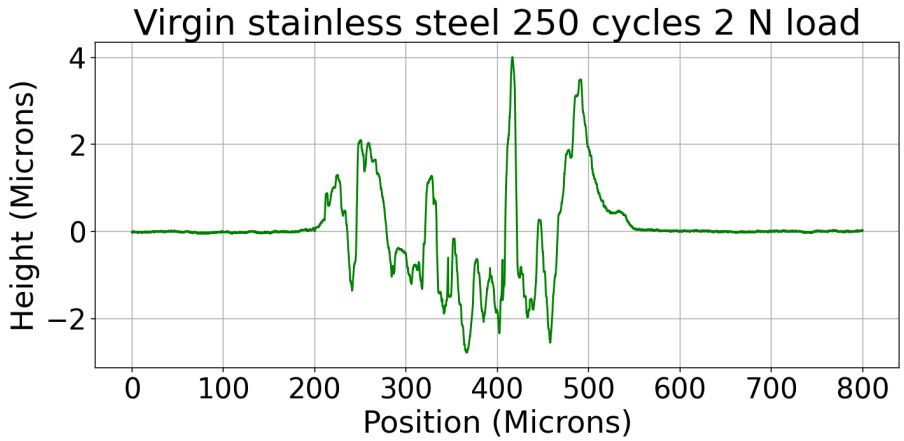

Figure A.21: This figure shows a virgin stainless steel sample. This figure shows the wear track recorded during line profiling measurement when equipped with a load of 2 N and during 250 cycles.

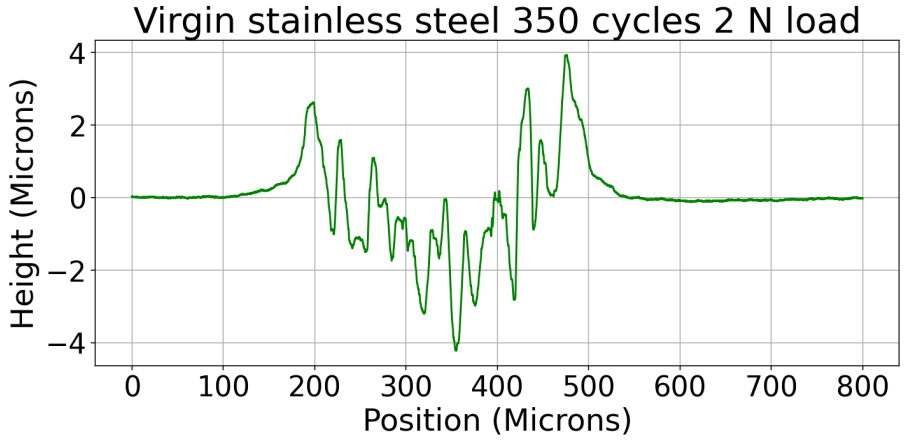

Figure A.22: This figure shows a virgin stainless steel sample. This figure shows the wear track recorded during line profiling measurement when equipped with a load of 2 N and during 350 cycles.

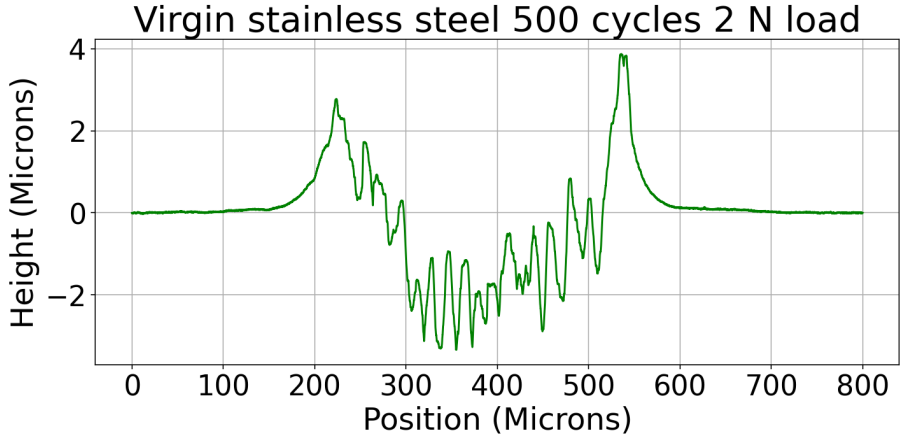

Figure A.23: This figure shows a virgin stainless steel sample. This figure shows the wear track recorded during line profiling measurement when equipped with a load of 2 N and during 500 cycles.

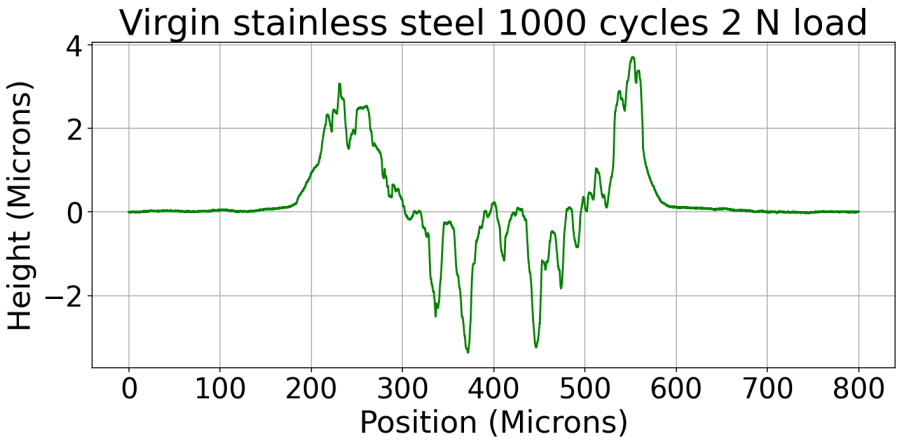

Figure A.24: This figure shows a virgin stainless steel sample. This figure shows the wear track recorded during line profiling measurement when equipped with a load of 2 N and during 1000 cycles.

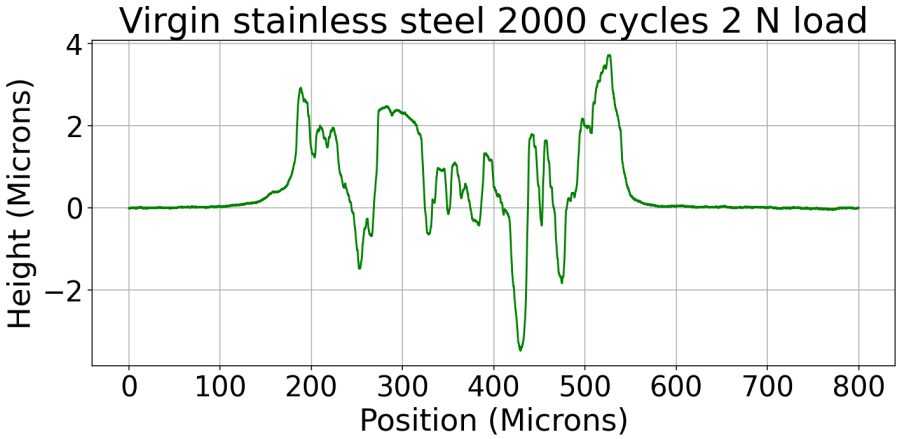

Figure A.25: This figure shows a virgin stainless steel sample. This figure shows the wear track recorded during line profiling measurement when equipped with a load of 2 N and during 2000 cycles.

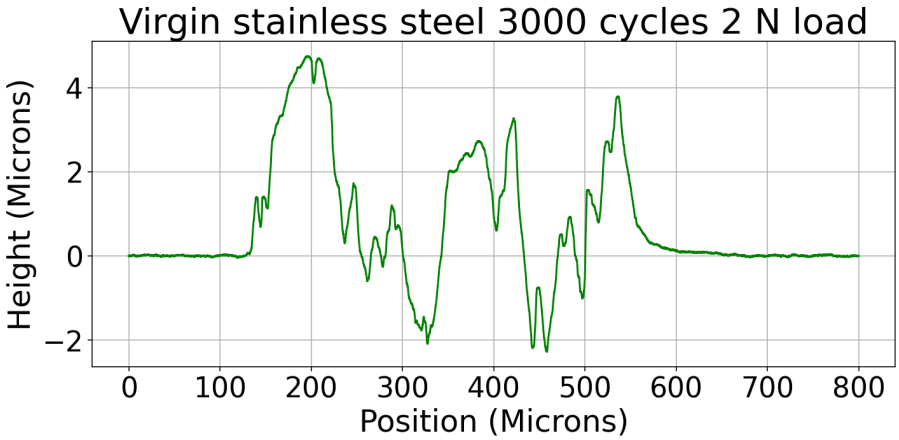

Figure A.26: This figure shows a virgin stainless steel sample. This figure shows the wear track recorded during line profiling measurement when equipped with a load of 2 N and during 3000 cycles.

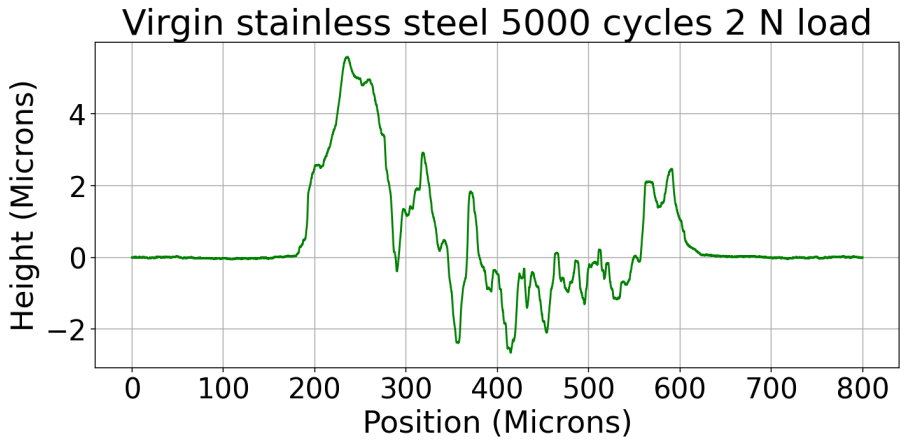

Figure A.27: This figure shows a virgin stainless steel sample. This figure shows the wear track recorded during line profiling measurement when equipped with a load of 2 N and during 5000 cycles.

A.1.4 Stainless Steel Line Profiling at 5 N

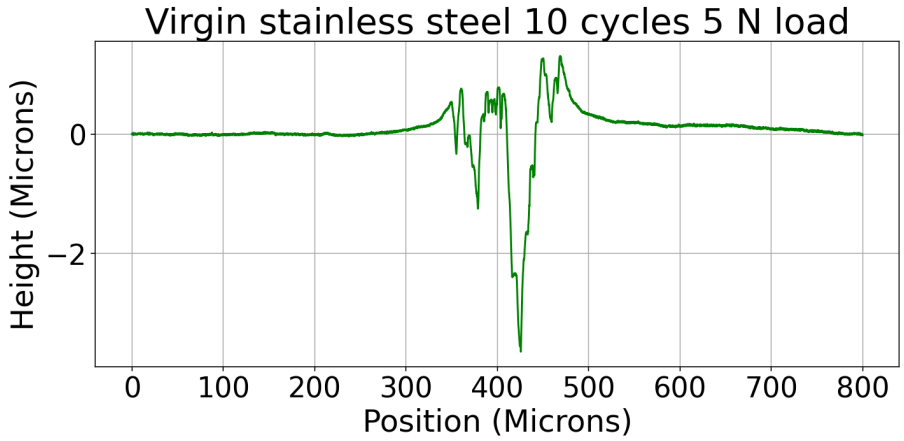

Figure A.28: This figure shows a virgin stainless steel sample. This figure shows the wear track recorded during line profiling measurement when equipped with a load of 5 N and during 10 cycles.

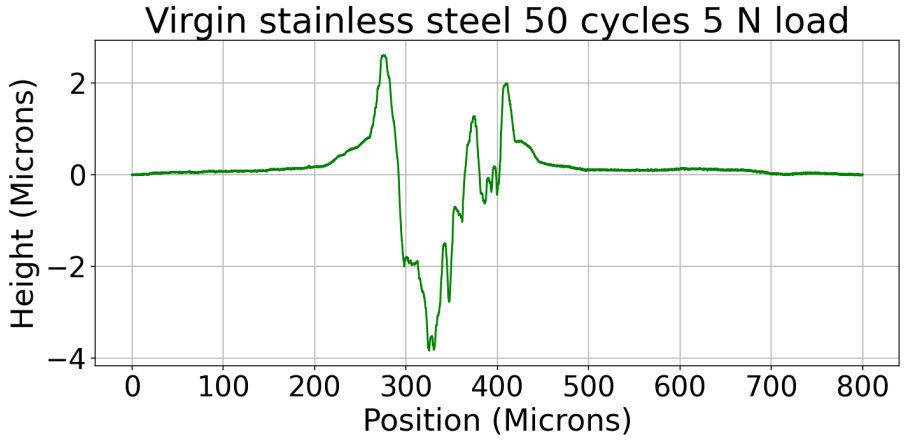

Figure A.29: This figure shows a virgin stainless steel sample. This figure shows the wear track recorded during line profiling measurement when equipped with a load of 5 N and during 50 cycles.

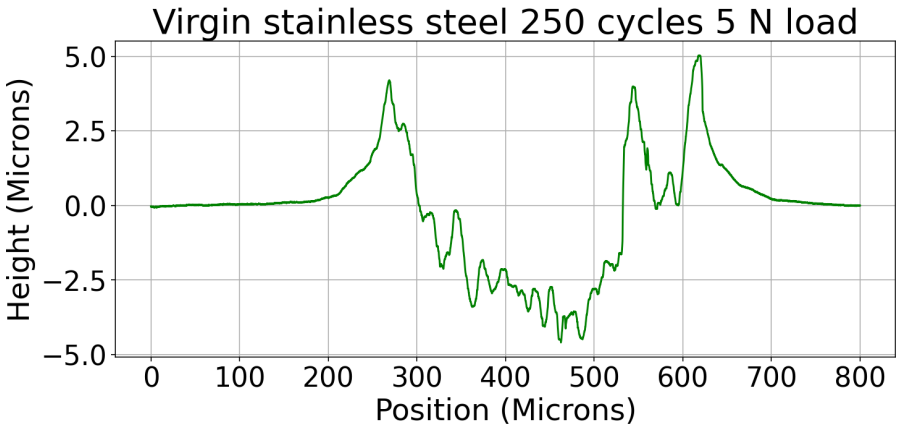

Figure A.30: This figure shows a virgin stainless steel sample. This figure shows the wear track recorded during line profiling measurement when equipped with a load of 5 N and during 250 cycles.

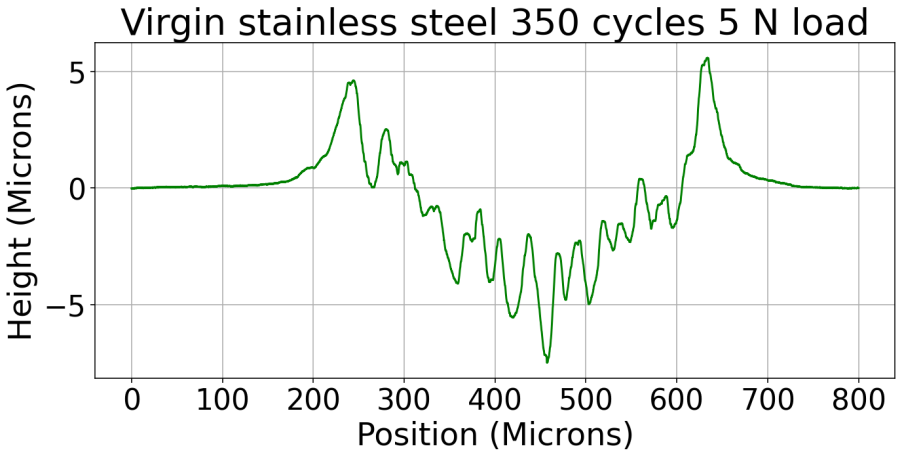

Figure A.31: This figure shows a virgin stainless steel sample. This figure shows the wear track recorded during line profiling measurement when equipped with a load of 5 N and during 350 cycles.

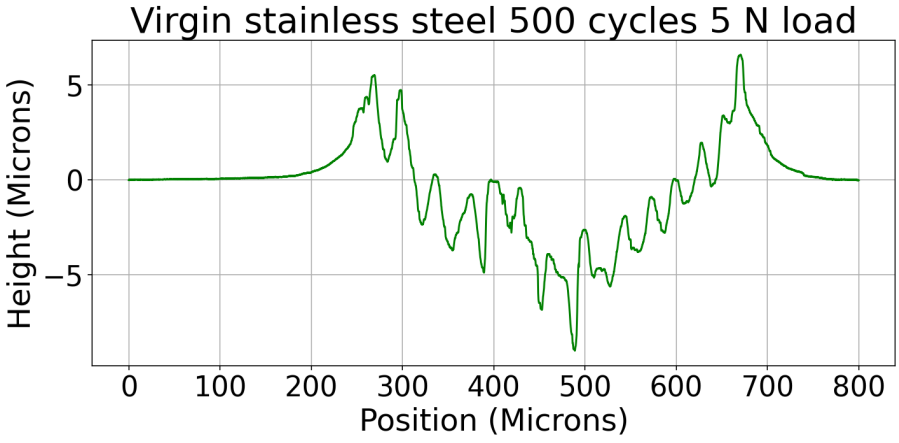

Figure A.32: This figure shows a virgin stainless steel sample. This figure shows the wear track recorded during line profiling measurement when equipped with a load of 5 N and during 500 cycles.

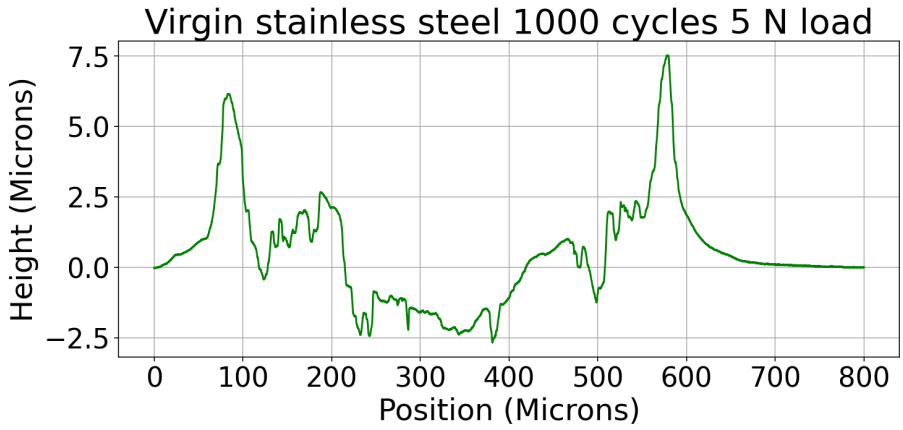

Figure A.33: This figure shows a virgin stainless steel sample. This figure shows the wear track recorded during line profiling measurement when equipped with a load of 5 N and during 1000 cycles.

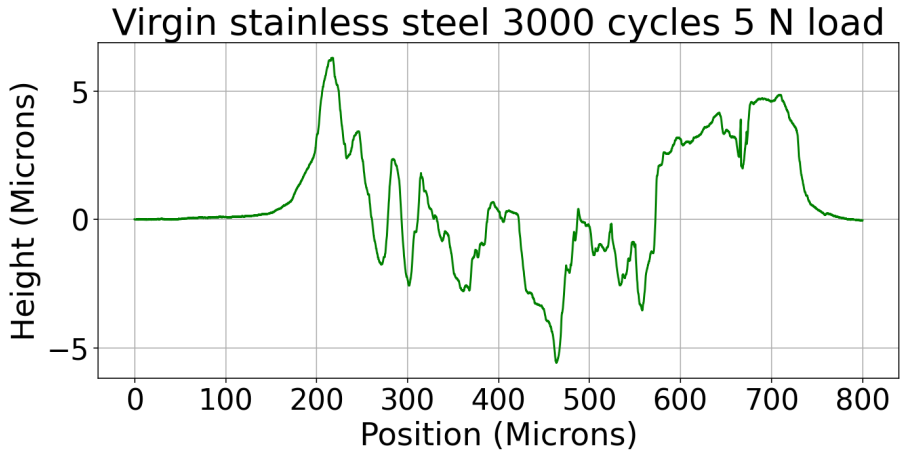

Figure A.34: This figure shows a virgin stainless steel sample. This figure shows the wear track recorded during line profiling measurement when equipped with a load of 5 N and during 3000 cycles.

A.1.5 Stainless Steel Line Profiling at 10 N

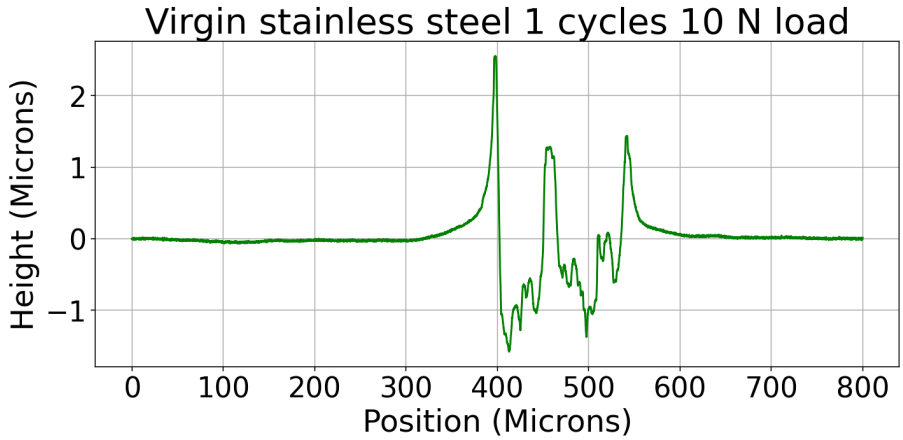

Figure A.35: This figure shows a virgin stainless steel sample. This figure shows the wear track recorded during line profiling measurement when equipped with a load of 10 N and during 1 cycle.

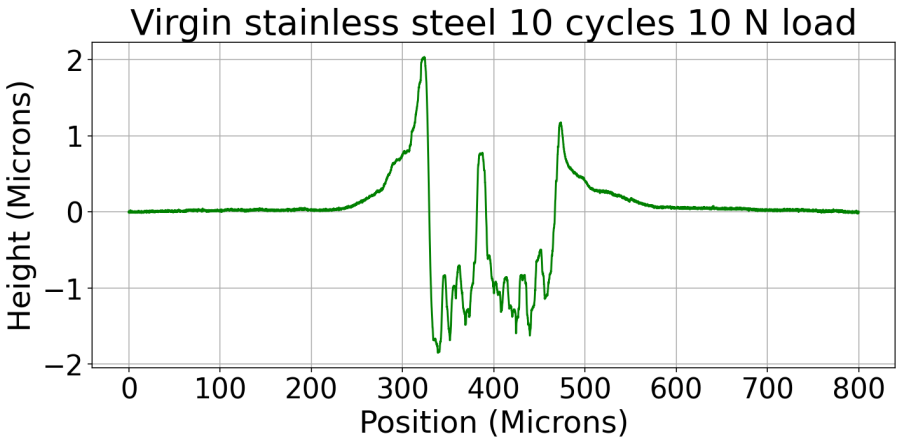

Figure A.36: This figure shows a virgin stainless steel sample. This figure shows the wear track recorded during line profiling measurement when equipped with a load of 10 N and during 10 cycles.

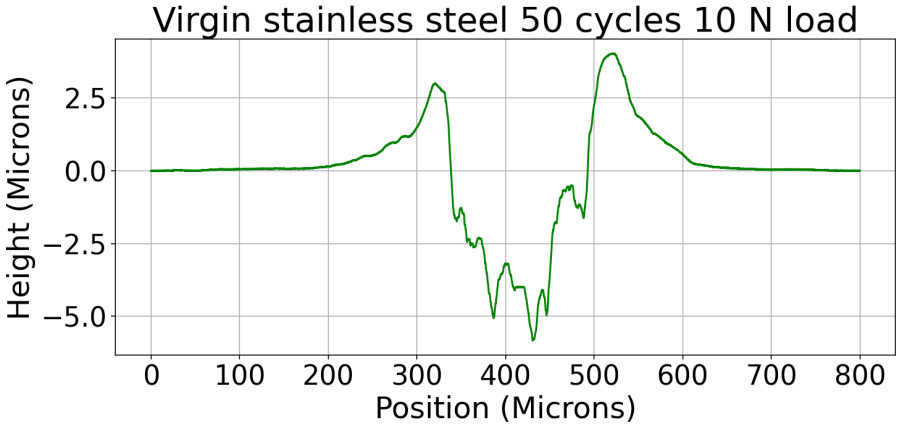

Figure A.37: This figure shows a virgin stainless steel sample. This figure shows the wear track recorded during line profiling measurement when equipped with a load of 10 N and during 50 cycles.

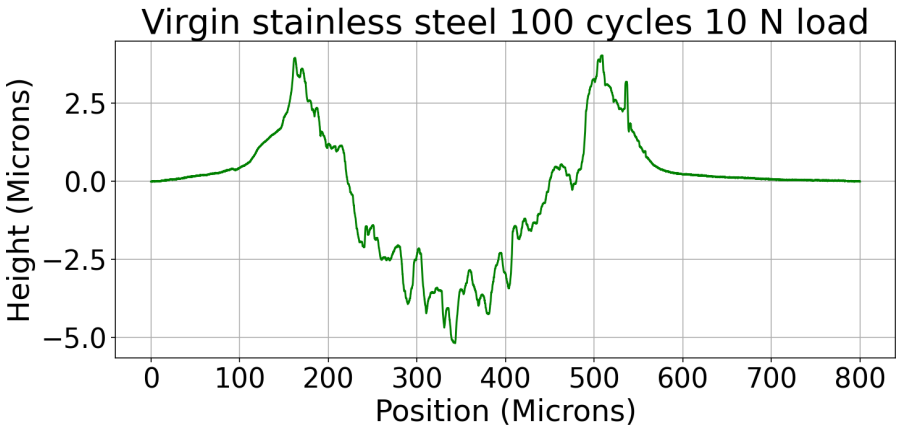

Figure A.38: This figure shows a virgin stainless steel sample. This figure shows the wear track recorded during line profiling measurement when equipped with a load of 10 N and during 100 cycles.

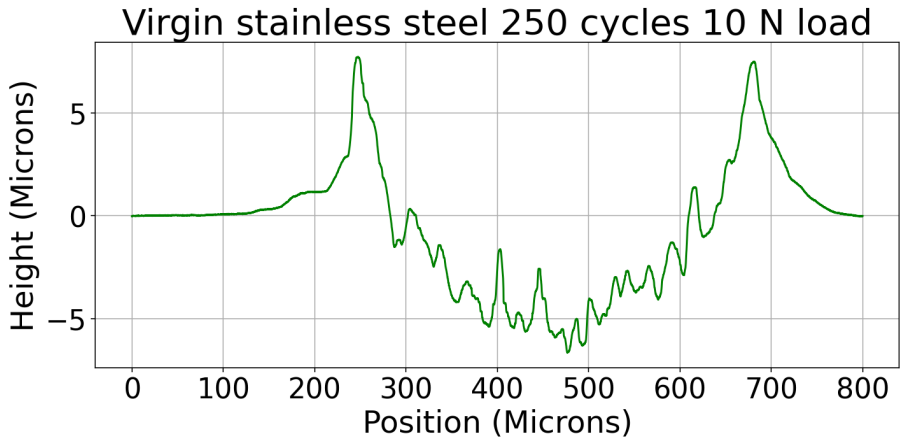

Figure A.39: This figure shows a virgin stainless steel sample. This figure shows the wear track recorded during line profiling measurement when equipped with a load of 10 N and during 250 cycles.

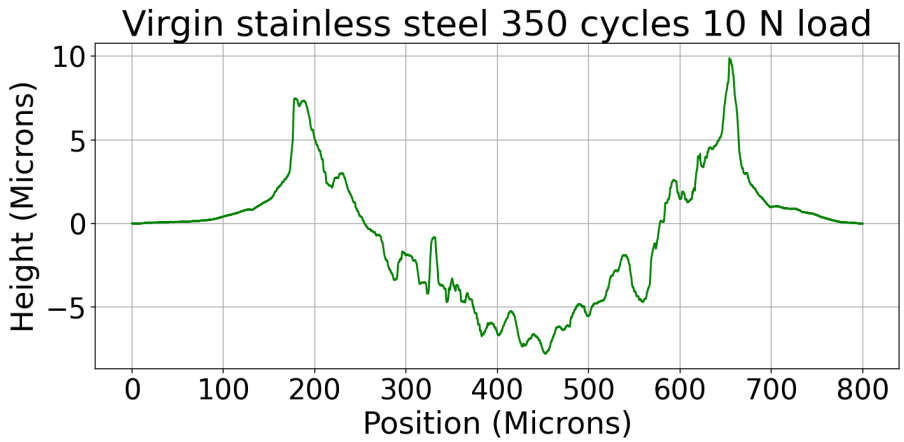

Figure A.40: This figure shows a virgin stainless steel sample. This figure shows the wear track recorded during line profiling measurement when equipped with a load of 10 N and during 350 cycles.

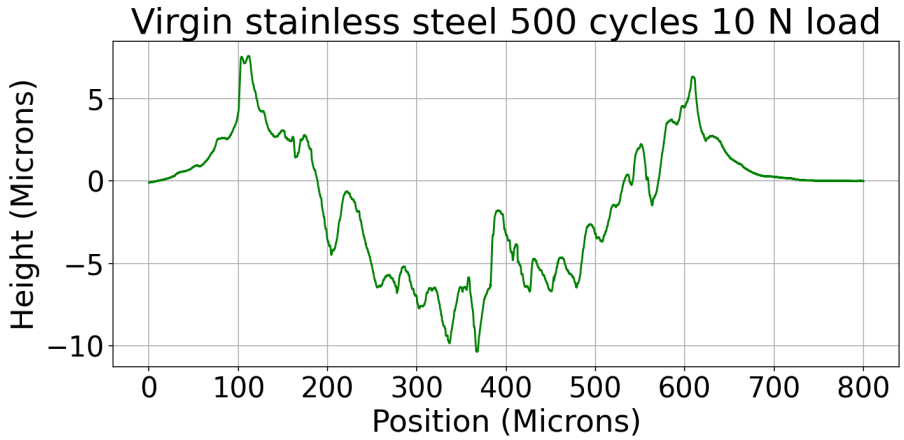

Figure A.41: This figure shows a virgin stainless steel sample. This figure shows the wear track recorded during line profiling measurement when equipped with a load of 10 N and during 500 cycles.

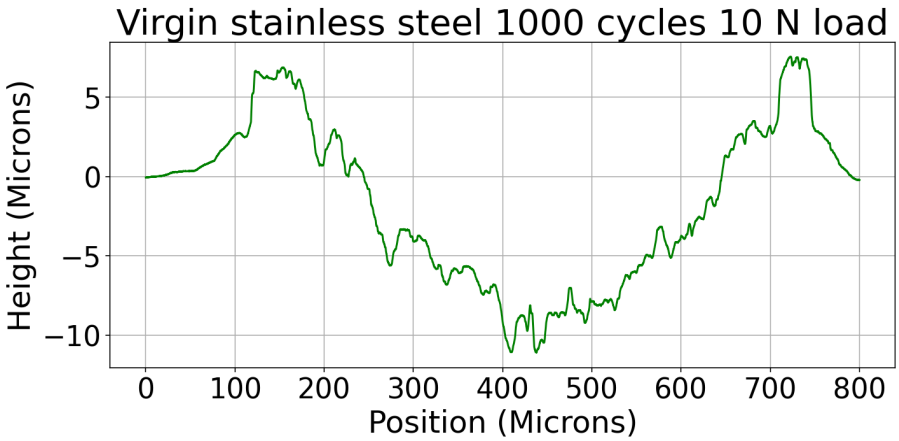

Figure A.42: This figure shows a virgin stainless steel sample. This figure shows the wear track recorded during line profiling measurement when equipped with a load of 10 N and during 1000 cycles.

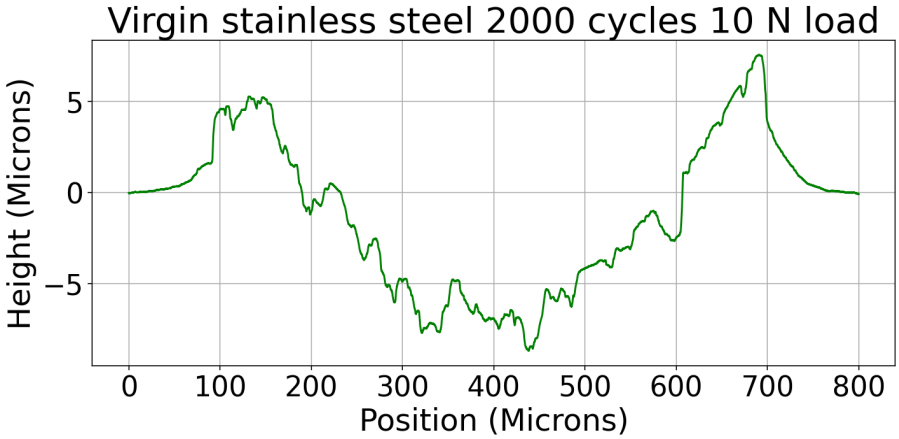

Figure A.43: This figure shows a virgin stainless steel sample. TThis figure shows the wear track recorded during line profiling measurement when equipped with a load of 10 N and during 2000 cycles.

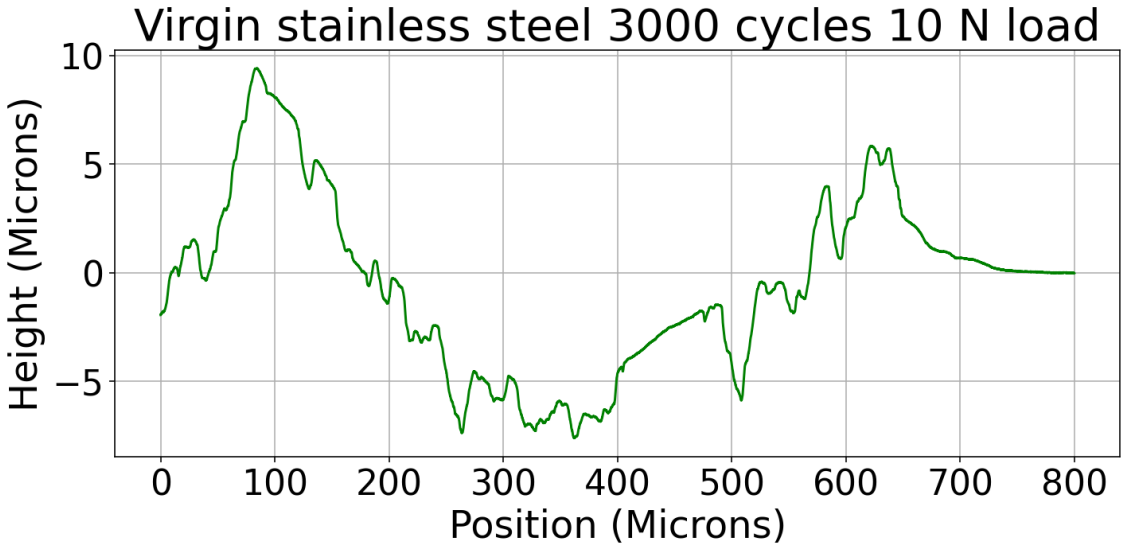

Figure A.44: This figure shows a virgin stainless steel sample. This figure shows the wear track recorded during line profiling measurement when equipped with a load of 10 N and during 3000 cycles.

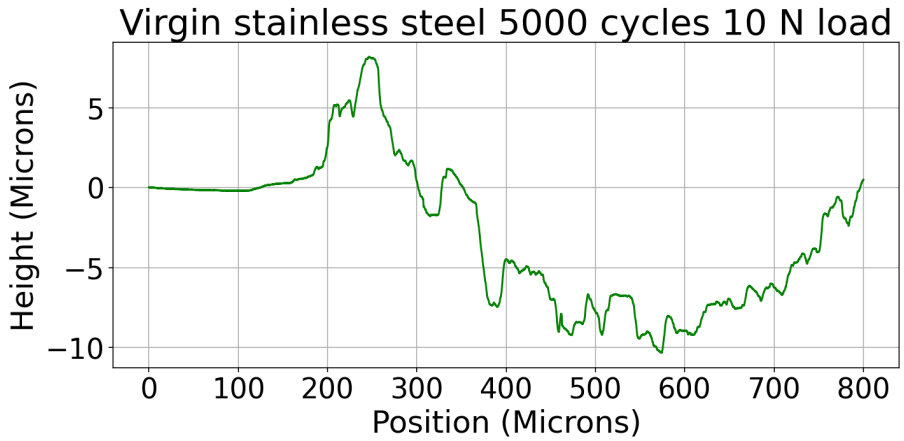

Figure A.45: This figure shows a virgin stainless steel sample. This figure shows the wear track recorded during line profiling measurement when equipped with a load of 10 N and during 5000 cycles.

A.2 All 1500 nm TiN Coated Line Profilings

A.2.1 1500 nm TiN Coated Line Profiling at 0.25 N

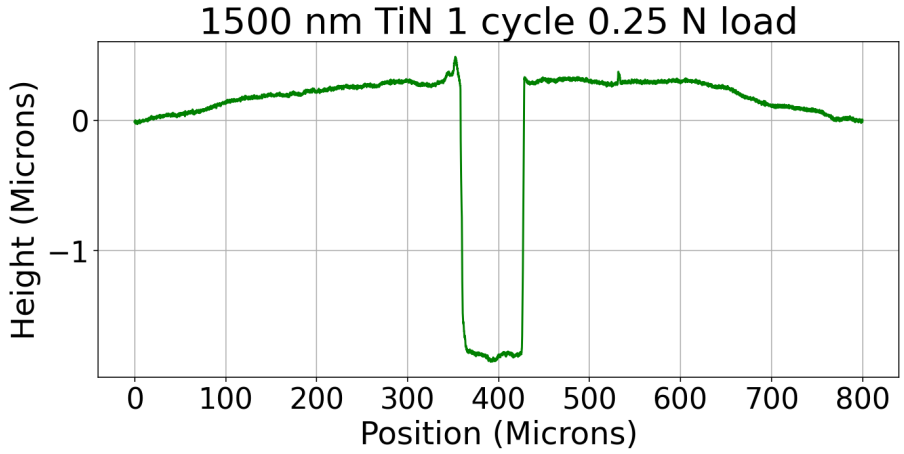

Figure A.46: This figure shows a 1500 nm TiN coated stainless steel sample. This figure shows the wear track recorded during line profiling measurement when equipped with a load of 0.25 N and during 1 cycle.

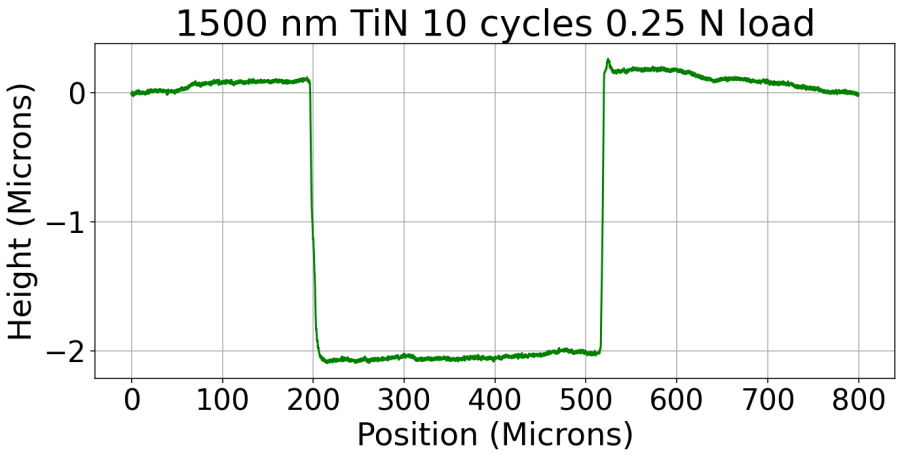

Figure A.47: This figure shows a 1500 nm TiN coated stainless steel sample. This figure shows the wear track recorded during line profiling measurement when equipped with a load of 0.25 N and during 10 cycles.

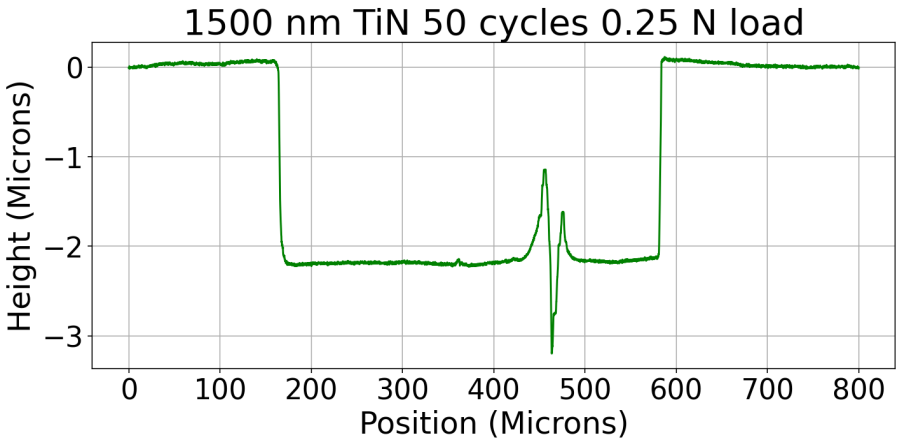

Figure A.48: This figure shows a 1500 nm TiN coated stainless steel sample. This figure shows the wear track recorded during line profiling measurement when equipped with a load of 0.25 N and during 50 cycles.

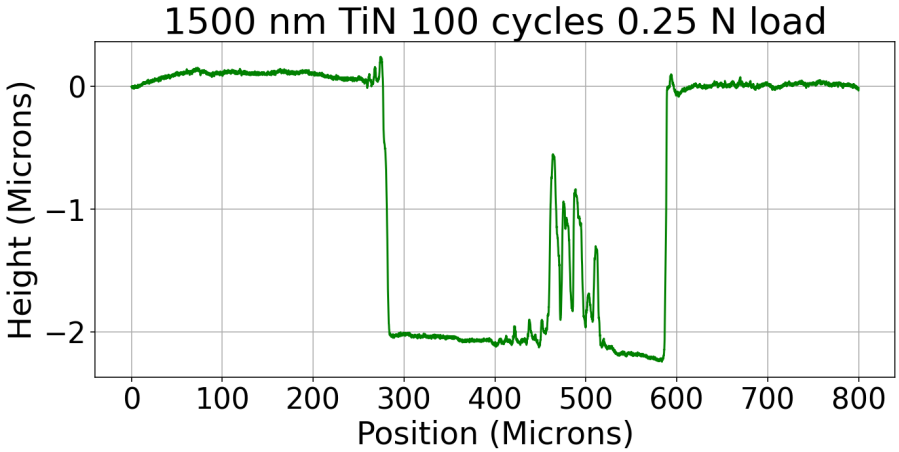

Figure A.49: This figure shows a 1500 nm TiN coated stainless steel sample. TThis figure shows the wear track recorded during line profiling measurement when equipped with a load of 0.25 N and during 100 cycles.

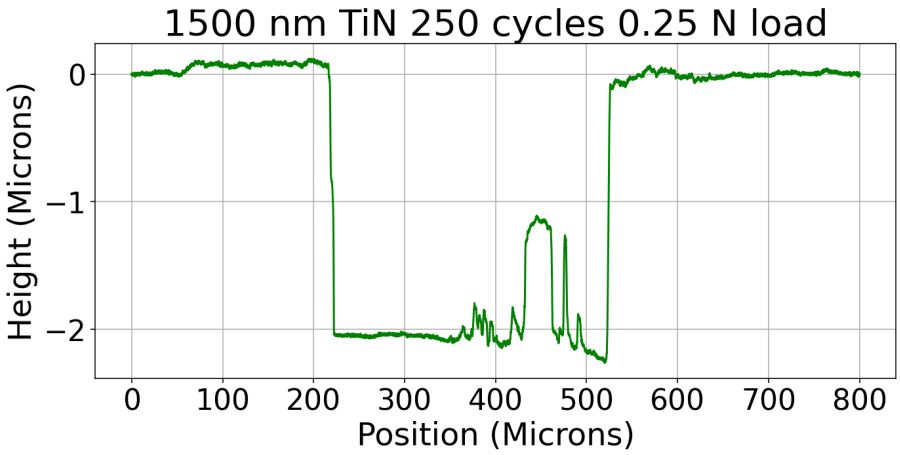

Figure A.50: This figure shows a 1500 nm TiN coated stainless steel sample. This figure shows the wear track recorded during line profiling measurement when equipped with a load of 0.25 N and during 250 cycles.

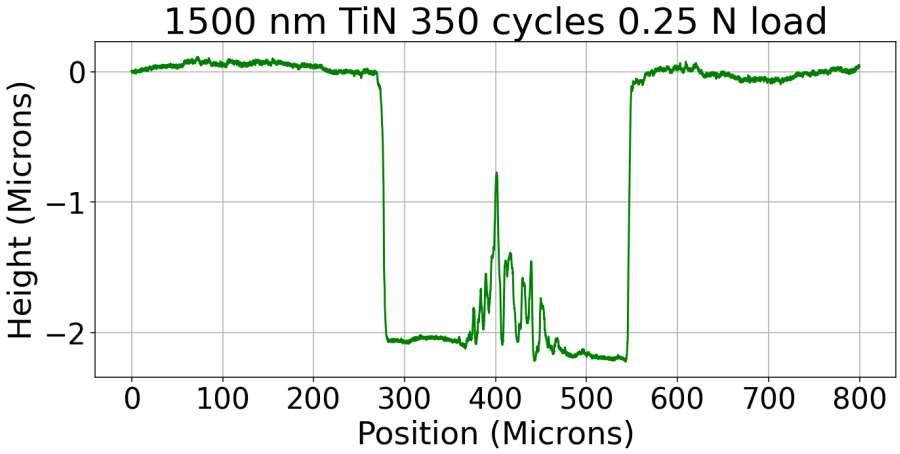

Figure A.51: This figure shows a 1500 nm TiN coated stainless steel sample. This figure shows the wear track recorded during line profiling measurement when equipped with a load of 0.25 N and during 350 cycles.

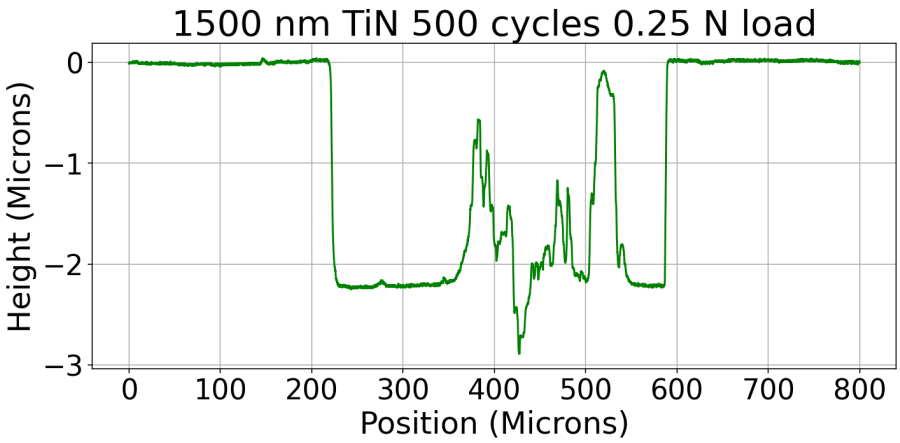

Figure A.52: This figure shows a 1500 nm TiN coated stainless steel sample. This figure shows the wear track recorded during line profiling measurement when equipped with a load of 0.25 N and during 500 cycles.

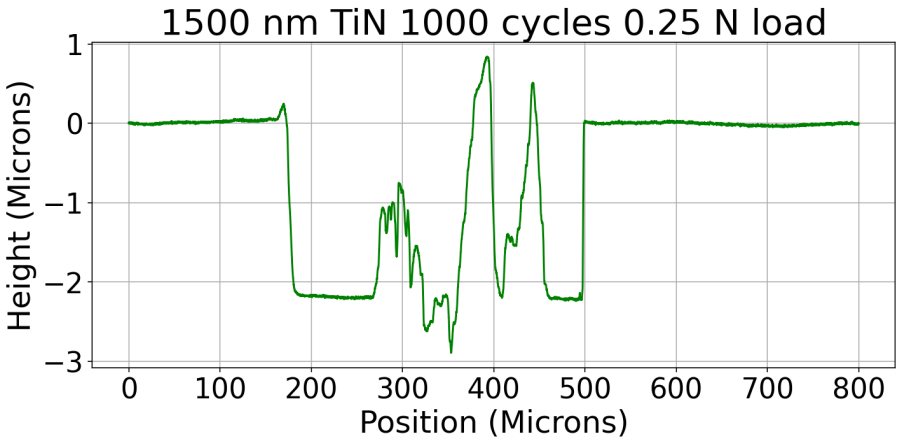

Figure A.53: This figure shows a 1500 nm TiN coated stainless steel sample. This figure shows the wear track recorded during line profiling measurement when equipped with a load of 0.25 N and during 1000 cycles.

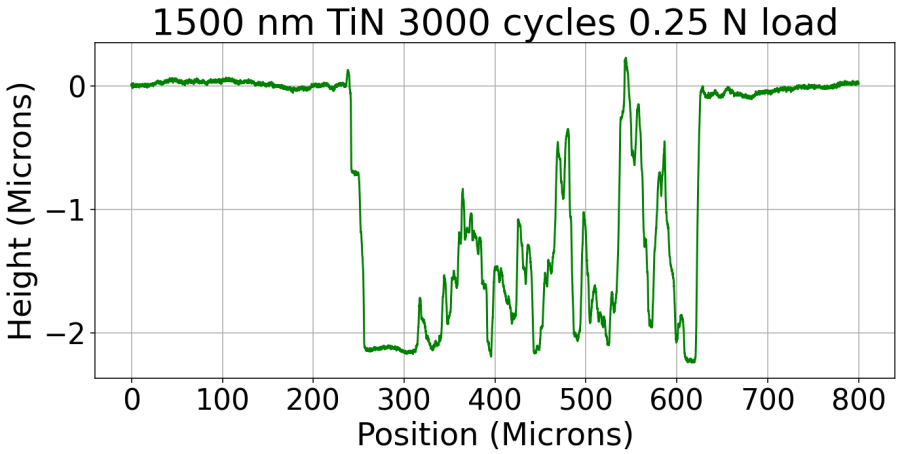

Figure A.54: This figure shows a 1500 nm TiN coated stainless steel sample. This figure shows the wear track recorded during line profiling measurement when equipped with a load of 0.25 N and during 3000 cycles.

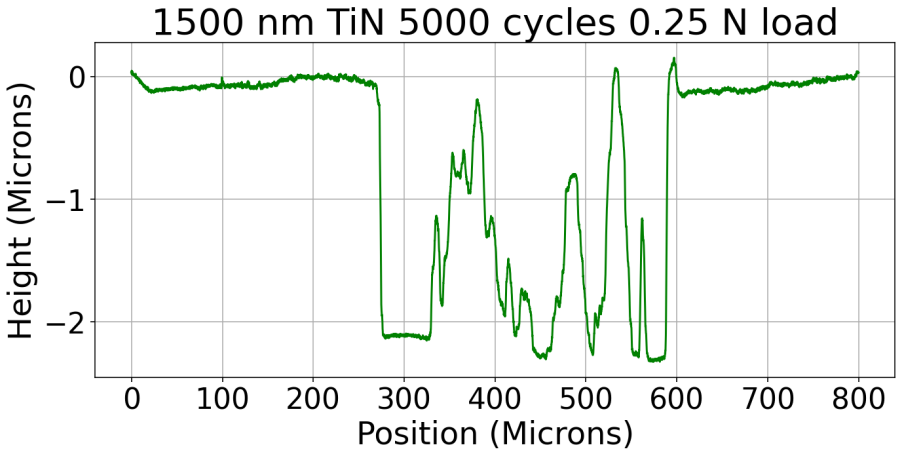

Figure A.55: This figure shows a 1500 nm TiN coated stainless steel sample. This figure shows the wear track recorded during line profiling measurement when equipped with a load of 0.25 N and during 5000 cycles.

A.2.2 1500 nm TiN Coated Line Profiling at 1 N

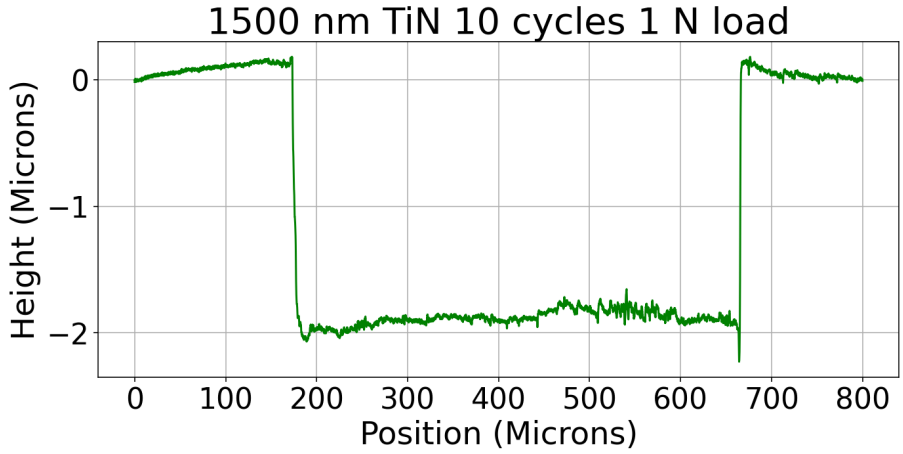

Figure A.56: This figure shows a 1500 nm TiN coated stainless steel sample. This figure shows the wear track recorded during line profiling measurement when equipped with a load of 1 N and during 10 cycles.

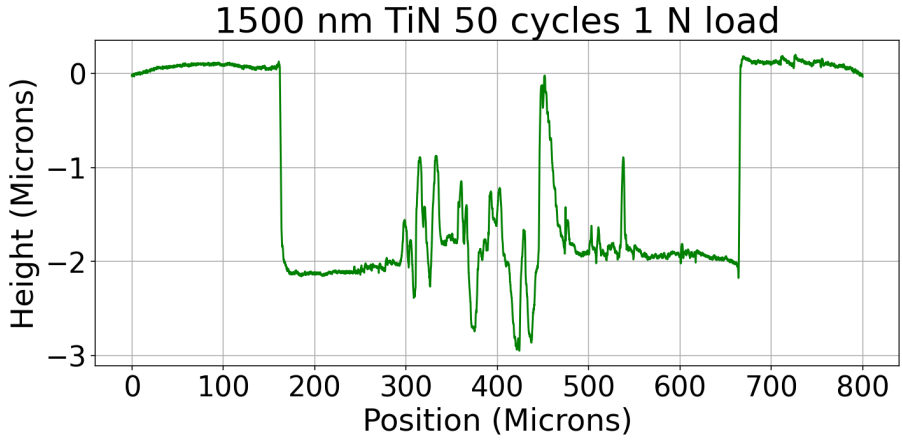

Figure A.57: This figure shows a 1500 nm TiN coated stainless steel sample. This figure shows the wear track recorded during line profiling measurement when equipped with a load of 1 N and during 50 cycles.

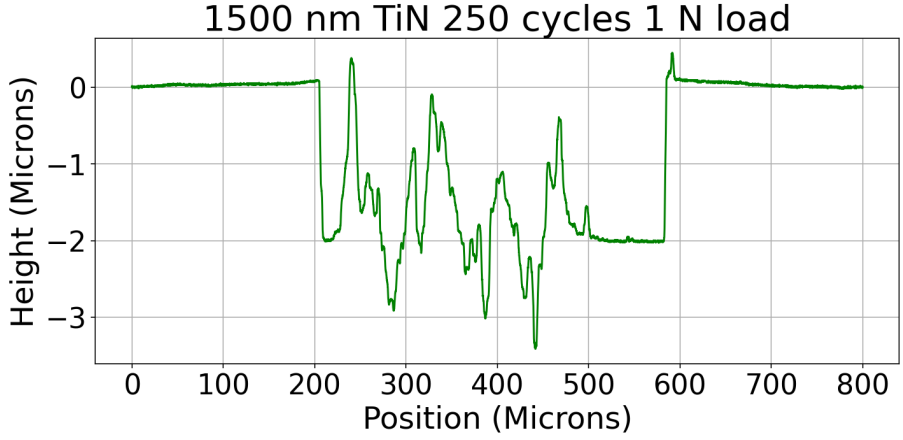

Figure A.58: This figure shows a 1500 nm TiN coated stainless steel sample. This figure shows the wear track recorded during line profiling measurement when equipped with a load of 1 N and during 250 cycles.

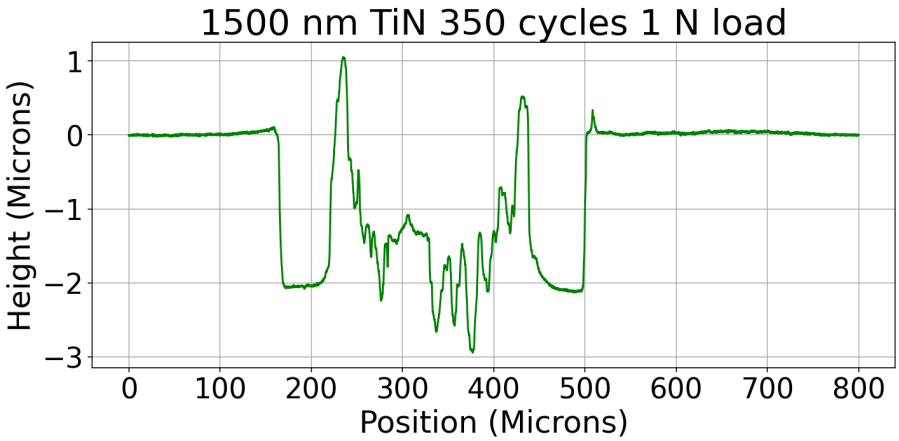

Figure A.59: This figure shows a 1500 nm TiN coated stainless steel sample. This figure shows the wear track recorded during line profiling measurement when equipped with a load of 1 N and during 350 cycles.

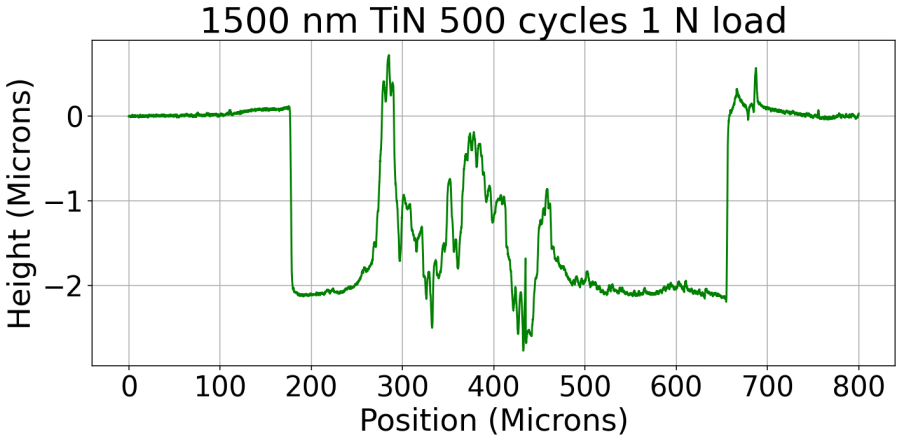

Figure A.60: This figure shows a 1500 nm TiN coated stainless steel sample. This figure shows the wear track recorded during line profiling measurement when equipped with a load of 1 N and during 500 cycles.

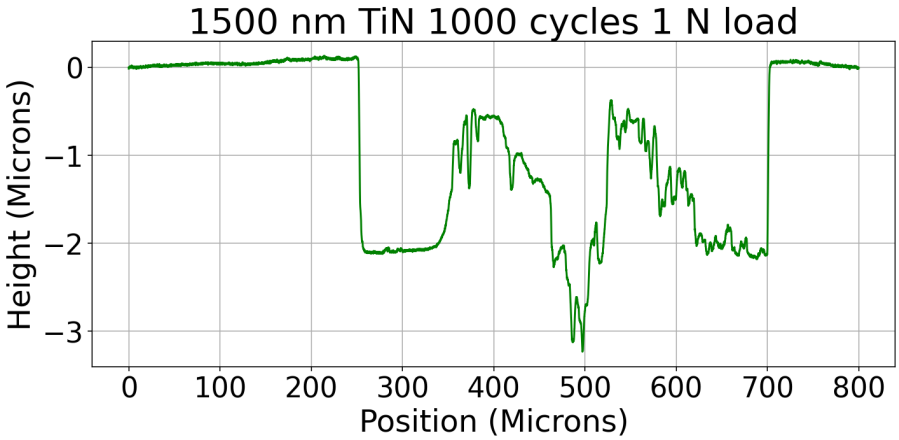

Figure A.61: This figure shows a 1500 nm TiN coated stainless steel sample. This figure shows the wear track recorded during line profiling measurement when equipped with a load of 1 N and during 1000 cycles.

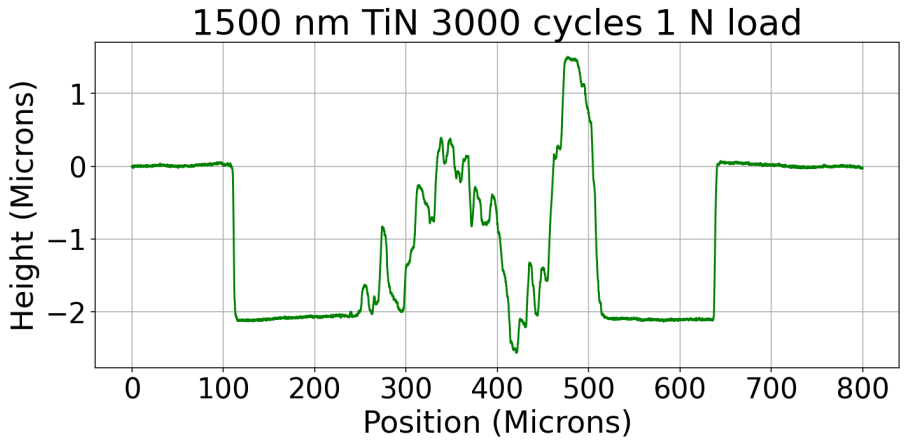

Figure A.62: This figure shows a 1500 nm TiN coated stainless steel sample. This figure shows the wear track recorded during line profiling measurement when equipped with a load of 1 N and during 3000 cycles.

A.2.3 1500 nm TiN Coated Line Profiling at 5 N

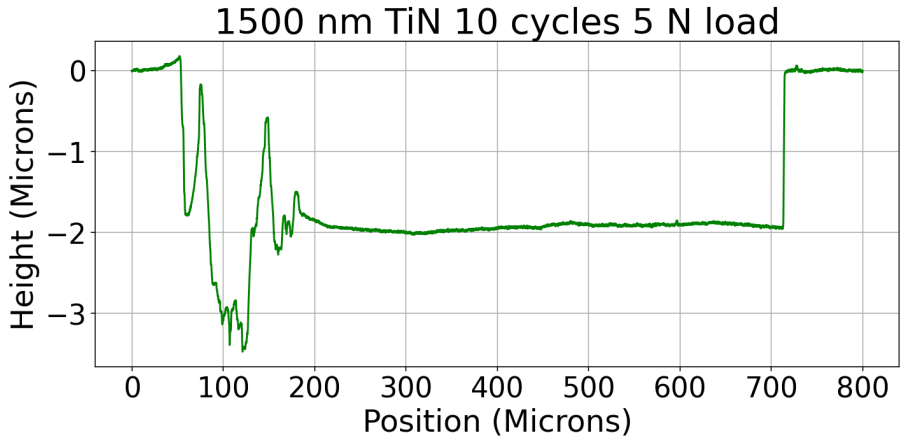

Figure A.63: This figure shows a 1500 nm TiN coated stainless steel sample. This figure shows the wear track recorded during line profiling measurement when equipped with a load of 5 N and during 10 cycles.

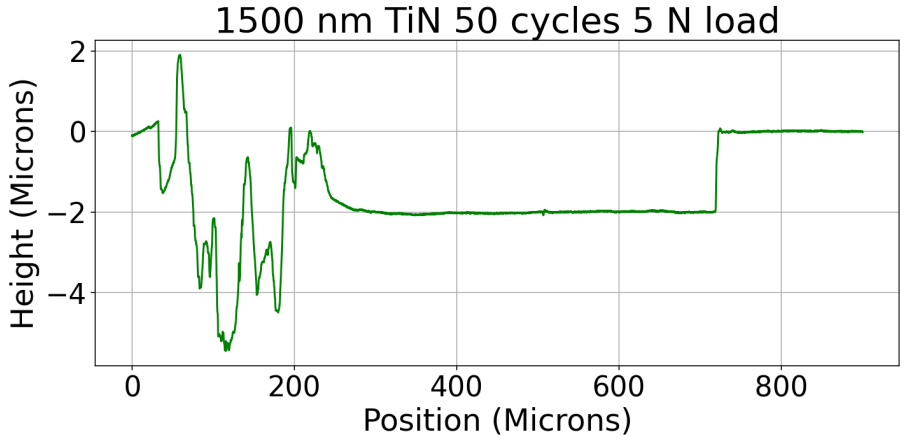

Figure A.64: This figure shows a 1500 nm TiN coated stainless steel sample. This figure shows the wear track recorded during line profiling measurement when equipped with a load of 5 N and during 50 cycles.

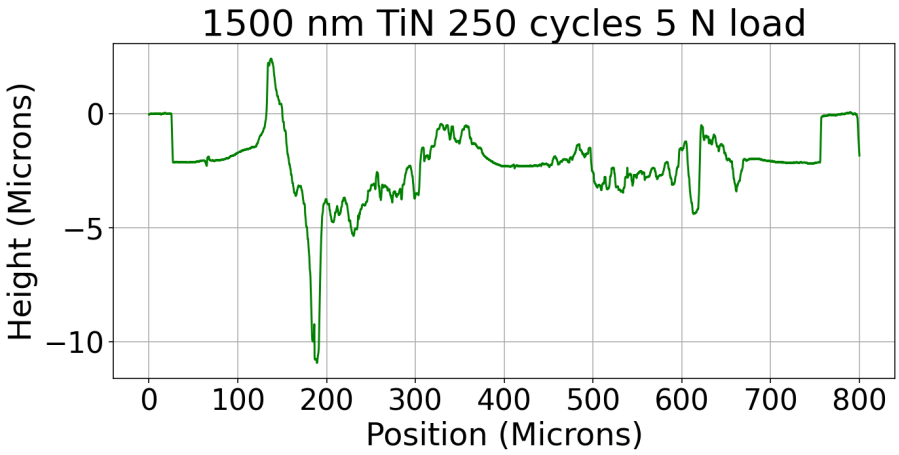

Figure A.65: This figure shows a 1500 nm TiN coated stainless steel sample. This figure shows the wear track recorded during line profiling measurement when equipped with a load of 5 N and during 250 cycles.

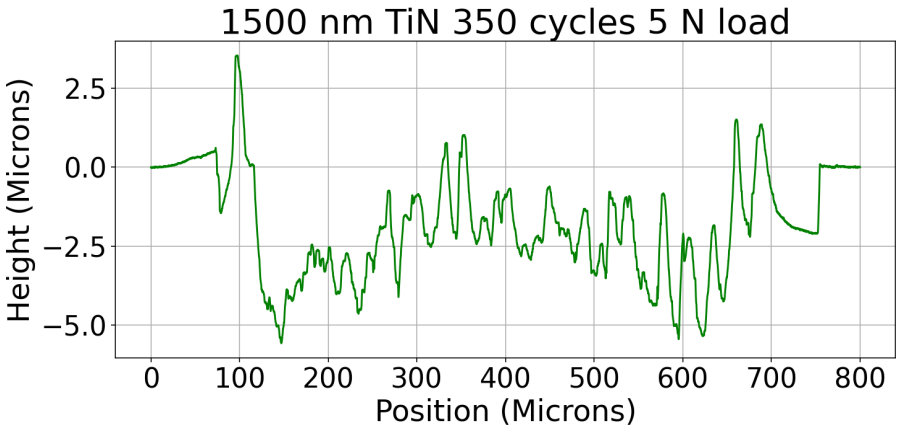

Figure A.66: This figure shows a 1500 nm TiN coated stainless steel sample. This figure shows the wear track recorded during line profiling measurement when equipped with a load of 5 N and during 350 cycles.

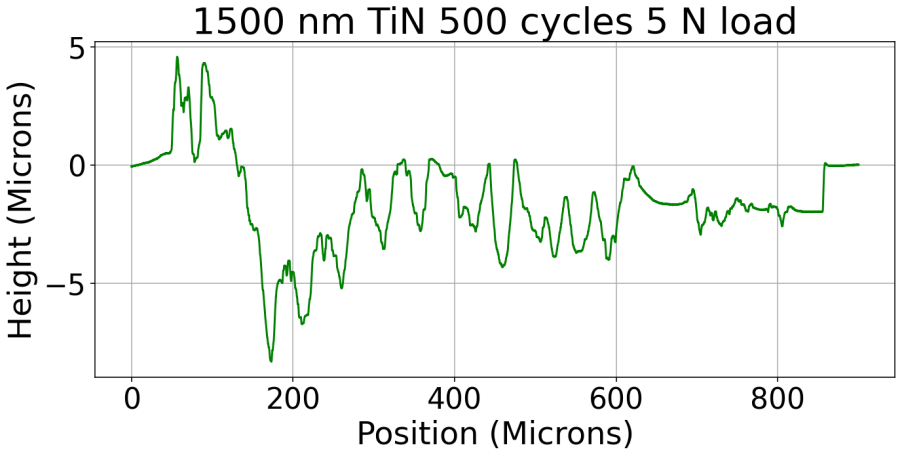

Figure A.67: This figure shows a 1500 nm TiN coated stainless steel sample. This figure shows the wear track recorded during line profiling measurement when equipped with a load of 5 N and during 500 cycles.

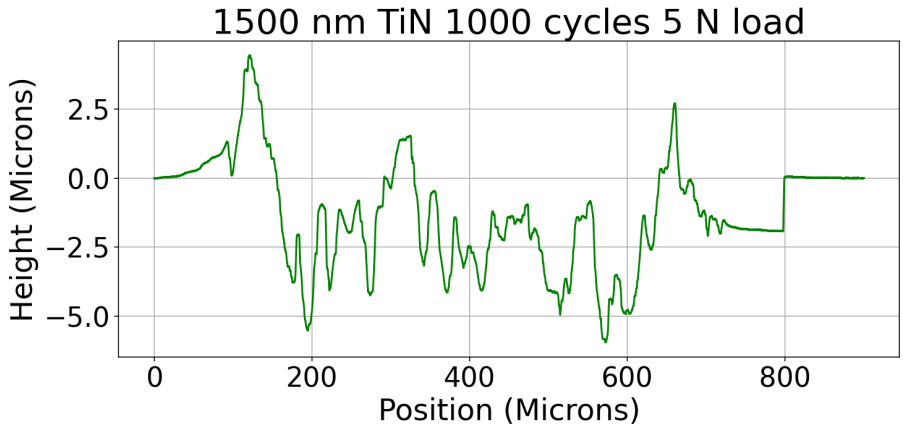

Figure A.68: This figure shows a 1500 nm TiN coated stainless steel sample. This figure shows the wear track recorded during line profiling measurement when equipped with a load of 5 N and during 1000 cycles.

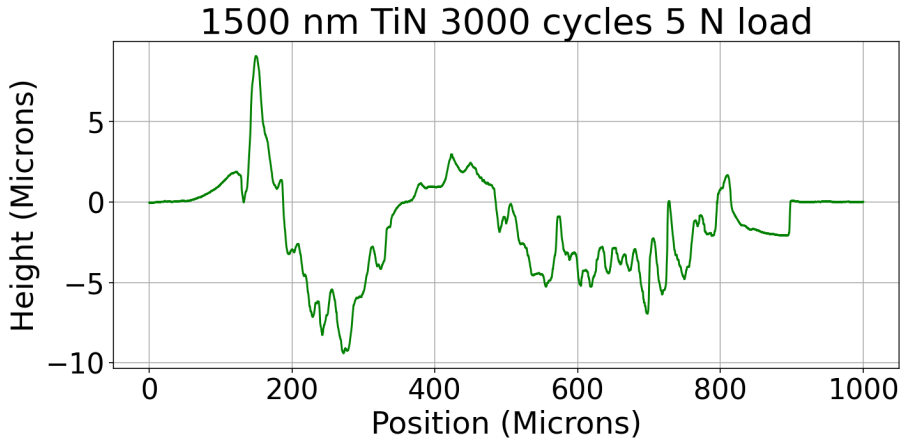

Figure A.69: This figure shows a 1500 nm TiN coated stainless steel sample. This figure shows the wear track recorded during line profiling measurement when equipped with a load of 5 N and during 3000 cycles.

A.2.4 1500 nm TiN Coated Line Profiling at 10 N

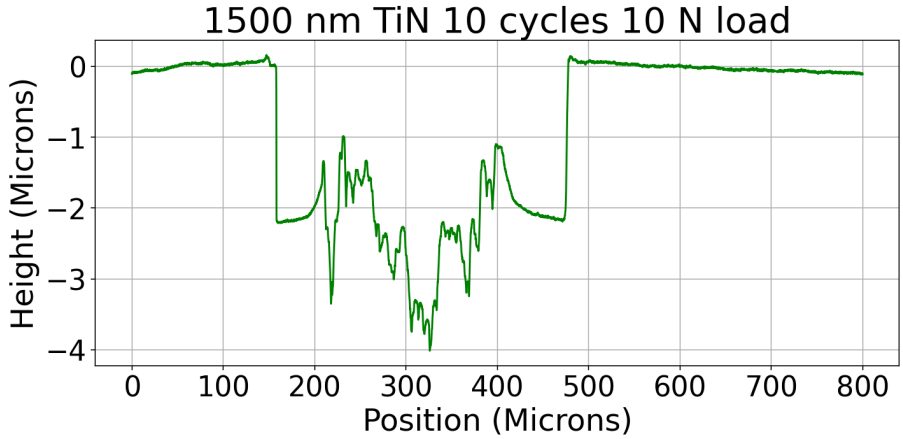

Figure A.70: This figure shows a 1500 nm TiN coated stainless steel sample. This figure shows the wear track recorded during line profiling measurement when equipped with a load of 10 N and during 10 cycles.

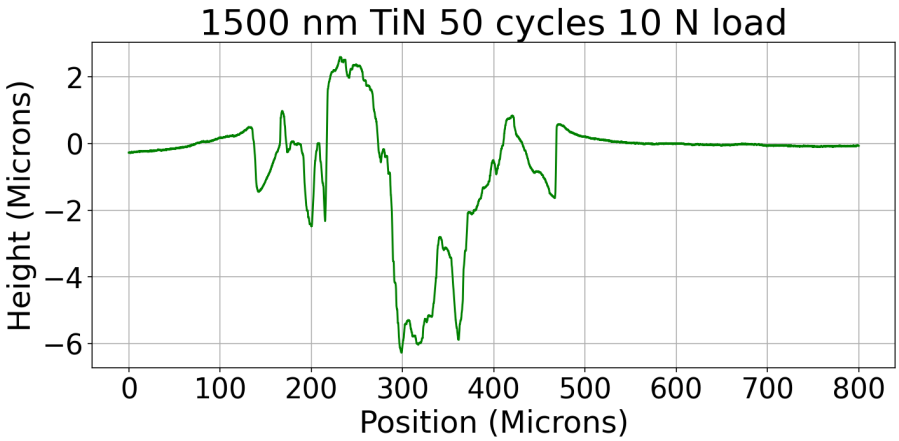

Figure A.71: This figure shows a 1500 nm TiN coated stainless steel sample. This figure shows the wear track recorded during line profiling measurement when equipped with a load of 10 N and during 50 cycles.

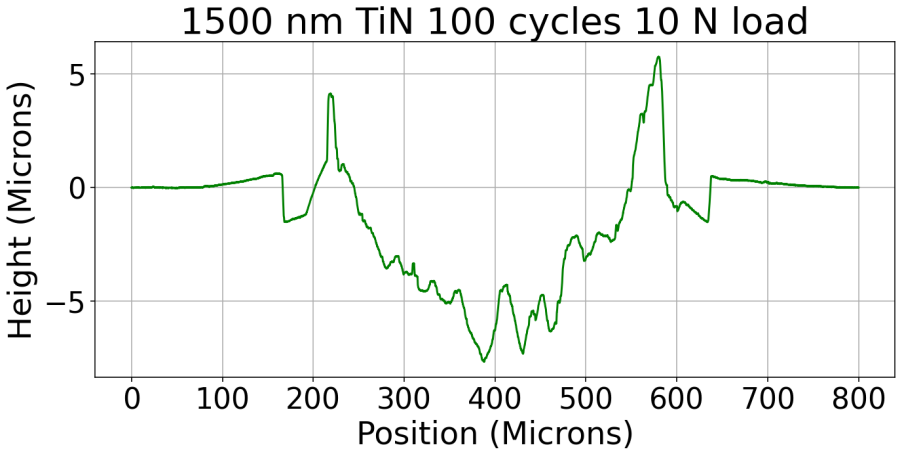

Figure A.72: This figure shows a 1500 nm TiN coated stainless steel sample. This figure shows the wear track recorded during line profiling measurement when equipped with a load of 10 N and during 100 cycles.

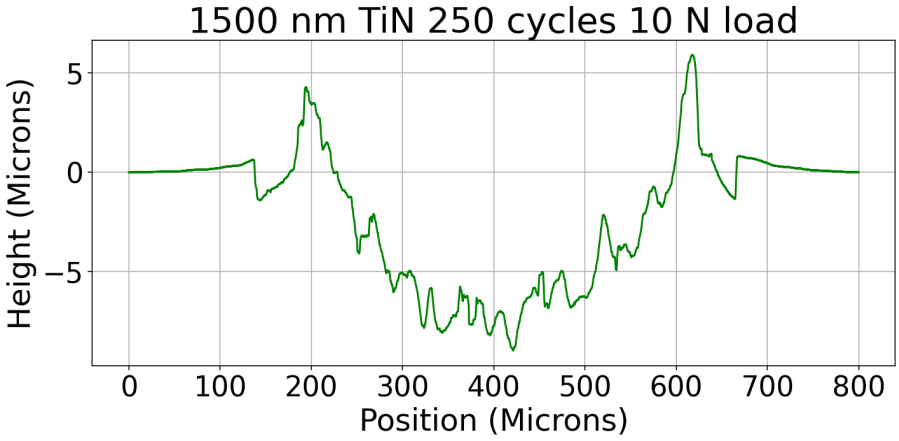

Figure A.73: This figure shows a 1500 nm TiN coated stainless steel sample. This figure shows the wear track recorded during line profiling measurement when equipped with a load of 10 N and during 250 cycles.

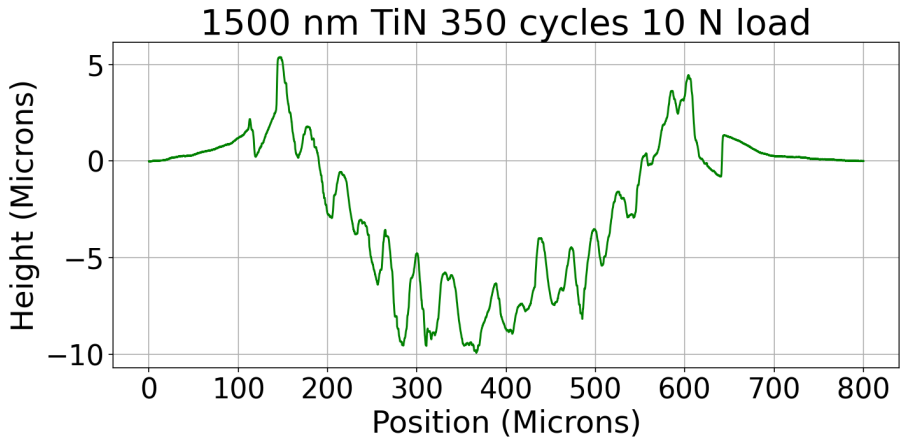

Figure A.74: This figure shows a 1500 nm TiN coated stainless steel sample. This figure shows the wear track recorded during line profiling measurement when equipped with a load of 10 N and during 350 cycles.

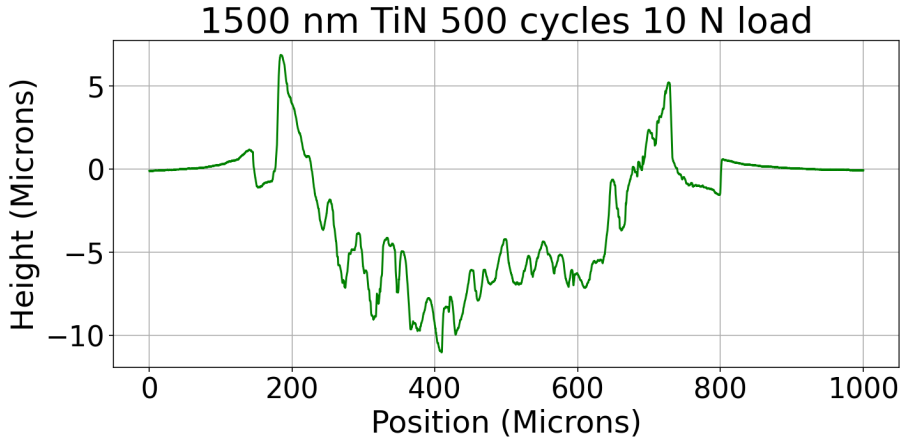

Figure A.75: This figure shows a 1500 nm TiN coated stainless steel sample. This figure shows the wear track recorded during line profiling measurement when equipped with a load of 10 N and during 500 cycles.

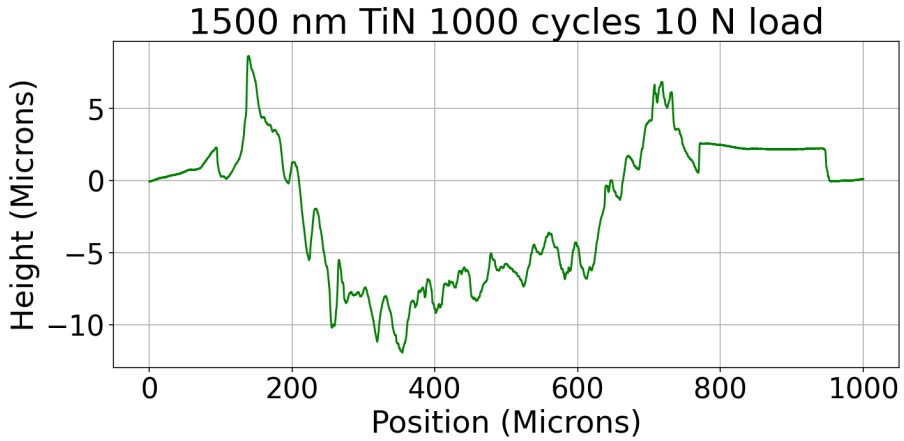

Figure A.76: This figure shows a 1500 nm TiN coated stainless steel sample. This figure shows the wear track recorded during line profiling measurement when equipped with a load of 10 N and during 1000 cycles.

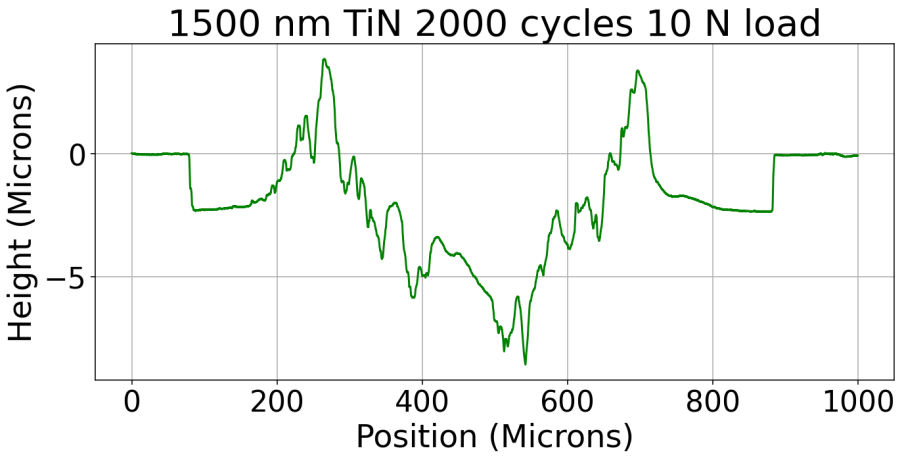

Figure A.77: This figure shows a 1500 nm TiN coated stainless steel sample. This figure shows the wear track recorded during line profiling measurement when equipped with a load of 10 N and during 2000 cycles.

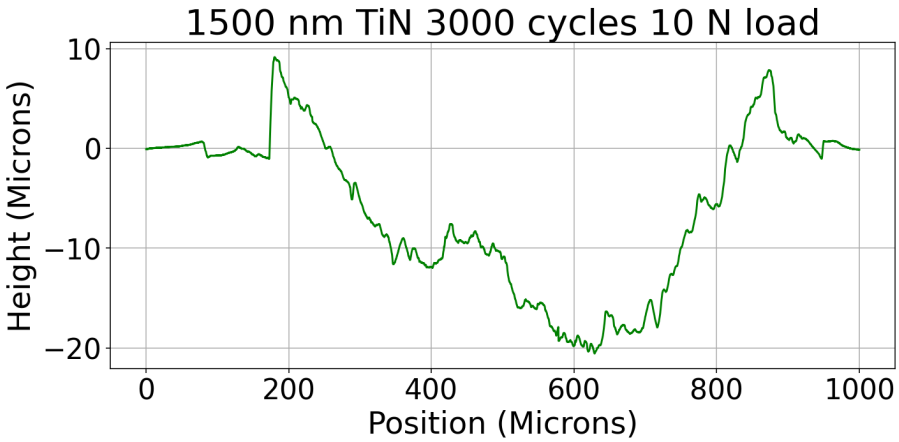

Figure A.78: This figure shows a 1500 nm TiN coated stainless steel sample. This figure shows the wear track recorded during line profiling measurement when equipped with a load of 10 N and during 3000 cycles.

A.3 All SEM Images of Wear Tracks on Stainless Steel Sample

SEM imaging of every wear track was done because the wear tracks vary quite a bit in quality when considering them through line profiling. The SEM images can help determine the cause of the shapes seen through line profiling.

A.3.1 SEM Images of Wear Tracks on Stainless Steel Sample at 0.25 N

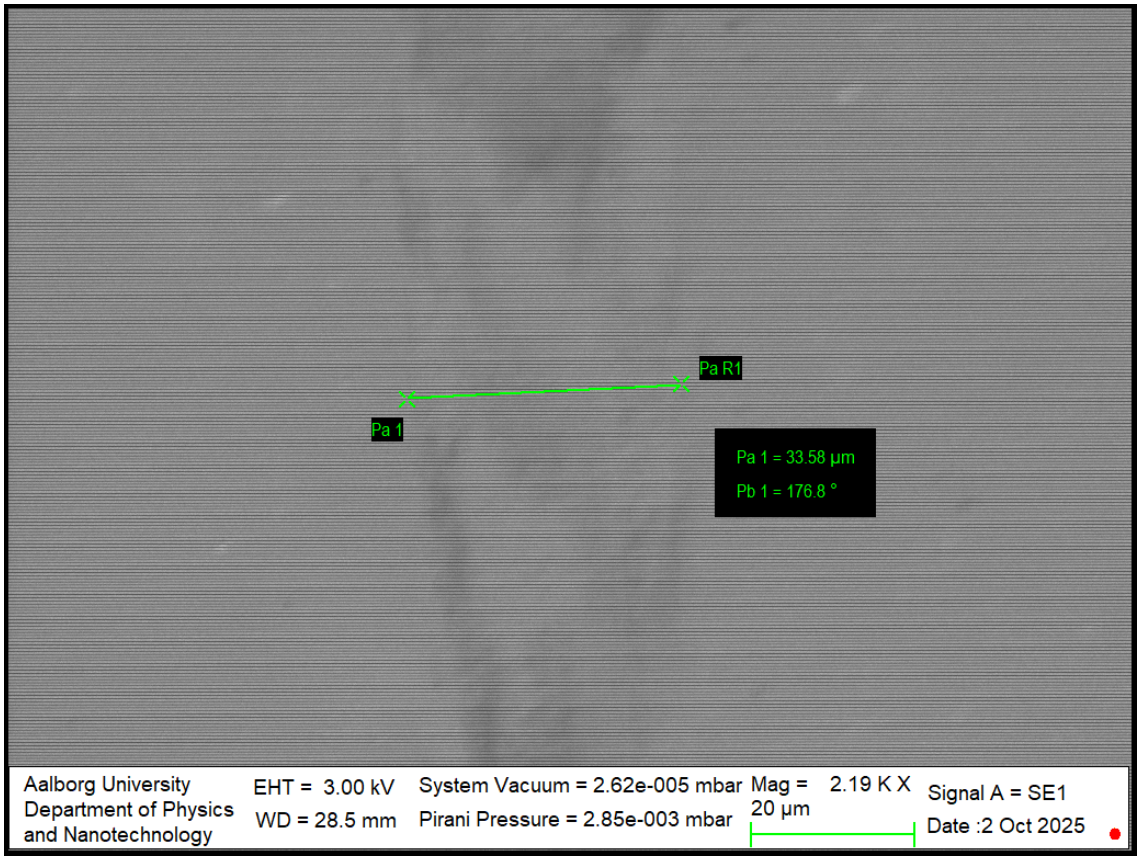

Figure A.79: This image shows a stainless steel sample. This image shows the wear track done on the sample by the TRB3 tribometer when equipped with a load of 0.25 N and during 1 cycle.

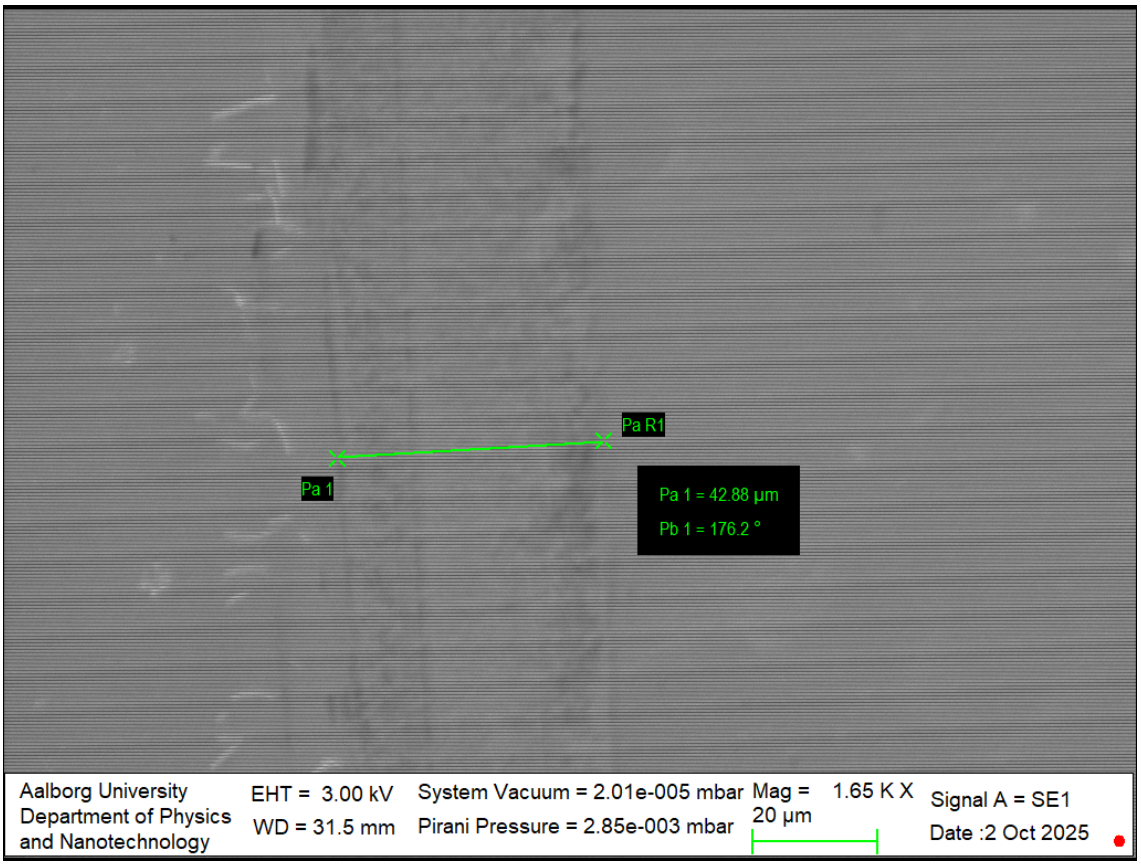

Figure A.80: This image shows a stainless steel sample. This image shows the wear track done on the sample by the TRB3 tribometer when equipped with a load of 0.25 N and during 10 cycles.

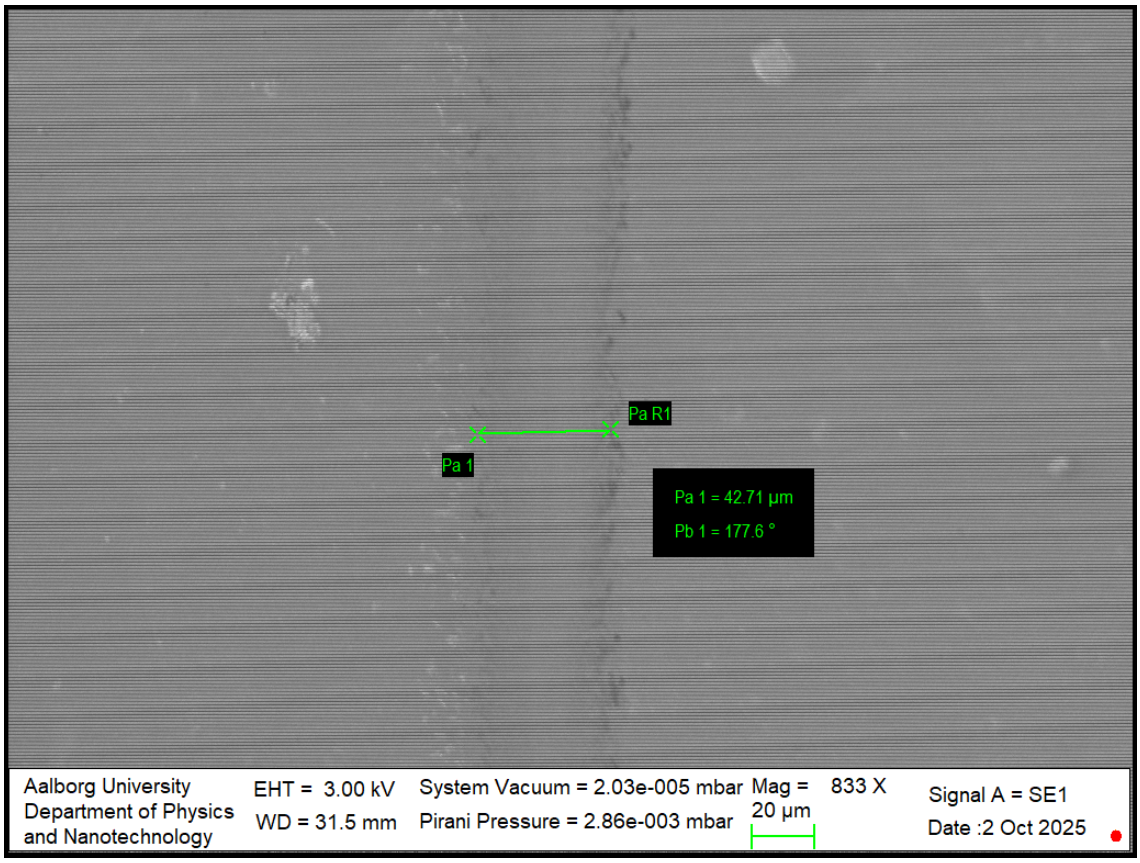

Figure A.81: This image shows a stainless steel sample. This image shows the wear track done on the sample by the TRB3 tribometer when equipped with a load of 0.25 N and during 50 cycles.

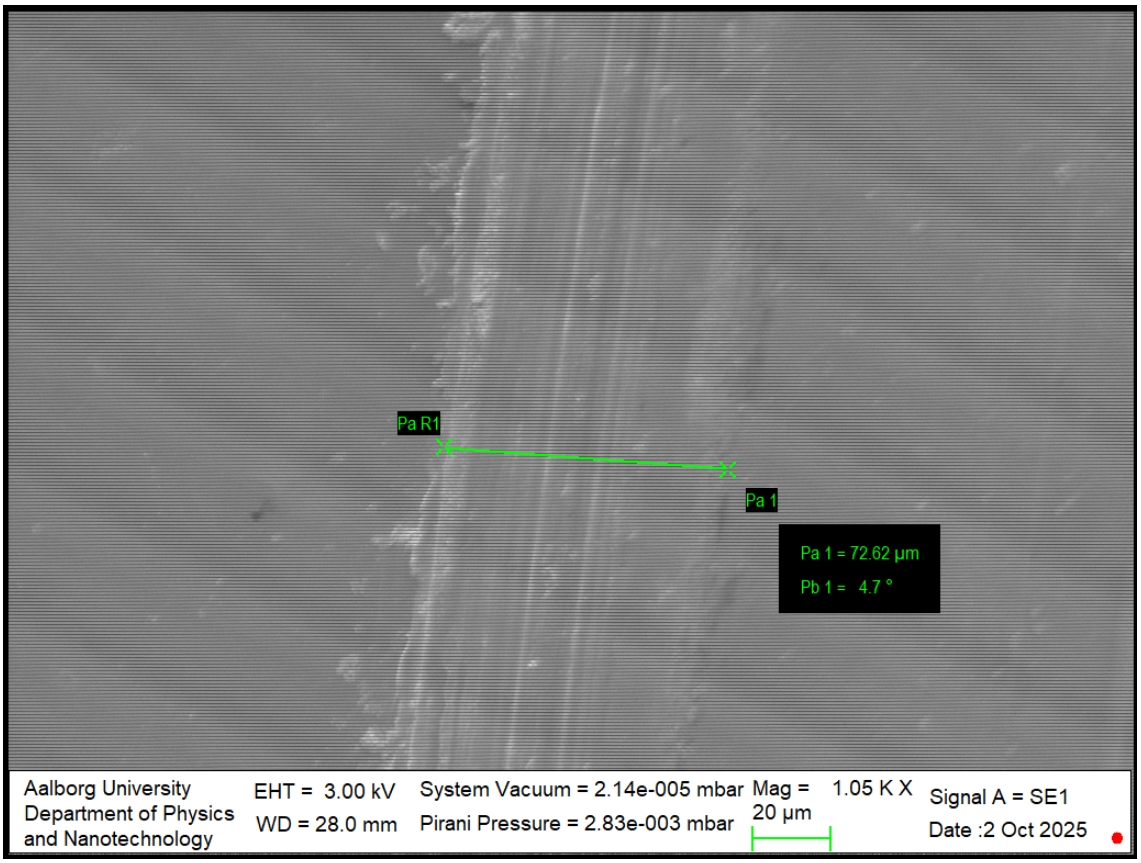

Figure A.82: This image shows a stainless steel sample. This image shows the wear track done on the sample by the TRB3 tribometer when equipped with a load of 0.25 N and during 100 cycles.

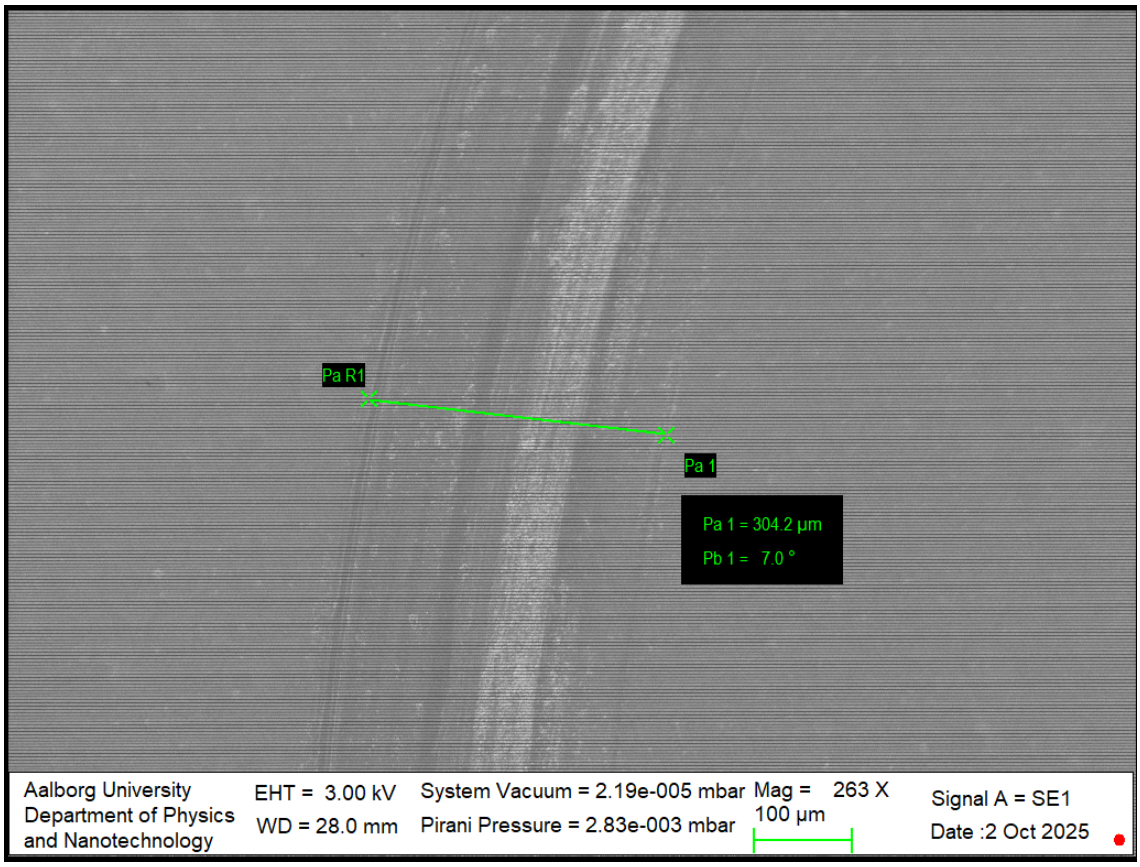

Figure A.83: This image shows a stainless steel sample. This image shows the wear track done on the sample by the TRB3 tribometer when equipped with a load of 0.25 N and during 250 cycles.

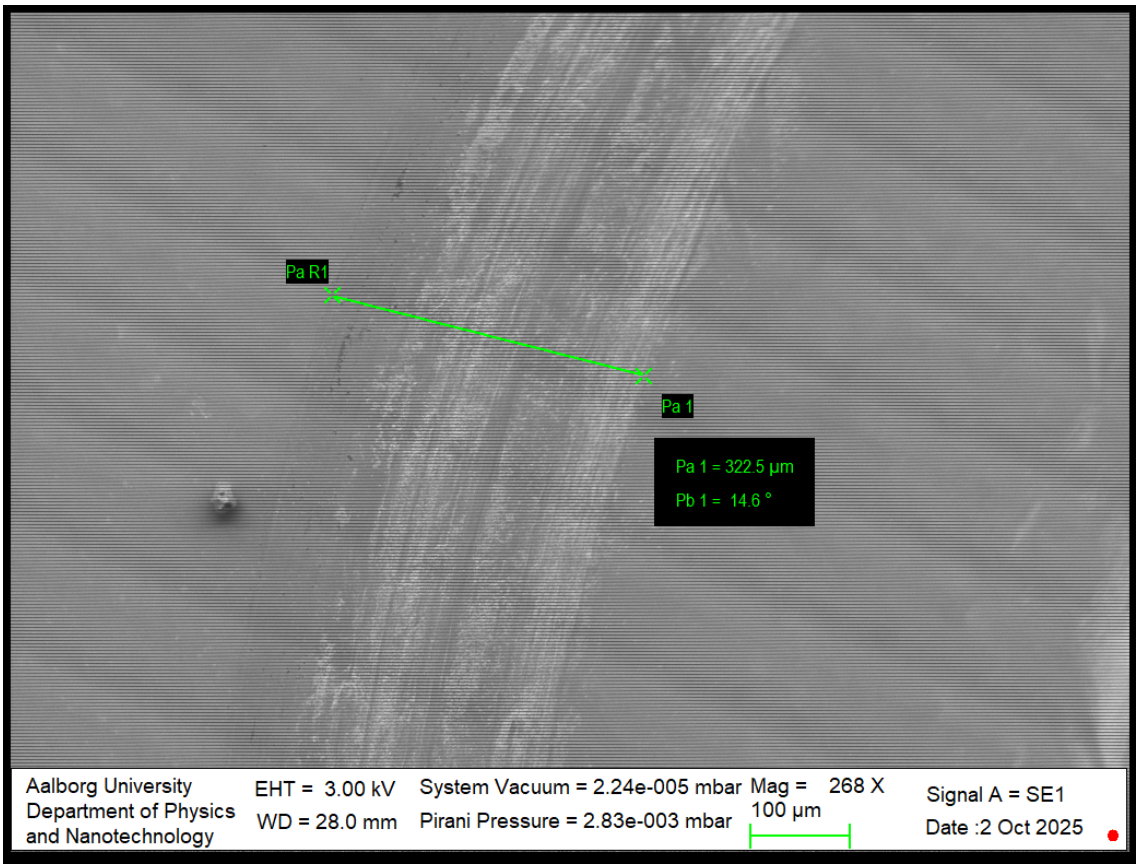

Figure A.84: This image shows a stainless steel sample. This image shows the wear track done on the sample by the TRB3 tribometer when equipped with a load of 0.25 N and during 350 cycles.

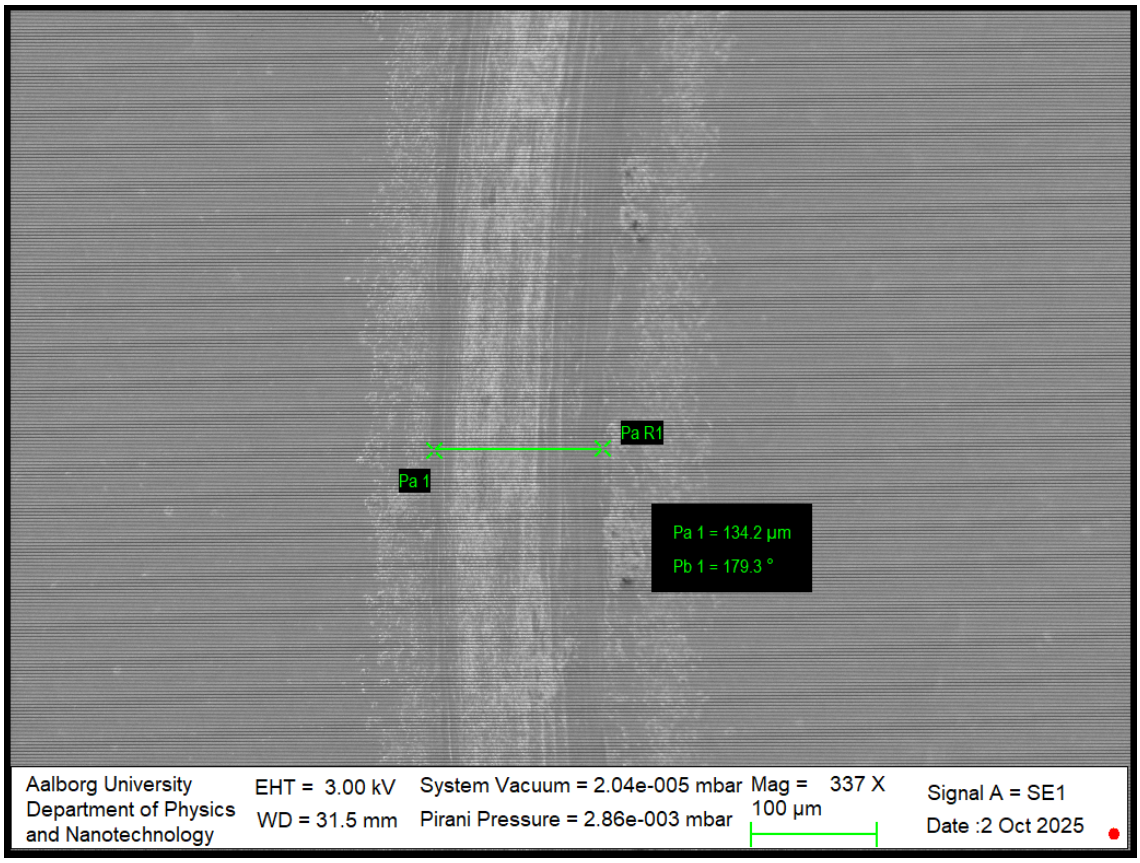

Figure A.85: This image shows a stainless steel sample. This image shows the wear track done on the sample by the TRB3 tribometer when equipped with a load of 0.25 N and during 500 cycles.

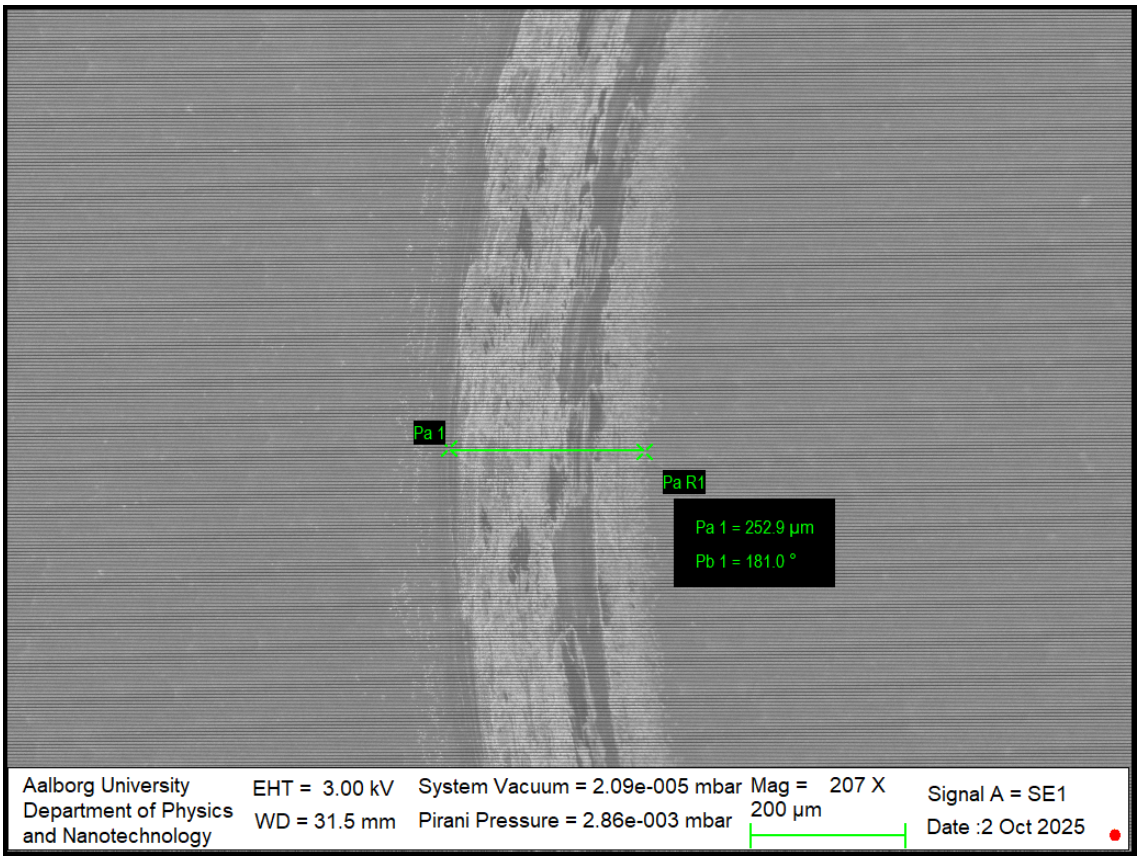

Figure A.86: This image shows a stainless steel sample. This image shows the wear track done on the sample by the TRB3 tribometer when equipped with a load of 0.25 N and during 1000 cycles.

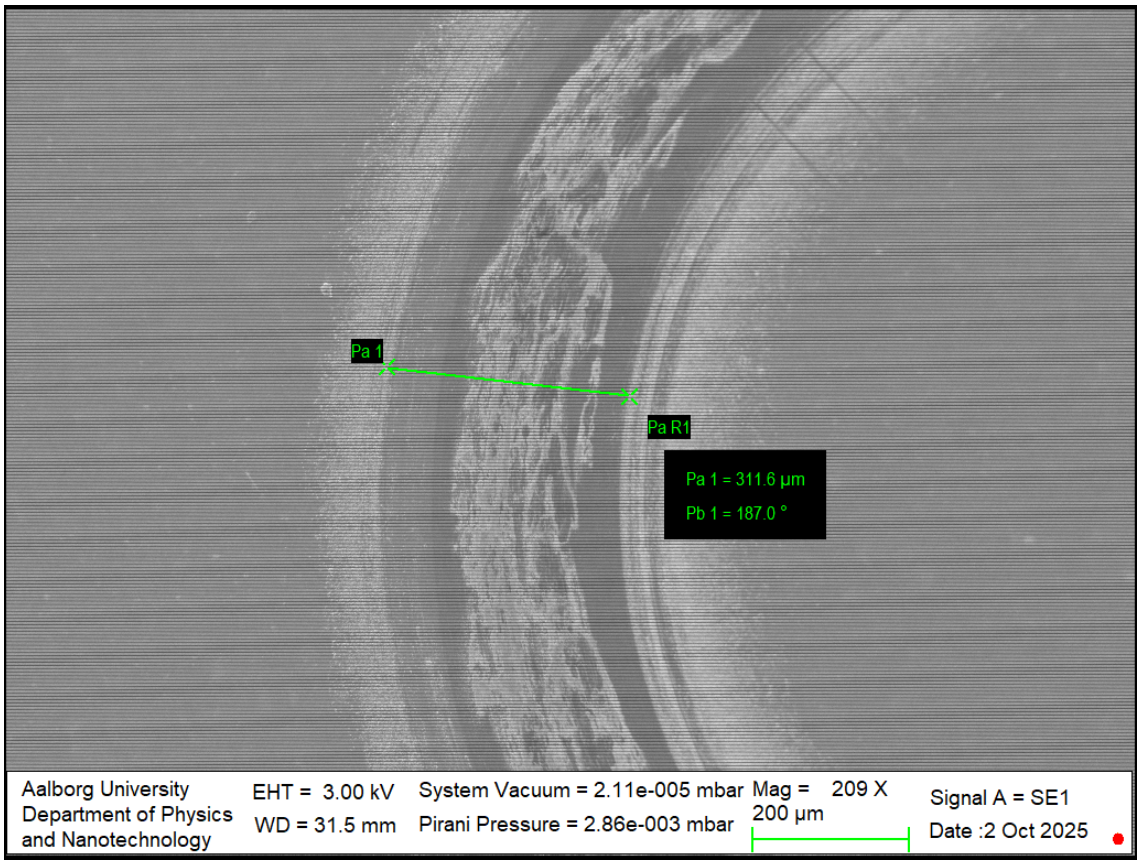

Figure A.87: This image shows a stainless steel sample. This image shows the wear track done on the sample by the TRB3 tribometer when equipped with a load of 0.25 N and during 2000 cycles.

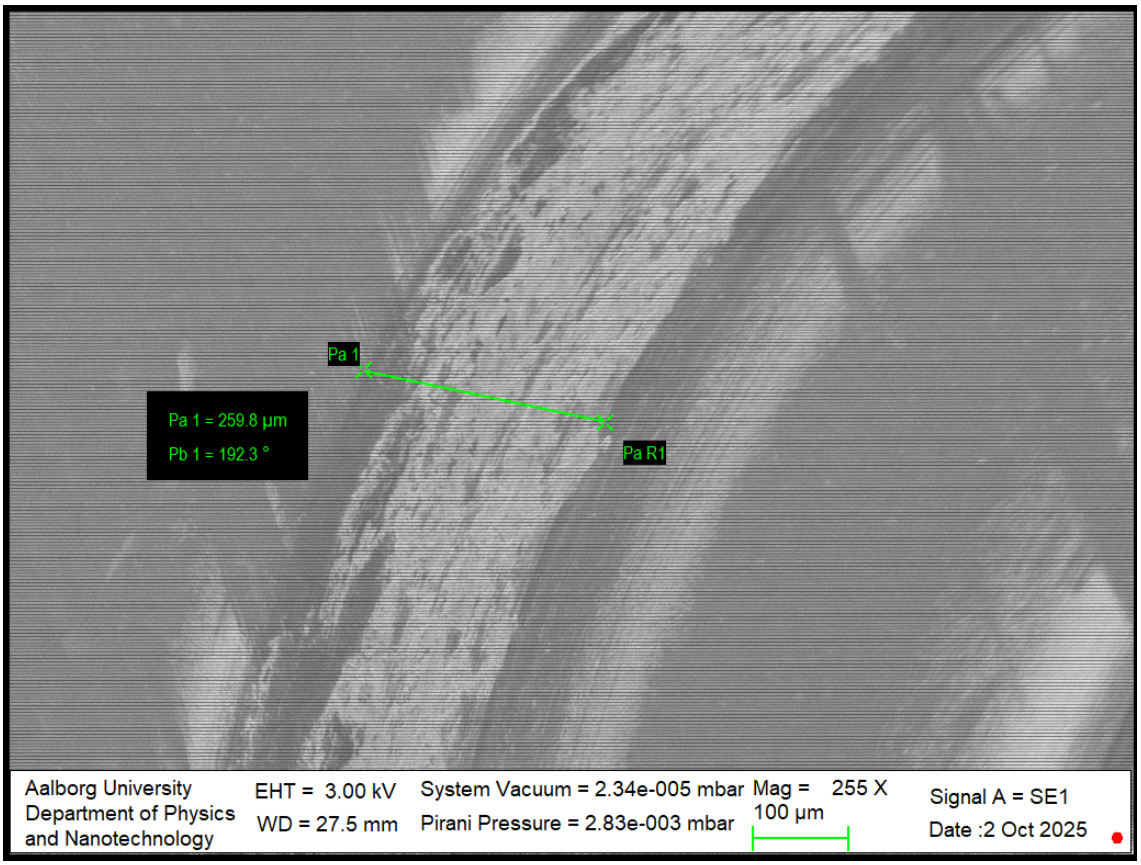

Figure A.88: This image shows a stainless steel sample. This image shows the wear track done on the sample by the TRB3 tribometer when equipped with a load of 0.25 N and during 3000 cycles.

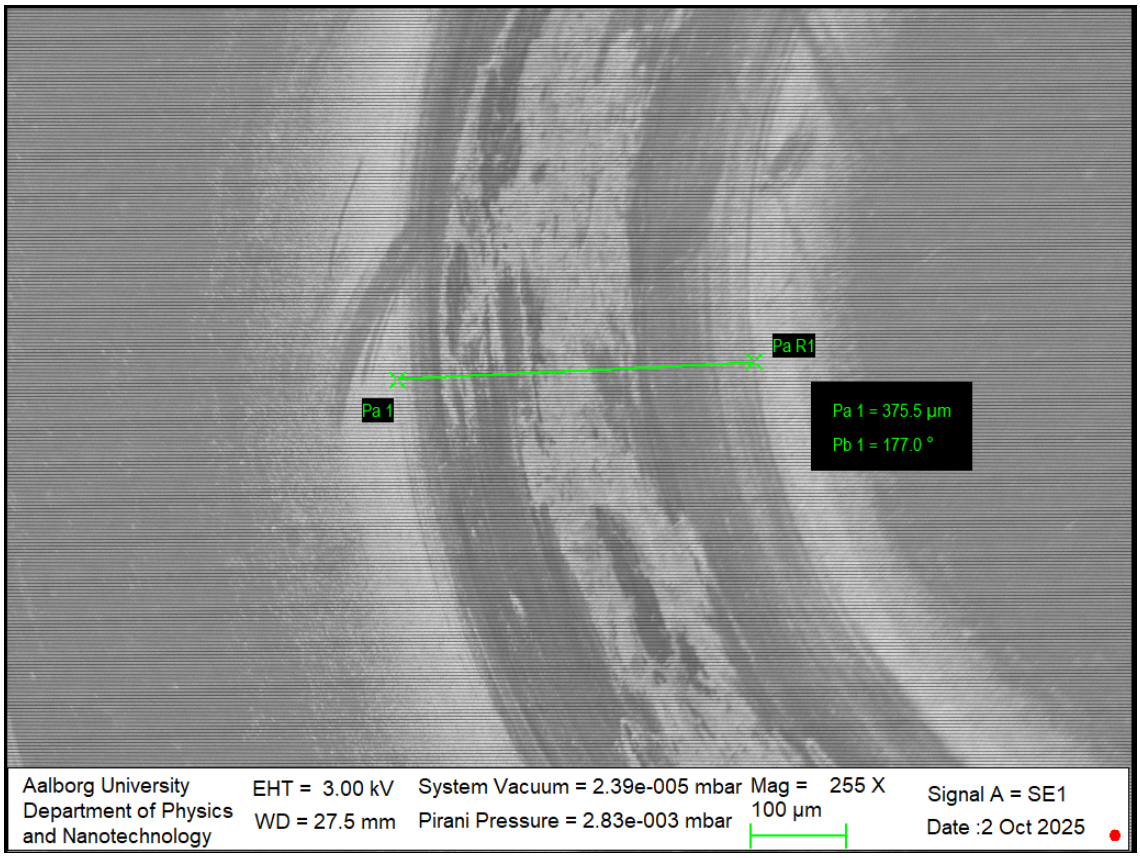

Figure A.89: This image shows a stainless steel sample. This image shows the wear track done on the sample by the TRB3 tribometer when equipped with a load of 0.25 N and during 5000 cycles.

A.3.2 SEM Images of Wear Tracks on Stainless Steel Sample at 1 N

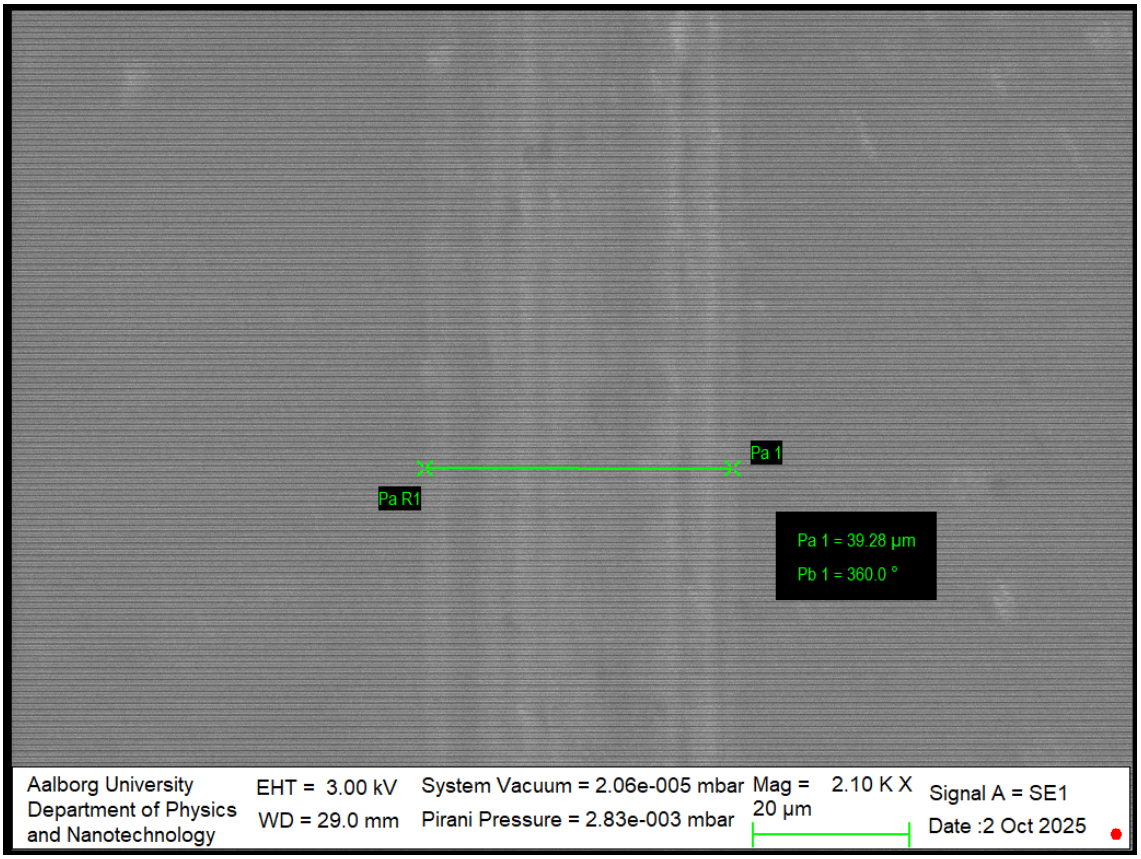

Figure A.90: This image shows a stainless steel sample. This image shows the wear track done on the sample by the TRB3 tribometer when equipped with a load of 1 N and during 1 cycle.

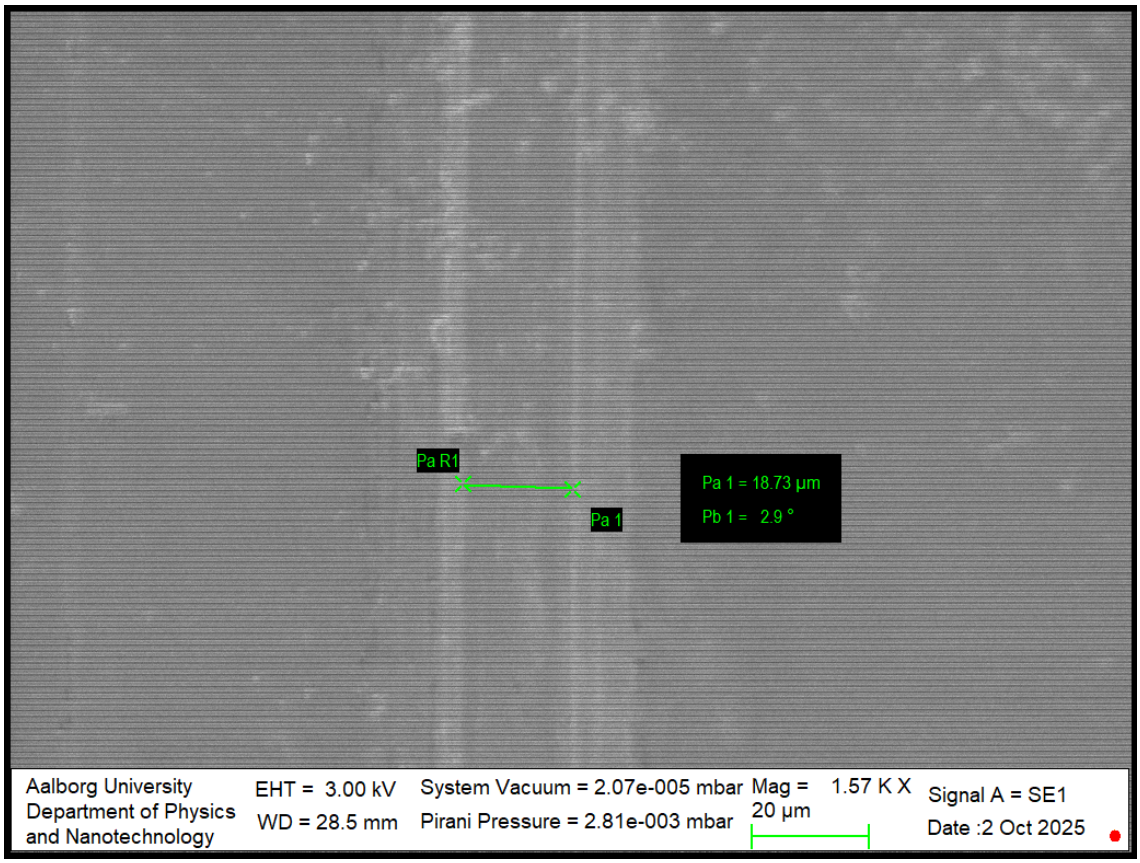

Figure A.91: This image shows a stainless steel sample. This image shows the wear track done on the sample by the TRB3 tribometer when equipped with a load of 1 N and during 10 cycles.

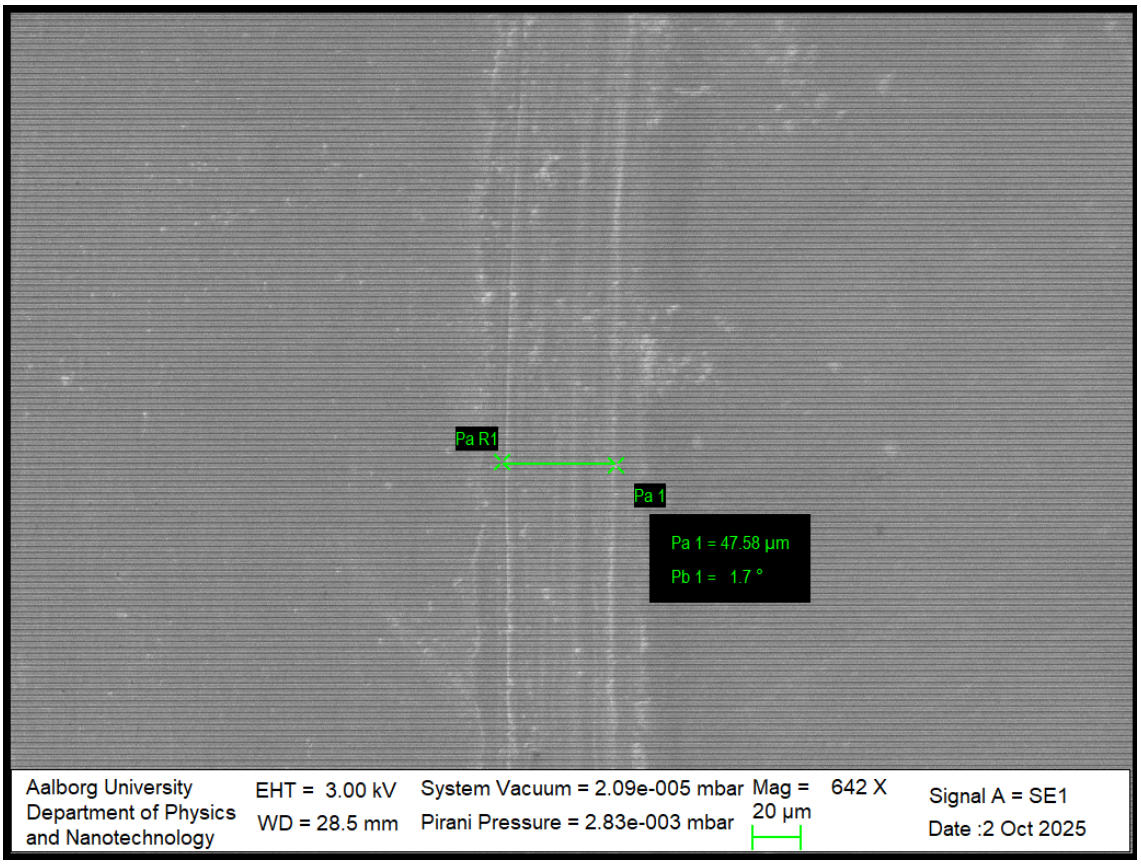

Figure A.92: This image shows a stainless steel sample. This image shows the wear track done on the sample by the TRB3 tribometer when equipped with a load of 1 N and during 50 cycles.

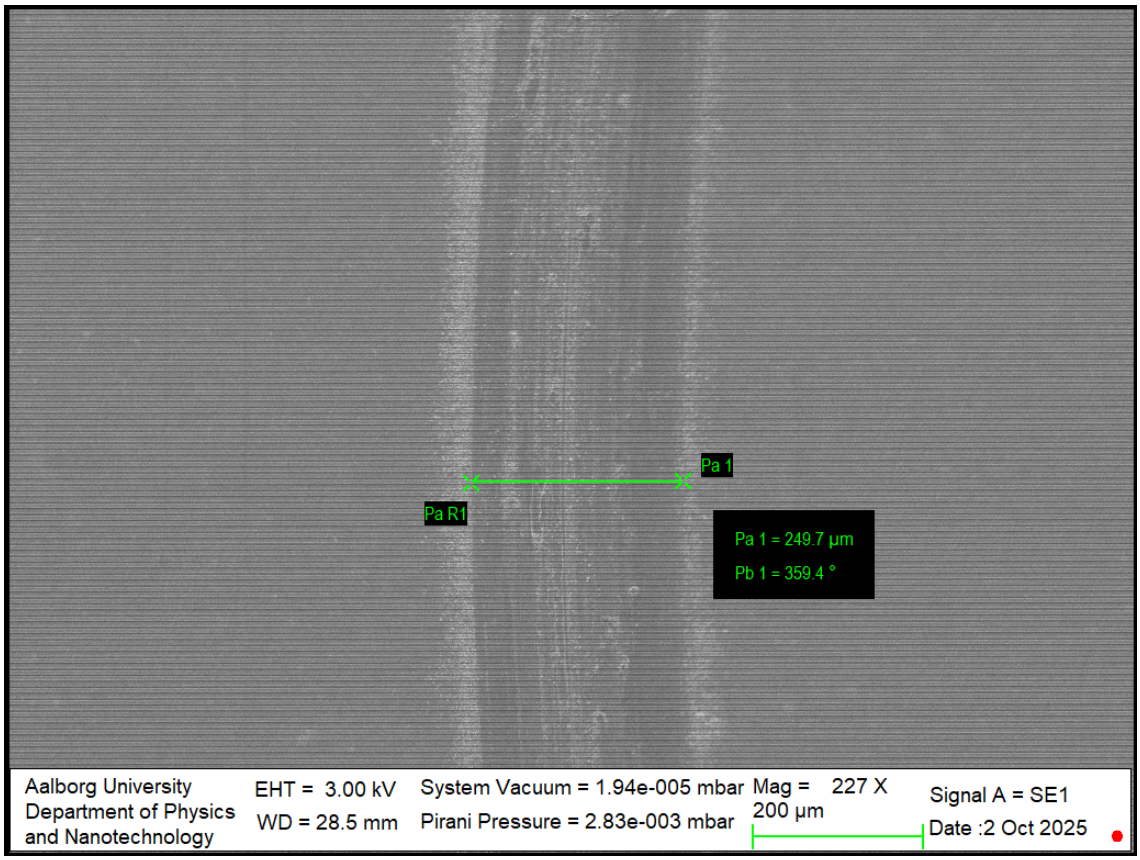

Figure A.93: This image shows a stainless steel sample. This image shows the wear track done on the sample by the TRB3 tribometer when equipped with a load of 1 N and during 100 cycles.

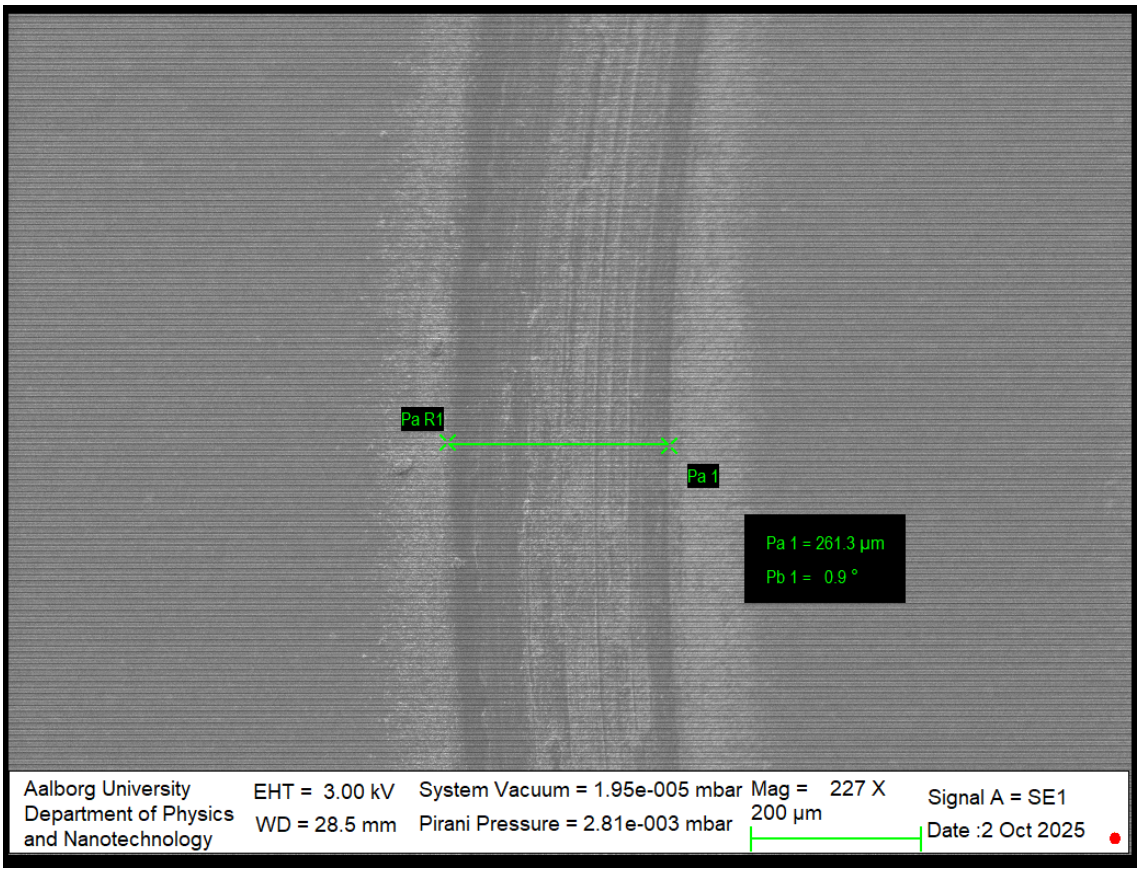

Figure A.94: This image shows a stainless steel sample. This image shows the wear track done on the sample by the TRB3 tribometer when equipped with a load of 1 N and during 250 cycles.

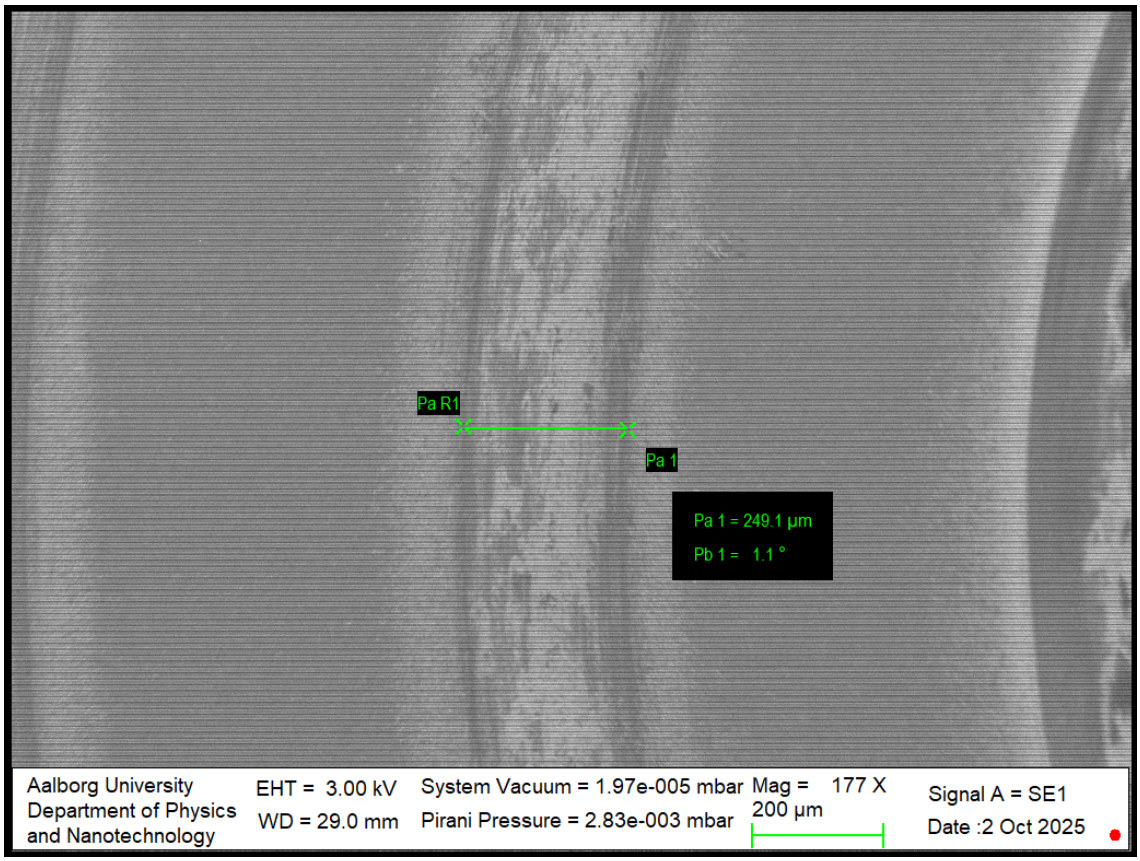

Figure A.95: This image shows a stainless steel sample. This image shows the wear track done on the sample by the TRB3 tribometer when equipped with a load of 1 N and during 350 cycles.

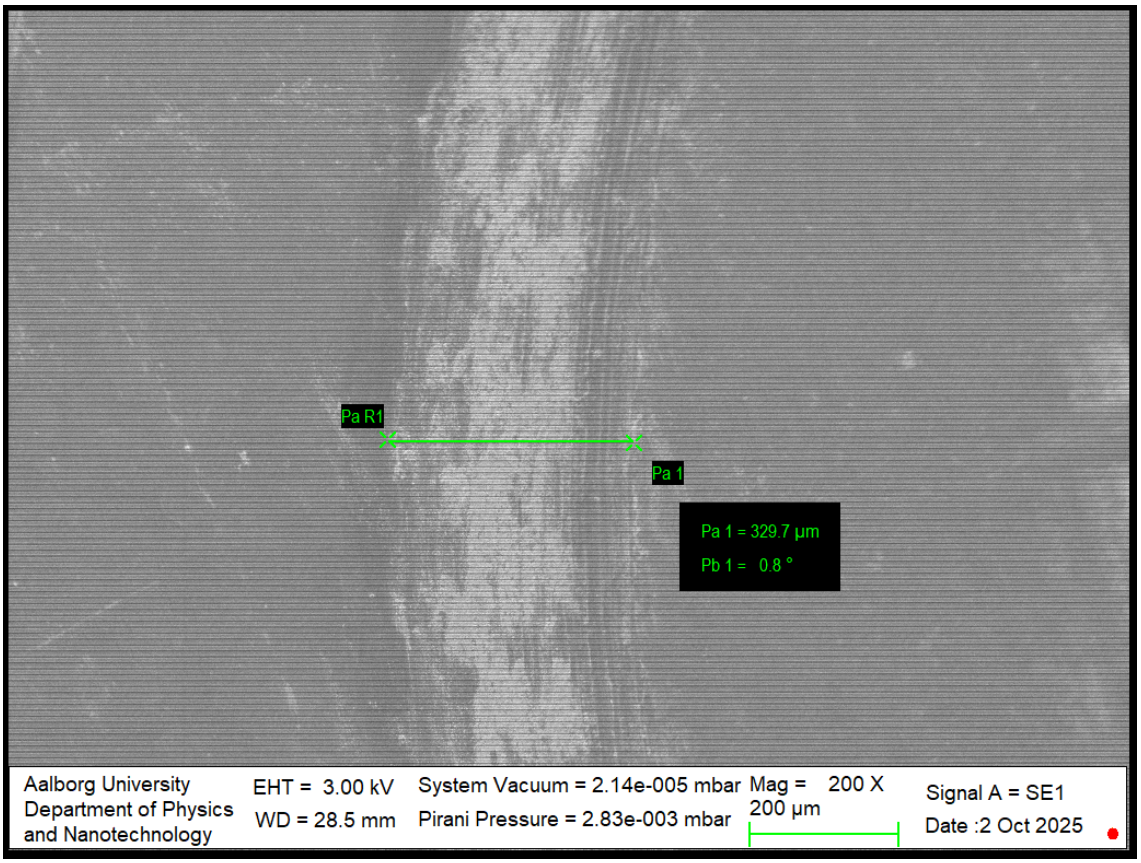

Figure A.96: This image shows a stainless steel sample. This image shows the wear track done on the sample by the TRB3 tribometer when equipped with a load of 1 N and during 500 cycles.

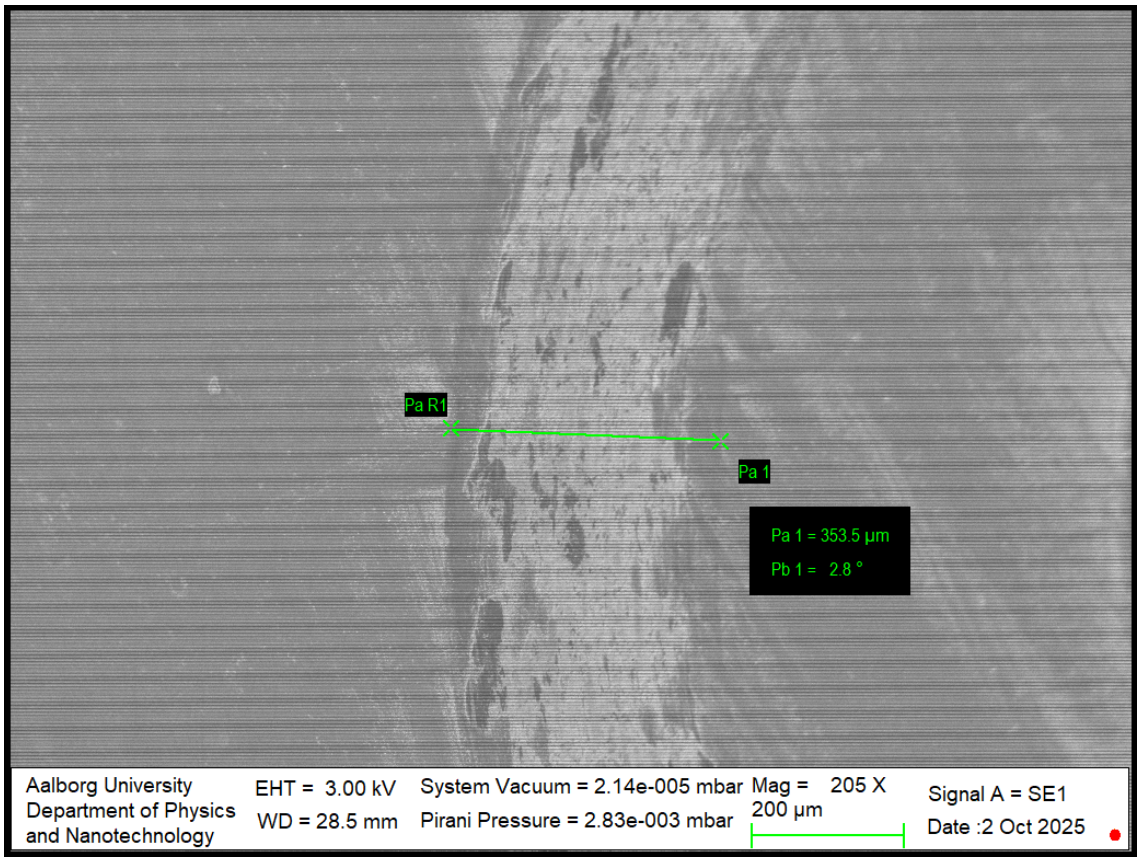

Figure A.97: This image shows a stainless steel sample. This image shows the wear track done on the sample by the TRB3 tribometer when equipped with a load of 1 N and during 1000 cycles.

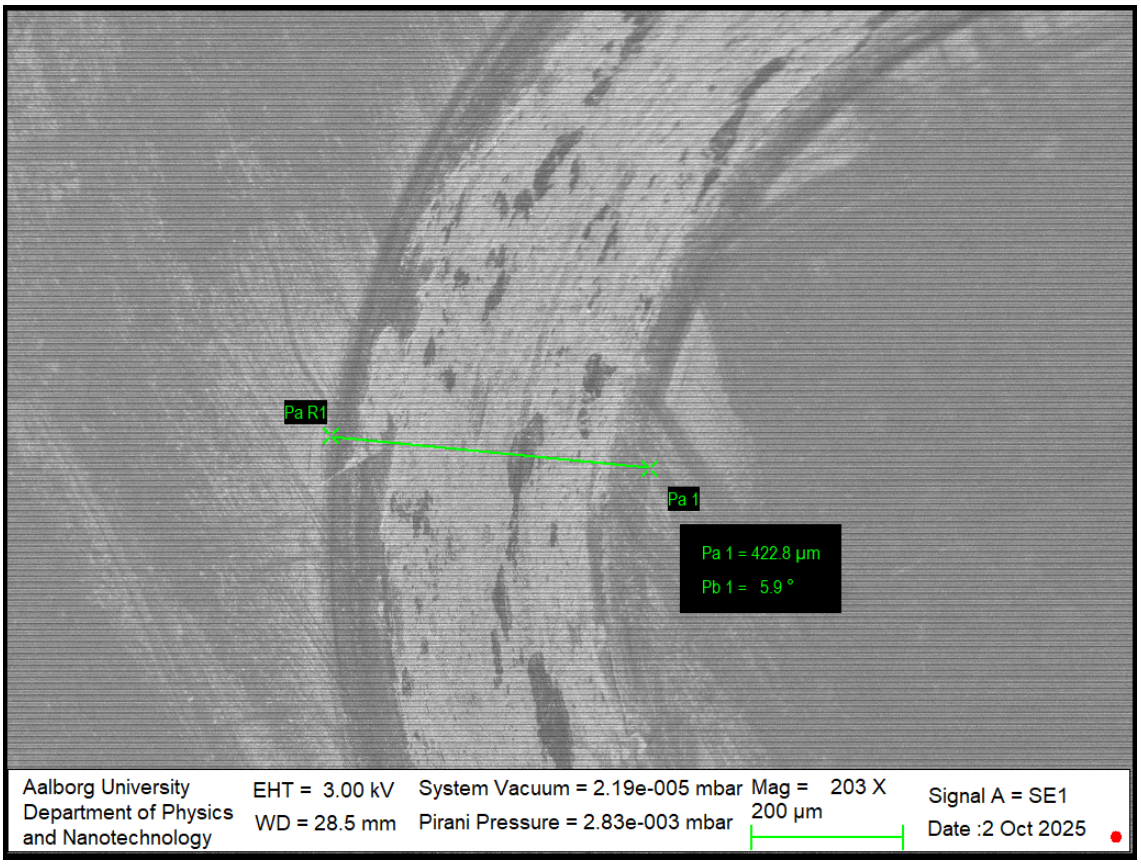

Figure A.98: This image shows a stainless steel sample. This image shows the wear track done on the sample by the TRB3 tribometer when equipped with a load of 1 N and during 2000 cycles.

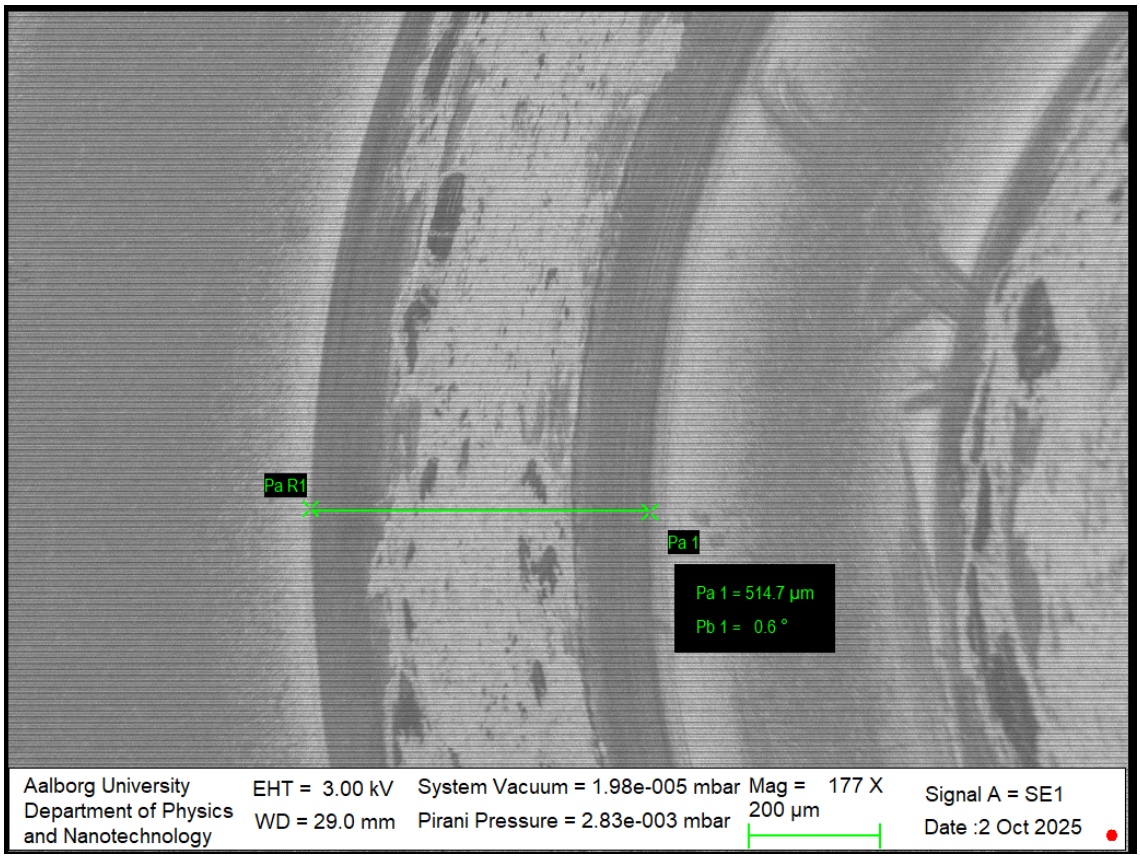

Figure A.99: This image shows a stainless steel sample. This image shows the wear track done on the sample by the TRB3 tribometer when equipped with a load of 1 N and during 3000 cycles.

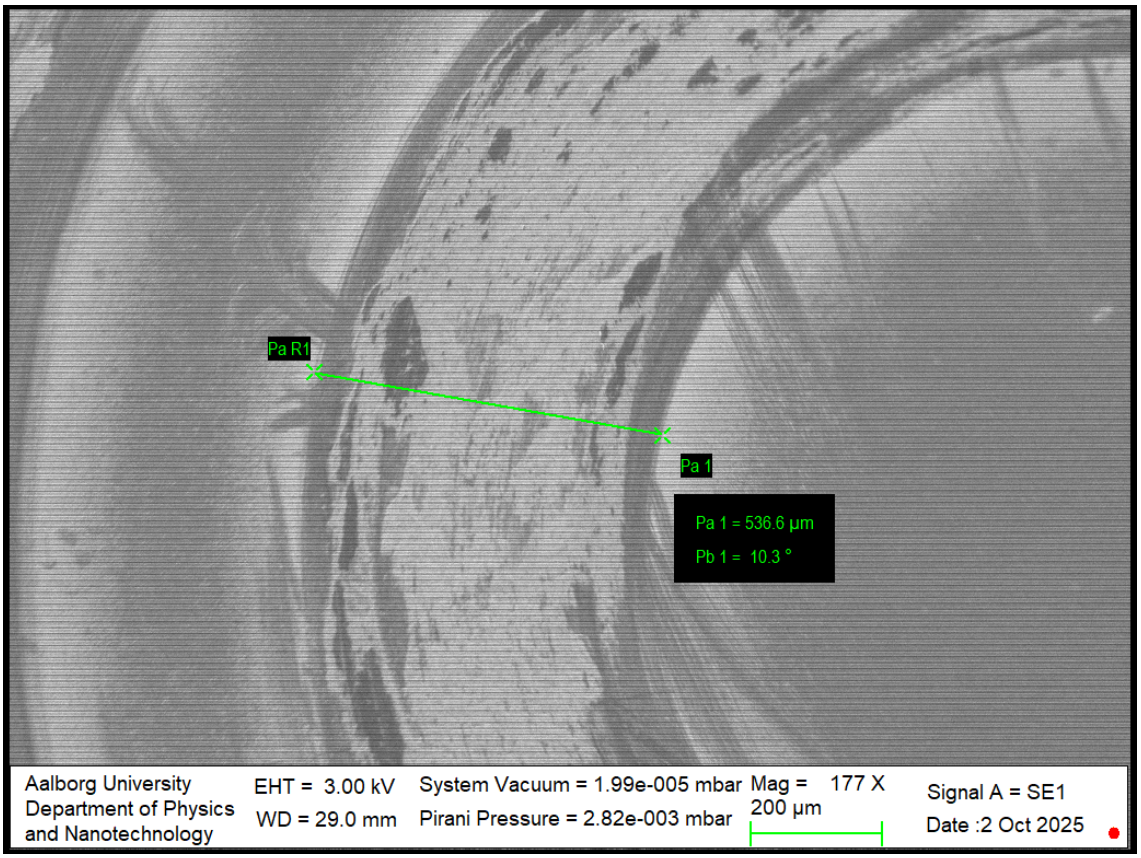

Figure A.100: This image shows a stainless steel sample. This image shows the wear track done on the sample by the TRB3 tribometer when equipped with a load of 1 N and during 5000 cycles.

A.3.3 SEM Images of Wear Tracks on Stainless Steel Sample at 2 N

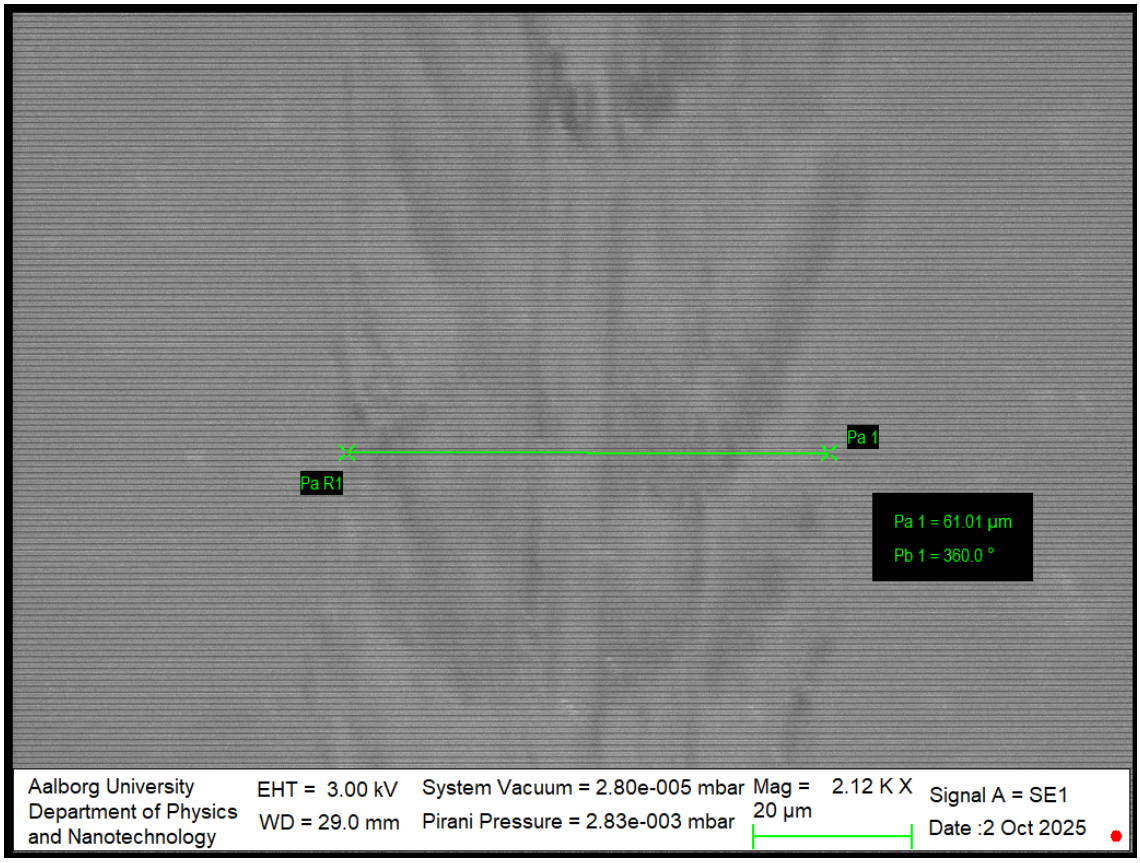

Figure A.101: This image shows a stainless steel sample. This image shows the wear track done on the sample by the TRB3 tribometer when equipped with a load of 2 N and during 1 cycle.

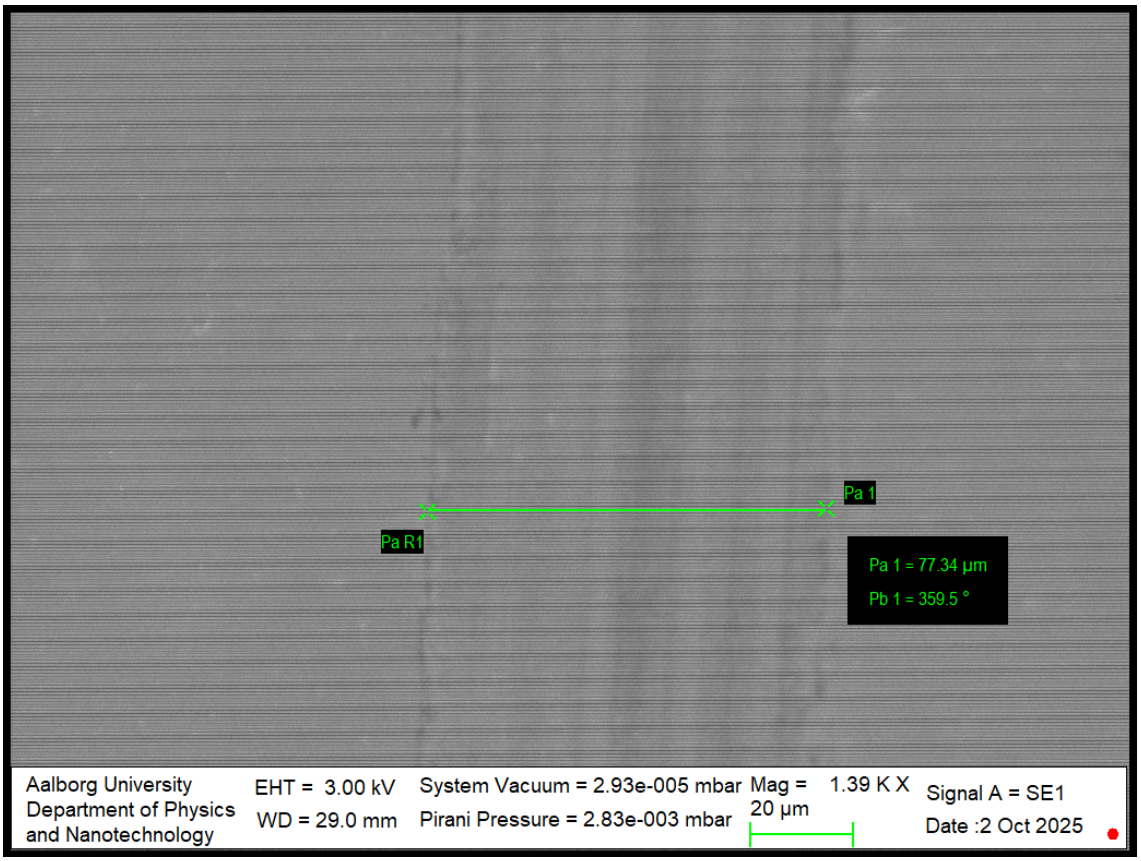

Figure A.102: This image shows a stainless steel sample. This image shows the wear track done on the sample by the TRB3 tribometer when equipped with a load of 2 N and during 10 cycles.

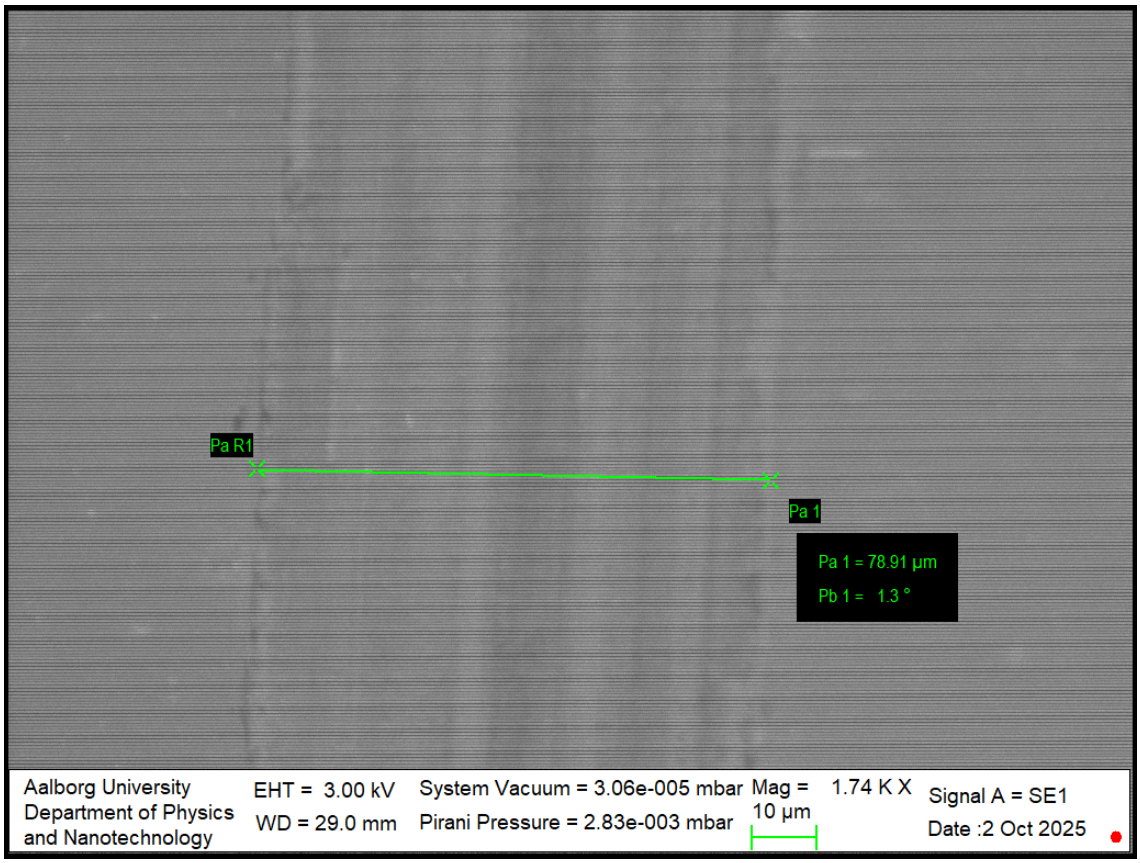

Figure A.103: This image shows a stainless steel sample. This image shows the wear track done on the sample by the TRB3 tribometer when equipped with a load of 2 N and during 50 cycles.

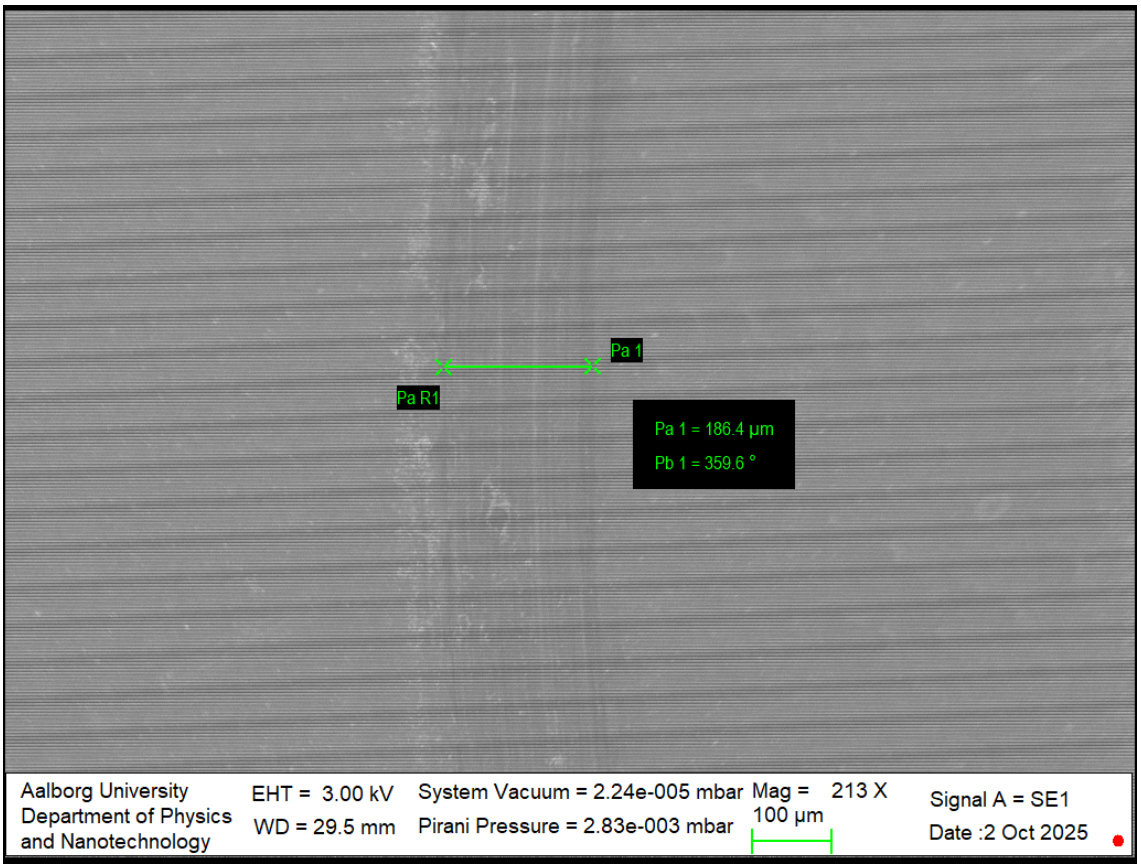

Figure A.104: This image shows a stainless steel sample. This image shows the wear track done on the sample by the TRB3 tribometer when equipped with a load of 2 N and during 100 cycles.

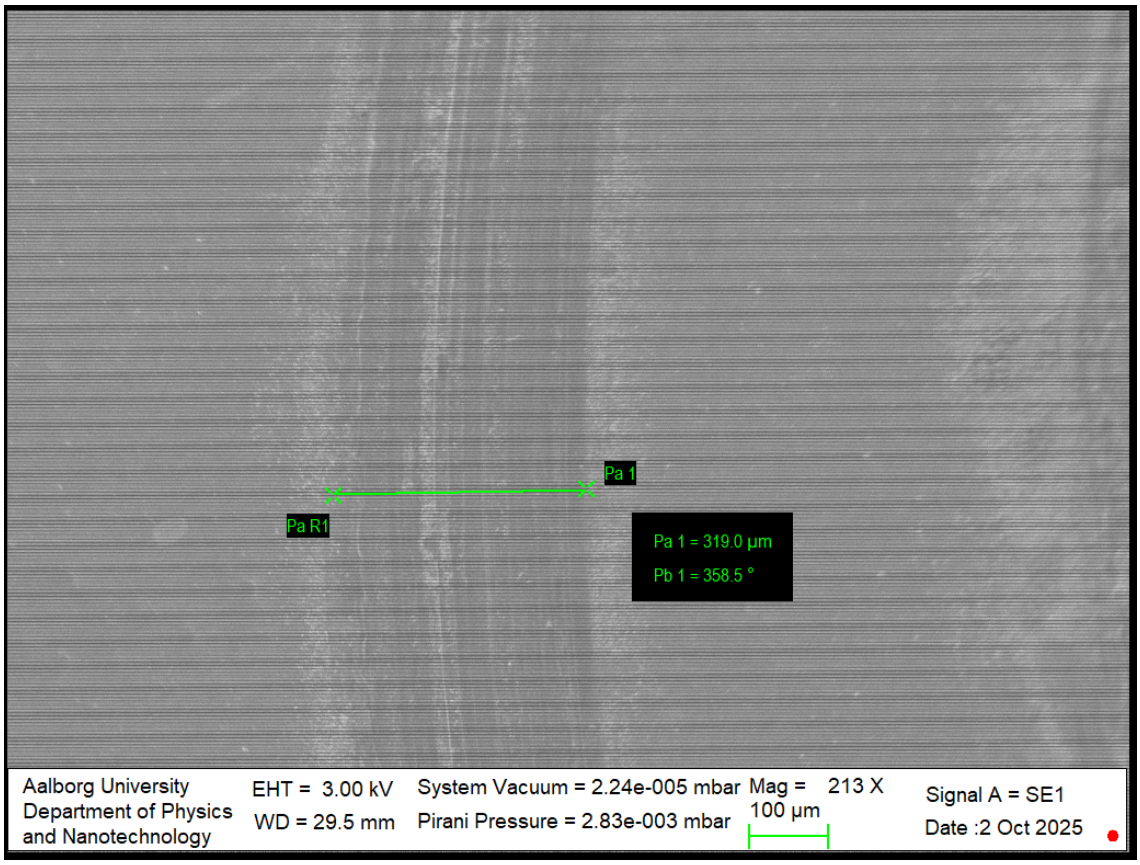

Figure A.105: This image shows a stainless steel sample. This image shows the wear track done on the sample by the TRB3 tribometer when equipped with a load of 2 N and during 250 cycles.

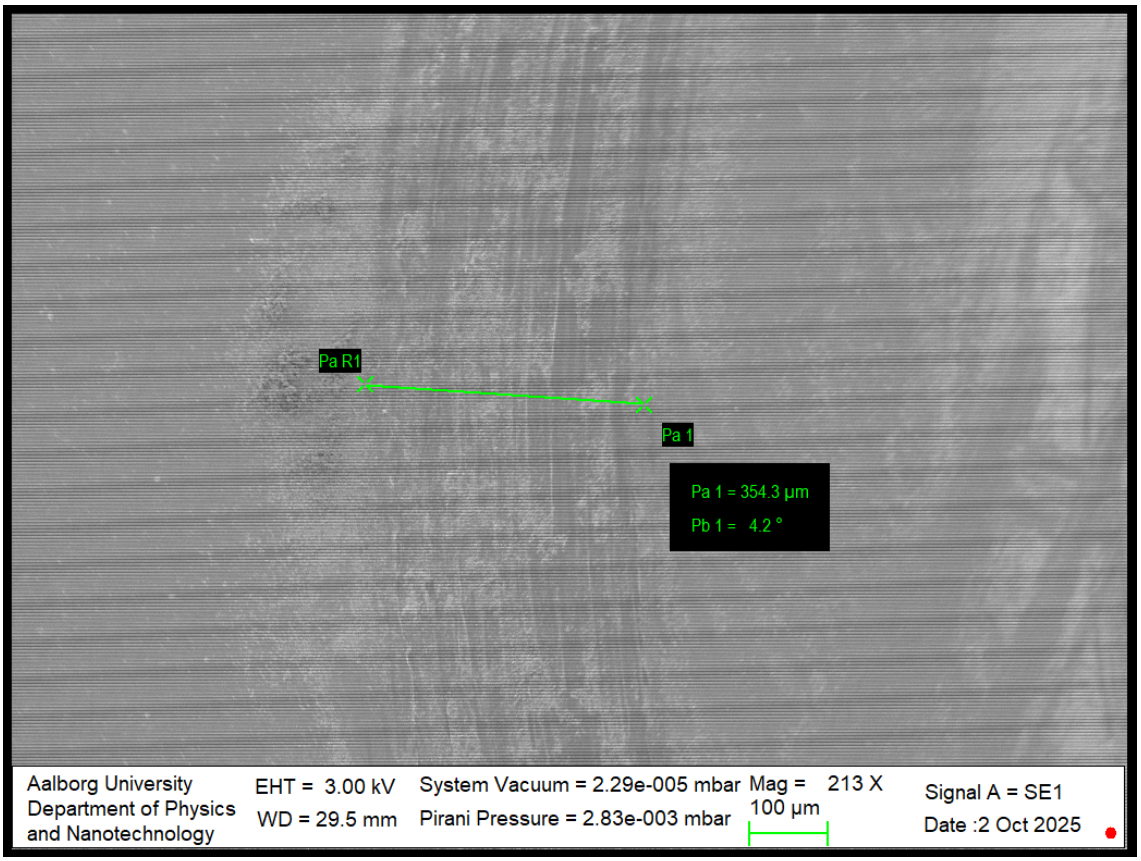

Figure A.106: This image shows a stainless steel sample. This image shows the wear track done on the sample by the TRB3 tribometer when equipped with a load of 2 N and during 350 cycles.

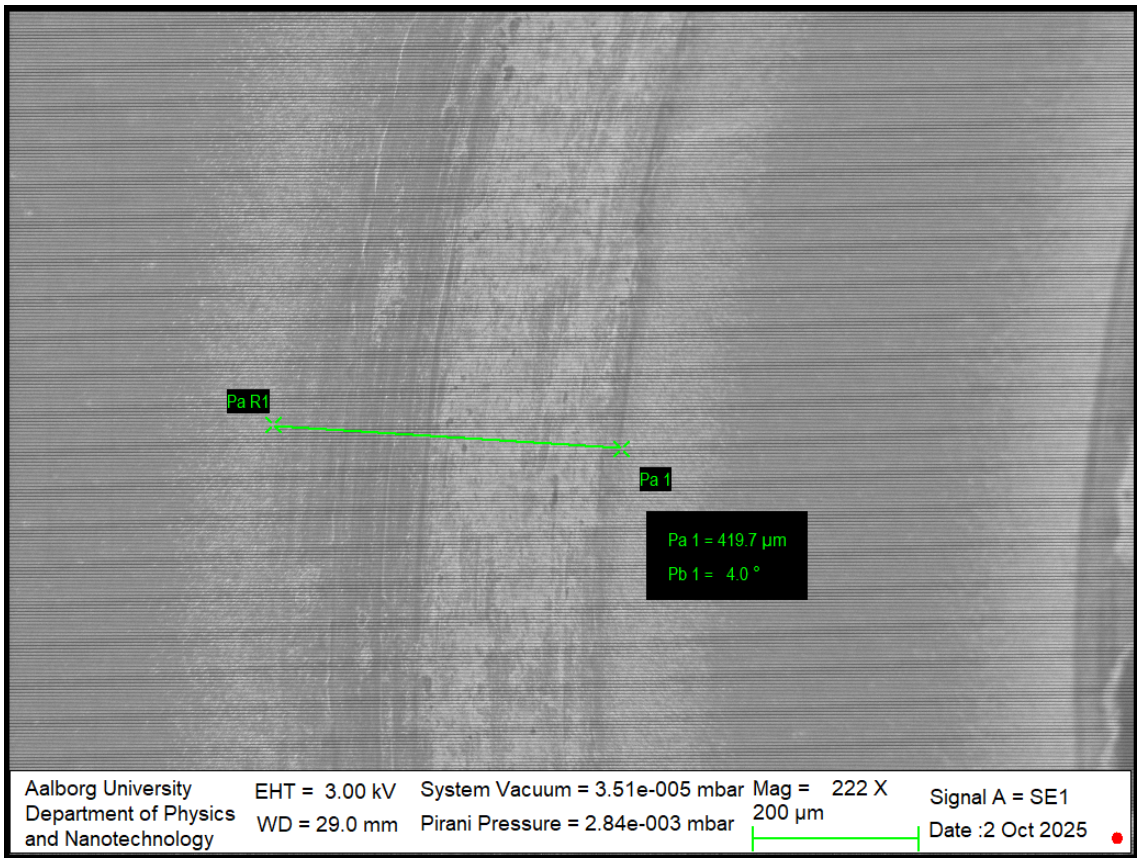

Figure A.107: This image shows a stainless steel sample. This image shows the wear track done on the sample by the TRB3 tribometer when equipped with a load of 2 N and during 500 cycles.

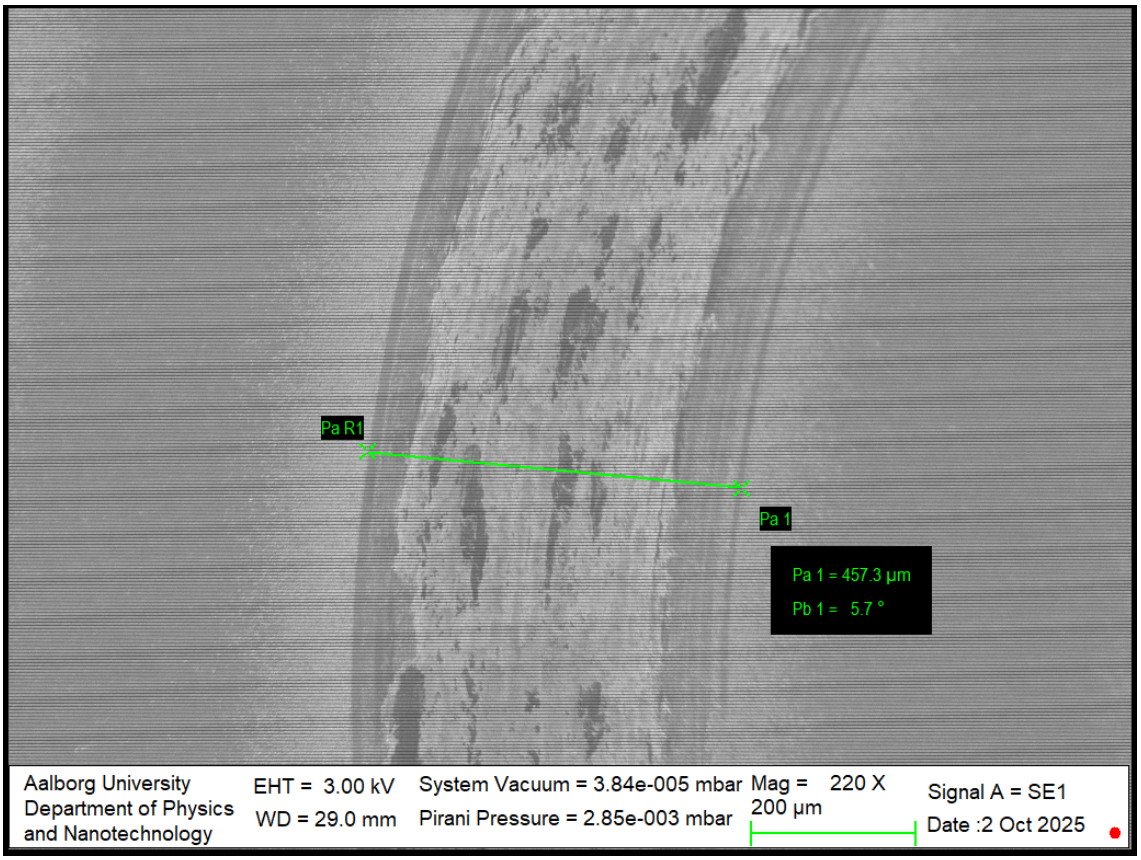

Figure A.108: This image shows a stainless steel sample. This image shows the wear track done on the sample by the TRB3 tribometer when equipped with a load of 2 N and during 1000 cycles.

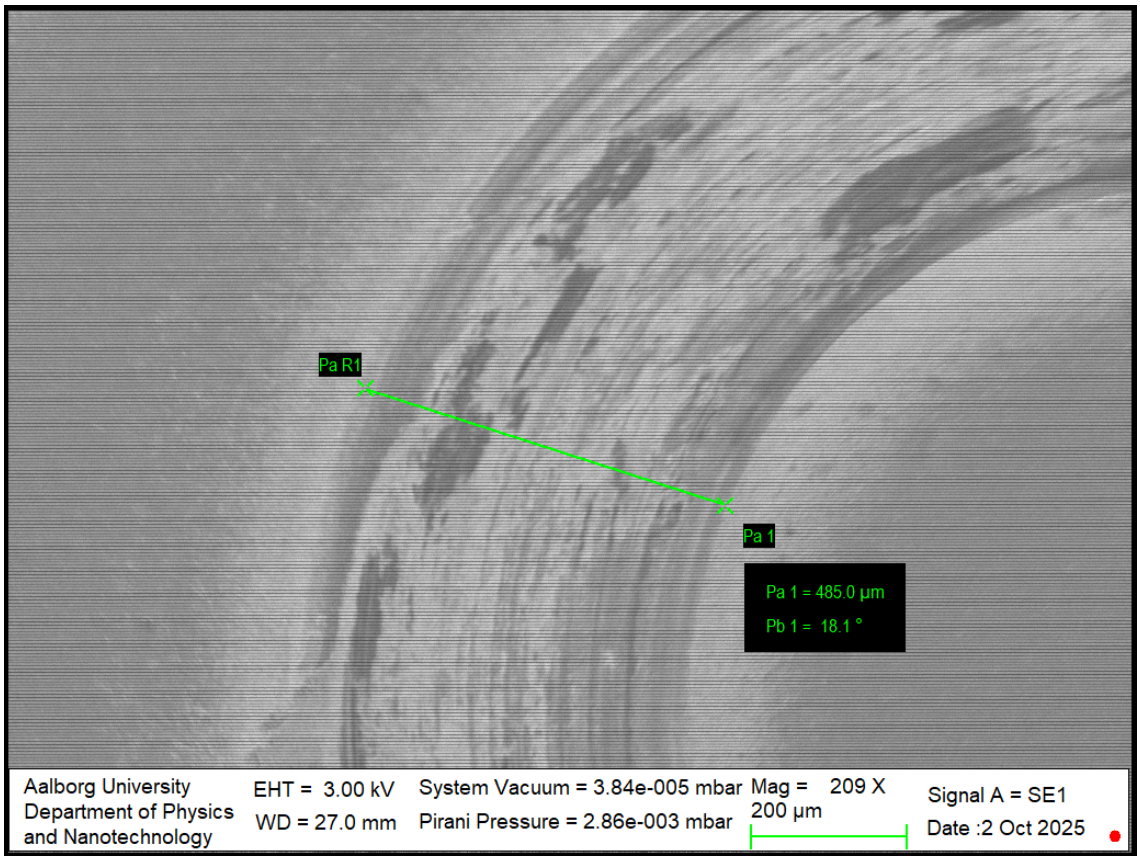

Figure A.109: This image shows a stainless steel sample. This image shows the wear track done on the sample by the TRB3 tribometer when equipped with a load of 2 N and during 2000 cycles.

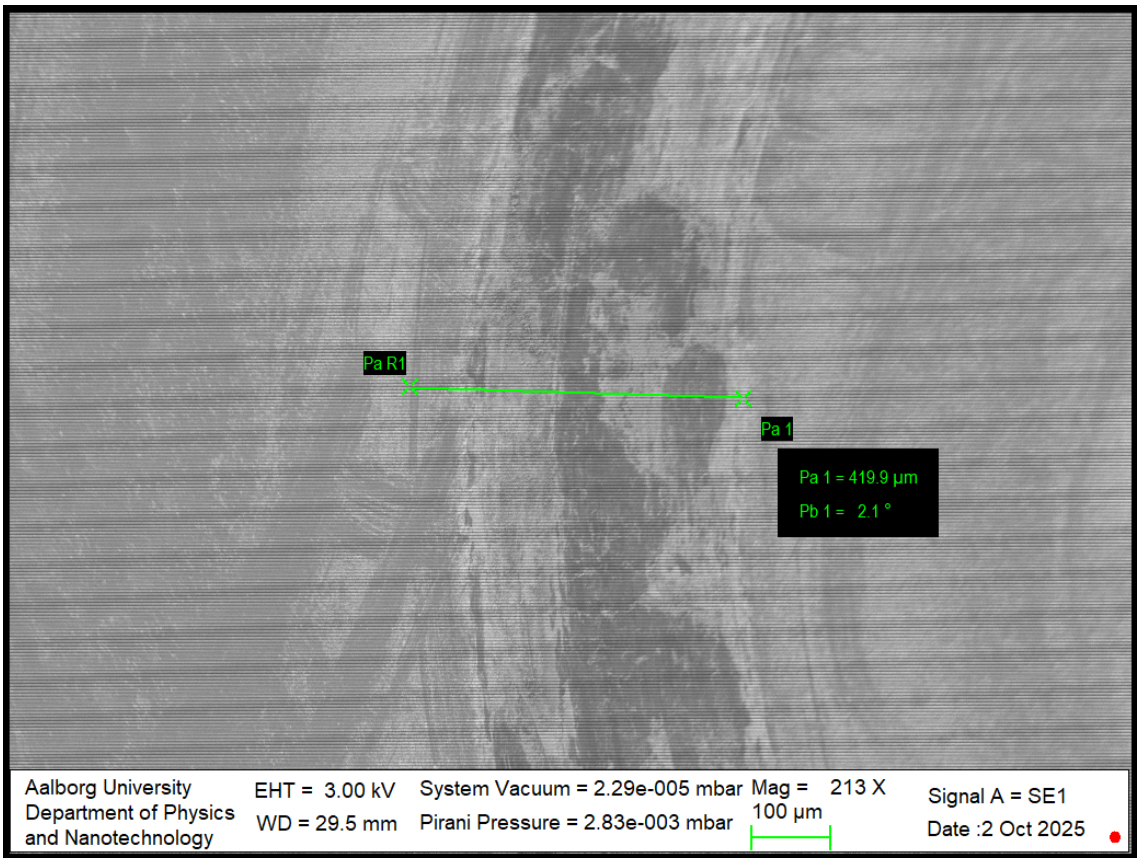

Figure A.110: This image shows a stainless steel sample. This image shows the wear track done on the sample by the TRB3 tribometer when equipped with a load of 2 N and during 3000 cycles.

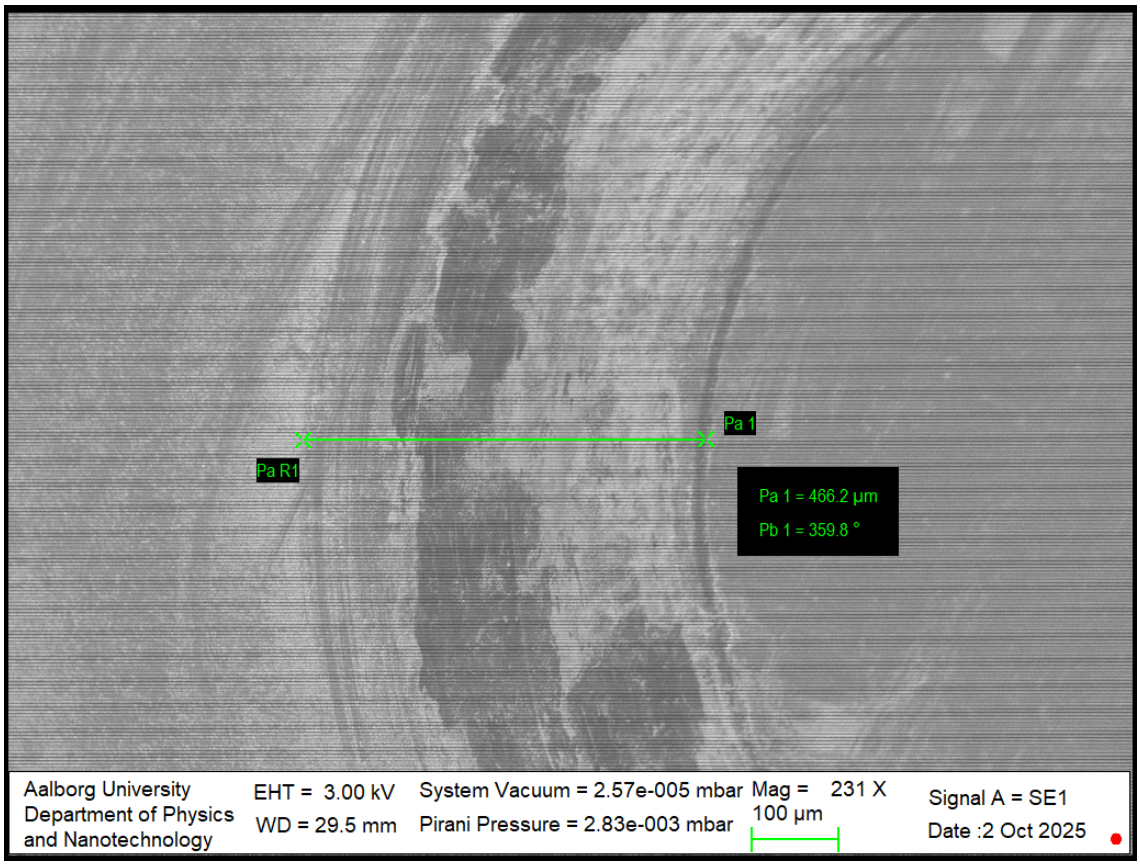

Figure A.111: This image shows a stainless steel sample. This image shows the wear track done on the sample by the TRB3 tribometer when equipped with a load of 2 N and during 5000 cycles.

A.3.4 SEM Images of Wear Tracks on Stainless Steel Sample at 5 N

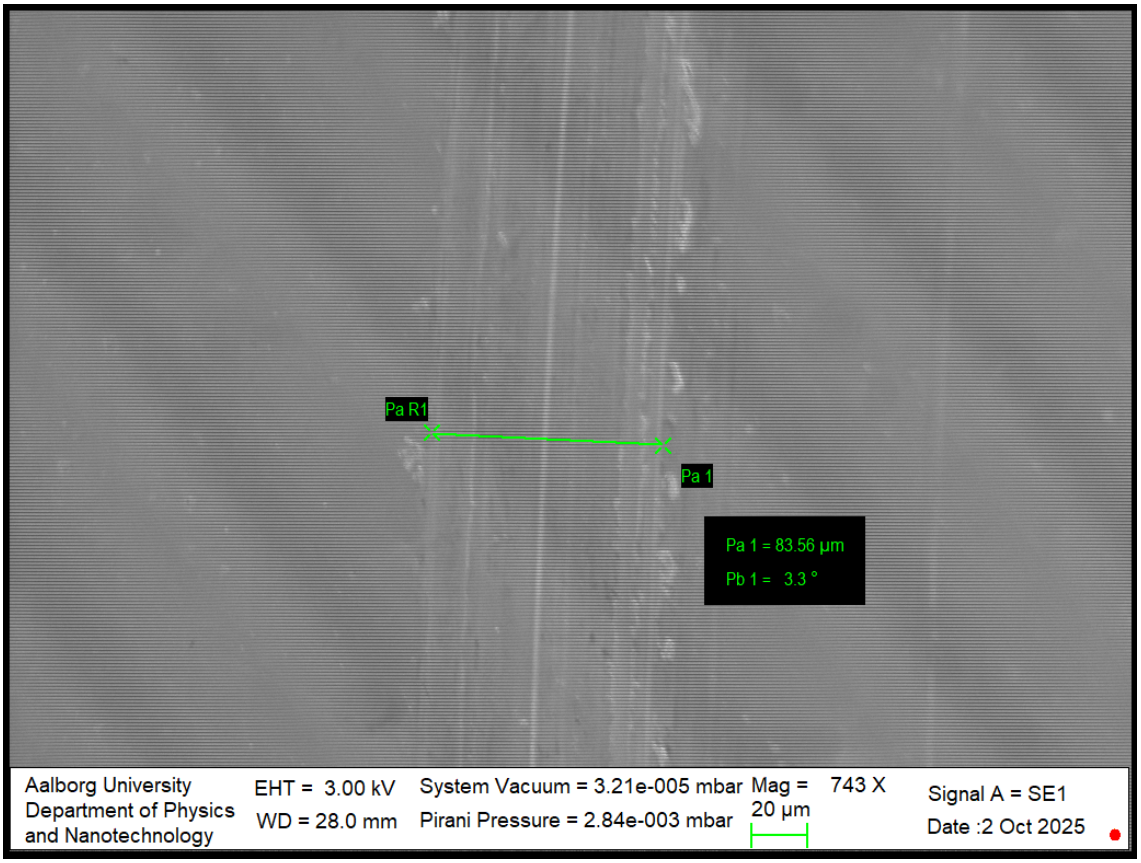

Figure A.112: This image shows a stainless steel sample. This image shows the wear track done on the sample by the TRB3 tribometer when equipped with a load of 5 N and during 1 cycle.

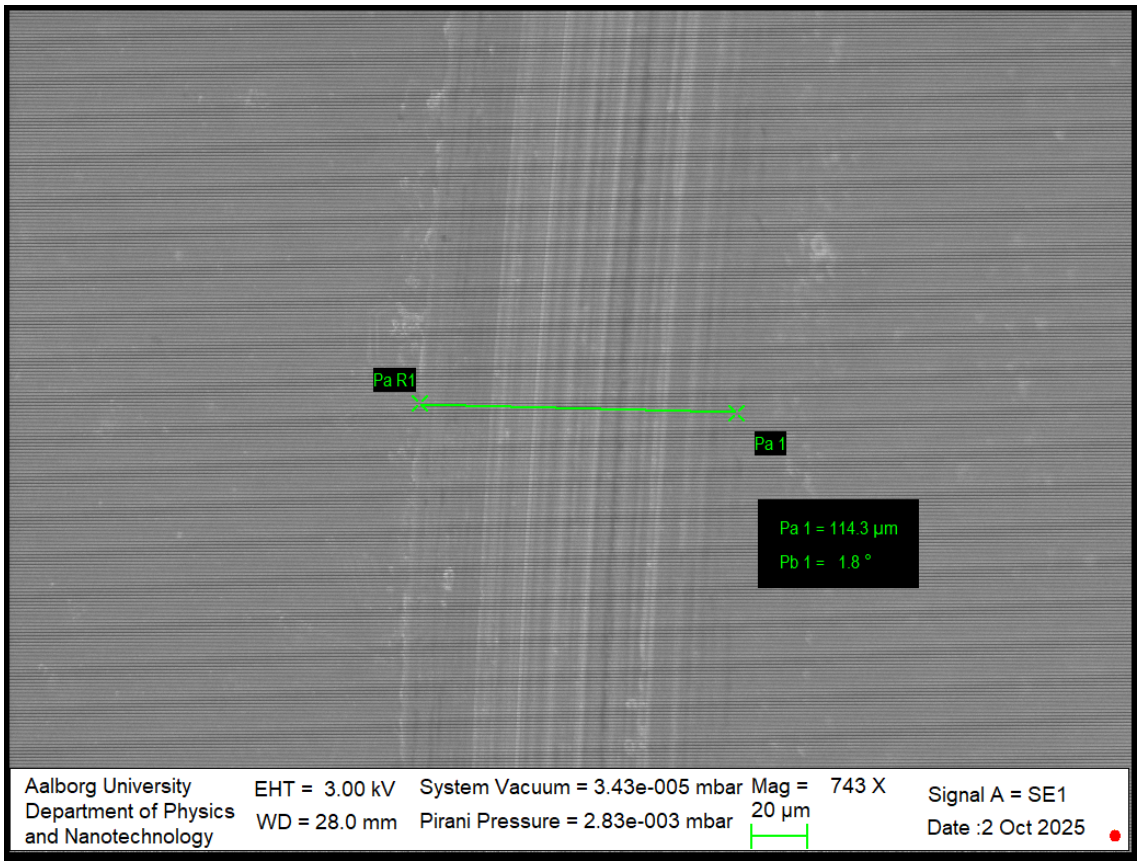

Figure A.113: This image shows a stainless steel sample. This image shows the wear track done on the sample by the TRB3 tribometer when equipped with a load of 5 N and during 10 cycles.

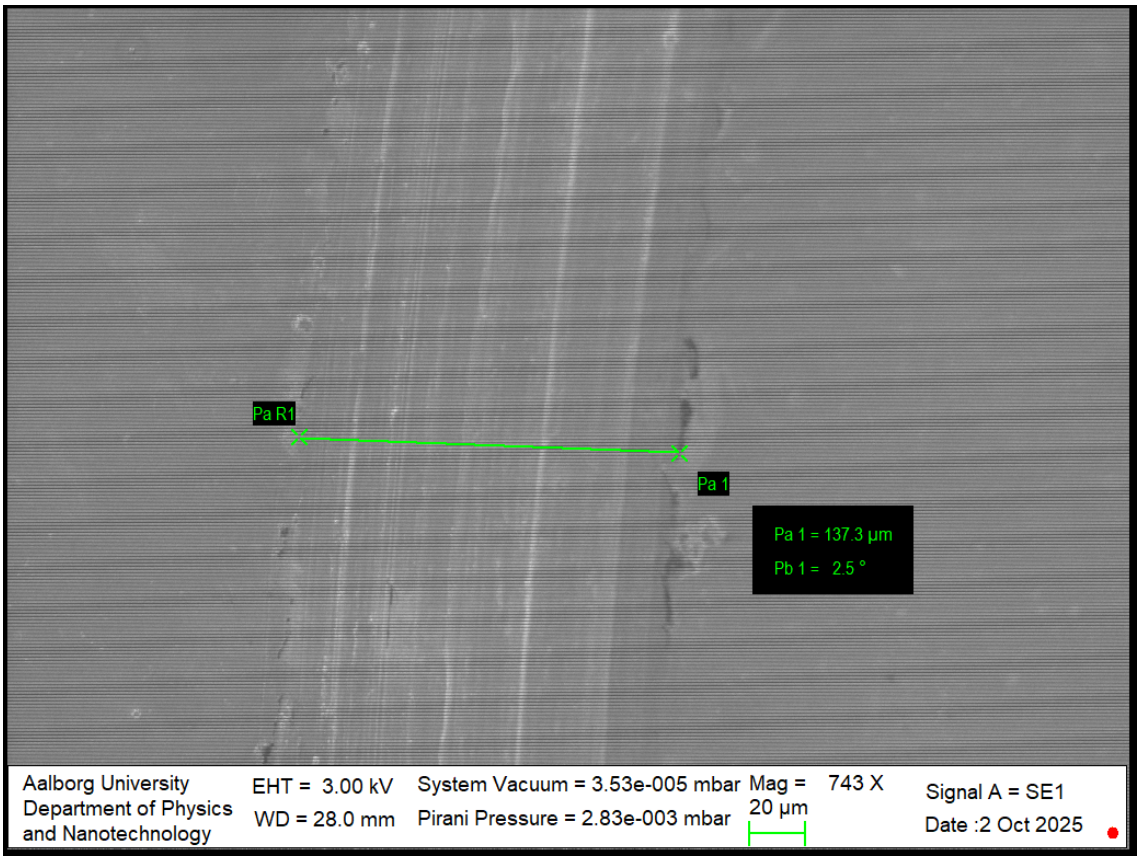

Figure A.114: This image shows a stainless steel sample. This image shows the wear track done on the sample by the TRB3 tribometer when equipped with a load of 5 N and during 50 cycles.

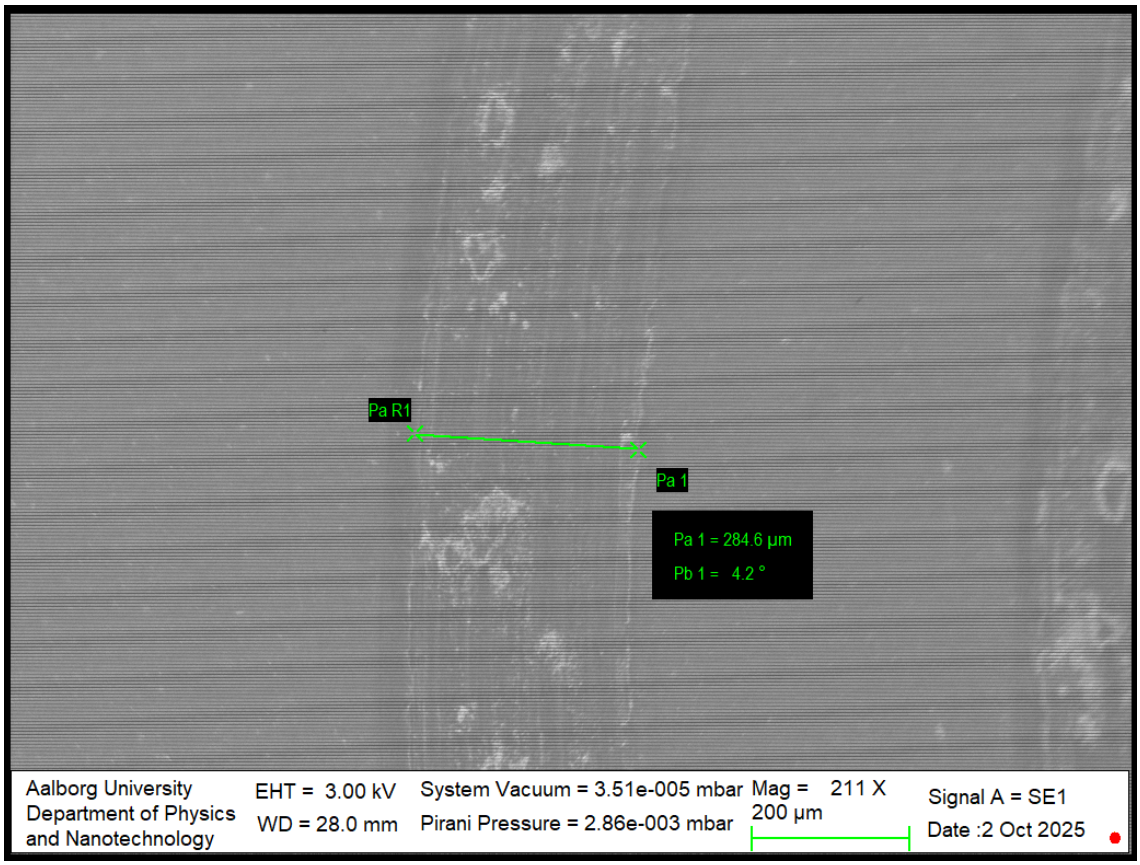

Figure A.115: This image shows a stainless steel sample. This image shows the wear track done on the sample by the TRB3 tribometer when equipped with a load of 5 N and during 100 cycles.

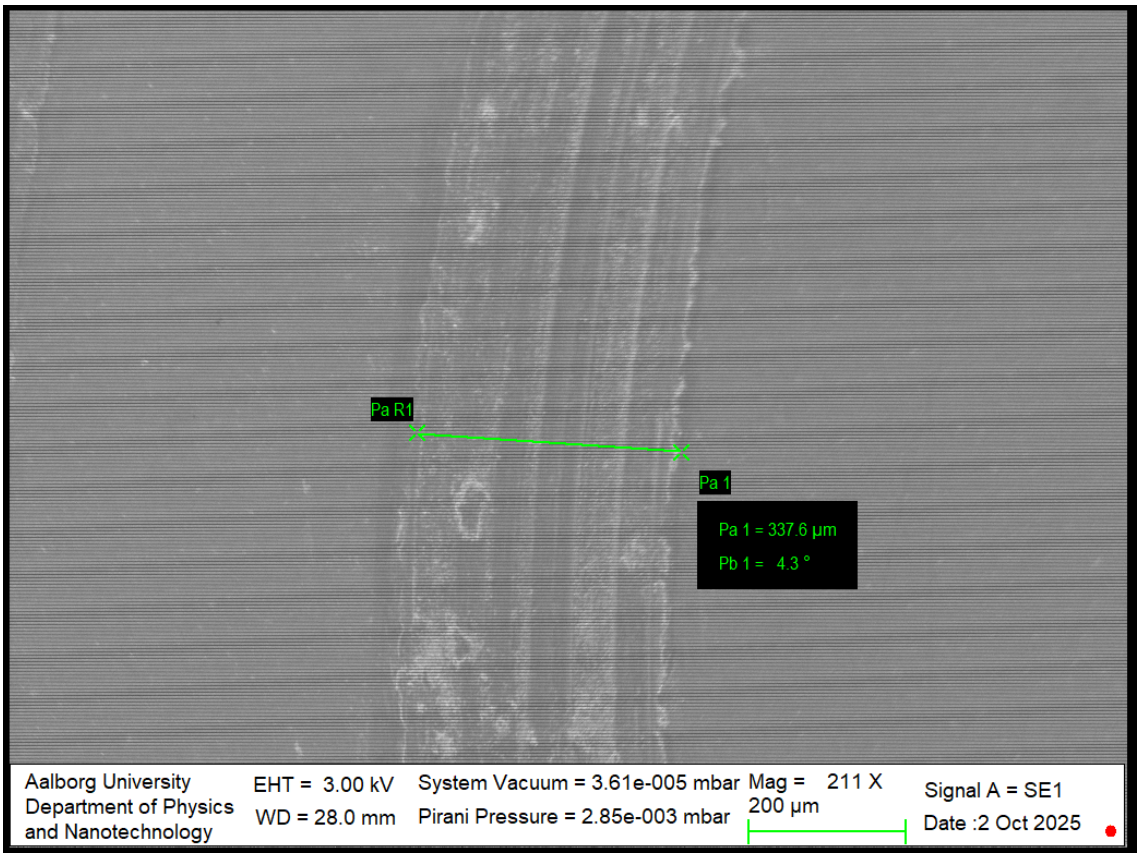

Figure A.116: This image shows a stainless steel sample. This image shows the wear track done on the sample by the TRB3 tribometer when equipped with a load of 5 N and during 250 cycles.

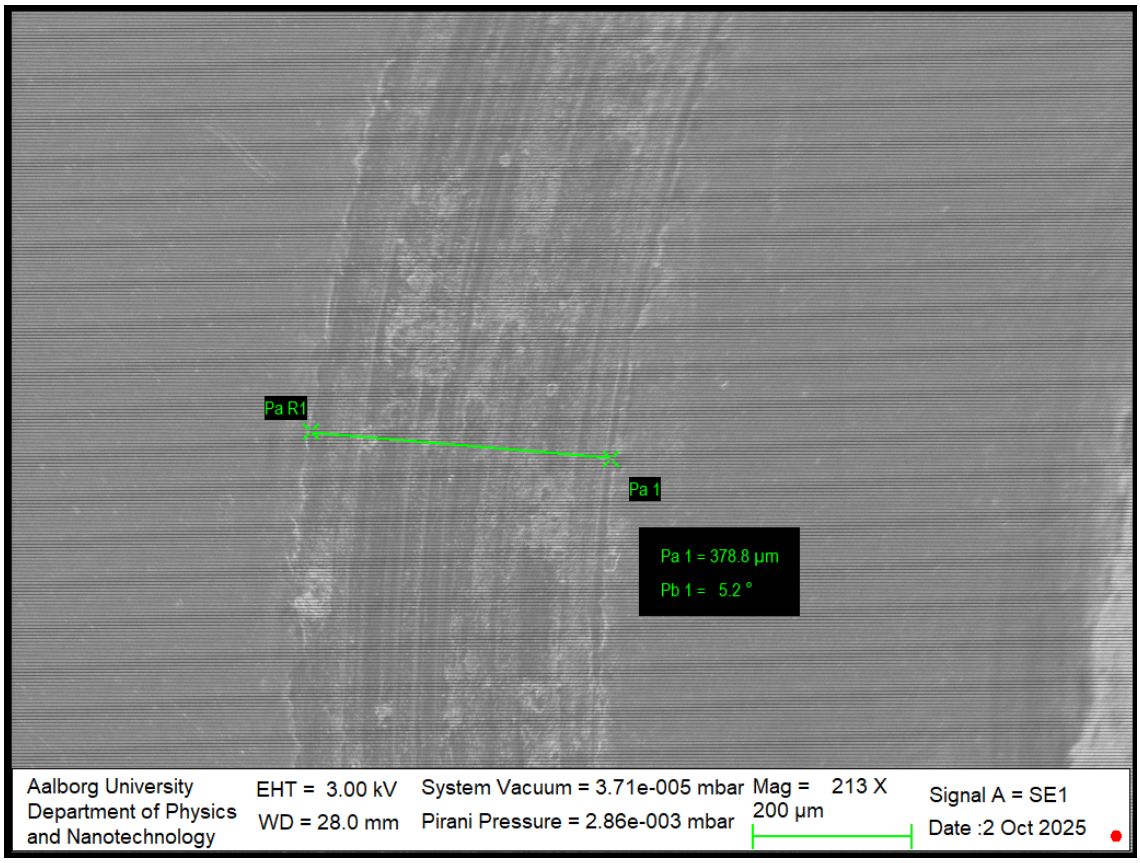

Figure A.117: This image shows a stainless steel sample. This image shows the wear track done on the sample by the TRB3 tribometer when equipped with a load of 5 N and during 350 cycles.

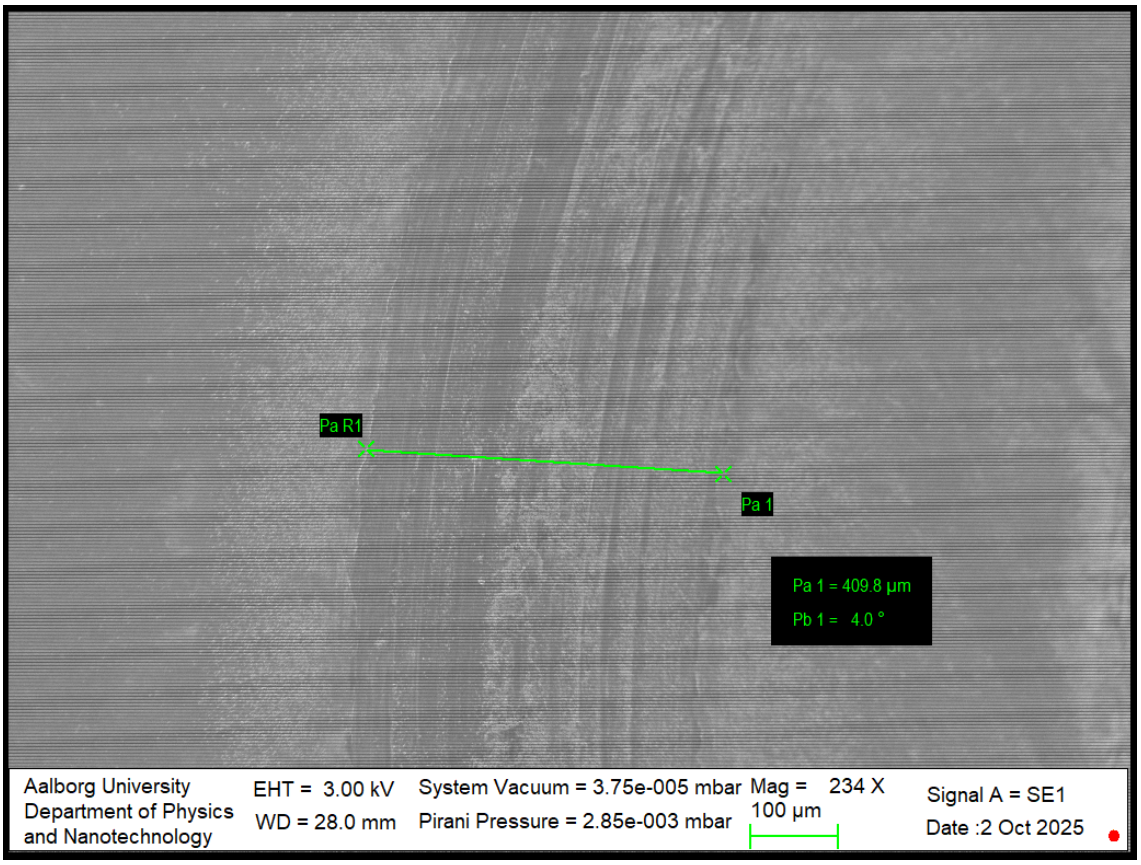

Figure A.118: This image shows a stainless steel sample. This image shows the wear track done on the sample by the TRB3 tribometer when equipped with a load of 5 N and during 500 cycles.

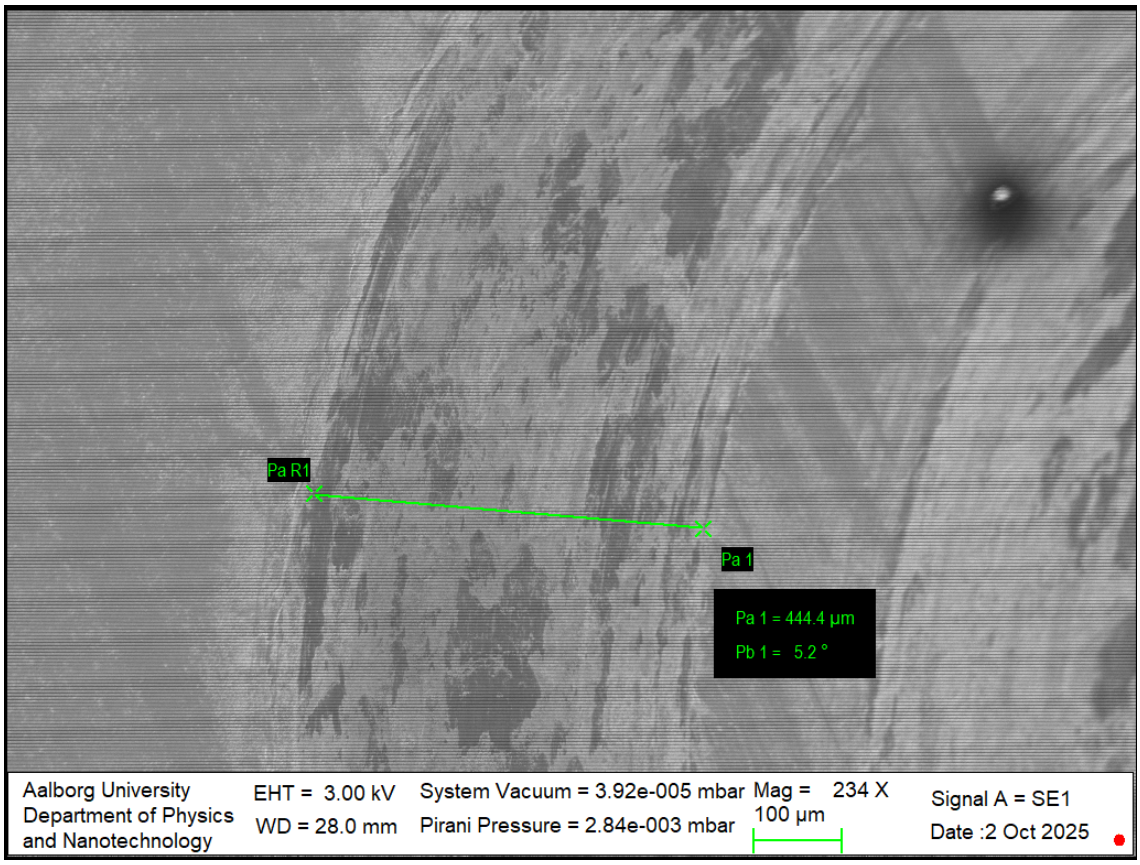

Figure A.119: This image shows a stainless steel sample. This image shows the wear track done on the sample by the TRB3 tribometer when equipped with a load of 5 N and during 1000 cycles.

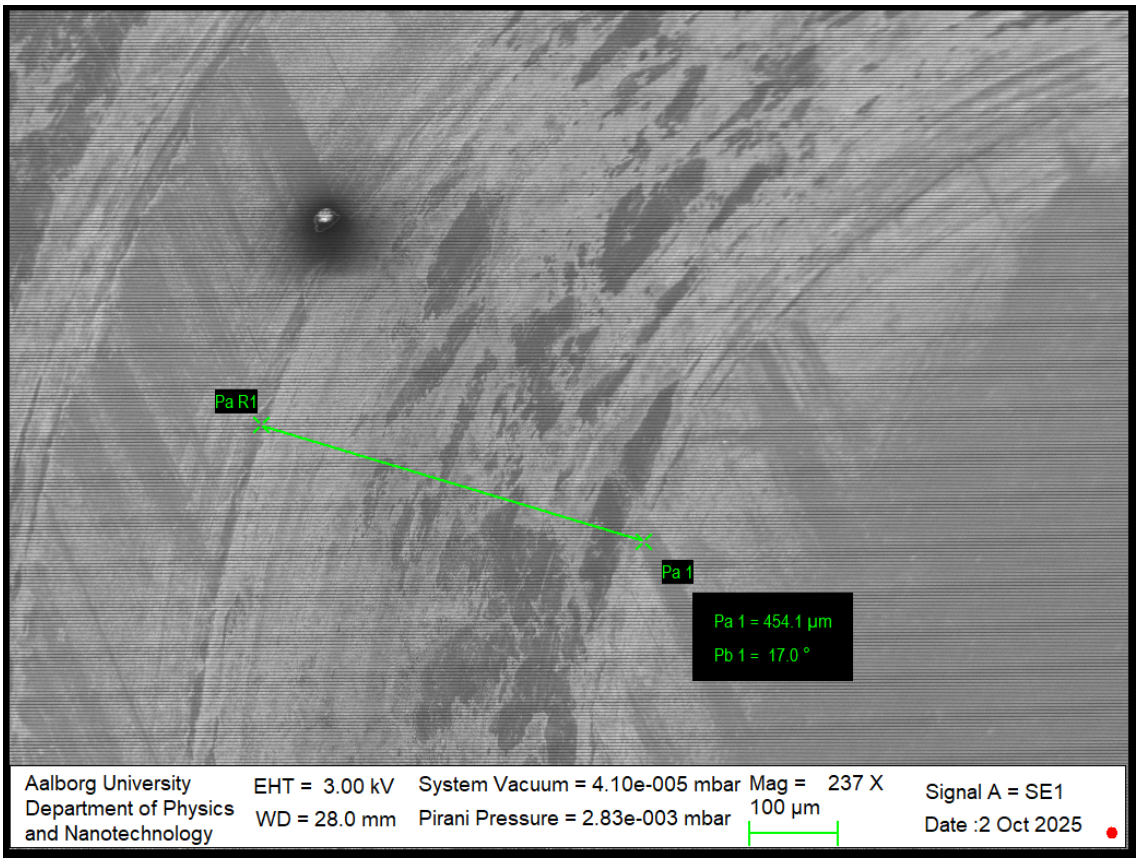

Figure A.120: This image shows a stainless steel sample. This image shows the wear track done on the sample by the TRB3 tribometer when equipped with a load of 5 N and during 2000 cycles.

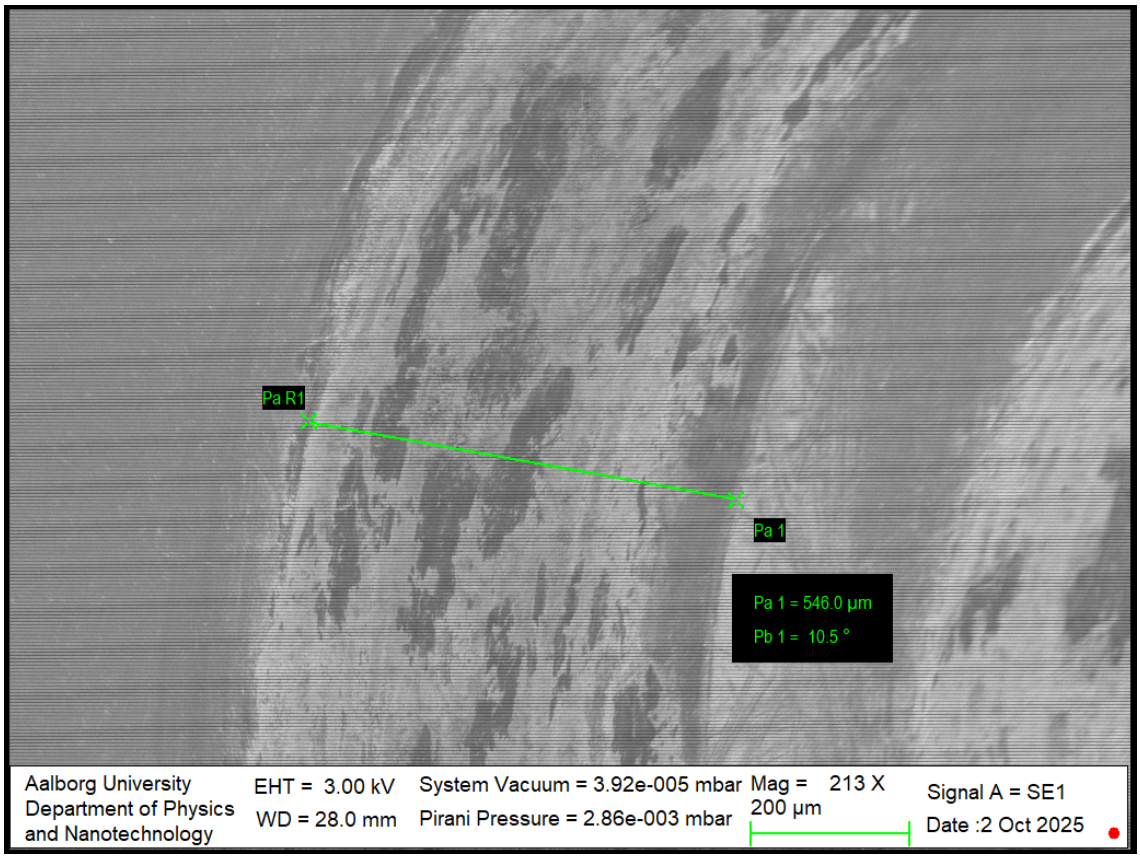

Figure A.121: This image shows a stainless steel sample. This image shows the wear track done on the sample by the TRB3 tribometer when equipped with a load of 5 N and during 3000 cycles.

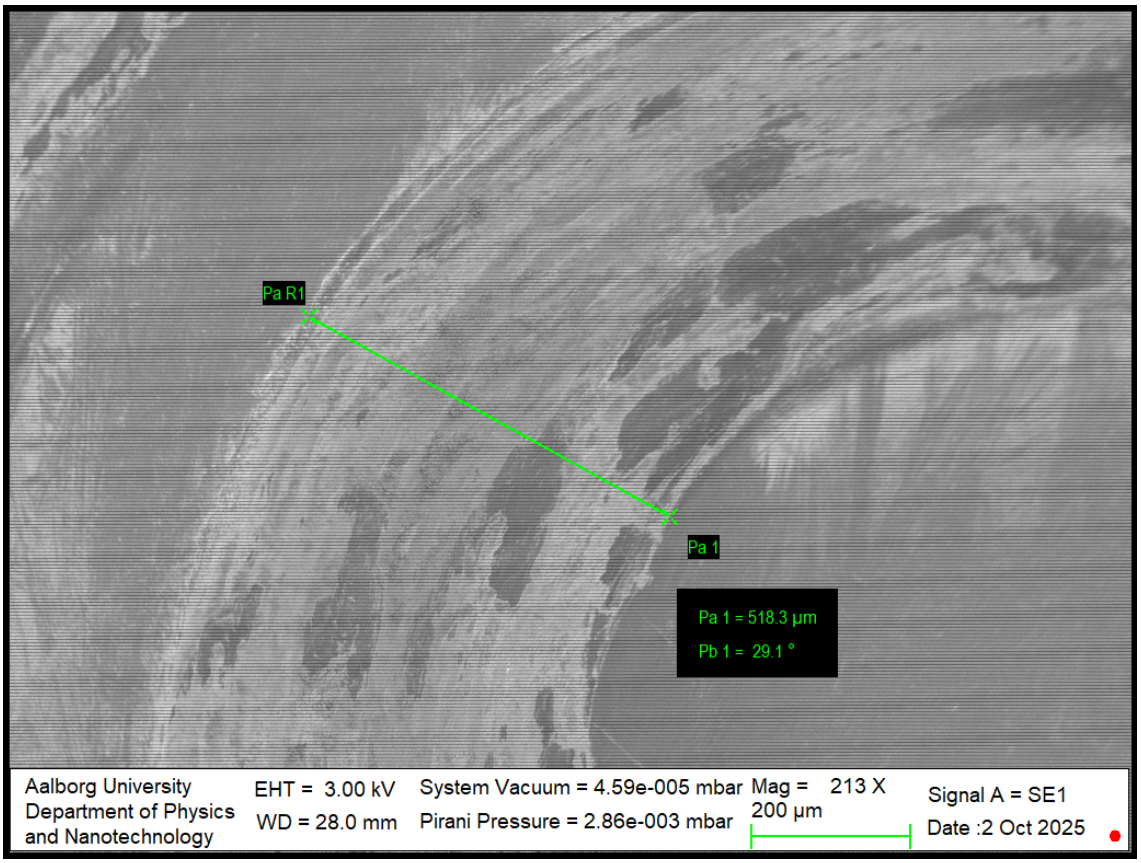

Figure A.122: This image shows a stainless steel sample. This image shows the wear track done on the sample by the TRB3 tribometer when equipped with a load of 5 N and during 5000 cycles.

A.3.5 SEM Images of Wear Tracks on Stainless Steel Sample at 10 N

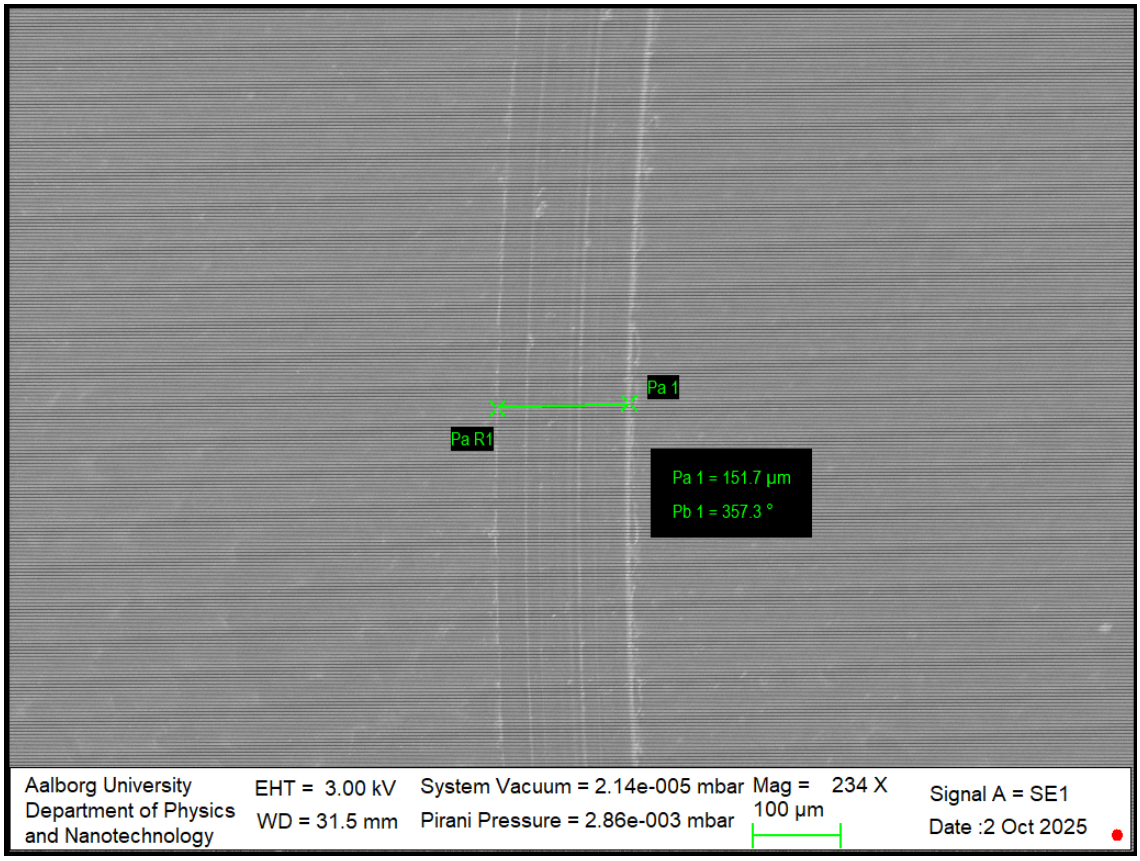

Figure A.123: This image shows a stainless steel sample. This image shows the wear track done on the sample by the TRB3 tribometer when equipped with a load of 10 N and during 1 cycle.

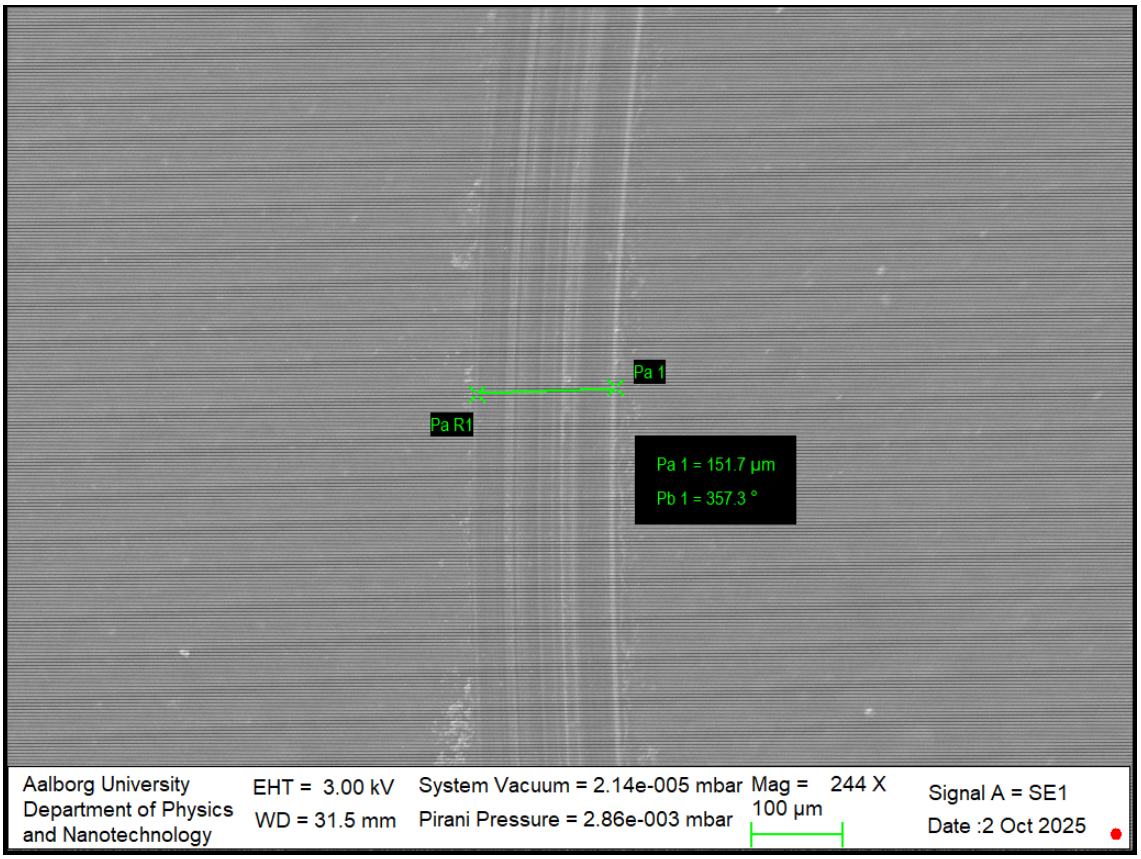

Figure A.124: This image shows a stainless steel sample. This image shows the wear track done on the sample by the TRB3 tribometer when equipped with a load of 10 N and during 10 cycles.

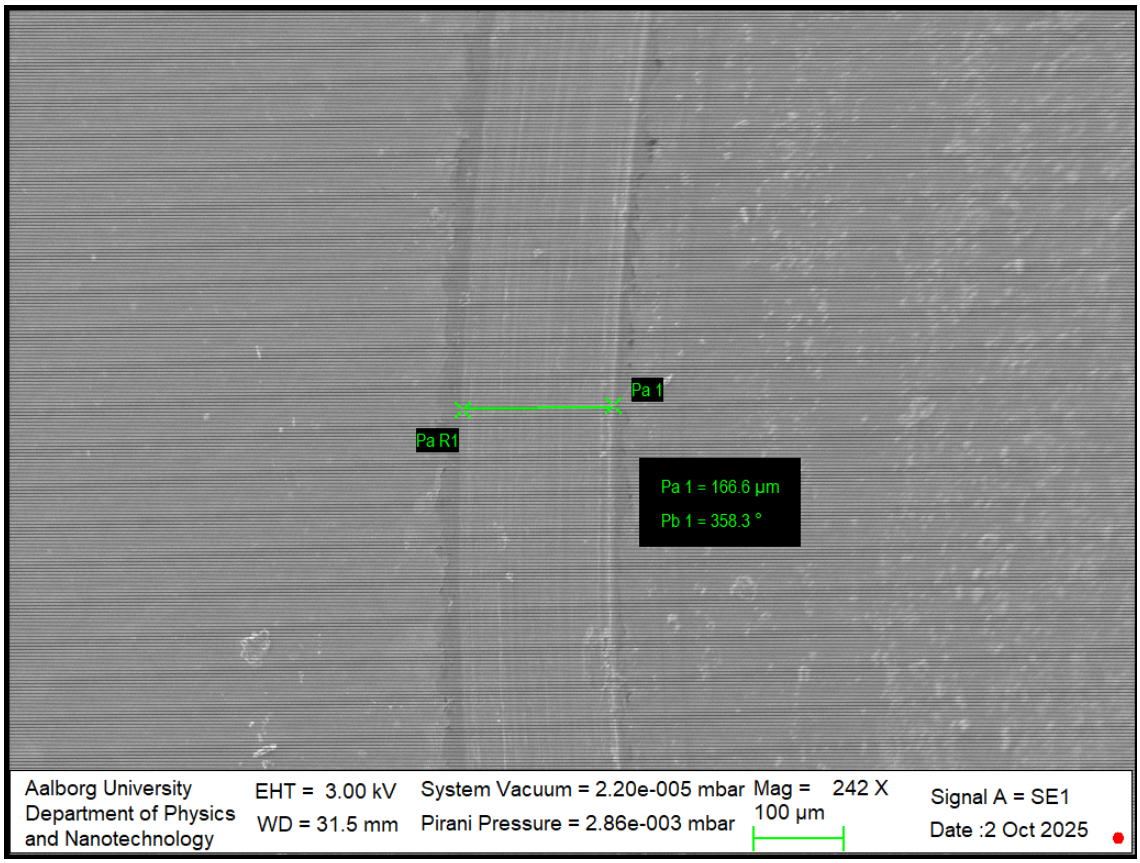

Figure A.125: This image shows a stainless steel sample. This image shows the wear track done on the sample by the TRB3 tribometer when equipped with a load of 10 N and during 50 cycles.

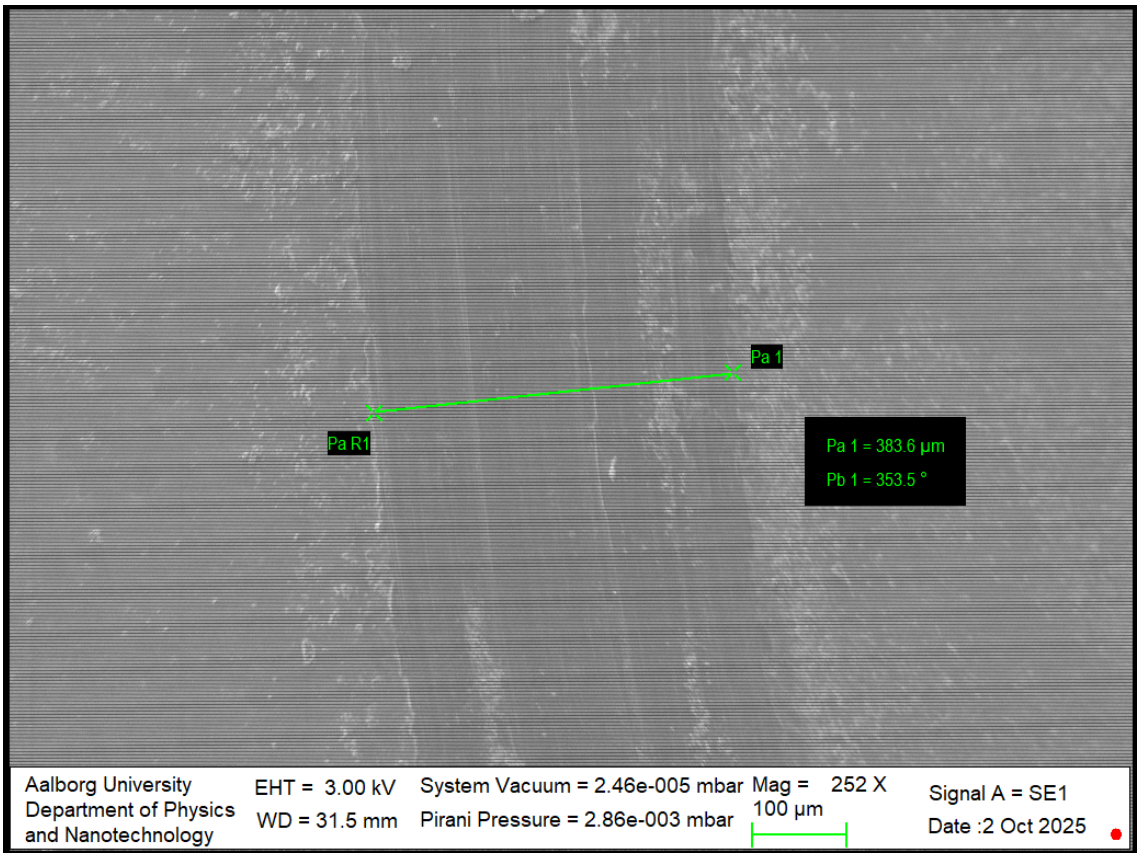

Figure A.126: This image shows a stainless steel sample. This image shows the wear track done on the sample by the TRB3 tribometer when equipped with a load of 10 N and during 100 cycles.

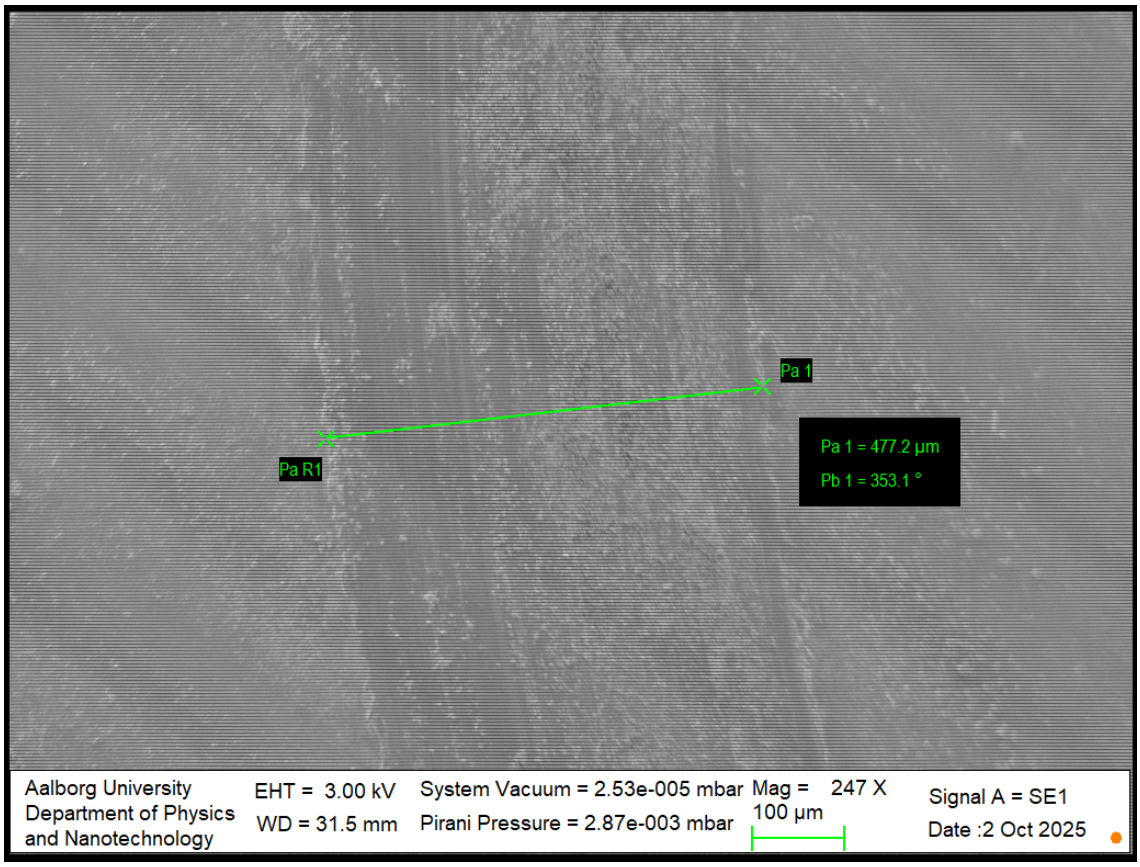

Figure A.127: This image shows a stainless steel sample. This image shows the wear track done on the sample by the TRB3 tribometer when equipped with a load of 10 N and during 250 cycles.

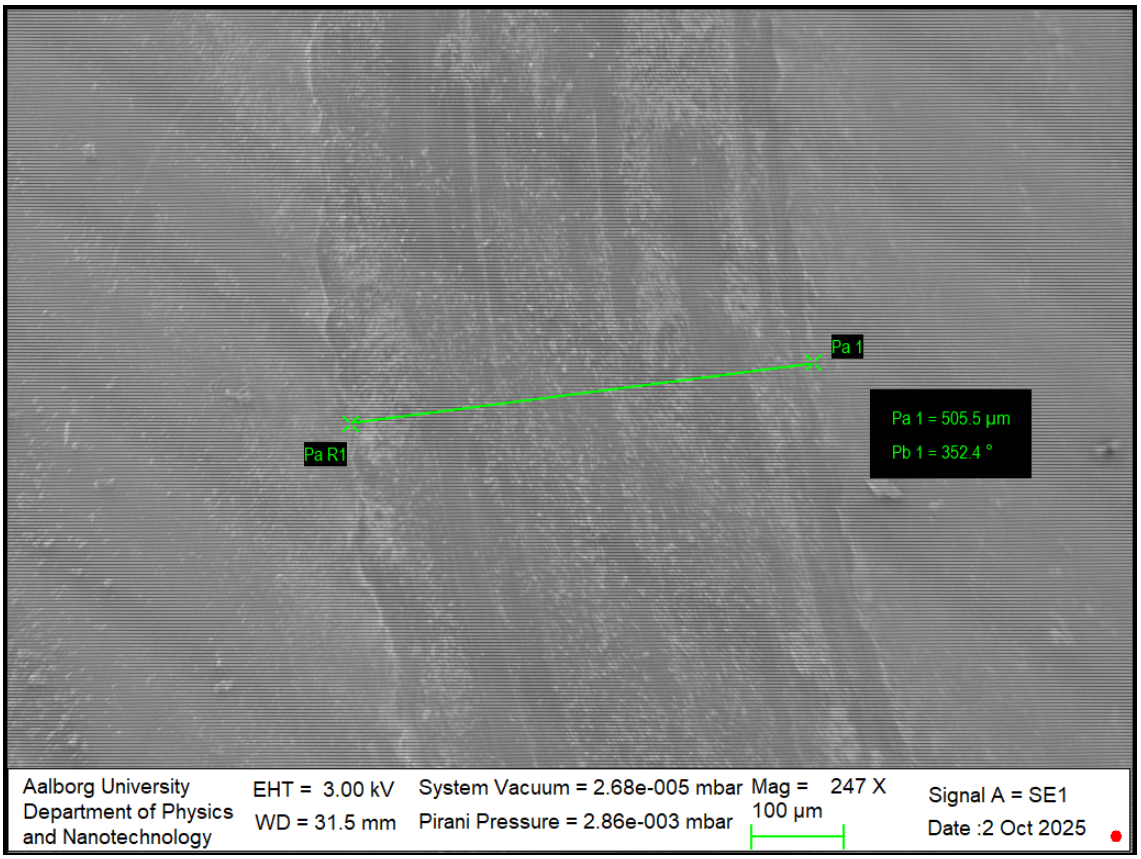

Figure A.128: This image shows a stainless steel sample. This image shows the wear track done on the sample by the TRB3 tribometer when equipped with a load of 10 N and during 350 cycles.

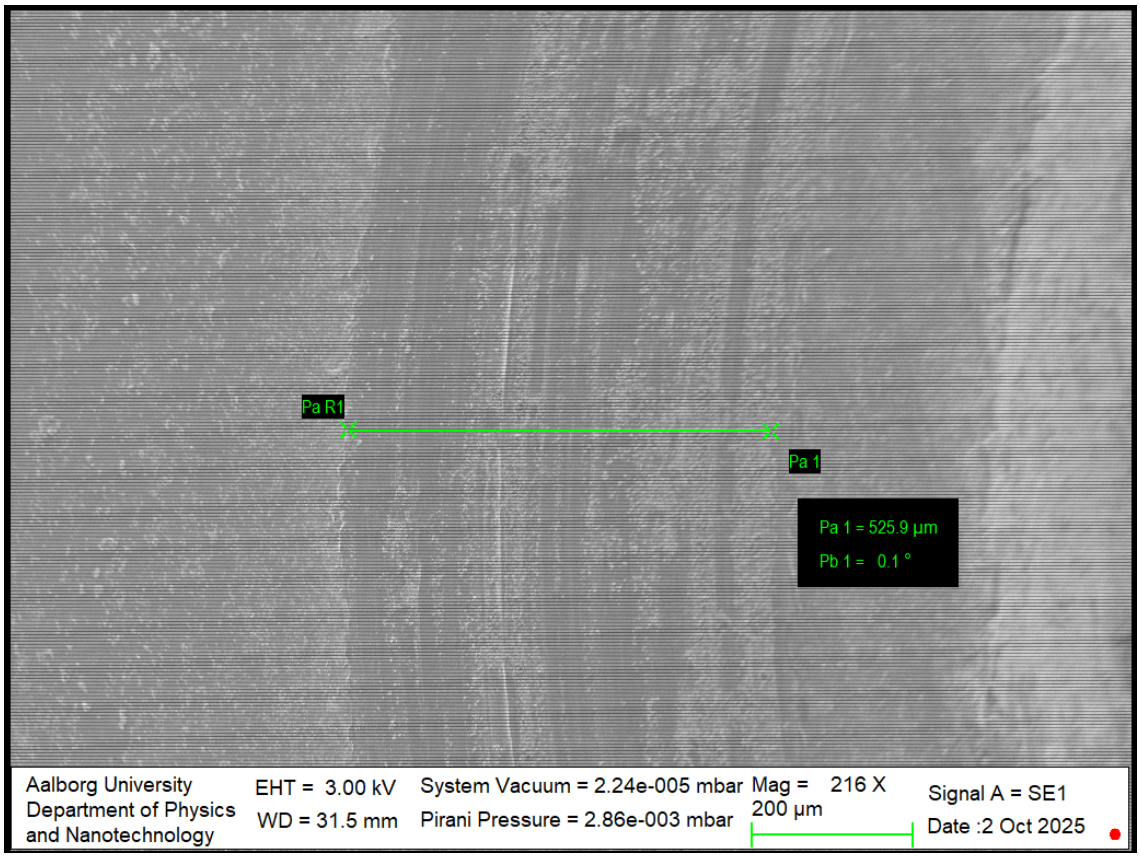

Figure A.129: This image shows a stainless steel sample. This image shows the wear track done on the sample by the TRB3 tribometer when equipped with a load of 10 N and during 500 cycles.

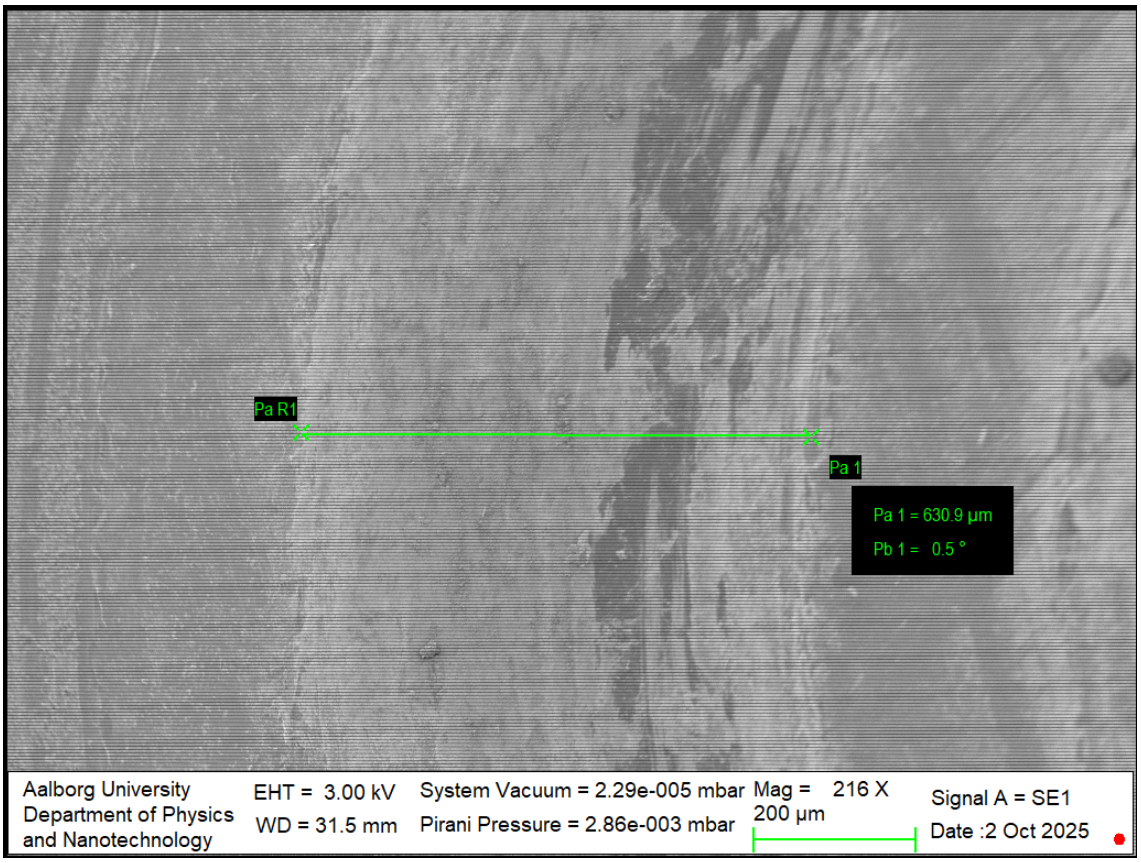

Figure A.130: This image shows a stainless steel sample. This image shows the wear track done on the sample by the TRB3 tribometer when equipped with a load of 10 N and during 1000 cycles.

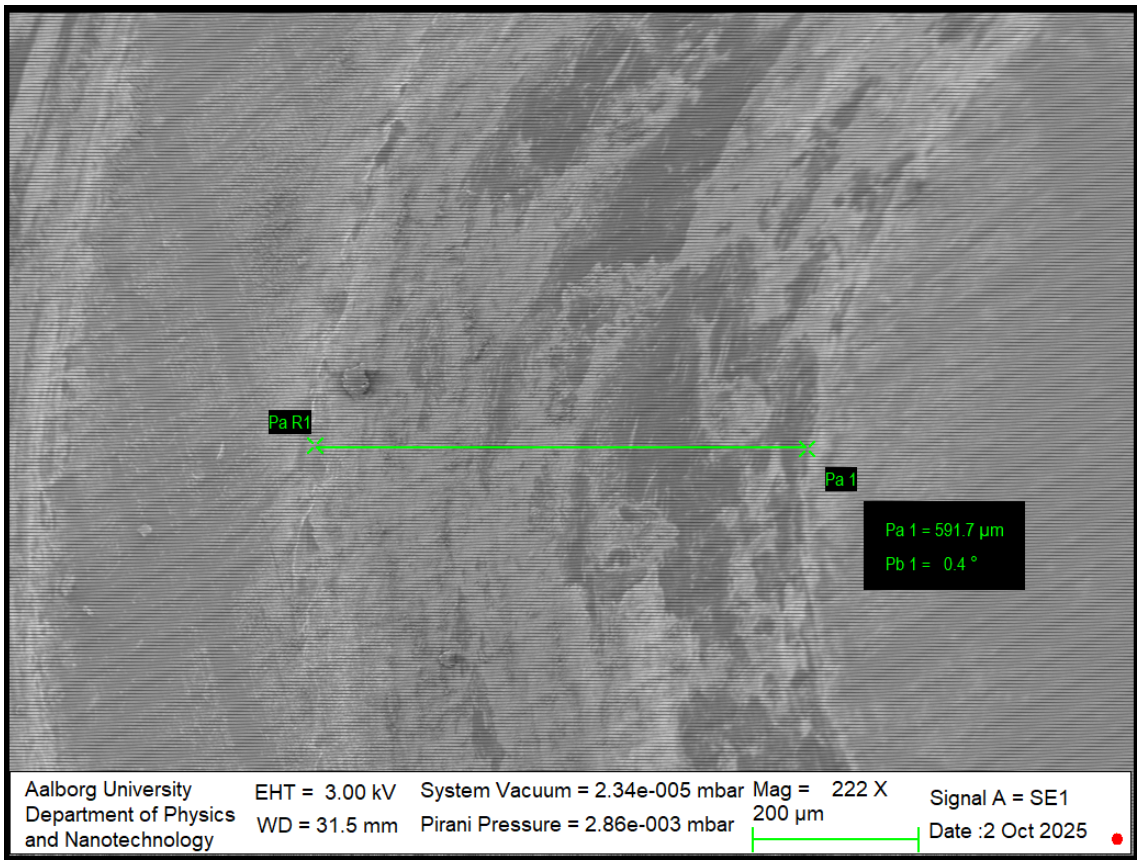

Figure A.131: This image shows a stainless steel sample. This image shows the wear track done on the sample by the TRB3 tribometer when equipped with a load of 10 N and during 2000 cycles.

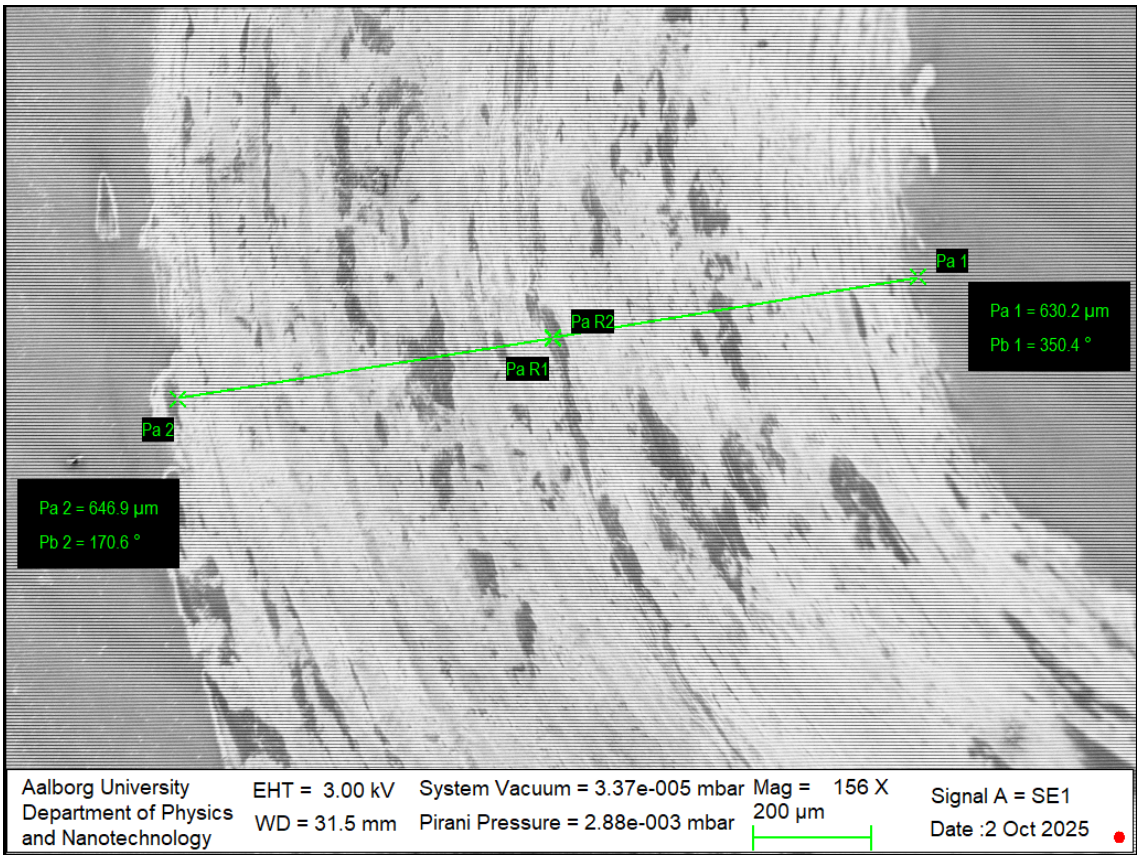

Figure A.132: This image shows a stainless steel sample. This image shows the wear track done on the sample by the TRB3 tribometer when equipped with a load of 10 N and during 5000 and 3000 cycles.

A.4 All SEM Images of Wear Tracks on 1500 nm TiN Coated Sample

A.4.1 SEM Images of Wear Tracks on 1500 nm TiN Coated Sample at 0.25 N

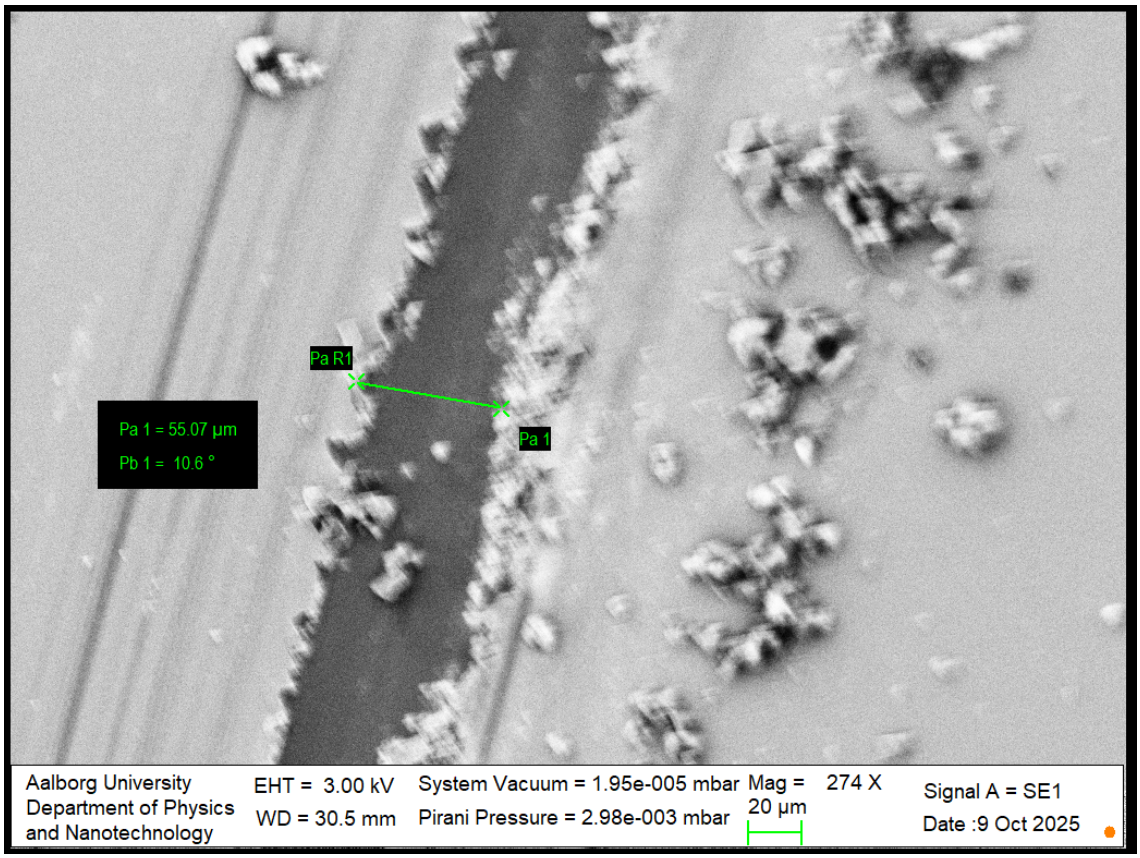

Figure A.133: This image shows a 1500 nm TiN coated stainless steel sample. This image shows the wear track done on the sample by the TRB3 tribometer when equipped with a load of 0.25 N and during 1 cycle.

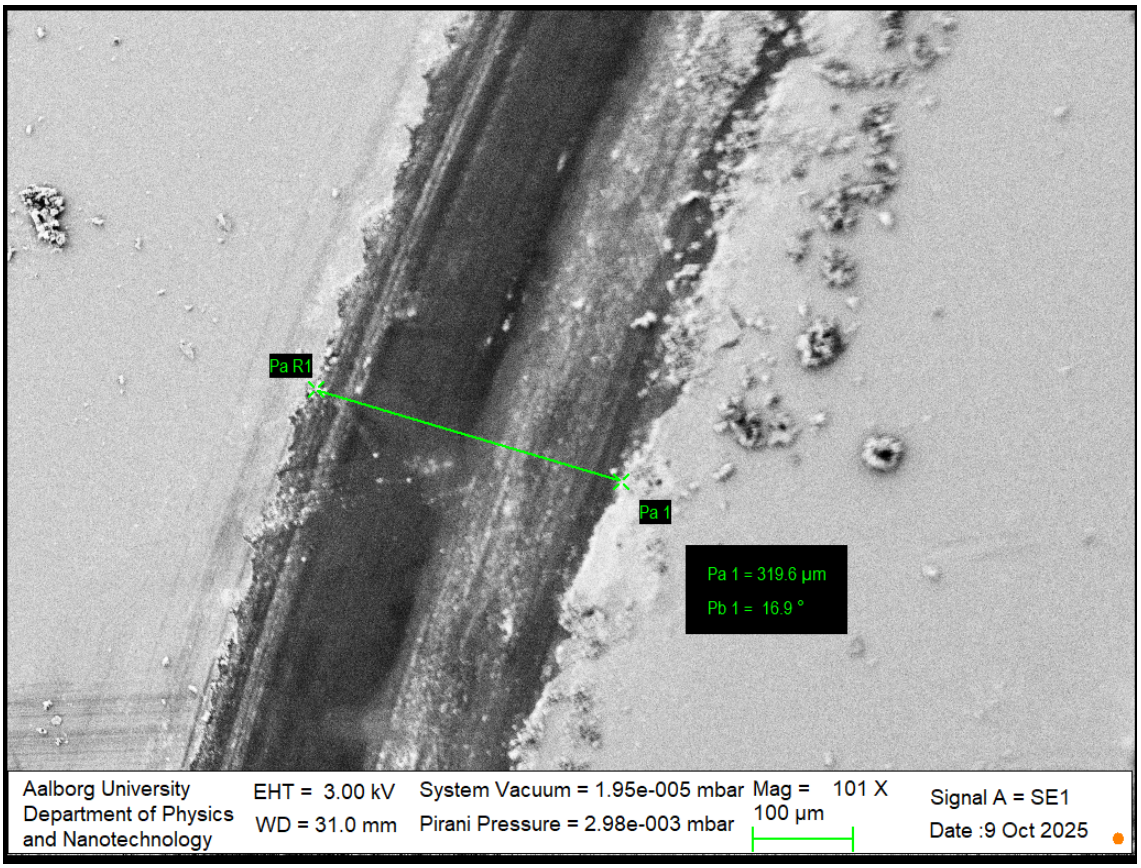

Figure A.134: This image shows a 1500 nm TiN coated stainless steel sample. This image shows the wear track done on the sample by the TRB3 tribometer when equipped with a load of 0.25 N and during 10 cycles.

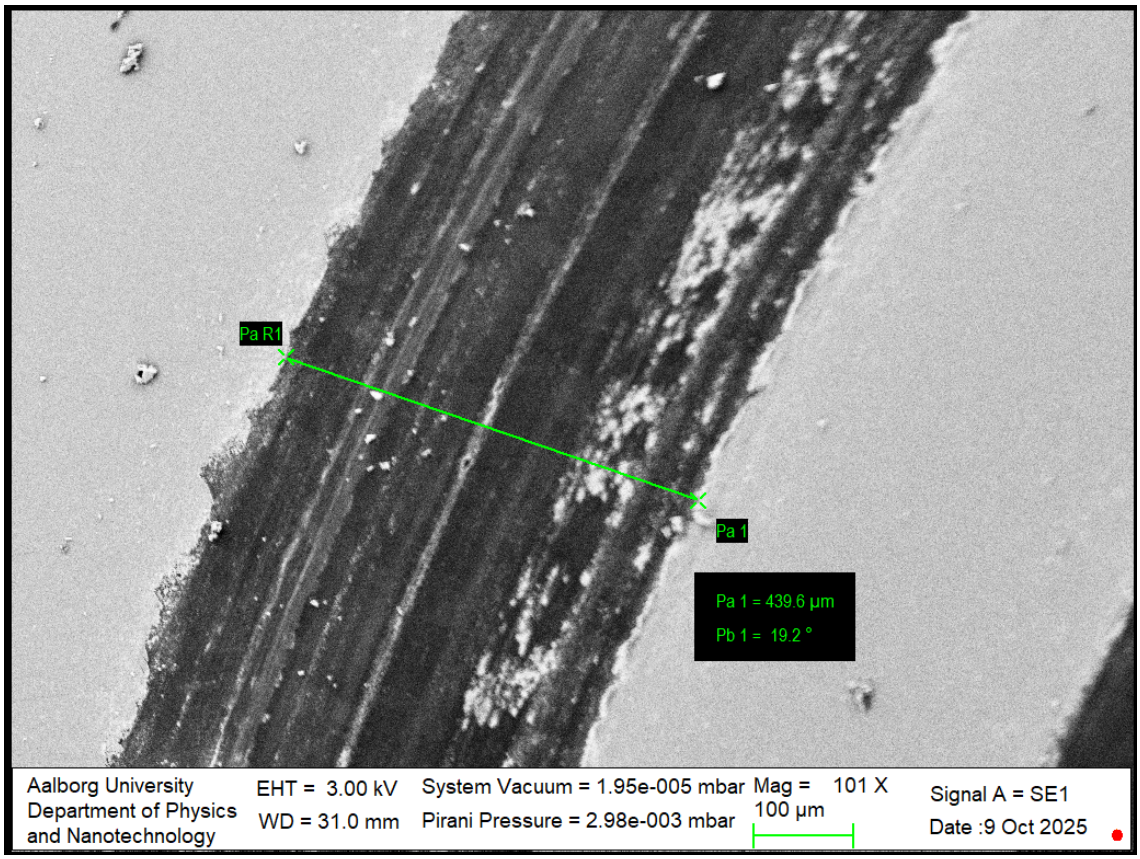

Figure A.135: This image shows a 1500 nm TiN coated stainless steel sample. This image shows the wear track done on the sample by the TRB3 tribometer when equipped with a load of 0.25 N and during 50 cycles.

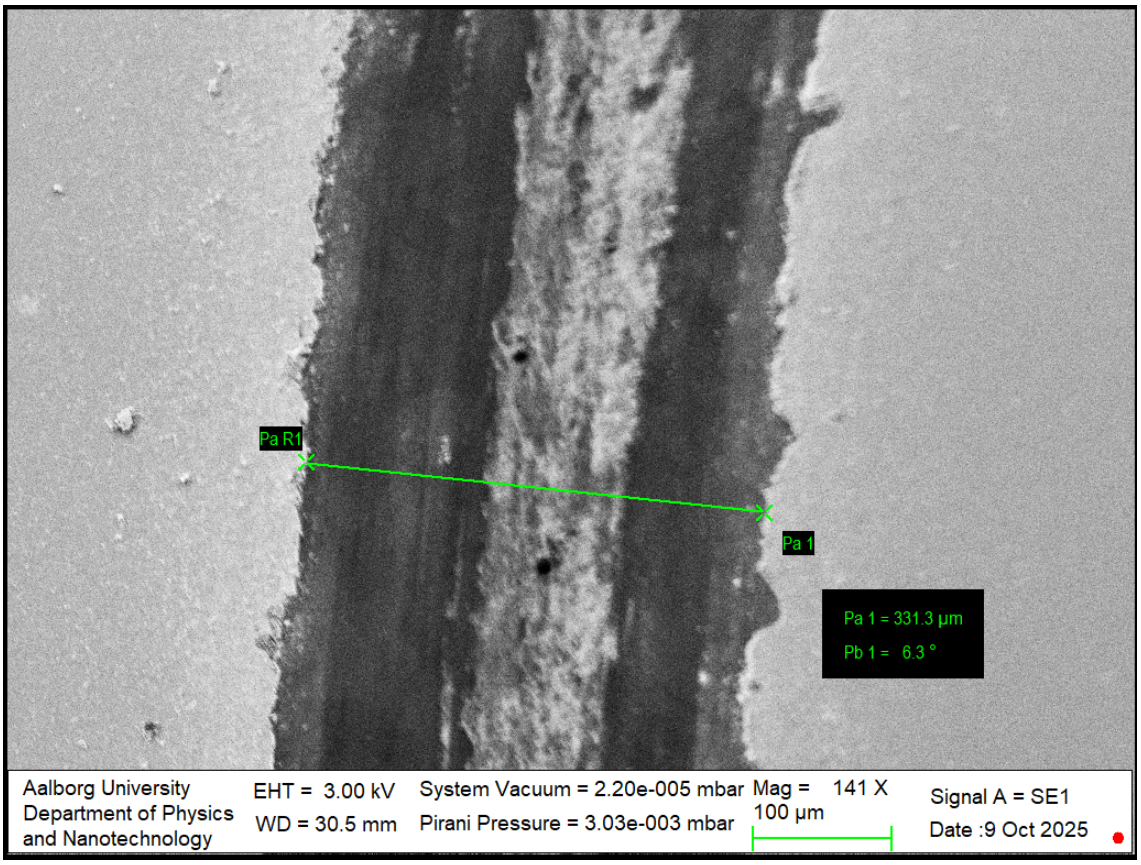

Figure A.136: This image shows a 1500 nm TiN coated stainless steel sample. This image shows the wear track done on the sample by the TRB3 tribometer when equipped with a load of 0.25 N and during 100 cycles.

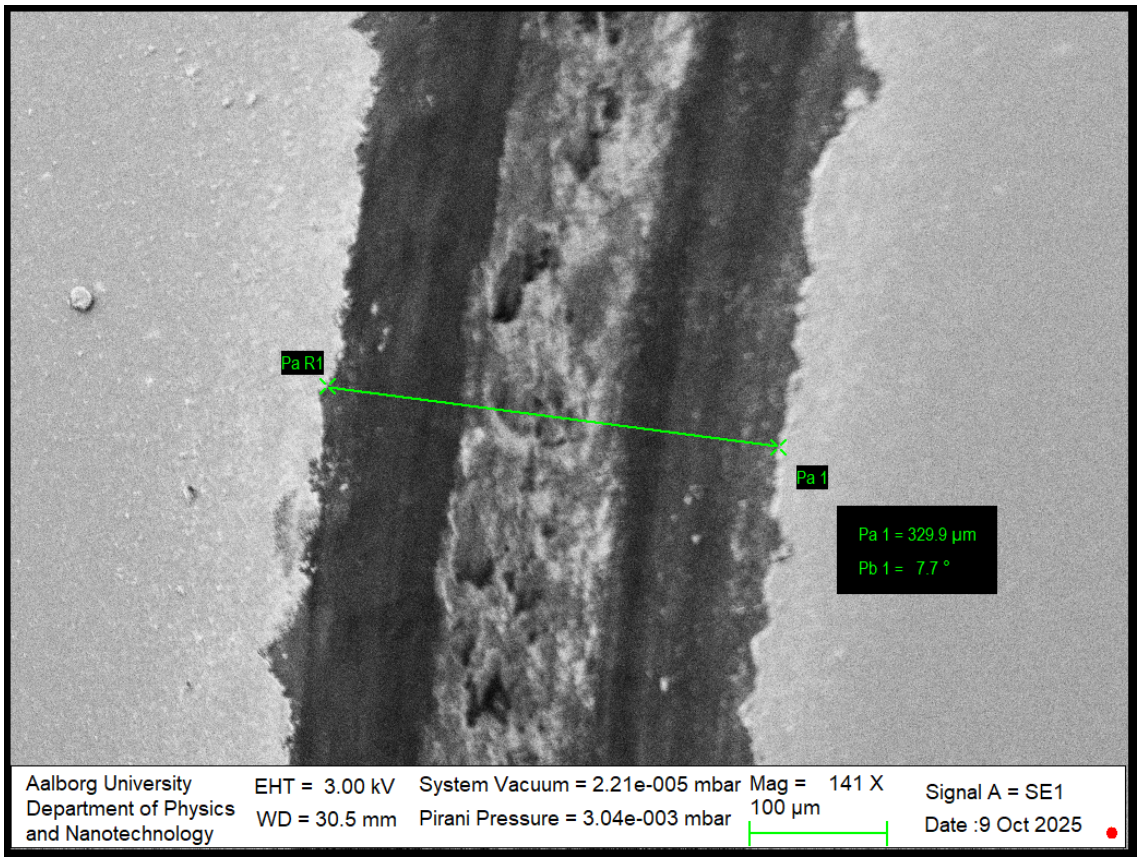

Figure A.137: This image shows a 1500 nm TiN coated stainless steel sample. This image shows the wear track done on the sample by the TRB3 tribometer when equipped with a load of 0.25 N and during 250 cycles.

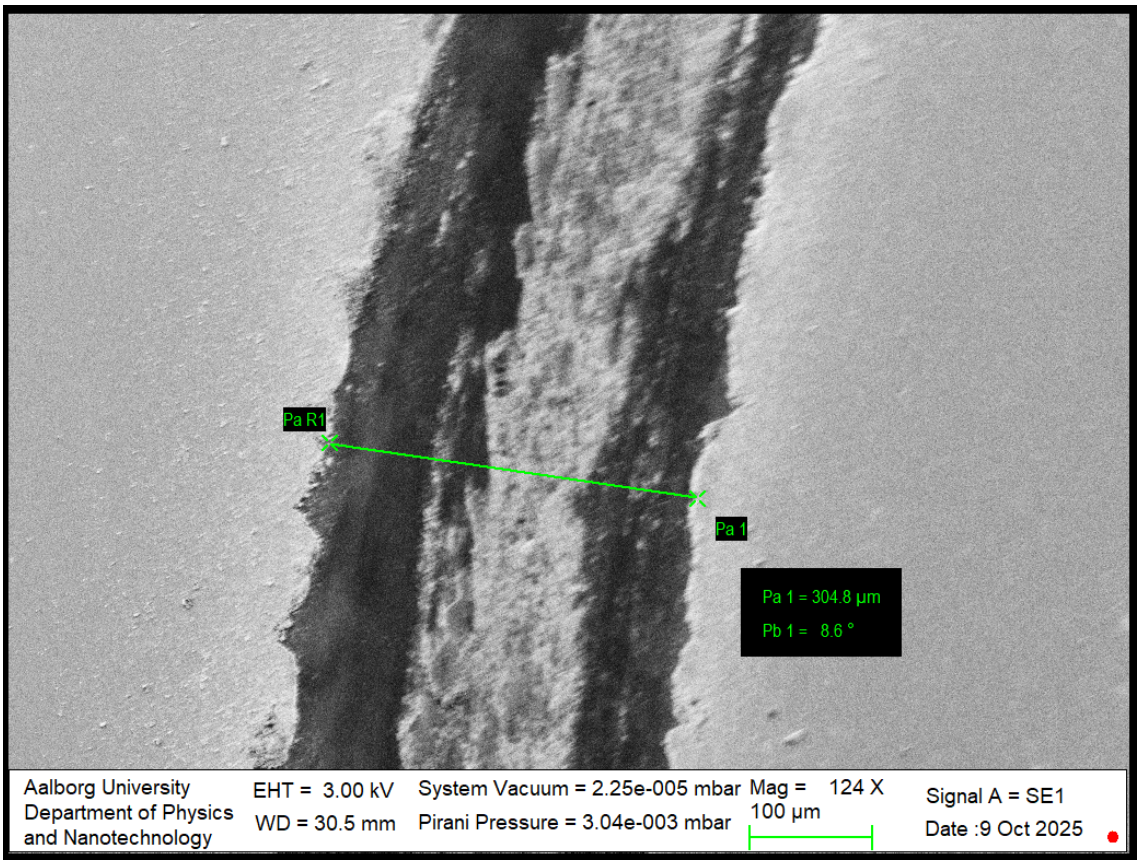

Figure A.138: This image shows a 1500 nm TiN coated stainless steel sample. This image shows the wear track done on the sample by the TRB3 tribometer when equipped with a load of 0.25 N and during 350 cycles.

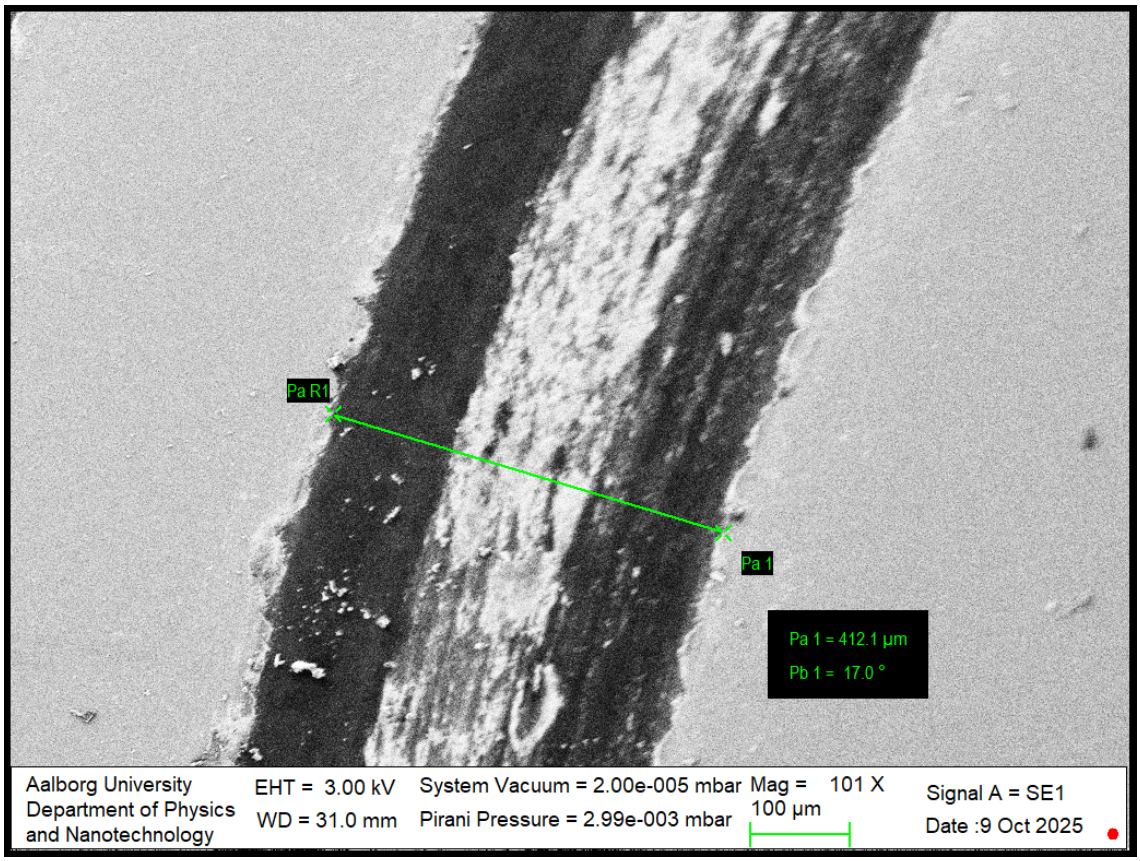

Figure A.139: This image shows a 1500 nm TiN coated stainless steel sample. This image shows the wear track done on the sample by the TRB3 tribometer when equipped with a load of 0.25 N and during 500 cycles.

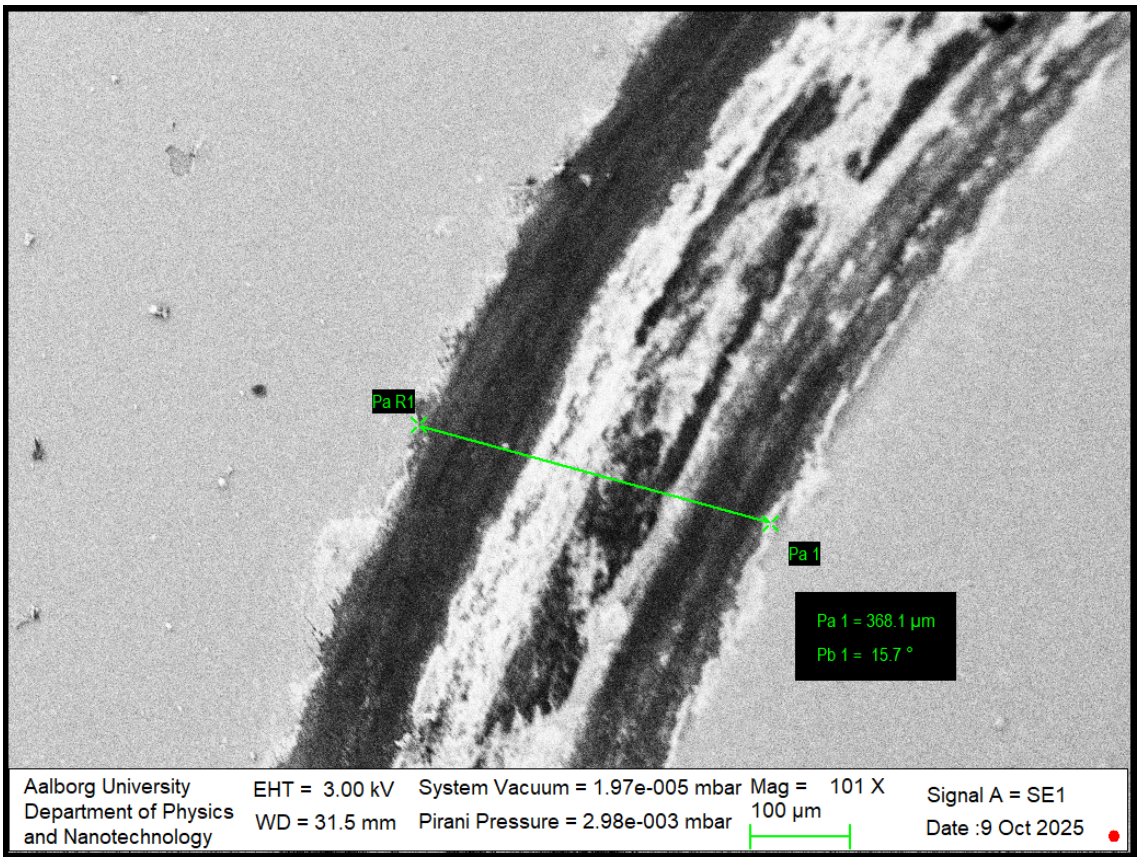

Figure A.140: This image shows a 1500 nm TiN coated stainless steel sample. This image shows the wear track done on the sample by the TRB3 tribometer when equipped with a load of 0.25 N and during 1000 cycles.

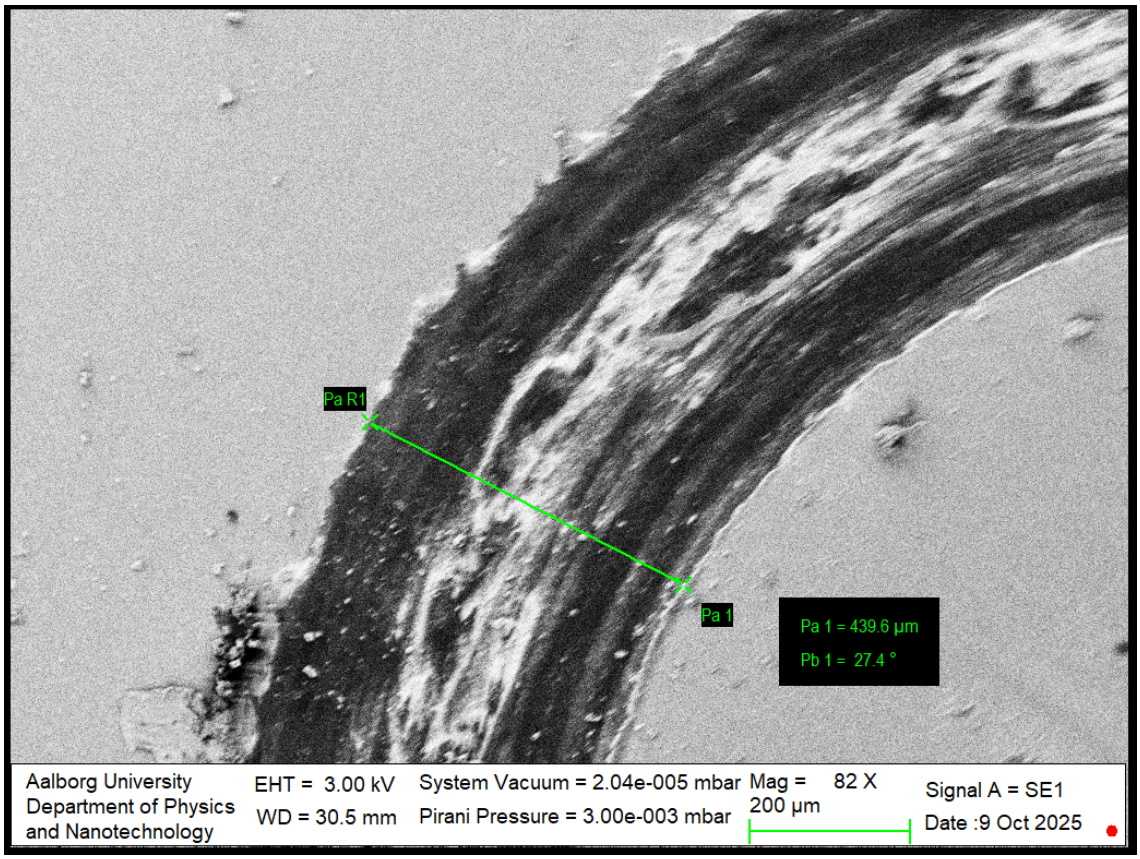

Figure A.141: This image shows a 1500 nm TiN coated stainless steel sample. This image shows the wear track done on the sample by the TRB3 tribometer when equipped with a load of 0.25 N and during 2000 cycles.

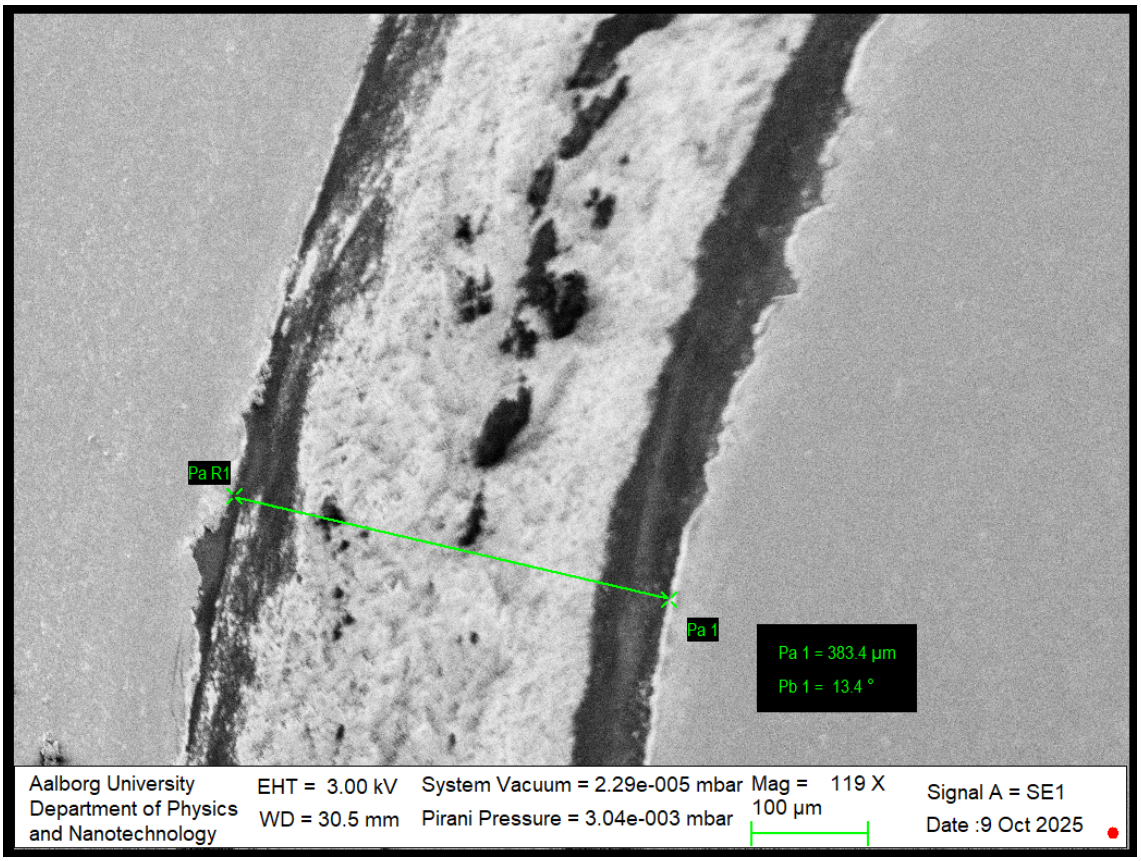

Figure A.142: This image shows a 1500 nm TiN coated stainless steel sample. This image shows the wear track done on the sample by the TRB3 tribometer when equipped with a load of 0.25 N and during 3000 cycles.

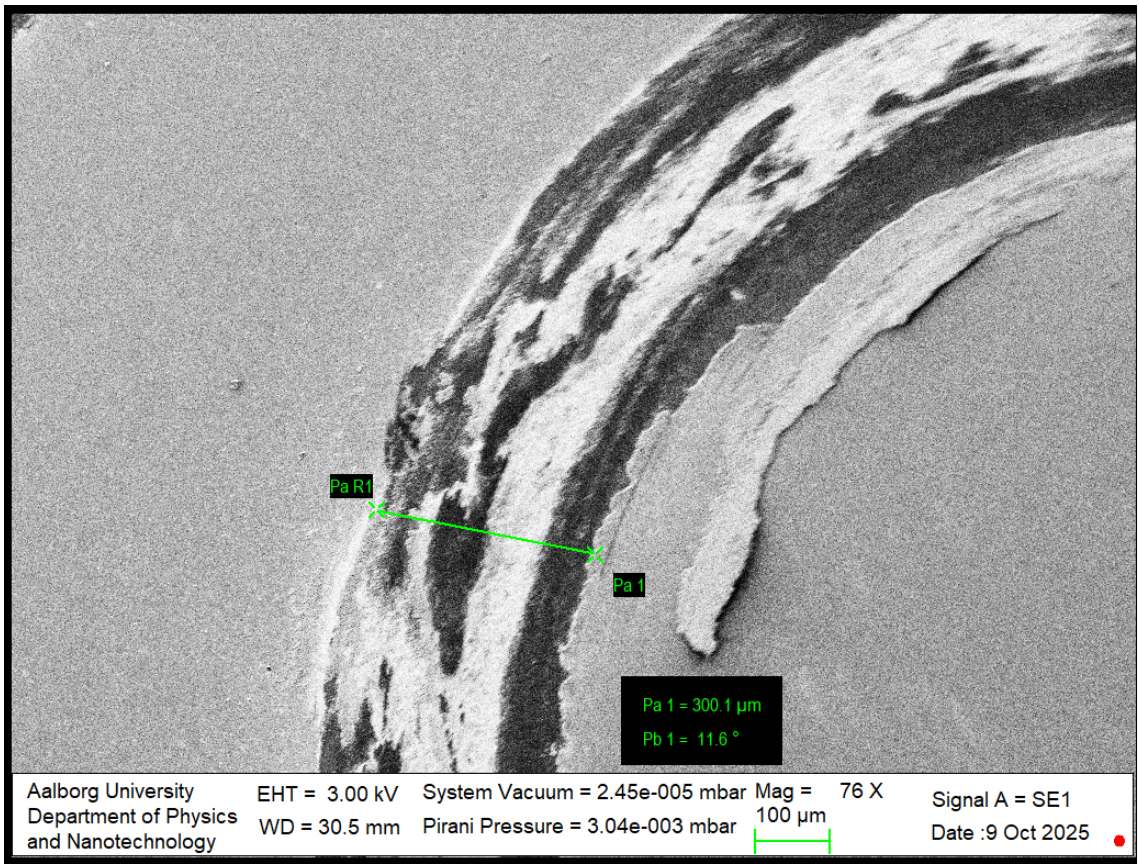

Figure A.143: This image shows a 1500 nm TiN coated stainless steel sample. This image shows the wear track done on the sample by the TRB3 tribometer when equipped with a load of 0.25 N and during 5000 cycles.

A.4.2 SEM Images of Wear Tracks on 1500 nm TiN Coated Sample at 1 N

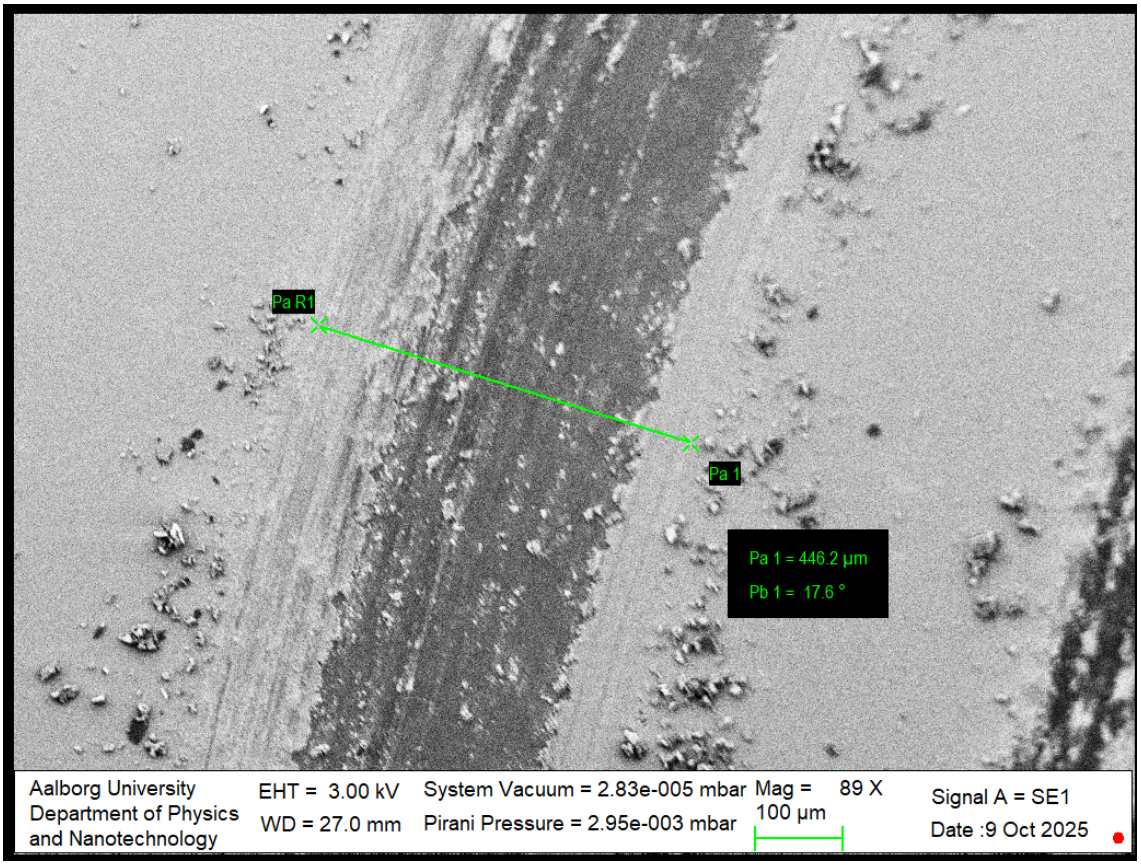

Figure A.144: This image shows a 1500 nm TiN coated stainless steel sample. This image shows the wear track done on the sample by the TRB3 tribometer when equipped with a load of 1 N and during 1 cycle.

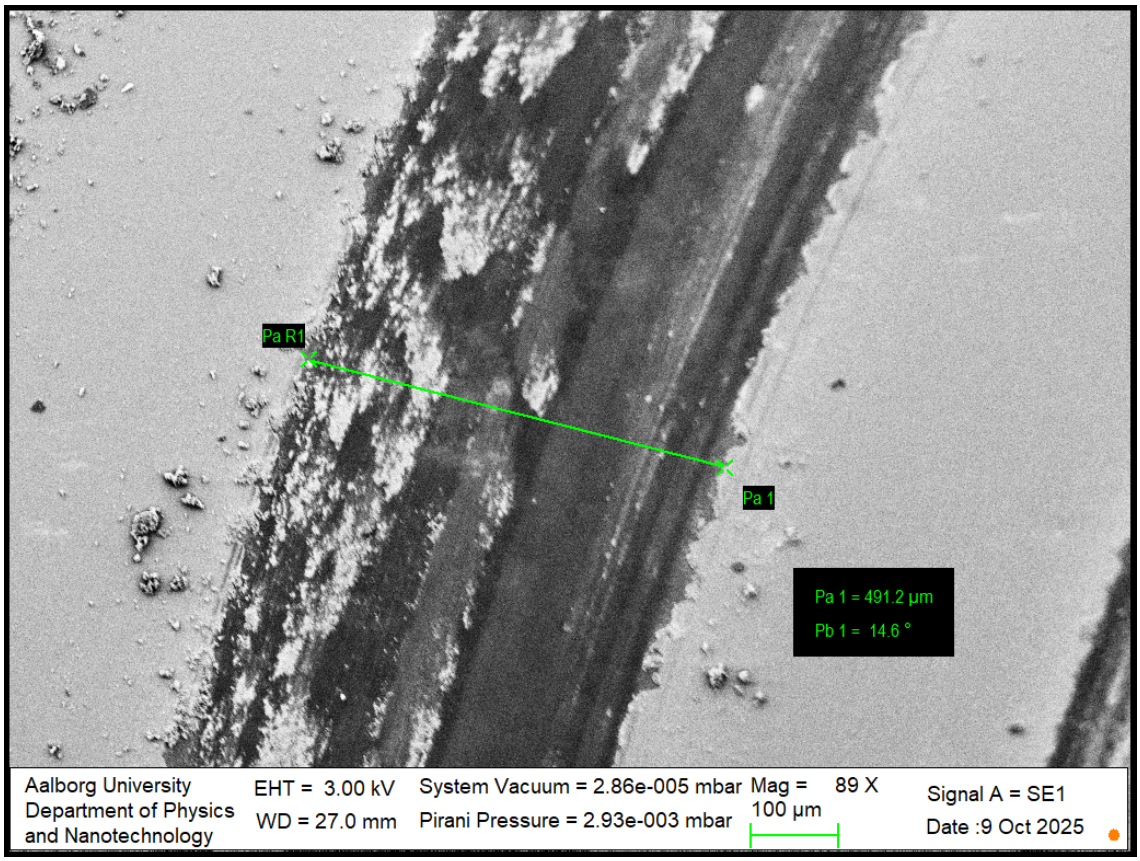

Figure A.145: This image shows a 1500 nm TiN coated stainless steel sample. This image shows the wear track done on the sample by the TRB3 tribometer when equipped with a load of 1 N and during 10 cycles.

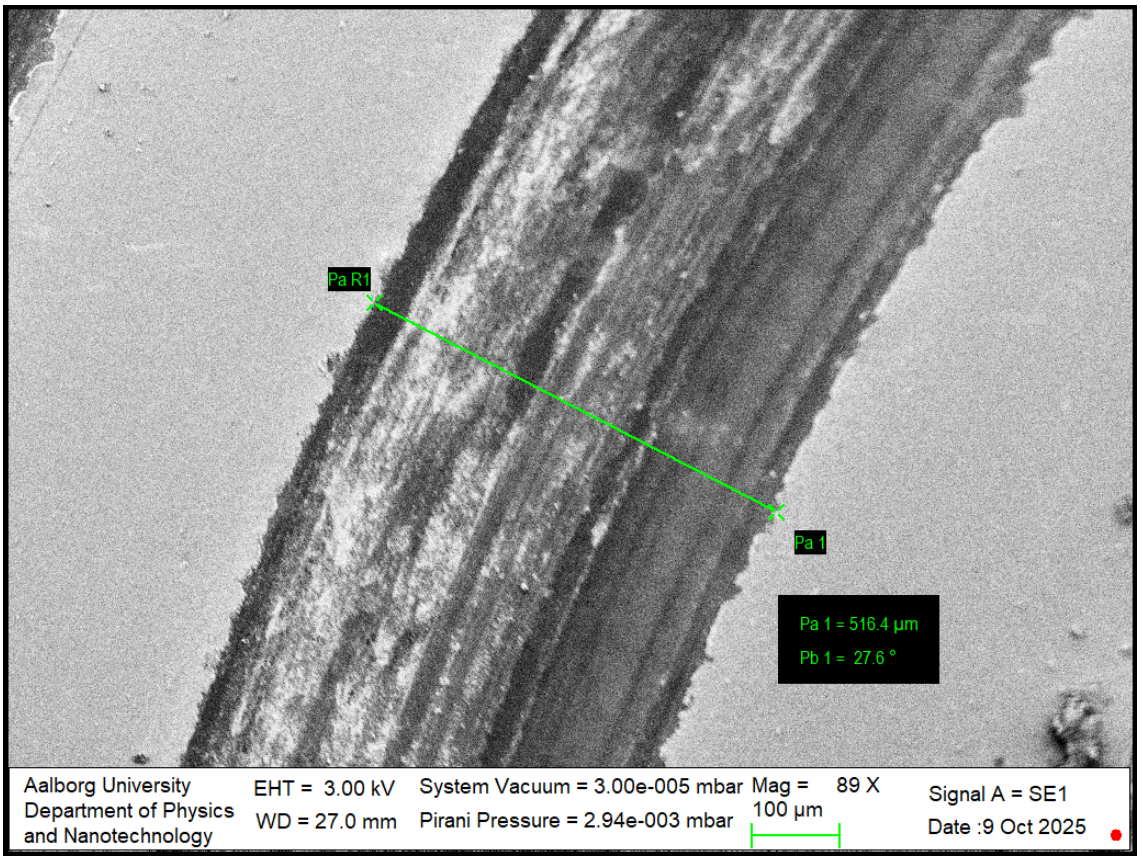

Figure A.146: This image shows a 1500 nm TiN coated stainless steel sample. This image shows the wear track done on the sample by the TRB3 tribometer when equipped with a load of 1 N and during 50 cycles.

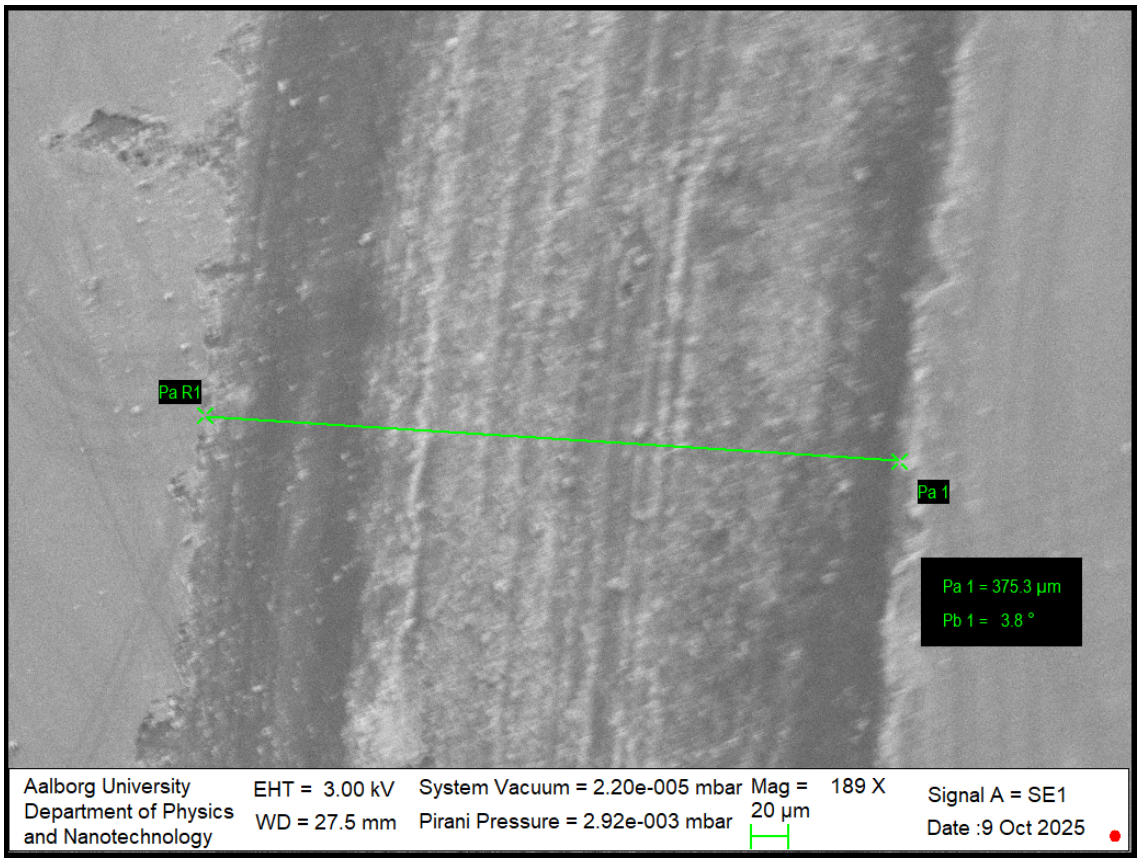

Figure A.147: This image shows a 1500 nm TiN coated stainless steel sample. This image shows the wear track done on the sample by the TRB3 tribometer when equipped with a load of 1 N and during 100 cycles.

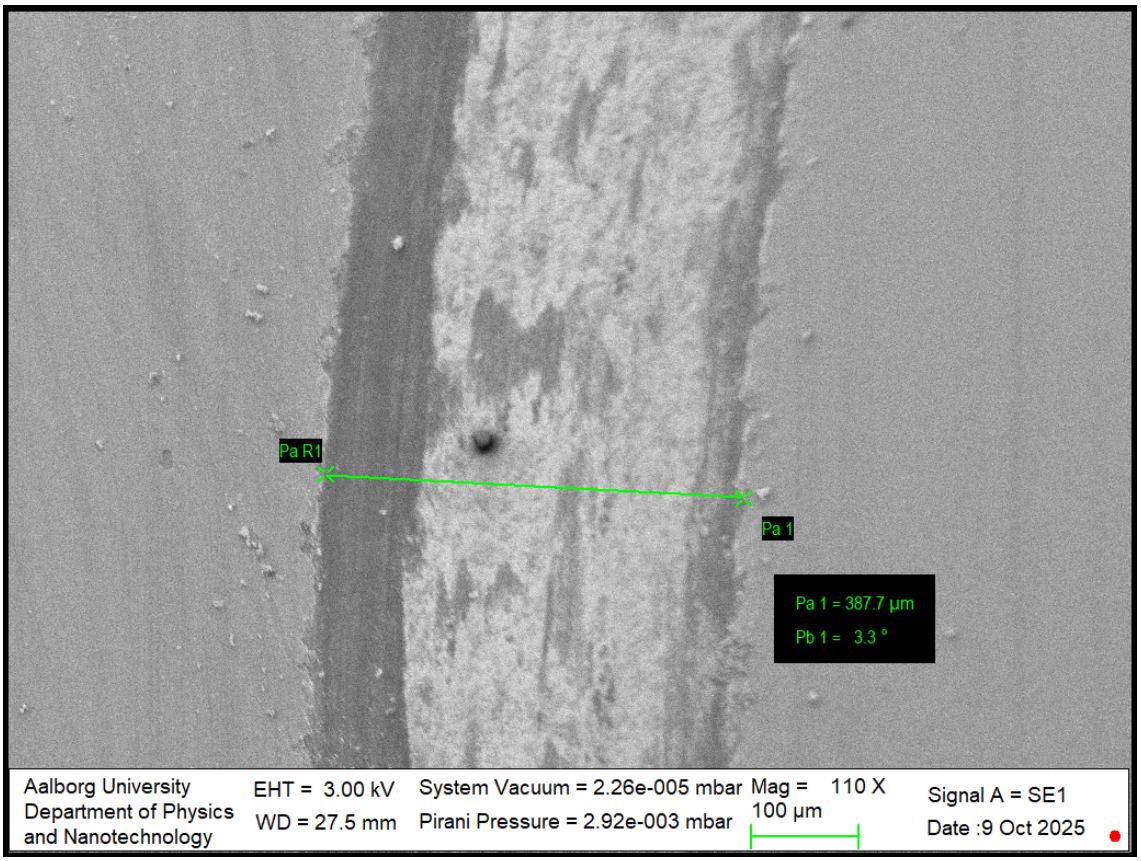

Figure A.148: This image shows a 1500 nm TiN coated stainless steel sample. This image shows the wear track done on the sample by the TRB3 tribometer when equipped with a load of 1 N and during 250 cycles.

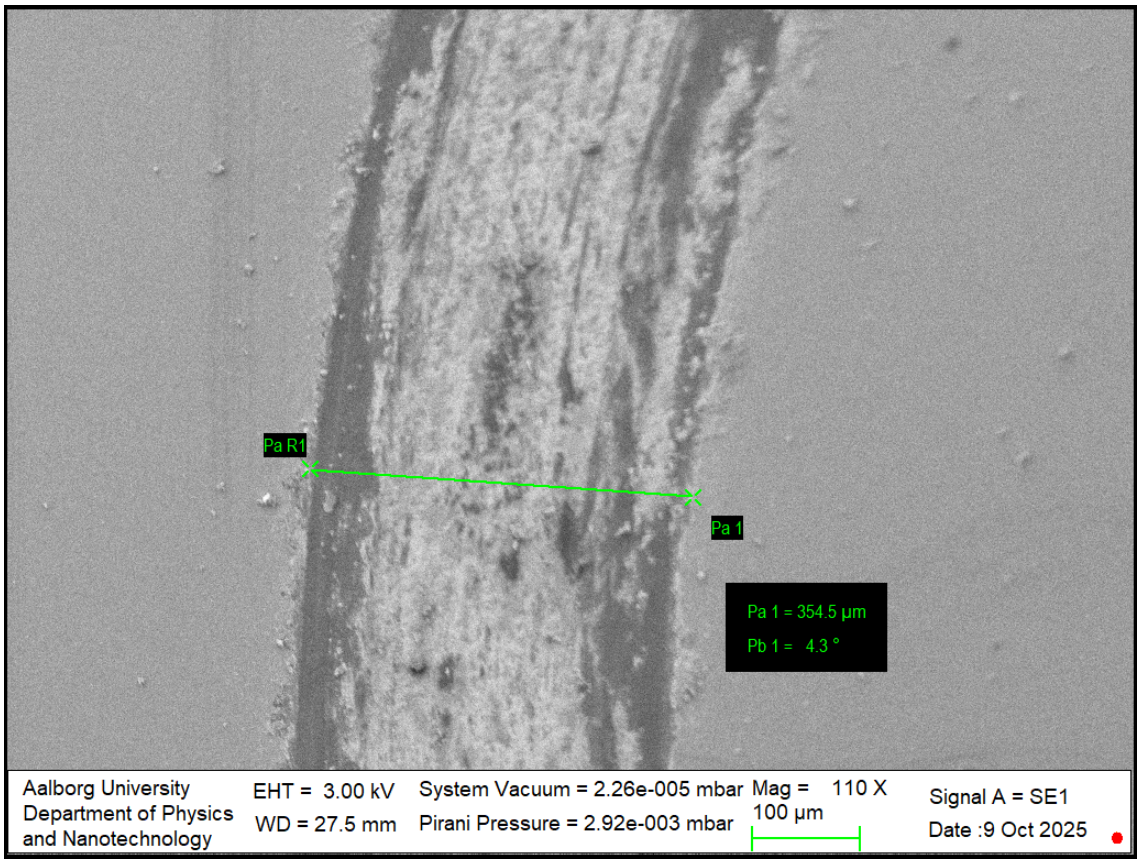

Figure A.149: This image shows a 1500 nm TiN coated stainless steel sample. This image shows the wear track done on the sample by the TRB3 tribometer when equipped with a load of 1 N and during 350 cycles.

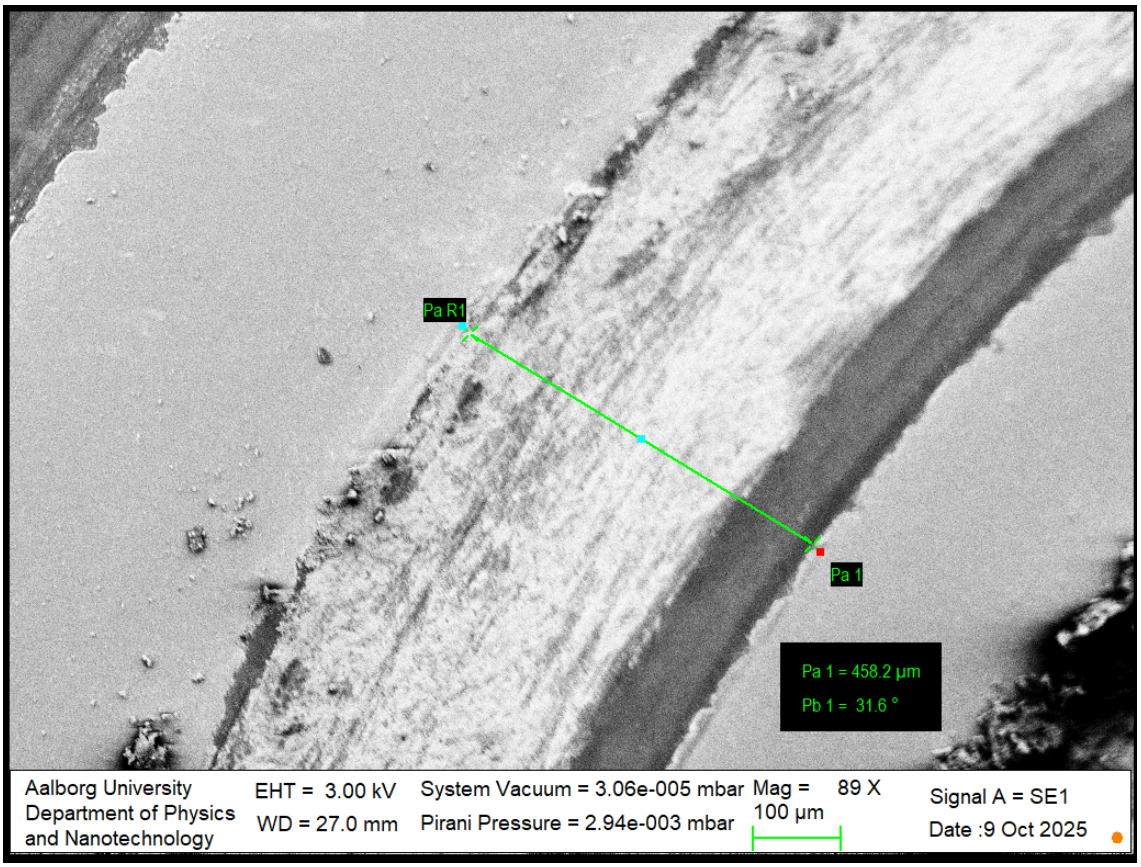

Figure A.150: This image shows a 1500 nm TiN coated stainless steel sample. This image shows the wear track done on the sample by the TRB3 tribometer when equipped with a load of 1 N and during 500 cycles.

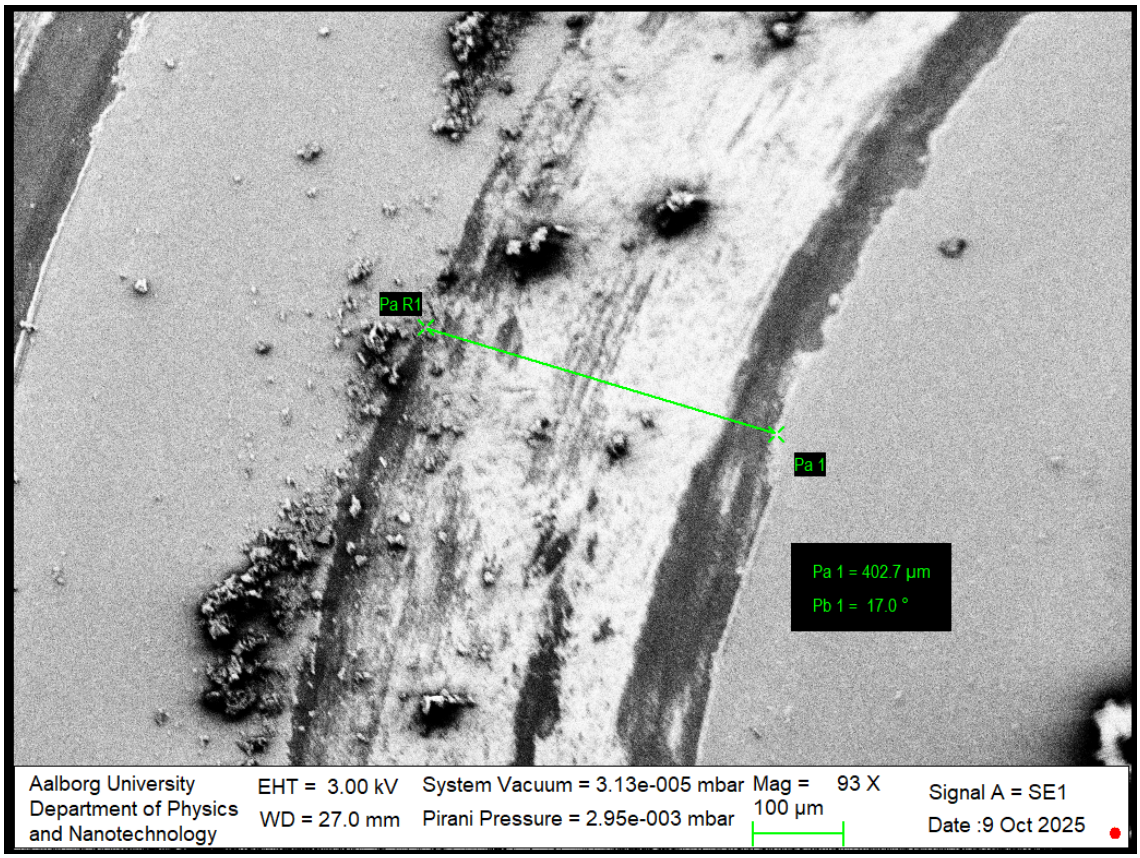

Figure A.151: This image shows a 1500 nm TiN coated stainless steel sample. This image shows the wear track done on the sample by the TRB3 tribometer when equipped with a load of 1 N and during 1000 cycles.

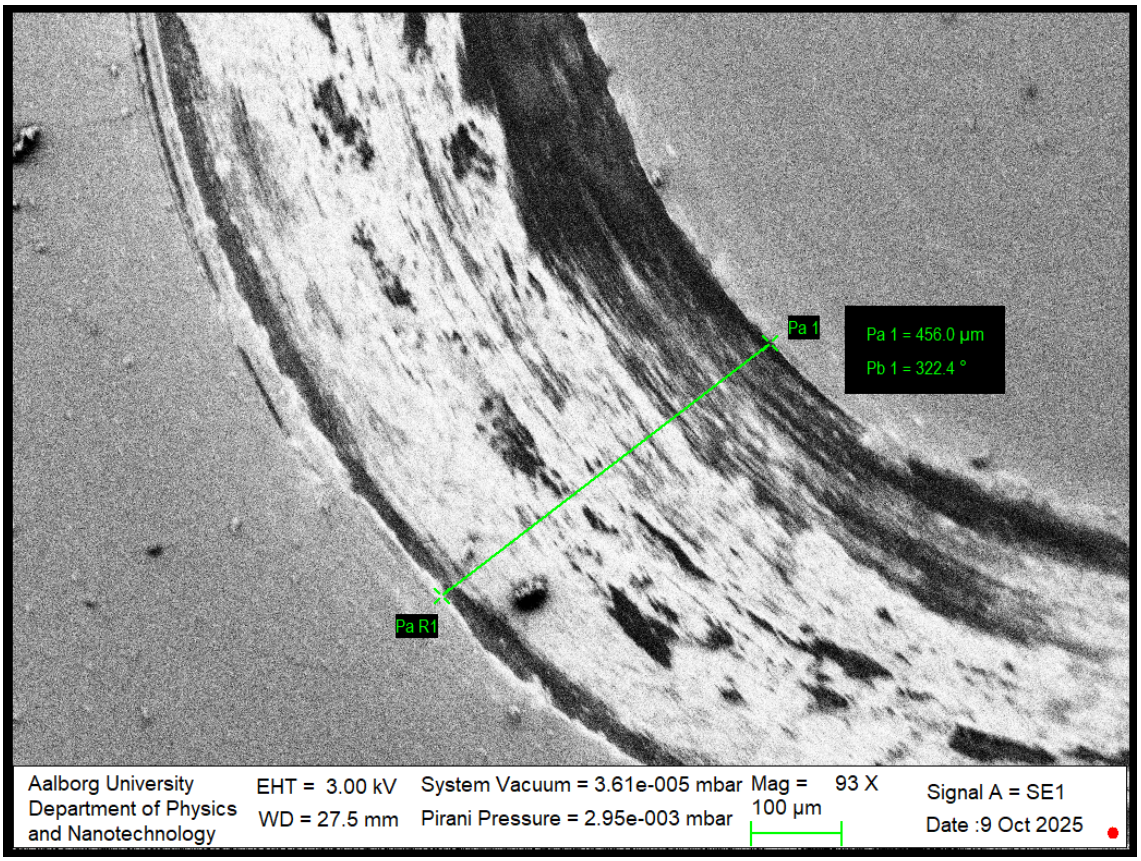

Figure A.152: This image shows a 1500 nm TiN coated stainless steel sample. This image shows the wear track done on the sample by the TRB3 tribometer when equipped with a load of 1 N and during 2000 cycles.

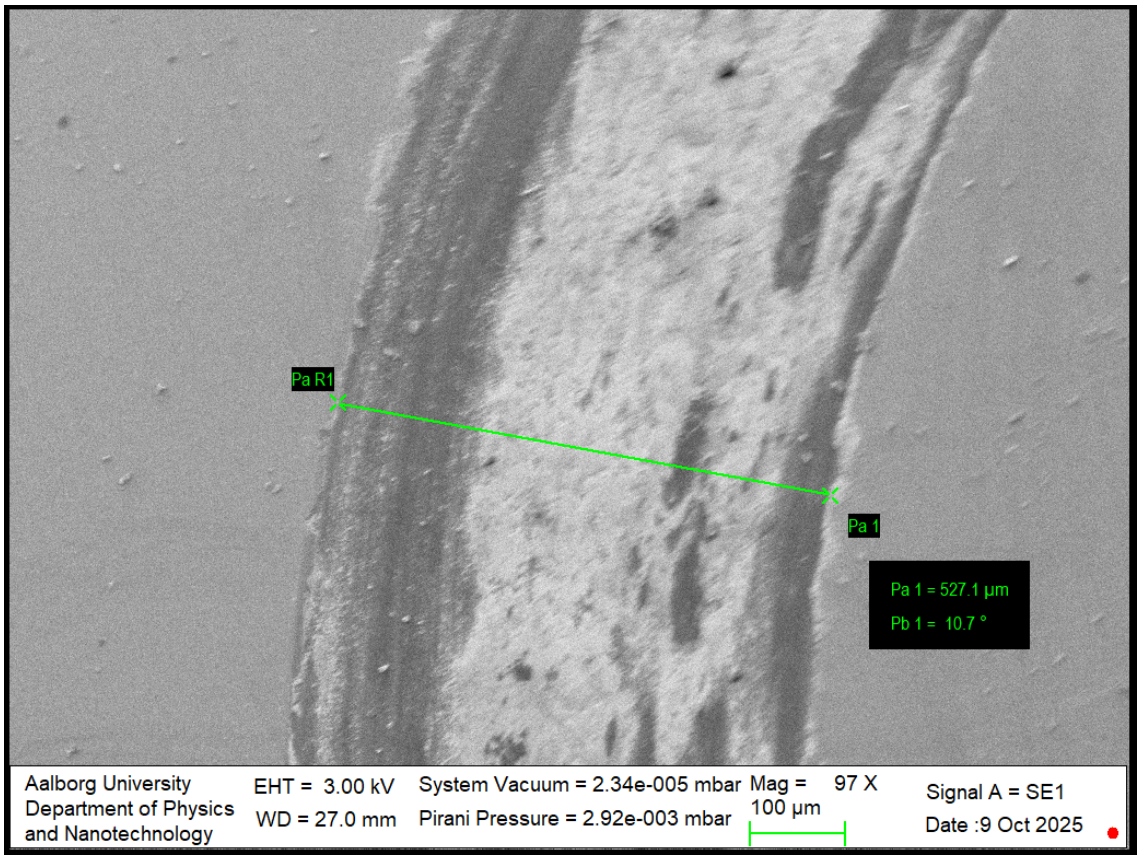

Figure A.153: This image shows a 1500 nm TiN coated stainless steel sample. This image shows the wear track done on the sample by the TRB3 tribometer when equipped with a load of 1 N and during 3000 cycles.

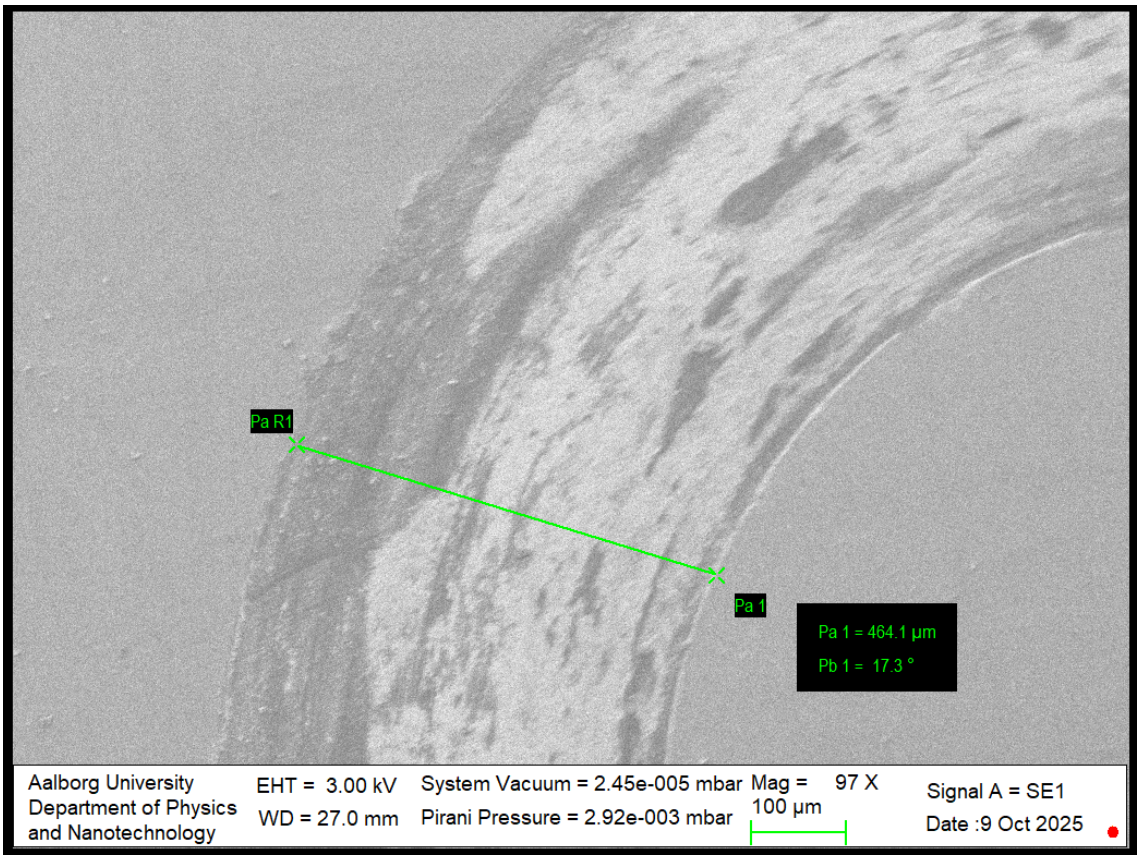

Figure A.154: This image shows a 1500 nm TiN coated stainless steel sample. This image shows the wear track done on the sample by the TRB3 tribometer when equipped with a load of 1 N and during 5000 cycles.

A.4.3 SEM Images of Wear Tracks on 1500 nm TiN Coated Sample at 2 N

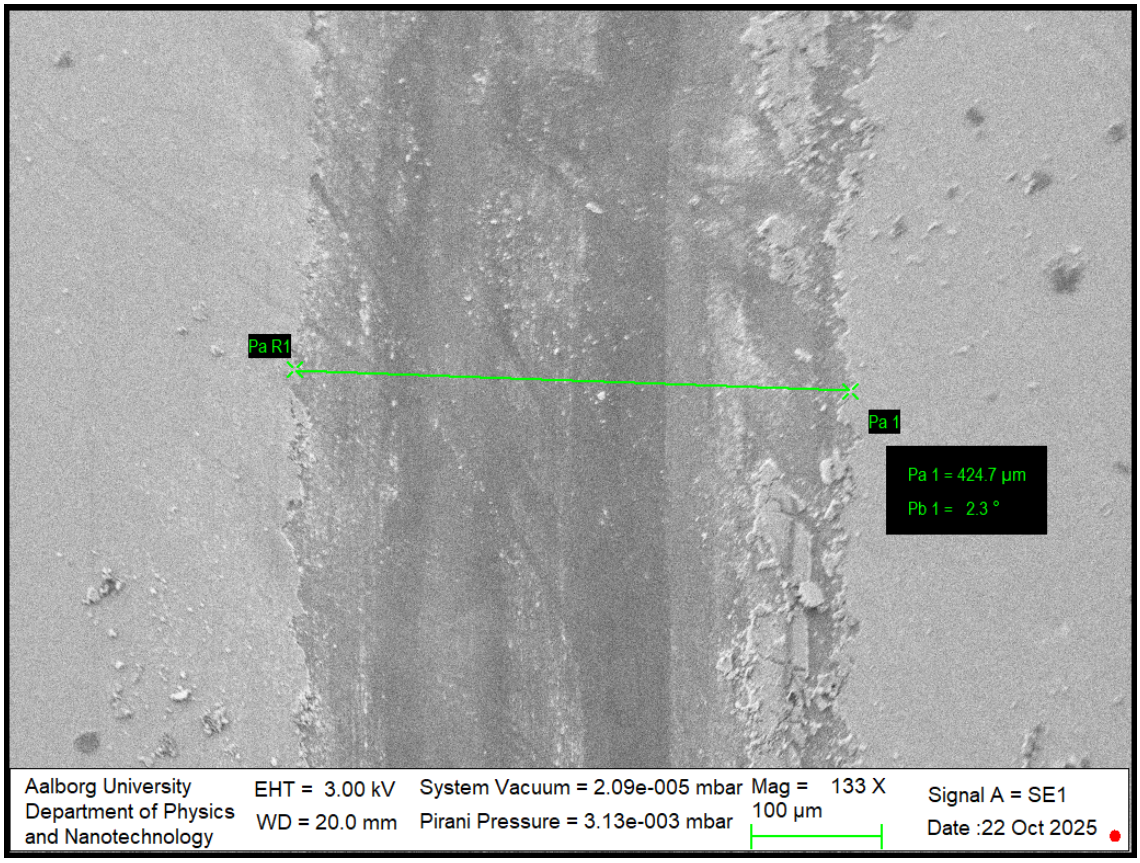

Figure A.155: This image shows a 1500 nm TiN coated stainless steel sample. This image shows the wear track done on the sample by the TRB3 tribometer when equipped with a load of 2 N and during 1 cycle.

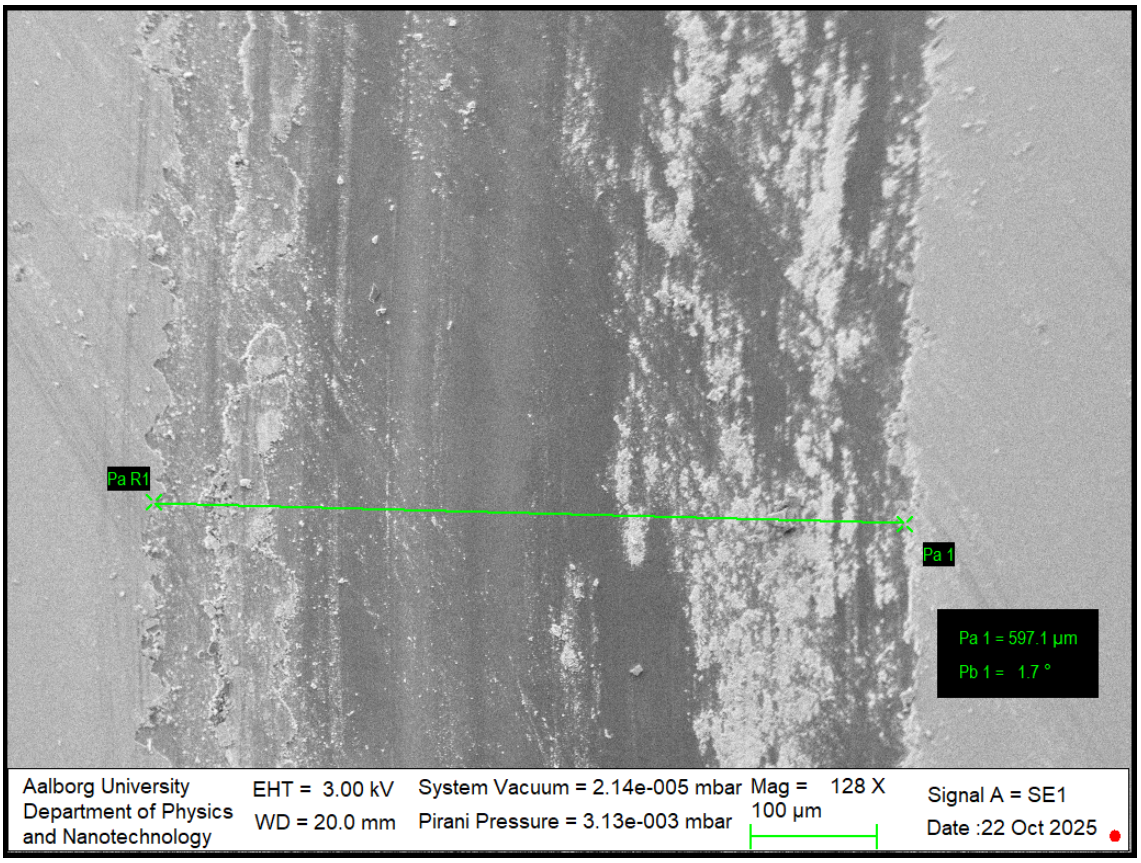

Figure A.156: This image shows a 1500 nm TiN coated stainless steel sample. This image shows the wear track done on the sample by the TRB3 tribometer when equipped with a load of 2 N and during 10 cycles.

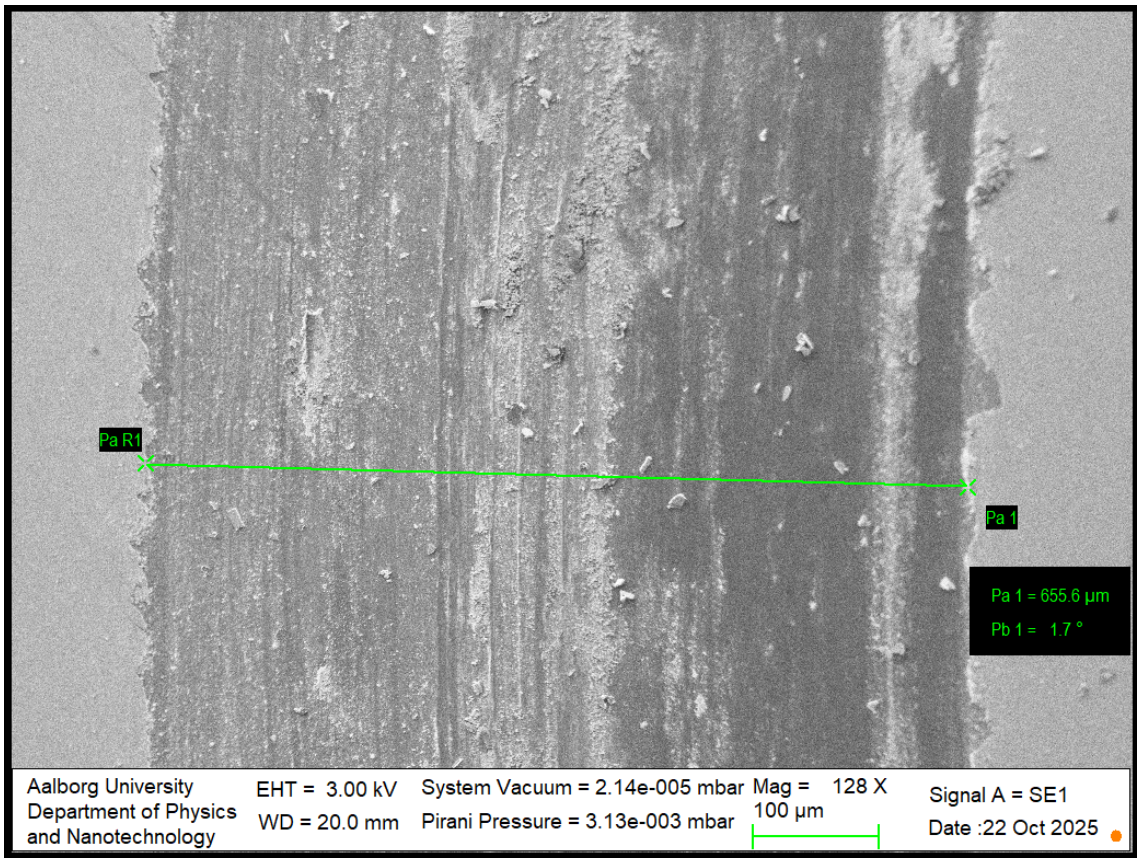

Figure A.157: This image shows a 1500 nm TiN coated stainless steel sample. This image shows the wear track done on the sample by the TRB3 tribometer when equipped with a load of 2 N and during 50 cycles.

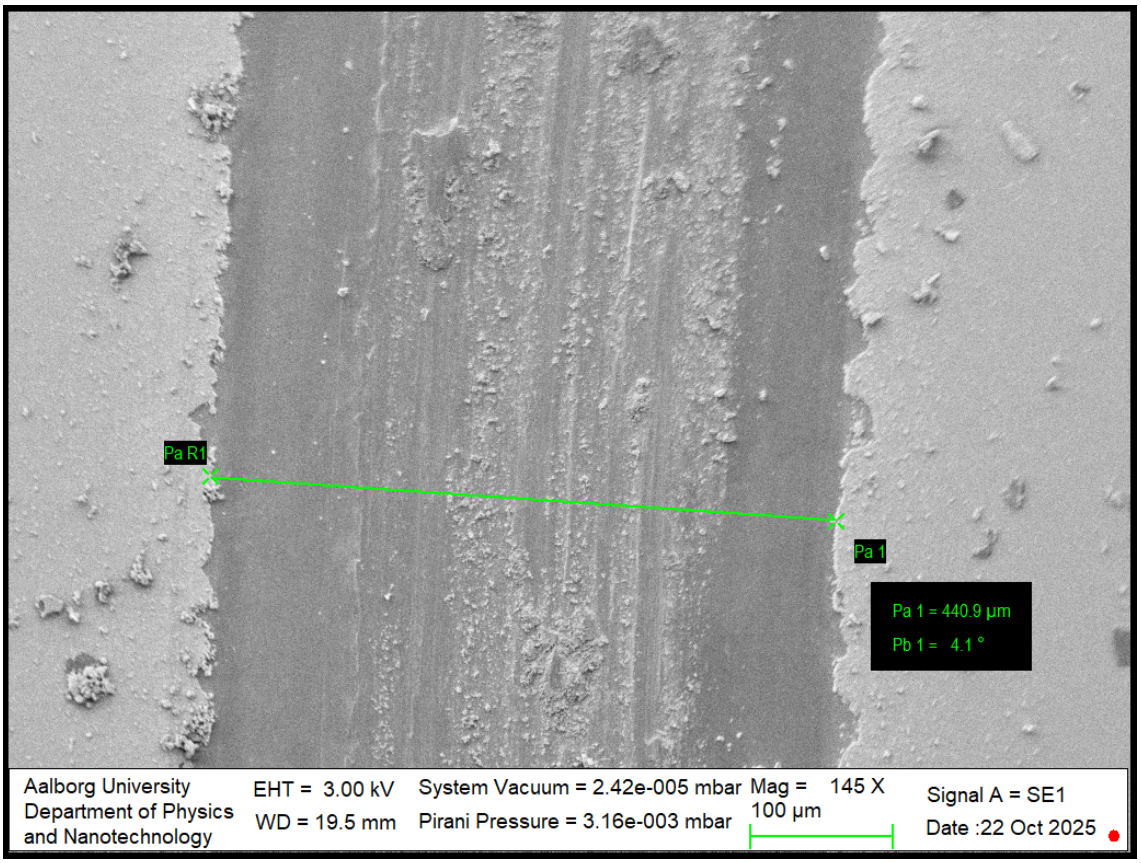

Figure A.158: This image shows a 1500 nm TiN coated stainless steel sample. This image shows the wear track done on the sample by the TRB3 tribometer when equipped with a load of 2 N and during 100 cycles.

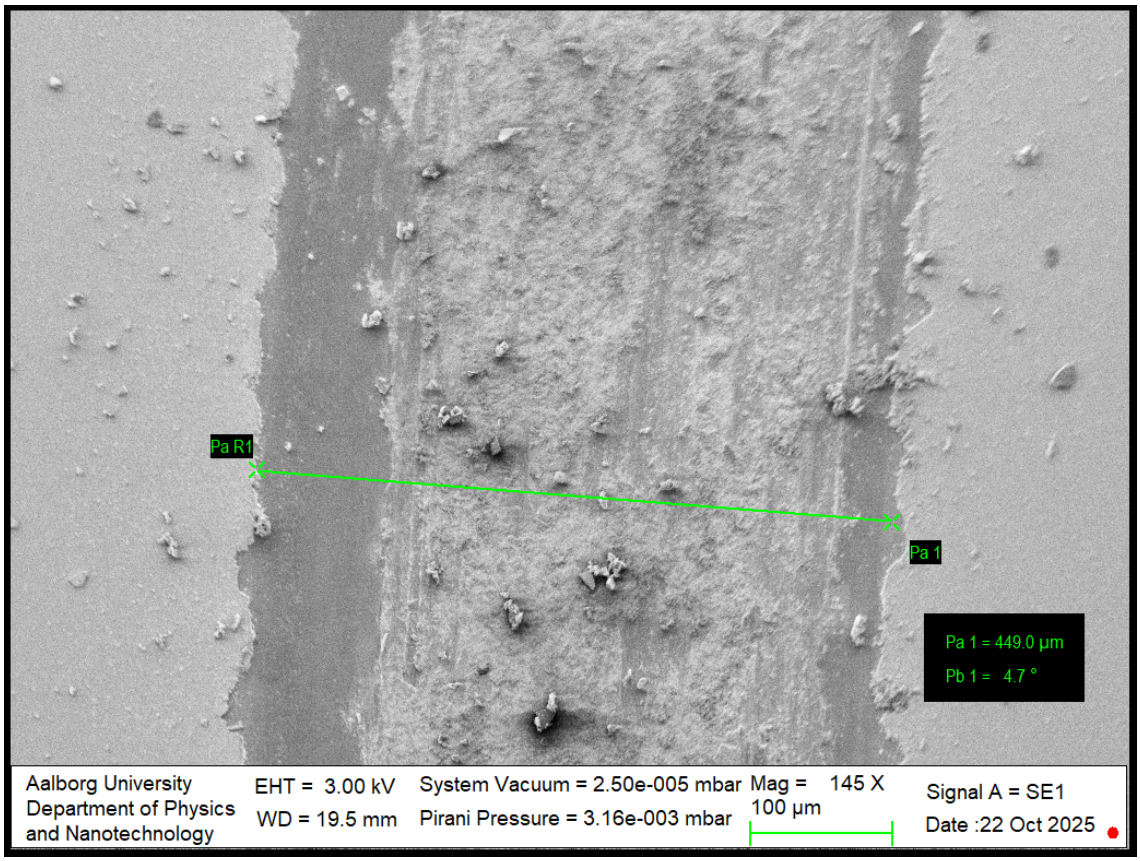

Figure A.159: This image shows a 1500 nm TiN coated stainless steel sample. This image shows the wear track done on the sample by the TRB3 tribometer when equipped with a load of 2 N and during 250 cycles.

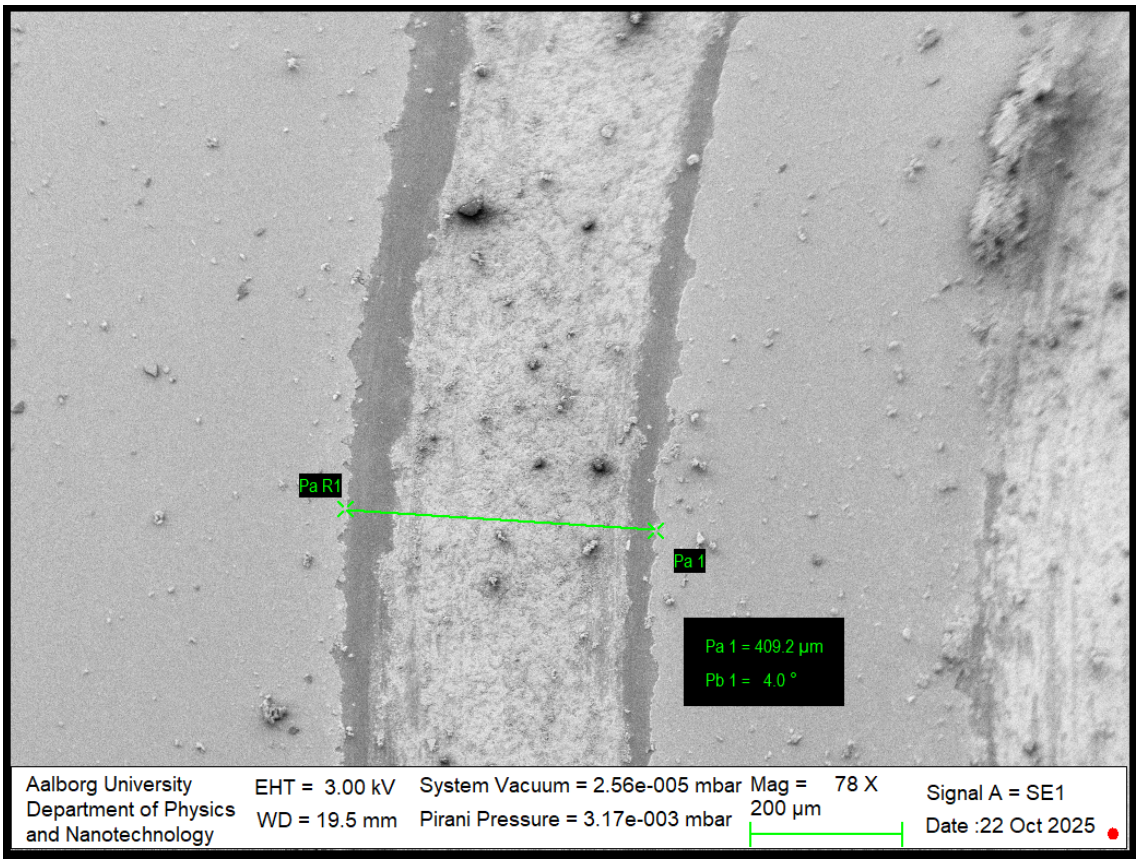

Figure A.160: This image shows a 1500 nm TiN coated stainless steel sample. This image shows the wear track done on the sample by the TRB3 tribometer when equipped with a load of 2 N and during 350 cycles.

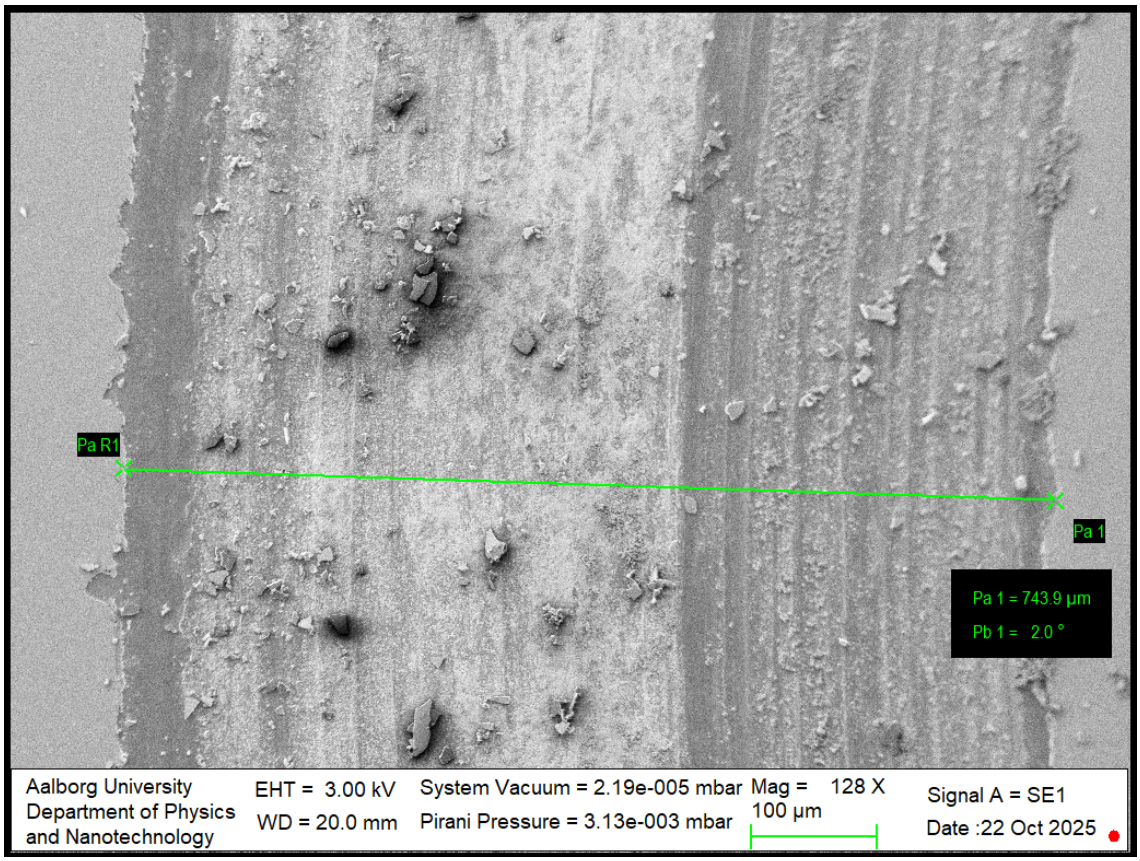

Figure A.161: This image shows a 1500 nm TiN coated stainless steel sample. This image shows the wear track done on the sample by the TRB3 tribometer when equipped with a load of 2 N and during 500 cycles.

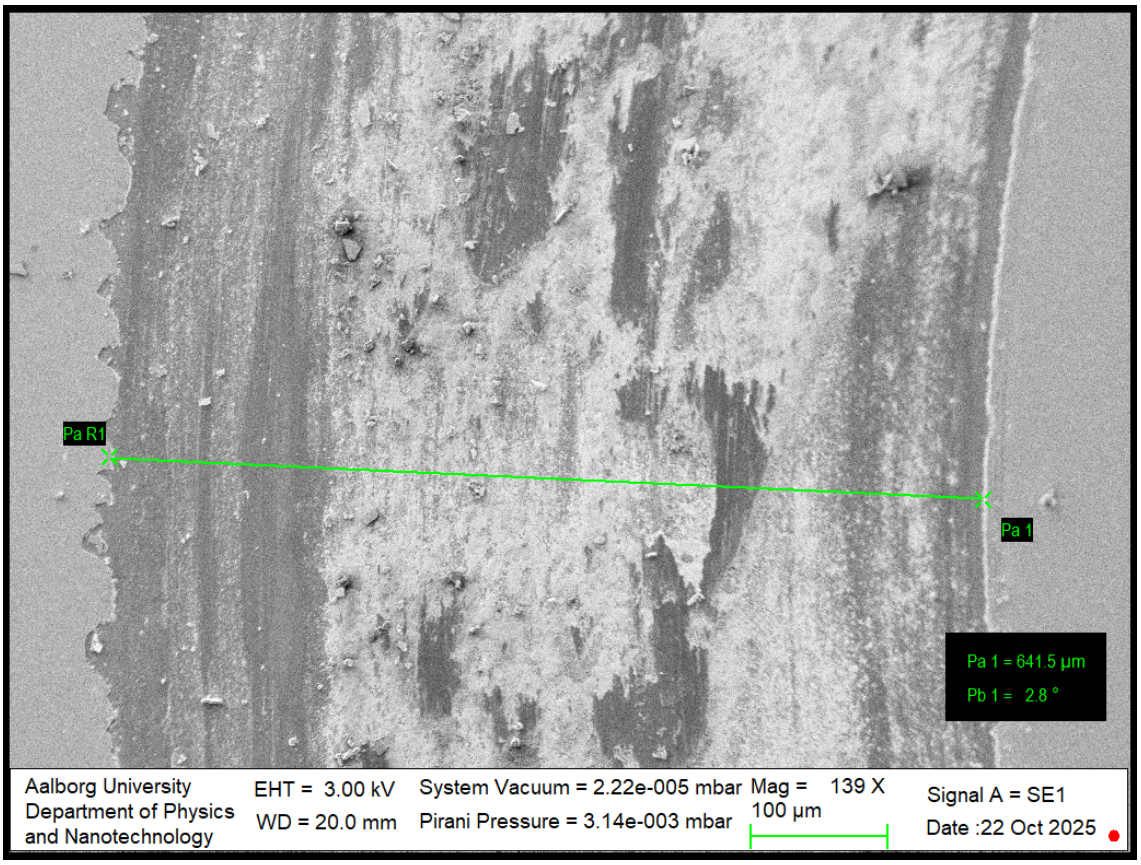

Figure A.162: This image shows a 1500 nm TiN coated stainless steel sample. This image shows the wear track done on the sample by the TRB3 tribometer when equipped with a load of 2 N and during 1000 cycles.

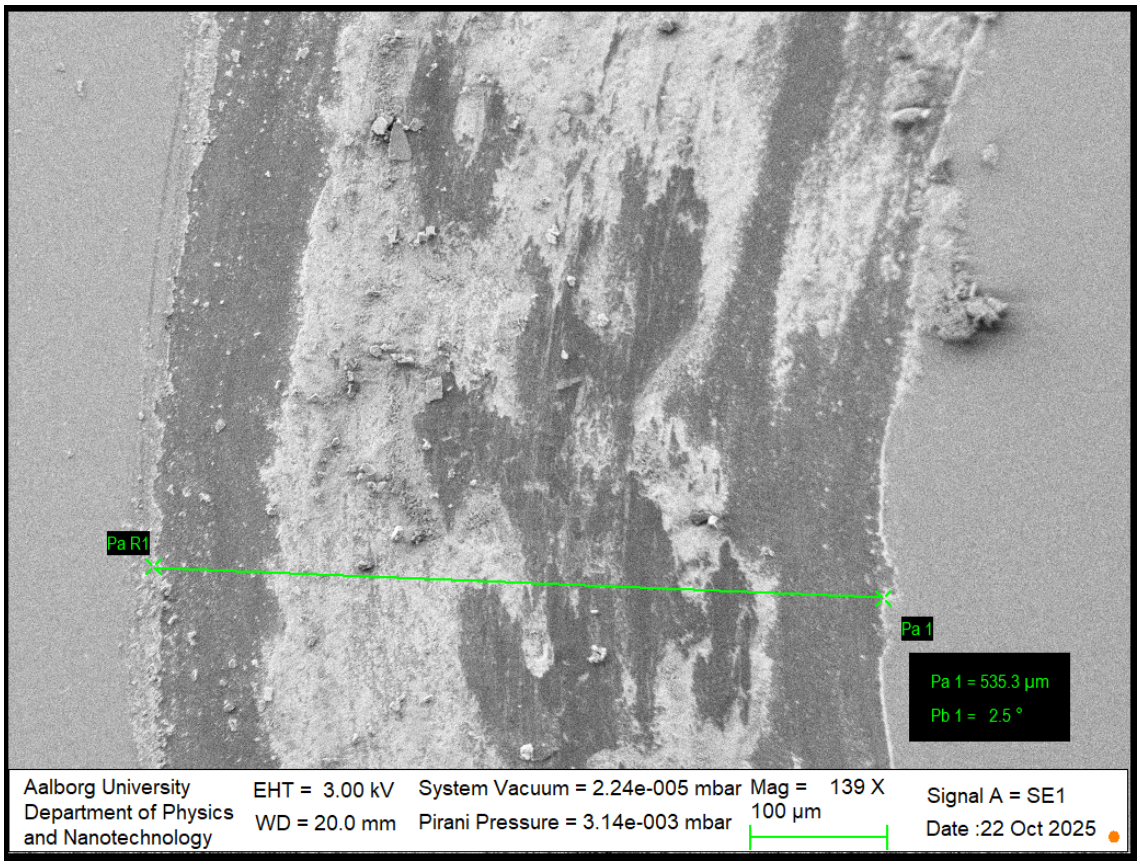

Figure A.163: This image shows a 1500 nm TiN coated stainless steel sample. This image shows the wear track done on the sample by the TRB3 tribometer when equipped with a load of 2 N and during 2000 cycles.

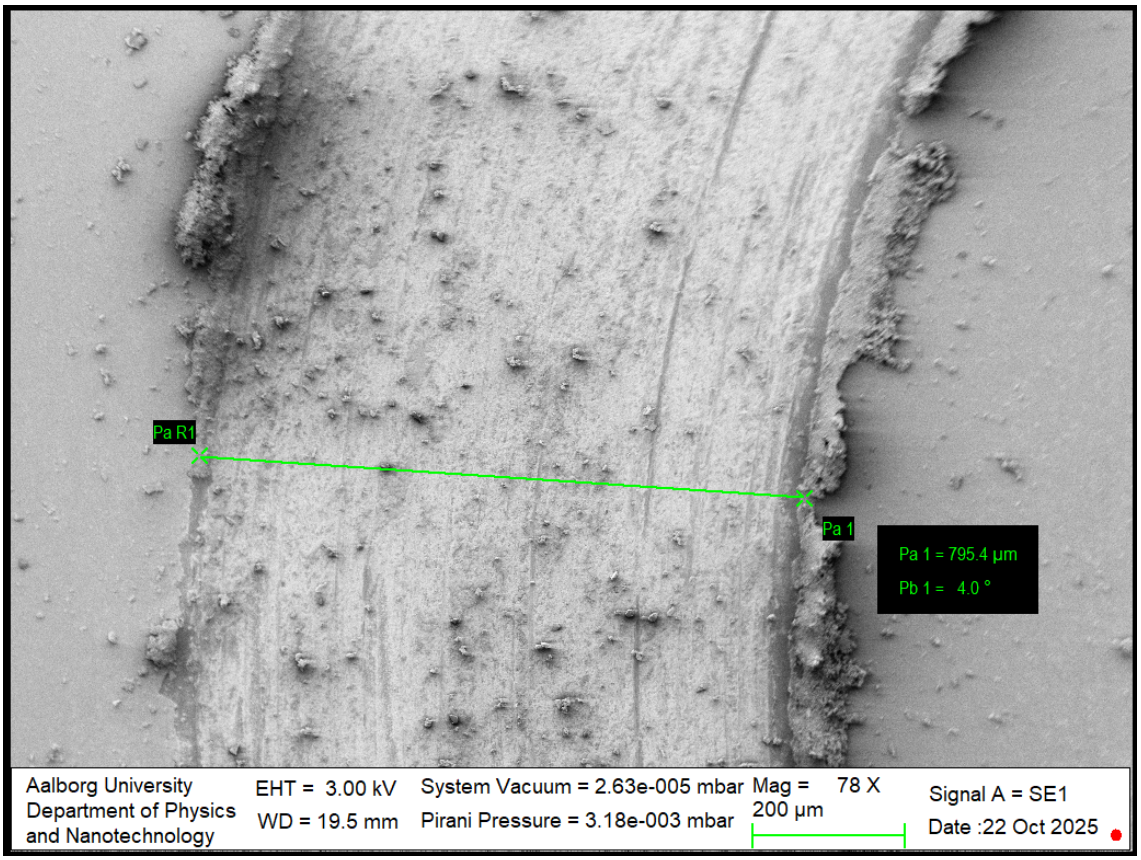

Figure A.164: This image shows a 1500 nm TiN coated stainless steel sample. This image shows the wear track done on the sample by the TRB3 tribometer when equipped with a load of 2 N and during 3000 cycles.

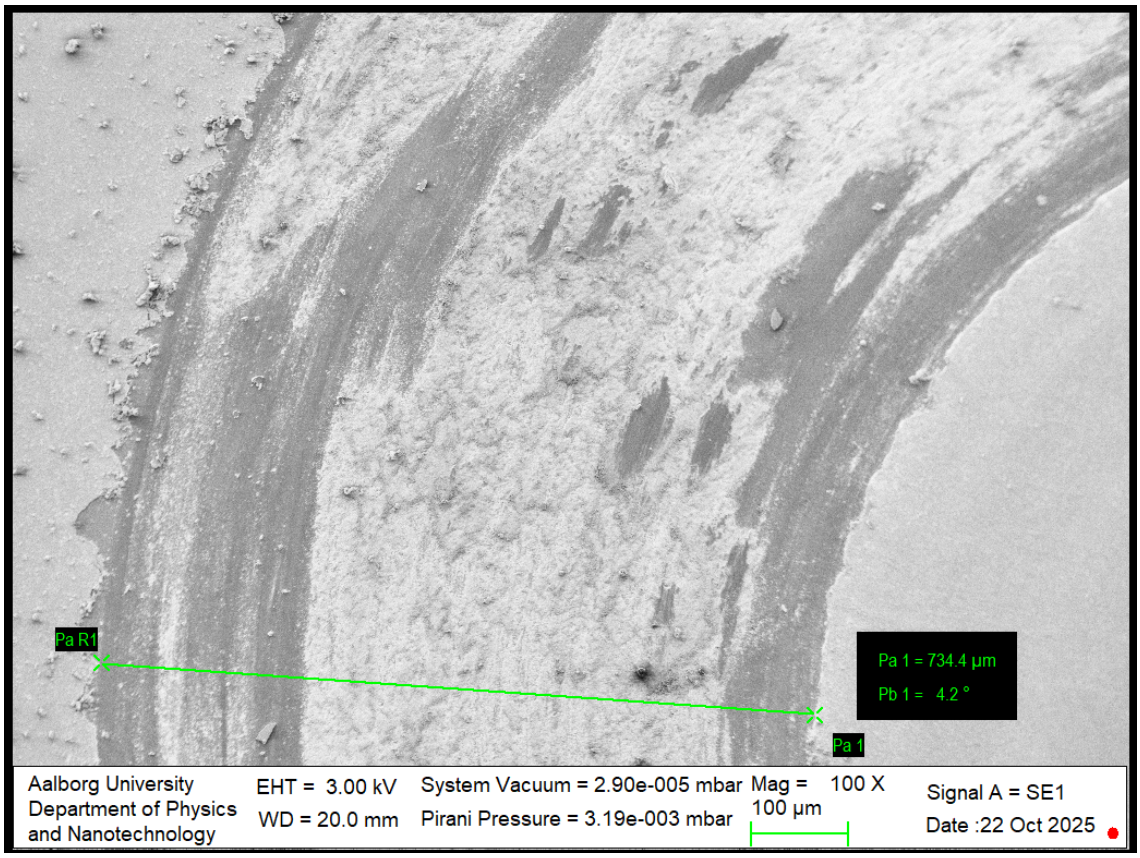

Figure A.165: This image shows a 1500 nm TiN coated stainless steel sample. This image shows the wear track done on the sample by the TRB3 tribometer when equipped with a load of 2 N and during 5000 cycles.

A.4.4 SEM Images of Wear Tracks on 1500 nm TiN Coated Sample at 5 N

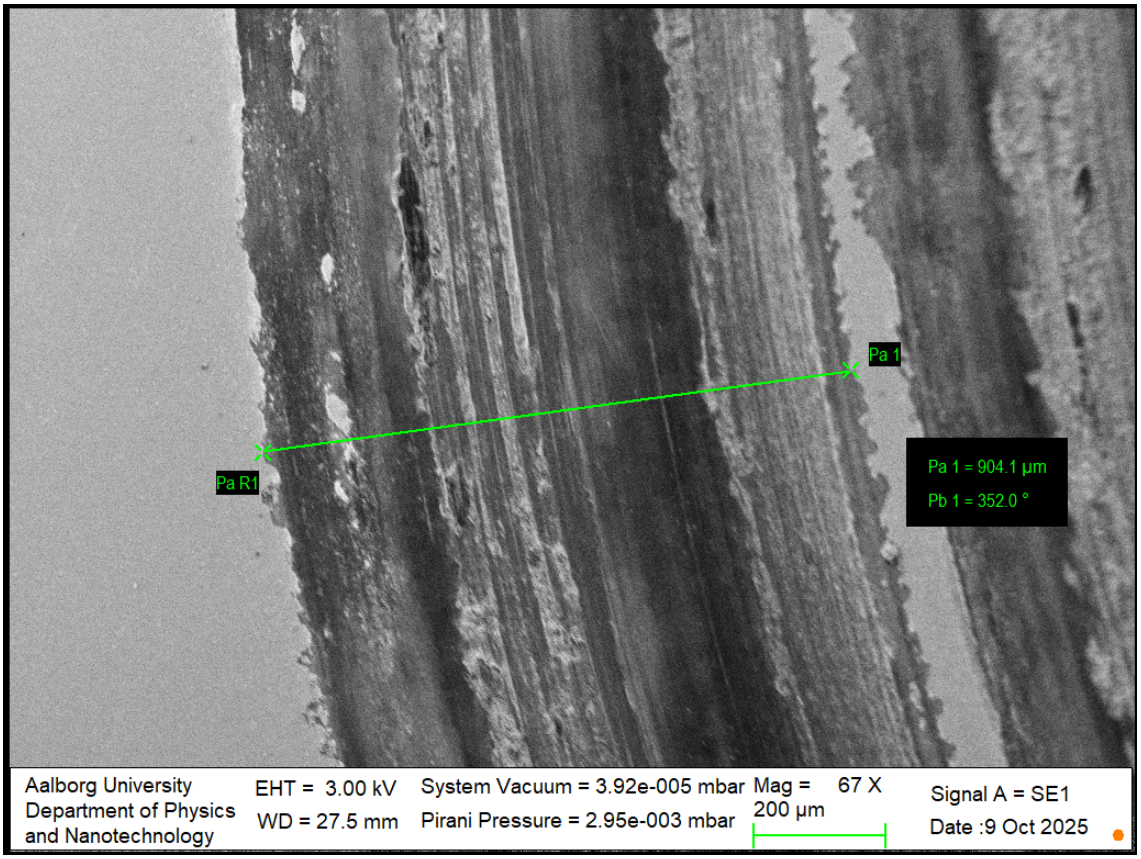

Figure A.166: This image shows a 1500 nm TiN coated stainless steel sample. This image shows the wear track done on the sample by the TRB3 tribometer when equipped with a load of 5 N and during 100 cycles.

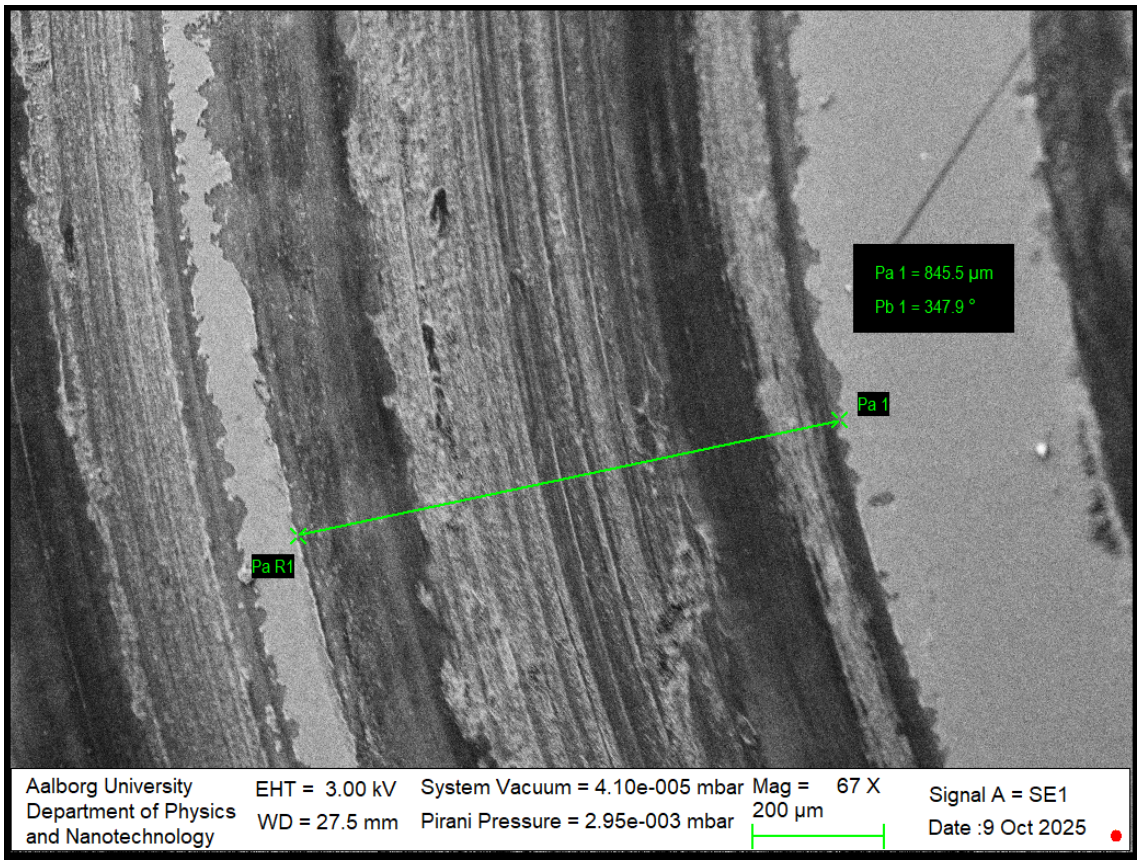

Figure A.167: This image shows a 1500 nm TiN coated stainless steel sample. This image shows the wear track done on the sample by the TRB3 tribometer when equipped with a load of 5 N and during 250 cycles.

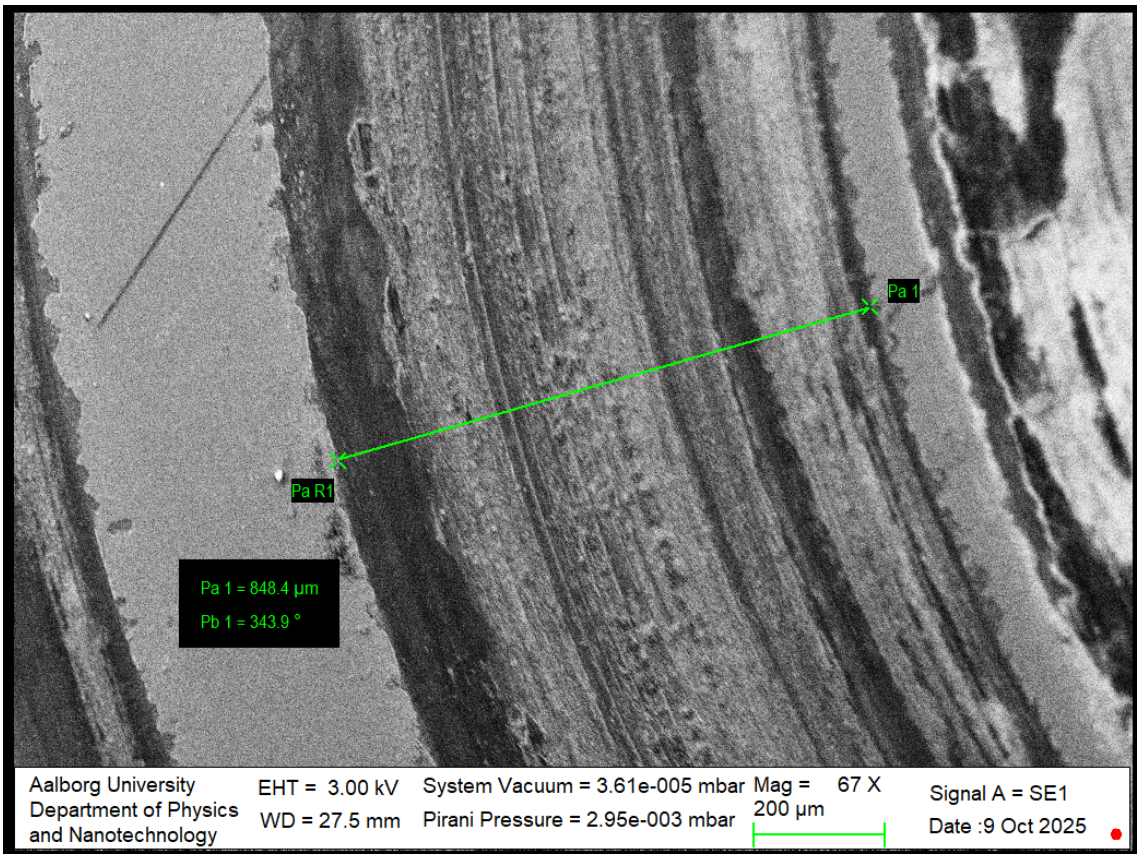

Figure A.168: This image shows a 1500 nm TiN coated stainless steel sample. This image shows the wear track done on the sample by the TRB3 tribometer when equipped with a load of 5 N and during 350 cycles.

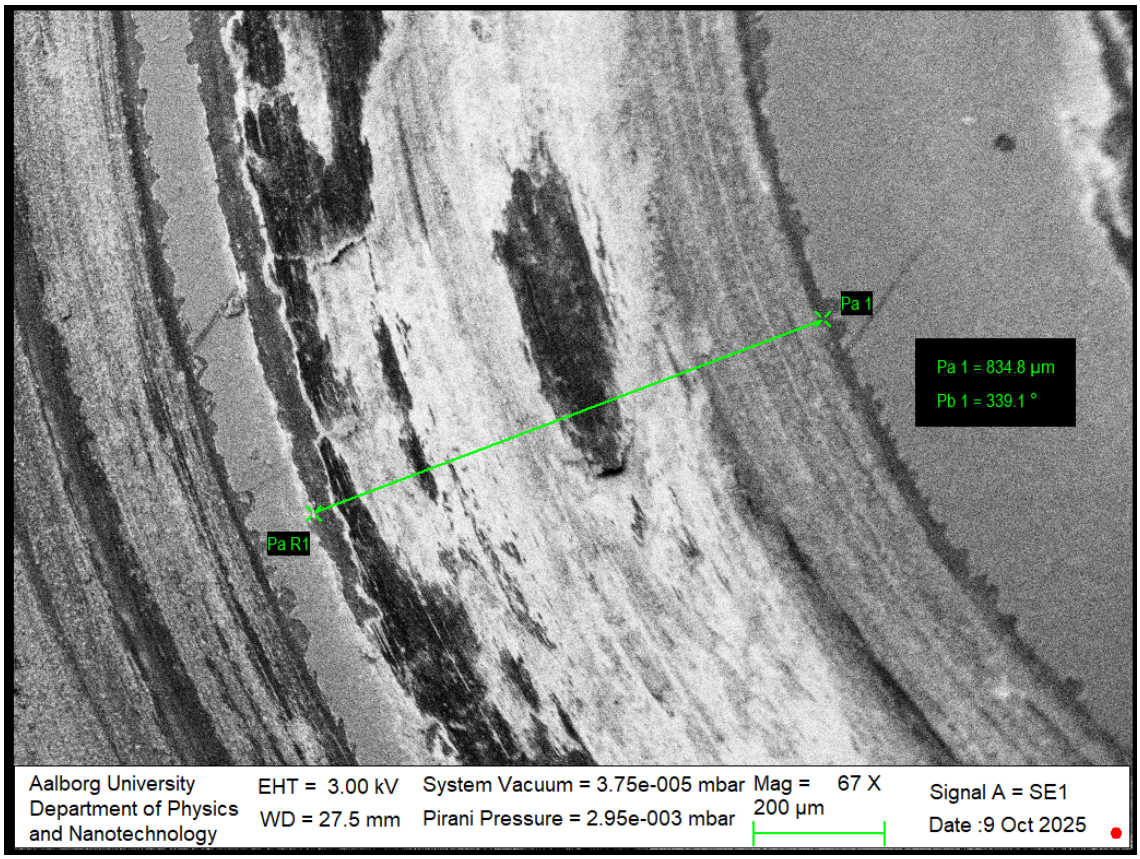

Figure A.169: This image shows a 1500 nm TiN coated stainless steel sample. This image shows the wear track done on the sample by the TRB3 tribometer when equipped with a load of 5 N and during 3000 cycles.

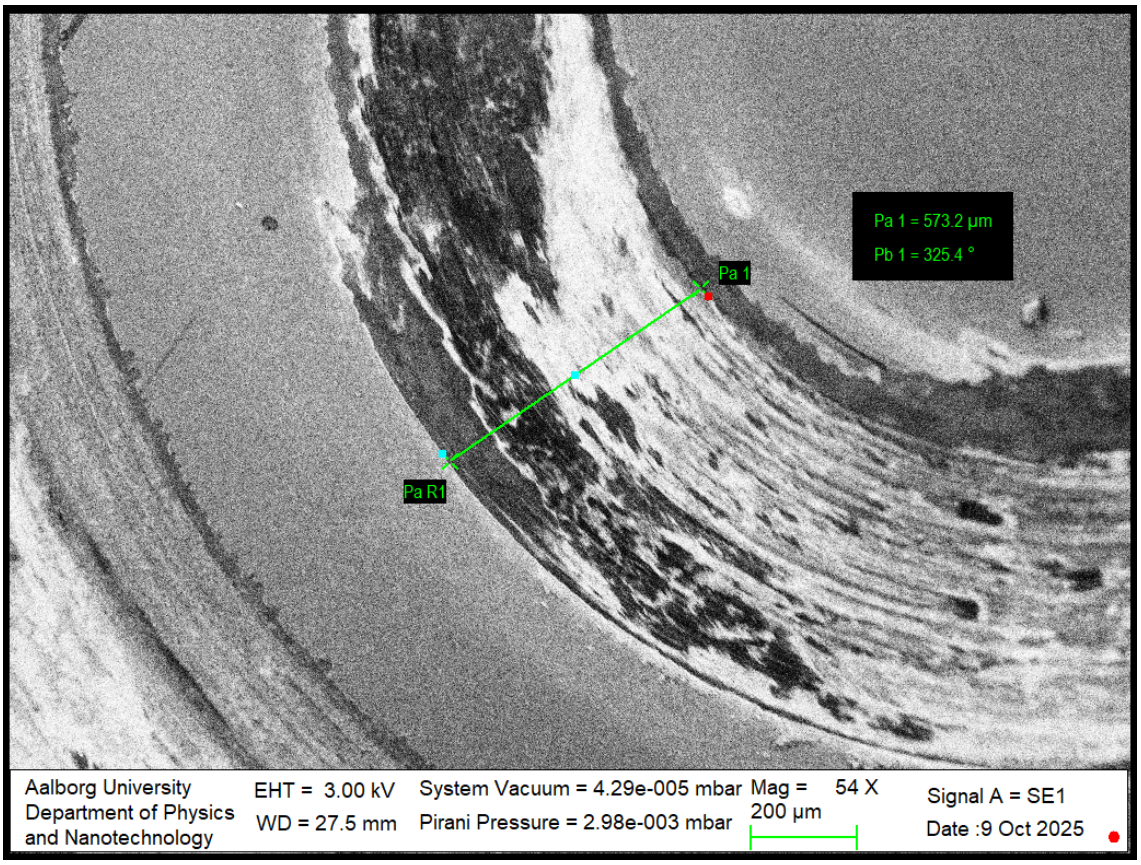

Figure A.170: This image shows a 1500 nm TiN coated stainless steel sample. This image shows the wear track done on the sample by the TRB3 tribometer when equipped with a load of 5 N and during 5000 cycles.

A.4.5 SEM Images of Wear Tracks on 1500 nm TiN Coated Sample at 10 N

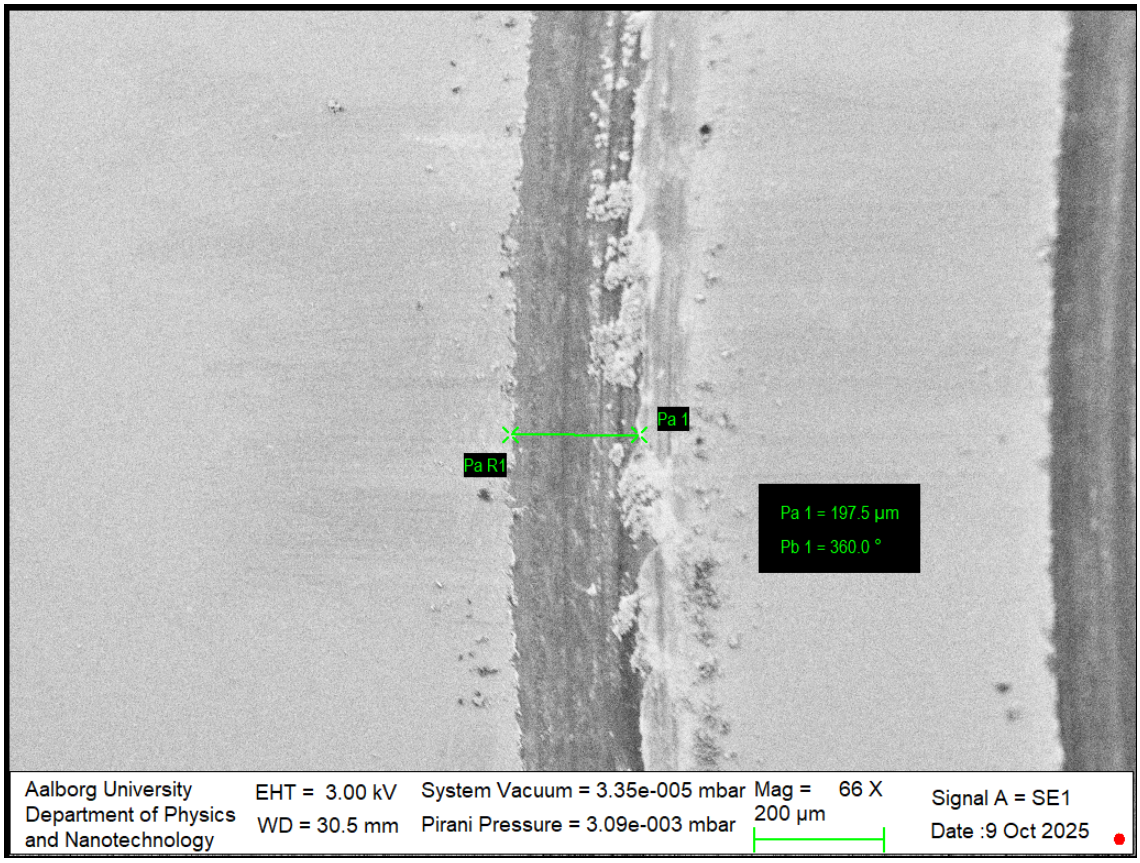

Figure A.171: This image shows a 1500 nm TiN coated stainless steel sample. This image shows the wear track done on the sample by the TRB3 tribometer when equipped with a load of 10 N and during 1 cycle.

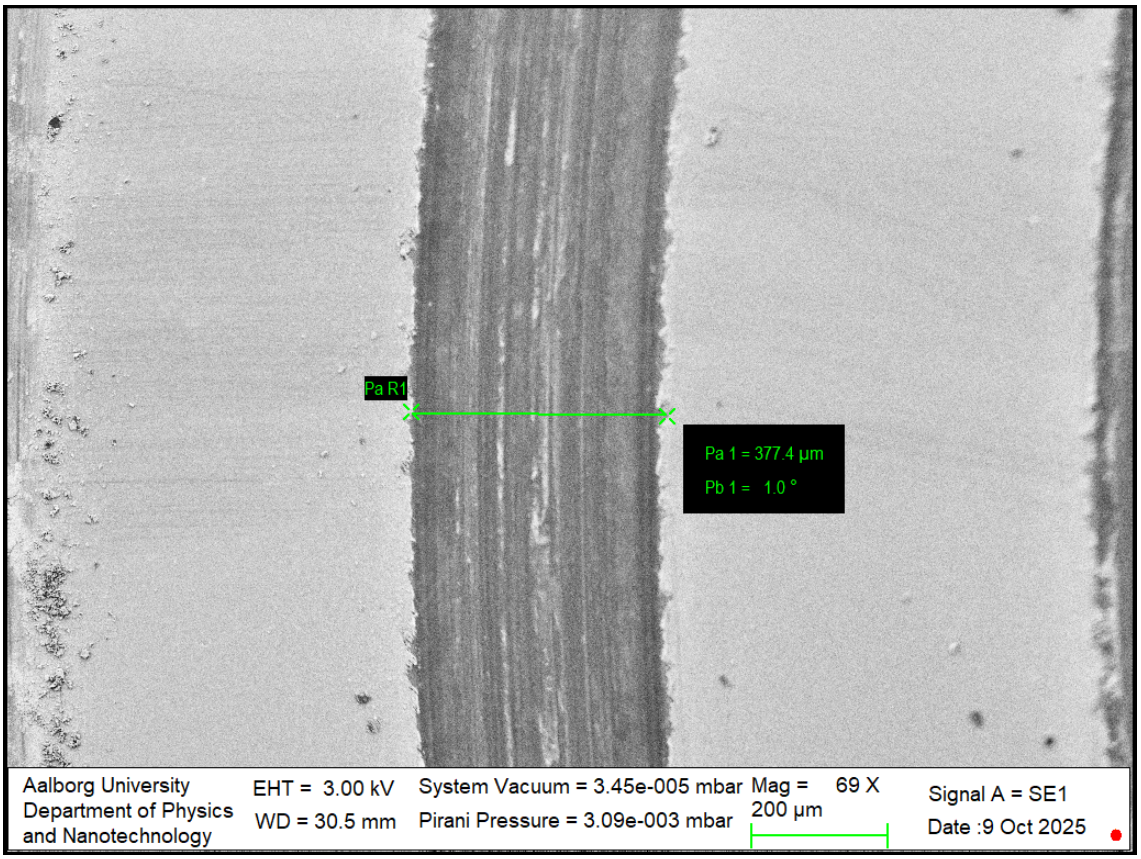

Figure A.172: This image shows a 1500 nm TiN coated stainless steel sample. This image shows the wear track done on the sample by the TRB3 tribometer when equipped with a load of 10 N and during 10 cycles.

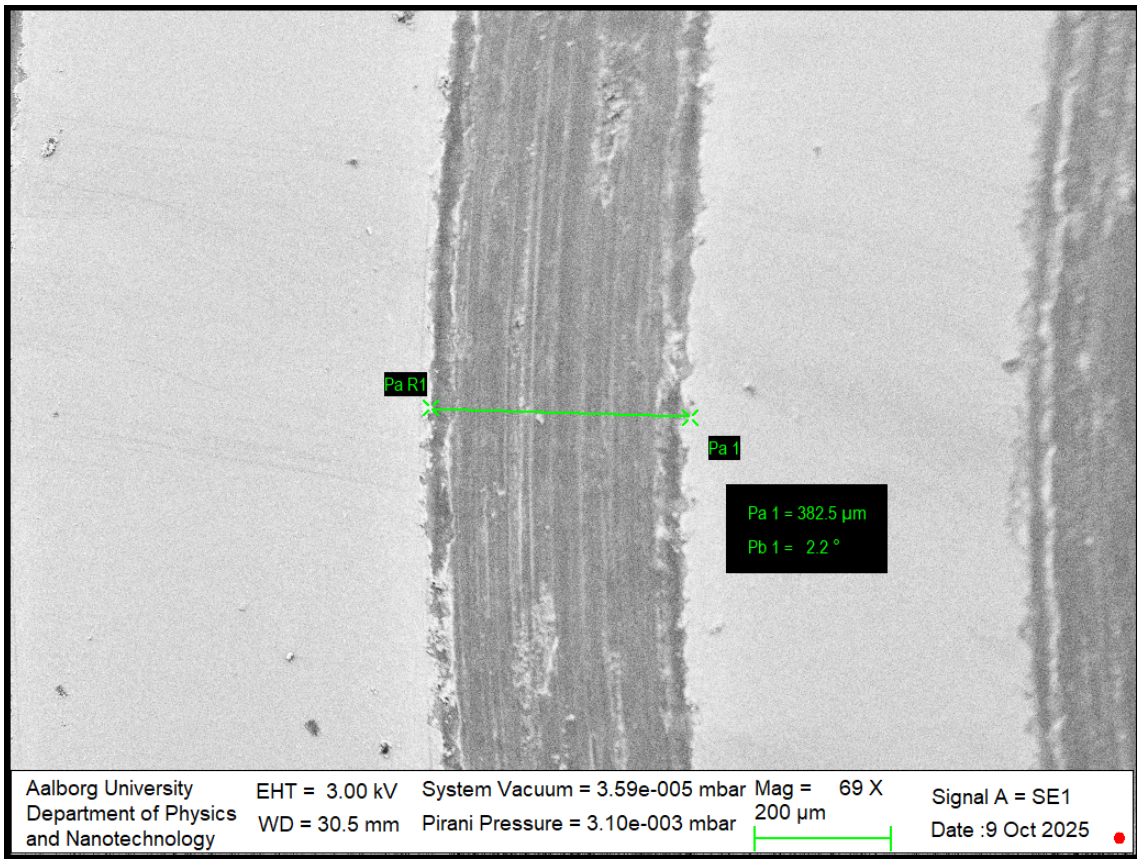

Figure A.173: This image shows a 1500 nm TiN coated stainless steel sample. This image shows the wear track done on the sample by the TRB3 tribometer when equipped with a load of 10 N and during 50 cycles.

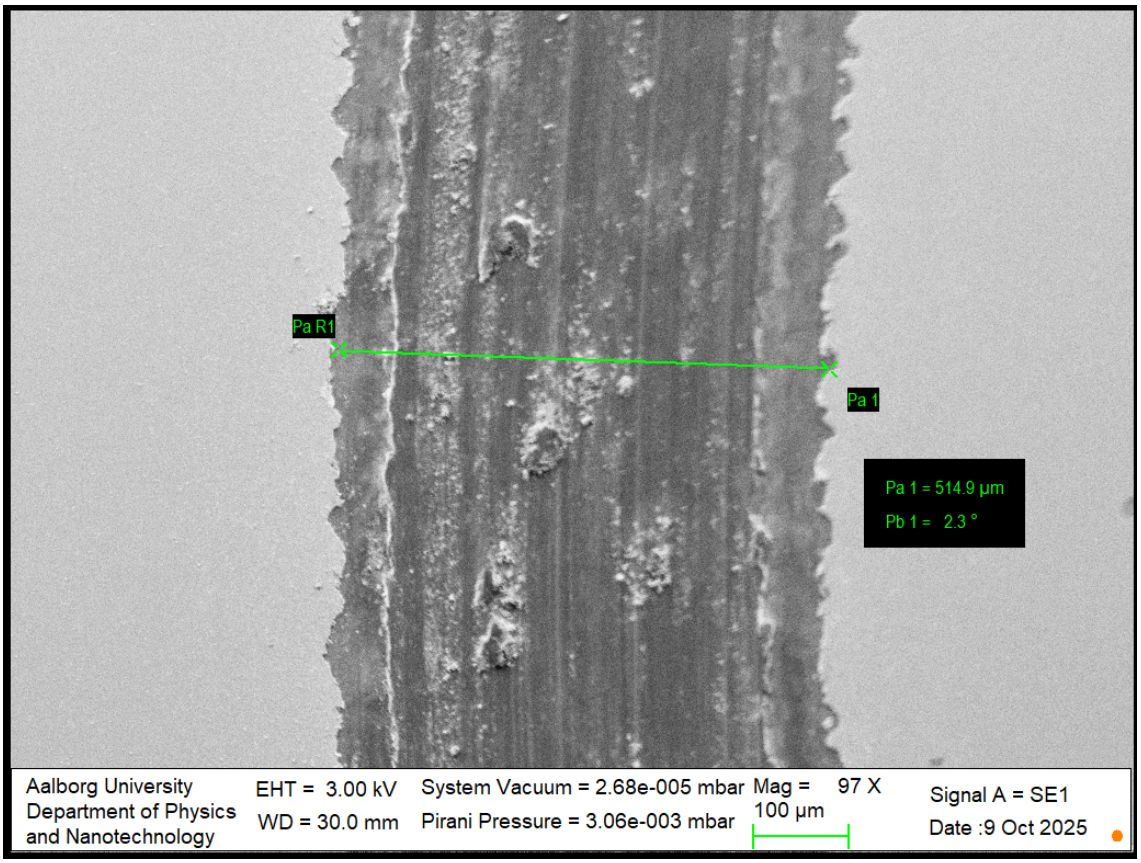

Figure A.174: This image shows a 1500 nm TiN coated stainless steel sample. This image shows the wear track done on the sample by the TRB3 tribometer when equipped with a load of 10 N and during 100 cycles.

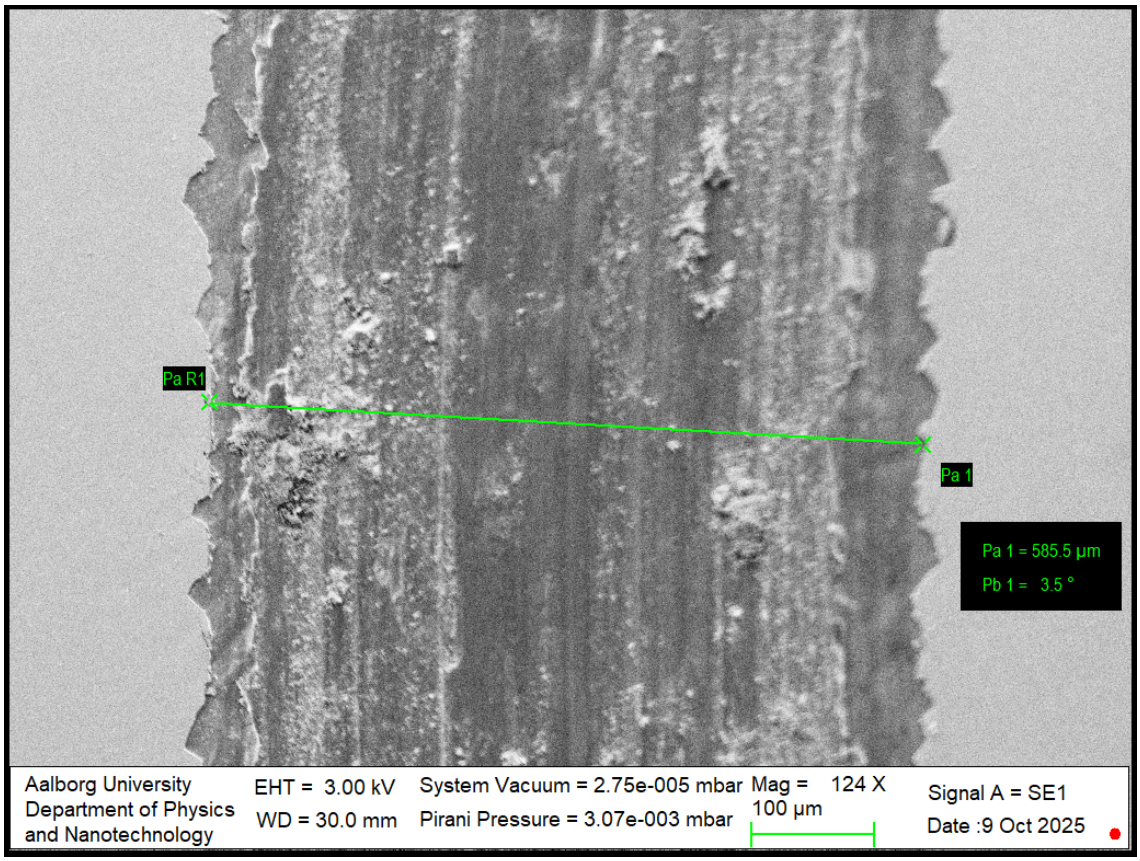

Figure A.175: This image shows a 1500 nm TiN coated stainless steel sample. This image shows the wear track done on the sample by the TRB3 tribometer when equipped with a load of 10 N and during 250 cycles.

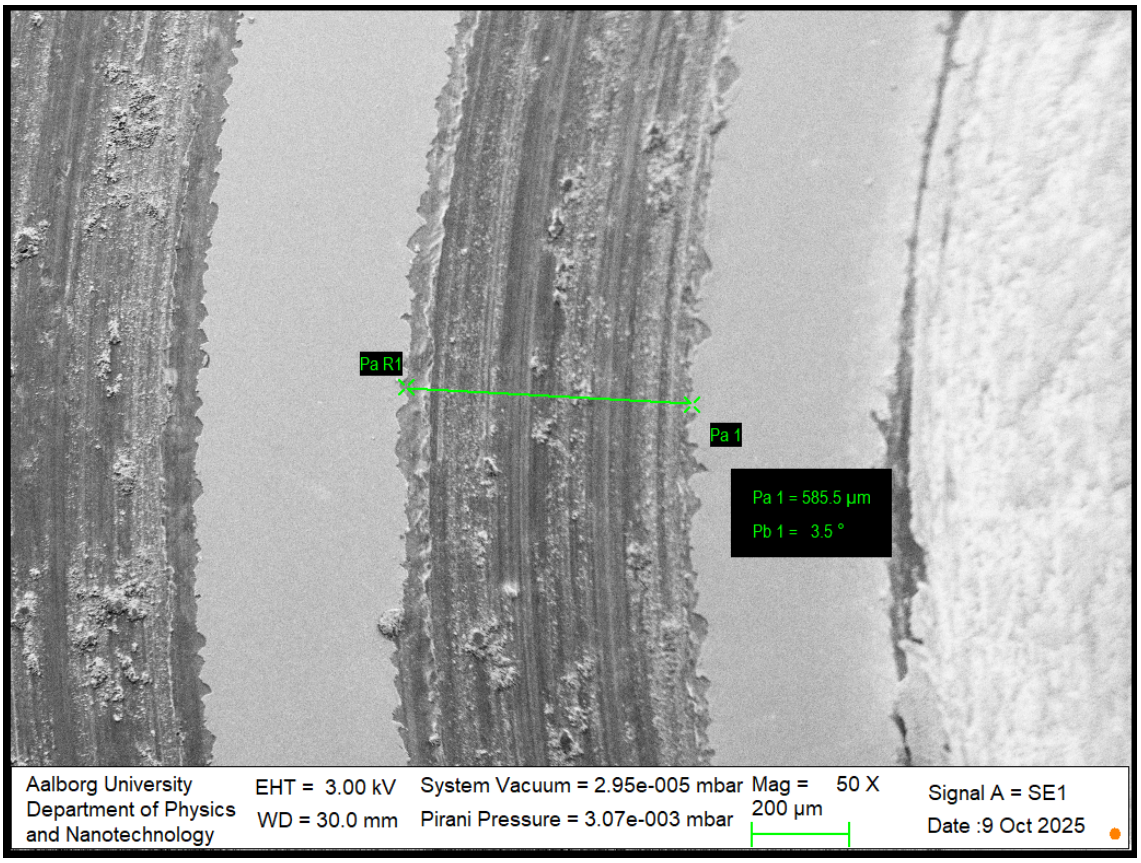

Figure A.176: This image shows a 1500 nm TiN coated stainless steel sample. This image shows the wear track done on the sample by the TRB3 tribometer when equipped with a load of 10 N and during 350 cycles.

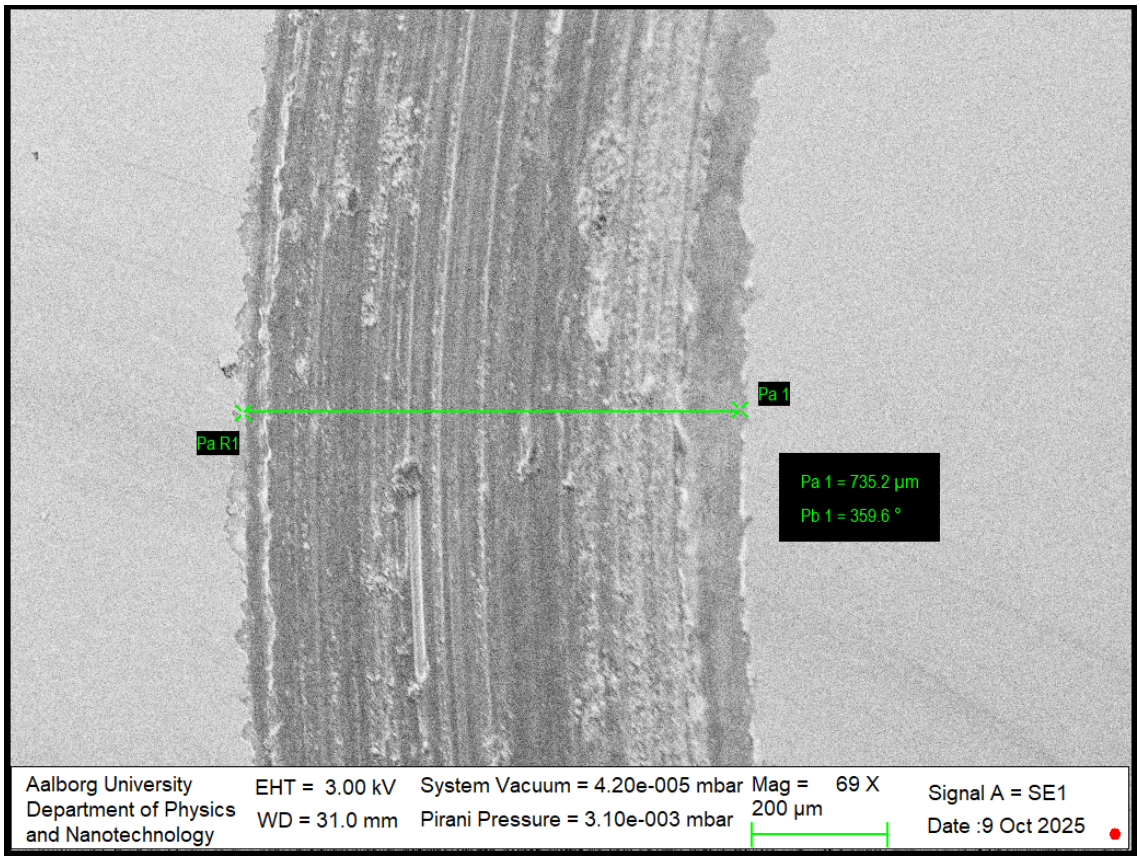

Figure A.177: This image shows a 1500 nm TiN coated stainless steel sample. This image shows the wear track done on the sample by the TRB3 tribometer when equipped with a load of 10 N and during 500 cycles.

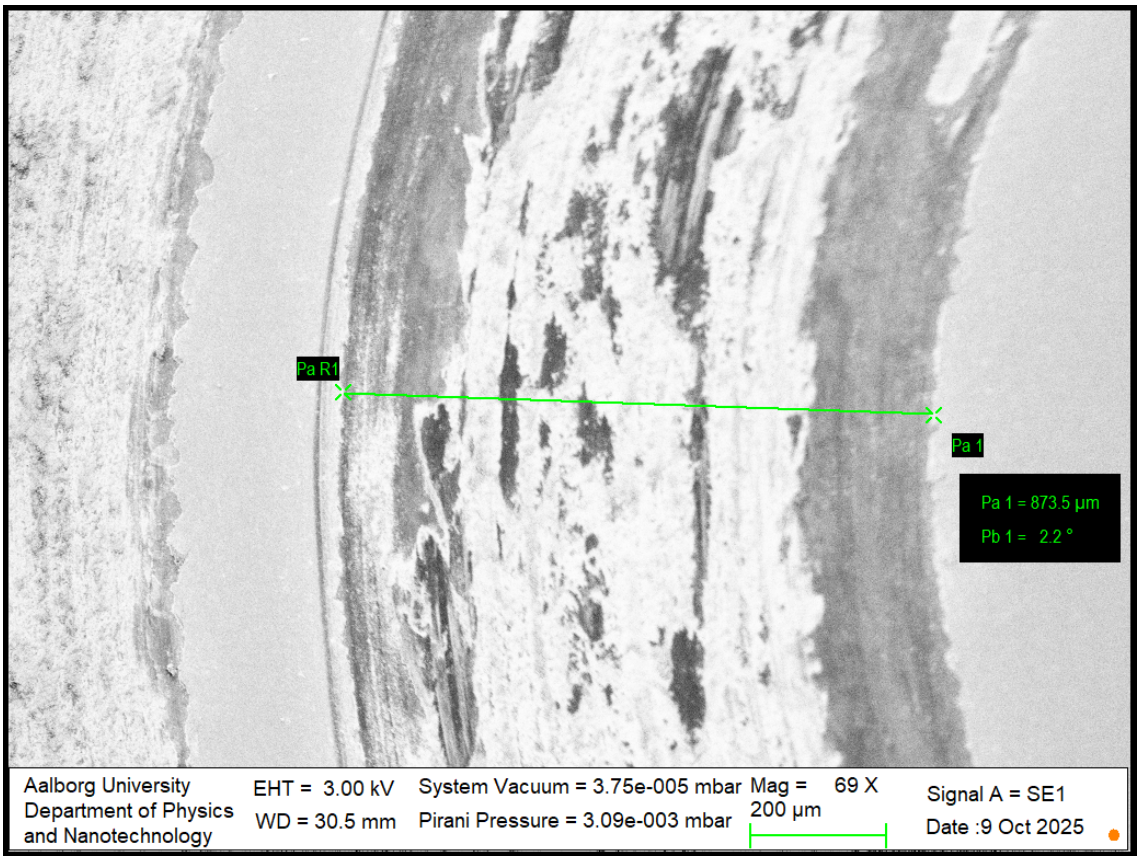

Figure A.178: This image shows a 1500 nm TiN coated stainless steel sample. This image shows the wear track done on the sample by the TRB3 tribometer when equipped with a load of 10 N and during 2000 cycles.

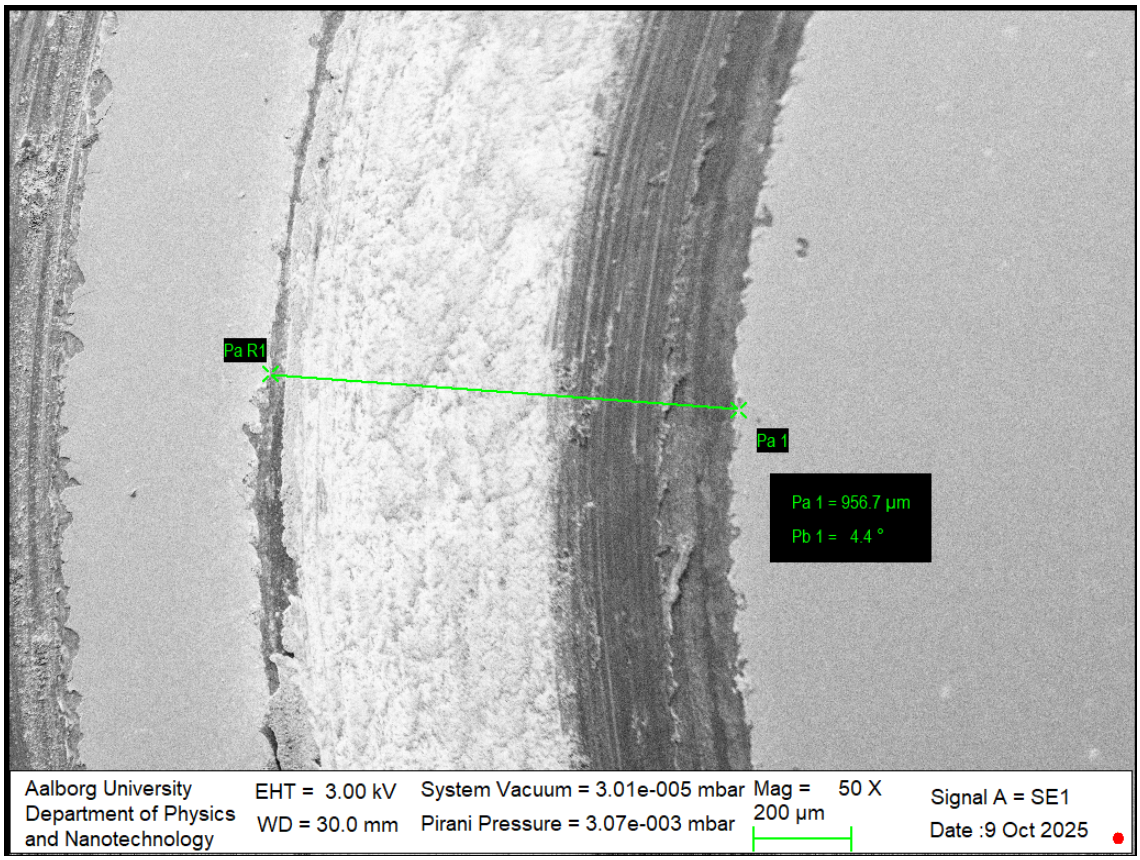

Figure A.179: This image shows a 1500 nm TiN coated stainless steel sample. This image shows the wear track done on the sample by the TRB3 tribometer when equipped with a load of 10 N and during 3000 cycles.

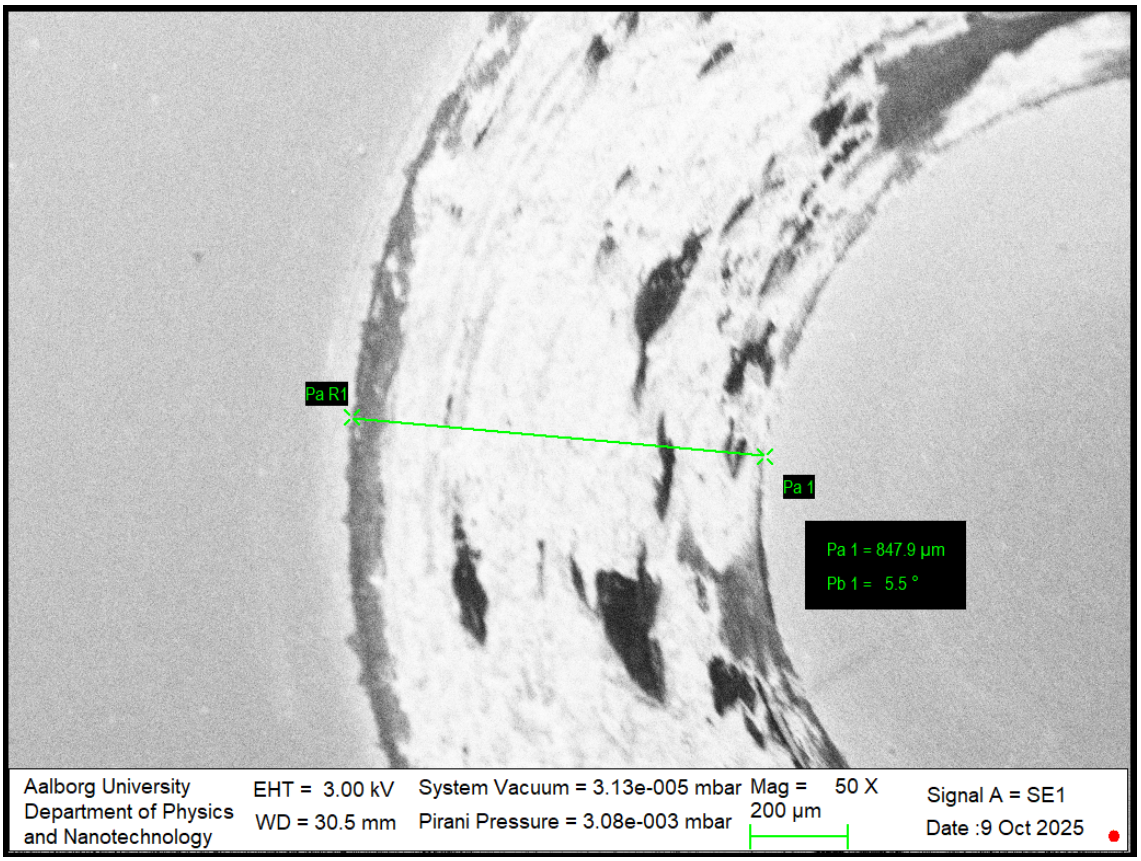

Figure A.180: This image shows a 1500 nm TiN coated stainless steel sample. This image shows the wear track done on the sample by the TRB3 tribometer when equipped with a load of 10 N and during 5000 cycles.

A.5 All Stainless Steel Hardness Measurements

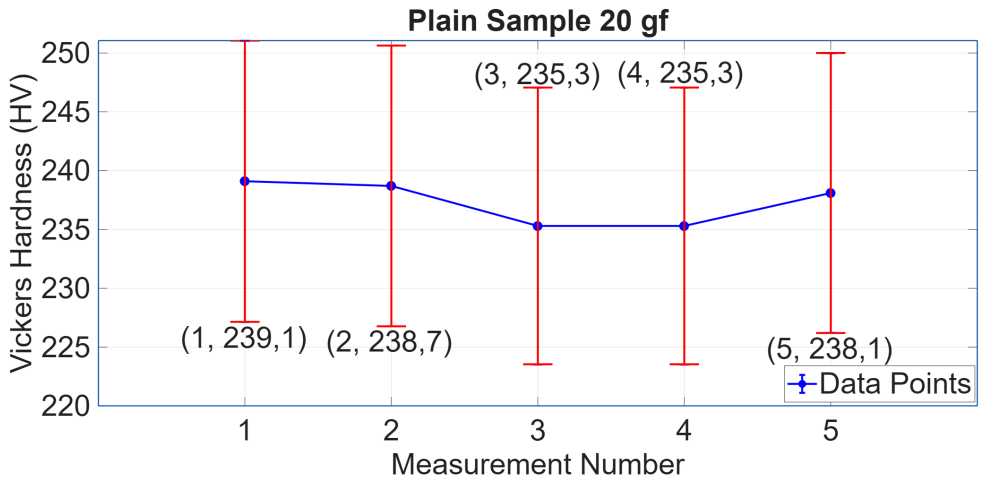

Figure A.181: This image shows a plain stainless steel sample. This image shows the hardness test results performed on Duramin-40 with load of 20 gf.

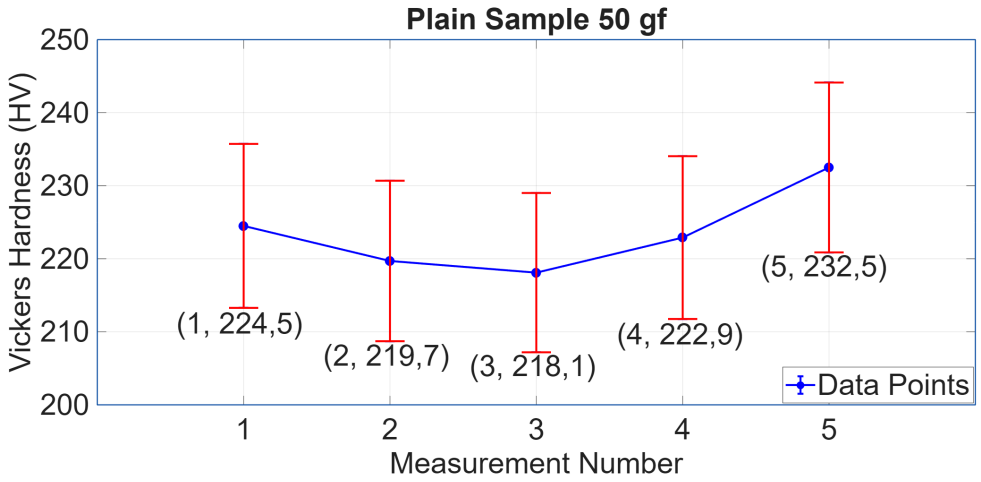

Figure A.182: This image shows a plain stainless steel sample. This image shows the hardness test results performed on Duramin-40 with load of 50 gf.

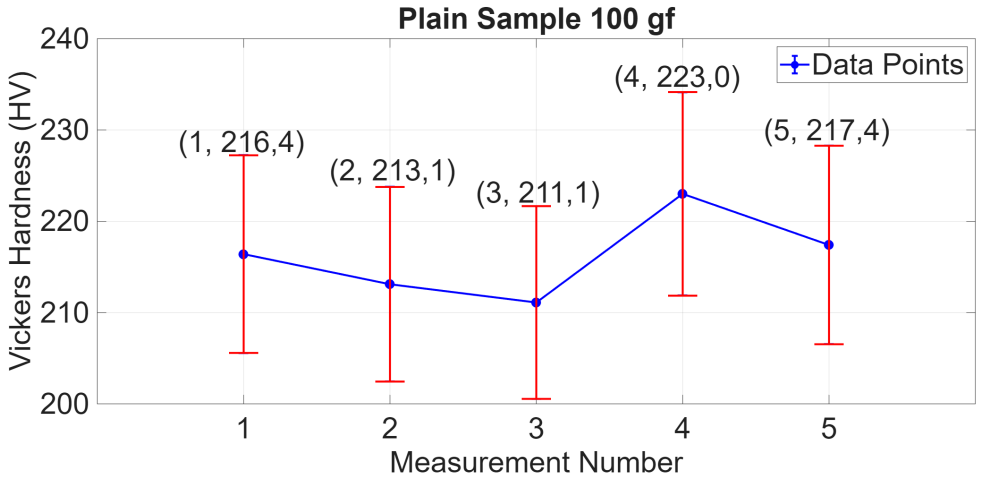

Figure A.183: This image shows a plain stainless steel sample. This image shows the hardness test results performed on Duramin-40 with load of 100 gf.

A.5.1 All 150 nm TiN Coated Hardness Measurements

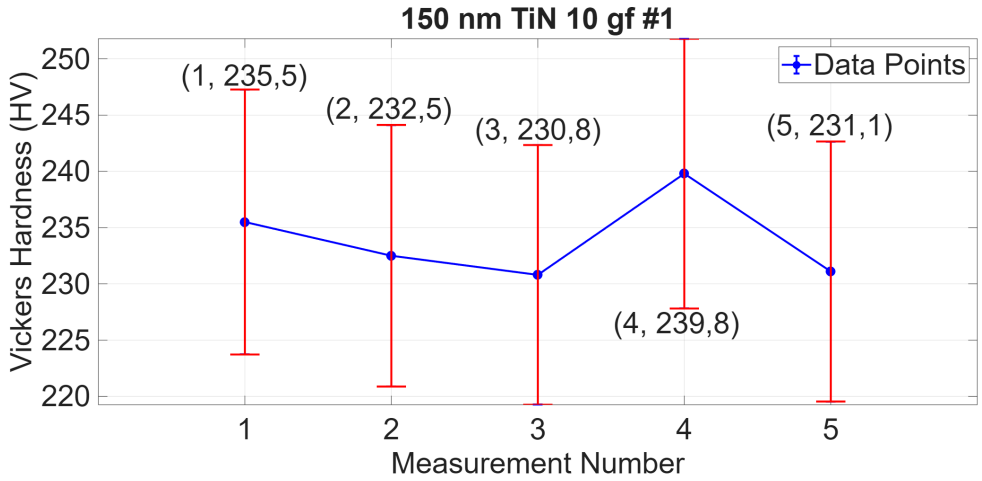

Figure A.184: This image shows a stainless steel coated with 150 nm TiN. This image shows the hardness test results performed on Duramin-40 with load of 10 gf.

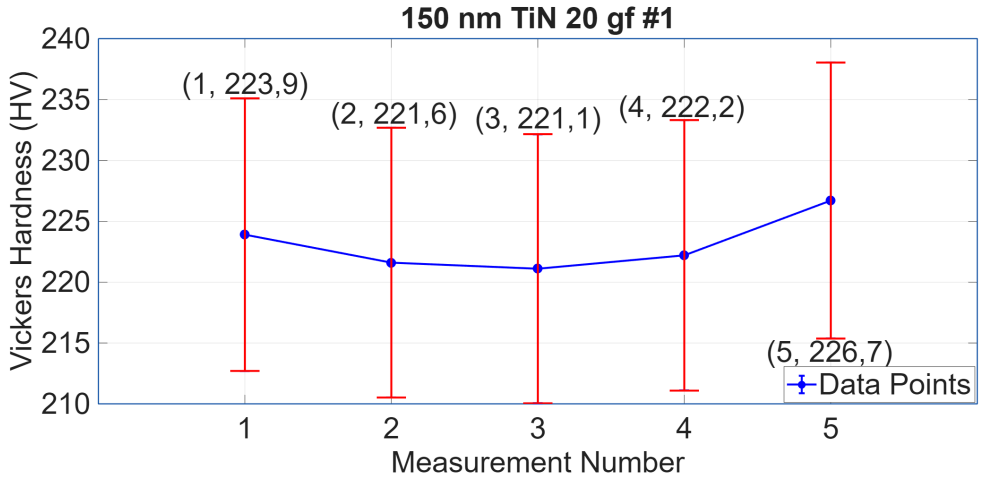

Figure A.185: This image shows a stainless steel coated with 150 nm TiN. This image shows the hardness test results performed on Duramin-40 with load of 20 gf.

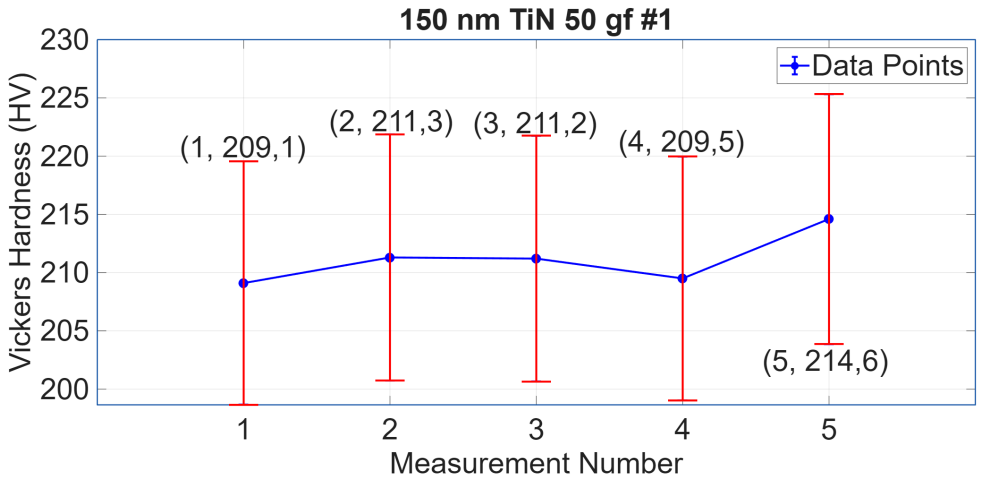

Figure A.186: This image shows a stainless steel coated with 150 nm TiN. This image shows the hardness test results performed on Duramin-40 with load of 50 gf.

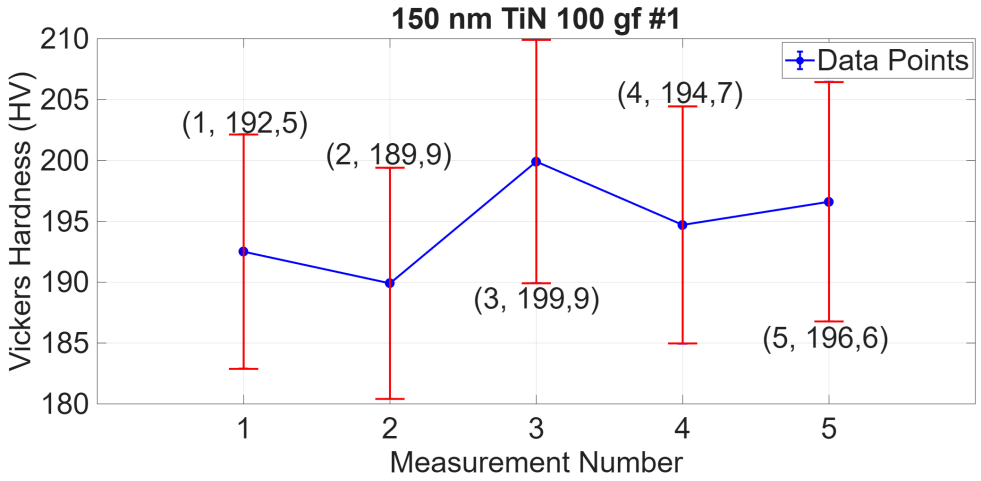

Figure A.187: This image shows a stainless steel coated with 150 nm TiN. This image shows the hardness test results performed on Duramin-40 with load of 100 gf.

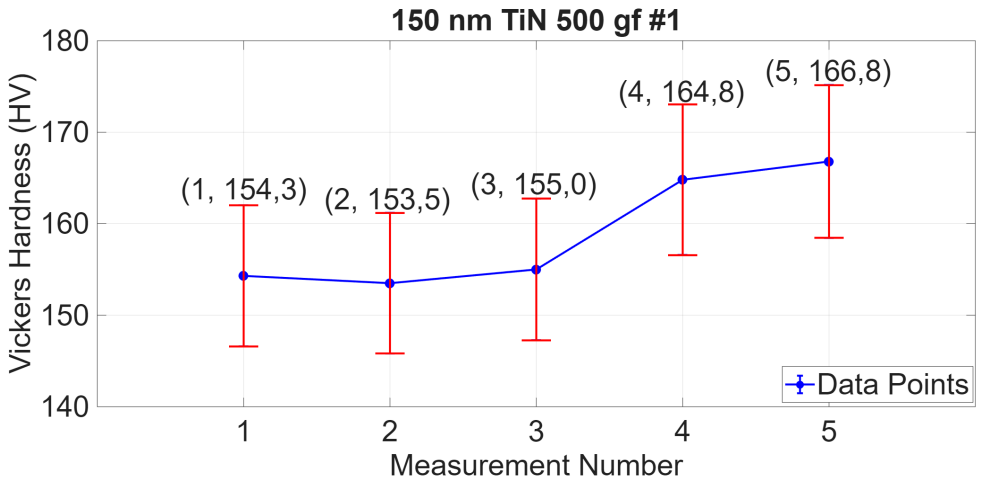

Figure A.188: This image shows a stainless steel coated with 150 nm TiN. This image shows the hardness test results performed on Duramin-40 with load of 500 gf.

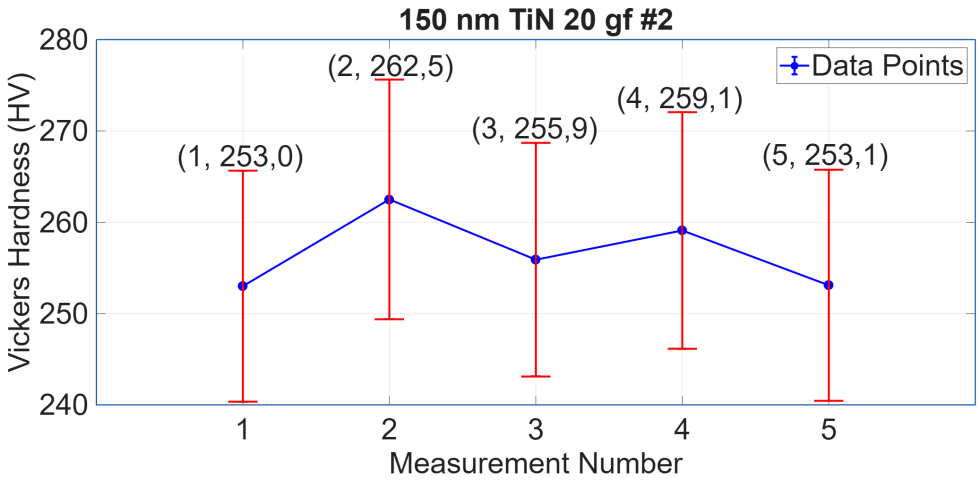

Figure A.189: This image shows a stainless steel coated with 150 nm TiN. This image shows the hardness test results performed on Duramin-40 with load of 20 gf.

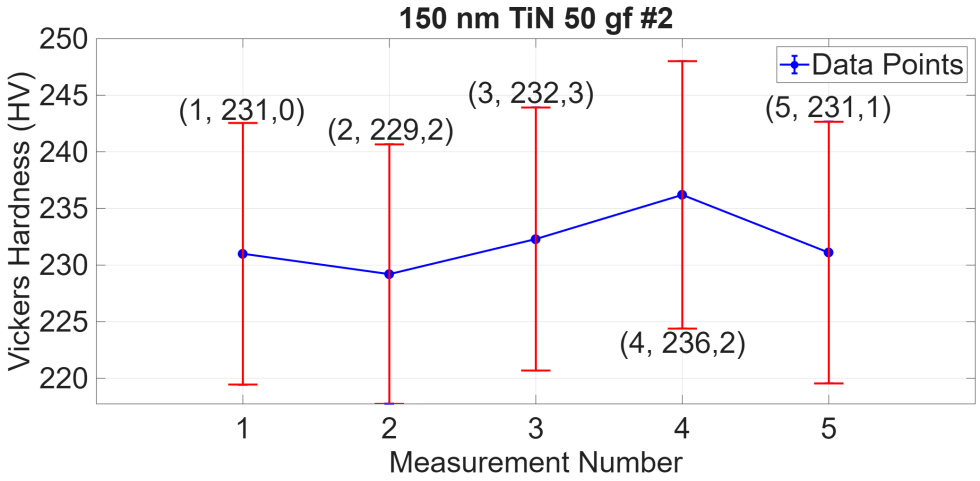

Figure A.190: This image shows a stainless steel coated with 150 nm TiN. This image shows the hardness test results performed on Duramin-40 with load of 50 gf.

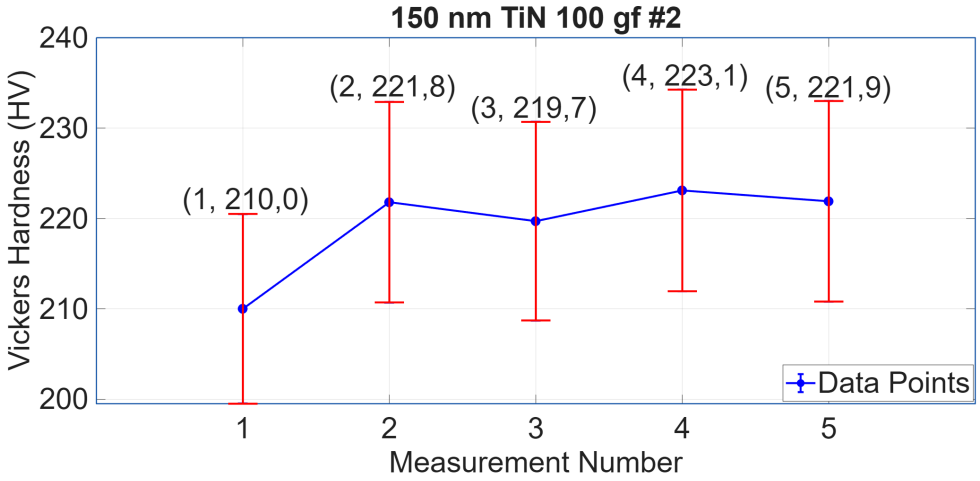

Figure A.191: This image shows a stainless steel coated with 150 nm TiN. This image shows the hardness test results performed on Duramin-40 with load of 100 gf.

A.5.2 All 300 nm TiN Coated Hardness Measurements

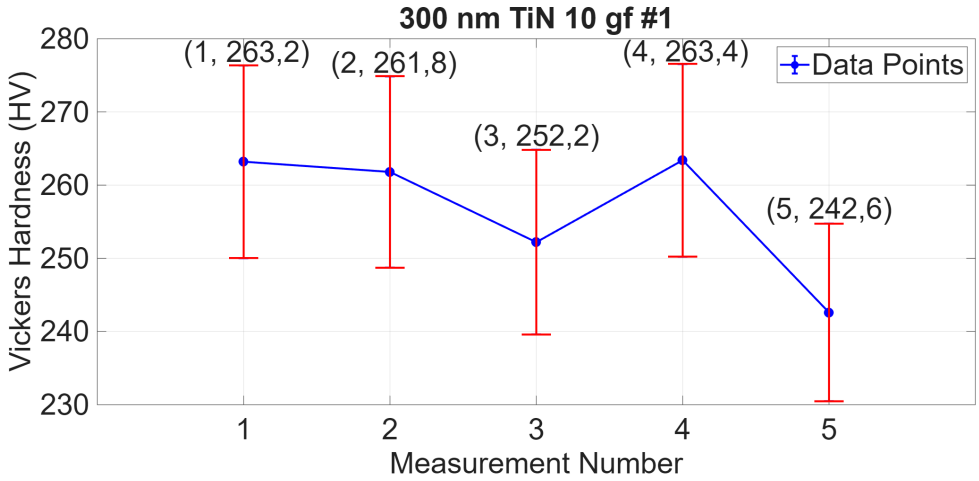

Figure A.192: This image shows a stainless steel coated with 300 nm TiN. This image shows the hardness test results performed on Duramin-40 with load of 10 gf.

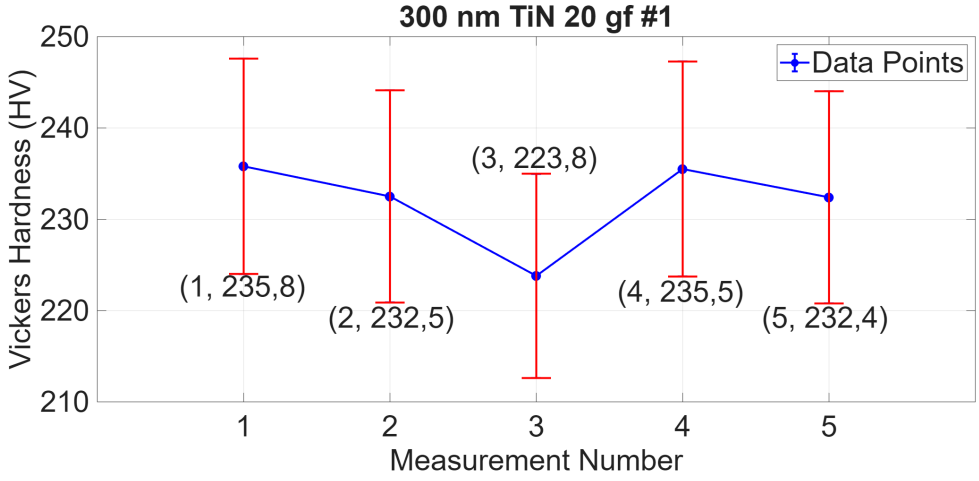

Figure A.193: This image shows a stainless steel coated with 300 nm TiN. This image shows the hardness test results performed on Duramin-40 with load of 20 gf.

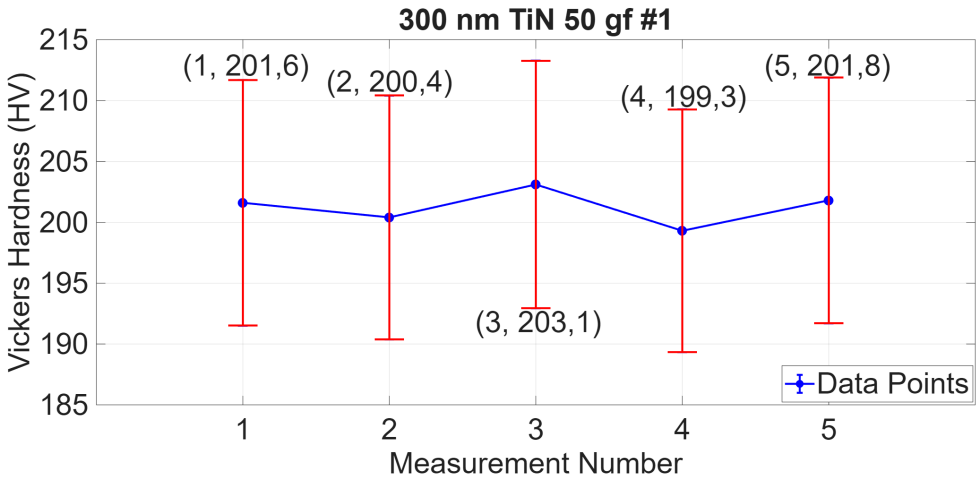

Figure A.194: This image shows a stainless steel coated with 300 nm TiN. This image shows the hardness test results performed on Duramin-40 with load of 50 gf.

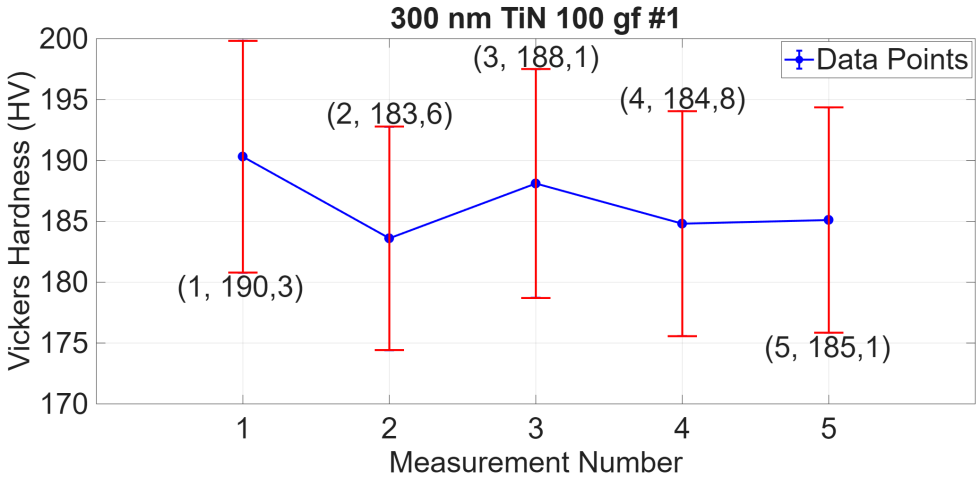

Figure A.195: This image shows a stainless steel coated with 300 nm TiN. This image shows the hardness test results performed on Duramin-40 with load of 100 gf.

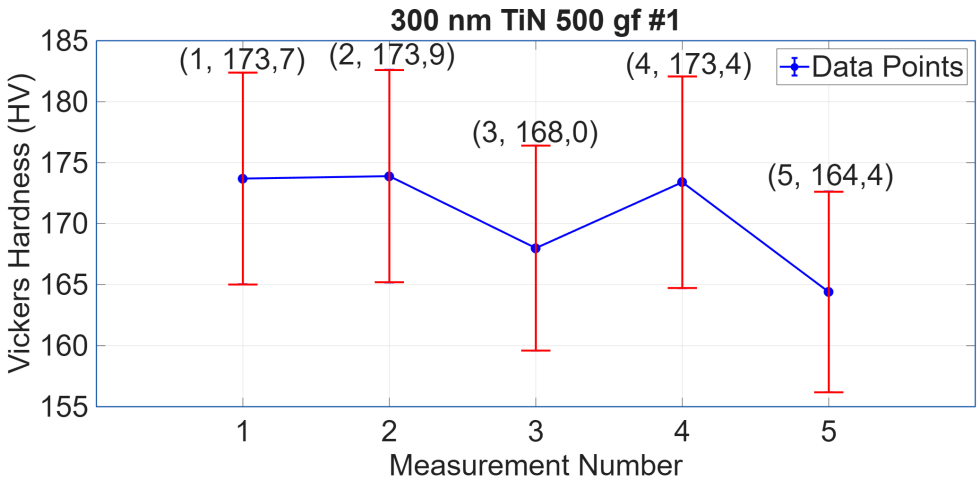

Figure A.196: This image shows a stainless steel coated with 300 nm TiN. This image shows the hardness test results performed on Duramin-40 with load of 500 gf.

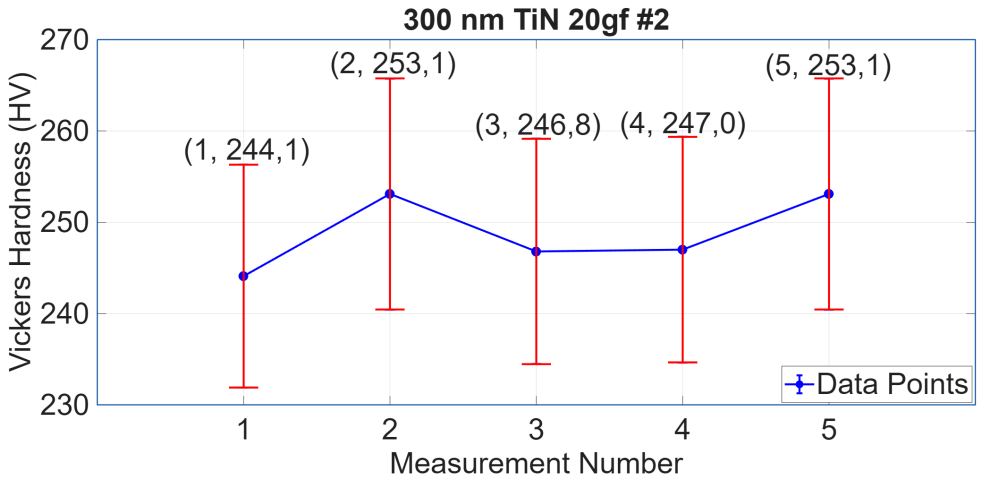

Figure A.197: This image shows a stainless steel coated with 300 nm TiN. This image shows the hardness test results performed on Duramin-40 with load of 20 gf.

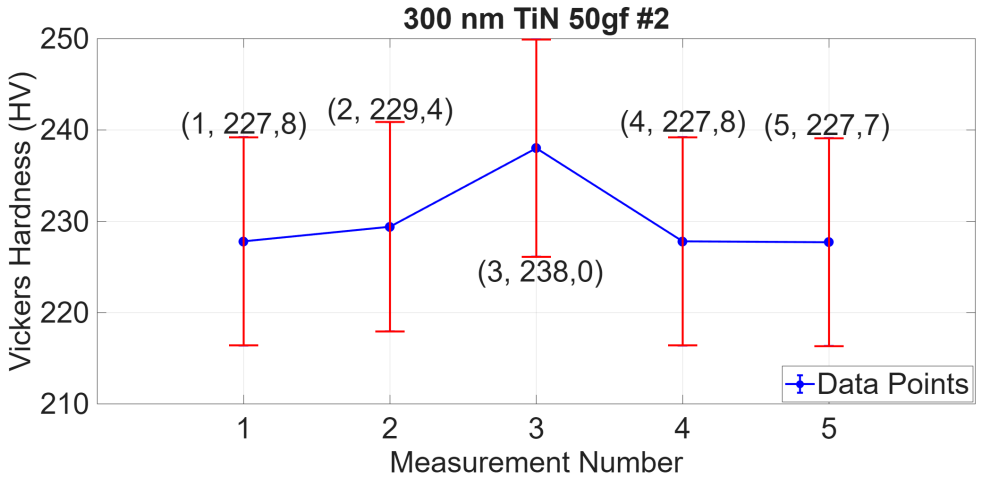

Figure A.198: This image shows a stainless steel coated with 300 nm TiN. This image shows the hardness test results performed on Duramin-40 with load of 50 gf.

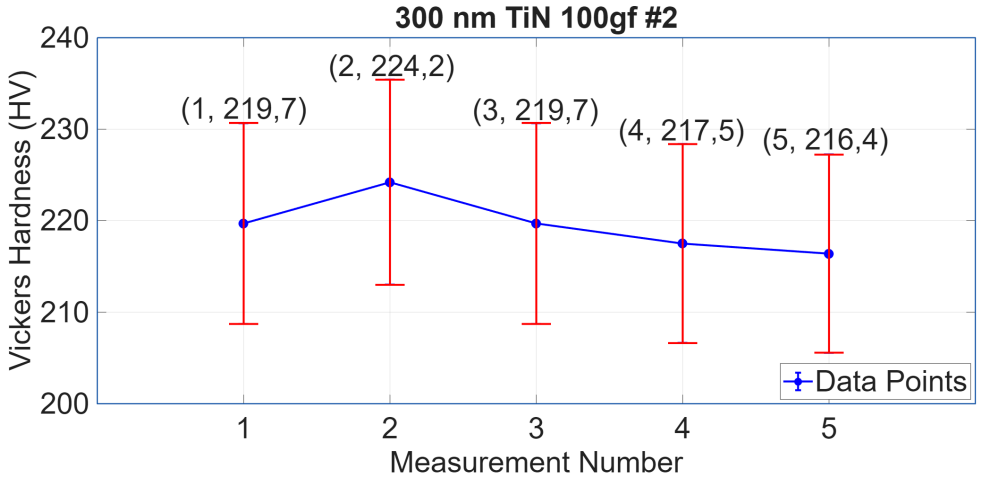

Figure A.199: This image shows a stainless steel coated with 300 nm TiN. This image shows the hardness test results performed on Duramin-40 with load of 100 gf.

A.5.3 All 1500 nm TiN Coated Hardness Measurements

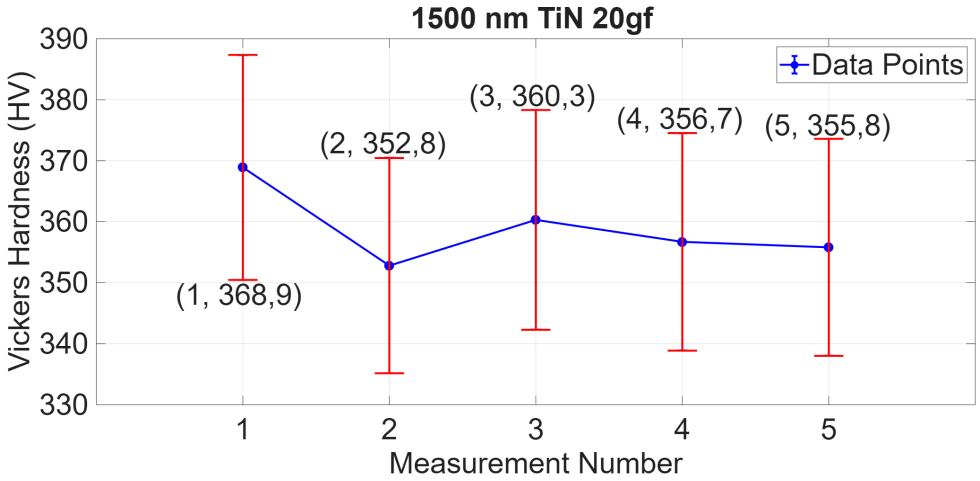

Figure A.200: This image shows a stainless steel coated with 1500 nm TiN. This image shows the hardness test results performed on Duramin-40 with load of 20 gf.

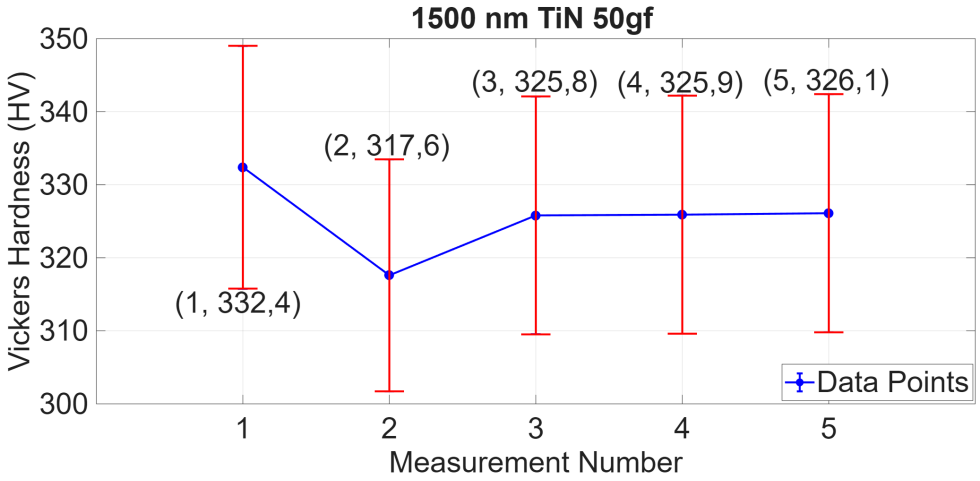

Figure A.201: This image shows a stainless steel coated with 1500 nm TiN. This image shows the hardness test results performed on Duramin-40 with load of 50 gf.

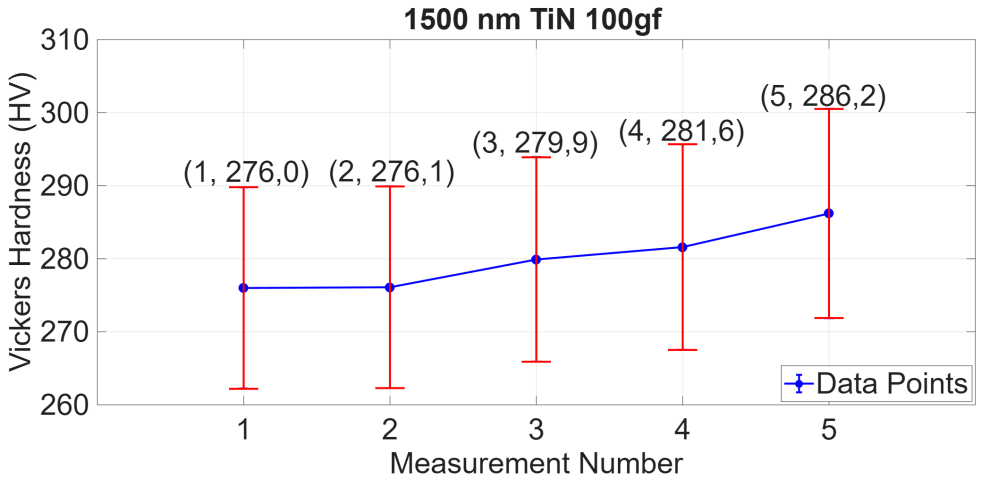

Figure A.202: This image shows a stainless steel coated with 1500 nm TiN. This image shows the hardness test results performed on Duramin-40 with load of 100 gf.

A.6 150 nm TiN Coated Stainless Steel Sample

A.6.1 300 nm TiN Coated Stainless Steel Sample

This section contains the tribometer and XR-2 results for two different samples. The description of those samples and some tribometry parameters are in the table below.

Sample Name	Sample Material	Diameter of the Sample	Coating Material and Thickness	Ball Material and Diameter	Linear Speed
Sample 1	Stainless Steel	2 cm x 2 cm	TiN 150 nm	Alumina 1 cm	2 cm/s
Sample 2	Stainless Steel	2 cm x 2 cm	TiN 300 nm	Alumina 1 cm	2 cm/s

Table A.1: This table shows the description of samples used in those measurements. The TiN coated samples are numerated sample 1 and 2. Furthermore, the table shows the information about the coating and tribometer ball for each sample.

Samples 1 and 2 were subjected to wear using the pin-on-disk tribometer with a 1 cm diameter alumina ball did not yield any proper information about the wear. The 1.0 cm diameter ball was chosen for these experiments since this ball is less rough on the material and it was suspected this would fix an issue of the coating being penetrated, as seen on Figure A.203, however it did not. These samples encountered the issue of the coating being ripped off even at the lowest possible load of 0.25 N and with the lowest possible cycle count i.e.

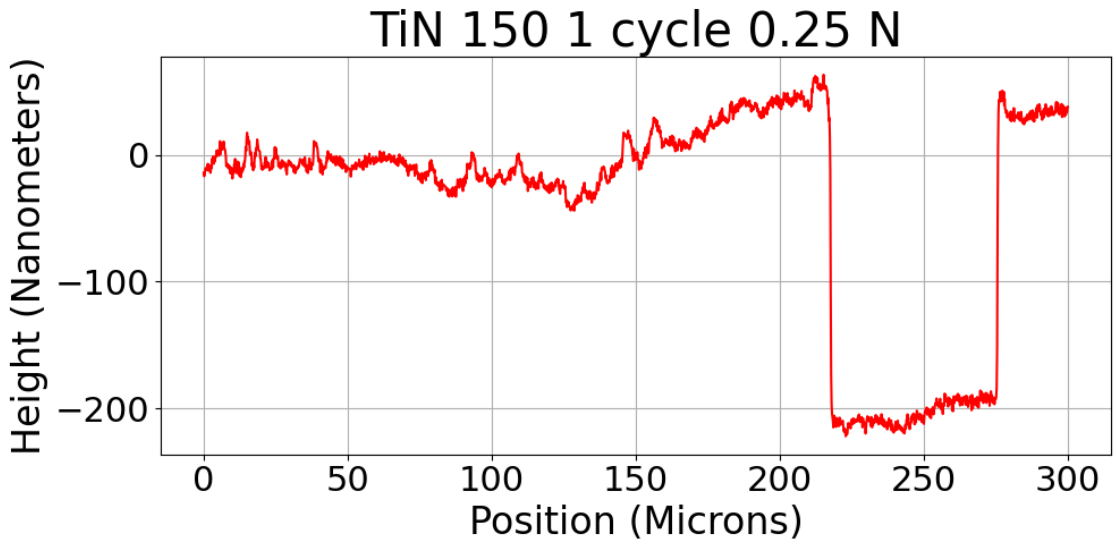

Figure A.203: This figure shows Sample 1. This figure shows the wear track the TRB makes in the sample when equipped with a load of 0.25 N and during only 1 cycle.

For Figure A.203 the wear rate is 4.4 10^{-2}mm^3/Nm, which is quite high, however, considering the figure this is likely due to the bad adhesion.
It is noteworthy that the tested TiN coatings are quite thin compared to typical industrial coatings which are often 5–10 μm. Thicker coatings generally sustain higher loads and cycle counts without delamination. The failure shown here is thus consistent with the claim that coating thickness is a critical parameter for tribological performance. The results from these samples is what initially showed the need to increase the thickness significantly.

A.7 AFM

The samples were tested on the AFM (Atomic Force Microscope) to ensure that some proper coating had indeed been done on the sample. This was done since initial ellipsometry measurements that were done yielded concerning results: that the coating contained no nitrate. Due to this the sample was put in the SEM, which showed nitrate for the same sample, however, the peaks of nitrate and titanium overlap so the exact amounts were somewhat unclear.
The AFM was supposed to be a measure the proportions between the two compounds, however, it was unable to do this since imaging does not directly differentiate between them. The AFM did indeed confirm some coating deposition, however, it was unable to tell us anything concrete about the proportion of titanium and nitrate. The AFM was also used in an attempt to capture the holes left by the DURAMIN-40 in the samples, however, the hole proved too deep for the cantilevers range.

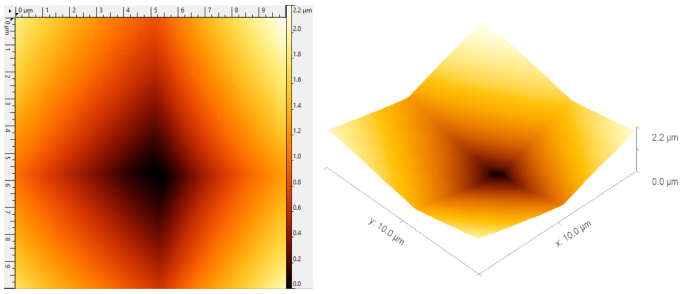

Figure A.204: AFM image of incomplete hole left by the DURAMIN-40 in a stainless steel sample.

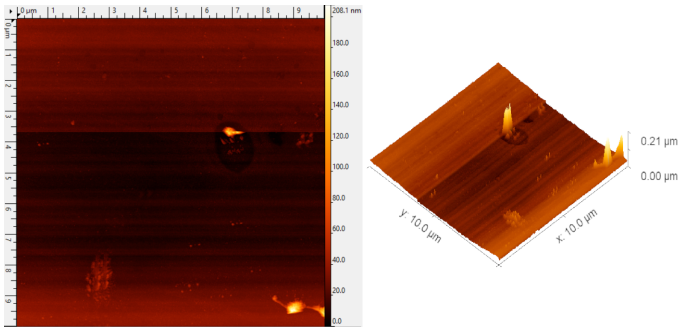

Figure A.205: AFM image of the surface of a stainless steel sample.

A.8 Friction Coefficient of Virgin Stainless Steel

A.8.1 Friction Coefficient of Virgin Stainless Steel 0.25 N

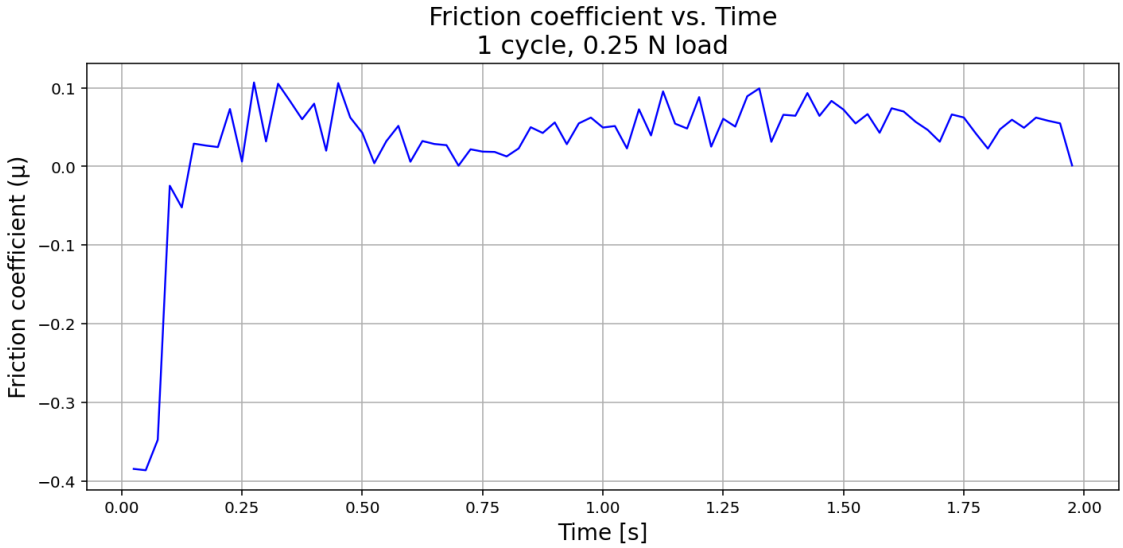

Figure A.206: This figure shows a virgin stainless steel sample. This figure shows the friction coefficient recorded during tribometry measurement when equipped with a load of 0.25 N and during only 1 cycle.

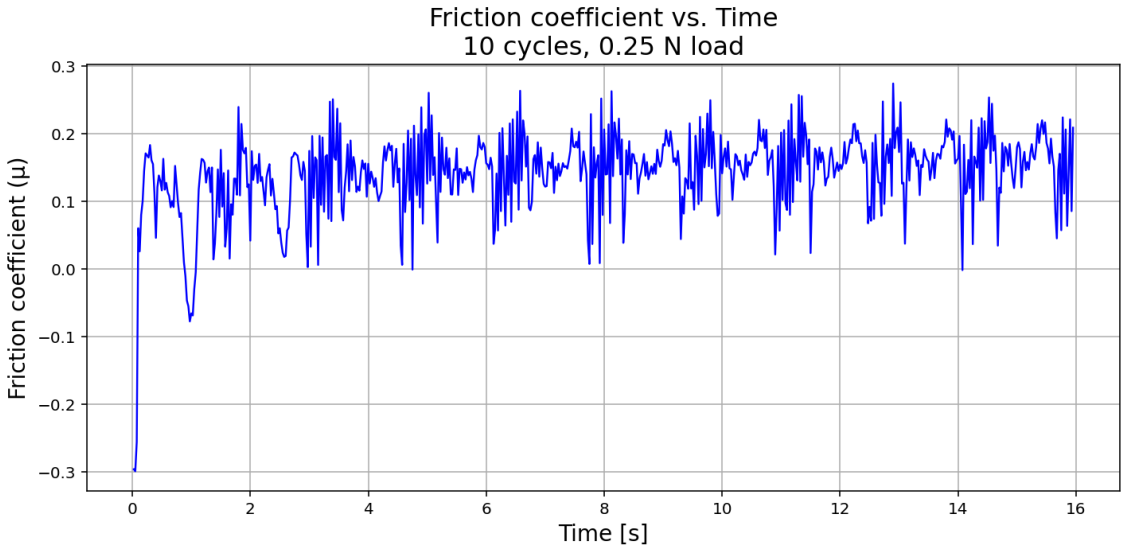

Figure A.207: This figure shows a virgin stainless steel sample. This figure shows the friction coefficient recorded during tribometry measurement when equipped with a load of 0.25 N and during only 10 cycles.

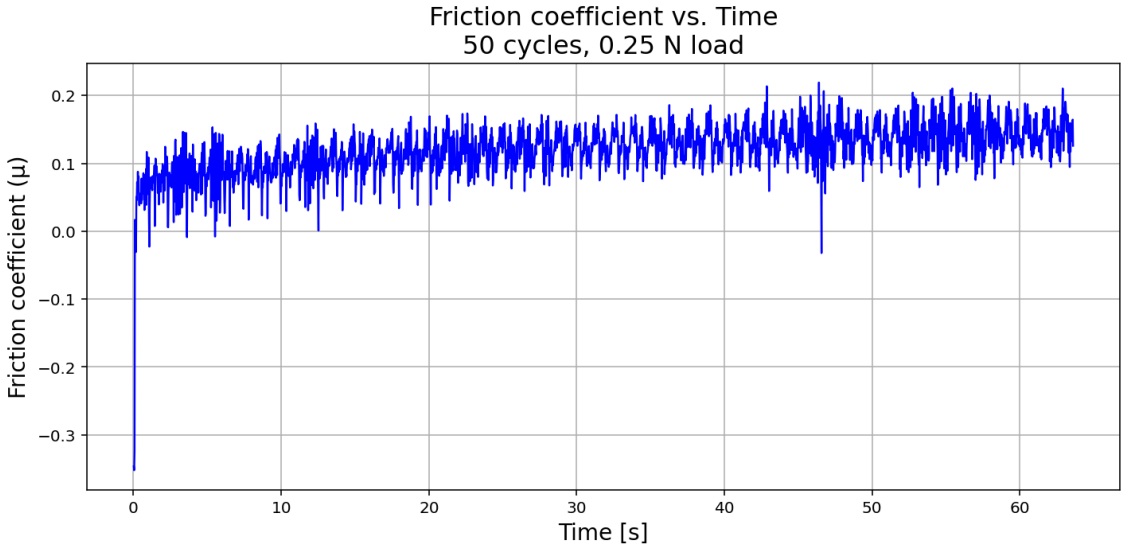

Figure A.208: This figure shows a virgin stainless steel sample. This figure shows the friction coefficient recorded during tribometry measurement when equipped with a load of 0.25 N and during only 50 cycles.

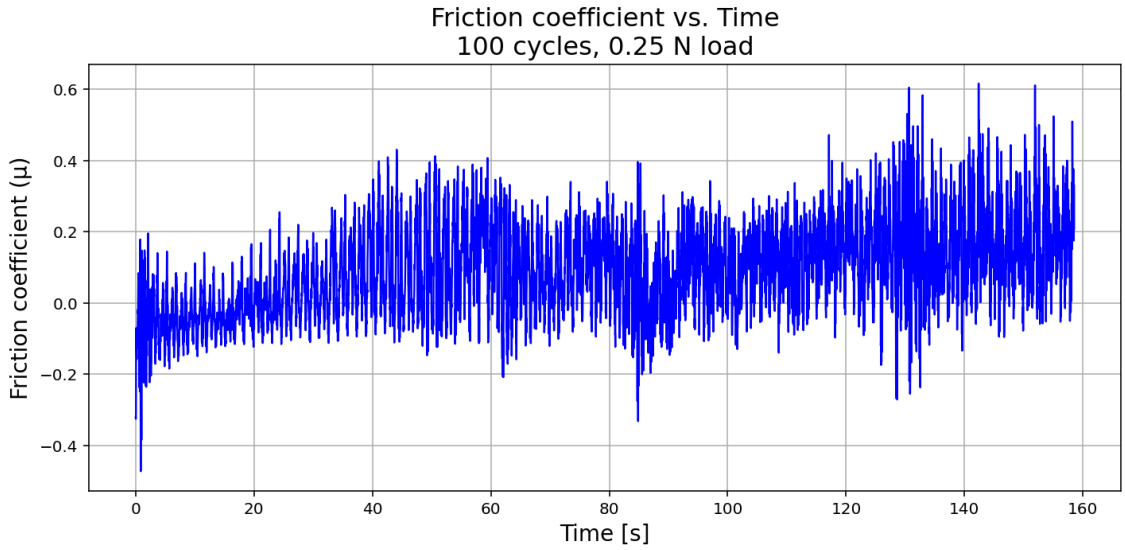

Figure A.209: This figure shows a virgin stainless steel sample. This figure shows the friction coefficient recorded during tribometry measurement when equipped with a load of 0.25 N and during 100 cycles.

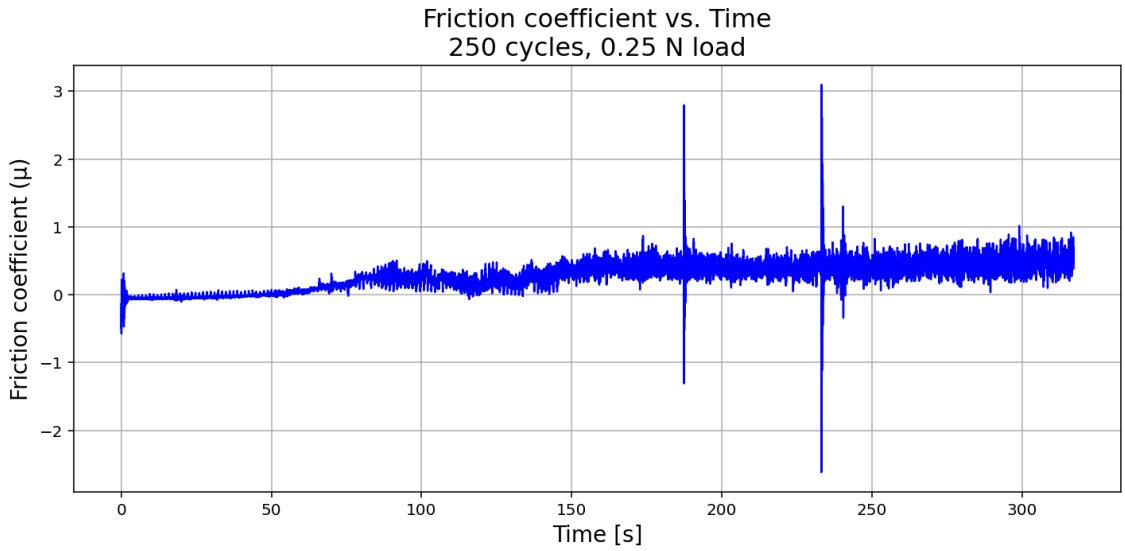

Figure A.210: This figure shows a virgin stainless steel sample. This figure shows the friction coefficient recorded during tribometry measurement when equipped with a load of 0.25 N and during 250 cycles.

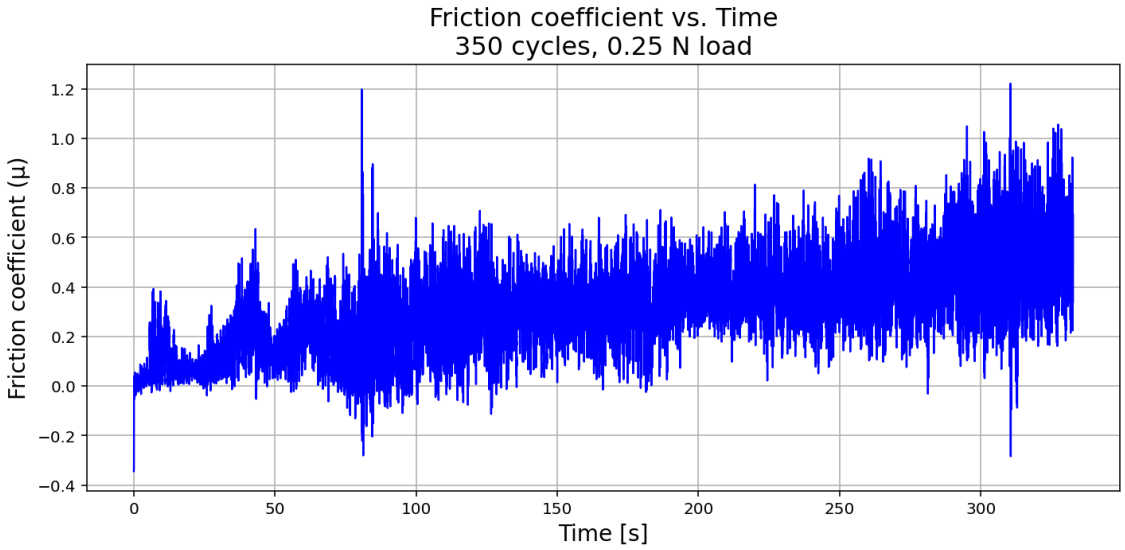

Figure A.211: This figure shows a virgin stainless steel sample. This figure shows the friction coefficient recorded during tribometry measurement when equipped with a load of 0.25 N and during 350 cycles.

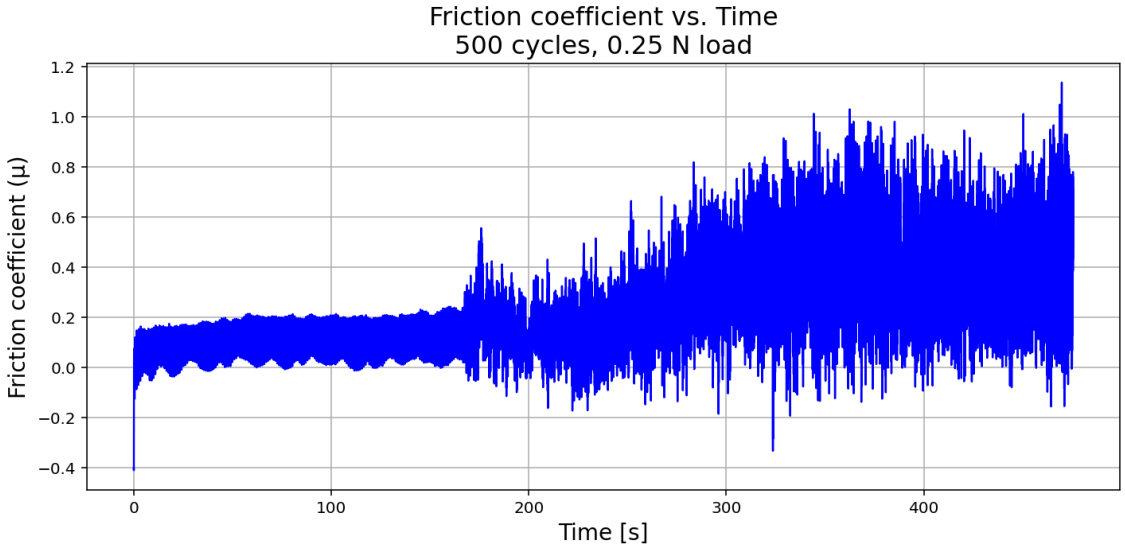

Figure A.212: This figure shows a virgin stainless steel sample. This figure shows the friction coefficient recorded during tribometry measurement when equipped with a load of 0.25 N and during 500 cycles.

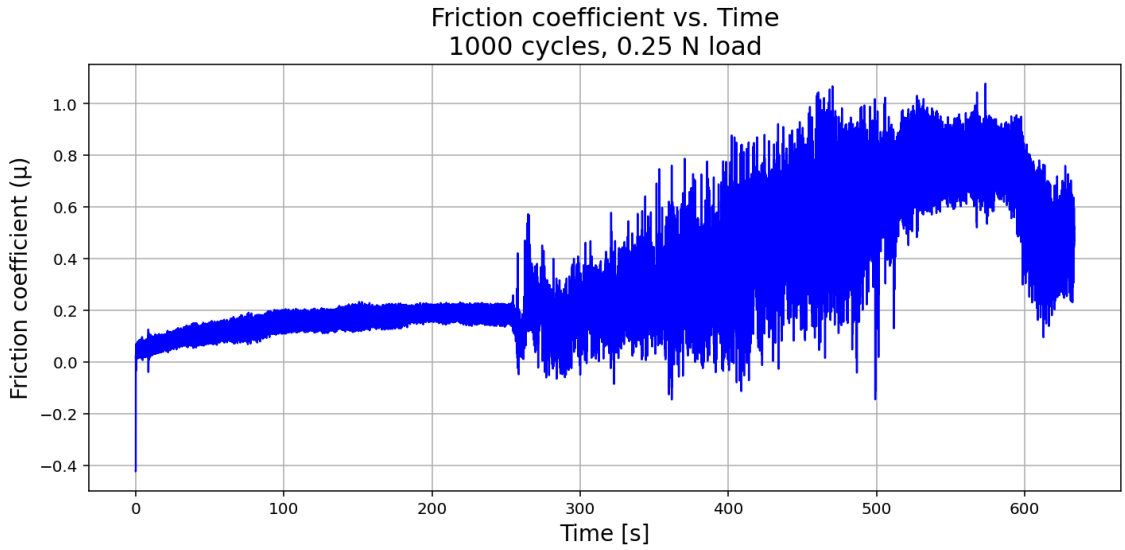

Figure A.213: This figure shows a virgin stainless steel sample. This figure shows the friction coefficient recorded during tribometry measurement when equipped with a load of 0.25 N and during 1000 cycles.

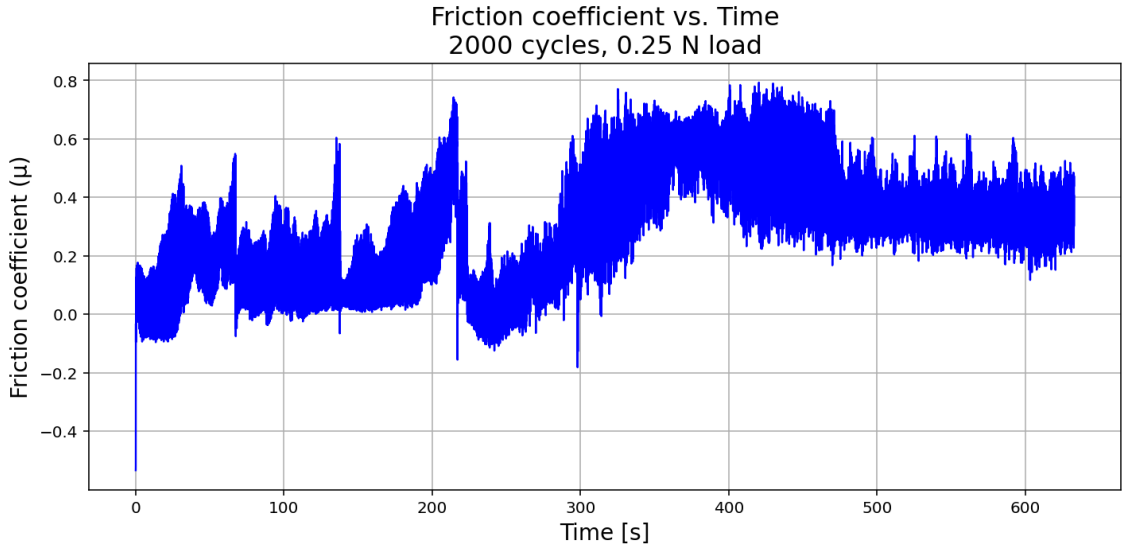

Figure A.214: This figure shows a virgin stainless steel sample. This figure shows the friction coefficient recorded during tribometry measurement when equipped with a load of 0.25 N and during 2000 cycles.

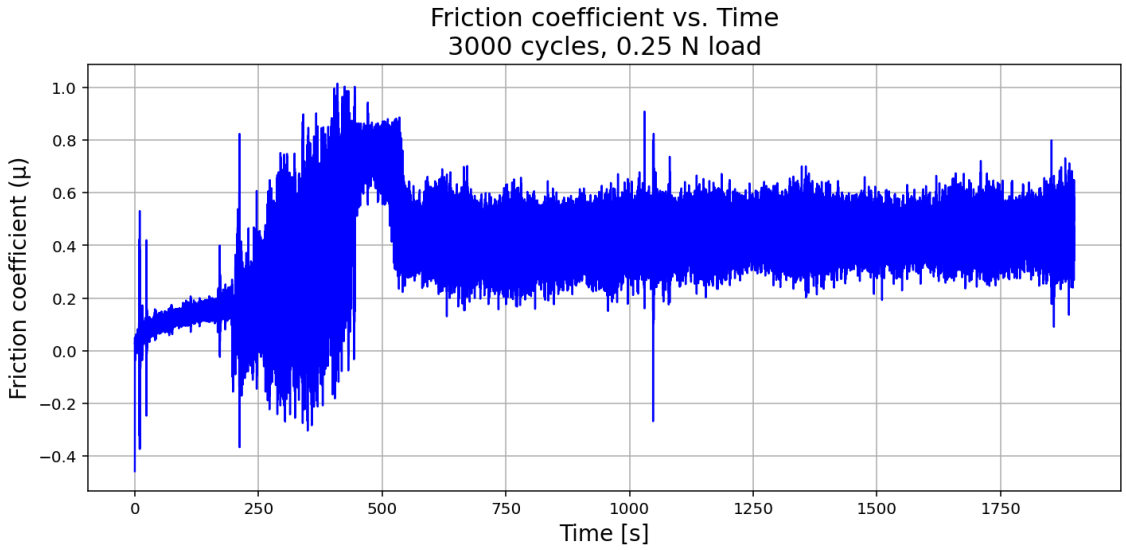

Figure A.215: This figure shows a virgin stainless steel sample. This figure shows the friction coefficient recorded during tribometry measurement when equipped with a load of 0.25 N and during 3000 cycles.

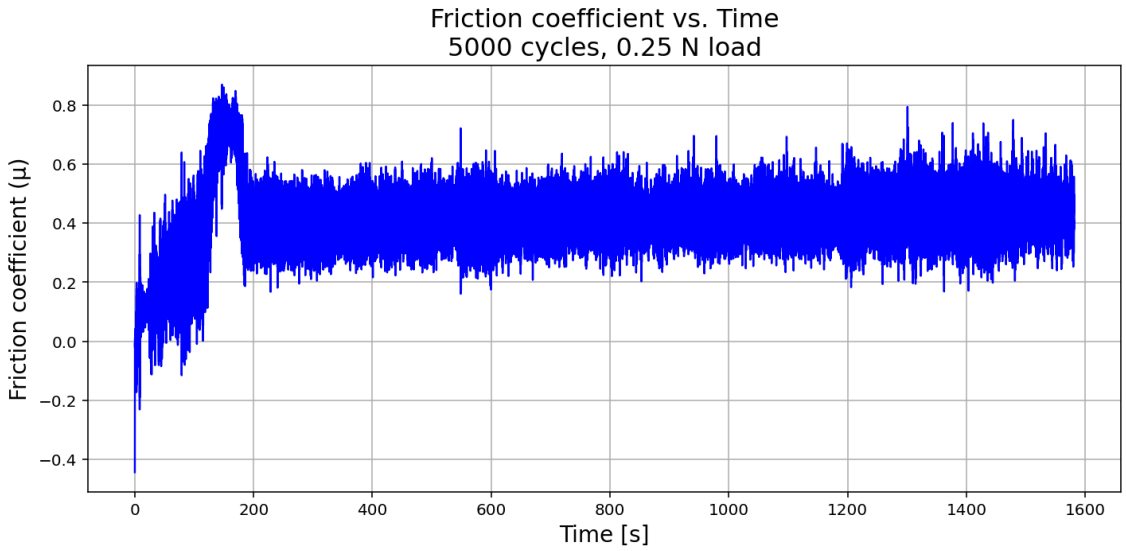

Figure A.216: This figure shows a virgin stainless steel sample. This figure shows the friction coefficient recorded during tribometry measurement when equipped with a load of 0.25 N and during 5000 cycles.

A.8.2 Friction Coefficient of Virgin Stainless Steel 1 N

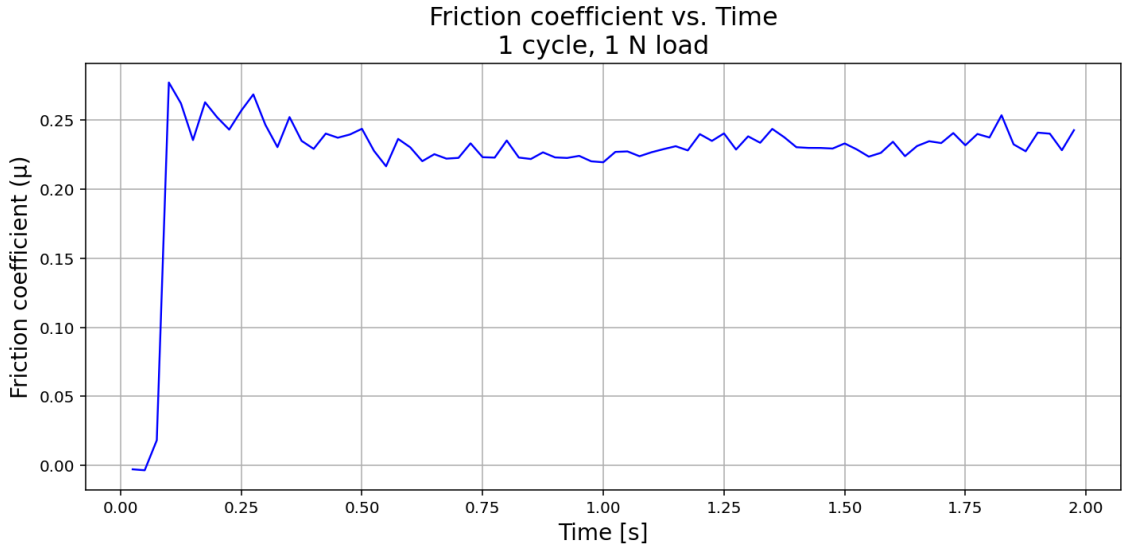

Figure A.217: This figure shows a virgin stainless steel sample. This figure shows the friction coefficient recorded during tribometry measurement when equipped with a load of 1 N and during only 1 cycle.

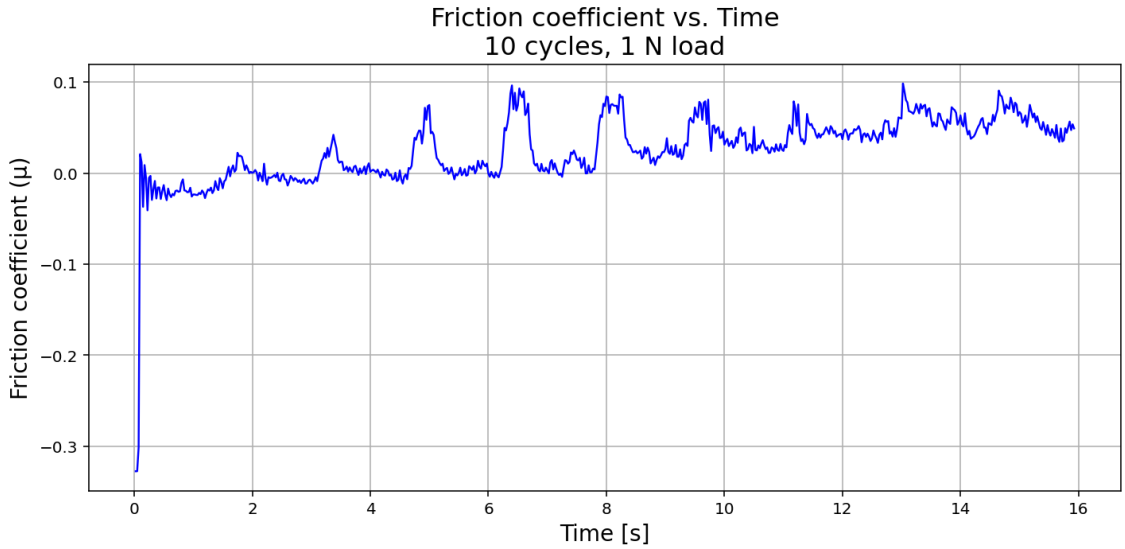

Figure A.218: This figure shows a virgin stainless steel sample. This figure shows the friction coefficient recorded during tribometry measurement when equipped with a load of 1 N and during only 10 cycles.

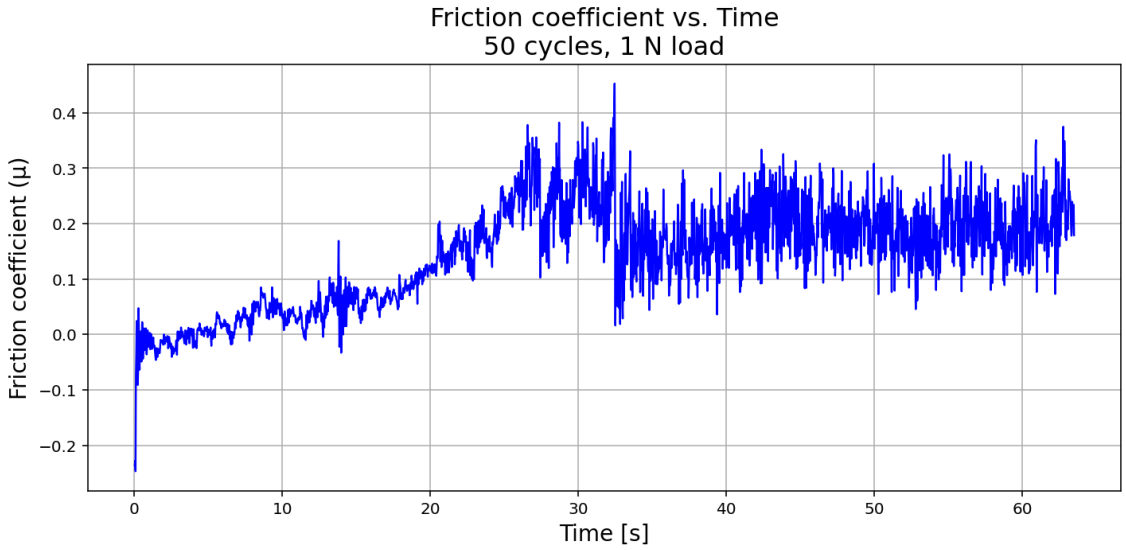

Figure A.219: This figure shows a virgin stainless steel sample. This figure shows the friction coefficient recorded during tribometry measurement when equipped with a load of 1 N and during only 50 cycles.

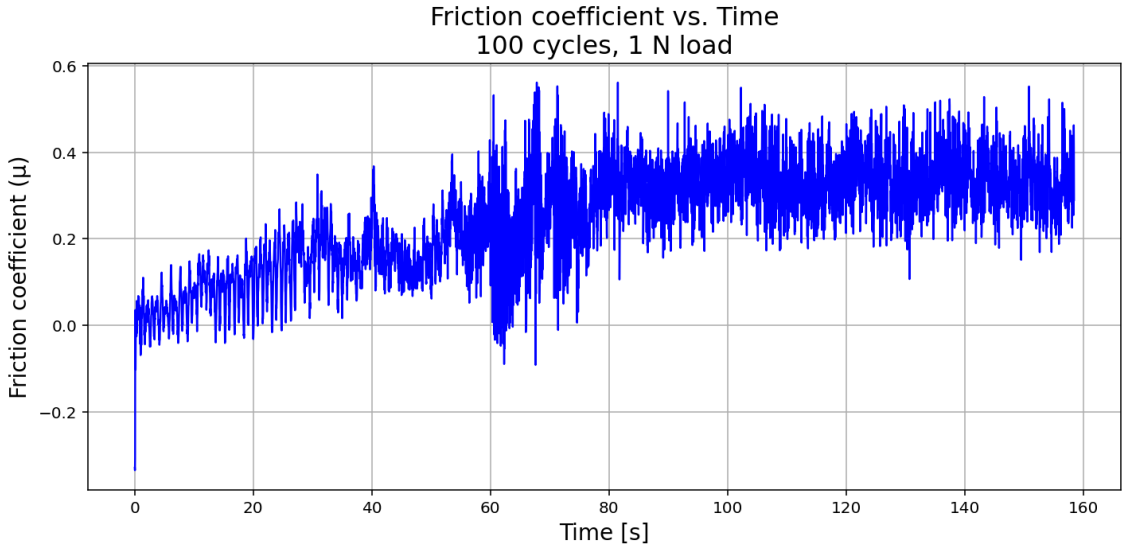

Figure A.220: This figure shows a virgin stainless steel sample. This figure shows the friction coefficient recorded during tribometry measurement when equipped with a load of 1 N and during 100 cycles.

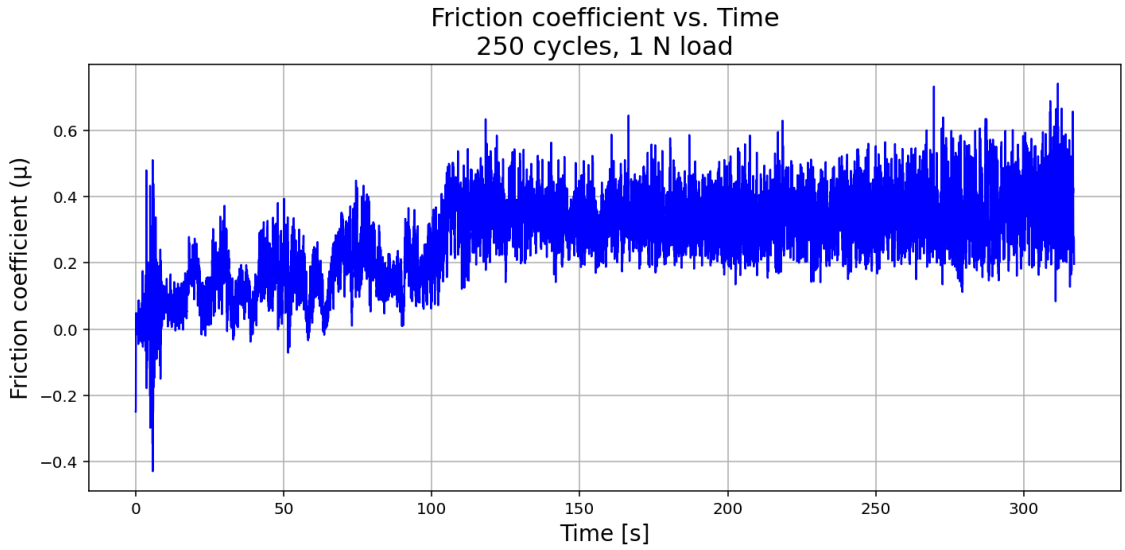

Figure A.221: This figure shows a virgin stainless steel sample. This figure shows the friction coefficient recorded during tribometry measurement when equipped with a load of 1 N and during 250 cycles.

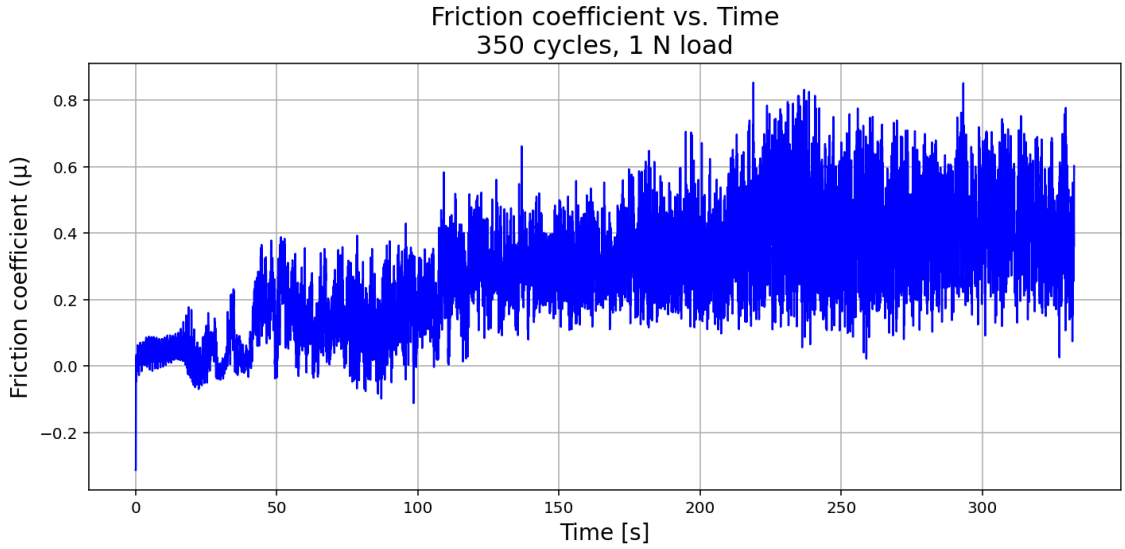

Figure A.222: This figure shows a virgin stainless steel sample. This figure shows the friction coefficient recorded during tribometry measurement when equipped with a load of 1 N and during 350 cycles.

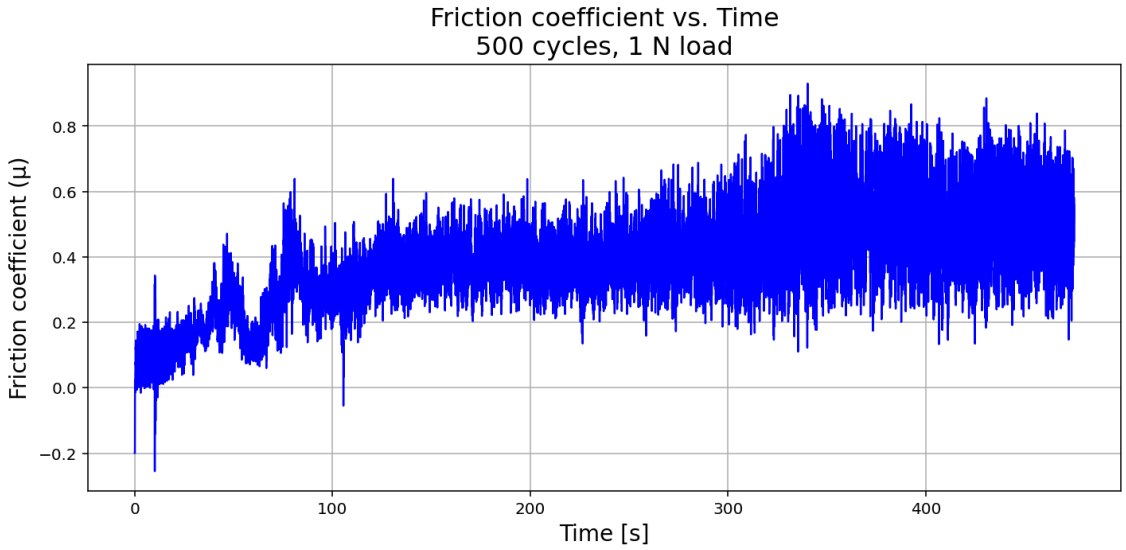

Figure A.223: This figure shows a virgin stainless steel sample. This figure shows the friction coefficient recorded during tribometry measurement when equipped with a load of 1 N and during 500 cycles.

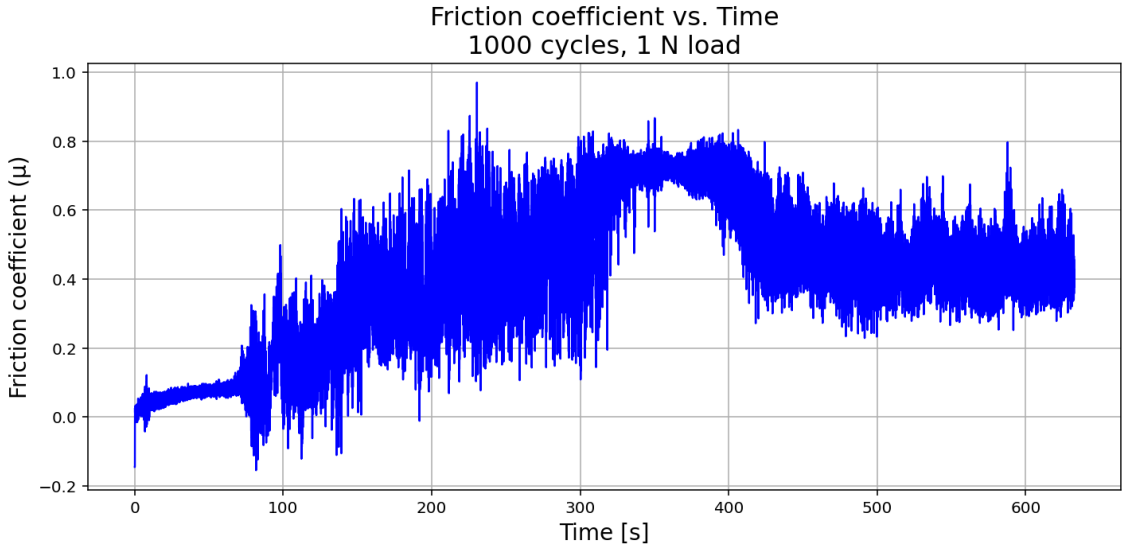

Figure A.224: This figure shows a virgin stainless steel sample. This figure shows the friction coefficient recorded during tribometry measurement when equipped with a load of 1 N and during 1000 cycles.

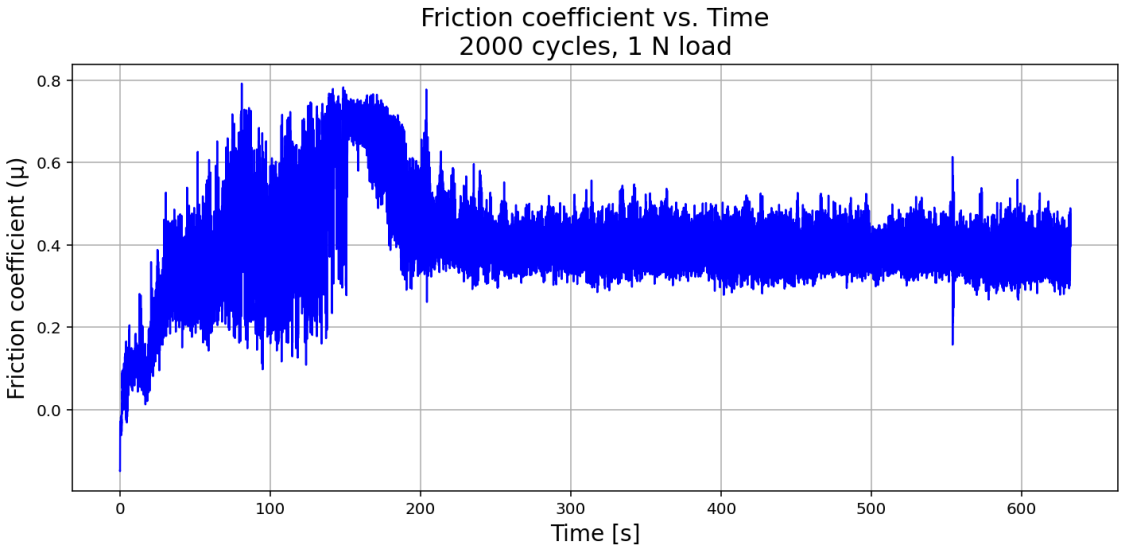

Figure A.225: This figure shows a virgin stainless steel sample. This figure shows the friction coefficient recorded during tribometry measurement when equipped with a load of 1 N and during 2000 cycles.

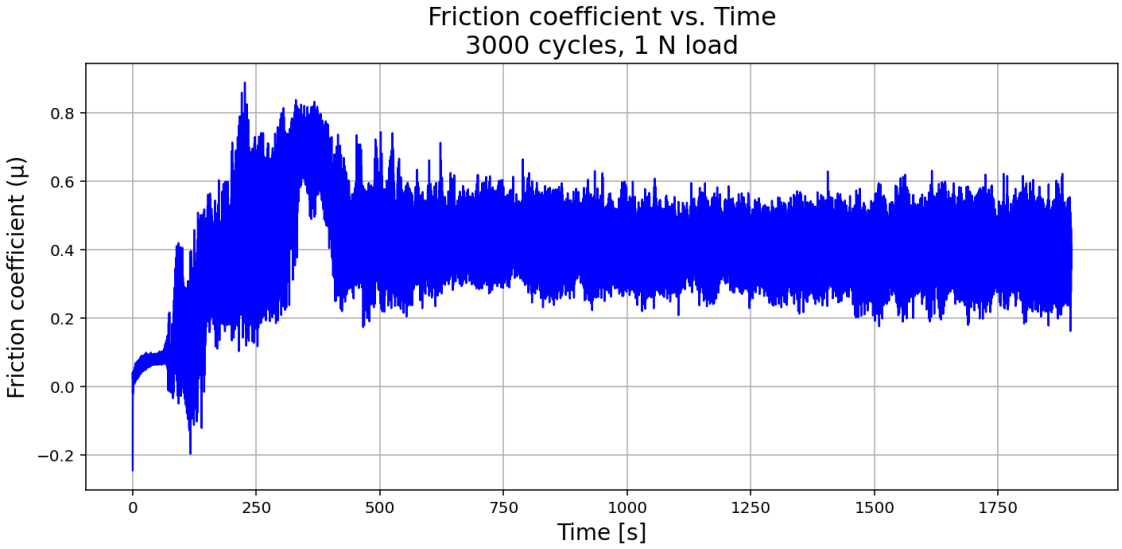

Figure A.226: This figure shows a virgin stainless steel sample. This figure shows the friction coefficient recorded during tribometry measurement when equipped with a load of 1 N and during 3000 cycles.

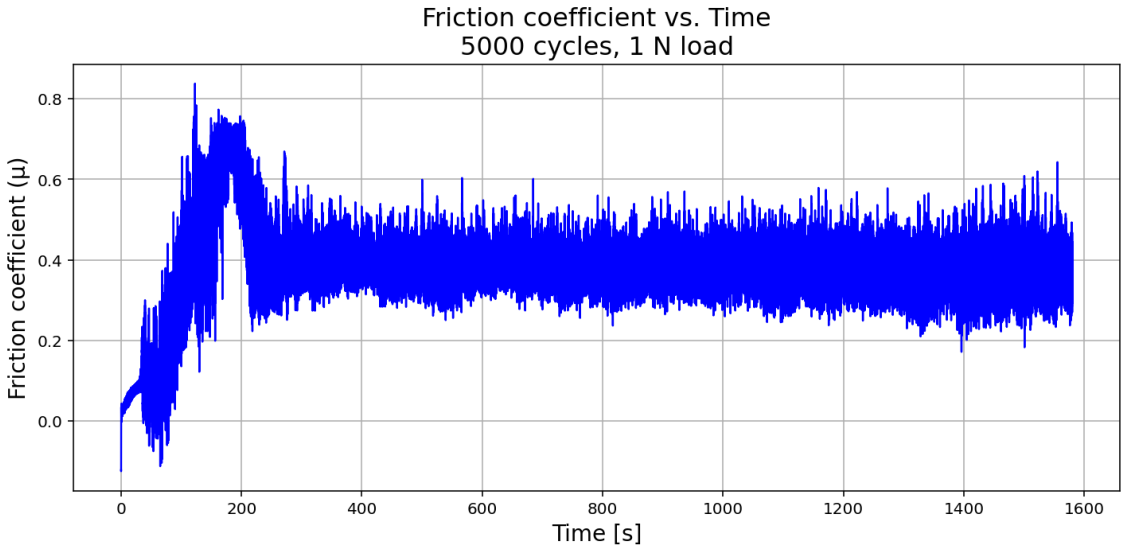

Figure A.227: This figure shows a virgin stainless steel sample. This figure shows the friction coefficient recorded during tribometry measurement when equipped with a load of 1 N and during 5000 cycles.

A.8.3 Friction Coefficient of Virgin Stainless Steel 2 N

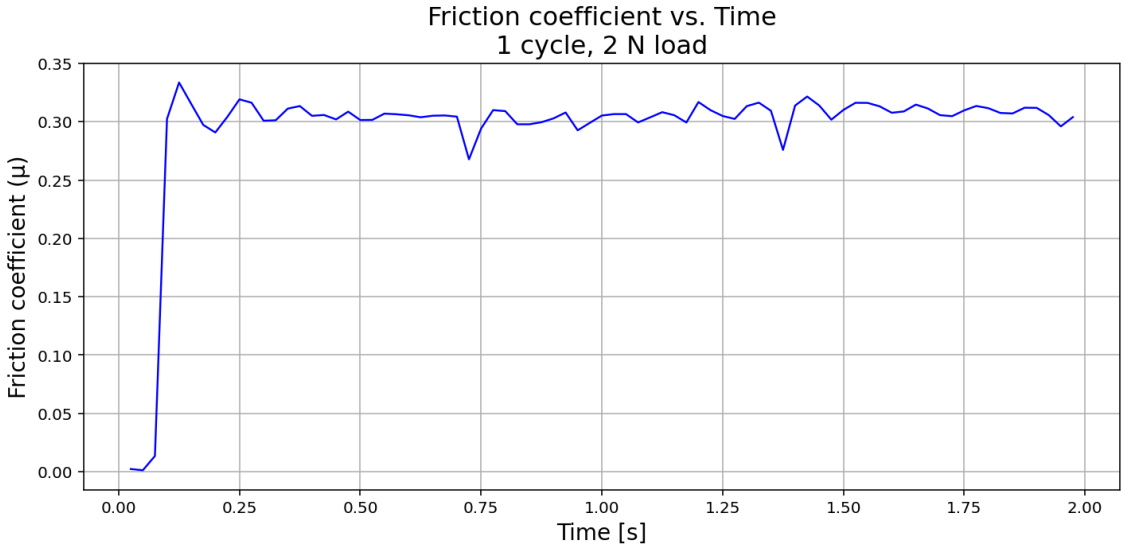

Figure A.228: This figure shows a virgin stainless steel sample. This figure shows the friction coefficient recorded during tribometry measurement when equipped with a load of 2 N and during only 1 cycle.

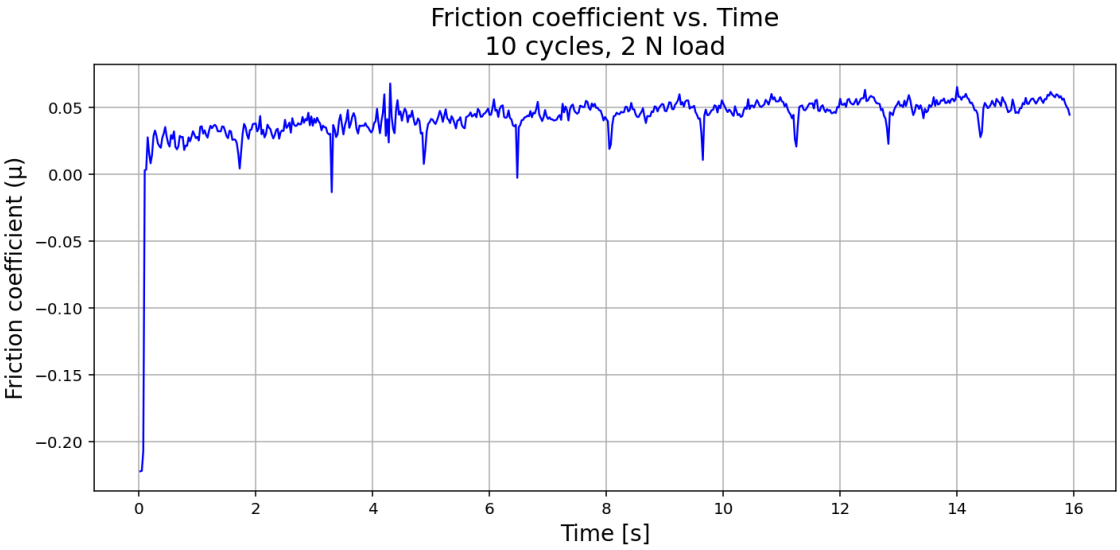

Figure A.229: This figure shows a virgin stainless steel sample. This figure shows the friction coefficient recorded during tribometry measurement when equipped with a load of 2 N and during only 10 cycles.

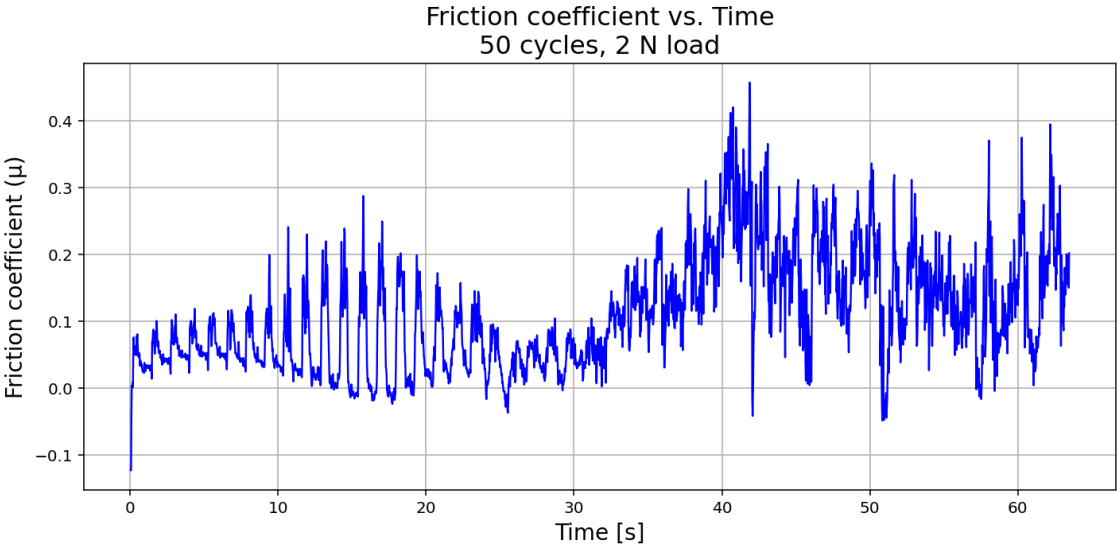

Figure A.230: This figure shows a virgin stainless steel sample. This figure shows the friction coefficient recorded during tribometry measurement when equipped with a load of 2 N and during only 50 cycles.

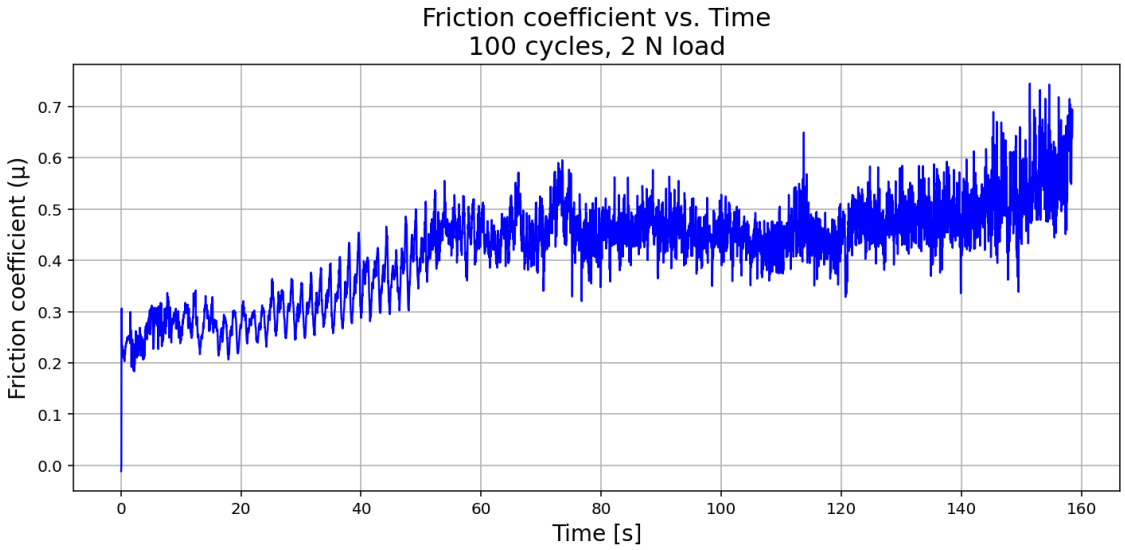

Figure A.231: This figure shows a virgin stainless steel sample. This figure shows the friction coefficient recorded during tribometry measurement when equipped with a load of 2 N and during 100 cycles.

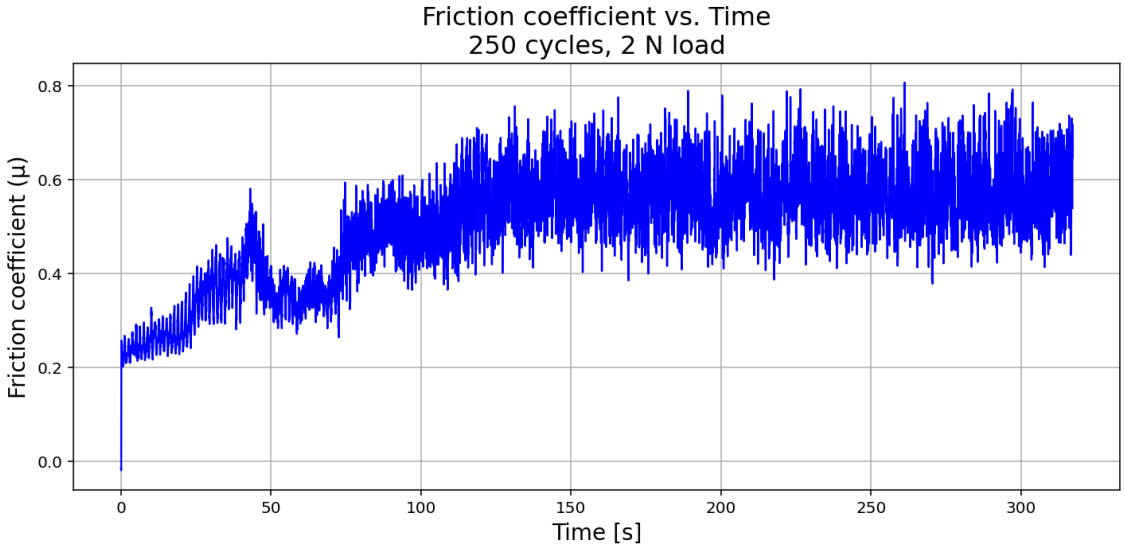

Figure A.232: This figure shows a virgin stainless steel sample. This figure shows the friction coefficient recorded during tribometry measurement when equipped with a load of 2 N and during 250 cycles.

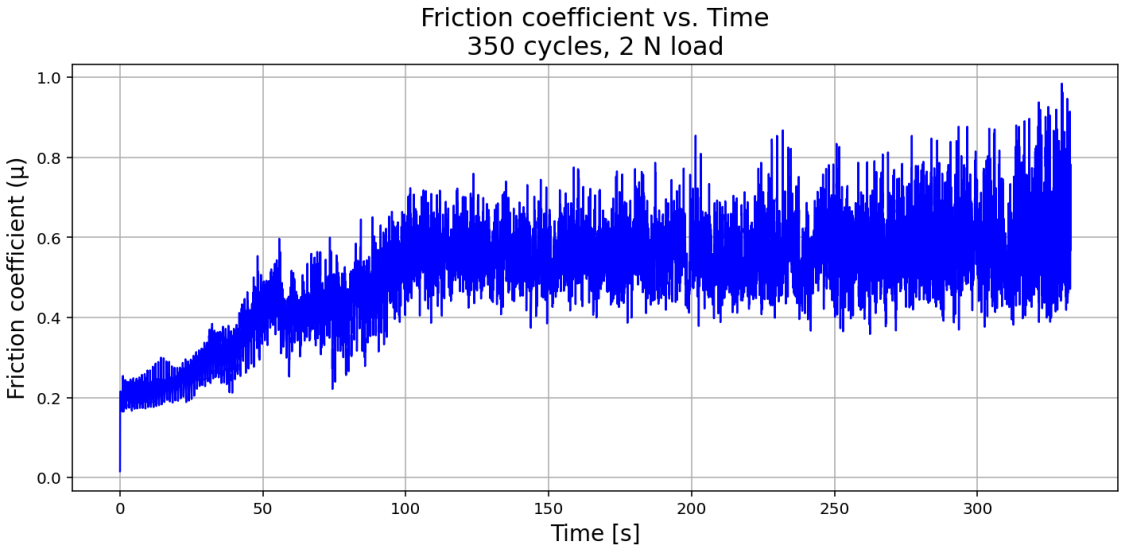

Figure A.233: This figure shows a virgin stainless steel sample. This figure shows the friction coefficient recorded during tribometry measurement when equipped with a load of 2 N and during 350 cycles.

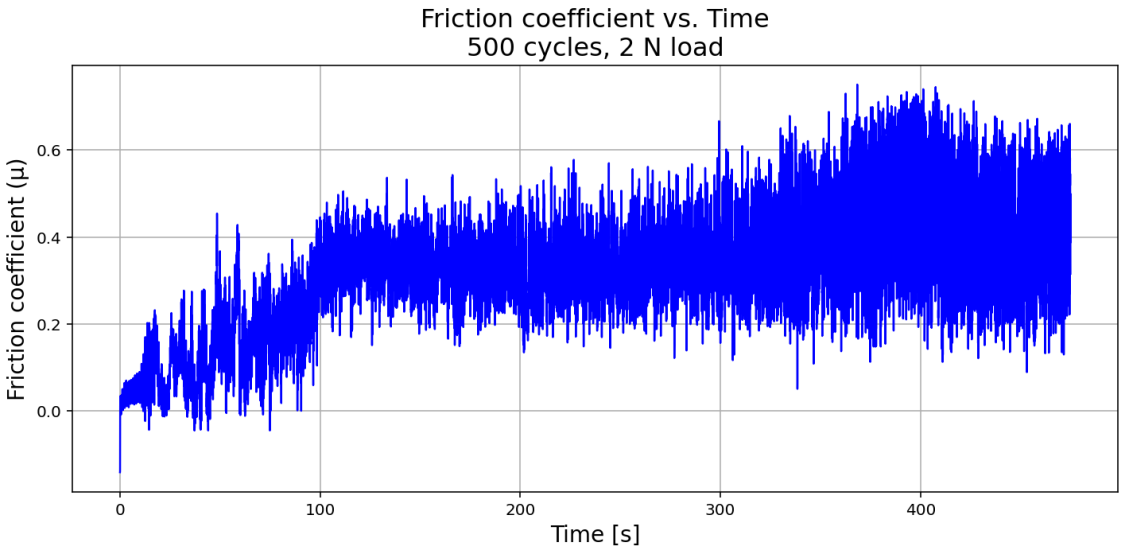

Figure A.234: This figure shows a virgin stainless steel sample. This figure shows the friction coefficient recorded during tribometry measurement when equipped with a load of 2 N and during 500 cycles.

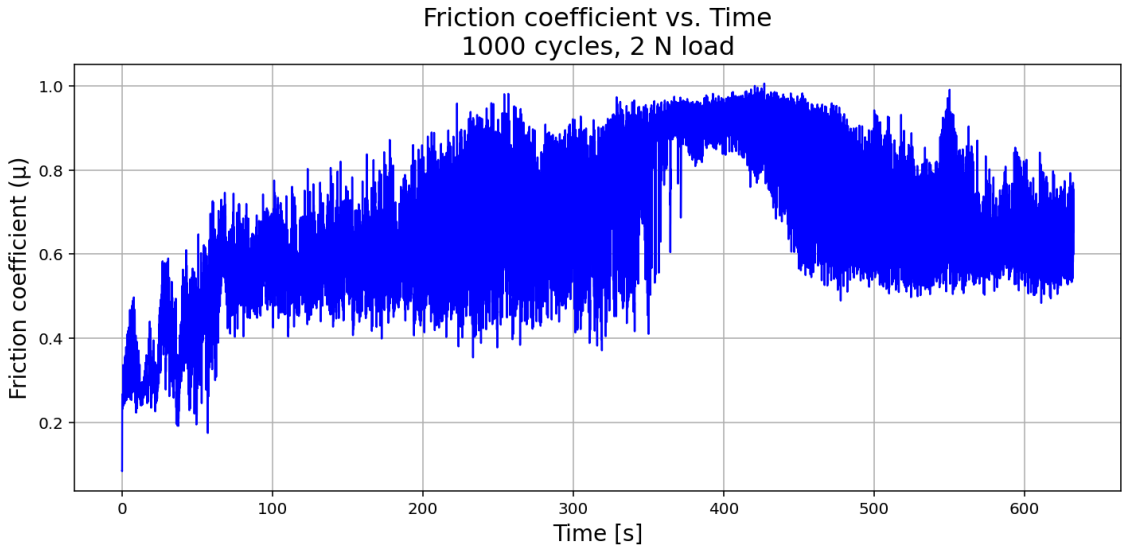

Figure A.235: This figure shows a virgin stainless steel sample. This figure shows the friction coefficient recorded during tribometry measurement when equipped with a load of 2 N and during 1000 cycles.

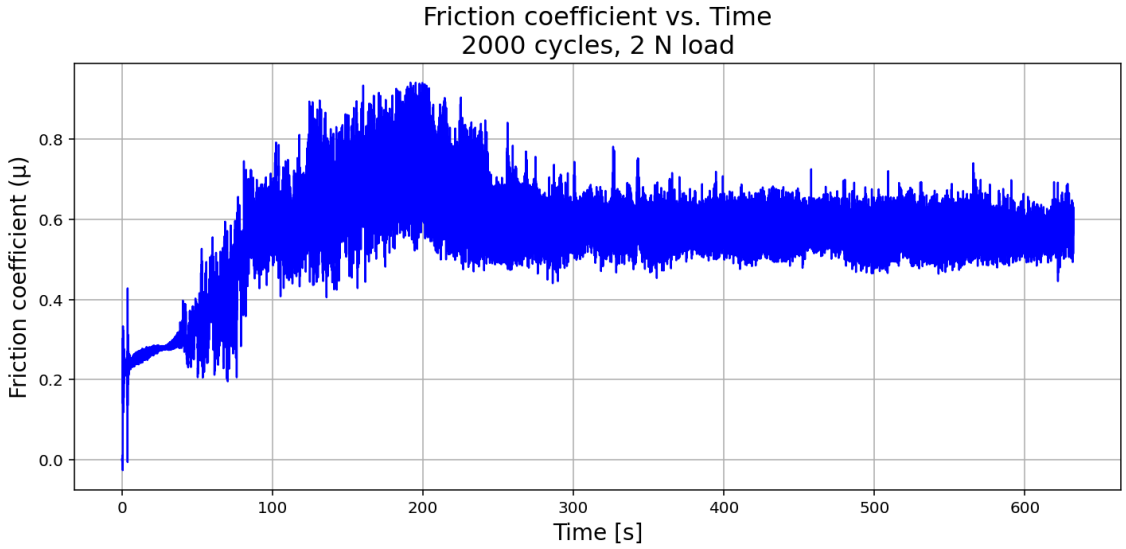

Figure A.236: This figure shows a virgin stainless steel sample. This figure shows the friction coefficient recorded during tribometry measurement when equipped with a load of 2 N and during 2000 cycles.

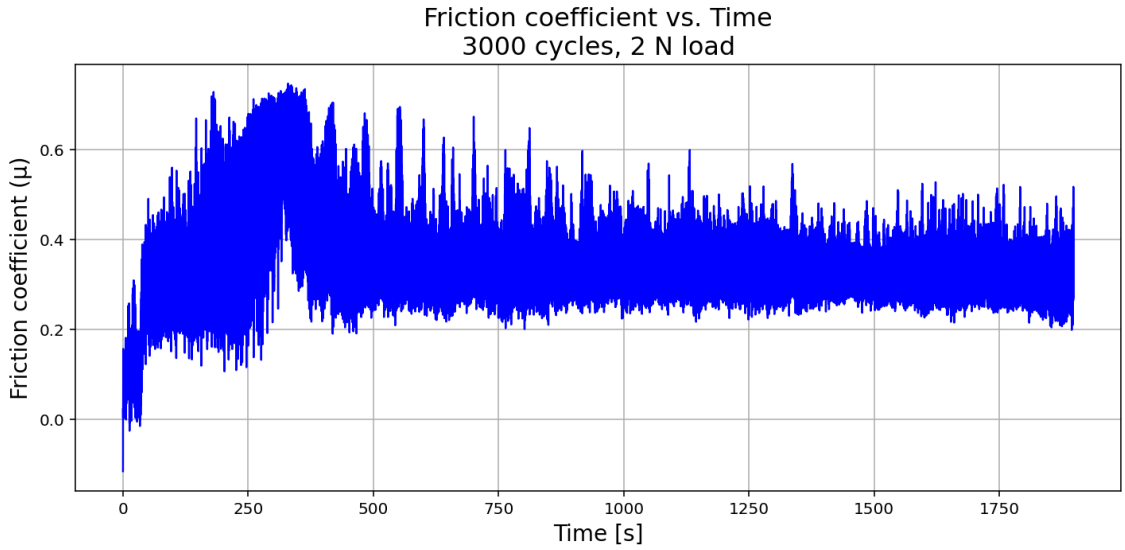

Figure A.237: This figure shows a virgin stainless steel sample. This figure shows the friction coefficient recorded during tribometry measurement when equipped with a load of 2 N and during 3000 cycles.

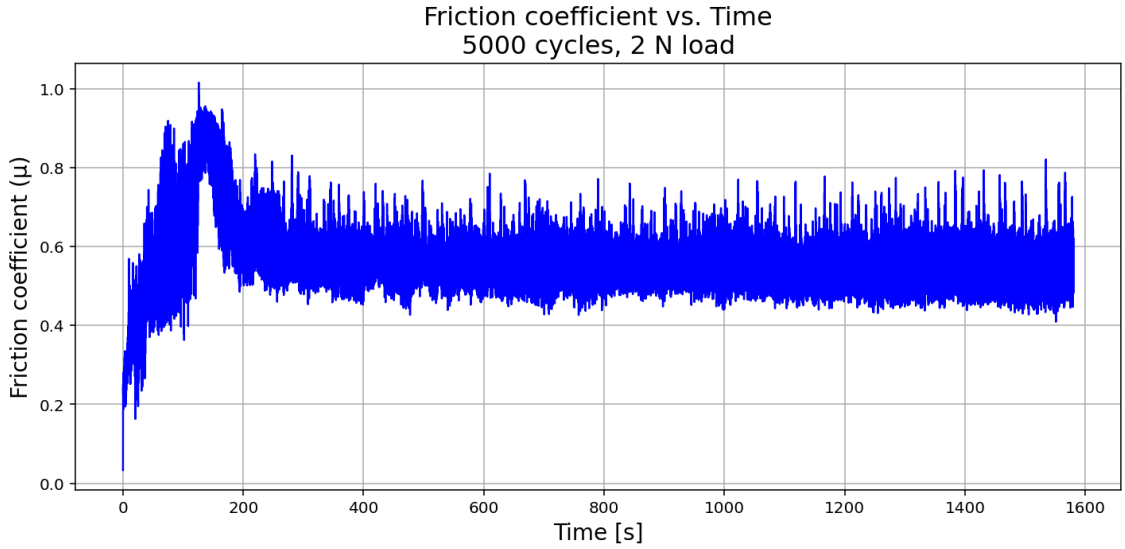

Figure A.238: This figure shows a virgin stainless steel sample. This figure shows the friction coefficient recorded during tribometry measurement when equipped with a load of 2 N and during 5000 cycles.

A.8.4 Friction Coefficient of Virgin Stainless Steel 5 N

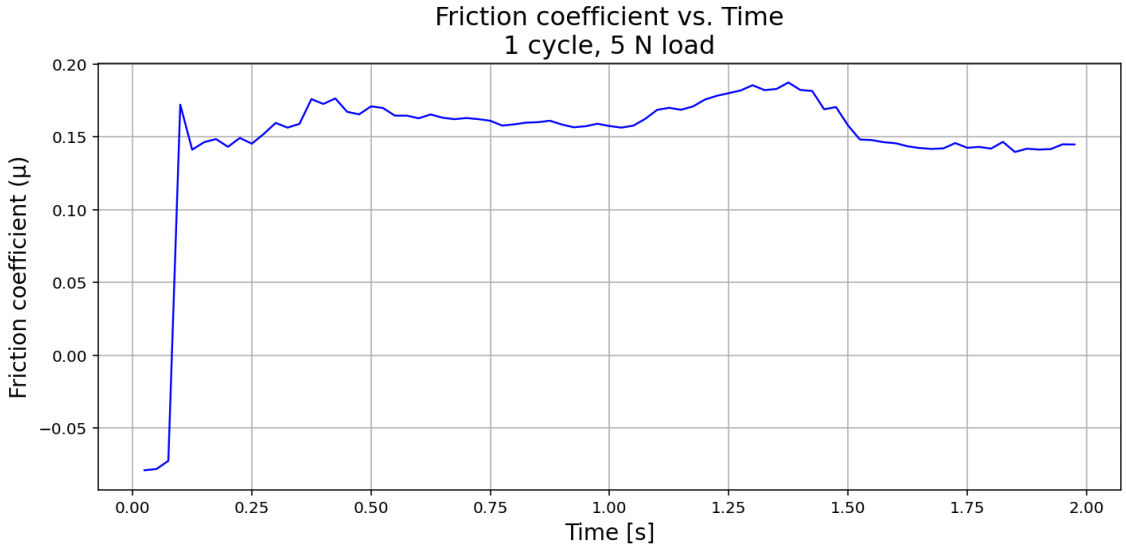

Figure A.239: This figure shows a virgin stainless steel sample. This figure shows the friction coefficient recorded during tribometry measurement when equipped with a load of 5 N and during only 1 cycle.

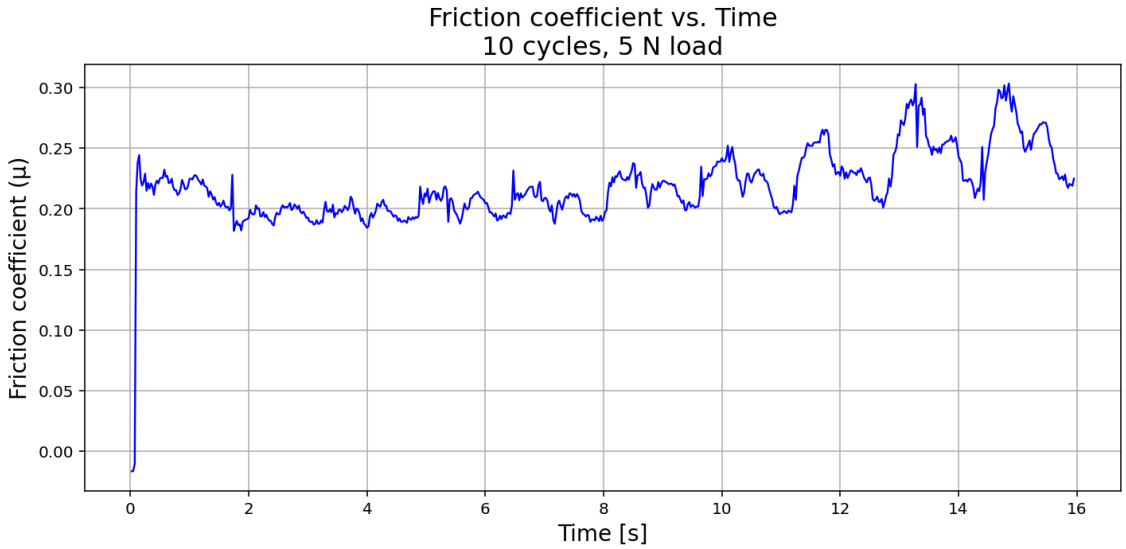

Figure A.240: This figure shows a virgin stainless steel sample. This figure shows the friction coefficient recorded during tribometry measurement when equipped with a load of 5 N and during only 10 cycles.

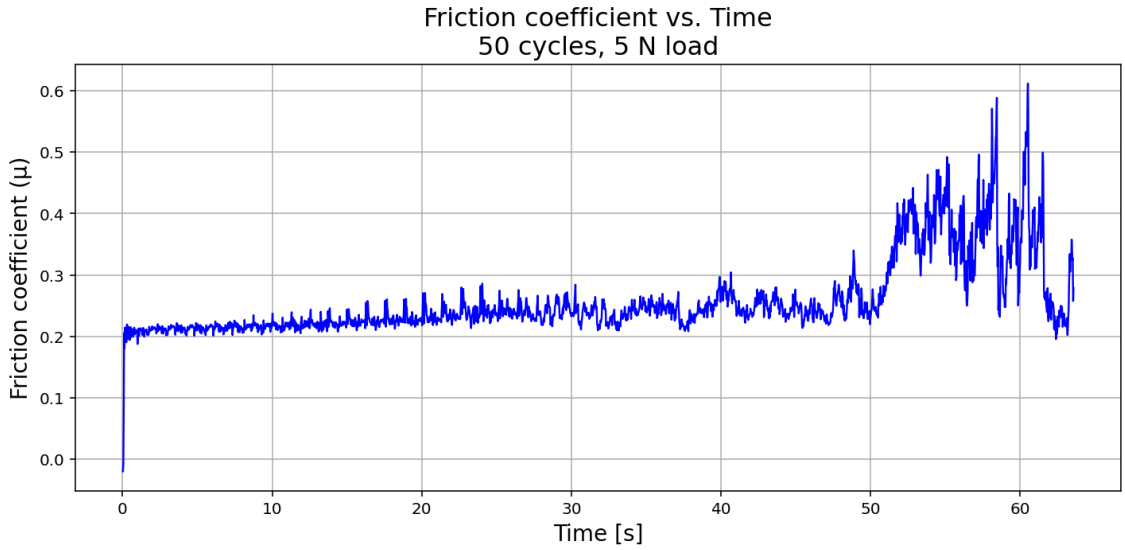

Figure A.241: This figure shows a virgin stainless steel sample. This figure shows the friction coefficient recorded during tribometry measurement when equipped with a load of 5 N and during only 50 cycles.

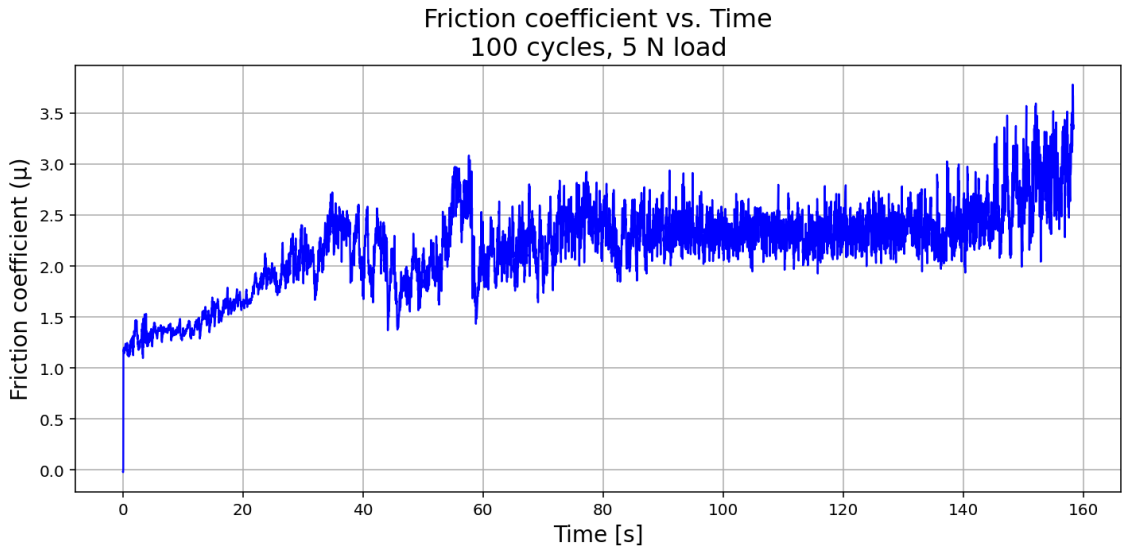

Figure A.242: This figure shows a virgin stainless steel sample. This figure shows the friction coefficient recorded during tribometry measurement when equipped with a load of 5 N and during 100 cycles.

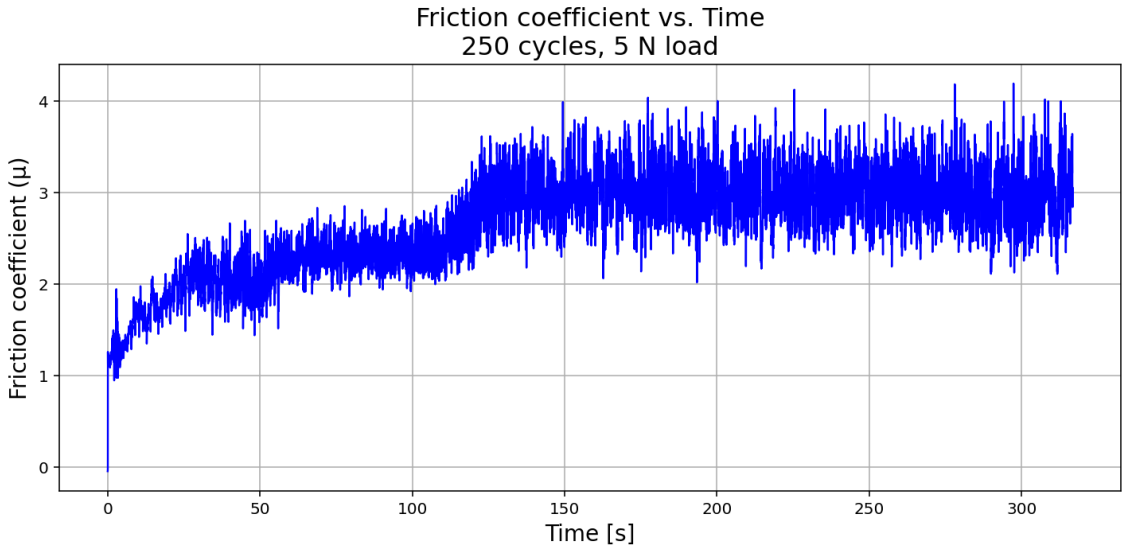

Figure A.243: This figure shows a virgin stainless steel sample. This figure shows the friction coefficient recorded during tribometry measurement when equipped with a load of 5 N and during 250 cycles.

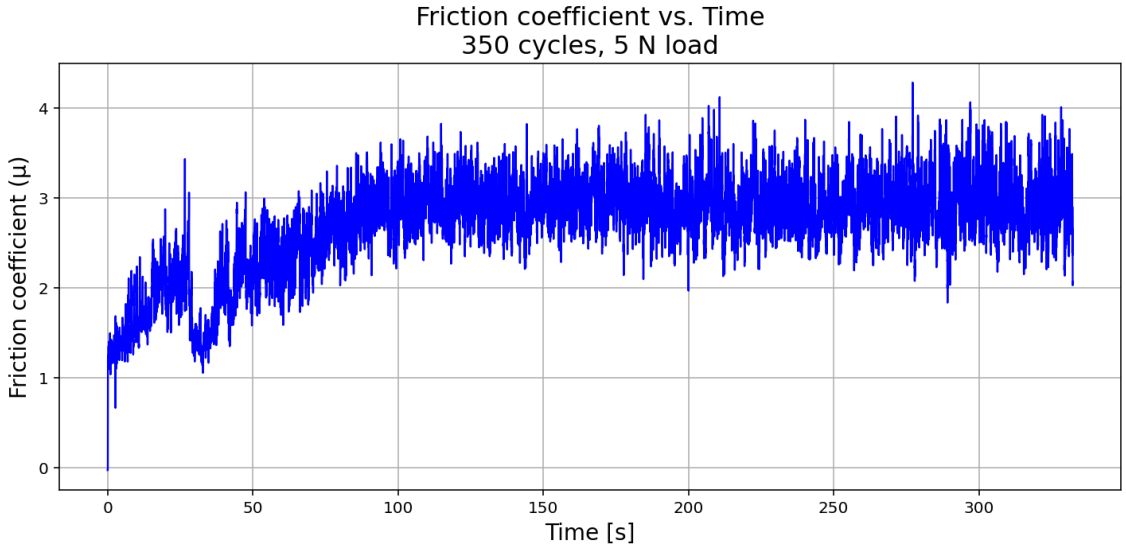

Figure A.244: This figure shows a virgin stainless steel sample. This figure shows the friction coefficient recorded during tribometry measurement when equipped with a load of 5 N and during 350 cycles.

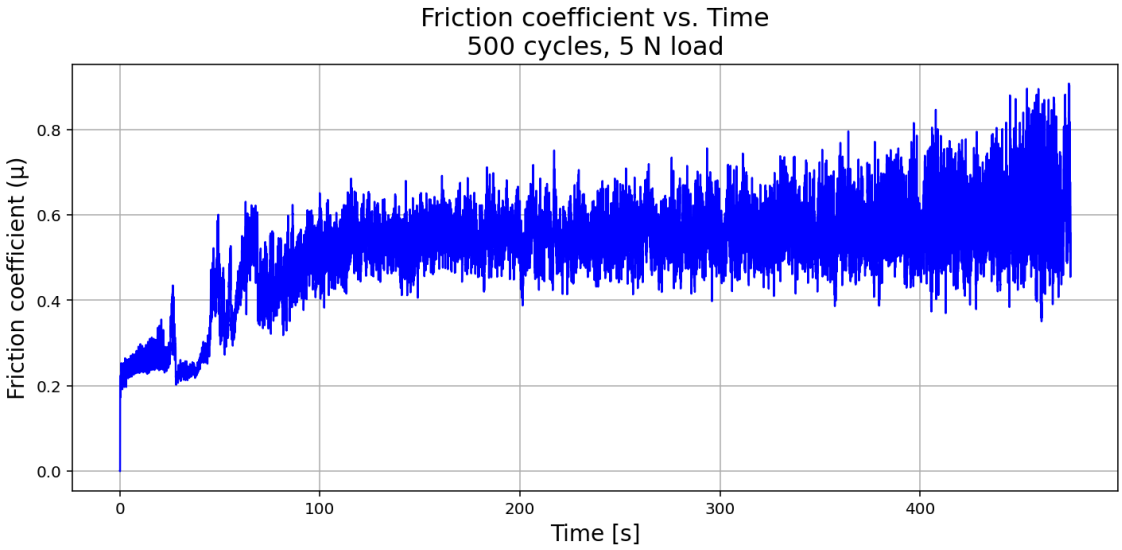

Figure A.245: This figure shows a virgin stainless steel sample. This figure shows the friction coefficient recorded during tribometry measurement when equipped with a load of 5 N and during 500 cycles.

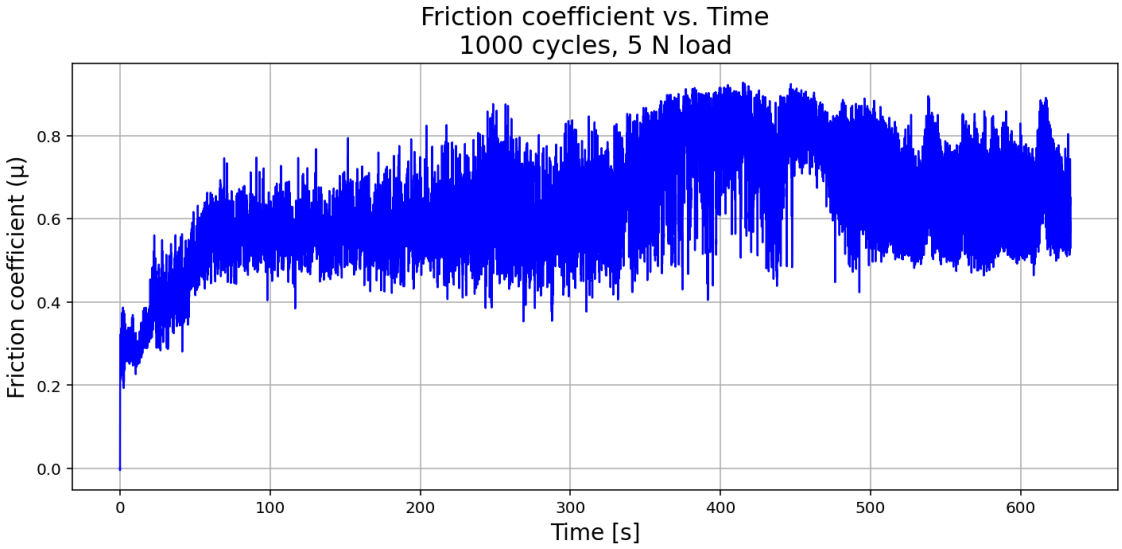

Figure A.246: This figure shows a virgin stainless steel sample. This figure shows the friction coefficient recorded during tribometry measurement when equipped with a load of 5 N and during 1000 cycles.

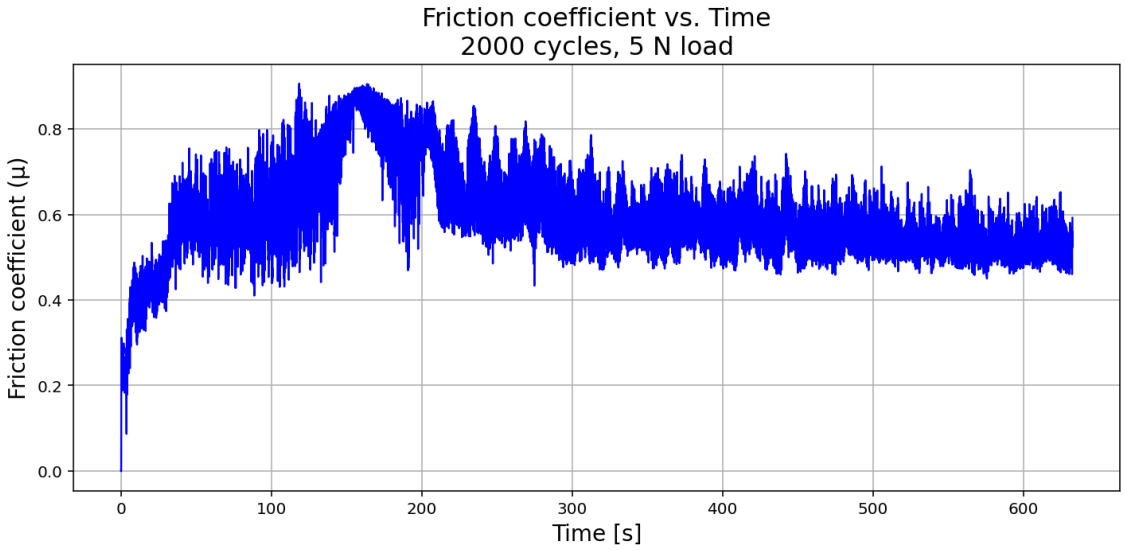

Figure A.247: This figure shows a virgin stainless steel sample. This figure shows the friction coefficient recorded during tribometry measurement when equipped with a load of 5 N and during 2000 cycles.

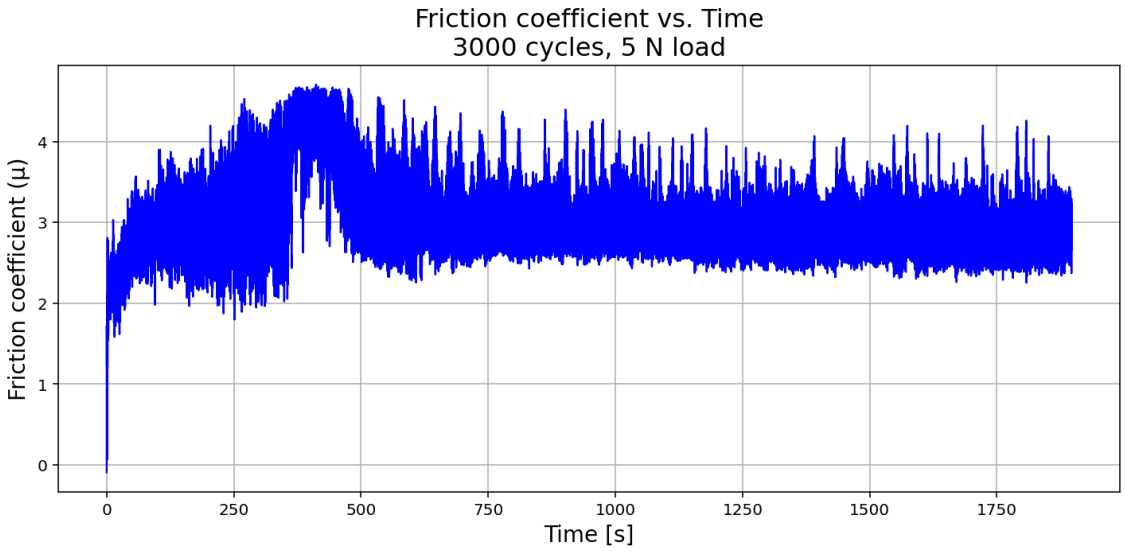

Figure A.248: This figure shows a virgin stainless steel sample. This figure shows the friction coefficient recorded during tribometry measurement when equipped with a load of 5 N and during 3000 cycles.

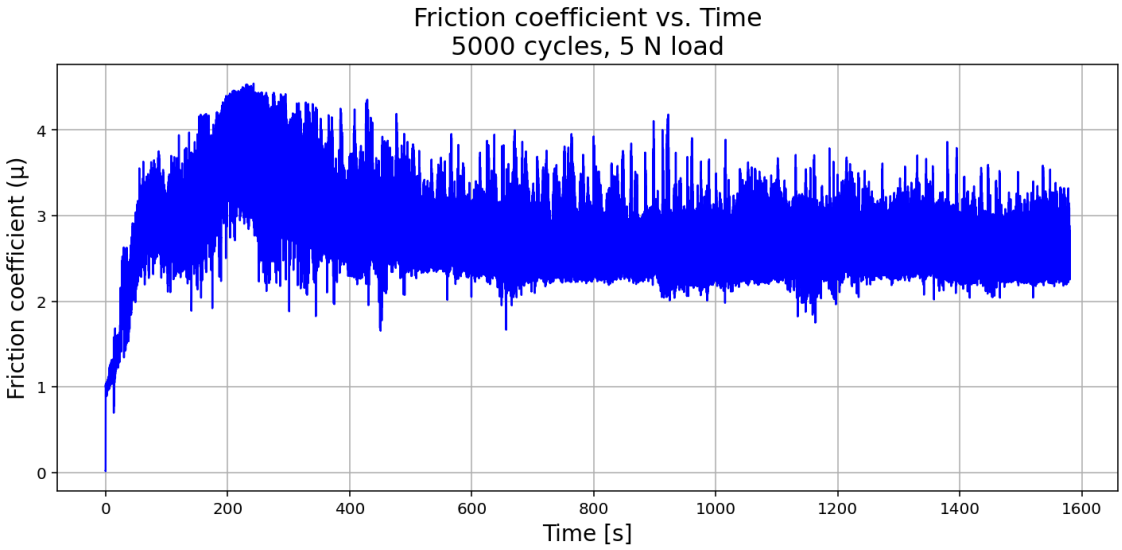

Figure A.249: This figure shows a virgin stainless steel sample. This figure shows the friction coefficient recorded during tribometry measurement when equipped with a load of 5 N and during 5000 cycles.

A.8.5 Friction Coefficient of Virgin Stainless Steel 10 N

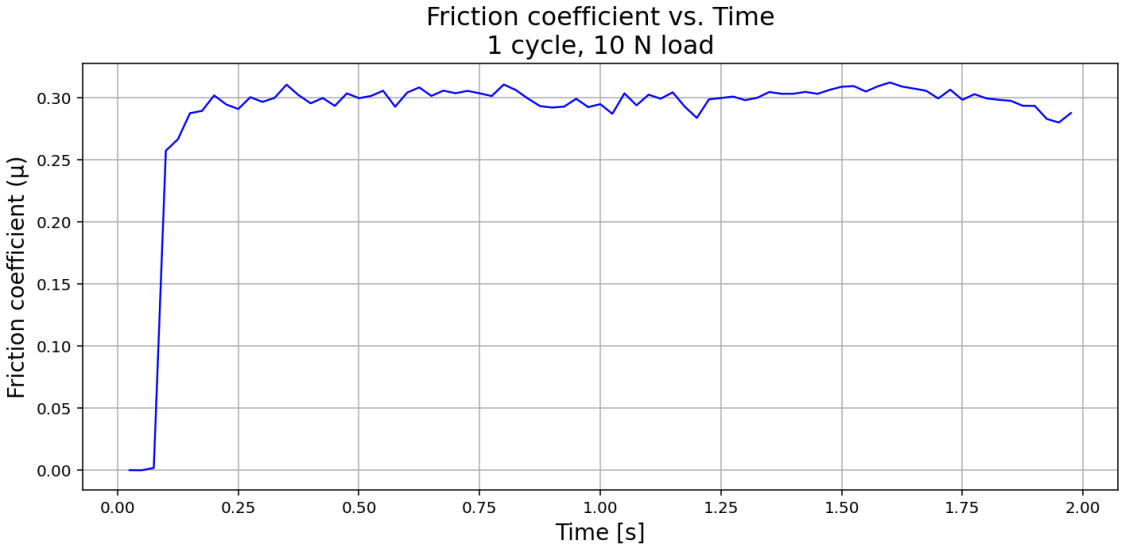

Figure A.250: This figure shows a virgin stainless steel sample. This figure shows the friction coefficient recorded during tribometry measurement when equipped with a load of 10 N and during only 1 cycle.

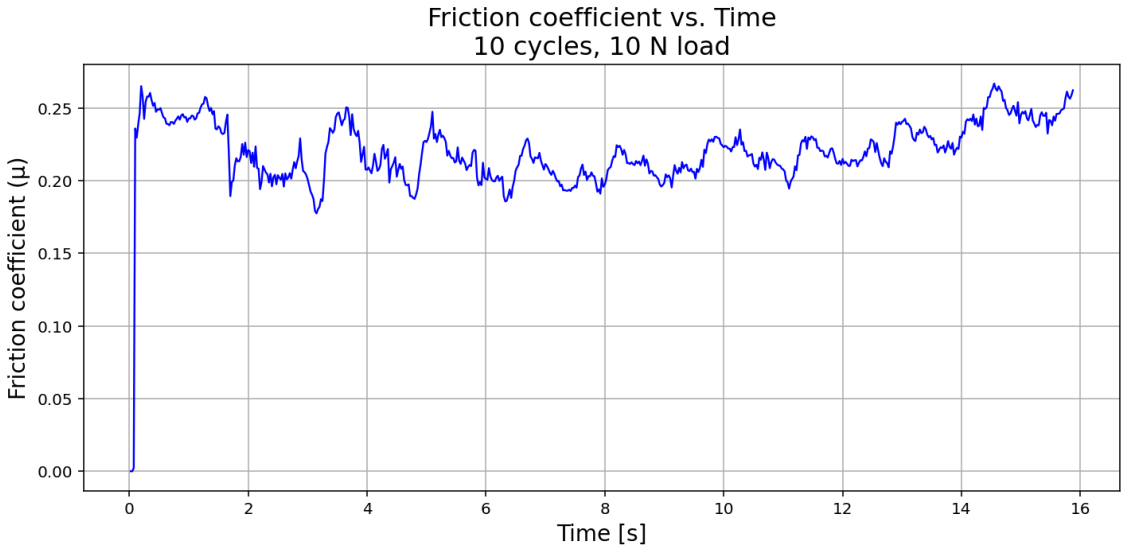

Figure A.251: This figure shows a virgin stainless steel sample. This figure shows the friction coefficient recorded during tribometry measurement when equipped with a load of 10 N and during only 10 cycles.

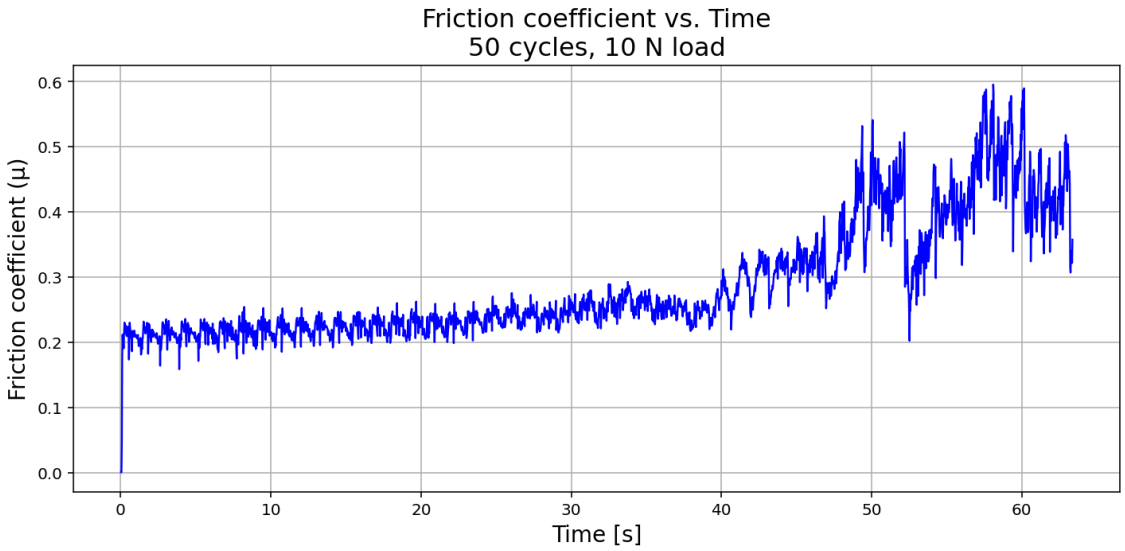

Figure A.252: This figure shows a virgin stainless steel sample. This figure shows the friction coefficient recorded during tribometry measurement when equipped with a load of 10 N and during only 50 cycles.

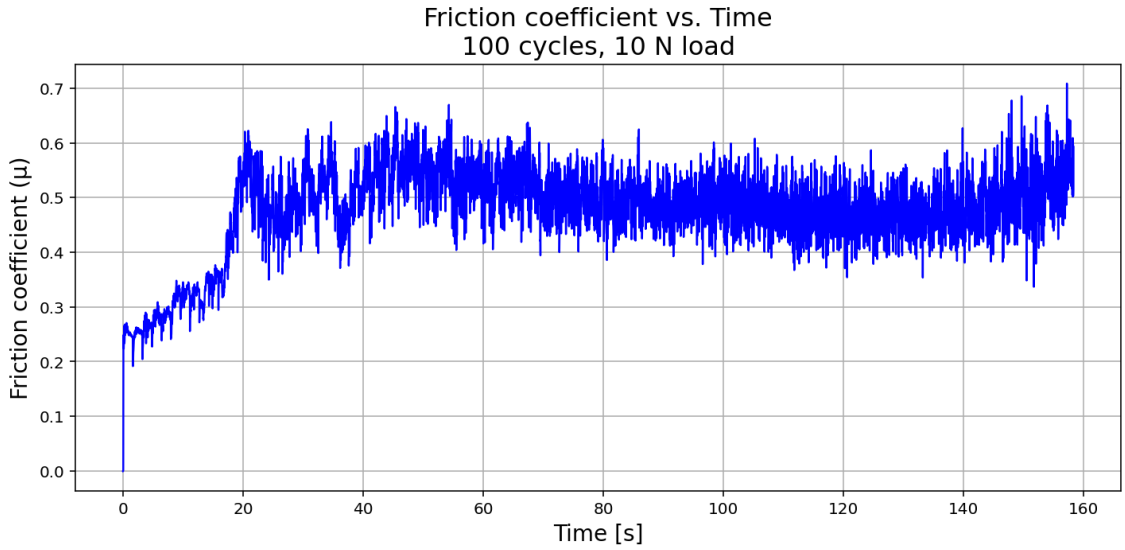

Figure A.253: This figure shows a virgin stainless steel sample. This figure shows the friction coefficient recorded during tribometry measurement when equipped with a load of 10 N and during 100 cycles.

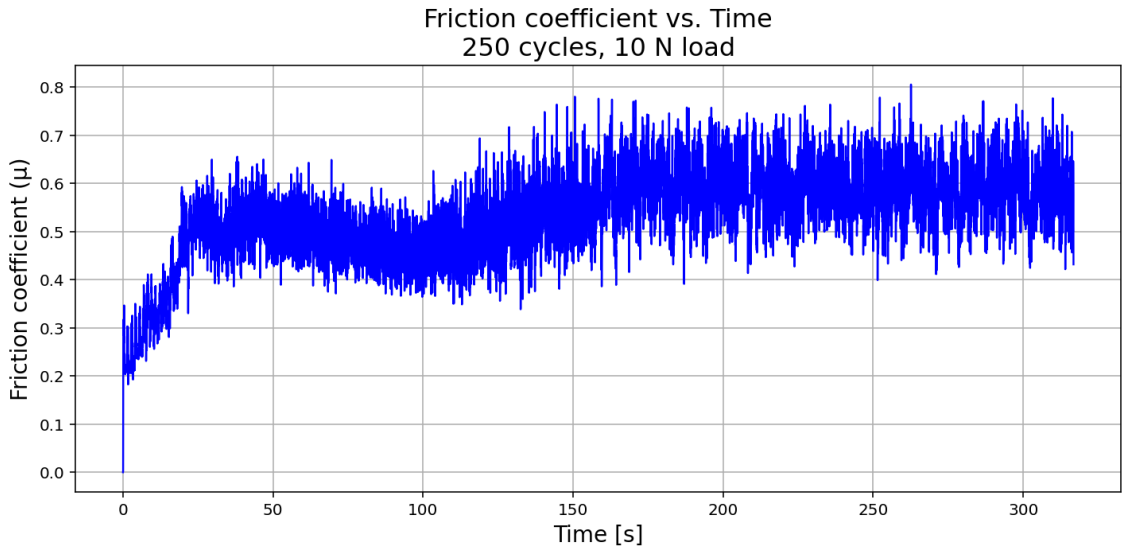

Figure A.254: This figure shows a virgin stainless steel sample. This figure shows the friction coefficient recorded during tribometry measurement when equipped with a load of 10 N and during 250 cycles.

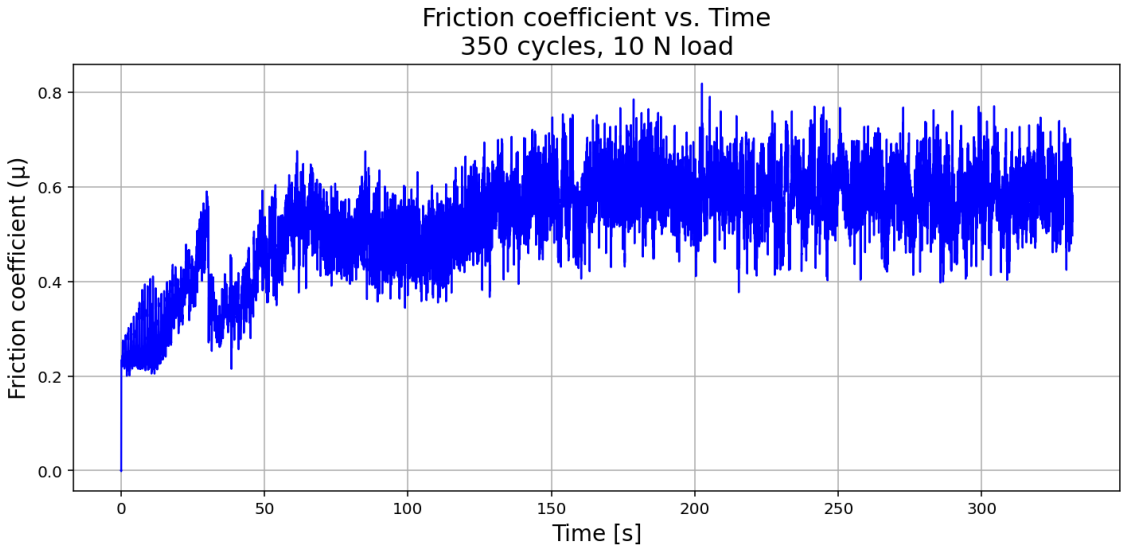

Figure A.255: This figure shows a virgin stainless steel sample. This figure shows the friction coefficient recorded during tribometry measurement when equipped with a load of 10 N and during 350 cycles.

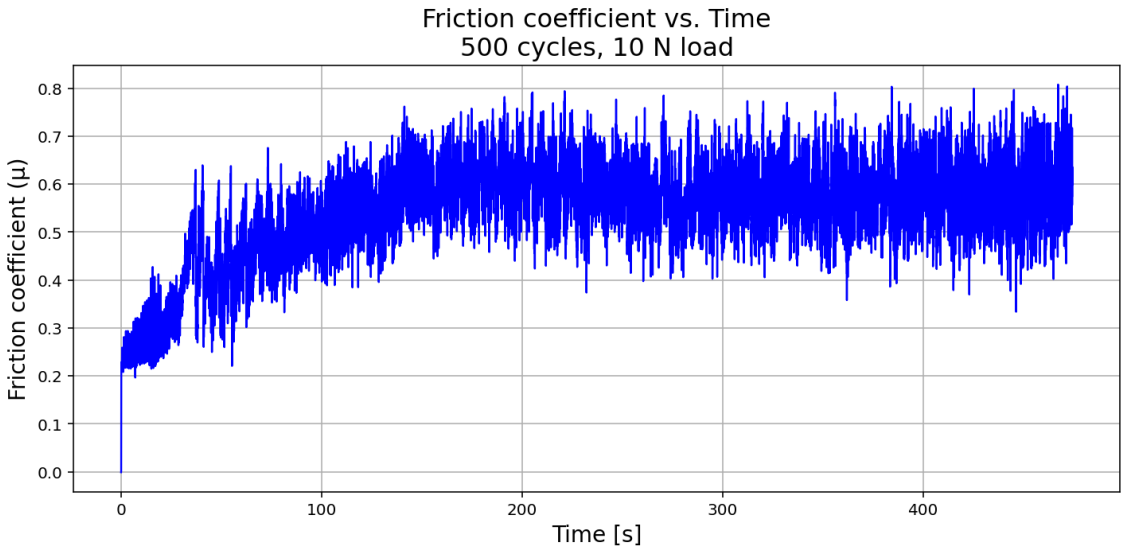

Figure A.256: This figure shows a virgin stainless steel sample. This figure shows the friction coefficient recorded during tribometry measurement when equipped with a load of 10 N and during 500 cycles.

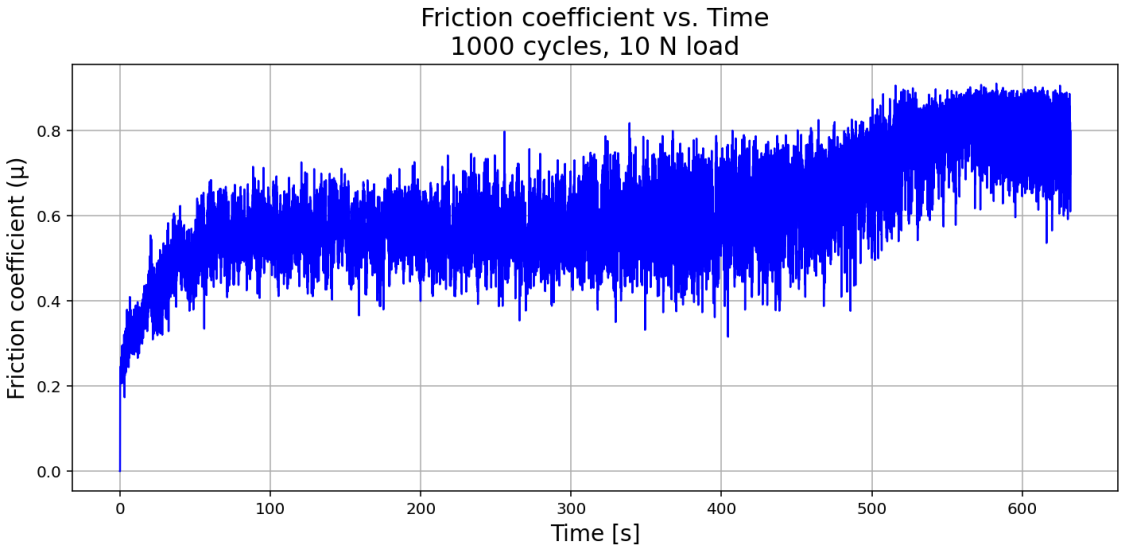

Figure A.257: This figure shows a virgin stainless steel sample. This figure shows the friction coefficient recorded during tribometry measurement when equipped with a load of 10 N and during 1000 cycles.

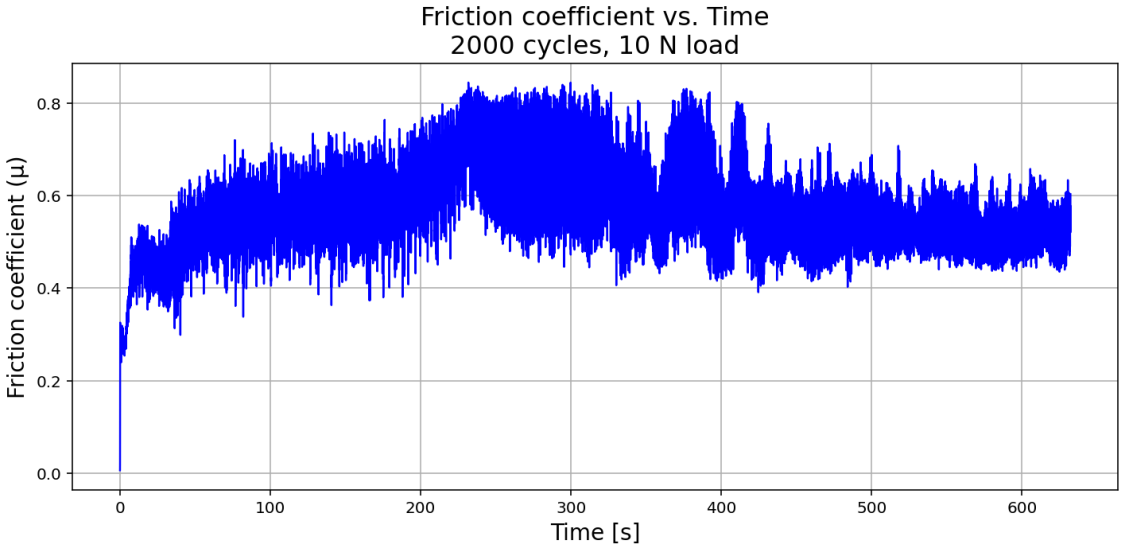

Figure A.258: This figure shows a virgin stainless steel sample. This figure shows the friction coefficient recorded during tribometry measurement when equipped with a load of 10 N and during 2000 cycles.

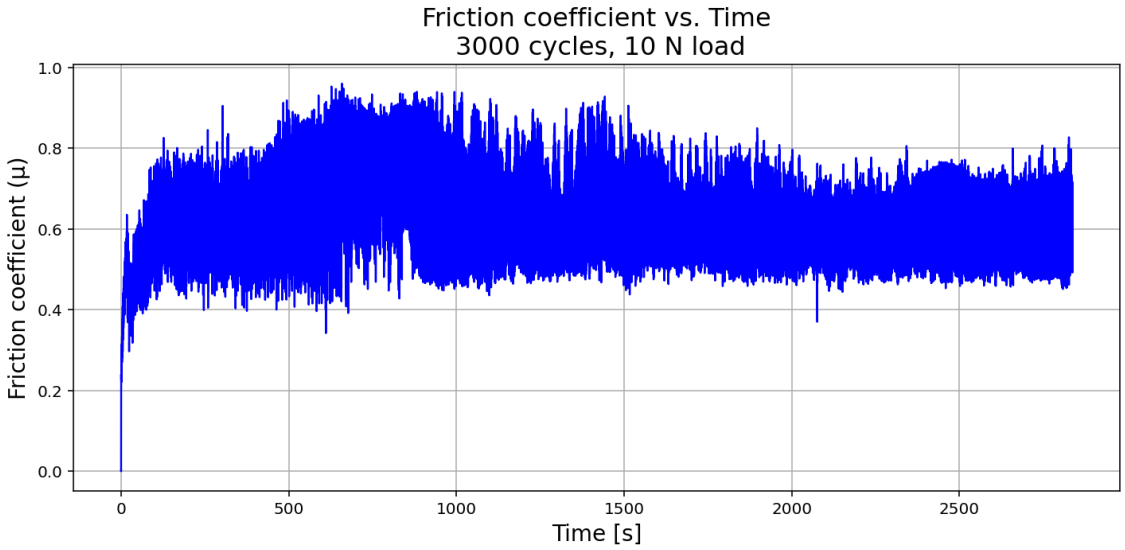

Figure A.259: This figure shows a virgin stainless steel sample. This figure shows the friction coefficient recorded during tribometry measurement when equipped with a load of 10 N and during 3000 cycles.

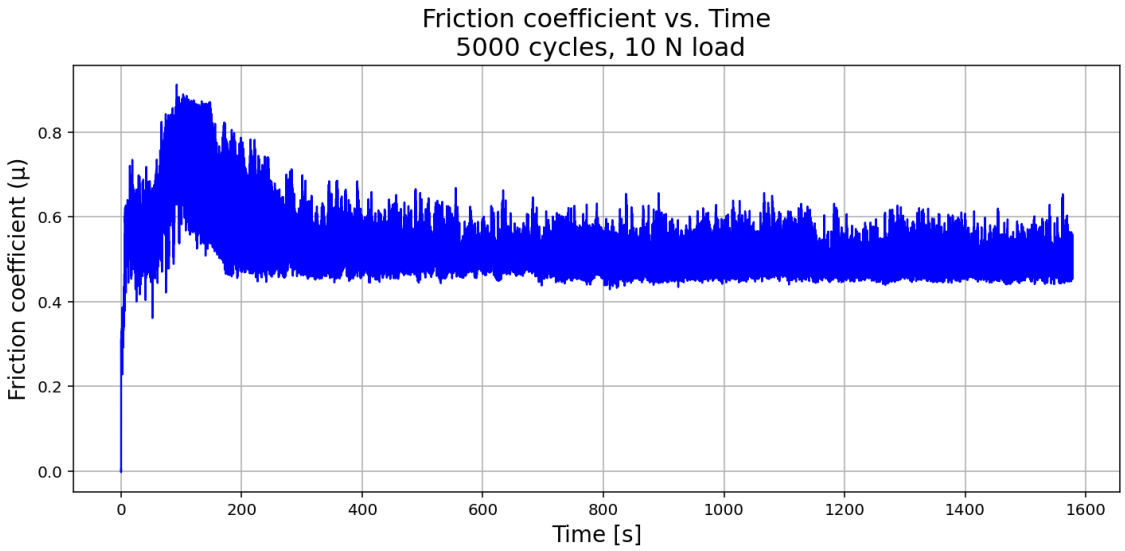

Figure A.260: This figure shows a virgin stainless steel sample. This figure shows the friction coefficient recorded during tribometry measurement when equipped with a load of 10 N and during 5000 cycles.

A.9 Friction Coefficient of 1500 nm TiN Coated Stainless Steel

A.9.1 Friction Coefficient of 1500 nm TiN Coated Stainless Steel 0.25 N

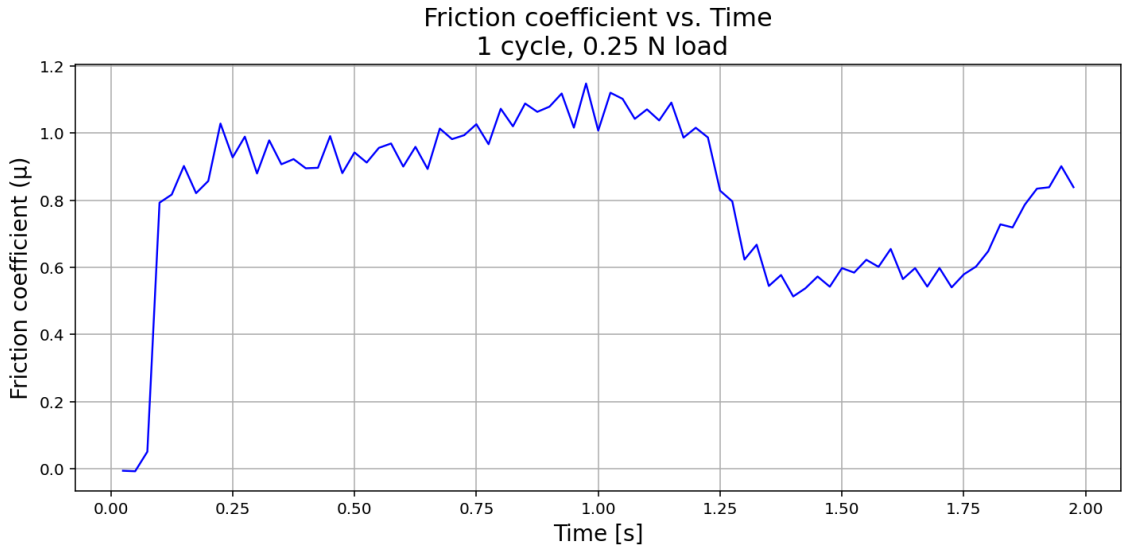

Figure A.261: This figure shows a 1500 nm TiN sample. This figure shows the friction coefficient recorded during tribometry measurement when equipped with a load of 0,25 N and during only 1 cycle.

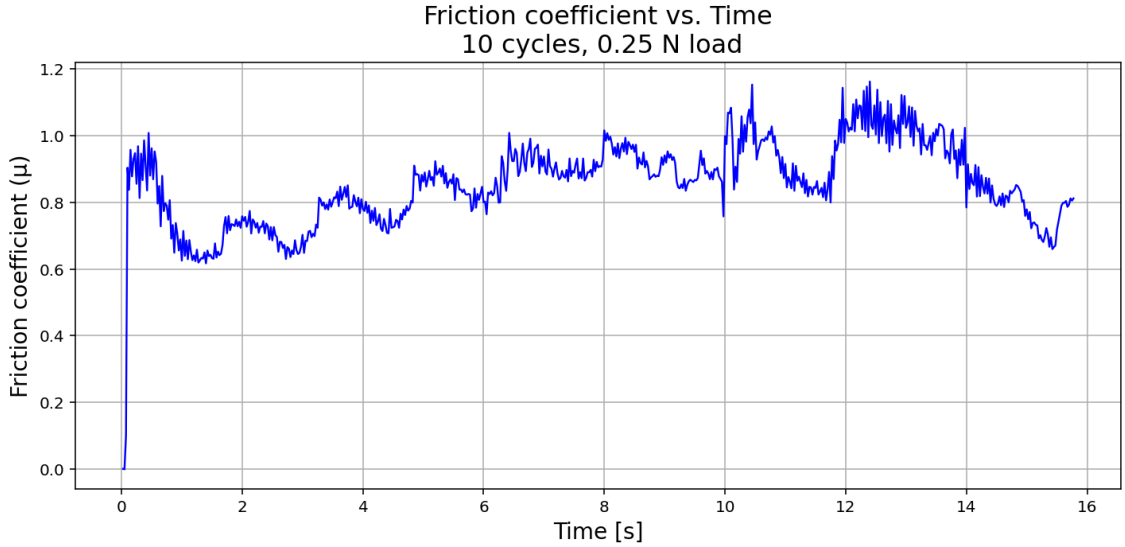

Figure A.262: This figure shows a 1500 nm TiN sample. This figure shows the friction coefficient recorded during tribometry measurement when equipped with a load of 0,25 N and during only 10 cycles.

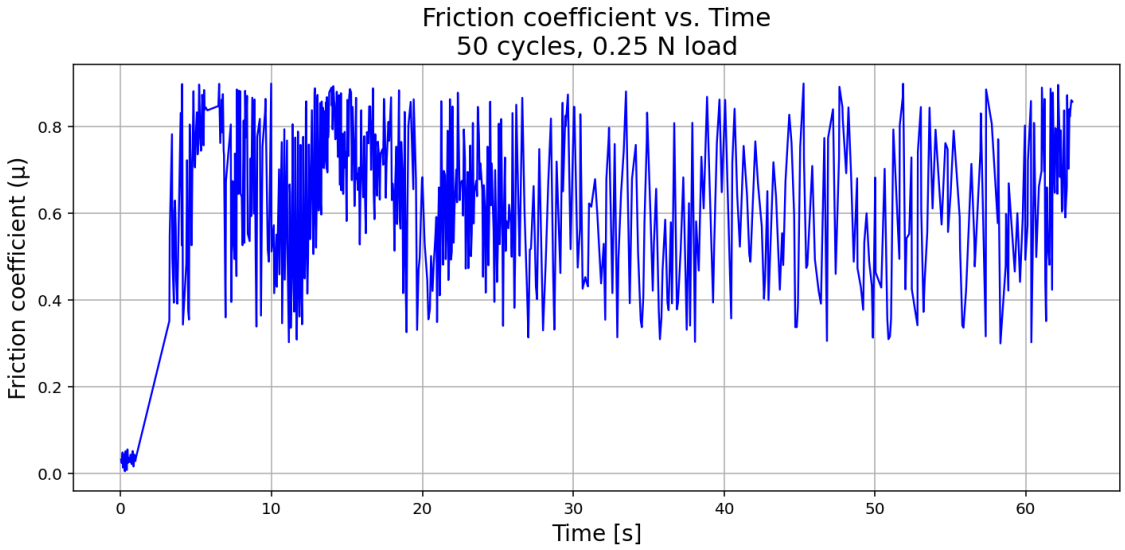

Figure A.263: This figure shows a 1500 nm TiN sample. This figure shows the friction coefficient recorded during tribometry measurement when equipped with a load of 0,25 N and during only 50 cycles.

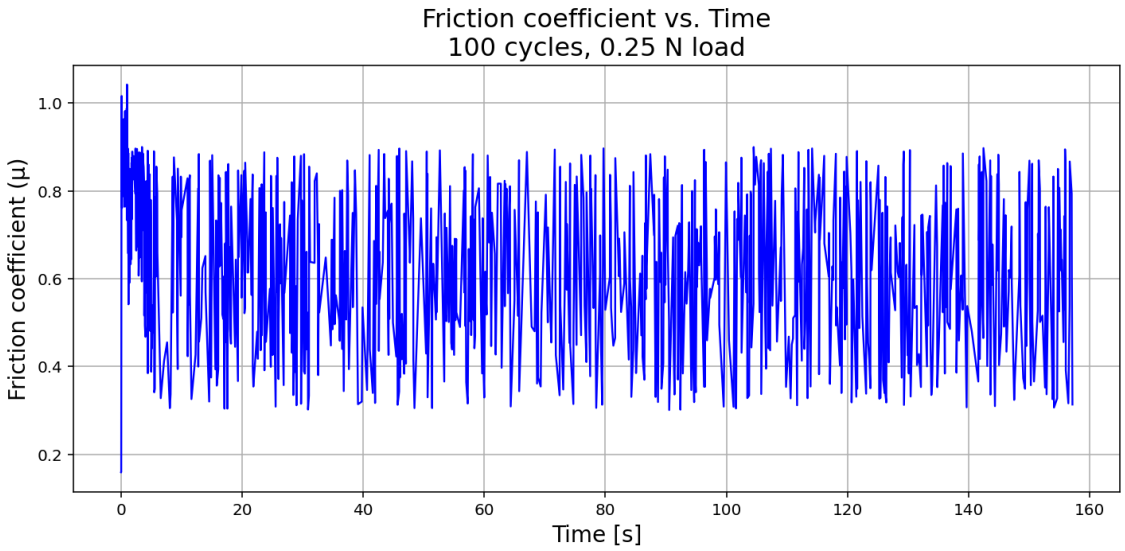

Figure A.264: This figure shows a 1500 nm TiN sample. This figure shows the friction coefficient recorded during tribometry measurement when equipped with a load of 0,25 N and during 100 cycles.

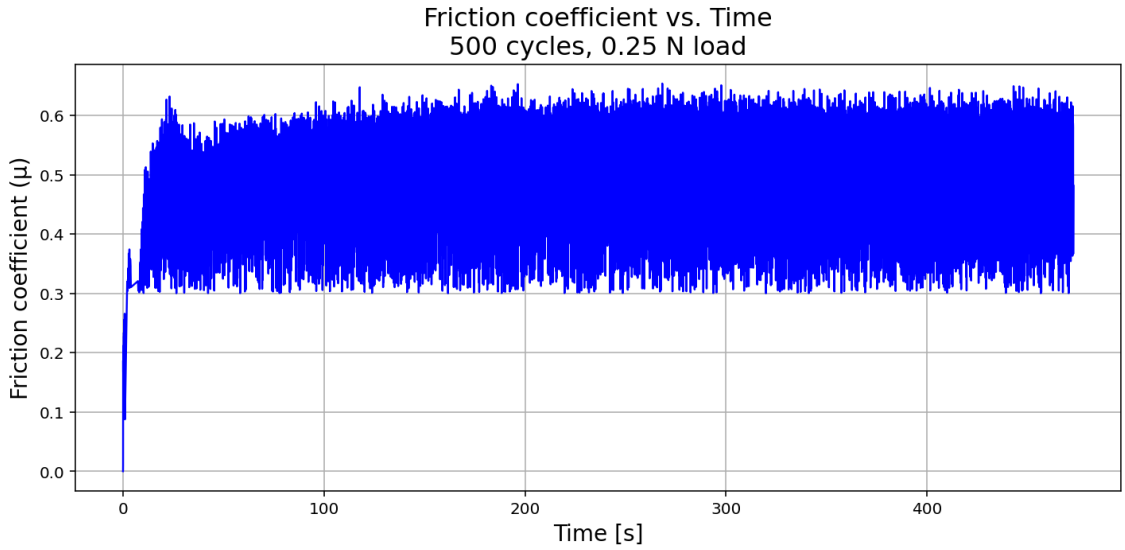

Figure A.265: This figure shows a 1500 nm TiN sample. This figure shows the friction coefficient recorded during tribometry measurement when equipped with a load of 0,25 N and during 500 cycles.

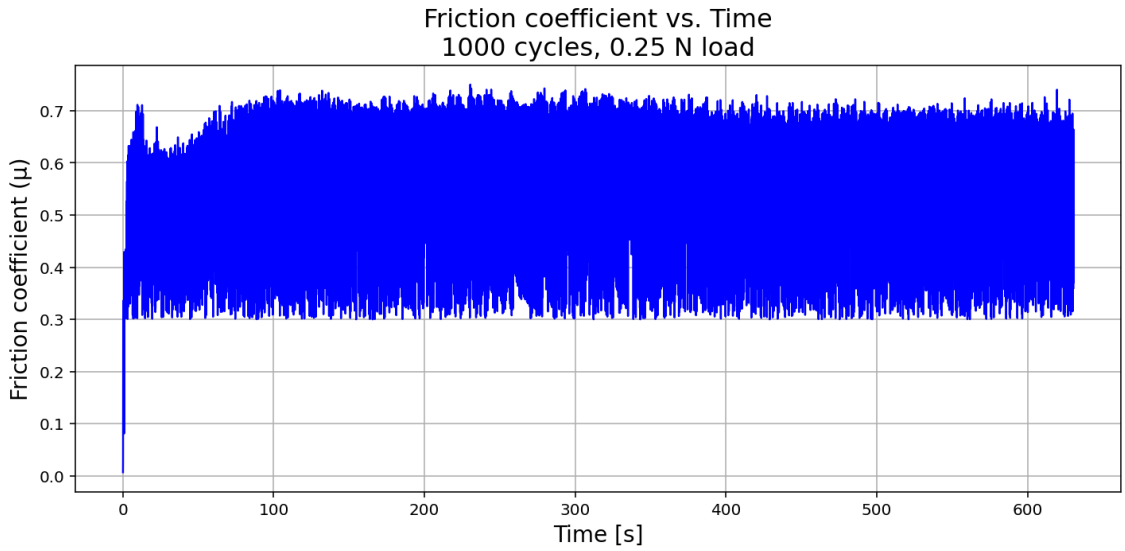

Figure A.266: This figure shows a 1500 nm TiN sample. This figure shows the friction coefficient recorded during tribometry measurement when equipped with a load of 0,25 N and during 1000 cycles.

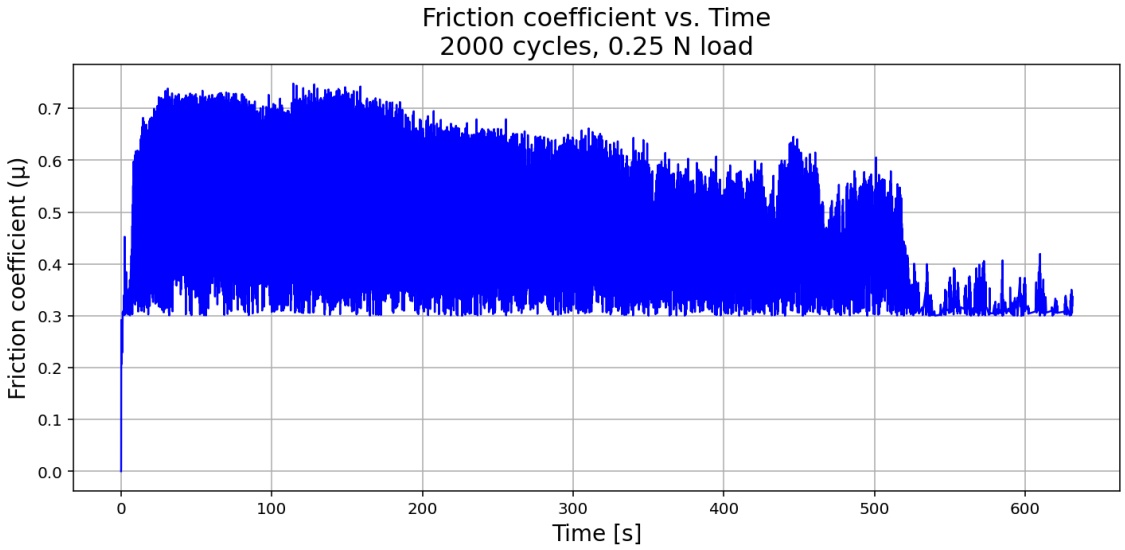

Figure A.267: This figure shows a 1500 nm TiN sample. This figure shows the friction coefficient recorded during tribometry measurement when equipped with a load of 0,25 N and during 2000 cycles.

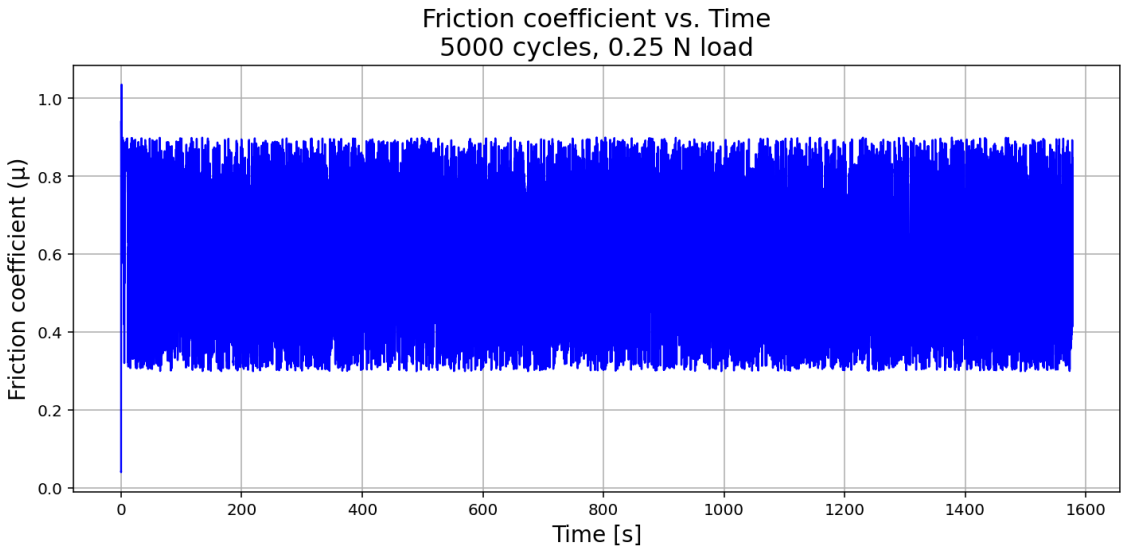

Figure A.268: This figure shows a 1500 nm TiN sample. This figure shows the friction coefficient recorded during tribometry measurement when equipped with a load of 0,25 N and during 5000 cycles.

A.9.2 Friction Coefficient of 1500 nm TiN Coated Stainless Steel 1 N

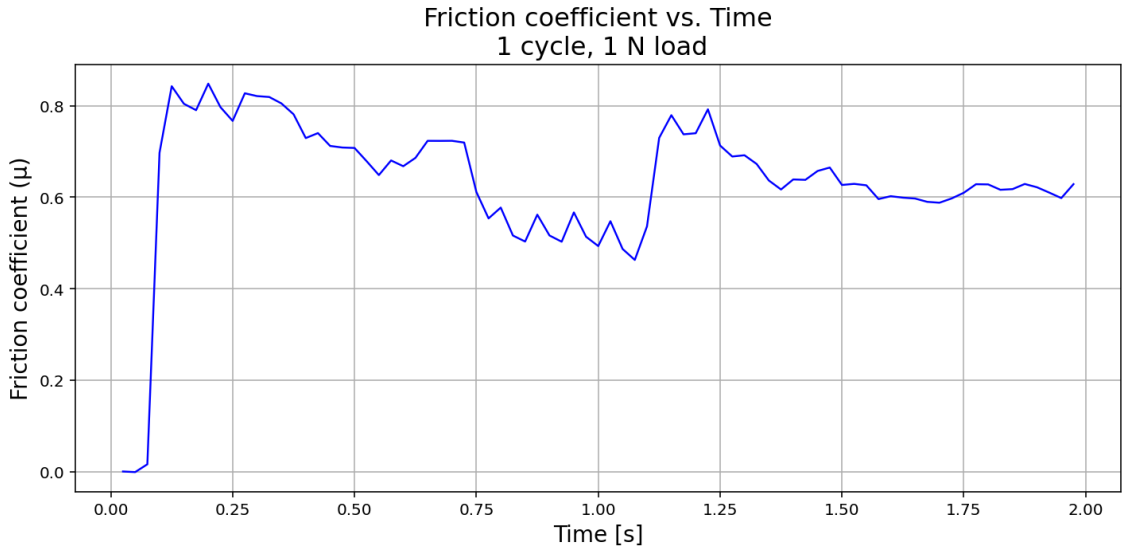

Figure A.269: This figure shows a 1500 nm TiN sample. This figure shows the friction coefficient recorded during tribometry measurement when equipped with a load of 1 N and during only 1 cycle.

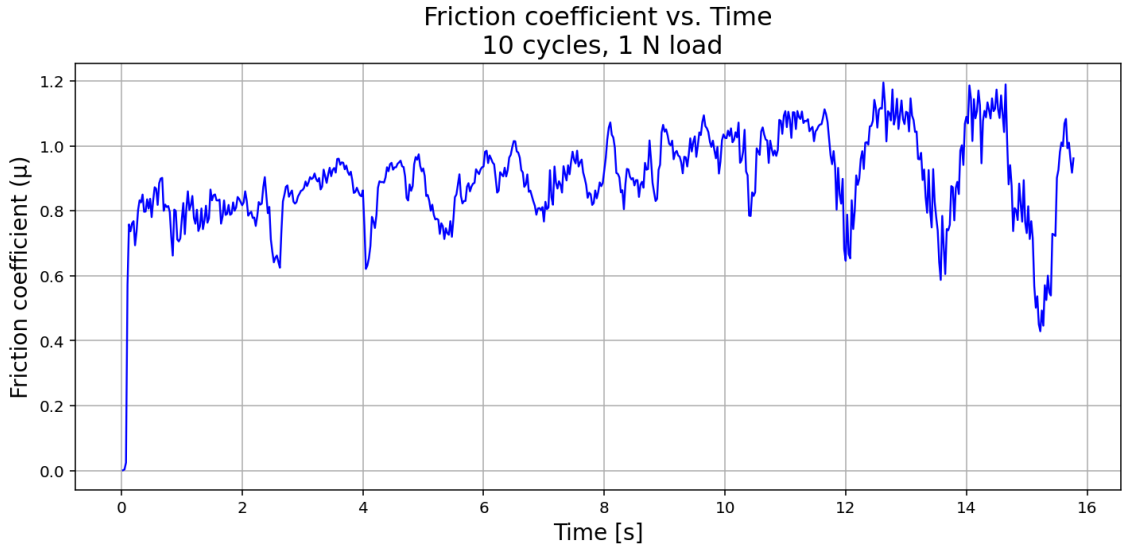

Figure A.270: This figure shows a 1500 nm TiN sample. This figure shows the friction coefficient recorded during tribometry measurement when equipped with a load of 1 N and during only 10 cycles.

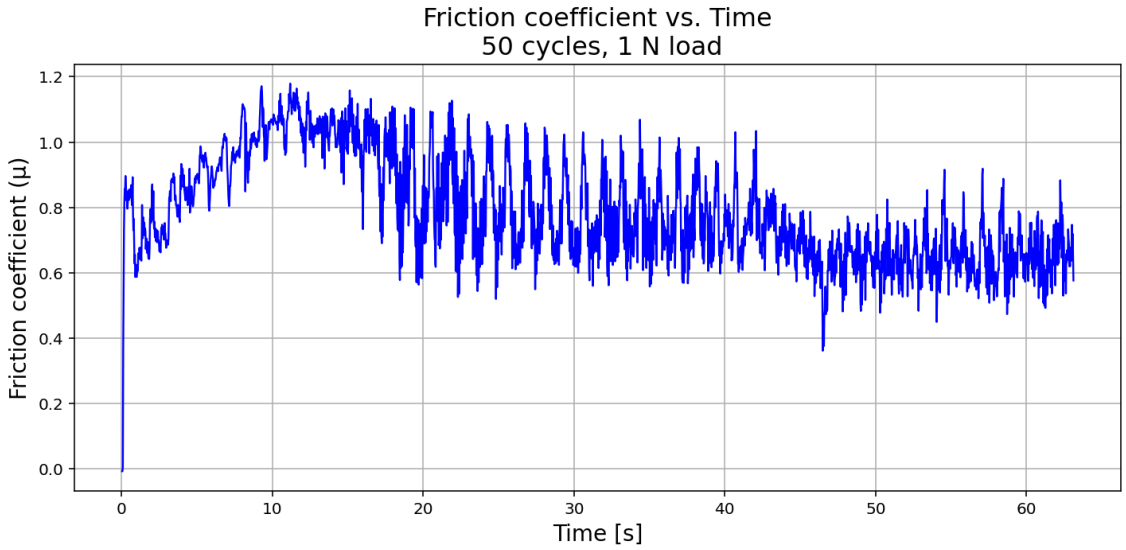

Figure A.271: This figure shows a 1500 nm TiN sample. This figure shows the friction coefficient recorded during tribometry measurement when equipped with a load of 1 N and during only 50 cycles.

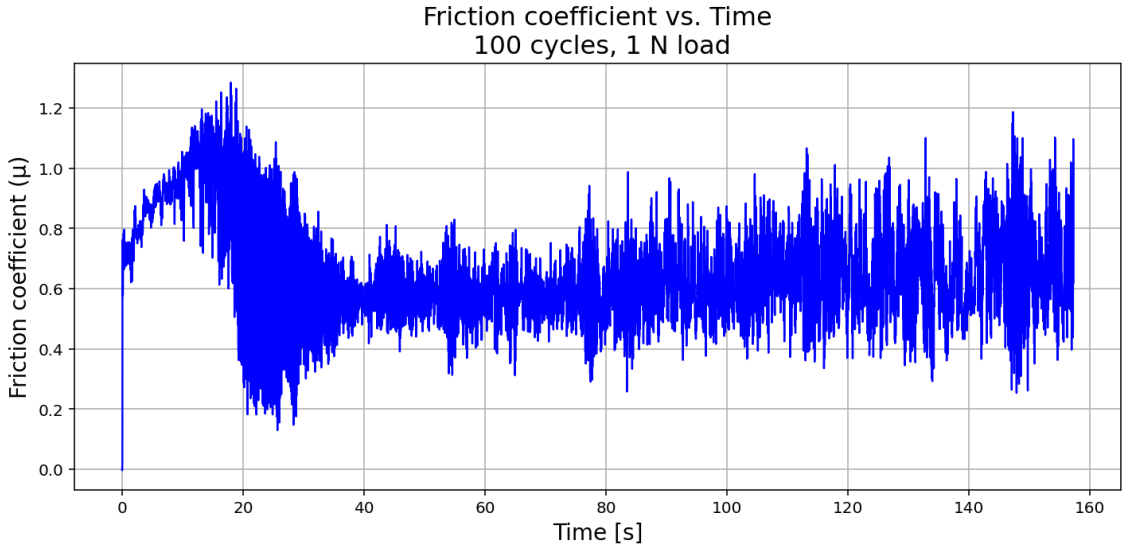

Figure A.272: This figure shows a 1500 nm TiN sample. This figure shows the friction coefficient recorded during tribometry measurement when equipped with a load of 1 N and during 100 cycles.

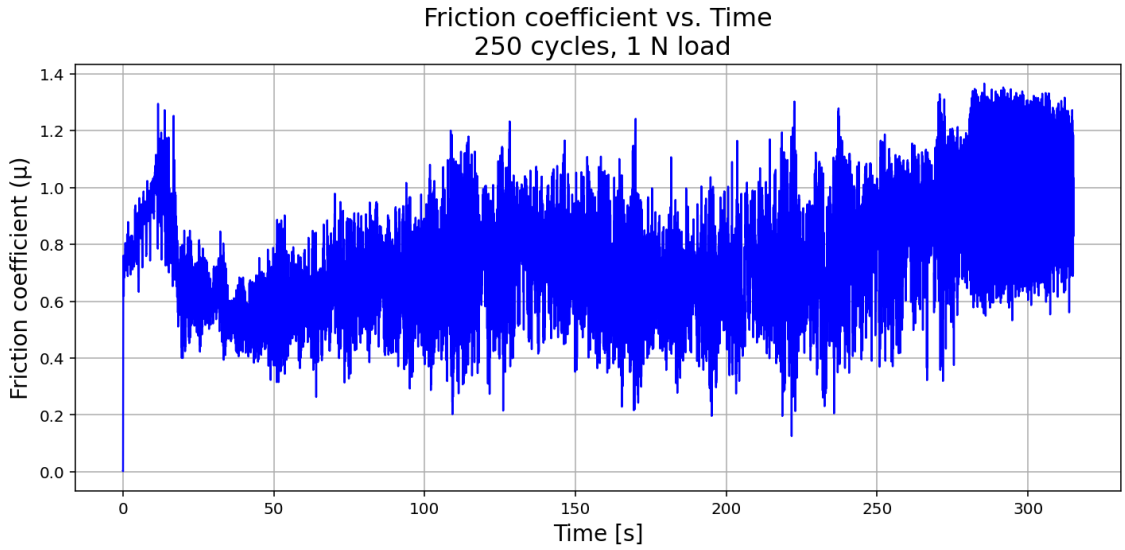

Figure A.273: This figure shows a 1500 nm TiN sample. This figure shows the friction coefficient recorded during tribometry measurement when equipped with a load of 1 N and during 250 cycles.

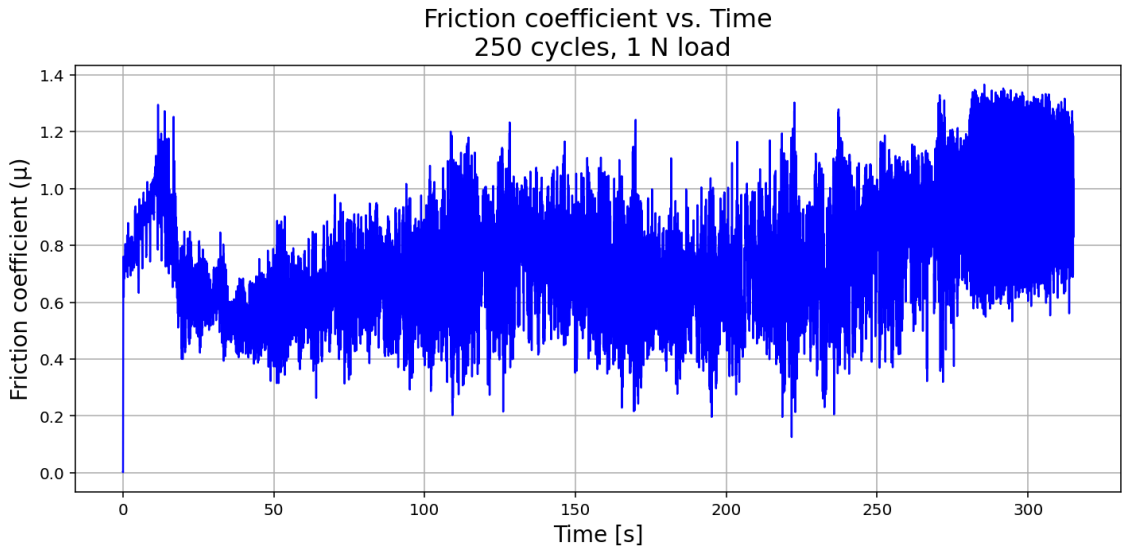

Figure A.274: This figure shows a 1500 nm TiN sample. This figure shows the friction coefficient recorded during tribometry measurement when equipped with a load of 1 N and during 250 cycles.

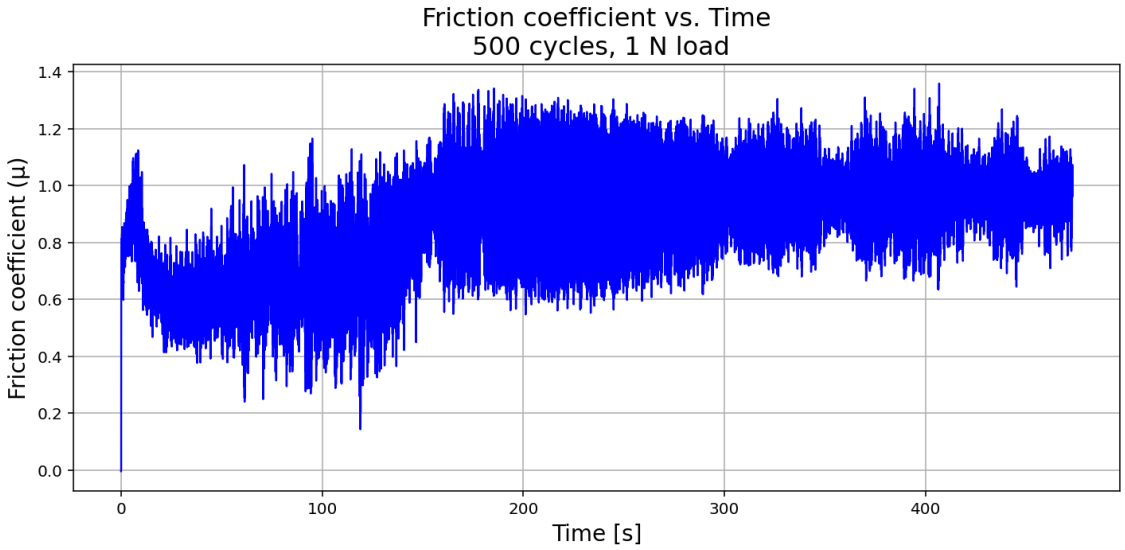

Figure A.275: This figure shows a 1500 nm TiN sample. This figure shows the friction coefficient recorded during tribometry measurement when equipped with a load of 1 N and during 500 cycles.

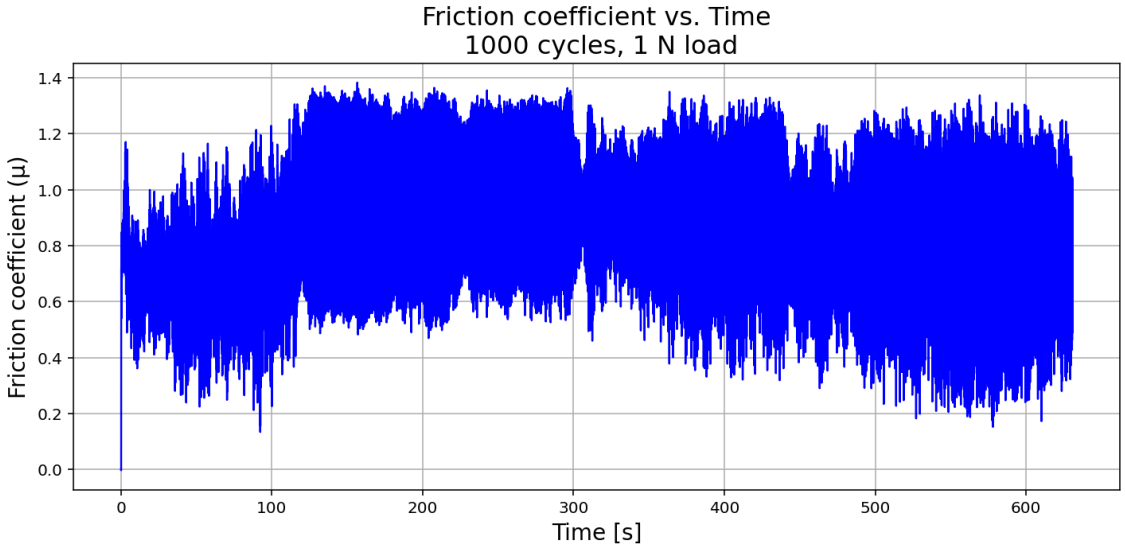

Figure A.276: This figure shows a 1500 nm TiN sample. This figure shows the friction coefficient recorded during tribometry measurement when equipped with a load of 1 N and during 1000 cycles.

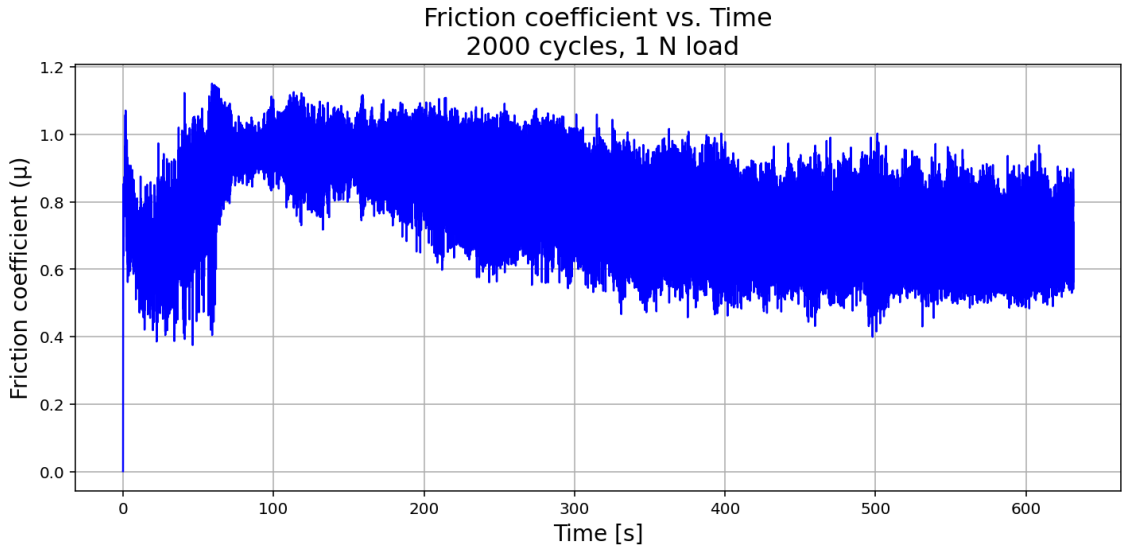

Figure A.277: This figure shows a 1500 nm TiN sample. This figure shows the friction coefficient recorded during tribometry measurement when equipped with a load of 1 N and during 2000 cycles.

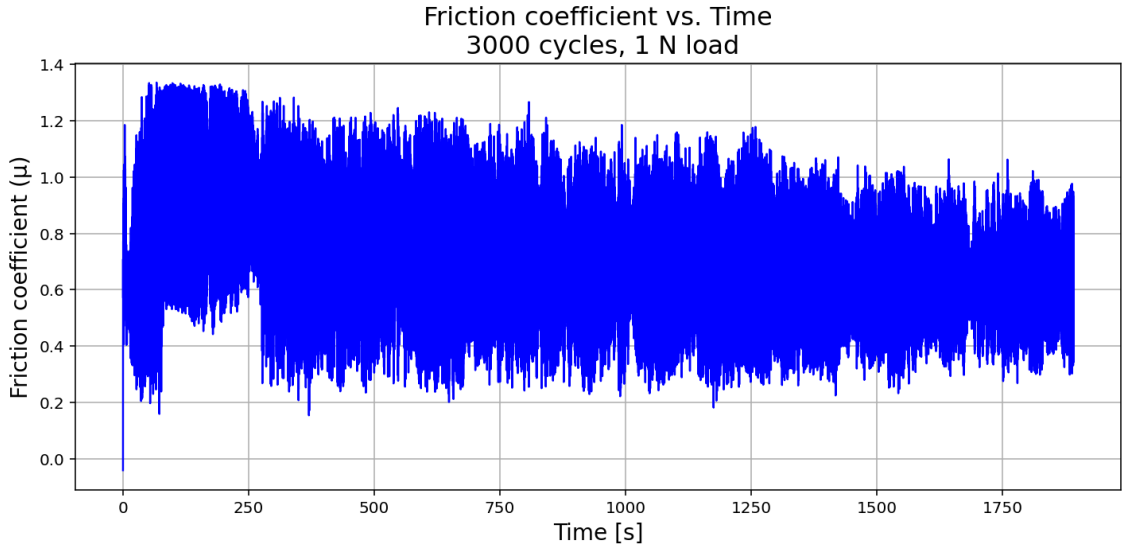

Figure A.278: This figure shows a 1500 nm TiN sample. This figure shows the friction coefficient recorded during tribometry measurement when equipped with a load of 1 N and during 3000 cycles.

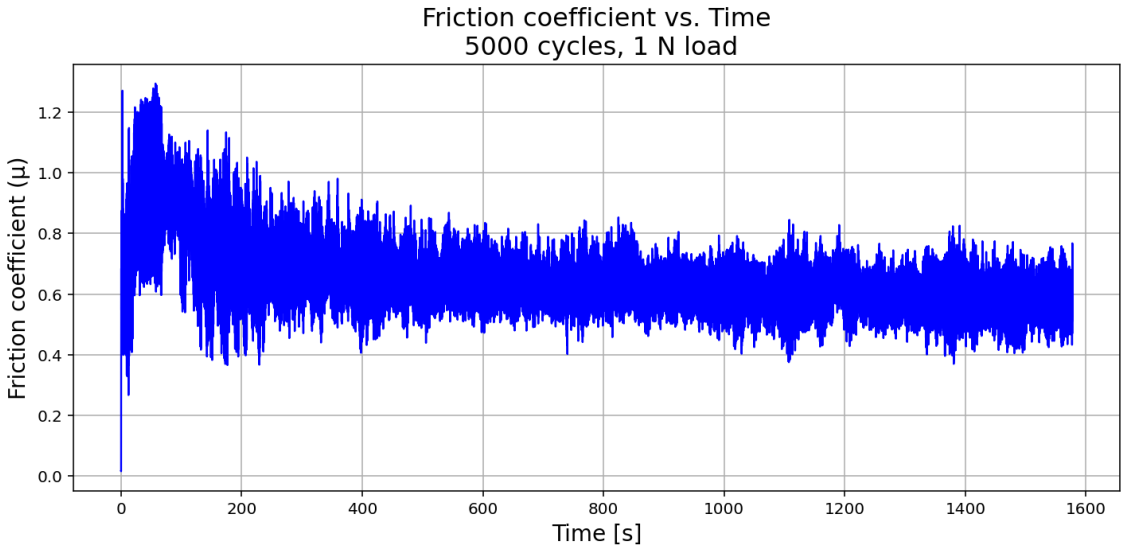

Figure A.279: This figure shows a 1500 nm TiN sample. This figure shows the friction coefficient recorded during tribometry measurement when equipped with a load of 1 N and during 5000 cycles.

A.9.3 Friction Coefficient of 1500 nm TiN Coated Stainless Steel 2 N

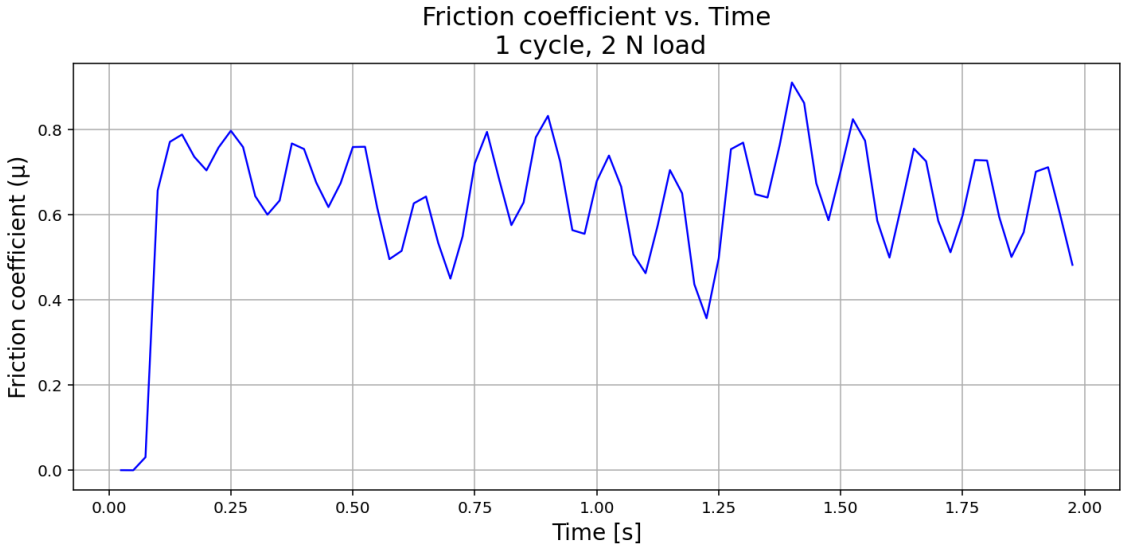

Figure A.280: This figure shows a 1500 nm TiN sample. This figure shows the friction coefficient recorded during tribometry measurement when equipped with a load of 2 N and during only 1 cycle.

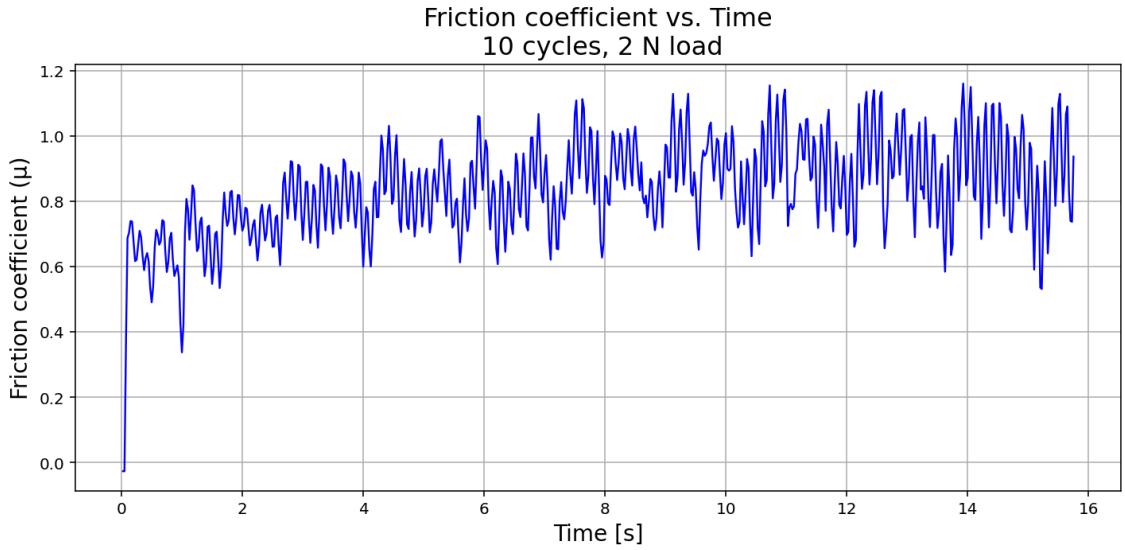

Figure A.281: This figure shows a 1500 nm TiN sample. This figure shows the friction coefficient recorded during tribometry measurement when equipped with a load of 2 N and during only 10 cycles.

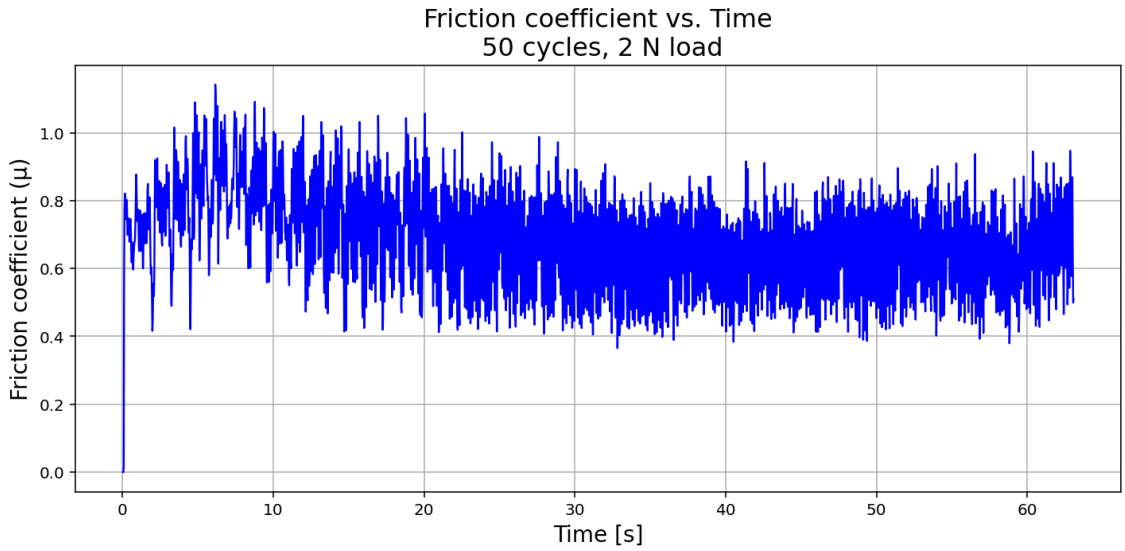

Figure A.282: This figure shows a 1500 nm TiN sample. This figure shows the friction coefficient recorded during tribometry measurement when equipped with a load of 2 N and during only 50 cycles.

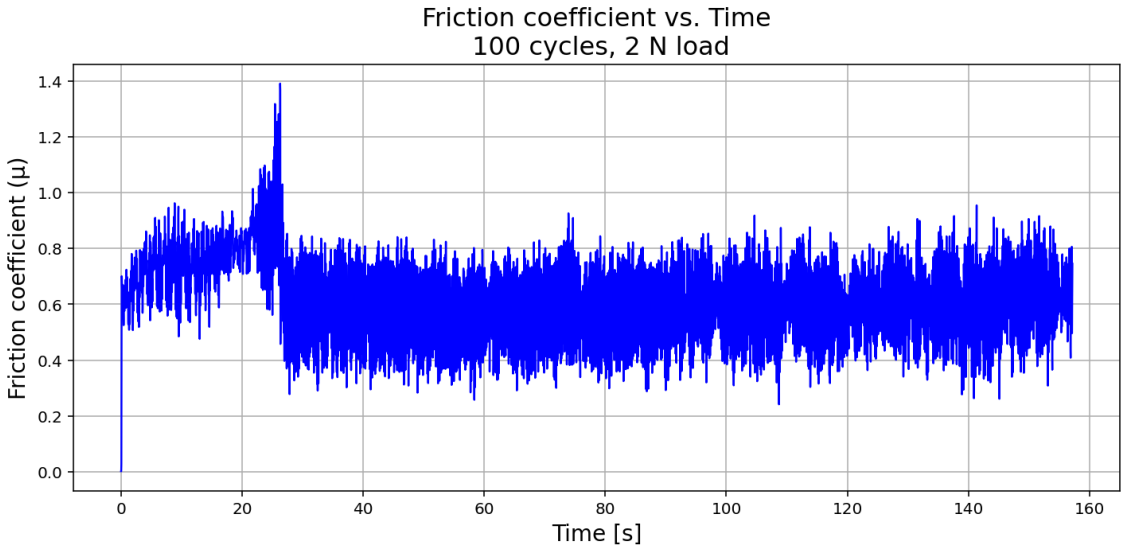

Figure A.283: This figure shows a 1500 nm TiN sample. This figure shows the friction coefficient recorded during tribometry measurement when equipped with a load of 2 N and during 100 cycles.

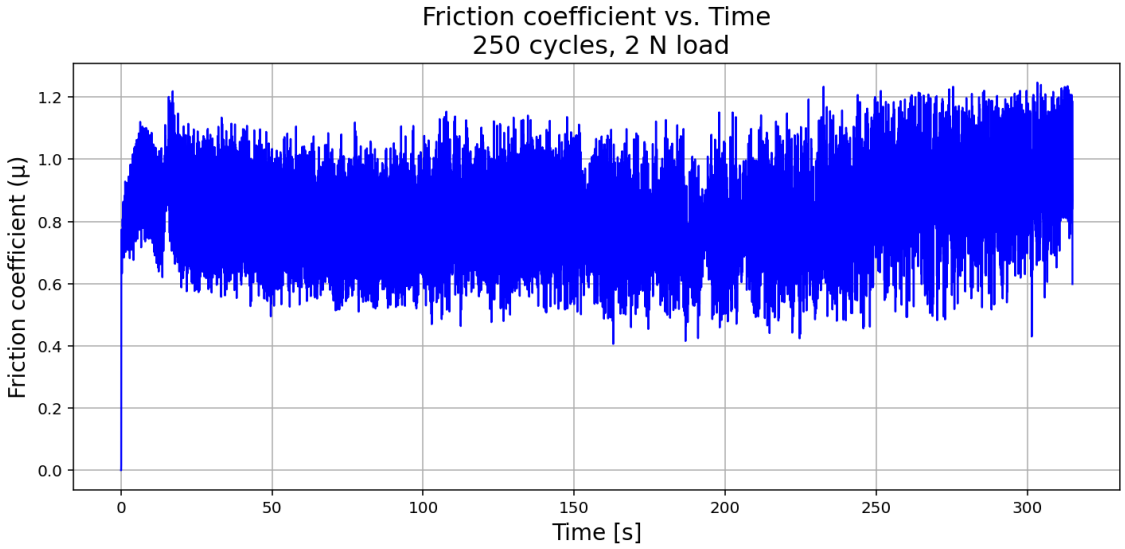

Figure A.284: This figure shows a 1500 nm TiN sample. This figure shows the friction coefficient recorded during tribometry measurement when equipped with a load of 2 N and during 250 cycles.

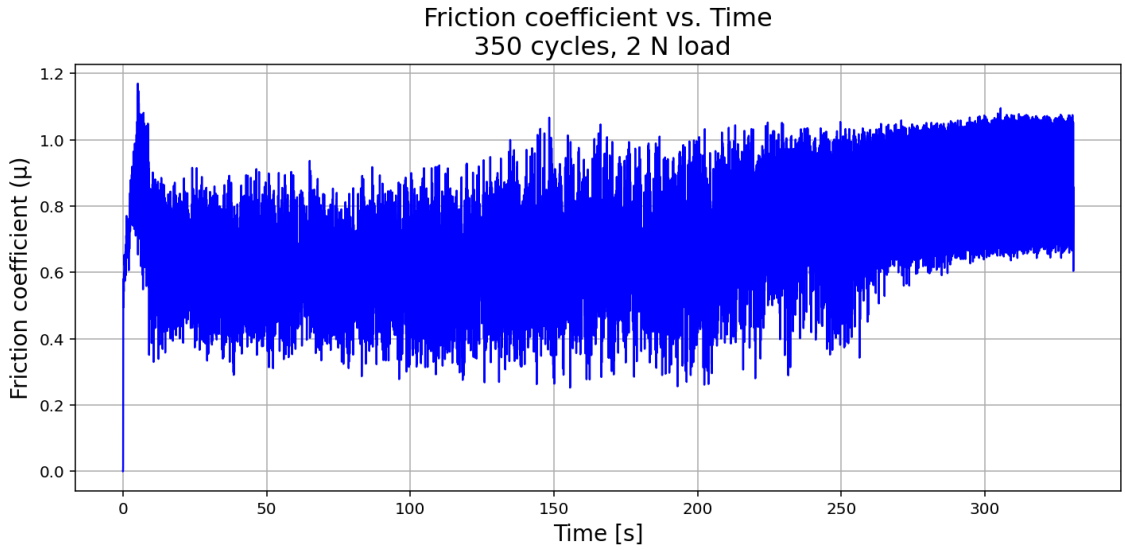

Figure A.285: This figure shows a 1500 nm TiN sample. This figure shows the friction coefficient recorded during tribometry measurement when equipped with a load of 2 N and during 350 cycles.

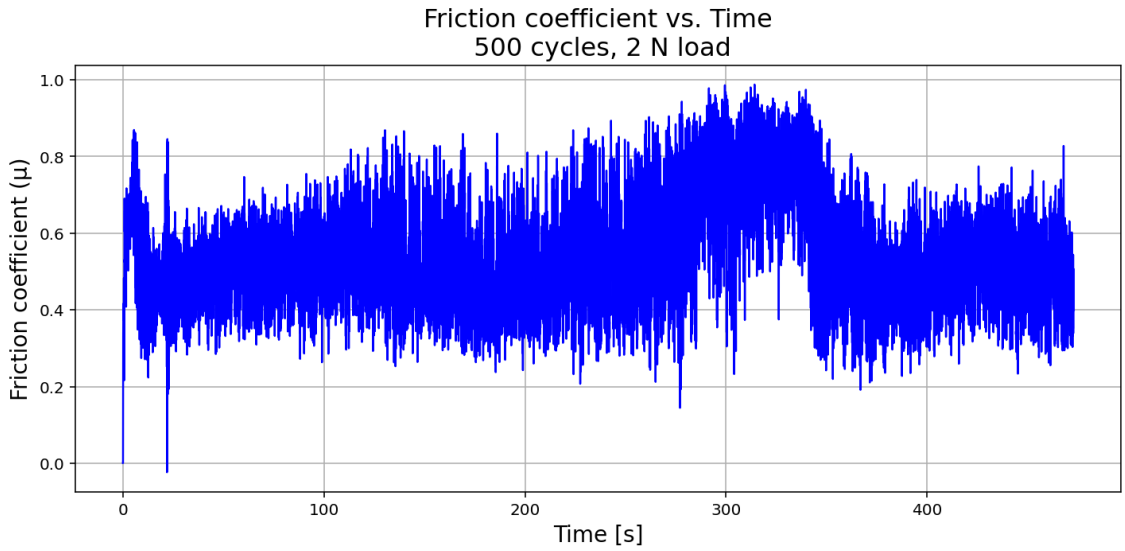

Figure A.286: This figure shows a 1500 nm TiN sample. This figure shows the friction coefficient recorded during tribometry measurement when equipped with a load of 2 N and during 500 cycles.

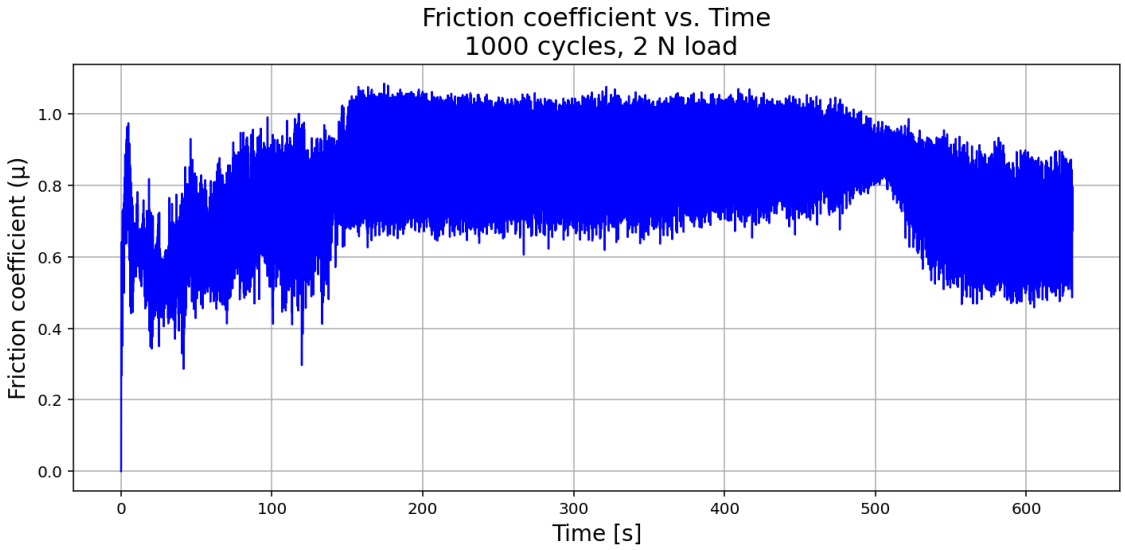

Figure A.287: This figure shows a 1500 nm TiN sample. This figure shows the friction coefficient recorded during tribometry measurement when equipped with a load of 2 N and during 1000 cycles.

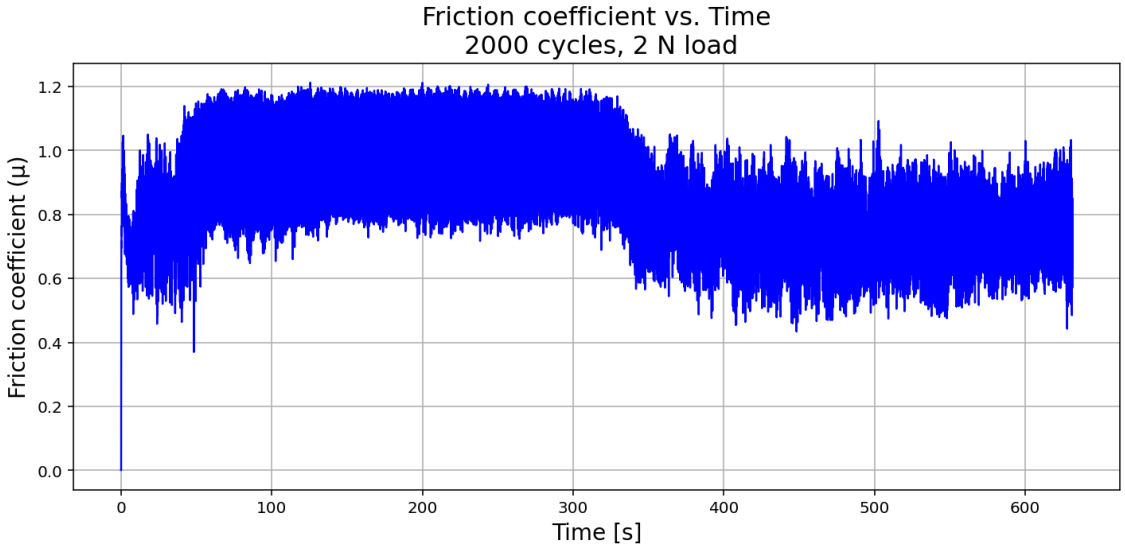

Figure A.288: This figure shows a 1500 nm TiN sample. This figure shows the friction coefficient recorded during tribometry measurement when equipped with a load of 2 N and during 2000 cycles.

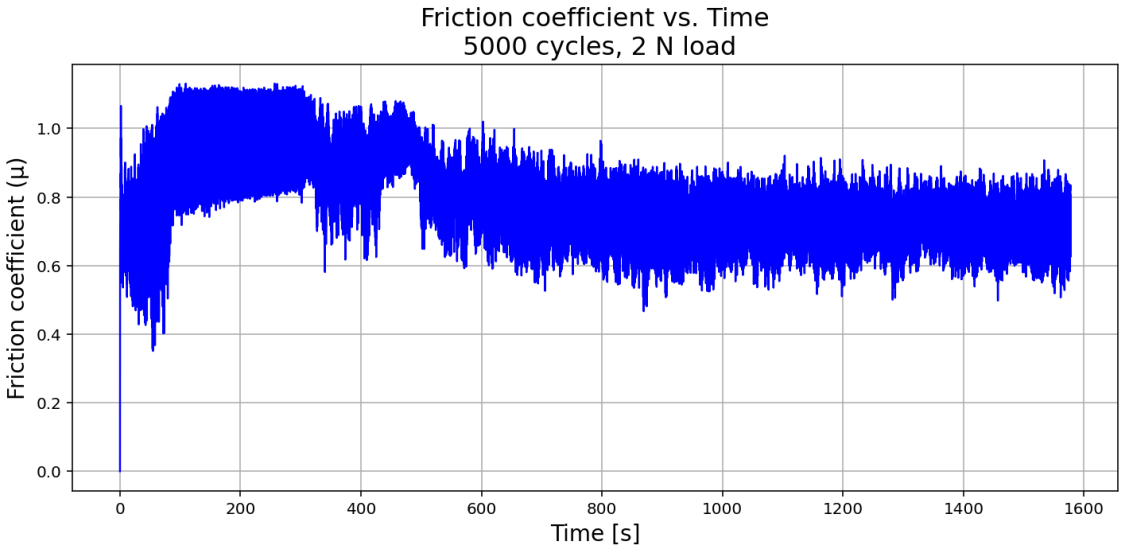

Figure A.289: This figure shows a 1500 nm TiN sample. This figure shows the friction coefficient recorded during tribometry measurement when equipped with a load of 2 N and during 5000 cycles.

A.9.4 Friction Coefficient of 1500 nm TiN Coated Stainless Steel 5 N

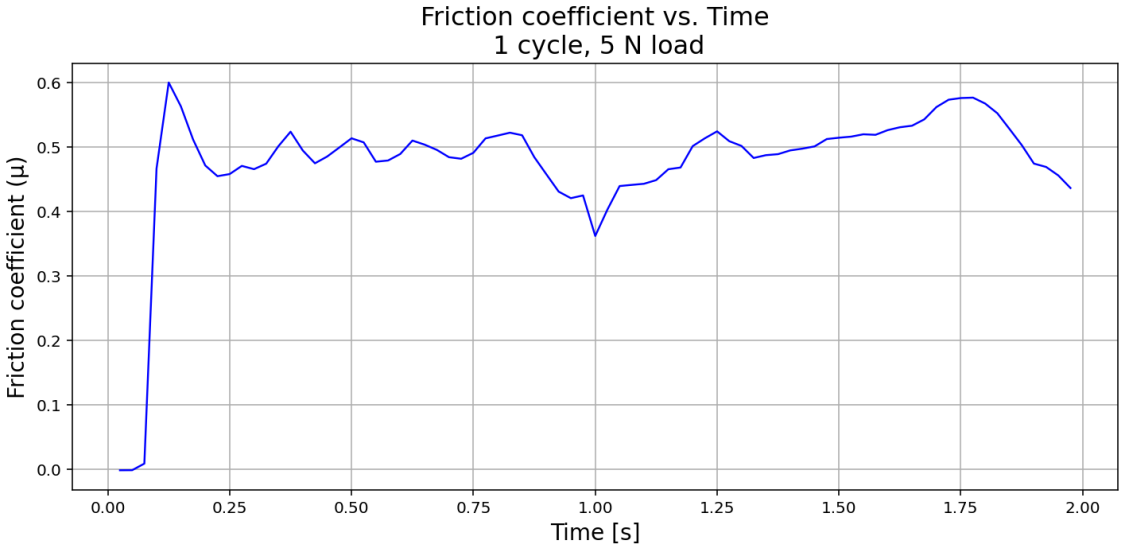

Figure A.290: This figure shows a 1500 nm TiN sample. This figure shows the friction coefficient recorded during tribometry measurement when equipped with a load of 5 N and during only 1 cycle.

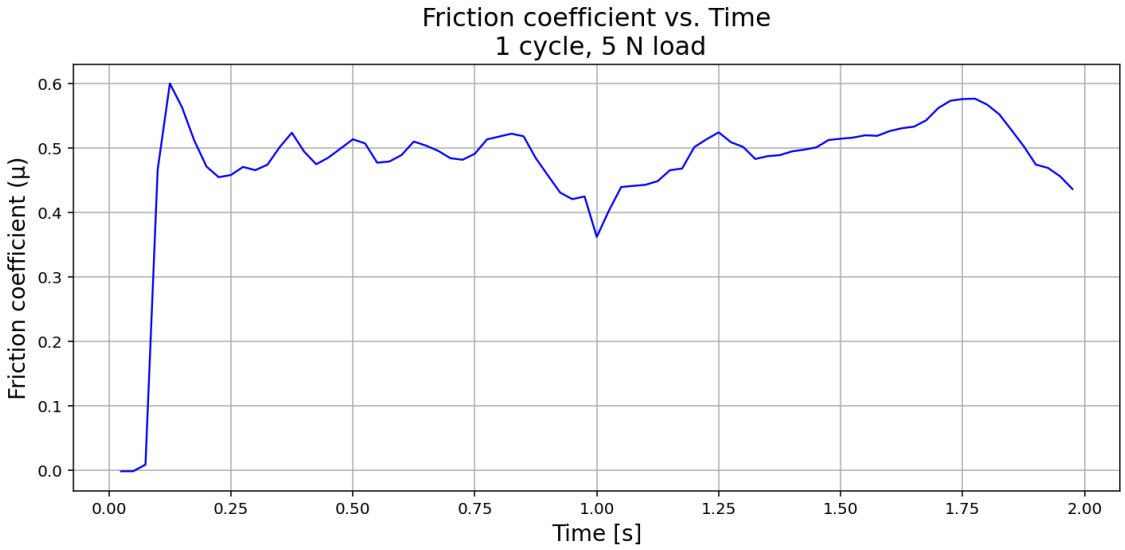

Figure A.291: This figure shows a 1500 nm TiN sample. This figure shows the friction coefficient recorded during tribometry measurement when equipped with a load of 5 N and during only 1 cycle.

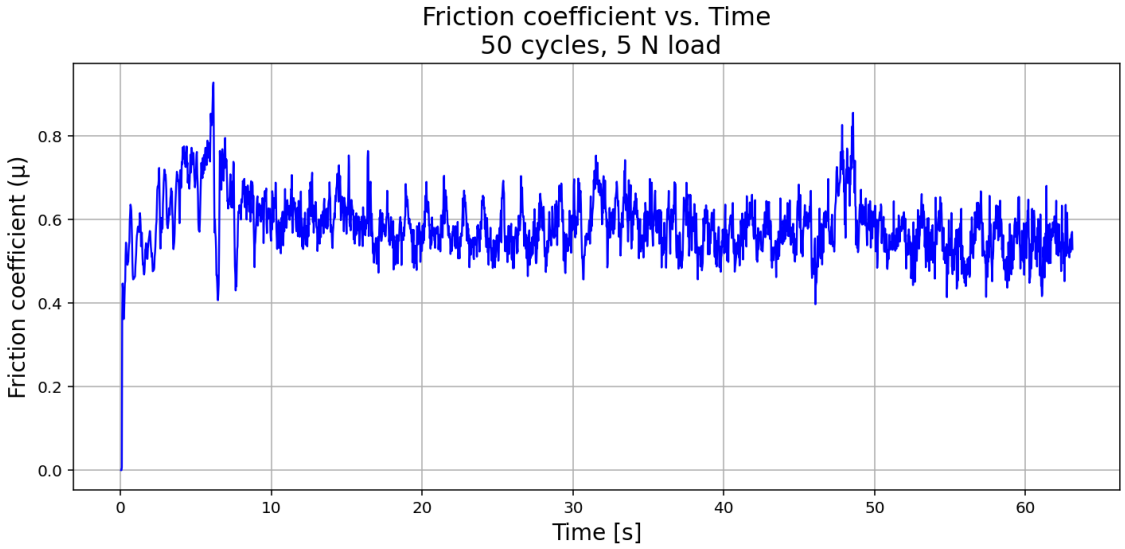

Figure A.292: This figure shows a 1500 nm TiN sample. This figure shows the friction coefficient recorded during tribometry measurement when equipped with a load of 5 N and during only 50 cycles.

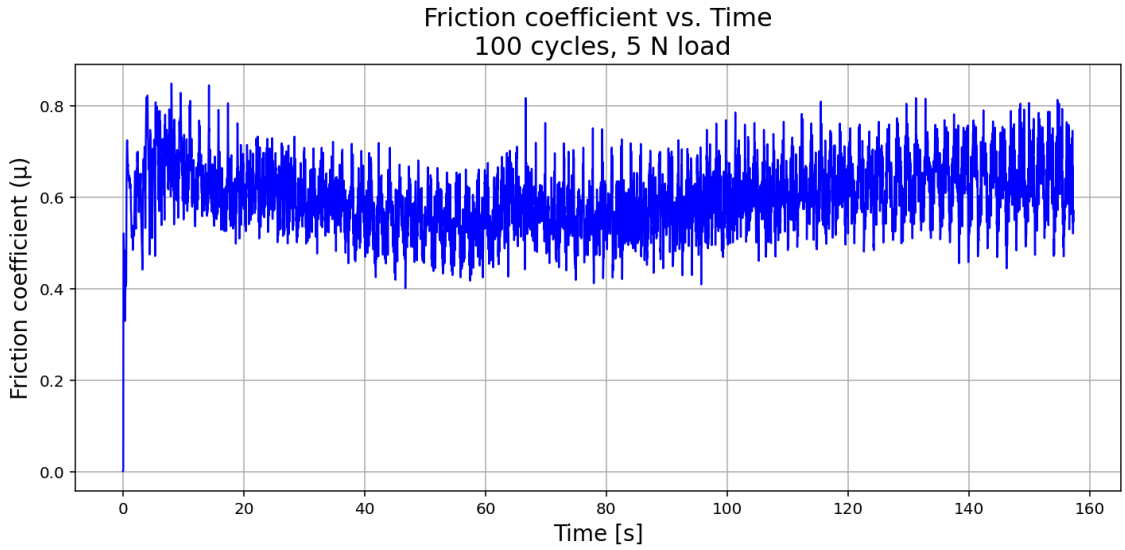

Figure A.293: This figure shows a 1500 nm TiN sample. This figure shows the friction coefficient recorded during tribometry measurement when equipped with a load of 5 N and during 100 cycles.

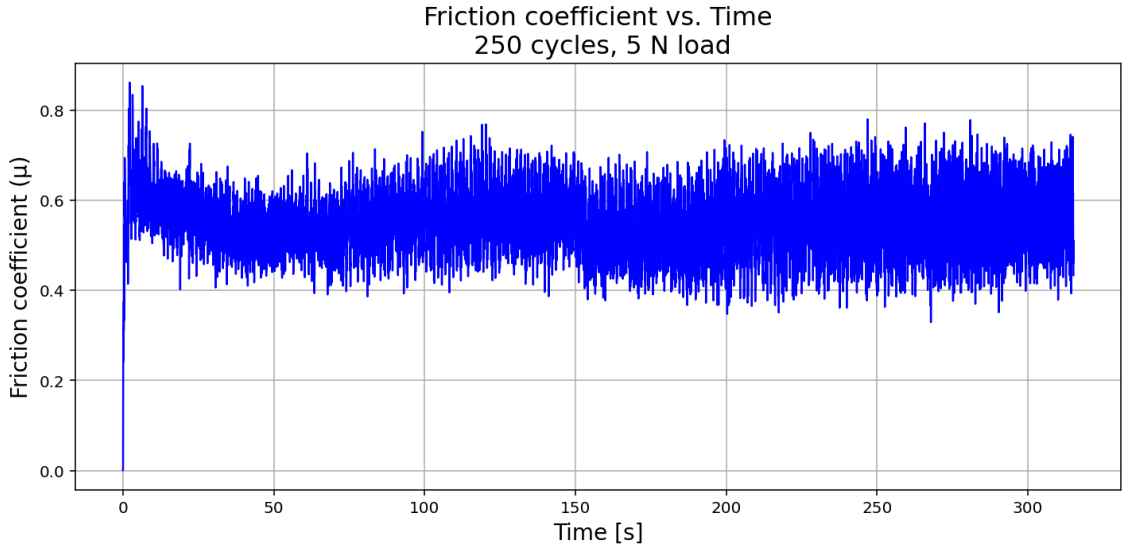

Figure A.294: This figure shows a 1500 nm TiN sample. This figure shows the friction coefficient recorded during tribometry measurement when equipped with a load of 5 N and during 250 cycles.

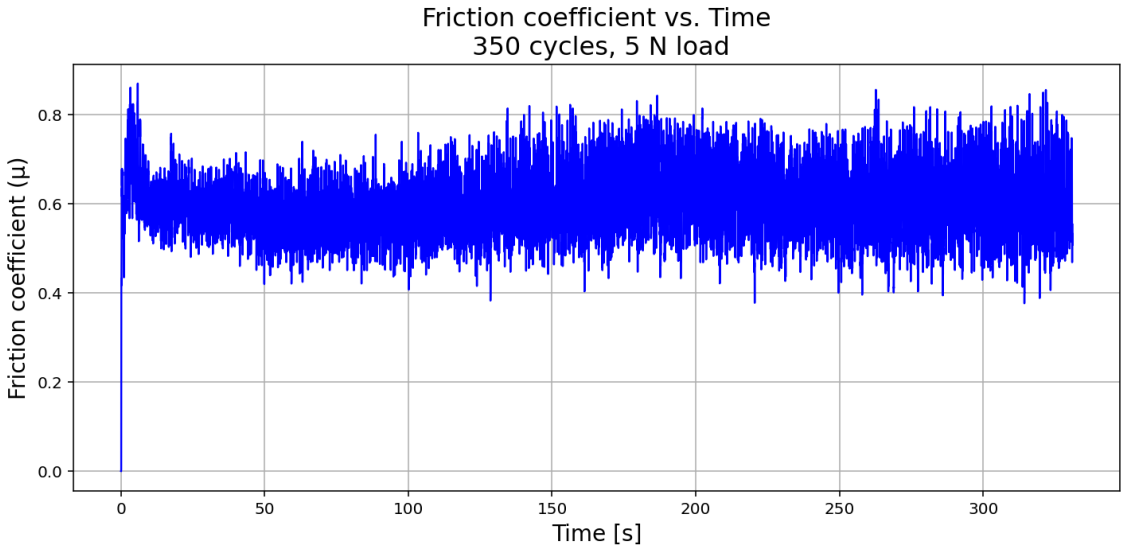

Figure A.295: This figure shows a 1500 nm TiN sample. This figure shows the friction coefficient recorded during tribometry measurement when equipped with a load of 5 N and during 350 cycles.

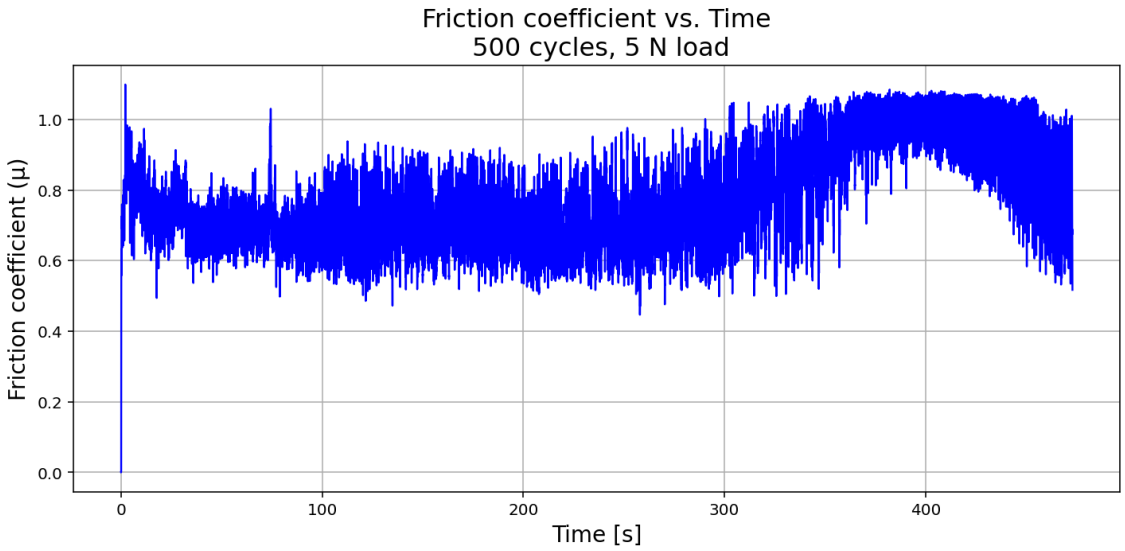

Figure A.296: This figure shows a 1500 nm TiN sample. This figure shows the friction coefficient recorded during tribometry measurement when equipped with a load of 5 N and during 500 cycles.

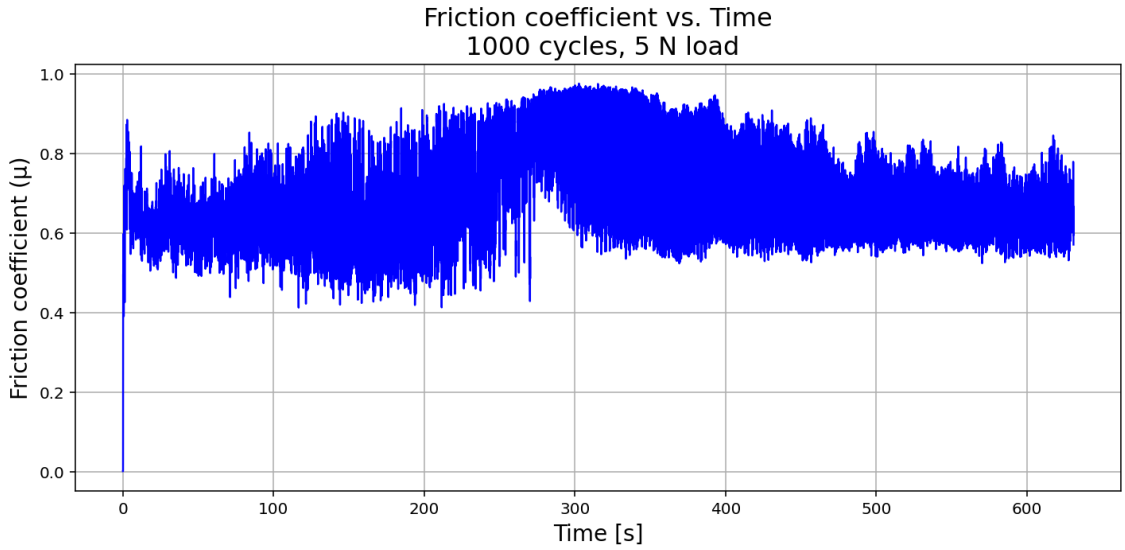

Figure A.297: This figure shows a 1500 nm TiN sample. This figure shows the friction coefficient recorded during tribometry measurement when equipped with a load of 5 N and during 1000 cycles.

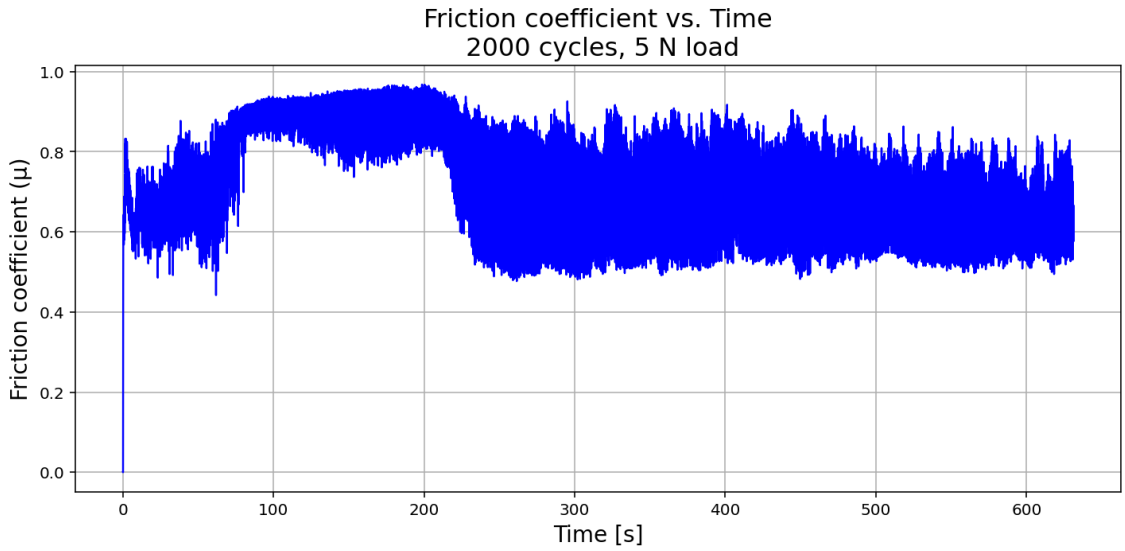

Figure A.298: This figure shows a 1500 nm TiN sample. This figure shows the friction coefficient recorded during tribometry measurement when equipped with a load of 5 N and during 2000 cycles.

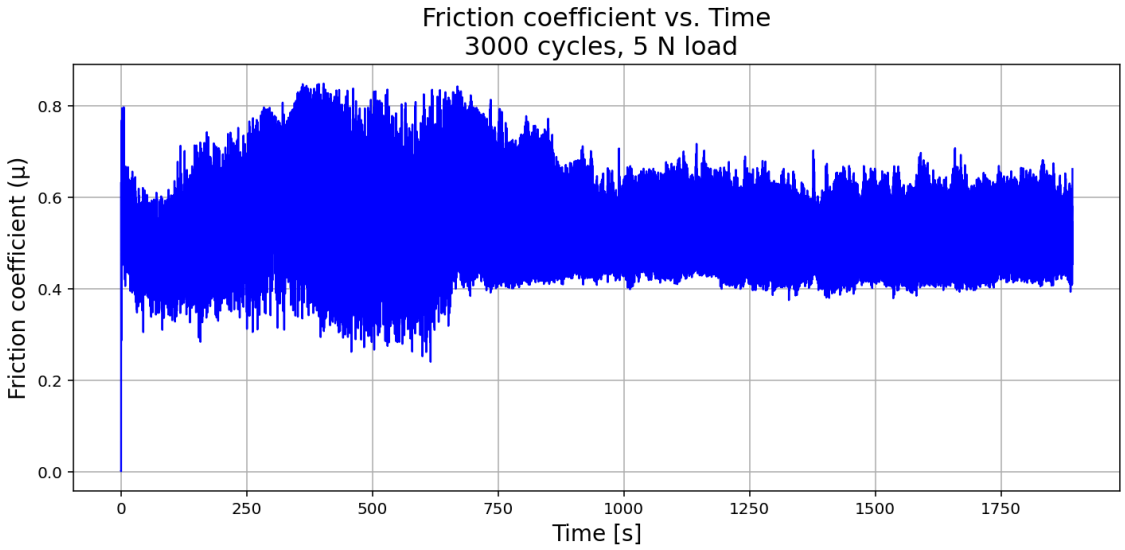

Figure A.299: This figure shows a 1500 nm TiN sample. This figure shows the friction coefficient recorded during tribometry measurement when equipped with a load of 5 N and during 3000 cycles.

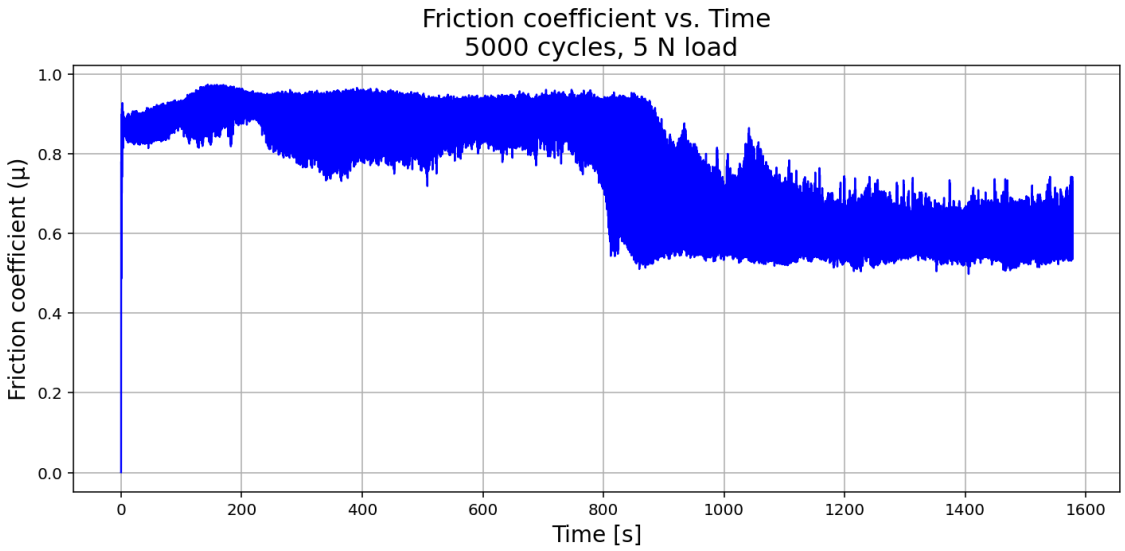

Figure A.300: This figure shows a 1500 nm TiN sample. This figure shows the friction coefficient recorded during tribometry measurement when equipped with a load of 5 N and during 5000 cycles.

A.9.5 Friction Coefficient of 1500 nm TiN Coated Stainless Steel 10 N

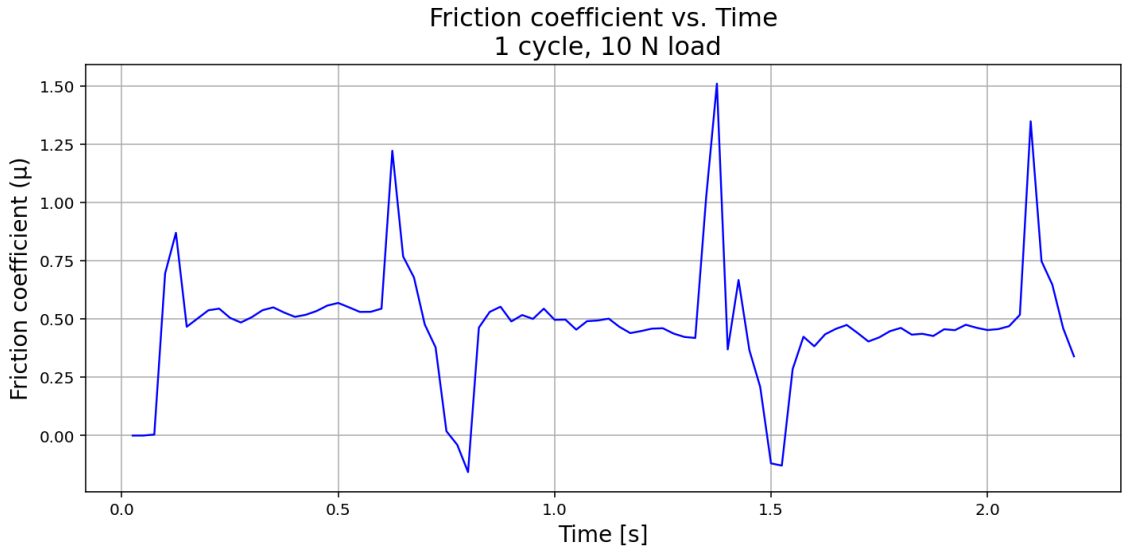

Figure A.301: This figure shows a 1500 nm TiN sample. This figure shows the friction coefficient recorded during tribometry measurement when equipped with a load of 10 N and during only 1 cycle.

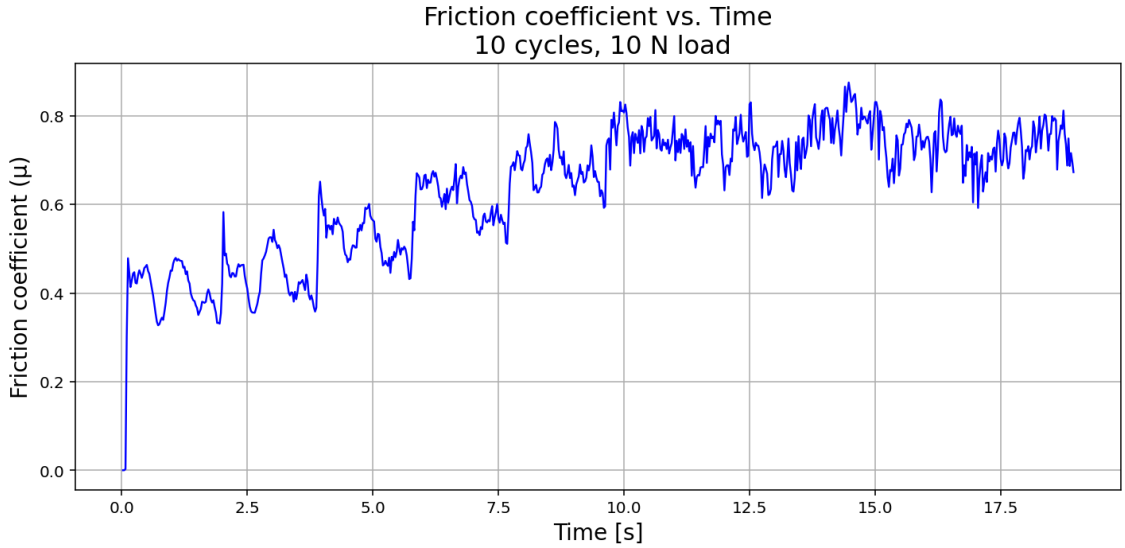

Figure A.302: This figure shows a 1500 nm TiN sample. This figure shows the friction coefficient recorded during tribometry measurement when equipped with a load of 10 N and during only 10 cycles.

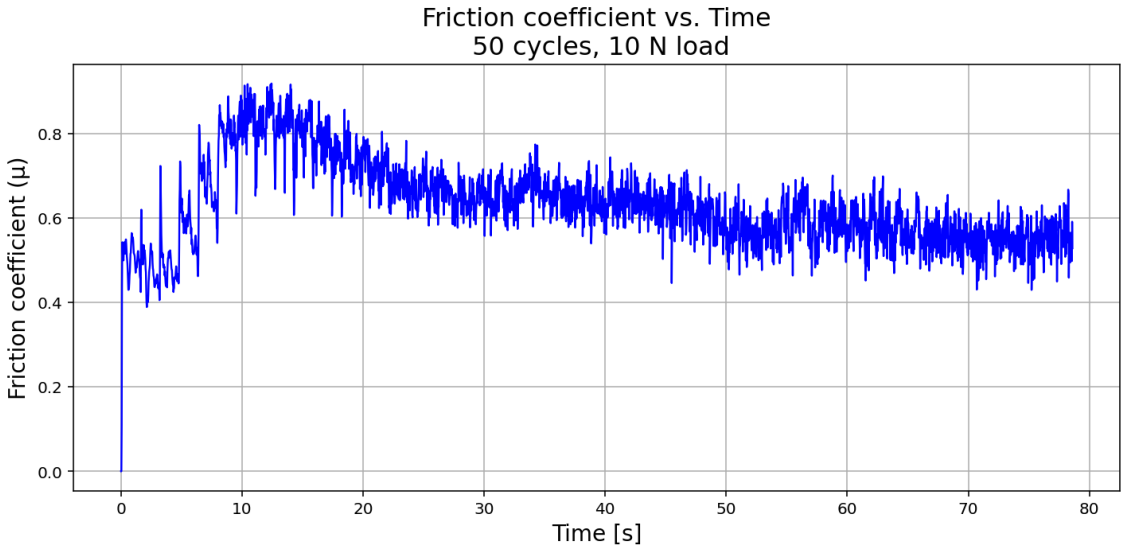

Figure A.303: This figure shows a 1500 nm TiN sample. This figure shows the friction coefficient recorded during tribometry measurement when equipped with a load of 10 N and during only 50 cycles.

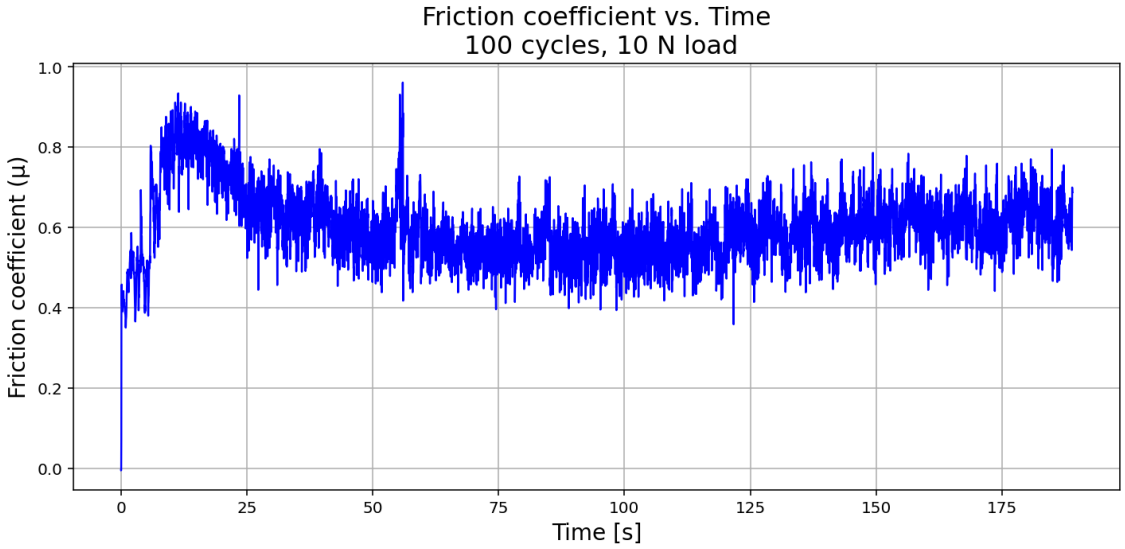

Figure A.304: This figure shows a 1500 nm TiN sample. This figure shows the friction coefficient recorded during tribometry measurement when equipped with a load of 10 N and during 100 cycles.

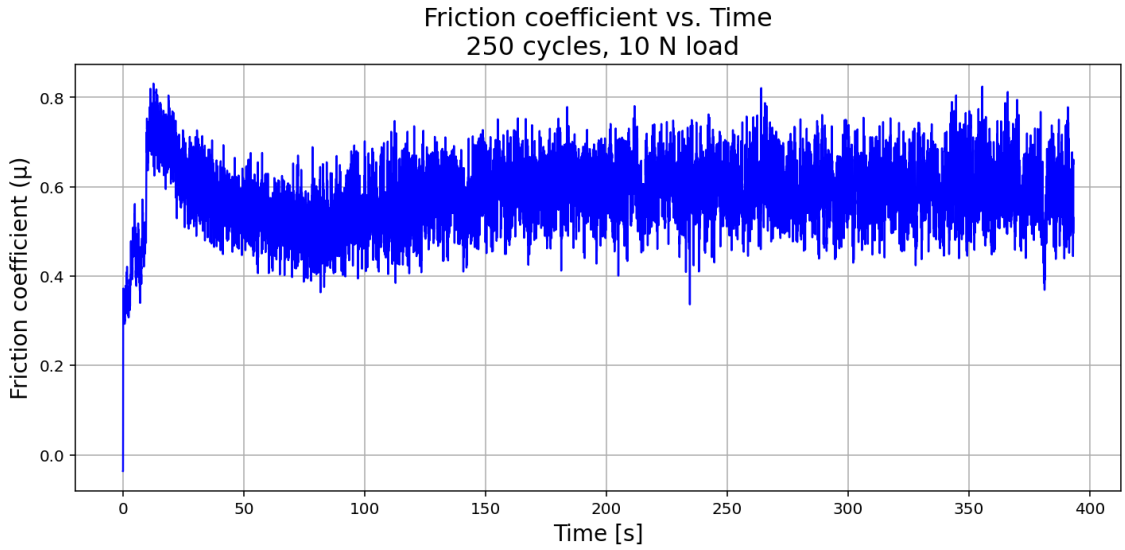

Figure A.305: This figure shows a 1500 nm TiN sample. This figure shows the friction coefficient recorded during tribometry measurement when equipped with a load of 10 N and during 250 cycles.

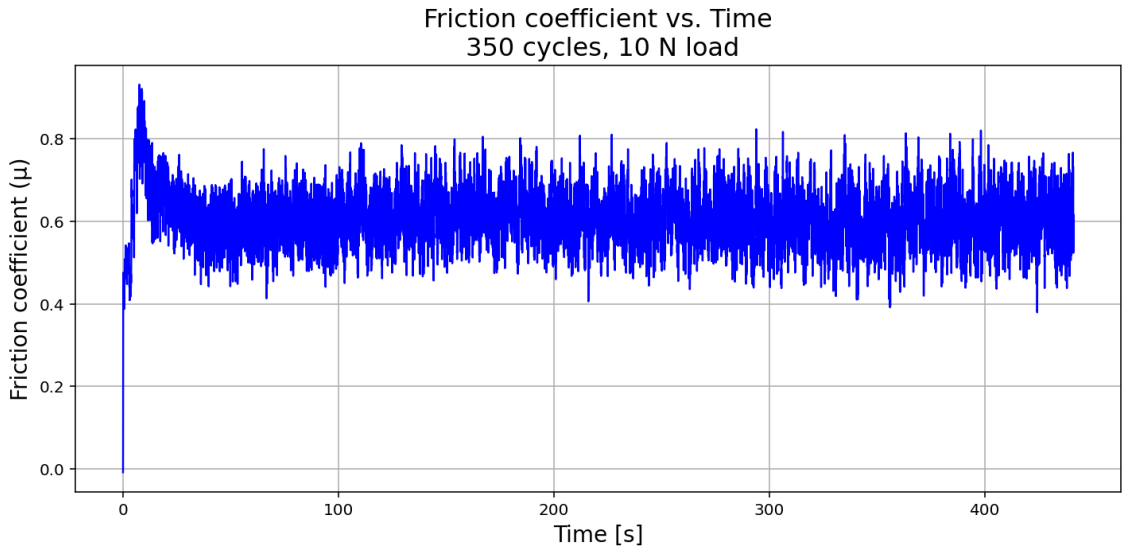

Figure A.306: This figure shows a 1500 nm TiN sample. This figure shows the friction coefficient recorded during tribometry measurement when equipped with a load of 10 N and during 350 cycles.

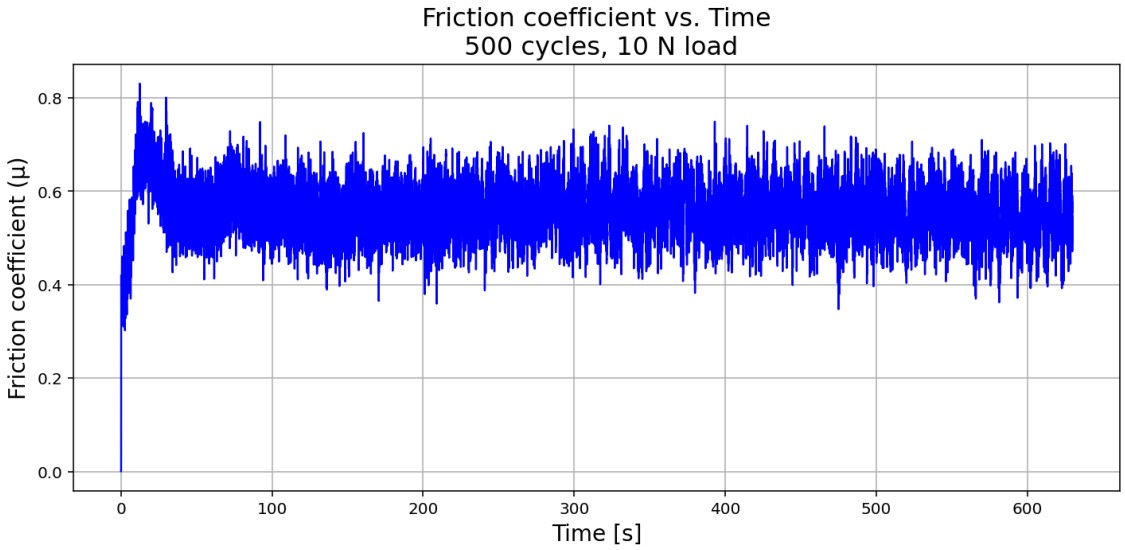

Figure A.307: This figure shows a 1500 nm TiN sample. This figure shows the friction coefficient recorded during tribometry measurement when equipped with a load of 10 N and during 500 cycles.

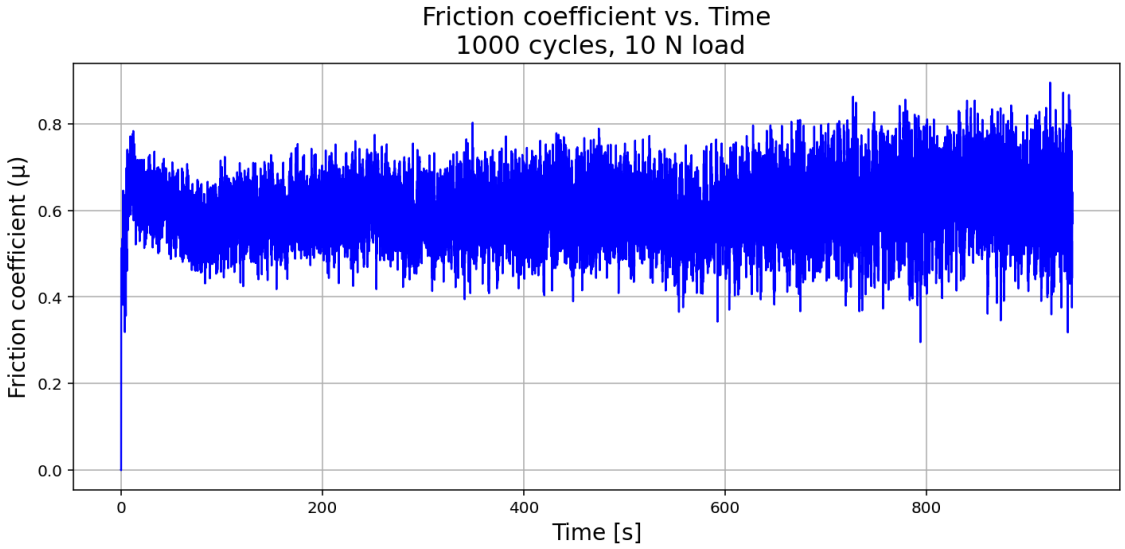

Figure A.308: This figure shows a 1500 nm TiN sample. This figure shows the friction coefficient recorded during tribometry measurement when equipped with a load of 10 N and during 1000 cycles.

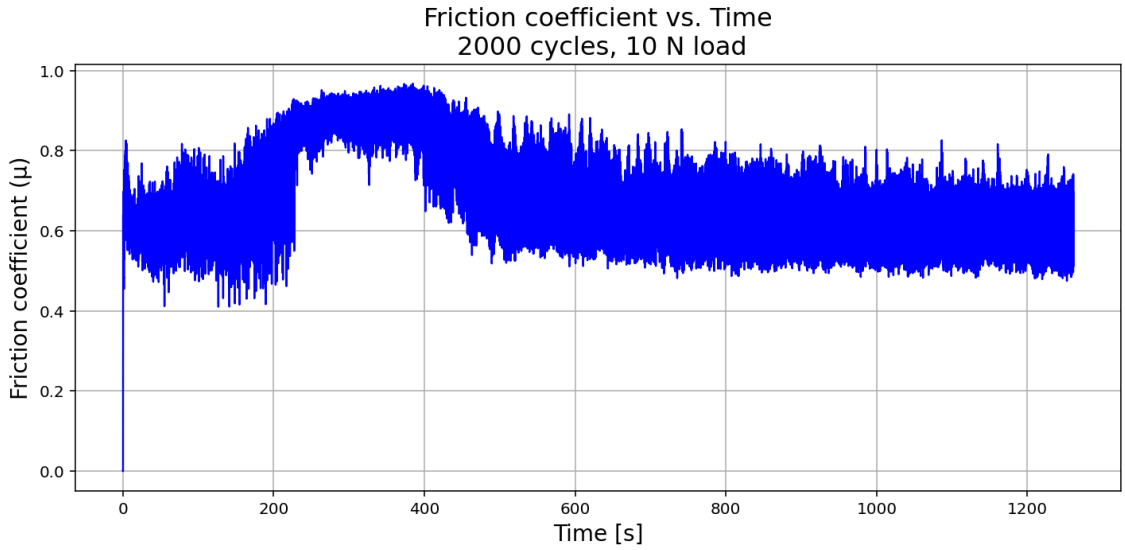

Figure A.309: This figure shows a 1500 nm TiN sample. This figure shows the friction coefficient recorded during tribometry measurement when equipped with a load of 10 N and during 2000 cycles.

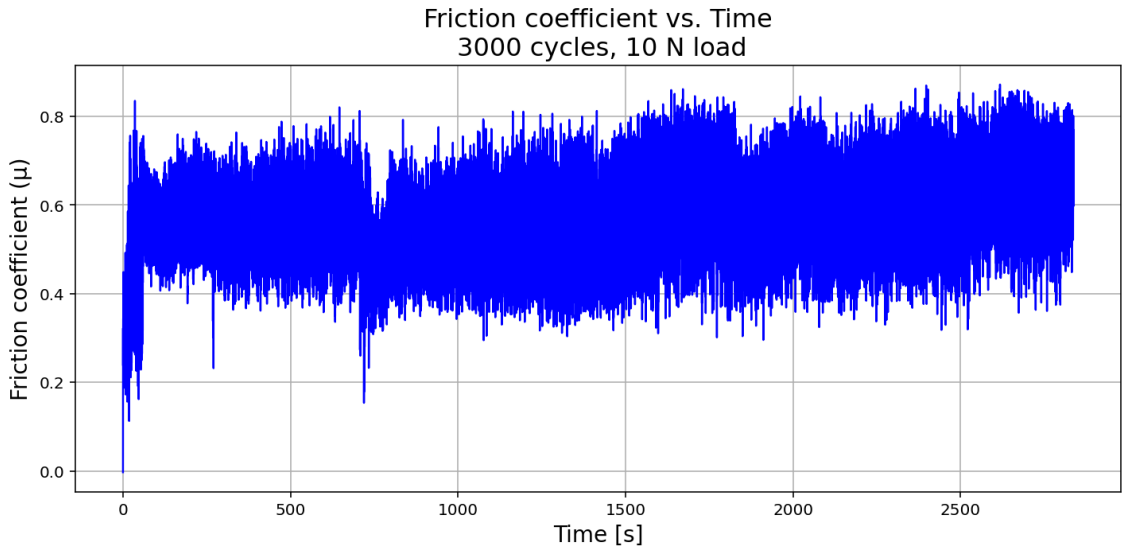

Figure A.310: This figure shows a 1500 nm TiN sample. This figure shows the friction coefficient recorded during tribometry measurement when equipped with a load of 10 N and during 3000 cycles.

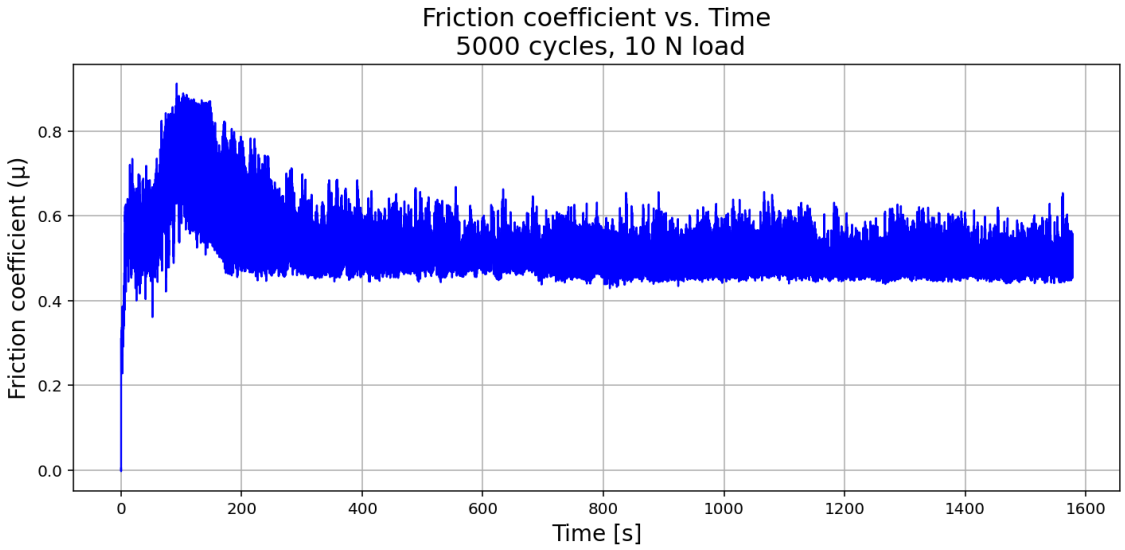

Figure A.311: This figure shows a 1500 nm TiN sample. This figure shows the friction coefficient recorded during tribometry measurement when equipped with a load of 10 N and during 5000 cycles.